Studies on sterol biosynthesis mutants of Arabidopsis

Margaret Leighton Pullen

Studies on sterol biosynthesis mutants of *Arabidopsis*

Volume 1 of 2

Thesis submitted for the degree of Doctor of Philosophy at the University of Durham

Margaret Leighton Pullen (Bsc. Liverpool, Msc. Durham)
Department of Biological and Biomedical Sciences
University of Durham

October 2005

Abstract

This thesis examines the gene promoter activity and morphological characteristics of mutants of *HYDRA1* (*HYD1*) and *HYDRA2/FACKEL* (*HYD2/FK*) (Mayer *et al.* 1991, Topping *et al.* 1997) from *Arabidopsis*. These loci are unique, and encode components of the sterol biosynthesis pathway (Schrick *et al.* 2000, Souter *et al.* 2002). Various patterning processes are disrupted in *hydra* mutants (Topping *et al.* 1997), and bulk sterol profiles are altered (Schrick *et al.* 2000, Souter *et al.* 2002). The mutants show heightened responses to auxin, and their phenotype is partly ameliorated by inhibition of ethylene signalling (Souter *et al.* 2002, 2004, He *et al.* 2003). Although much previous attention has been given to the analysis of their phenotype, the precise basis of the pleiotropic defects seen in the *hydra* mutants have not been attributed to any single phenomenon.

This thesis examines the *hydra* mutants' body patterning and morphology, and aims to test the hypothesis that *hydra* mutants are defective in pattern coordination across the radial axis. The basis of phenotypic rescue through reduced ethylene perception, as conveyed by the *ethylene insensitive2* (*ein2*) mutation (Alonso *et al.* 1999), is also examined using anatomical and transgenic markers of pattern definition and phytohormone signalling response.

Mutants at the *hydra* loci have a substantial inter-sibling variability, including duplication or dissociation of the longitudinal axis. Reporter activity of the *HYDRA1* (*HYD1*) promoter implies an association of gene activity with stipules, and functional epidermal cells and ground tissue in both root and shoot tissues at the point of cell differentiation. Reporter expression defines a radial gradient across the root longitudinal axis which is maximal in the differentiation zone. All cell types highlighted by pHYD1::GUS activity sow anomalous cellular patterning in the root and rosette of *hydra* mutant

seedlings, although pattern definition in lateral organs of the inflorescence stem appear relatively normal. Tissues of the *hydra* embryo and vegetative rosette have ectopic cell division activity; this persists in cotyledons beyond the point where wild-type cotyledon development has ceased.

Reduced ethylene perception via *ein2* appears to confer a partial rescue of the *hydra* phenotype by facilitating an earlier transition from cell division to cell fate commitment, thus allowing greater coordination between cells in longitudinal cell files. This phenomenon may be attributable to enhanced auxin transport. In contrast, shoot dorsiventral cues are variably skewed or reversed, correlating with a loss of stipular function, in a manner independent of ethylene signalling. Other phytohormone signalling systems, as revealed by reporter constructs for auxin, cytokinin and gibberellin responsive genes, show a varied activity between seedlings. All of these responses appear anomalous in *hydra* single mutants, some with distinct differences between the two mutant sibling populations. These responses are partly modulated by *ein2* in the *hydra-ein2* double mutants, although *ein2* itself has little or no effect on reporter activity. In particular the distinctive differences in cytokinin positional response between the two *hydra* mutants are abolished by the presence of *ein2*.

HYDRA gene activity appears to modulate radial patterning and differentiation-associated processes. The mutant shoot phenotypes suggest a role for sterols in the definition of organ lateral boundaries and coordinated centrolateral expansion in flattened organs. In the mutant root, the control of the transition from division to differentiation in cortex cells is disrupted in *hydra* and may reflect a disrupted phosphate perception. As *HYDRA* gene activity is associated specifically with functional cells in the epidermis, this suggests that sterols may activate a mechanism for the timed differentiation of 'target cells'. Models are proposed to integrate the *HYDRA* gene expression data and the *hydra* mutant phenotype into a functional scheme of plant development.

Declaration

All work recorded in this thesis is original unless otherwise acknowledged in the text or by references, and has not been previously submitted for a degree in this or any other university.

Statement of Copyright

Acknowledgements

Thanks go to my supervisor, Prof. Keith Lindsey, for advice, encouragement, and a degree of freedom such as is rarely afforded to a PhD student. I am similarly grateful to everyone from our lab team, past and present, for their generosity with advice, time, and general good humour. I should particularly like to mention Jen for her enduring calm under all circumstances, Kerrie and Gill for a lot of laughter, Stu for molecular biology advice and (ahem) moving a considerable amount of compost, Ellie for extra-ordinary perceptiveness (and timely supplies of chocolate), and Nick for being there during an abysmally timed house move. Mrs Christine Richardson contributed invaluable assistance with the sectioning, confocal work, and appeared not to mind my persistent dumb questions. My 'students' Prof. Xianlong Zhang and Duncan Wiles are noted for their hard work and patience, and Dr Fatimeh (Roya) Zarinkamar for the histology advice, friendship, and faith in me both in and out of the lab.

This work has benefited from the financial support of the University of Durham, and use of facilities at Department of Biological and Biomedical Sciences. Thanks also to our many collaborators who generously shared their seed lines and advice; you are all mentioned in context.

To Mr Roy Biggs and Dr Anthony Parton; I am indebted to you both for teaching me to begin to learn how to see. I am grateful to you Roy for being prepared to make me angry, and to you Anthony for making me feel like everything was my own discovery. I shall not forget this generosity.

A huge thank-you to Greg; my wonderful and insightful husband, and for my loving and supportive family, and to my friends, all of whom have put up with the neglect without complaint as I plodded my way through the writing.

To all of the above, this is our achievement, not just mine. We shall celebrate and give thanks.

"If I have seen further it is by standing upon the shoulders of giants"

(Sir Isaac Newton)

This thesis is dedicated to my giants.

Three generations of extraordinary women;

The late Margaret Mountain *née* Leighton

June Margaret Franks *née* Mountain

Megan Tafner *née Franks*

Two extraordinary men;

John Franks

The late Fr. Anthony M Cunningham

An extraordinary friend;

Madelaine Beryl Coyne *née* Ellerton

Contents

Volume 1

Volume 2

Chapter 1

Aspects of pattern formation during plant development

1.1 Abstract

This chapter introduces the context of current thinking in plant development, and appraises some of the evidence concerning pattern formation within the plant body. Much recent work has focused upon embryogenesis, particularly using the model species *Arabidopsis*. This species is used as a case study to illustrate some of the new molecular genetic data on plant pattern formation, against a background of anatomically based 'classical' studies of development. The expression of selected genes from *Arabidopsis* are considered as a means of genetically defined cellular identity during the establishment of pattern within the plant body, with emphasis on the definition of longitudinal and radial axes. These processes, and the resultant patterning and morphology, are influenced by signalling cascades involving phytohormones such as auxin, and modulated by the internal sterol environment of the seedling.

Bulk sterols affect the properties of membranes, whilst others act as precursors to signalling molecules such as cholesterol and the brassinosteroids. Screens for altered patterning in embryos and seedlings have identified genes encoding some components of plant sterol biosynthesis. Analysis of the sterol composition of these mutants reveal a modulated sterol environment in the plant body, and a complexity of biochemical pathways which are distinct to plants. Amongst these, the *hydra* mutants of *Arabidopsis* are disrupted in single genes from the early in the isoprenoid metabolic pathway which generates 24-methylated sterols. Their seedling lethal phenotypes are reviewed as potential examples of defective radial pattern formation, and possible sterol-mediated mechanisms affecting pattern formation are reviewed.

1.2 Axioms and axes in the study of plant development

1.2.1 Plant development's developmental axis

Within the discipline of biology, 'development' refers to the progression of events by which a multi-cellular organism resolves a mature adult form from a single celled zygote. In animals the adult body plan, with its characteristic numbers of organs and tissue types, is defined during embryogenesis, often in a rudimentary form. Post-embryonic growth then concerns the enlargement and maintenance of this body. In contrast, plant embryogenesis defines a 'primary body', consisting of a cylindrical arrangement of vascular conducting tissues enclosed in protective layers of ground tissue and epidermis, and ending in apical meristems. These meristems undergo an indeterminate and repetitive development throughout the life of the plant, generating a 'secondary body' comprised of a range and variable number of structures not found within the embryo (Steeves & Sussex 1989).

Historically, developmental biology has involved the derivation of general principles from the study of comparative anatomy and morphology. This approach was revolutionized by the discovery of the genetic basis of heredity, resulting in the application of new molecular tools and technologies to re-examine old questions, and the adoption of single species as 'model systems' for exploration of specific gene function. In one model system, the fruit fly *Drosophila*, the isolation of embryonic genes facilitated significant and rapid advances in the understanding of early developmental processes (Nüsslein-Volhard & Weischaus 1980, Nüsslein-Volhard 1991). The success of this approach prompted the search for genes expressed during plant embryogenesis, often using *Arabidopsis* as a model system (e.g. Mayer *et al.* 1991, Meinke 1991a. 1991b, Lindsey & Topping 1993, Goldberg *et al.* 1994). This framework brought ideas and concepts from animal development into the interpretation of plant molecular

genetic data. Plant genes were sought, and found, that had homology to known genes responsible for patterning of animal embryos, e.g. the *POLYCOMB* and *HOMEOBOX* (*HOX*) genes first discovered in *Drosophila*, and many groups of transcriptional activator proteins.

An abundance of transcription factors have been found in plant genomes. Some, including the MYB protein family, are common to plant and animal development, whilst others such as the HD-Zip class, are unique to plants and may mediate unique plant patterning processes (Schena & Davis 1992, Martin & Paz-Ares 1997). Early analyses of these and other genes were therefore evaluated within the framework of animal development, leading to an interpretation of plant mutants using the idea of the embryo as a series of connected compartments along an apical-basal axis (e.g. Jürgens *et al.* 1991, Mayer *et al.* 1991, Laux *et al.* 2004). By this route other concepts from animal embryogenesis such as cell lineage defining cell fate, and the independence of embryonic and post-embryonic growth, were adopted into analyses of plant embryogenesis (Kaplan & Cooke 1997).

Recent work has shown that many of these ideas are misconceptions when applied to plant development. Studies involving laser ablation and excision of specific tissues have re-established the former view of precedence of the positional context over cell lineage (Berger *et al.* 1998b, Lim *et al.* 2000). In addition, molecular genetic studies have confirmed the role of certain genes in the directing of specific cell fates in a position-dependent manner (Lee & Schiefelbein 1999, Masucci *et al.* 1996, Wada *et al.* 1997). Kaplan and his coauthors, along with other groups, are beginning a re-synthesis of the vast body of early (pre-1990's) work in comparative plant morphology, wherein classic comparative anatomical studies provide a context for the interpretation of molecular genetic results (Kaplan & Cooke 1997, Kaplan 2001a, b). Other ideas from animal biology, such as maternal effects upon the developing embryo, and lateral inhibition between cells during pattern definition (e.g. leopard spots, zebra stripes, and trichome spacing from *Drosophila*), have endured as relevant comparisons, and are now receiving greater attention.

1.2.2 Axes can be defined within the *Arabidopsis* plant body

Axial patterning phenomena amongst the dicotyledons have been most comprehensively studied to date in the 'model' species *Arabidopsis thaliana*. In this species, the sequence of cell divisions from the first division of the zygote, and the resultant organization of the embryo, has been catalogued and is typically interpreted as a stylized programme under tight developmental control. The first transverse division of the zygote, separating cell lineages that form the embryo-proper and its suspensor, have been interpreted as defining apical-basal and radial axes in the plant body (Goldberg *et al.* 1994, Mayer & Jürgens 1998, Vroemen *et al.* 1996, 1999, Laux *et al.* 2004). However the 'pattern formation' process within the plant, by which cell fates are adopted in a position-dependent manner, is still "...A concept in search for a molecular mechanism" (Mayer & Jürgens 1998).

The plant body can be considered as having three planes of section through which the primary axes are discernible, as illustrated in Fig. 1.1.

1. Longitudinal or apical-basal; this includes the longitudinal axis of shoot lateral organs, which arise around the meristem flanks in lateral positions as outgrowths in the apical direction. Within the plant, 'distal' or 'acropetal' indicates a position towards the extreme of this axis, although applying this definition to the shoot and root apices appears to indicate opposing directions in the plant body.
2. Radial; in the median plane from the centre towards the periphery. Growth of dicotyledons is characterized by a radial organogenesis around the shoot apex, in a helical, whorled or opposite (distichous) 'phyllotaxy'. In the flattened *Arabidopsis* leaf, the radial axis spans the leaf width in the adaxial-abaxial (central-peripheral) direction. This axis is also termed 'dorsiventral'; in botanical terms, 'dorsal' and 'ventral' have been applied to erect leaves as they appear at the primordial stage, so the 'ventral' or back corresponds to the abaxial

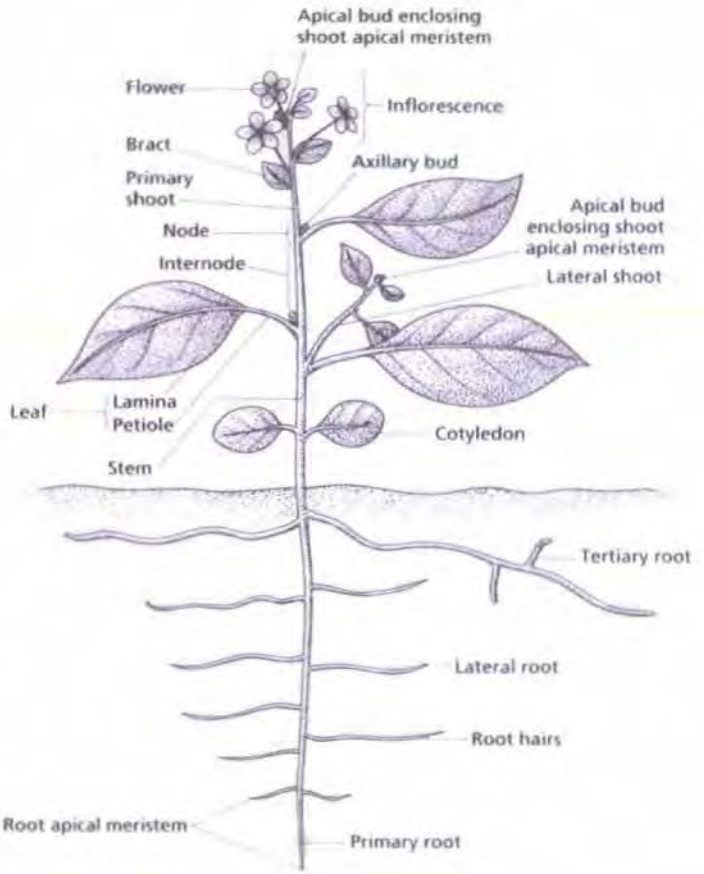

(a) Annotated generalized plant structure

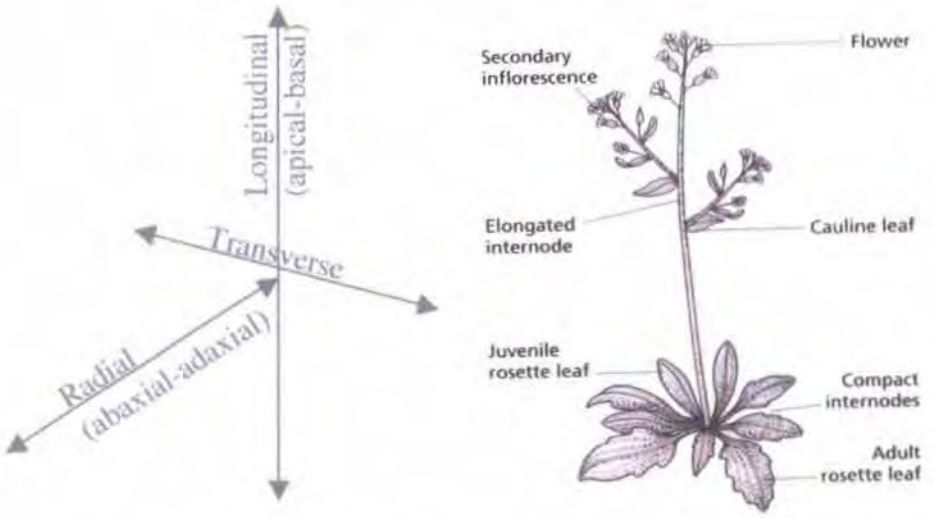

(b) Planes of section

Figure 1.1 Axes and morphological structures in dicotyledons

Diagrams adapted from Leyser & Day (2003)

(outer) side (Kaplan & Cooke 1997). There is some confusion over this definition in recent botanical literature, both with the allocation of 'dorsal' and 'ventral' (e.g. Hudson & Waites 1998), and use of the term 'dorsoventral', another misconception from animal development (e.g. Waites *et al.* 1999, Sessions & Yanofsky 1999, Reinhardt *et al.* 2004)

3. Transverse; at right angles to the long axis of the shoot. A transverse section of the plant body reveals the organization of the apical basal axis in radial layers. Most dicotyledonous leaves expand 'centrolaterally', in the transverse plane at right angles to both the longitudinal and radial sections, and develop a lamina which has parallel abaxial and adaxial surfaces separated by a mesophyll layer. Transverse sections of leaves from most species of plant vary substantially in shape at different points along the leaf apical-basal axis.

In addition, a bilateral symmetry can be defined in the embryo from the inception of the two cotyledon primordia either side of the shoot apical meristem. This pattern is the instigation of the helical, whorled or alternate phyllotaxy seen around the meristem periphery in post-embryonic growth. Primordia develop at different growth stages, and hence in different positions; this results in the temporal instigation of organ differentiation, broadly defining the organ type within the hierarchy of the shoot.

1.2.3 Longitudinal organization of the dicotyledon plant body is established across the apical radial axis

The dicotyledonous shoot apical meristem (SAM) establishes a population of stem cells from its first inception in the globular-stage embryo, and maintains them in an undifferentiated state throughout the life of the plant. The SAM has a structure which is comprised of layers of cytologically differentiated cells, shown diagrammatically in Fig. 1.2. In longitudinal

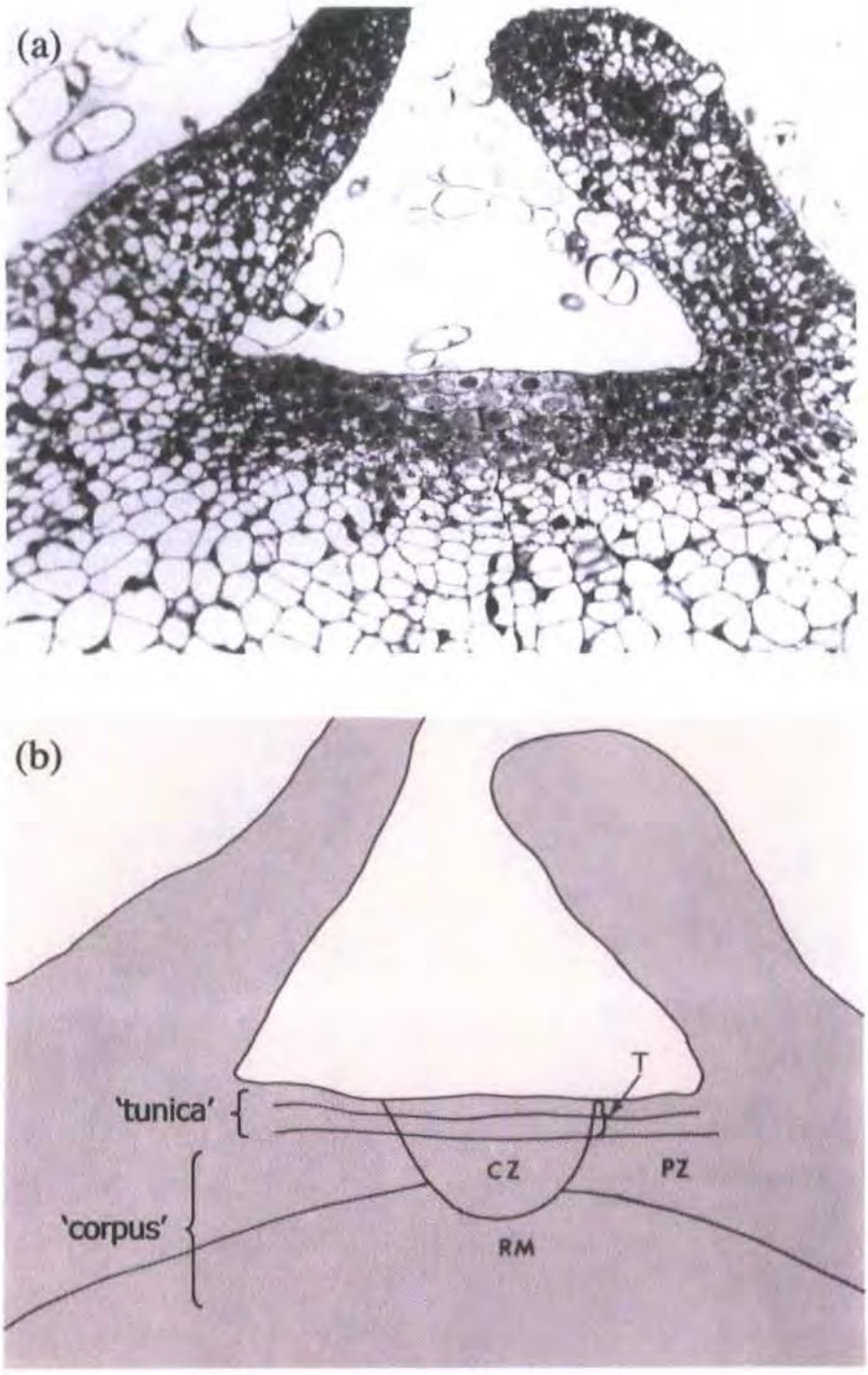

Figure 1.2 Zonation of the shoot apical meristem in *Helianthus annuus*

(a), median longitudinal section of the shoot apical meristem of *Helianthus annuus*, x340; (b), diagrammatic illustration of the same apex shown in (a). Key; CZ, central zone; PZ, peripheral zone, RM, rib meristem, T, tunica. The 'tunica-corpus' concept of longitudinal stratification of cell layers, can be used to define the organization of cells in longitudinal sections of angiosperm apices, along with some examples from other plant groups. The tunica and corpus regions are anatomical reflections of the pattern of cell division activity at the apex. This varies substantially between species.

Diagrams taken from Steeves & Sussex (1989).

section, the outer cell layers over the structure comprise small, densely stained cells, lying above an area of larger cells with greater vacuolation. These zones have traditionally been termed the 'tunica' and 'corpus', and are a pattern common throughout the angiosperms (Steeves & Sussex 1989). The outer cell layers of the tunica, termed L1 and L2, are strongly connected by plasmodesmata, and the inner layer, termed L3, incorporates the upper cell layer of the 'corpus'. The cell layers which form the precursors to the L1, L2 and L3 layers of the SAM are distinguishable in the *Arabidopsis* embryo by the heart stage (Barton & Poethig 1993).

Roots throughout the flowering plant taxa can be variably specialised, and have multiple radial layers of cells, though all show a similar organisation at their apices, in which longitudinal files of mature and maturing cells converge on a small region below the root cap, containing initial cells around a quiescent centre (Steeves & Sussex 1989). Within this zone, the boundaries of a meristematic area are not definable histologically in the way that the SAM can be delineated. *Arabidopsis* has a 'closed' root meristem, in that all cell files can be easily traced and originate from specific initial cells. Other species with an 'open' meristem have a more plastic developmental fate for cells derived from the meristem initials. Serial transverse sections along the longitudinal axis of the juvenile seedling proceeding proximally from the root apex reveal a radial patterning sequence over a developmental time course.

The *Arabidopsis* root meristem, illustrated in the diagram in Fig. 1.3, is patterned by a well characterised series of division events. Divisions in initial cells adjacent to the quiescent centre (QC) generate a radially organised structure (Dolan *et al.* 1993), in which longitudinally organised cell files differentiate in radial layers, and new cells adopt a positionally defined pattern (Van den Berg *et al.* 1995). On the distal side of the quiescent centre, columella initial cells derive the root cap columella. These cells are surrounded by a ring of 16 lateral root cap initials, giving rise to both the epidermis and the lateral root cap (Dolan *et al.* 1993). Adjacent to the lateral root cap initials on the proximal side of the

(i)

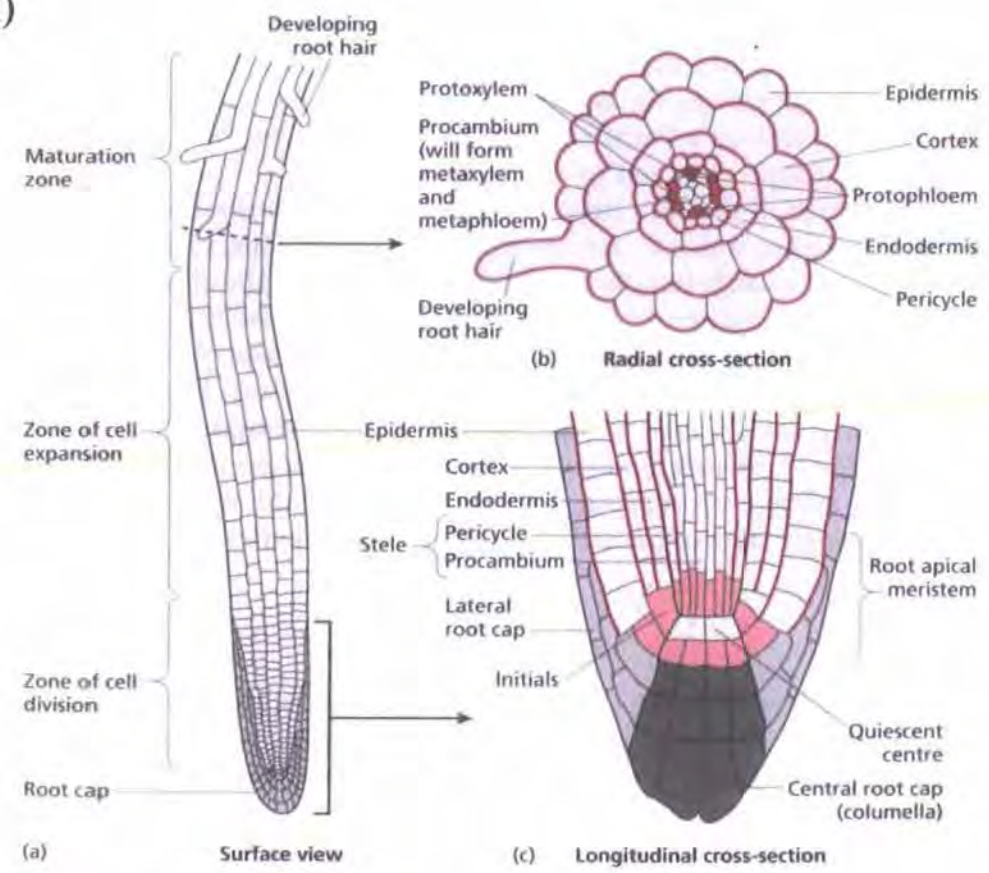

Figure 1.3 The *Arabidopsis* root apex

(i) Anatomical diagram of the *Arabidopsis* root apical region showing longitudinal patterning and zonal progression of differentiation across the radial axis (from Leyser & Day (2003) *Mechanisms in Plant Development* Blackwell, Oxford.

(ii) A model for cell division patterns at the primary root meristem of *Arabidopsis thaliana*, after Dolan *et al.* (1993). Diagram A shows the root apex as in (i), colour-coded for cell identity. B shows the initials around the central region (the quiescent centre), annotated with the numbers of different types of initials. C shows division patterns in these initials and their derivatives which generate cell layers; shown as dashed lines (first division), dotted lines (second division) and third (striped) divisions in the transverse plane.

(ii)

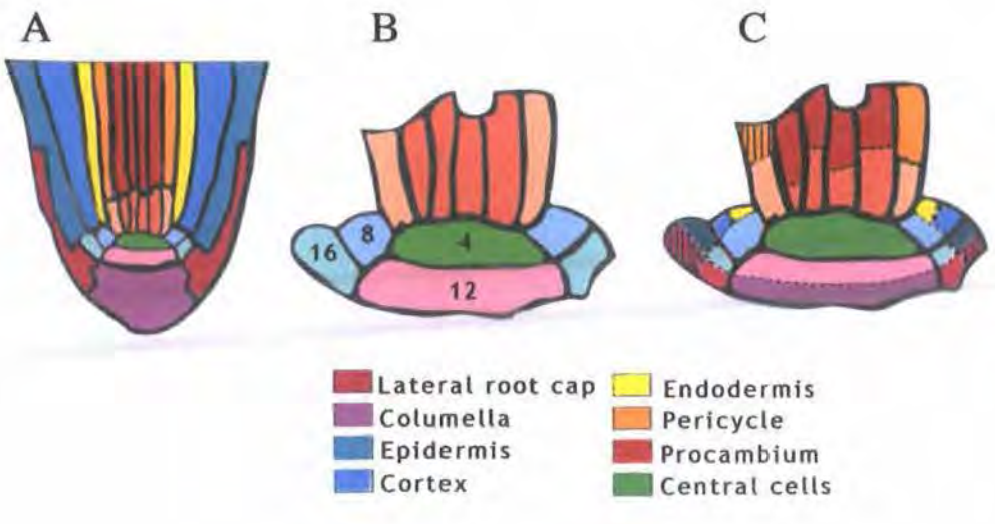

quiescent centre, a ring of 8 cortical initial cells give rise to cortical daughters, which divide periclinally to produce two radial cell layers; the cortex and endodermis. The remaining initials, towards the centre of the radial layer, derive cells of the pericycle and vascular stele.

1.3. Pattern definition

1.3.1 The plant body pattern is established during embryogenesis in a manner distinct to the plant group.

1.3.1.1 Dicotyledons

In the model species *Arabidopsis*, as in the sporophyte generation of most dicotyledons, the development of an organized embryo from the initial zygote progresses through a series of recognizable shape changes. This progression begins with the initial division of the zygote into a smaller apical cell and a larger basal cell. In *Arabidopsis* the basal cell undergoes a filamentous growth to form the suspensor, whilst the apical cell forms the 'embryo proper' (Lindsey & Topping 1993). Initial symmetrical divisions form an 'octant' of 8 isodiametric cells, followed by a 'globular' stage where internal cell layers are resolved, a 'heart' stage where the shoot apical meristem devolves its first two organs (the cotyledons), a 'torpedo' stage of elongation, and later stages involving the maturation of the embryo prior to dormancy. This sequence is illustrated in Fig. 1.4.

In *Arabidopsis*, as in *Capsella bursa-pastoris* and other Brassicaceae, a protoderm is formed at the octant-globular transition by asymmetric, periclinal divisions (parallel with the surface) to resolve a 16-cell 'globular' form with an outer and inner cell layer of 8 cells each. This is followed by further periclinal and anticlinal divisions to distinguish a 3-layered structure comprising an inner procambium surrounded by a ground tissue layer and outer protoderm (Mayer *et al.* 1991, Scheres *et al.* 1994).

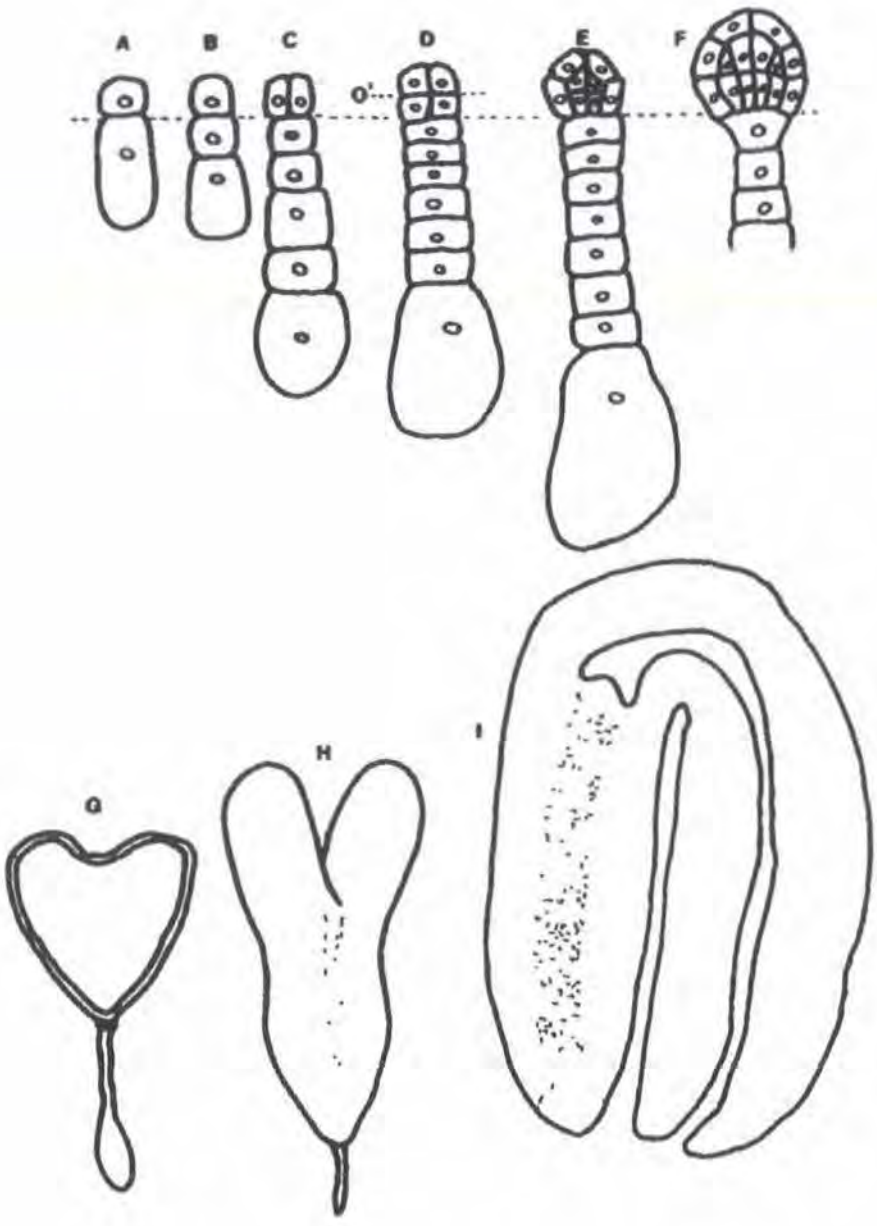

Figure 1.4 Schematic representation of *Arabidopsis thaliana* embryogenesis (from Lindsey & Topping 1993)

The model dicotyledonous species *Arabidopsis* has small embryos, hence a minimal cell number, making cellular pattern definition easy to discern.
A-C, pro-embryonic stages. A shows the two which result from the initial asymmetric division of the zygote. B and C illustrate the development of these lineages into the embryo proper (apical cell) and suspensor (basal cell). The dotted line represents the clonal boundary between these two regions. D, octant stage, showing the position of the so-called O' boundary between the upper and lower domain of the embryo proper; E-F, globular stage; G, heart stage, H, torpedo stage; I, cotyledonary (mature embryo) stage.

Elongation of the central cells then resolves a discernible apical-basal morphology within the cell mass, and the embryo begins to appear flattened at the apex as the shoot apical meristem (SAM) initiates, prior to early cotyledon expansion when a bilateral symmetry becomes apparent.

The subsequent elongation of the *Arabidopsis* embryo resolves a central region of cells which form the precursors to the seedling hypocotyl, below which the hypophysis divides to produce the precursors of a root meristem, first differentiating a root cap columella (Scheres *et al.* 1994, 1995). As the embryo elongates during the torpedo stage, the suspensor starts to degenerate. Later cell divisions in the lower hypocotyl and root zone are not as regular, with some cells producing tangential cell walls, that become 'normalized' in alignment, possibly by inner pressure from the cell mass (Scheres *et al.* 1995).

The orientation of cell division events within the dicotyledon embryo proper that establish this internal radial organization is not prescriptive in all species. Steeves & Sussex (1989) point out that some dicotyledons have a variable or obscure pattern of cell division. Two well-studied examples include carrot (*Daucus carota*) where cleavage patterns have been shown to be variable, and cotton (*Gossypium hirsutum*) where cell wall orientation appears to be completely irregular. Citing these and other examples, Kaplan & Cooke (1997) offer the explanation that the supposedly invariable cell division patterns seen in *Capsella* and *Arabidopsis* are related more to the physics of their small size and uniform growth than to any basis of form generation.

1.3.1.2 Monocotyledons

In monocotyledon embryogenesis, the shape-based definition of developmental stages cannot be applied. Monocot embryos initiate only a single cotyledon, and consequently do not proceed through a heart stage. Neither do they have a clear longitudinal or radial symmetry. However the earlier stages share certain similarities with the 'classic' dicotyledonous

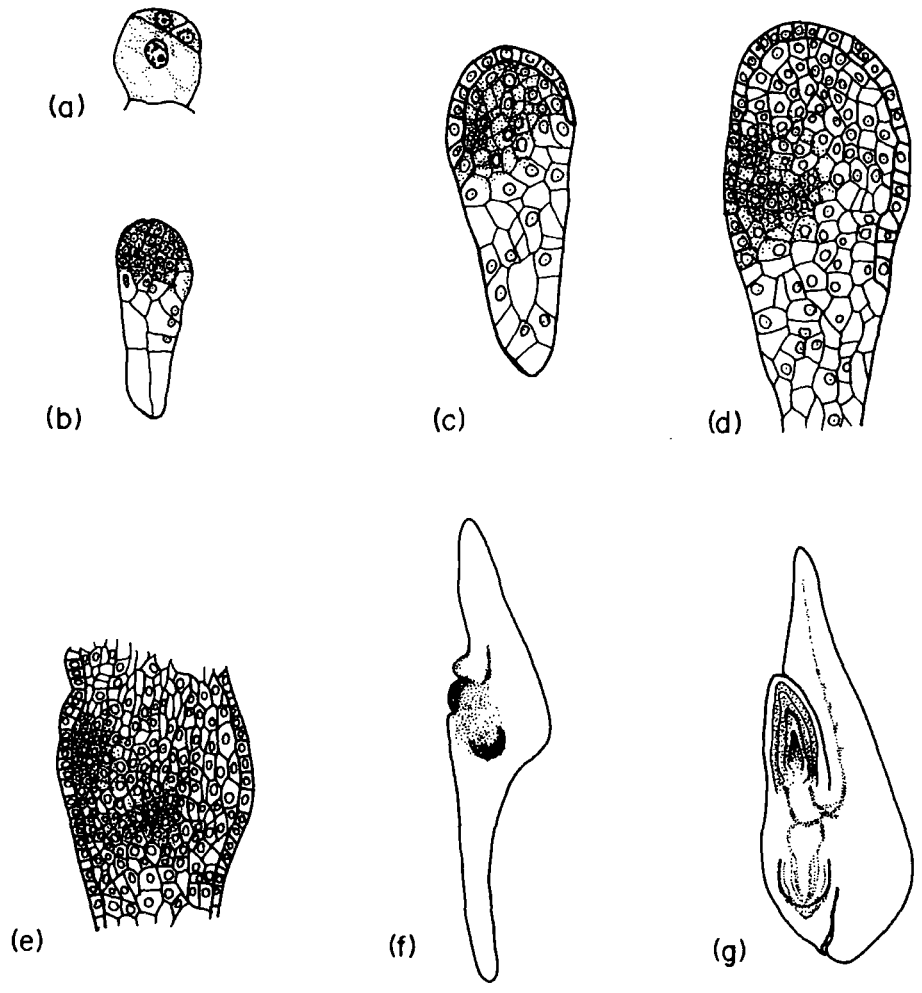

Figure 1.5 Embryogenesis in *Zea mays*

(a) Three-celled embryo showing first division of the terminal cell. (b) Six-day embryo sowing embryo proper and suspensor. (c) Seven-day embryo showing delimitation of protoderm in embryo proper. (d) Nine-day embryo showing increased cytoplasmic density (on the left) in the region where the meristems arise. (e) Eleven day embryo showing superficial position of the shoot apical meristem and internal origin of the root apical meristem. (f) Thirteen-day embryo showing shoot and root apical meristems. (g) Forty-four day, fully developed embryo. (a-d), x140; (e), x125; (f), x42; (g), x8.5.

Diagram reproduced from Steeves & Sussex (1989).

series as outlined for *Arabidopsis*. In the monocotyledon species *Zea mays* (maize), shown in Fig. 1.5, the first division of the zygote is asymmetrical and produces a smaller apical cell and larger basal cell. The apical cell then divides vertically, to give two isodiametric cells, although later divisions are irregular both in orientation and sequence (Poethig *et al.* 1986). The result is a club-shaped embryo, where the suspensor tissue is integral to the overall cell mass, and is distinct from embryo-proper only in its larger cell size and greater vacuolation. The shoot meristem develops from an area of cytoplasmically-dense cells in a lateral position, and the root meristem differentiates internally within the cell mass at the basal end near the suspensor. A strand of procambium then differentiates through the embryo axis between the two meristems. The remainder of the embryo proper is involved in the formation of the scutellum; a shield-like organ often interpreted as a cotyledon homologue. The suspensor then continues to enlarge, and the shoot meristem initiates up to 6 leaves.

1.3.1.3 Gymnosperms

A great diversity is found in the embryo development of gymnosperms. The taxon is characterized by a period of free nuclear division at the beginning of embryo development. The large egg, contained within the female sex organ (the archegonium), is situated at the micropylar end of the cellular female gametophyte. After fertilization, the zygote nucleus divides, but no cell walls arise to separate the daughter nuclei until many nuclei are present in the cytoplasmic mass. Wall formation occurs and partitions the embryo into uninucleate cells of similar size. Cells further from the micropyle then undergo more rapid divisions, resolving a marked axial gradient in cell size with the smallest cells at the apical region. These small cells give rise to the shoot and root apices and cotyledons, whilst the larger cells (comprising two thirds of the embryo volume) divide more slowly, are vacuolated, and are interpreted by some as constituting a suspensor (reviewed in Steeves & Sussex 1989).

The free nuclear stage of gymnosperm embryogenesis is highly variable between species. This range encompasses a spectrum from a single division of the zygote prior to wall formation in *Sequoia* (redwood), 2 in the Cupressaceae, 256 in *Ginkgo*, and over 1000 in the cycad *Dioon edule*. Another feature of the gymnosperms is the incidence of polyembryony, where multiple embryos arise from a single zygote after wall formation within the multinucleate mass, as in *Pinus* species.

1.3.1.4 Lower plants

Embryogenesis in the lower plants encompasses "...a bewildering array of embryonic types" (Steeves & Sussex 1989), although these authors suggest that the general patterns in lower plant development has many similarities to that of higher plants. Citing examples from the leptosporangiate ferns, they describe a process commencing with placement of the first zygotic cell division parallel to the long axis of the archegonium, the second division perpendicular to the first, and further synchronous divisions to produce an octant. Further divisions produce a globular mass within which differentiation begins in the part of the embryo which gives rise to the 'foot', followed by the first leaf, root and then shoot apex. In contrast to the higher plants, ferns form roots exclusively from the shoot, and do not develop a spatially separated root system. This distinctive pattern results from a unipolar embryo organization, with the first root arising at an oblique angle rather than diametrically opposite the shoot (Groff & Kaplan 1988).

1.3.2 Dormancy and seed set

The onset of dormancy has been traditionally taken as the end-point of embryogenesis. However this does not always occur in the developing seed. *In vitro* cultures of oat zygotic embryos (Triplett & Quatrano 1982) and somatic embryos of carrot (Ammirato 1983) proceeded to the seedling stage without dormancy unless supplemented by ABA. In diverse plant

species, the dormancy phase can occur at various points in the 'classic' sequence, from a rudimentary globular stage as in orchids (Arditti 1992) to the case in some grasses where the dormant seed has several sets of leaf primordia and shoot-borne roots (Hetz *et al.* 1996, Kaplan & Cooke 1997). The lower vascular plants have no interruption of growth to distinguish a distinct embryonic phase; here the embryo develops directly into a juvenile plant that bursts out of the parental gametophyte tissues, and rapidly becomes independent (Steeves & Sussex 1989).

These observations imply a continuum of development from the onset of iterative growth in the developing embryo of all multicellular plants, which is paused by dormancy in seed plants, but is not interrupted. This interpretation is given further confirmation by molecular genetic data; genes isolated for their activity early in embryogenesis, e.g. *AtML1* (Lu *et al.* 1996) *AtLTP1* (Vroemen *et al* 1996), *POLARIS* (Topping & Lindsey 1997, Casson *et al.* 2002) and *EXORDIUM* (Topping & Lindsey 1997; Farrar et al. 2003), also show activity in post-germination growth.

There is a convincing body of evidence that suggests that ABA induces dormancy and seed maturation. Certain viviparous mutants of maize have reduced ABA sensitivity (Robichaud *et al.* 1980), and many grass species develop vivipary in certain parts of their geographical range. Studies in *Arabidopsis* imply that environmental factors such as light, temperature and water availability, affect germination through the mediation of gibberellins (Chory 1997, Karssen *et al.* 1999). This implies that the instigation of dormancy is determined or modulated by environmental factors, and that the physiological response to these factors is implicit to the plant species' ecology.

1.3.3 Establishment of a longitudinal axis

1.3.3.1 The division axis of the zygote can vary between species

The smaller apical and larger basal cell resulting from the first division of the *Arabidopsis* zygote follow different developmental fates (Mansfield & Briarty 1991); the basal daughter cells dividing to produce a file of 7-9 highly vacuolated cells of the suspensor filament, and the apical cell undergoing multiple divisions to produce an 'octant' of isodiametric cells. Definition of the *Arabidopsis* apical-basal axis has been interpreted with reference to the transverse direction of cell wall placement in the initial division of the zygote This interpretation has been reinforced by studies of the polarity of the cell contents prior to division (Mansfield & Briarty, 1991, Vroemen *et al.* 1999).

Most, though not all, of the dicotyledonous species follow the *Arabidopsis* model of an initial transverse division in its zygote. Kaplan & Cooke (1997) cite at least 19 dicotyledonous species analyzed in the embryological literature, in which the zygotes undergo longitudinal, oblique or even variable first divisions instead of the expected transverse division. From a comparison of cell dimensions in these zygotes, these authors conclude that the plane of the first division coincides with the minimum dimensions of the cell. When the zygote is longer than wide, the minimum dimension will be the transverse dimension, and the first wall forms across the cell in a transverse plane. For zygotes that are wider than they are long, the minimum dimension will be longitudinal, and the first wall consequently forms along this longitudinal plane. In isodiametric zygotes, the first wall forms in an oblique plane. Kaplan & Cooke (1997) conclude that

> *"...the initial division, like most divisions in plant cells, is oriented according to the overall geometry of the zygote, thereby obeying the principles of minimum surface area; in the absence of other physical forces, an incipient wall occupies the plane within the dividing cell that represents the position of minimum surface area (Errera, 1886)."*

Kaplan & Cooke (1997) also suggest two other conclusions from their survey of dicotyledon embryogenesis. These are;

1. As growing zygotes acquire characteristic shapes before their first division, the division plane must be a consequence and not a cause of polarized growth,
2. As species examined developed a suspensor regardless of the cell division orientation, that this orientation is not essential for establishing the embryonic axis. Rather, this initial zygotic division is purely coincidental and reflects, but does not establish, the underlying polarity of dicotyledon embryos.

1.3.3.2 Zygote internal polarization appears to result from external cues

In the absence of an innate polarity, it remains for the zygote to derive a polarizing signal from its environment. The dicotyledon zygote is in initial contact with the micropyle - the aperture between the integuments of the ovule through which the pollen tube grows, and comprising the boundary tissue allowing communication between the maternal sporophyte and gametophyte. The suspensor remains connected to this structure until its degeneration at round the heart stage. There is a discernible apical-basal polarity in the gymnosperm embryo which develops in the placement of cell division events after cell wall deposition; this is also oriented in relation to the micropyle. This connection could therefore provide an initial environmental cue to prompt the polarization of the zygote.

Molecular genetic evidence from *Arabidopsis* now reinforces the idea of a signal reaching the zygote via the maternal tissues, e.g. the *DICER-LIKE1* gene, required for zygote development (Ray *et al.* 1996, Golden *et al.* 2002). Null alleles of *DCL1* have a zygotic embryo-lethal phenotype (Schwartz *et al.* 1994), while weaker alleles can be rescued if the mother plant is heterozygous but not homozygous for the mutation, indicating a maternal (sporophyte) component in the functioning of this gene during embryogenesis. The action of DCL1 in plants appears to be similar to DICER function in animals; the protein is nuclear localized, and is required for the production of short micro-RNA molecules, involved in gene silencing (Papp

et al. 2003, Bernstein *et al.* 2001, Ketting *et al.* 2001). This suggests the possibility that various maternal micro-RNAs (miRNAs) could affect many aspects of embryo development by direct or indirect means.

In contrast, the unipolar ferns lack a micropylar structure. The egg is contained within an elongated flask-like structure, the archegonium, which opens at maturity to allow the entrance of a multi-flagellated sperm. Following fertilization, the zygote divides parallel to the long axis of the archegonium. A parallel can be drawn from studies on the establishment of polarity in zygotes of the algae *Fucus* and *Pelvetia*, where light, or sperm entry in the absence of light, provides an environmentally-triggered cue which is used for zygote polarization (Roberts & Brownlee 1995, Shaw & Quatrano 1996, Hable & Kropf 2000). This process is disrupted by brefeldin A, an inhibitor of vesicle transport (Shaw & Quatrano 1996), implying that directed vesicle trafficking is a requirement to establish internal polar organization.

1.3.3.3 Cellular polarization is required for co-ordination but not establishment of a longitudinal axis in *Arabidopsis*

Once the *Arabidopsis* zygote has divided in a polar fashion, a distinction is made between the cells by the appearance of the PIN7 auxin transport protein in the basal daughter cell, localized to the apical cell wall. This protein then mediates auxin flux into the apical cell (Friml *et al.* 2003). Mutations in either *PIN7*, or the *WOX2* gene which is specifically expressed in the apical daughter cell, have similar phenotypes in which the initial division patterns of the apical cell appear disorganized (Friml *et al.* 2003, Haecker *et al.* 2004). In these mutants, cellular disorganization persists only into the globular stage of *Arabidopsis* embryogenesis; this suggests that early cellular organization within the very young embryo does not impede the establishment of differential cell fate, and that patterning processes occurring within the cell mass are responsible for resolving the body pattern of the embryo.

Studies on the effects of mutations in the *GNOM* gene of *Arabidopsis* suggest that the asymmetry of the initial division of the zygote is not a requirement for the establishment of a longitudinal axis in the embryo-proper. In *gnom* zygotes, the initial cell expansion proceeds without elongation, and the enlarged zygote divides symmetrically to produce daughter cells of equivalent size (Mayer *et al.* 1991, 1993; Shevell *et al.* 1994). The basal cell forms a normal, though shortened suspensor, but the apical cell shows an abnormal development. Cells divide with abnormal placement of the intervening cell wall, resulting in a range of sibling morphologies in the embryo proper. Most *gnom* embryos are cone-shaped; lacking a root, and with reduced and fused cotyledons around the apex, although some form a spherical mass of tissue with no obvious signs of a longitudinal axis (Mayer *et al.* 1991).

The *AtLTP1* gene, encoding a lipid transfer protein, is initially expressed in all protoderm cells but its expression becomes restricted to the apical region (around the upper hypocotyl and cotyledons) from the heart stage (Vroemen *et al* 1996), thereby acting as a marker of apical polarity. When introduced into *gnom*, the cone-shaped embryos expressed a GUS-fusion marker of *LTP1* in the expected position around the apex. In ball-shaped *gnom* embryos, this marker showed variable expression including normal positioning (relative to the suspensor), reversed polarity, and (seldom) examples of no polarity (Vroemen *et al* 1996). Expression of the *POLARIS* gene, marking the position of the developing root, was also expressed in the correct position in $gnom^{emb30}$ embryos where an obvious apical-basal pattern could be seen, and in other positions in ball-shaped embryos (Topping & Lindsey 1997). These observations suggest that in the loss or absence of normal cues that determine the apical-basal axis, a new longitudinal axis can arise *de novo*.

1.3.4 Radial pattern definition

1.3.4.1 Radial pattern is established during embryogenesis

Radial pattern definition is evident from early in the establishment of cellular organization within the plant body. In *Arabidopsis* embryogenesis, the transition from 'octant' to 'globular' stages (i.e. 8 to 16 cells) involves synchronized cell division which resolves two layers of narrower outer cells and larger inner cells. These cell divisions are usually interpreted as being asymmetric, although should the walls form in a position which maintains the minimum cell dimensions between two cells of equal volume, this same pattern would be predicted. This round of cell division produces a 16-cell embryo with a radial organization of outer and inner layers; this arrangement has a maximal geometric packing efficiency, and an organization in which the cells have a maximal possible wall contact.

After this point, subsequent cell divisions are oriented that preserve the transverse symmetry across the plant growth axis. Mutant analysis in *Arabidopsis* has identified genes which are defective in this process (Scheres *et al.* 1995). Coordinated asymmetric divisions of the inner cell layer define a central zone of small narrow cells with their long axes in line with the suspensor. The shoot meristem develops at the apical pole in coordination with these cell files, which run longitudinally between the apex and base of the embryo. Inception of the apical meristem triggers cotyledon development and marks the anatomical shift from the radial 'globular' to bilateral 'heart' stages of pattern organization. The embryonic root then develops at the basal pole from the first adjacent suspensor cell (the hypophysis), which divides to form the embryonic root meristem quiescent centre (QC) and root cap.

1.3.4.2 Radial cues around the shoot apex generate lateral organs

The dicotyledon SAM is organized in a radial arrangement, with anatomical zonation of cell identity (central, peripheral and rib zones) common to all dicotyledonous species (Steeves & Sussex 1989) as shown in Fig. 1.6. Organ primordia arise around the meristem from the peripheral zone (PZ). Cell

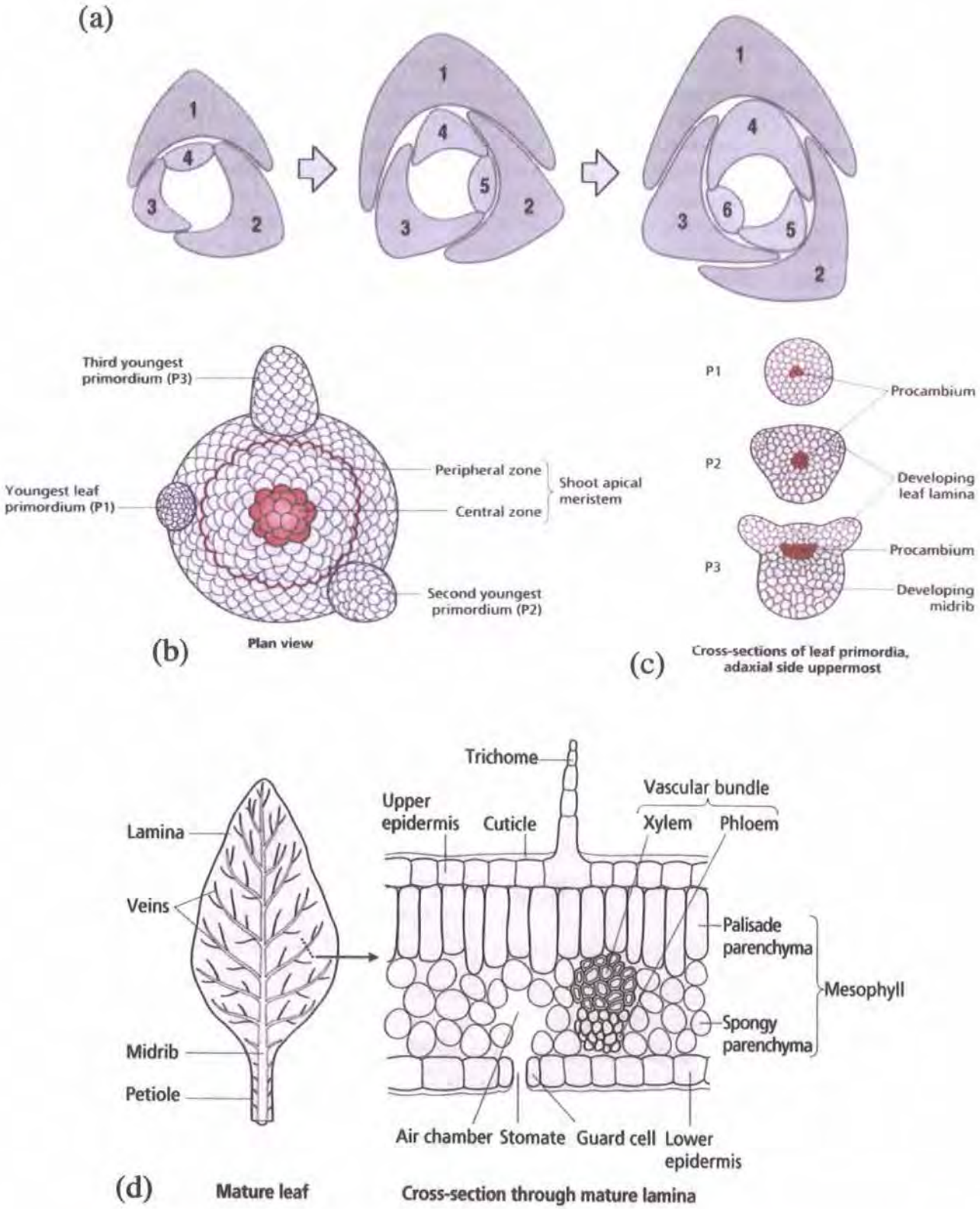

Figure 1.6 Dicotyledon phyllotaxy and leaf cellular organization

(a); stylized representation of a dicotyledon shoot apical meristem in transverse section, and (b); in plan view, showing a spiral arrangement of new primordia (i.e. the phyllotactic series). (c); sections of the young primordia shown in (b). (d); section through a mature leaf to shown the differential arrangement of cells between abaxial (lower) and adaxial (upper) surfaces.

Diagrams from Wolpert (1998) and Leyser & Day (2003).

proliferation increases the cell numbers throughout the surface layers of the meristem (the 'tunica'), and possibly in deeper tissues as well, resulting in a 'protrusion' of cells in a position around the radial axis at a position predictable with reference to the existing organ primordia. This regular pattern about the growth axis is termed 'phyllotaxy', and its pattern is characteristic of the species. Leaves may occur singly at each node, in pairs, or in whorls of three or more. Where primordia arise singly, they form a helical pattern ascending the stem in order of decreasing age, referred to as the 'generative spiral' The position of emergence of a new primordium is influenced by the presence of other primordia around the apex, and surgical experiments on the shoot apex have established that a lateral inhibition phenomenon is involved, shown recently to be dependent upon intercellular transport of the phytohormone auxin (Snow & Snow 1931, Reinhardt *et al.* 2003, 2004).

Lateral organs emerge and develop by a complex set of processes not yet fully understood, but generating a recognizable pattern. The dicotyledon lamina is organized as a layer of mesophyll cells derived mostly from L2 but also from L3 of the meristem, surrounded by an L1 derived epidermis. In most dicotyledons, a transverse section of the lamina presents a differential cellular arrangement across the radial axis, with the upper (i.e. inner, adaxial) face displaying a layer of elongated specialized cells clustered beneath the epidermis with their long axes radially aligned; the palisade mesophyll. Other cells within this layer are also specialized, and form an abaxial 'zone' within the tissue, containing spongy mesophyll organized with contact to intercellular air spaces, vascular strands of abaxially oriented phloem and adaxially-oriented xylem (the 'collateral' pattern), and other specialized cells including those of the bundle sheath, which form a layer around the vascular network. Cells of the bundle sheath may be further defined across the radial axis. Wysocka-Diller *et al.* (2000) have shown that the SCARECROW (SCR) protein, defining endodermal cell identity in the root and hypocotyl of *Arabidopsis,* is also found in close abaxial association with the vascular tissues as they 'invade' new primordia around the meristem.

1.3.4.3 Signals from established tissues maintain the root radial pattern

The root apex of all higher plants contains a meristem organized around a quiescent centre (QC) of mitotically relatively inactive cells, surrounded by 'initials' which give rise to the different radial cell layers of the root. This fundamentally similar form has diverse means of organization between species, according to the cellular anatomy of the root tip. Root meristems are classifiable as 'open' or 'closed'. In an 'open' meristem there is no discrete boundary between the root proper and the root cap tissues, making it difficult to trace cell files to distinct initials. In closed meristem roots such as *Arabidopsis*, convergence of cell files to a cytologically distinct QC make it straightforward to identify putative initials in median longitudinal sections (Clowes 1981).

Surgical and laser ablation studies in the roots of closed meristem species *Arabidopsis* and *Zea mays* have examined the phenomena by which patterning is defined in the establishment and maintenance of the root apical meristem, and the arrangement of cell layers around the root growth axis (Van den Berg *et al.* 1995, Lim *et al.* 2000). In *Arabidopsis*, the root apical meristem produces columella root cap cells on its outer face, lateral root cap and epidermal cell files from a single row of initials at the margin, and initials giving rise to the ground tissue and vascular procambium layers (Dolan *et al.* 1993).

Laser ablation of the QC results in a re-specification of procambial cells to QC and columella initial identity (Van den Berg *et al.* 1995). This involves a signal coming from the established tissues further up the root radial axis. The endodermal layer in *Arabidopsis* is defined by expression of the SCARECROW (SCR) protein, which is transcribed in response to SHORT ROOT; a transcription factor produced by cells of the pericycle and vascular cylinder (Helariutta *et al.* 2000). The SCR protein is also present in cells of

the QC (Wysocka-Diller *et al.* 2000). The maize homologue of SCR, also expressed in the endodermis, was shown to appear successively in cells adjacent to the endodermis at the cut surfaces; this signal spread across the root radial axis between the endodermal cell files, recruiting cells to the new cell fate, and generating a new QC and root cap upon joining of the 'invading ends' (Lim *et al.* 2000).

Laser ablation of a single cortical initial in the *Arabidopsis* root meristem results in an 'invasion' of the area by expansion of cells of the pericycle, followed by periclinal division to generate new cortical initials in the outer cells, whilst the inner cells remain part of the pericycle (Van den Berg *et al.* 1995). Along with clonal analyses (Kidner *et al.* 2000), these experiments make clear that cell position, and not lineage, defines cell fate across the root radial axis. Other radially-defined positional cues active within the root include the specification of new phloem and procambium by differentiating xylem strands (Mähönen *et al.* 2000), and initiation of lateral root primordia from pericycle cells in direct contact with underlying protoxylem (Dubrovsky *et al.* 2001).

1.4 Radial cellular organization in *Arabidopsis* has a molecular-genetic basis

1.4.1 Radial patterning in the *Arabidopsis* globular embryo

The earliest molecular-genetic markers to appear in the embryo proper are the homeobox genes *ARABIDOPSIS THALIANA MERISTEM LAYER 1* (*AtML1*) and *PROTODERMAL FACTOR2* (*PDF2*) (Lu *et al.* 1996, Abe *et al.* 2003), which appear in the small apical cell after the first zygotic division, and persist in the protoderm (outer cell layer) through to the end of embryogenesis. In the 'octant' embryo, both of these genes are expressed

in all of the cells. At this 8 to 16 cell transition, *AtML1* and *PDF2* expression is found in the outer layer but not the inner layer (Lu *et al.* 1996, Abe *et al.* 2003), and comprises a radially-organized differential gene expression within the cell mass. This means that on the basis of gene expression, the radial organization of the embryo proper is the first 'pattern' to be established.

A subsequent synchronized division of all cells in the embryo proper places anticlinally-oriented walls between cells of the protoderm layer, and periclinal walls in the inner cells, resulting in a three-layered structure. This round of division can also be viewed in terms of preserving an equivalent cell volume and minimum cell dimension, as the middle layer of cells are narrower in a transverse plane across the embryo (Kaplan & Cooke 1997). The basic body organization is now present, with an outer protoderm, an inner ground tissue and a procambium in the centre.

At this three-layer globular stage of *Arabidopsis* embryogenesis, the inner procambial layer of cells activates expression of the *SHORTROOT* (*SHR*) gene, and then divides to create an outer pericycle and inner core of vascular precursors (Helariutta *et al.* 2000). The SHR protein then induces *SCARECROW* (*SCR*) expression in the surrounding ground tissue (Nakajima *et al.* 2001), followed by a subsequent division of this layer to form the cortex and endodermal cell layers (Di Laurenzio *et al.* 1996). SCR appears first in the hypophysis, and then resolves to the lens-shaped cell which will form the QC, prior to extension of the SCR signal into the ground tissue cell layer. This expression pattern extends upwards as the embryo enters the transition stage to heart. As this morphological change takes place, the ground tissue cells divide asymmetrically and sequentially from the base, giving two radial layers in which the inner layer maintains SCR activity (Wysocka-Diller *et al.* 2000). The cortex and endodermis each comprise 8 cell files, a pattern which persists into the seedling root (Dolan *et al.* 1993, Scheres *et al.* 1995).

Another radially partitioned gene activity is seen from the transcription factor *MONOPTEROS* (*MP*) (Przemeck *et al.* 1996, Hardtke & Berleth 1998). A transcriptional signal appears first in the apical daughter cell of the first zygotic division, is throughout all cells of the octant embryo, and then becomes confined to the sub-epidermal cells at the early globular stage. At the heart stage, gene activity becomes enhanced in the central layers as they adopt procambial cell identity, with a less strong signal in the cortex (Steinemann *et al.* 1999, Ulmasov *et al.* 1999). The *MP* gene encodes an Auxin Response Factor (ARF), which binds to the promoters of auxin-inducible genes and regulates their transcription. Gene activity appears to include a role in the longitudinal coordination of cell files, as in the *mp* mutant, cells fail to elongate fully, producing a seedling with a reduced and discontinuous vasculature. Another interpretation could be in the pathway regulating cellular polarity, as the apical daughter cell of the *mp* zygote divides transversely, rather than vertically as in wild-type, and the placement of division planes in the globular embryo is highly irregular.

After the anatomical resolution of the central cell files, the homeodomain protein *AthB8* is transcribed, in a manner which defines the procambium (Baima *et al.* 1995). This gene is the earliest known vascular tissue cell fate marker (Scarpella *et al.* 2004), appearing at the pre-procambial stage. Expression of this transcription factor commences in the young heart stage embryo, with a stronger activity at the root apex, and appearing to progress towards the apex as the embryo elongates into torpedo stage. Later activity defines the procambial traces in the embryonic cotyledons, by which point the whole embryonic provascular network is apparent. This successive acropetal 'recruitment' of cell identity is also seen in post-embryonic development, where procambial strands extend from the established cotyledon traces below the SAM into the incipient primordia as they emerge (Baima *et al.* 2001). Transcription of *AthB8* is auxin-responsive, and gene expression is limited by *MP* in wild-type plants (Mattsson *et al.* 2003).

1.4.2 Radial partitioning of the *Arabidopsis* embryonic shoot apex

The expression domains of some currently known transcription factors around the *Arabidopsis* embryonic shoot apex are shown schematically in Fig. 1.7. The first molecular-genetic indication of SAM development concerns expression of the *WUSCHEL* (*WUS*) homeobox gene during embryogenesis at the 16-cell stage. Transcripts appear in the 4 sub-epidermal cells which comprise the inner cell layer in the apical half of the embryo (Laux *et al.* 1996, Mayer *et al.* 1998), i.e. just after the radial distinction between cell layers has been established by *AtML1*. The signal persists at the apex through the next round of cell division that resolves the ground tissue and procambium, and during which the inner procambial cells appear as elongated in the longitudinal axis. Expression is maintained by asymmetric division within this four-cell domain, placing the *WUS* expressing cells in the sub-epidermis beneath the presumptive shoot meristem in the late globular embryo (Laux *et al* 1996, Mayer *et al.* 1998).

AINTEGUMENTA (*ANT*), an *APETALA2*-like gene (Elliot *et al.* 1996), shows expression first in a few cells at the apex of the 32 cell stage embryo, and rapidly develops activity in a ring around the apex of the embryo at the early globular stage (Long & Barton 1998). The region defined by *ANT* is absent from the central cells which lie directly above the cells expressing *WUS*.

Another pattern which establishes in the early globular embryo involves the functionally redundant *CUP-SHAPED COTYLEDON* (*CUC*) genes, encoding NAC domain proteins which are putative transcription factors homologous to the petunia NO APICAL MERISTEM proteins (Aida *et al.* 1999, Takada *et al.* 2001, Souer *et al.* 1996). *CUC2* expression appears first in isolated patches of apical cells, then develops in a stripe across the apex of the

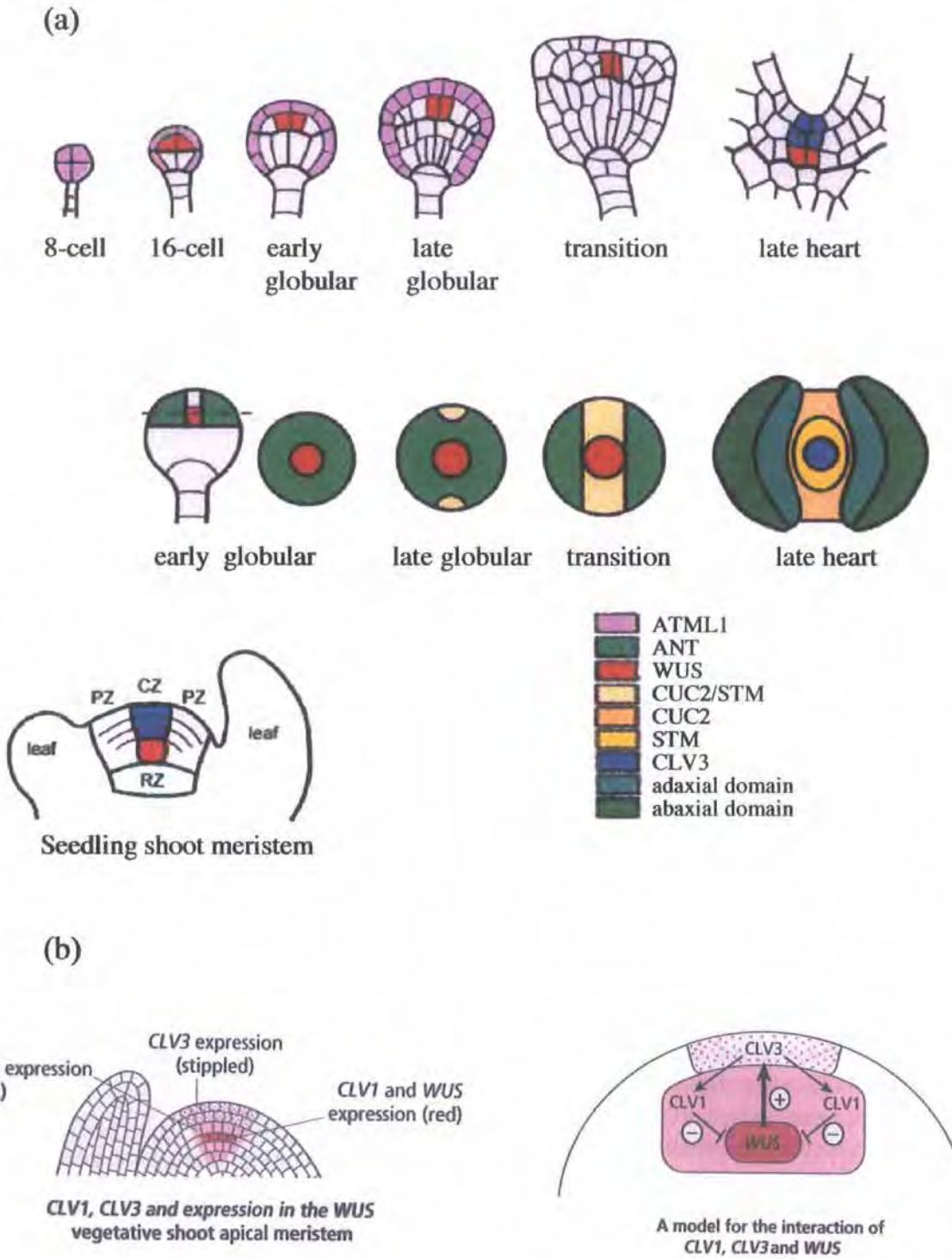

Figure 1.7 Molecular markers of radial cell identity and positioning in *Arabidopsis*

(a) The development of radial domains during *Arabidopsis* embryogenesis; (b) The *WUS/CLV1/CLV1* feedback loop.

Diagrams adapted from Laux *et al.* (2004) and Leyser & Day (2003).

globular embryo, in a position which is followed in the late globular phase by expression of the *SHOOTMERISTEMLESS* (*STM*) gene, encoding a homeodomain transcription factor from the knotted class. These two gene expression domains are almost overlapping; both are found in the L2 and L3 layers, but *STM* expands into the L1 layer. Activity of the *CUC* genes provide the first molecular definition of a bilateral axis.

STM transcripts appear in a single off-centre cell at the embryo's apex within the region defined by *ANT*, followed closely by another point of activity in a cell on the opposite side of the apex. This activity begins as the globular embryo begins to flatten, and expands into a solid band across the apex at the transition to heart stage, defining a region between the emerging cotyledon primordia (Long *et al.* 1996, Long & Barton 1998). Concurrently, the ring of *ANT* expression seen in the globular embryo becomes displaced into the incipient cotyledon primordia, and organ-specific gene expression is initiated (Long & Barton 1998).

Mutants of *stm* fail to maintain meristem function, and lack the tunica-corpus organization of the SAM (Endrizzi *et al.* 1996). Weaker alleles have meristems which initiate true leaves but abort at the seedling stage, whilst null *stm* seedlings do not initiate true leaves, and develop a swollen ring of tissue around the meristem periphery between the cotyledons (Endrizzi *et al.* 1996, Long & Barton 1998). *STM* expression therefore corresponds to areas of the meristem where lateral organ outgrowth is inhibited, and *ANT* becomes excluded from the *STM* domain into the region of cotyledon primordial growth (Elliott *et al.* 1996).

Transcription of the *UNUSUAL FLORAL ORGANS* (*UFO*) gene appears in the L2 and L3 layers at the globular-heart transitional embryo apex, within the 'striped' domain of *STM* expression, and encompassing the region defined by *WUS*. Gene activity appears to be positively regulated by STM; *UFO* expression becomes more intense through the heart stage, and resolves into a cup-shaped domain at the base of the central zone (Long & Barton 1998). Shortly after the appearance of *UFO* transcripts, *CLAVATA1* (*CLV1*)

gene activity appears in the central zone in the L2 and L3 layers, and *CLAVATA3* (*CLV3*) in the L1 and L2 layers of the early heart stage apex, in a zone above and overlapping with the *WUS* domain (Laux *et al.* 1996, Long & Barton 1998, Schoof *et al.* 2000, Brand *et al.* 2002).

STM expression in later embryogenesis appears to require *WUS* function, which in turn requires *CLAVATA3* (*CLV3*) activity from the heart stage onwards (Schoof *et al.* 2000). A feedback loop involving these three proteins defines their respective domains, and maintaining meristem homeostasis for the life of the plant, is active from the heart stage onwards (Schoof *et al.* 2000, Brand *et al.* 2000, 2002). The role of *UFO* in vegetative SAM patterning is unknown, but as its transcriptional activity defines the boundary of the *STM* domain at its margin with the *CLV* domain margin, and its presence may contribute to a verification of the domain boundary. Activity of these genes produces a well-defined radial arrangement in transverse section across the shoot apex.

1.4.3 Radial organization of the *Arabidopsis* embryonic root axis involves procambial and vascular-derived signals

During *Arabidopsis* embryogenesis, definition of the vascular procambium begins anatomically with asymmetric cell divisions at the transition from octant to globular stages, under control of the SHR protein, producing a column of long narrow cells in the centre of the embryo (Scheres *et al.* 1995, Helariutta *et al.* 2000). The position of the SAM is established and maintained by the *WUS* domain in a region above this column (Laux *et al.* 1996). Definition of further radial layers continues via SCR protein activity, commencing in the hypophysis of the globular embryo (Wysocka-Diller *et al.* 2000). Synchronously with the timed appearance of SCR gene expression in the hypophysis, the *WUSCHEL-RELATED HOMEOBOX5* (*WOX5*) gene is transcribed, and retains activity in the inner lens-shaped daughter

cell and its subsequent derivatives, which form the quiescent centre, and was also noted in vascular primordia of the cotyledons at around the heart stage (Haecker *et al.* 2004).

Other *WOX* gene activities define the root region at various stages of embryo development (Haecker *et al.* 2004). In the octant embryo, the upper layer of cells expresses *WOX2* strongly, with some weaker expression in the lower layer; the lower layer and hypophysis express *WOX9*, and the hypophysis and suspensor express *WOX8*. In the globular embryo these expression boundaries resolve more specifically along the longitudinal and radial axes; *WOX2* is confined to the apical region (enveloping the domain defined by *WUS*), *WOX9* becomes limited to the lower radial tier of epidermal cell files around the hypophysis, and *WOX8* is confined to suspensor cells below the hypophysis. These three *WOX* genes initially define domains around *WOX5*, becoming separated through later intervening cell divisions.

Expression of the procambial marker *AthB8* from the heart stage (Baima *et al.* 1995) means that vascular identity is defined after the establishment of the pericycle and endodermal layers by SHR and SCR. Another component of the vascular circuitry involves the MYB coiled-coil protein ALTERED PHLOEM DEVELOPMENT (APL) (Bonke *et al.* 2003), which functions as a transcription factor necessary for phloem formation. The *apl* mutant has ectopic xylem characteristics in the phloem cell position, suggesting an additional role for the protein in negative regulation of xylem development. This suggests a lateral inhibition mechanism similar to the action of WER in the root epidermis, where action of a MYB protein specifies one cell fate whilst repressing another. Another gene present in the pericycle and vascular cylinder is *WOL/CRE1,* which encodes a putative receptor protein implicated in cytokinin response (Scheres *et al.* 1995, Mähönen *et al.* 2000, Inoue *et al.* 2001). Mutation of the *WOL* locus also suggest the involvement of a non-cell autonomous signal, as *wol* mutants also have ectopic proliferation of xylem and an absence of phloem (Mähönen *et al.* 2000). The *wol* and *shr* mutant phenotypes are additive,

implying that these genes are involved in independent processes (Scheres *et al.* 1995).

1.4.4 Radial patterning genes at the shoot apex define bilateral cues and organ polarity

A bilateral axis is imposed upon the embryo, by a mechanism including expression of the *CUC* genes in a stripe across the apex (Aida *et al.* 1999), and displacement of *ANT* expression into the zones of cotyledon primordia by *STM* expression (Long & Barton 1998). The cotyledon primordia then differentiate beyond this zone, not simultaneously but in a very close sequence (Woodrick *et al.* 2000). Cotyledon expansion is accompanied by extension of the procambial cell file pattern, resulting in longitudinally coordinated files of cells of the proto-stele and provasculature, which branch beneath the SAM. The positioning of the SAM, and its relationship to the vasculature of the upper hypocotyl and cotyledons, is therefore established during embryogenesis.

A similar reciprocal radial pattern as seen between *STM* and *ANT* across the embryonic apex, appears in post-germination SAM maintenance. This involves *STM* and the MYB domain transcription factor *ASYMMETRIC LEAVES 1* (*AS1*) (Byrne *et al.* 2000), a homologue of the *PHANTASTICA* gene of *Antirrhinum*. *AS1* has been proposed as having a role in the specification of founder cell identity in lateral organ primordia. *STM* appears to suppress the expression of *AS1* in the central domain. SAMs are formed in correct positions in *stm-as1* double mutants. As *AS1* is already transcribed in the cotyledons before *STM* expression appears, it is possible that *STM*'s function is primarily to counteract *AS1* activity, and maintain undifferentiated cell states in the centre.

Further elaboration of the radial pattern is seen in the cotyledon primordia. Transverse partitioning is indicated by the *WUSCHEL*-related

homeobox genes *PRESSED FLOWER/WOX3* and *WOX1*: these genes are expressed respectively at the margins of cotyledon primordia at heart stage, and throughout cotyledon primordia from heart through torpedo stage (Haecker *et al.* 2004). Dorsiventral patterning genes of the HD-Zip (Homeodomain-leucine zipper) III class (i.e. PHABULOSA (PHB), PHAVOLUTA (PHV) and REVOLUTA (REV)) appear in the cotyledon primordia from the early inception of these organs (Emery *et al.* 2003. Prigge *et al.* 2005).

Other genes involved in definition of the abaxial-adaxial axis include the abaxial fate-promoting GARP transcription factors, encoded by the *KANADI* (*KAN*) genes and the *YABBY* gene family of transcription factors. *KANADI* genes comprise a functionally redundant family with four members in *Arabidopsis* (Keersetter *et al.* 2001, Emery *et al.* 2003, Eshed *et al.* 2004). Combined loss of function at *KANADI* loci results in adaxialization of developing leaves. *KAN* and *PHB/PHV/REV* genes appear to establish abaxial-adaxial domains within the leaf by mutual suppression (Eshed *et al.* 2001). Members of the *YABBY* class (Siegfried *et al.* 1999, Sawa *et al.* 1999, Kumaran *et al.* 2002) are regulated at the transcriptional level; the promoter of the *FILAMENTOUS FLOWER* (*FIL*) locus contains elements which both promote gene expression throughout the primordium, and repress transcription on the adaxial side, implying an active exclusion from the adaxial domain (Watanabe & Okada 2003). The role of YABBY genes is unclear in the promotion of adaxial cell fate, but double mutants of *fil* and *yabby3* produce adaxialised leaves when *KAN* function is compromised (Kumaran *et al.* 2002, Eshed *et al.* 2004).

REV, *CNA*, *PHV* and *PHB* play key overlapping roles in the establishment of bilateral symmetry at the shoot apical meristem (Prigge *et al.* 2005). Double and triple loss-of-function mutant studies with these genes indicate a complex set of overlapping, distinct and antagonistic functions. *REV* is essential in conjunction with *PHB* or *PHV* and for patterning of the apical region of the embryo, and mutations in *CNA* or *AthB8* partially suppress the *rev* and *ref-phb* mutations (Prigge *et al.* 2005). Mutation of *AthB8* does not

have a discernible phenotype, although over-expression of the wild-type gene produces ectopic formation of xylem (Baima *et al.* 2001).

1.5 Sterols as agents of pattern definition and morphology in plant development

1.5.1 A potential mechanism for sterol signalling during morphogenesis?

The HD-Zip III family of transcription factors in *Arabidopsis* comprises 5 members; *REV*, *PHV* and *PHB*, *AthB8* and CORONA (*CNA*). These genes encode proteins with a putative sterol binding (START) domain (Kallen *et al.* 1988, Ponting & Avarind 1999, Prigge *et al.* 2005). The only member of this gene family with a loss-of-function phenotype is *REV* (Prigge *et al.* 2005). These *rev* mutants have defects in cell polarity and coherence of the vascular tissue, auxin transport, leaf development and meristem maintenance (Talbert *et al.* 1995, Zhong *et al.* 1997, 1999, Zhong & Ye 1999, 2001, Otsuga *et al.* 2001). Gain of function mutations in *PHB* and *PHV* show strong adaxialization of lateral organs; these mutations are within the START domain (McConnell *et al.* 2001, Emery *et al.* 2003). However it is unclear whether the mutant defects result from a modified sterol interaction, or is due to a disruption of microRNA binding (Rhoades *et al.* 2002, Tang *et al.* 2003).

Other genes encoding proteins with a putative START domain in *Arabidopsis* include *GL2*, involved in epidermal patterning in both root and shoot tissues (Rerie *et al.* 1994, Ponting & Avarind 1999), and *AtML1*, suggesting that sterols may modulate various regulatory protein functions (McConnell *et al.* 2001). A promoter-reporter of GL2 transcription has been noted for mis-expression in the root epidermis of *hydra2* (Souter *et al.* 2002). Expression

of *AtML1* has not yet been characterized in the mutants, although this gene is specific to the embryonic protoderm; a tissue layer which is indistinctly defined in the *hydra* embryo (Topping *et al.* 1997).

MicroRNAs are conserved as a post-transcriptional regulatory mechanism throughout the eukaryotes, and target multiple cleavage sites found in many regulatory genes in *Arabidopsis,* including members of large families of transcription factors (e.g. CUC1 and CUC2, APETALA2, PHV and PHB) (reviewed by Carrington & Ambros 2003). They function as negative regulators, conferring a specificity mechanism to complexes which inhibit protein synthesis in animals, and promoting degradation of mRNA targets in plants. START domains have been demonstrated to be functional sites for microRNA cleavage of mRNA *in vitro* (Tang *et al.* 2003), suggesting the possibility of a role for miRNAs in regulating plant morphogenesis.

The START domain has been proposed to convey negative regulation via binding of a sterol ligand, as is thought to operate in animal systems. This was suggested as a mechanism to explain why gain of function *phb* and *phv* mutant genes are constitutively active; however similar dominant mutations in *rev* have been interpreted as resulting primarily if not solely from the disruption of miRNA regulation (Emery *et al.* 2003). Their results imply that a common genetic programme dependent upon miRNAs is common to both apical and vascular meristems in the angiosperm shoot. However miRNAs are an abaxial-derived signal. There is strong evidence, based on laser-ablation, for an L1-specific meristem-derived adaxializing signal involved in radial partitioning of leaf primordia (Reinhardt *et al.* 2004).

Down-regulation of START-containing regulatory proteins via miRNA is specific to the mRNA, i.e. acts at the pre-translational level. A proposed sterol-mediated activity would operate via interaction with the protein, at the post-translational level. The protein architecture of the START region in the human cholesterol binding and transfer protein StAR, was found to be well designed to bind and solublise lipid monomers (Tsujishita & Hurley

2000). Sterols therefore may be implicated in targeting the START domain in signalling proteins, whilst miRNA targeting limits the translation of these proteins. In combination, these two mechanisms could permit a positive reinforcement mechanism (at the protein level) combined with a negative regulatory mechanism (at the mRNA level). Such a mechanism could potentially operate diverse patterning processes, e.g. involving positive reinforcement within a specific cell and lateral inhibition in adjacent cells (e.g. GL2-mediated trichome and atrichoblast patterning within the epidermis), and longer range signals between layers for tissue-wide radial differentiation of cell identity.

1.5.2 Sterol biosynthesis in animals, fungi and higher plants proceeds via distinct metabolic routes

Sterols comprise a biochemically diverse group of lipidic compounds which are derived from the 5-carbon molecule isoprene; they constitute essential, ubiquitous components found throughout the eukaryotes. In bulk they affect membrane architecture, regulating fluidity via the ordering of acyl chains, and modulate the water permeability of the phospholipid bilayer (Hartmann 1998, Schaller 2004). Sterols also comprise the biosynthetic precursors of minute amounts of biologically active molecules, e.g. steroid hormones such as cholesterol in mammals, ecdysteroids in insects, ferns and higher plants (Costet-Corio *et al.* 1993), and the higher plant-specific brassinosteroids (Bishop & Yokota 2001).

The isoprenoid pathway derives a diverse range of compounds from a common precursor; a 5-carbon phosphorylated isoprene called isopentenyl phosphate (IPP). In plants, IPP is synthesized by two metabolic routes; firstly in the cytoplasm from Acetyl-CoA via mevalonate (the MVA pathway), and secondly in plastids from pyruvate and glyceraldehyde-3-phosphate via 2-C-methyl-D-erithrytol-4-phosphate (MEP). These two schemes, leading to IPP, are summarized in Fig. 1.8. The MVA pathway

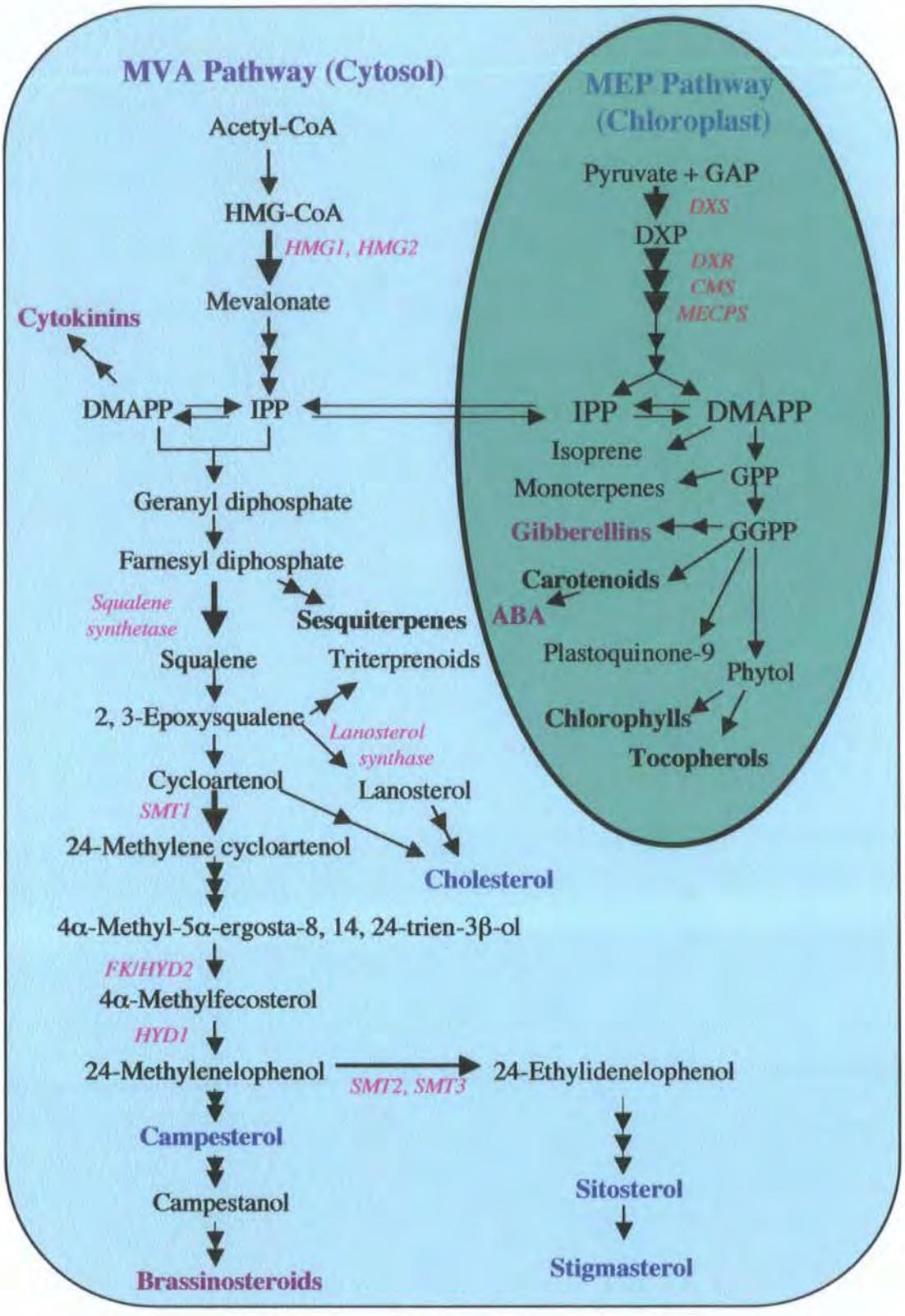

Figure 1.8 Context of phytosterol biosynthesis in *Arabidopsis*

Adapted from Estevez *et al.* 2001 (*J Biol Chem* **276**; 22901-9), Suzuki *et al.* 2004 and Ori *et al.* 1999. Abbreviations: ABA, abscisic acid; CMS,4-diphosphocytidyl- 2-C-methyl-D-erythritol synthase; DMAPP, dimethallyl diphosphate; DXP, 1-deoxy-D-xylulose 5-phosphate; DXR, 1-deoxy-D-xylulose-5-phosphate reducto-isomerase; DXS, 1-deoxy-D-xylulose-5-phosphate synthase; GGPP, geranyl-geranly diphosphate; GPP, geranyl diphosphate; HMG1,2, hydroxymethyl glutaryl CoA-reductase 1 and 2; IPP, isopentenyl diphosphate; MECPS, 2-C-methyl- D-erythritol-2.4-cyclodiphosphate synthase; MEP, 2C-methyl-D-erythritol 4-phosphate; MVA, Mevalonate; SMT1, *STEROL METHYLTRANSFERASE1;* SMT2/SMT3, *STEROL METHYL TRANSFERASE2* and *3*.

supplies substrates required for the production of sesquiterpenes, triterpenes, sterols and brassinosteroids (Newman & Chappell 1999), whereas the MEP pathway derives quinones, carotenoids, chlorophyll side chains, and the phytohormones ABA and GA (Lichtenthaler 1999). IPP is also a precursor for the biosynthesis of cytokinins, via its isomer dimethallyl diphosphate (DMAPP) (Gan & Amasino 1995, Ori *et al.* 1999). In mammals and yeast, IPP synthesis proceeds only via the MVA pathway, whilst the MEP pathway is found in all plastid bearing eukaryotes, indicating that the genes encoding these enzymes are cyanobacterial in origin (Lange *et al.* 2000).

The overall biosynthetic flux leading to sterols in higher plants appears to be under the control of the 3-hydroxy-3-methylglutaryl coenzymeA reductase (HMGR) enzyme. HMGR over-expression in *Hevea brasiliensis* resulted in an increased overall accumulation of sterols, and the *hmg1* loss of function mutation in *Arabidopsis* reduced overall sterol content (Gondet *et al.* 1992, Suzuki *et al.* 2004). HMGR is negatively regulated by light (Learned 1996). There is a metabolic flux of IPP between the plastid and the cytosol (Nagata *et al.* 2002). As most of the carbon found in higher plant sterols originates from the MVA route under normal physiological conditions, this metabolic cross-talk between the MVA and MEP pathways may be important (Schaller 2004).

Sterol synthesis proceeds from IPP by the combining these 5-C units to make the 30-C compound squalene, which is oxidized and subsequently cyclized. In plants, the major product of these early biosynthetic steps is a plant specific sterol, cycloartenol, whereas in yeast and mammals lanosterols are produced. Certain single codon changes in the *Arabidopsis* cycloartenol synthase result instead in the production of lanosterol (Hart *et al.* 1999, Segura *et al.* 2002); also a functional *Arabidopsis* lanosterol synthase was recently characterized (Kolesnikova *et al.* 2006). Sterol synthesis via the tetracyclic lanosterol is less metabolically costly than via the pentacyclic cycloartenol, which requires an additional enzymatic step

to open the extraneous cyclopropyl ring (Heintz *et al.* 1974). These data imply that cycloartenol and its derivatives have plant specific functions.

Some structural variation exists between sterol molecules throughout the eukaryotes.

- Sterols from fungi and higher plants differ from those of vertebrates by the presence of an extra alkyl group at the C-24 position (Nes 2000). These are added by sterol methyltransferase enzymes at separated biochemical steps, each followed by a demethylation step (annotated in the scheme in Fig. 1.8).
- The two methyl groups present on C-4 of cycloartenol require removal for its conversion into functional sterol compounds. In animals and fungi, these are removed successively much earlier in biosynthesis, whereas in plants their removal occurs subsequently to the methylation steps affecting C-24.
- Plant species synthesize several pathway end products, e.g. campesterol, sitosterol, stigmasterol and isofucosterol in genetically defined proportions, in contrast to mammals where the only sterol product is cholesterol.

1.5.3 Sterol mutant isolation and genetic characterization

The plant sterol biosynthesis pathway below IPP can be considered as having three biosynthetic domains (Lindsey *et al.* 2003), annotated on the scheme in Fig. 1.9. The first domain (A) concerns the steps which derive 4-methylene lophenol from squalene. Below this point, the pathway branches into two domains, distinguished by the activity of a C-28 methyltransferase. This enzyme produces 24-ethylidene lophenol, from which are derived the more abundant sterols including the membrane components sitosterol and stigmasterol (via domain B). The third domain (C) produces the membrane sterol campesterol, which is present in very

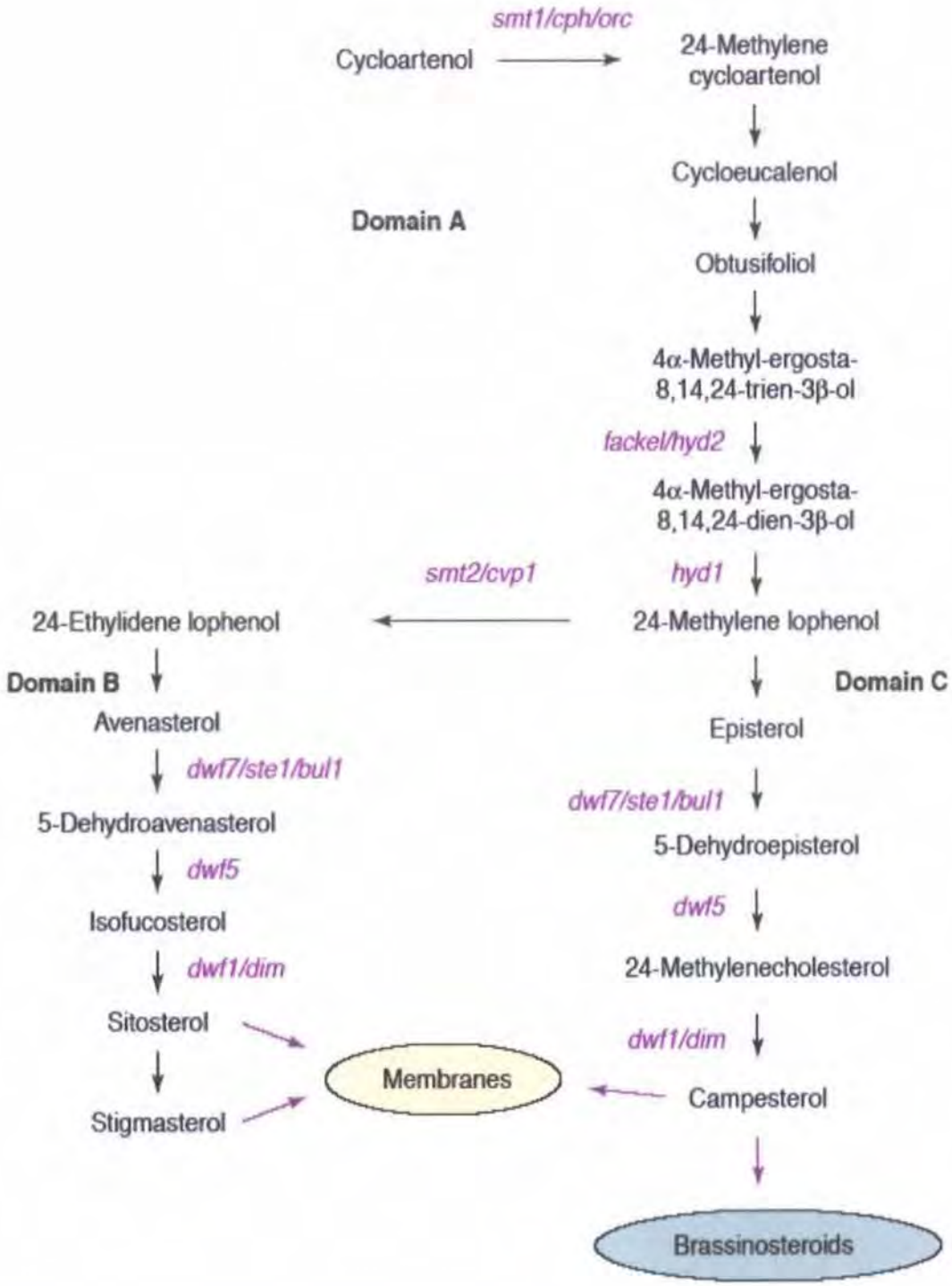

Figure 1.9 Plant sterol biosynthesis downstream of cycloartenol

Scheme taken from Lindsey *et al.* (2003). Annotations refer to known biosynthetic mutants from *Arabidopsis thaliana*.

small amounts under normal physiological conditions, and is itself is a precursor of the brassinosteroids.

Arabidopsis mutants for a number of the sterol biosynthetic genes have been isolated from a range of mutant screens for defective root morphology, cell patterning, vascular patterning and embryogenesis. Their phenotypes imply a relationship between sterols and morphogenesis, cell differentiation, cellular polarity and patterning processes at the tissue level. The mutants known in *Arabidopsis* are included as annotations to the scheme in Fig. 1.9. Certain of these mutants, analyzed for their sterol profiles, were found to contain sterol products downstream of the biosynthetic steps shown in the figure in addition to lesser amounts of novel sterols, revealing that the current scheme is incomplete and grossly oversimplified in the plant context.

Several *Arabidopsis null* mutants are known for genes encoding domain A enzymes upstream of *smt2/cvp1*. These mutants (*smt1/cph/orc, cyp51, fk/hyd2* and *hyd1*) are seedling lethal, have variable phenotypes resulting from anomalies in embryonic patterning, and have low levels of brassinosteroids (BRs), but cannot be rescued by exogenous BR application (Topping et al., 1997, Schrick *et al.* 2000, Jang *et al.* 2000, Schaeffer *et al.* 2001, Kim *et al.* 2005). This is in contrast to the mutants of domains B and C, which have phenotypes that respond to exogenous BR application (reviewed in Lindsey *et al.* 2003). The *smt2/cvp1* mutant, at the junction between these upper and lower domains, does not have the seedling lethal phenotype of domain A mutants above it in the pathway; this may be the result of substantial redundancy in the *SMT2* and *SMT3* genes, although single mutations in either of these loci resulted in reduced sitosterol and stigmasterol levels (Carland *et al.* 2002). All of the early pathway mutants except *cvp1* show defective embryogenesis; Kim *et al.* (2005) report a post-heart stage maturation defect, whilst other mutants show earlier patterning anomalies (Topping et al., 1997, Schrick *et al.* 2000, Jang *et al.* 2000, Schaeffer *et al.* 2001). The *cvp1* mutation does not become apparent until post-germination differentiation of the vasculature reveals a

disjointed cotyledon xylem trace (Carland *et al.* 2002). These authors also note that the severity of the *cvp1* phenotype, isolated in a Columbia background, is enhanced in the ecotype Landsberg erecta (Ler). The relative proportions of three of the main membrane sterols in *Arabidopsis* domain A mutants are summarized in Table 1.1.

The *hydra* mutants of *Arabidopsis* were first isolated in mutagenesis screens for seedling defective patterning (Topping *et al.* 1997). Mutations at the *HYDRA1* (*HYD1*) and *HYDRA2* (*HYD2*) loci have a similar seedling lethal phenotype, resulting from patterning defects established during embryogenesis (Topping *et al.* 1997). *HYD2* was later found to be allelic to the *FACKEL* (*FK*) gene (Souter *et al.* 2002), first isolated by Mayer *et al.* (1991) in a screen looking for altered body organization of the *Arabidopsis* embryo, and interpreted as a 'central domain deletion'. Later independent isolation of another mutant allele of *fk*, this time as a putative cytokinin response mutant, was similarly interpreted as a central domain deletion (Jang *et al.* 2000), resulting in "*...cotyledon vascular bundles [which] met at the top of the root system, indicating that a typical hypocotyl was missing, and the hypocotyl-like structure was [comprised of] fused petioles*".

Cloning of the *HYDRA* genes revealed them to encode components of the plant sterol biosynthesis pathway; *HYD1* encodes a Δ8-Δ7 sterol isomerase (Souter *et al.* 2002, Grebenok *et al.* 1988), and *HYD2/FK* encodes a sterol C-14 reductase (Schrick *et al.* 2000, Marcireau *et al.* 1992). An analysis of single and double mutants between *hydra1*, *hydra2/fk* and *smt2* revealed a complex interaction between pathway components, and the production of variable proportions of sterols found at low levels in wild-type plants, along with novel sterol compounds (Schrick *et al.* 2002). Expression of a p*FACKEL*::GUS reporter in the *fackel* mutant background showed a strong up-regulation of its own transcription, and enhanced *FK/HYD2* mRNA production by exogenous treatment with the phytohormone compounds Indole-acetic acid (auxin), brassinolide, gibberellic acid and cytokinin (He *et al.* 2003). *SMT2* mRNA was similarly found to have a phytohormone

responsive transcription, being induced strongly by ethylene and moderately by cytokinin, whilst *SMT3* was induced strongly by cytokinin; both responded moderately to auxin, but not to brassinosteroid or gibberellic acid (Carland *et al.* 2002).

Table 1.1: Sterol content for different *Arabidopsis* mutants from domain A of the isoprenoid biosynthetic pathway

	% Concentration of sterol compared with wild type			
Mutant	**Sitosterol**	**Stigmasterol**	**Campesterol**	Refs
smt1-1	57%	ND	131%	Diener *et al.* 2000
orc	57%	Trace	124%	Willeemsen *et al.* 2003
cyp51-A2-3	25%	33%	12%	Kim *et al.* 2005
fk-J79	50%	ND	51%	Jang *et al.* 2000
fk-X224	Trace	118%	Trace	Schrick *et al.* 2000
fk-hyd2	4%	322%	0%	Souter *et al.* 2002
hyd1	2%	182%	12%	Souter *et al.* 2002
cvp1-1	43%	44%	377%	Carland *et al.* 2002
cvp1-3	29%	51%	359%	Carland *et al.* 2002
cvp1-4	35%	57%	350%	Carland *et al.* 2002

Data represent the percentage concentration of each sterol compared with wild type levels. ND indicates no data.

1.5.4 Morphology of the *hydra* mutant phenotype

Mutations at the *HYDRA* loci result in a highly pleiotropic phenotype, illustrated in Fig. 1.10. The first sign of cellular defects are visible from the three-layer stage of the globular embryo (Topping *et al.* 1997, Schrick *et al.* 2000), where the innermost cells fail to elongate and produce daughters of similar size, rather than the elongated cells found in wild-type. Schrick *et al.*(2004) report ultrastructural defects from this stage common to both *hydra* mutants and *smt1/cph/orc*; these include incomplete cell walls, aberrant cell wall thickenings, and ectopic deposits of callose and lignin. Seedling morphology of all three mutants is

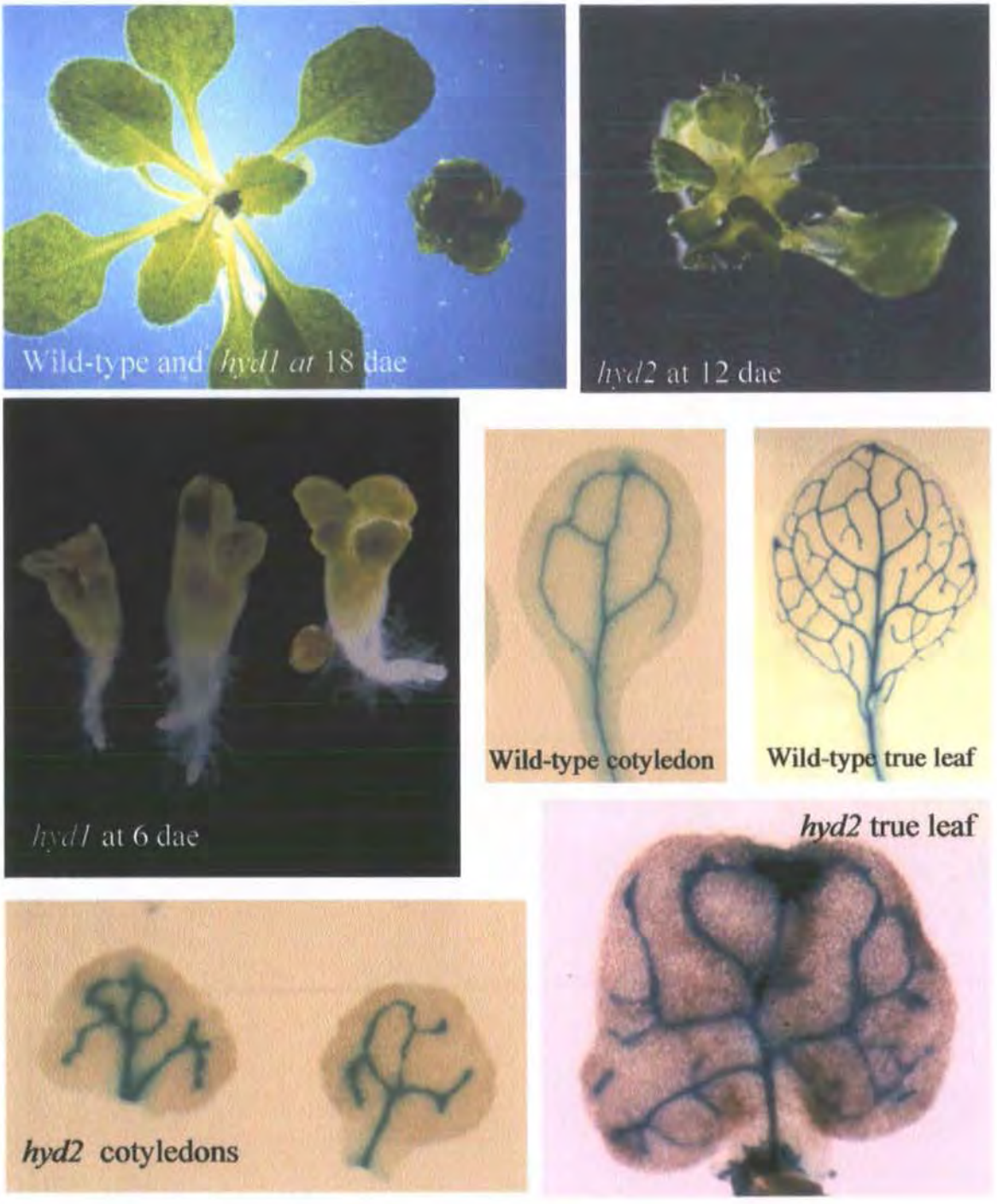

Figure 1.10 The *hydra* mutant phenotype

(a), *hyd1* and wild-type at 18 dae, illustrating the stunted phenotype of these mutants; (b) and (c) show detail of *hyd1* and *hyd2* younger seedlings. (d) and (e) respectively show a cotyledon and true leaf from a wild-type plant expressing the p*PIN1*::GUS promoter-reporter construct, which highlights the vasculature. This same reporter in *hydra* mutants, as for *hyd2* in (g) and (h), reveals a highly irregular vasculature in anomalously shaped leaves.

compromised, although the defects in *smt1* are not as severe as in *hyd1* and *hyd2* The *hydra* sibling population has variable morphology; the shoot apex carries a variable number of cotyledons from 1 to 7, some with cotyledon trichomes (Topping *et al.* 1997). The mutants are stunted, with short, widened hypocotyls, and irregularly shaped leaves compressed in the proximo-distal axis (Topping *et al.* 1997).

At the cellular level, seedlings have varied cell shapes and more isodiametric cells than in wild type (Topping *et al.* 1997). The vasculature is reticulate as in wild-type leaves, but is often interrupted. Multiple cell layers have been noted in the hypocotyl (Topping *et al.* 1997) and leaf (Jang *et al.* 2000), along with modulated levels of vascular differentiation (Jang *et al.* 2000). Hypocotyl tissues appeared to have excessive numbers of ground tissue cells and a disorganized endodermis (Topping *et al.* 1997). The *hyd1* mutant was reported as having excessive numbers of xylem in the vascular bundles (Topping *et al.* 1997), whilst *hyd2/fk* was noted for excessive division of phloem companion and vascular parenchyma cells, with reduced differentiation of xylem (Jang *et al.* 2000). Jang *et al.* (2000) also found enlarged cortical cells beneath the shoot apical meristem which showed exaggerated expansion in the lateral direction. Meristem patterning is disrupted; Schrick *et al.* (2000) describe aberrant placement of *STM* transcripts in *hyd2* mutant embryos, with variably broadened or asymmetric distributions of mRNA. Both *hydra* mutants were noted for compromised root meristem viability (Topping *et al.* 1997, Souter *et al.* 2002).

The precise nature of the defects found within the *hydra* mutants have not been pinned to a consequence of any single patterning or cell regulatory process, although the phenotype has been variably interpreted as "...defective in patterning of apical-basal structures" (Schrick *et al.* 2000), lacking a central domain (Mayer *et al.* 1991, Jang *et al.* 2000), and as "...defective in the control of cell shape in embryos and seedlings" (Topping *et al.* 1997). The mutants correctly express positional reporters of apical-basal polarity (Topping *et al.* 1997, Topping & Lindsey 1997). The apical L1

layer reporter construct p*LTP1*::GUS shows activity in the leaf epidermis down to the hypocotyl-cotyledon boundary; this domain separation can be seen in *hydra*, defining an upper boundary to the hypocotyl (Souter 2002), and refuting an interpretation of these mutants as a hypocotyl deletion.

A number of the vascular patterning defects noted in *hydra* mutants are also reported in the HD-Zip III class mutants *rev*, *phb* and *phv*. The adaxial fate-promoting *REV* gene lies in the same pathway and upstream of the meristem identity genes *WUS*, *STM* and *CLV* (Otsuga *et al.* 2001). The altered sterol environment and problems in meristem maintenance of the *hydra* phenotype suggests that sterols could mediate a role in meristem-derived radial signalling.

1.6 Aims of this work

This thesis aims to reassess the *hydra* mutants for defects in radial tissue organization and coordination throughout the plant body. If *hydra* mutants are essentially radially defective, then radial structures within the seedling, i.e. roots, hypocotyls, and the radially-patterned shoot apex would display patterning problems. These tissues have already been noted for patterning anomalies in the *hydra* mutants, although these defects have not been studied in detail.

As radial patterning is coordinated throughout the longitudinal axis of the plant, problems would also be anticipated in coordination of longitudinally aligned cell files such as in the epidermis and vasculature. Should the HYDRA protein function in the modulation of a sterol-mediated signalling pathway affecting pattern definition across the radial axis, then a radially-differentiated distribution of gene expression could be anticipated, perhaps in association with meristematic regions. If the modified sterol composition of the mutant plants affects the functioning of START-containing patterning genes, then their activity would also be expected to

show modulation. The *GL2* gene has already been shown to have a modulated activity (Souter *et al.* 2002).

Finally, if radial signalling is implicated in the *hydra* mutant phenotype, then this mechanism would either interact with, or be integrated as a component of, the endogenous phytohormone signals, namely auxin and ethylene, which modulate radial tissue morphology and cell identity. The mutants have enhanced auxin responses, and are noted for ethylene-associated patterning defects which are partially rescued by chemical inhibition of ethylene perception (Souter *et al.* 2002).

This work examines the expression activity of the *HYD1* promoter throughout development, and its responses to a range of phytohormone and inhibitor treatments. The cell and tissue types highlighted by reporter activity are then examined for their patterning and morphology. The activity of selected patterning genes and the positioning of phytohormone-responsive tissues is assessed in the mutants using a range of reporter constructs. The contribution of ethylene to the pleiotropic mutant phenotype is then assessed by examining morphology, cellular patterning and reporter construct expression in *hydra-ein2* double mutants.

Chapter 2

Materials and Methods

2.1 Abstract

This chapter presents an ordered account of all materials and procedures used to obtain the results described subsequently in this thesis.

The methods chosen to investigate radial patterning phenomena in the *hydra* mutants have adopted a combined approach. Methods from 'classical' anatomical and developmental studies have been applied in conjunction with the powerful tools now available from the emerging discipline of molecular biology, specifically in the form of promoter-reporter constructs and protein fusions.

2.2 Materials

2.2.1 Chemicals

All chemicals used in the following experiments were analytical reagent grade. All chemicals were obtained from Sigma-Aldrich (Poole, UK), Fisher Scientific Ltd (Loughborough, UK), and BDH (Lutterworth, UK) unless otherwise stated. X-Gluc and IPTG were obtained from Melford Laboratories Ltd (Suffolk, UK), and X-Gal from Bioline (London, UK).

2.2.2 Reagents for molecular biology

Restriction endonucleases and T4 DNA ligase were obtained from Promega (Southampton, UK). Taq DNA polymerase and Hyperladder™IV were from Bioline (London, UK).

The TOPO-TA cloning kit was obtained from Invitrogen (Paisley, UK). The Plasmid Midi kit (for low copy number plasmids) and QIAquick® gel extraction kit were from Qiagen LTD (Surrey, UK). The GenElute™Plasmid Miniprep kit (for high copy number plasmids) was supplied by Sigma.

Oligodeoxynucleotide primers used in PCR reactions were obtained from MWG-Biotech (Ebersberg, Germany). The sequences of primers used in this work are shown in Appendix 2.

2.2.3 DNA sequences

The promoter region of the *HYDRA1* gene was isolated from the Wassileskia (Ws) ecotypic background by D. Lourdas via plasmid rescue, and was supplied by Dr J. Topping.

2.2.4 Bacterial strains and culture conditions

Bacterial culture media

Luria-Bertani (LB) culture media was made up according to the following recipe (after Ausubel *et al.* 1997), and autoclaved at 121°C for 20 minutes.

LB broth

10g/l "Select" tryptone

5g/l "Select" yeast extract

5g/l NaCl

LB agar

As above, but including 15g/l Bacto-agar (Difco, UK) prior to autoclaving.

E. coli

The *E.coli* strain XL1-blue MRF (Jerpseth, 1992) was used to prepare competent cells, and as a plasmid host.

The TOP-10 *E.coli* strain used as a host for pCR2.1-TOPO was supplied as part of the TOPO-TA cloning kit (Invitrogen; Paisley, UK).

The *E.coli* strain HB101 was used as a carrier for the pRK2013 plasmid, described below.

All of these cultures were grown in LB broth with constant shaking, or on LB-agar plates at 37°C.

Agrobacterium

The *Agrobacterium tumefaciens* C58C3 strain (Dale *et al.* 1989) was used for transformation of the p*HYD1*::GUS construct into *Arabidopsis thaliana* ecotype Col-0. The strain retains the virulence factors required for T-DNA transfer and insertion into plant genomic DNA, but has been disabled so not to cause crown gall disease. C58C3 carries a chromosomal streptomycin resistance marker, allowing antibiotic selection using 100µg/ml.

Agrobacterium cultures were grown in LB broth or on LB agar plates at 30°C.

Storage of bacterial cultures

Aliquots from fresh overnight cultures of all bacterial strains were combined in equal volume with sterile 50% glycerol in Eppendorf tubes, and stored either at -20°C for short-term use, or flash-frozen in liquid nitrogen and kept at -80°C for extended periods.

Bacterial selection

Stock solutions of antibiotics were prepared by dissolving in distilled water, filter-sterilising using 0.2µm pore Acrodiscs™ (Gelman, Northampton, UK), and added to liquid or molten bacterial growth media as required. The following list includes the antibiotics used in this study.

- Ampicillin (Sigma); made as 1000x stock and stored at -20°C, used for selection of bacterial plasmids.
- Augmentin (Beecham Research, UK); made fresh as 1000x stock, used for removal of *Agrobacterium tumefaciens* after plant transformation.
- Kanamycin sulphate (Sigma); made as 1000x stock and stored at -20°C, used for selection of bacterial plasmids and transformed plants.
- Methicillin (Sigma); made as 1000x stock and stored at -20°C, used for selection of bacterial plasmids in conjunction with Ampicillin, to limit growth of secondary satellite colonies on LB-agar plates.
- Nalidixic acid (Sigma); made as 1000x stock and stored at -20°C, used for selection of bacterial plasmids.
- Streptomycin sulphate (Sigma); made as 1000x stock and stored at -20°C, used for selection of bacterial plasmids.

Where blue-white colour selection of recombinants was required, 40µg/ml X-Gal (substrate) and 100µg/ml IPTG (to induce expression of the *LacZ* gene) were added at the same time as the antibiotic, to the molten LB agar prior to pouring the plates. Blue-white selection allows identification of

recombinants because insertion of the cloned fragment disrupts *LacZ*, and colonies appear white instead of blue.

2.2.5 Plasmid vectors

The following plasmids were used in this project. Where appropriate, vector diagrams with restriction sites can be seen in Appendix 3.

pCR®2.1 TOPO from Invitrogen (Paisley, UK) is used for cloning DNA fragments generated by PCR. The vector is supplied as a linearised plasmid with single overhanging thymidine residues, used as compatible 'sticky' ends to match with the overhanging adenine residues appended to PCR products by Taq DNA polymerase.

pΔ-GUS-CIRCE (kindly supplied by Dr I. M. Evans, University of Durham, UK), is based upon pCIRCE, a derivative of pBIN19 (Bevan, 1984), which incorporates the multiple cloning site and GUS cassette from pGUS-1 (Topping *et al.* 1991). The pCIRCE plasmid is a wide host range binary cloning vector for *Agrobacterium*-mediated transfer into plant cells. The GUS cassette from pGUS-1 contains the β-Glucuronidase gene from *E.coli*, followed by the NOS terminator; this is inserted into pΔ-GUS-CIRCE in the *LacZ* gene, and so this vector does not have blue/white selection.

The pRK2013 plasmid is a Naladixic acid-resistant broad host range 'helper', required for the introduction of binary vectors into *Agrobacterium* by tri-parental mating (Topping *et al.* 1991). Tri-parental mating is used here to move the T-DNA construct carrier pΔ-GUS-CIRCE into *Agrobacterium* strain C58C3, which contains the virulence loci necessary for T-DNA transfer. During tri-parental mating, pRK2013 mobilizes itself into both *Agrobacterium* C58C3 and *E. coli* strain XL1-blue, using the mobilizing (mob) functions present in *E. coli* HB101. The presence of pRK2013 then mobilizes itself and pΔ-GUS-CIRCE back into both *E. coli* HB101 and *Agrobacterium* C58C3. Antibiotic selection procedures then

separate *Agrobacterium* carrying pΔ-GUS-CIRCE from the two *E. coli* strains.

2.2.6 Plant lines

Plant lines carrying seedling-lethal mutations at two loci, designated *hydra1* (*hyd1*) and *hydra2* (*hyd2*), were isolated in screens of EMS and T-DNA mutagenised populations (Topping et al. 1997). These lines, and their respective ecotypes in *Arabidopsis thaliana* (C24 and Wassilewskia), were supplied by Professor Keith Lindsey (University of Durham). Of these, several alleles of *hyd1* are available; *hyd1-1* is a point mutation in the C24 background, and *hyd1-2, hyd1-3* and *hyd1-4* are in Ws. One allele is available for *hyd2* in the Ws background. In order to minimise the number of background controls required, and in order to distinguish the *hyd1* phenotype more clearly, most analyses were performed on *hyd1-2* and *hyd2*, using a Wassilewskia (Ws) control. Therefore wherever *hyd1* is mentioned in this study, it will refer to the *hyd1-2* allele unless specified otherwise.

The Columbia-0 strain of *Arabidopsis*, used as a host for transformation of the p*HYD1*::GUS construct, was obtained from the Nottingham Arabidopsis Stock Centre (Nottingham, UK). The two full-length p*HYD1*::GUS constructs (respectively from Ws and Col) were supplied ready-transformed into Col-0 by Dr J. Topping, for analysis alongside the deletion series made for this study.

The *ethylene insensitive-2* (*ein2*) mutant in a Columbia ecotype background, donated by Joe Ecker, was used to provide an ethylene-reduced signalling environment in which to study *hydra* development.

The transformed marker lines containing promoter-reporter and protein-reporter fusion constructs listed in Table 2.1 below, were donated from the sources indicated.

Construct	Donor	Original reference
CYC1At::CDB::GUS	M-T Hauser	Hauser & Bauer, 2000
DR5::GUS	J Murfett/ T Guilfoyle	Ulmasov *et al.* 1997
p*PIN1*::GUS	K. Palme	(unpublished)
p*ACS1*::GUS	M. Van Montague/ Rodriguez-Pousada	Rodriguez-Pousada *et al.* 1993
p*AthB8*::GUS	S Baima	Baima *et al.* 1995
p*GASA3*::GUS	J Mundy	Raventos *et al.* 2000
p*IAA2*::GUS	R. Swarup/ M. Bennett	Swarup *et al.* 2001
p*ARR5*::GUS	J. Kieber	D'Agostino *et al.* 2000
p*PHB*::GUS	J. Bowman	(unpublished)
p*REV*::GUS	J. Bowman	(unpublished)
p*YAB*::GUS	J. Bowman	Siegfried *et al.* 1999
SCR::GFP	J. Benfey	Wysocka-Diller *et al.* 2000
GFP::TUA6	T. Hashimoto (via P. Hussey)	Ueda *et al.* 1999

Table 2.1; Promoter-reporter and protein-reporter fusion constructs

2.3 Methods

2.3.1 Plant Growth Conditions

2.3.1.1 Soil-based greenhouse culture

Arabidopsis plants used for genetic crosses, segregating mutant lines and bulking of seed, were grown in a 5:1 mixture of Gem multi-purpose compost and horticultural silver sand (both from LBS Horticulture LTD, Lancashire, UK), to ensure adequate drainage. Seeds were sown in small pots and pre-chilled at 4°C for three days to break dormancy, before transfer to normal growing conditions (22°C, 16 hours light: 6 hours dark). Germinating seedlings were transferred at 5-10 days after emergence (dae) into 24-well standard tray inserts (LBS Horticulture LTD, Lancashire, UK) containing the standard compost-sand mixture, placed on damp capillary matting. Plants were watered from above using a fine nozzle. Separate pools of seeds from individual plants were obtained using the Aracon system (BetaTech, Belgium).

All compost was treated as standard with "Intercept" systemic insecticide (Levinton Horticulture LTD, UK), at a rate of 64mg/24-well tray. The mite *Amblyseius cucumeris* (Syngenta, UK) was introduced every 6 weeks onto the aerial parts of the plant as a biological control against thrips.

Parent plants carrying the *hydra* mutation were identified by screening for the presence of mutant embryos. Mature ovules were dissected from siliques prior to senescence, mounted on standard microscope slides (BDH, UK) in 0.5M KOH for one minute to clear the tissues, and gently squashed using a coverslip to allow ovules to emerge from the testa. The ovules were then examined using an Olympus SZH10 research stereomicroscope (Olympus Optical Company LTD, London, UK).

Genetic crosses were made under a Zeiss STEMI SV8 dissecting stereomicroscope (Carl Zeiss LTD, Welwyn Garden City, Herts, UK). Flowers were selected on the basis of age; examples were chosen for relative maturity of the stigma prior to dehiscence of pollen from the anthers, and all other siliques and unsuitable flowers were removed from the stem. Young flowers were emasculated, using fine watchmakers forceps (BDH, UK) to gently remove immature anthers, and then mature pollen from the male parent was transferred manually to the stigma, again with forceps. The stem below the crossed flower was labelled, and the plants returned to the greenhouse for silique development. Siliques were harvested upon maturity, but prior to senescence and pod shatter.

2.3.1.2 Culture under sterile conditions

All seedlings for analysis were grown in sterile Petri dishes using $^1/_2MS_{10}$ media (Appendix 1), with plate margins sealed using Micropore™ medical tape (Industricare Ltd, Leicestershire, UK). Prior to germination, seeds were stratified for 7 days in the dark at 4°C to promote and synchronise germination. Plates were then transferred to a growth chamber at 22 ± 2°C set at 'long days' (16 hours light: 6 hours dark). 'Dark-grown' plates were treated exactly as those in the light, except that Petri dishes were wrapped in aluminium foil prior to placement in the growth chamber.

Surface-sterilisation of seeds is necessary for germination on nutrient rich medium to prevent contamination by fungi or bacteria. Sterilisation was carried out in a laminar flow cabinet, and solutions were transferred between tubes using a fresh sterile transfer pipette for each seed sample. Aliquots of seeds were placed in 7ml plastic bijou bottles (BDH) and exposed to 70% v/v ethanol for 20-30 seconds to partially de-wax the testa. Samples were then immersed for 15-30 minutes in 10% v/v commercial bleach solution with a drop of Tween 20 detergent to enhance wetting and penetration. The seeds were then washed thoroughly in 4-6 changes of sterile distilled water before being plated immediately onto germination

medium ($^1/_2MS_{10}$). All washings were collected and filtered through paper towels to remove stray seeds, for autoclaving and disposal.

Seedlings for analysis at early post-germination stages (prior to 10dae) were harvested directly from germination plates. Seedlings for later analysis were transferred at 5dae onto square Petri dishes (Fred Baker, UK) under sterile conditions using flame-sterilised forceps, and grown vertically at an angle of approximately 70°.

2.3.1.3 Culture under semi-sterile conditions

The small amounts of F1 seed derived from genetic crosses were germinated in semi-sterile conditions prior to transplantation for greenhouse growth. This involved filling small Petri dishes (Sterilin) with autoclaved Gem perlite (LBS Horticulture LTD, Lancashire, UK) and moistening the granules with a sterile 1% (w/v) solution of Gamborgs B5 basal medium with minimal organics (Sigma). Seeds were then scattered over the surface, where they could be clearly seen against the white granules, and stratified in the usual way prior to germination in a growth cabinet.

2.3.2 Screening

2.3.2.1 Screening for mutant seedlings

The *hydra* mutants of *Arabidopsis* are seedling lethal, and require nutrient-enriched growth conditions for survival. Hence these mutant plants are maintained via a heterozygous parent line, and grown on $^1/_2MS_{10}$ media in sterile conditions, where they appear in a 1:3 ratio with plants of wild-type morphology (Topping *et al.* 1997). Due to the compromised germination rate of these mutants, seeds require synchronising by chilling for 7 days at

4°C. Upon germination, *hydra* mutants are easily distinguished with the aid of a dissecting microscope, by the severe morphology of their phenotype.

Crossed F2 progeny were screened to identify *ein2* mutant homozygotes. This locus encodes a central component of the ethylene signalling pathway (Alonso *et al.* 1999), and *ein2* mutants have been identified by screens for insensitivity to both exogenous and endogenous ethylene (Guzman & Ecker 1990, Roman *et al.* 1995). These plants were selected, greenhouse grown, and subsequently screened to derive *hydra* parental lines within a homozygous *ein2* background.

Selection for *ein2* was conducted in two ways. Dark germination and growth for 4-5 days in media supplemented with 40μM ACC (ACPC) distinguished the *ein2* mutants by their etiolated morphology, whilst non-mutant plants show a strong triple response under these conditions. Light grown seedlings were transferred at 4-5 days after exposure to light (dae), to vertical plates containing 10μM ACC, alongside wild-type and *ein2* parental control plants. Root lengths of all seedlings were marked at the point of transfer, and *ein2* homozygotes identified by their enhanced root elongation response over the subsequent three days.

2.3.2.2 Screening for molecular markers

Molecular markers that demonstrate a response to certain signalling pathways or gene activities, can be used to gain insight into the positioning of cell types and cellular responses within the plant body. A comparison of promoter-reporter expression patterns in wild-type plants with those in the *hydra* mutants, were used in this study to infer cellular positional information in these mutants. Some protein-fusion markers, such as those highlighting intracellular components by fusing native proteins with GFP, again in comparison with wild-type results are able to reveal aspects of the internal functioning of the mutant cells *in-vivo*.

Plant lines carrying promoter- or protein- fusion constructs made using a bacterial gene encoding the β-glucuronidase enzyme (GUS), were screened by incubating seedlings in a 1mM solution of X-Gluc (5-bromo-4-chloro-3-indolyl-β-D-glucuronic acid), as described in section 2.4.3.

Seedlings expressing GFP constructs were mounted in water and screened under fluorescence using the BY2A (GFP) filter on a Nikon Optiphot-2 stereomicroscope, (Nikon UK Ltd, Surrey, UK) prior to bulking seed for confocal analysis.

2.3.3 Histology and microscopy

2.3.3.1 Morphological analysis of embryos and whole seedlings

Shoot morphology

To visualise the 3D morphology of shoots, whole seedlings at all stages of development were mounted in the desired orientations on 0.5% agarose in a Petri dish, and examined using a Zeiss STEMI SV8 dissecting stereomicroscope, an Olympus SZH10 stereomicroscope or a Leica MZ125 stereomicroscope (Leica Instruments, Heidelberg, Germany). Material to be photographed was mounted in agarose as above, and then the Petri dish flooded with 40% glycerol to submerge the seedling and reduce glare. Images were captured digitally using a Photometrics Coolsnap™ CF camera (Roper Scientific Inc, Trenton, New Jersey, USA) with Openlab 3.11 software. Larger specimens were displayed on agarose plates and photographed using a tripod-mounted Nikon Coolpix 5000 digital camera (Nikon UK Ltd, Herts, UK).

Root epidermal morphology

General examination of root morphology was carried out with samples mounted on agarose as described above, but without glycerol immersion. Higher power magnification involved mounting samples on microscope slides under coverslips. This typically resulted in distortion to the more delicate *hydra* tissues, and so 4 dae seedings were transferred under sterile conditions to a 1-2mm thick film of $^1/_2MS_{10}$ medium on a 20x50mm microscope coverslip, covered with a semi-permeable membrane and left to grow for another 5 days immersed in $^1/_2$ MS_{10} liquid at an angle of approximately 30°. This enabled the roots to grow down through the medium and along the surface of the coverslip. Microscopic examination was then possible without distortion, by peeling away the membrane and mounting the coverslip directly onto a microscope slide. By this method, the root samples were sufficiently embedded in the medium that the structure and morphology of root hairs was preserved, allowing examination at higher magnification.

Phyllotaxy

Plants were analysed at 12 dae to assess the patterns of primordial initiation. Due to difficulties in interpretation of patterning in duplicated meristems, *hydra* mutant plants were chosen that showed a single apparent point of primordial initiation around the SAM. The *hydra* seedlings were first fixed in FPA (50ml 96% ethanol, 5ml Propionic acid, 10ml 37% Formaldehyde, 35ml dH2O) for 1 hour, and then replaced in dH2O; this de-coloured the youngest primordia, and made them easier to visualise with top light (using a Leica CLS 150X swan-neck cool illumination lamp) . All mutant and control plants were then mounted in agarose and photographed under glycerol as described above.

2.3.3.2 Patterning phenomena

Xylem vessels

Leaf material was prepared for visualisation of xylem vessels and cleared epidermal cells using standard light microscopy after Carland *et al.* (1999). Samples were fixed for 1 hour in 3:1 ethanol:acetic acid, cleared overnight in 25% chloral hydrate, and dehydrated through an ethanol series (30%, 50%, 70% for 1 hour each before 96% overnight). After dehydration, leaf tissues were mounted on microscope slides in 50% v/v glycerol, and vascular traces and epidermal patterning were examined using light and dark field microscopy.

Visualization of procambial tissue in whole-mount embryos

The p*AthB8*::GUS reporter construct (Baima *et al.* 1995) is a marker of pre-procambial cell fate; GUS activity is visible in these cells prior to their anatomical resolution as narrow procambial cell files (Scarpella *et al.* 2004). Developing siliques were harvested from plants heterozygous for *hyd* mutations, and carrying the p*AthB8*::GUS transgene, the testa punctured with a fine tungsten histology needle, and the embryos vacuum-infiltrated with X-Gluc in buffer (described in Section 2.3.2 below). Reporter activity highlights the provascular strands by localization of β-glucuronidase activity. GUS-stained embryos were dissected from their seed coat, and mounted in a clearing mixture of 8:2:1 (w:v:v) chloral hydrate:glycerol:water.

Embryos were mounted under a coverslip, and examined with a Zeiss Axioscop stereomicroscope (Carl Zeiss Ltd, Herts, UK) using DIC/Nomarski optics. Images were captured digitally using a Photometrics Coolsnap™ CF camera (Roper Scientific Inc, Trenton, New Jersey, USA) with Openlab 3.11 software.

General patterning of cells in the epidermis

Material for staining was fixed, cleared and dehydrated as described for xylem vessels above, then stained for 5 minutes with safranin-O (1% w/v in 95% ethanol), dipped momentarily into 95% ethanol to wash out excess stain, and immediately counterstained for 15 seconds in fast green (0.1% w/v in 95% ethanol) before re-hydrating through 70, 50 and 30% v/v

ethanol, and finally dH_2O. This staining method highlighted both the vascular strands and trichome cells of the epidermis in red, while areas of dense cells (such as stipules) were counterstained in green.

Cotyledon epidermal patterning and stomatal ontogeny

The ontogeny of stomatal clusters was examined using epidermal prints in agarose, with a method adapted from Mathur & Koncz (1997) by Xavier Torres-Contreras (*pers comm.*). Cotyledon adaxial surfaces are a useful model system with which to study stomatal density and distribution because they are easily accessible, they lack trichomes in wild type plants, and undergo a relatively few cell division events during post-germination growth (Geisler & Sack, 2002). The cell division activity which takes place in the adaxial epidermis is in association with the division and differentiation of meristemoids; the precursors that form guard mother cells. Cotyledon mesophyll layers grow almost entirely through cell expansion in the post-germination phase (Tsukaya *et al.* 1994). Cotyledon adaxial patterning lacks the longitudinally elongated central cell files found above the primary veins of true leaves, and so gives an even field of expansion across the width of the lamina. Also, because these leaves lack trichomes, in wild type plants all epidermal cells are potentially available for commitment to guard mother cell fate (Bean *et al.* 2002).

General cotyledon patterning was examined by making single agarose impressions of cotyledons from mutant and control plants. In order to study the ontogenic sequence of stomatal clusters, sequential impressions of the same leaf surfaces were necessary. Seedlings were grown under standard sterile conditions, and the plants handled using flame-sterile forceps. Cotyledons from selected plants were used to produce epidermal prints between 6 and 10dae.

A 6% solution of agarose was made using distilled water, melted in a microwave and kept in a molten state using a waterbath. Microscope slides were warmed on a hotplate prior to applying a drop of molten agarose, and allowing this to cool for a few seconds before use. Epidermal prints were

made by placing plant samples onto the agarose in the desired orientation, and supporting them with fine forceps until the agarose solidified. The agarose was then allowed to cool completely, before removal of the sample. To help protect the seedlings against dessication during handling, the microscope slides were kept in closed Petri dishes, and the plants transferred back to culture plates as rapidly as possible. The slides were then stored in 30% (v/v) ethanol at 4°C prior to examination.

The imprints were examined with a Zeiss Axioscop stereomicroscope (Carl Zeiss Ltd, Herts, UK) using DIC/Nomarski optics. Photographs were captured digitally using a Photometrics Coolsnap™ CF camera (Roper Scientific Inc, Trenton, New Jersey, USA) and Openlab 3.11 software. Because the leaf surfaces were curved, or in the case of the *hydra* mutants often uneven, multiple digital images were required in different focal planes; composite images were constructed from these using Adobe Photoshop 4.

2.3.3.3 Histochemical analysis

Callose

To visualise callose in sieve tube elements in seedlings, aniline blue was used according to the method of Carland et al (1999). Leaf material was fixed in 3:1 (v/v) ethanol:acetic acid for 1 hour, then treated for 1 hour in 2M NaOH. This was neutralised briefly by washing with 50mM Sodium Phosphate buffer, pH6.8, then stained overnight in a freshly filtered solution of 0.0005% (w/v) aniline blue in phosphate buffer. Stained material was mounted in 50% (v/v) glycerol, and visualised under UV light using a broad band filter to detect 4',6-diamino-2-phenlyindole. Fluorescence images were captured by a Photometrics Coolsnap™ CF camera and handled in Openlab 3.11 software, and then the same leaf area was photographed under light field illumination to show the xylem trace.

The images were superimposed in Openlab, to show the relationship between xylem and phloem tracery in the leaf.

β-glucuronidase (GUS)

Histochemical localised β-glucuronidase enzyme (GUS) activity was observed by incubating fresh seedlings in a 1mM solution of X-Gluc (5-bromo-4-chloro-3-indolyl-β-D-glucuronic acid; Melford Labs Ltd, Suffolk), carried in a buffer comprising 0.1M sodium phosphate at pH 7.0, 10mM EDTA, 0.1% Triton-X100 and 6mM potassium ferri/ferrocyanide to inhibit diffusion of the reaction intermediate. The ferri/ferrocyanide concentration is higher than is typically used for GUS staining; this concentration was increased because the *hydra* mutants typically showed higher levels of tissue diffusion of the resultant blue precipitate than is observed in wild-type plants.

Plant material carrying a GUS reporter construct was incubated for the optimal derived time and temperature, found by subjecting the plant line carrying the construct to a comprehensive developmental staining analysis. These times are shown in Table 2.2. All plant lines were initially stained by incubation at 37°C, though a slower incubation at room temperature was found to give a less diffuse signal, and so this method was used preferentially in later analyses. The p*CYC1At*::CDB::GUS line was also fixed in 90% acetone for 15 minutes on ice prior to incubation (as described by Donnelly *et al.* 1999), to halt cells in the process of dividing.

Young embryos were stained by first puncturing the testa of fresh (undessicated) seeds using a tungsten wire histology needle, or mature embryos were imbibed in water for 24h and dissected out of the seed coat completely, prior to vacuum-infiltration with X-Gluc buffered solution.

For all samples, tissues were then cleared in 70% ethanol prior to mounting on agarose or microscope slides in 50% glycerol. Slide samples for higher

resolution examination were mounted in 8:2:1 (w:v:v) chloral hydrate:glycerol:water.

Table 2.2; Optimal GUS staining times and temperatures

Construct	Optimal staining time & temperature
CYC1At::CDB::GUS	16 h rt
DR5::GUS	3h 37°C or 16h rt
p*ACS1*::GUS	8h 37°C or 24h rt
p*AthB8*::GUS	3h 37°C or 16h rt
p*GASA1*::GUS	3h 37°C or 16h rt
p*IAA2*::GUS	3h 37°C or 16h rt
p*ARR5*::GUS	3h 37°C or 16h rt
p*PIN1*::GUS	6 h 37°C or 24h rtC
p*PHB*::GUS	36h 37°C or 5 days rt
p*REV*::GUS	1h 37°C or 8h rt
p*YAB*::GUS	12h 37°C 36h rt

2.3.3.4 Preparation of material for wax embedding and sectioning

Material was fixed in 3:1 (v/v) methanol:acetic acid overnight at -20°C, then washed in PBS three times for 15 minutes each. Samples were then dehydrated by immersing them each for an hour in an ethanol series (10%, 30%, 50%, 70%, 90%, 96%), followed by 1 hour in 1% safranin-O (w/v) in 96% (v/v) ethanol (to surface-stain the samples and make them more visible

later in the paraffin block), and finally in 96% (v/v) ethanol overnight. Samples were then vacuum-infiltrated through a series of (v/v) (96%) ethanol:Histoclear in ratios of 3:1, 2:1, 1:1, 1:2, and 1:3 and 100% Histoclear for 1 hour each, before overnight incubation in fresh Histoclear at 4°C.

Samples for embedding were then infiltrated by adding a layer of melted Paraplast paraffin wax to the Histoclear, and incubated at room temperature for 12 hours. A second layer of paraffin was added and left to incubate at 42°C for 12 hours. Samples were then kept at 50°C for subsequent infiltration stages. Half of the solution around the samples was replaced with molten paraffin for 3 hours, followed by two more washings with paraffin respectively for 3 hours and overnight. After a final wash in paraffin for one hour, the samples were labelled and embedded in moulds.

The wax block was trimmed using a razor blade and mounted on a wooden block in the desired orientation using molten paraplast. Serial sections of 5-10μm were cut on a Leitz 1512 rotary microtome, transferred into drops of water onto Superfrost Plus™ slides (BDH) which are ready-coated with a positively-charged ionic layer to aid adhesion of sections, and dried on a heating block set at a low temperature.

Slides were washed three times in Histoclear and incubated for 20 minutes in the solution before being de-paraffinised using an ethanol series of 100%, 96%, 80%, 70%, 50%, 25% and dH_2O for 10 minutes each.

Sections were stained with 1% w/v Safranin-O in dH_2O for 30 minutes, washed three times with dH_2O, incubated in 1% w/v Methyl Green in dH_2O. After another three washings in dH_2O, the slides were dried as above and mounted in DPX mounting medium, covered with a coverslip and left to harden overnight.

An alternative method of fixation and embedding, using Historesin, was found to give superior morphological preservation. This method is described below in section 2.3.3.5.

2.3.3.5 Resin Embedding

Plant material carrying GUS reporter genes were incubated in X-Gluc as described. Stained material was rinsed three times in 0.1M phosphate buffer pH 7.

After staining, samples were fixed in a fresh solution of Karnovsky's fixative. A 4% paraformaldehyde, 4% glutaraldehyde solution was made by dissolving paraformaldehyde in de-ionised water at 60°C, adding 0.1M KOH dropwise to bring the pH above 8. The solution was cooled, and brought to pH 7 using 0.1m HCl. Glutaraldehyde was then added, and combined with 1 volume of 0.2M phosphate buffer (pH 7) to give a (w/v) 4% paraformaldehyde, (v/v) 4% glutaraldehyde solution in 0.1M phosphate buffer. Samples were placed into this fixative for 3 hours on ice at 4°C, then the bathing solution replaced with fresh fixative for incubation overnight at 4°C, to ensure penetration into the internal tissues. After this all traces of fixative were removed by rinsing the samples three times in 0.1M phosphate buffer, for at least 30 minutes each time.

Samples were then embedded using the method recommended for the Historesin™ Embedding kit (Leica instruments, Heidelberg, Germany), as follows. After fixation, samples were dehydrated through an ethanol series comprising 1 hour in each of 30, 50, 70 and 95% (v/v) ethanol, with a final wash in 95% ethanol overnight. Infiltration solution was prepared by mixing 50ml of Basic Resin liquid with 1 packet (0.5g) of Activator. Each sample was then incubated at 4°C in the following solutions, under vacuum for the first 30 minutes;

- 3:1 v/v ethanol/Infiltration solution for 6 hours,
- 1:1 v/v ethanol/Infiltration solution overnight,

- 1:3 v/v ethanol/Infiltration solution for 6 hours,
- Infiltration solution overnight.

Embedding medium was prepared by mixing 15ml of Infiltration solution with 1ml of Hardener, and used immediately. Flat bottom embedding (BEEM) capsules (Agar Scientific, Stanstead, UK) were filled with Embedding Medium, the samples oriented in this medium using forceps, and left to harden overnight with closed lids.

Capsules were cut away from the hardened resin using razor blades, and the resin trimmed prior to mounting on the cutting block of a Reichert Ultracut ultramicrotome. 50µm sections were cut from samples using a glass knife, and floated onto water on Superfrost Plus™ pre-coated microscope slides (BDH), then left to evaporate on a hotplate. Samples were then mounted in DPX (Fisons Scientific Equipment, Loughborough, UK).

The sections were examined with a Zeiss Axioscop stereomicroscope (Carl Zeiss Ltd, Herts, UK) using DIC/Nomarski optics. Photographs were captured digitally using a Photometrics Coolsnap™ CF camera (Roper Scientific Inc, Trenton, New Jersey, USA) and Openlab 3.11 software.

2.3.3.6 Confocal microscopy

GFP visualization

Fresh seedlings carrying GFP constructs were mounted in dH_2O under a large (32x24mm) zero-thickness coverslip, and examined using a Zeiss LSM510 microscope, argon laser excitation at 488nm and emission filter at 505-530nm. The *SCR*::GFP reporter was used to overlay transmission images of root tissues to show the location of the fluorescence signal.

Counterstaining was attempted by incubation for 1 minute in 10μg/ml propidum iodide, with samples then transferred to water prior to slide mounting, and observed promptly, overlaying the TRIT-C red channel (propidium iodide) onto the FIT-C green (GFP). This treatment extinguished most of the GFP signal in all *hyd* mutant samples, and was abandoned.

Images were captured digitally using the integral LSM software.

Embryo and root internal cellular patterning

Embryos were dissected from desiccated seeds imbibed overnight, or fresh ovules were punctured with a fine tungsten histology knife, and prepared using the following method, as described by Bougourd *et al.* (2000). This method was also found effective for staining and examining cell layers in young root tissues.

Naked embryos and immature seeds were transferred to 15% v/v ethanol in a 70μm nylon cell strainer (Falcon 2350) resting in a 6-well plate (Falcon 3046, both from; Becton-Dickinson Labware Europe, Le Pont de Claix, France). Embryos were dehydrated through an ethanol series (15%, 50%, 70%, 96%, and twice at 100% (v/v) for 15-30 minutes each) before being left for 3h-overnight in 100% ethanol. Material was then re-hydrated (though 96%, 70%, 50% and 15% (v/v) ethanol) before washing twice with dH_2O, again for 15-30 minutes each. A 0.5% (w/v) stock solution of Aniline Blue in sodium phosphate buffer pH 6.5, was freshly filtered and used to make a staining solution of 1:20 dilution in more buffer; this was used to stain the embryos for 30 minutes, followed by three successive washings and two 15 minute soaks in fresh dH_2O. The material was then dehydrated and re-hydrated again, through the series described.

Embryos were transferred to microscope slides and mounted in Hoyer's solution (9g gum arabic, 60g chloral hydrate, 6ml glycerol, 15ml dH_2O) under a coverslip. Slides were left for several days to harden, and

examined by confocal microscopy using the FIT-C argon laser at 140nm excitation, 550-585nm emission.

Visualization of cortical microtubular arrays

Cortical microtubules demonstrate a helical arrangement during cell expansion in longitudinally oriented *Arabidopsis* cell files, and are known to be modulated by ethylene (Roberts *et al.* 1985). The angle of orientation of these microtubular arrays in hypocotyl epidermal cell files was used in this study as a means both to assess the direction of expansion growth in *hydra* mutant hypocotyl cells, and to compare the effect of *ein2* on the axis of cellular expansion.

Using the *TUA-6*::GFP protein fusion reporter (Ueda *et al.* 1999) to highlight the cortical microtubular arrays in *Arabidopsis* hypocotyl cells, light-grown *hydra1* and *hydra1-ein2* seedlings at 4-6 dae were compared against their respective Ws and *ein2* backgrounds for alignment of the cortical microtubular arrays in expanding regions of the hypocotyl. (Unfortunately, *hyd2* mutants could not be analysed for cortical microtubular arrays with the *TUA-6*::GFP construct, as this transgene was found to demonstrate genetic linkage with the *HYD2* locus, and did not co-segregate with the mutant *hyd2* gene in the time available.) Photographs of the directionally expanding hypocotyl region were taken at x40 using confocal microscopy as described above.

2.3.3.7 Scanning Electron Microscopy

Seedlings grown on vertical agar plates were vacuum-infiltrated for 30 minutes with 4% paraformaldehyde in 1M Phosphate buffer, pH 7.5 before dehydration through a series of 30, 50, 70, 90, 96 and 100% ethanol, incubating in each solution for at least 1 hour, before washing twice in dry acetone. Samples were loaded into cradles and placed into an E3100 Jumbo Critical Point Drying Apparatus, where the acetone was replaced with liquid carbon dioxide under pressure, and heated gently using a water

jacket to raise the temperature to the 'critical point' where the CO_2 lyophilises from a liquid to a gaseous phase, drying the tissue samples with minimal structural disruption.

The dried samples were transferred and mounted, using a fine brush, onto metal stubs (Agar Scientific, UK) carrying double-sided adhesive discs, before coating with an electron-dense layer of gold-palladium of 5-50Å, using a Polaron sputter coating machine. Samples were stored in a sealed cabinet over silica gel prior to observation using a JEOL IC848 SEM. Images were digitally captured and processed using Adobe Photoshop 4.

2.3.4 Exogenous hormone response experiments

Exogenous hormone response experiments present a rapid, though crude, means of assessing the responsiveness of seedlings to known plant signalling molecules. It is noted that under these circumstances the applied compounds may be present at levels unrepresentative of the seedling's usual physiology, and many of the compounds themselves are analogues of natural compounds so may not accurately reflect the plant's response to natural active forms of the relevant pathway components. However in comparison between the mutants and their control backgrounds, these treatments may reveal qualitative differences in responses which can indicate differences in the mutant's physiology in relation to its respective wild-type control.

All phytohormone and inhibitor compounds were made up as 10mM (1000X) stock solutions in the relevant solvents, and filter-sterilised using 0.2µm pore Acrodisks™ (Gelman, UK) prior to use. These chemicals were introduced into molten media, cooled to around 55°C, before vertical plates were poured and allowed to cool. Seedlings were transferred at 6 dae onto these vertical plates, supplemented with these compounds and over the concentration ranges listed below. Response was assessed by

changes in root and shoot morphology, in relation to seedlings grown on un-supplemented media. Wild-type and *ein2* control seedlings were assessed for their response after 7 days exposure to supplemented media. The *hydra* mutant plants, which have a much slower growth rate, were left for longer; 14-21 days after transfer, in order to assess their response.

Phytohormones and inhibitor compounds

The following list of compounds was used across the concentrations indicated, to assess growth responses.

Auxins

1 and 10μM 1-NAA; (biologically active auxin analogue)

1 and 10μM 2-NAA (inactive auxin analogue)

These two isomers of naphthalene-1-acetic acid (NAA) were chosen because these compounds enter plant cells by diffusion, and so circumvent problems with uptake (Delbarre *et al.* 1996). Stock solutions were made using filter-sterilised 70% (v/v) ethanol.

Inhibitors of polar auxin transport

25μM TIBA (2,3,5-triiodobenzoic acid); a synthetic auxin transport inhibitor which is itself transported in a polar manner. It acts in the cell to inhibit auxin efflux (Thompson *et al.* 1973; Cande & Ray, 1976) and mimics the reduction in polar auxin transport caused by the *pin1* mutation of *Arabidopsis* (Okada *et al.* 1991).

10μM 1-NOA (naphthoxy-1-acetic acid); a compound which specifically inhibits the auxin influx carrier AUX1, with minimal effects on auxin efflux (Imhoff *et al.* 2000). Addition of NOA to the growth medium phenocopies the *aux1* mutation, though does not affect auxin efflux, and has no auxin-like activity (Parry *et al.* 2001).

Stock solutions of both compounds were made using filter-sterilised 70% (v/v) ethanol.

Abscissic Acid

0.1, 1 and 10μM ABA; a phytohormone. A stock solution was made by dissolving the compound in sterile dH_2O.

Gibberellic Acid

0.1, 1 and 10μM GA_3; a phytohormone. A stock solution was made by dissolving the compound in sterile dH_2O.

Brassinosteroids

0.1, 1 and 10μM Epibrassinolide; a steroid phytohormone. A stock solution was made fresh, using filter-sterilised 70% (v/v) ethanol

Cytokinins

1 and 10μM BAP (6-benzyl-amino purine); a cytokinin. A stock solution was prepared by dissolving the compound in 0.5M HCl.

Ethylene

1, 10 and 100μM ACC (1-aminocyclopropane-1-carboxylic acid); also known as ACPC. This is the ethylene precursor, produced during biosynthesis of ethylene in plants, and the enzyme ACC synthase is the rate-limiting step in this pathway. ACC oxidases are in all tissues, and convert ACC to ethylene. A stock solution of ACC was made in sterile dH_2O.

10 and 100μM Silver thiosulphate

Silver ions are know to inhibit ethylene responses when applied to plant tissues (Beyer, 1976, 1979); they are thought to block the signalling pathway by binding to the ethylene receptor ETR1, in competition with the Cu^{++} co-factor used by this protein (Rodriguez *et al.* 1999). Silver thiosulphate was chosen for use in this study rather than silver nitrate, due to the lesser toxicity and greater mobility within the plant, of the

thiosulphate ion; $[Ag(S_2O_3)_2]^{3-}$. A 10mM stock solution of silver ions was made by combining equal volumes of stocks of 20mM silver nitrate, and 80mM sodium thiosulphate, both in dH_2O. The nitrate solution was added drop-wise to the thiosulphate, with regular mixing using a vortex to avoid the formation of a precipitate.

2.3.5 Construction and analysis of a *HYD1* molecular reporter

A promoter-reporter deletion series was constructed for *HYD1*, using the β-glucuronidase enzyme from *E.coli*. The strategy for construction of the promoter-GUS reporter deletion series for *HYD1* is shown in Diagram 2.1. Methods indicated in the scheme are described below. The enzymes and antibiotic selection used at each stage are detailed in the diagram. Primary transformants (T1 plants) were selected by kanamycin segregation and grown on under greenhouse conditions. This T2 generation was assessed for kanamycin segregation and preliminary GUS staining. From these, transformant lines were selected for detailed developmental analysis of expression, and in response to exogenous phytohormone treatments.

2.3.5.1 PCR

Standard PCR

Cloning of the *HYD1* promoter regions from the Ws template (obtained by plasmid rescue) used *Taq* DNA polymerase (Bioline, UK) under standard PCR conditions with the Mg^{++} free 10x reaction buffer and 50mM $MgCl_2$ stock solutions supplied with the enzyme. Oligodeoxynucleotide primers were obtained from MWG-Biotech as lyophilised pellets, and were re-suspended to make 100pM stock solutions, from which 20pM working concentrations were made, using sterile dH_2O.

The standard PCR reaction contained the following components, assembled on ice in a sterile 0.5ml microcentrifuge tube. .

- 10-100ng DNA template
- 2.5µl primer 1 [forward] (2pM final concentration)
- 2.5µl primer 2 [reverse] (2pM final concentration)
- 1.5µl 50mM $MgCl_2$ (1.5mM final concentration)
- 5µl Mg^{++} free 10x reaction buffer
- 1µl 10mM dNTP mix
- 2.5 units of *Taq* DNA polymerase

The volume was then made up to 50µl with sterile dH_2O

Reactions were overlain with a drop of mineral oil and placed in a DNA Thermal Cycler (Perkin Elmer; CA, USA). Amplification was carried out as follows; an initial 2 minutes denaturation at 94°C, followed by 30 cycles comprising 1 minute denaturation at 94°C, 1 minute annealing at 55°C and extension at 72°C for 1 minute per kilobase of expected product. A final extension step of 10 minutes at 72°C was performed after amplification. An aliquot of 10-20µl of the reaction product was checked using agarose gel electrophoresis.

Colony PCR

Bacterial colonies grown from single cells transformed with plasmid DNA, were patched onto a numbered grid on selective plates, and grown overnight at 37°C before checking for the desired insert by colony PCR. The reaction mixture was set up on ice in bulk without *Taq*, in a 1.5ml sterile Eppendorf tube, allowing 20µl for each of N+1 reactions (the extra quantity allowed for pipetting errors).

The following formula was used to calculate the volumes of the various components.

- 10x Mg^{++} free 10x reaction buffer [N + 1] x 2µl
- 10mM dNTP mix [N + 1] x 0.5µl
- Primer 1 [forward] [N + 1] x 0.5µl

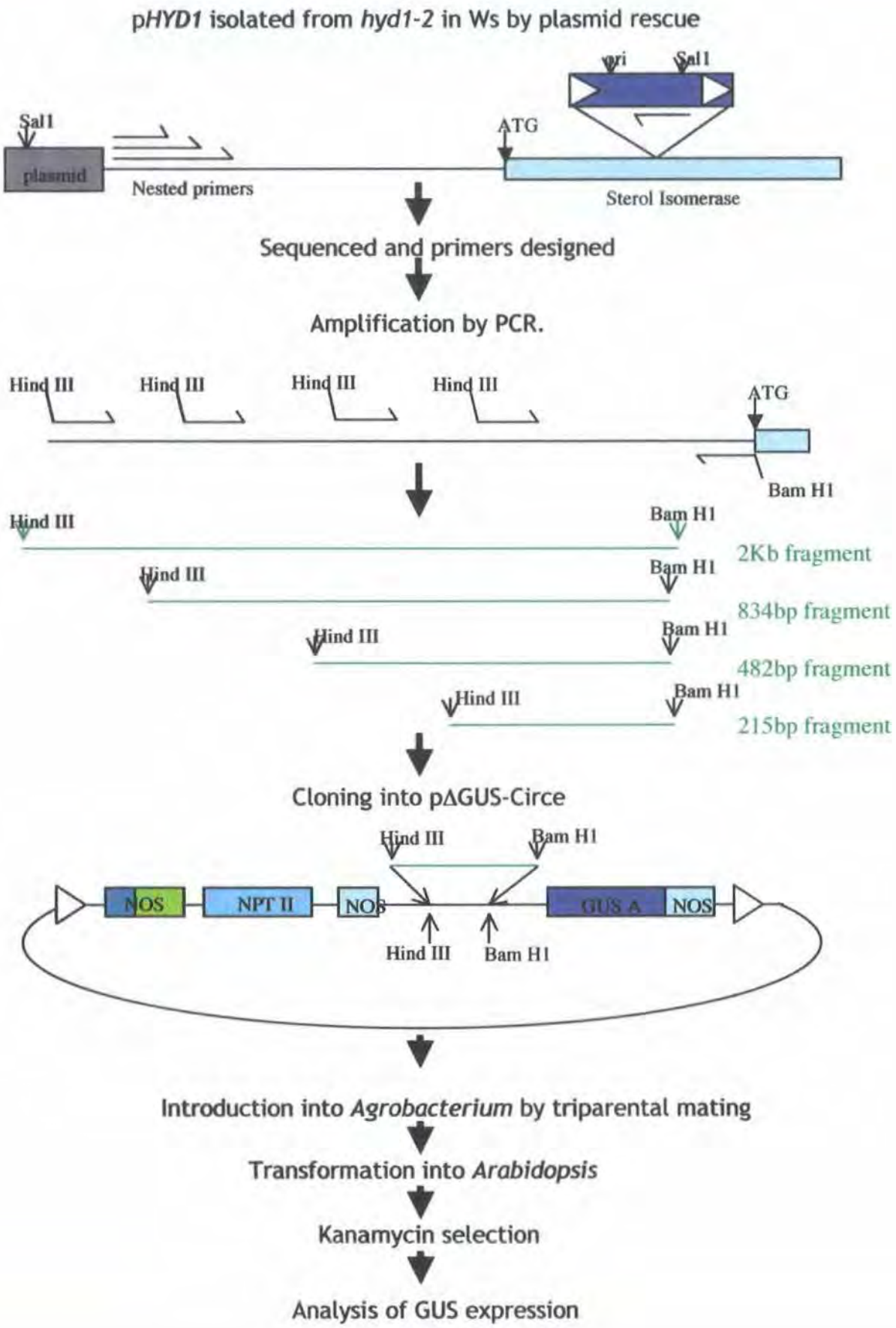

Figure 2.1 Construction of a p*HYD1*::GUS deletion series

- Primer 2 [reverse] [N + 1] x 0.5µl
- 50mM $MgCl_2$ [N + 1] x 0.5µl
- dH_2O to make the total volume up to; [N + 1] x 20µl

The mixture was mixed gently then pipetted into 20µl aliquots in 0.5ml sterile microcentrifuge tubes, 0.1µl *Taq* added, the tube contents overlain with mineral oil, and the PCR thermal cycle reaction carried out under the conditions described above. 10µl of each reaction product was checked using agarose gel electrophoresis.

2.3.5.2 DNA agarose gel electrophoresis

Agarose gel electrophoresis for separation of DNA fragments was carried out as described by Sambrook *et al.* 1989.

Gels were used at from 0.7% to 2% (w/v) agarose in 1x TAE buffer (40mM Tris-acetate pH 8.0, 1mM EDTA), using higher percentages of agarose to resolve smaller fragments and vice-versa. The agarose-buffer mixture was heated in a microwave to melt and dissolve the gel, and allowed to cool to around 50°C before adding 0.1µg/ml of ethidium bromide. The molten agarose was then poured immediately into a prepared gel tray, and allowed to solidify at room temperature before use.

Gels were submerged in the electrophoresis tank in 1x TAE buffer prior to loading. DNA samples were mixed with 1/6 volume of 6x loading dye, before transfer by pipette into the gel lanes. One gel lane of each row would be loaded with DNA markers (Hyperladder I or Hyperladder IV, supplied by Bioline, UK), to enable quantification and approximate sizing of fragments. Electrophoresis was performed at 5-10V/cm. DNA was visualised, photographed and printed using a Gel Doc 1000 UV trans-illuminator system, with Molecular Analyst software, version 2.1.1 (Bio-Rad).

2.3.5.3 DNA manipulation

Digestion with restriction endonucleases

Vectors and inserts were prepared for cloning using restriction endonucleases, obtained from Promega Ltd, and the reactions carried out according to the manufacturer's instructions. Typically, this would involve assembling the following mixture in an Eppendorf tube;

- 1µl of 10X reaction buffer,
- 1µl of the enzyme(s) each at 10units/µl,
- 0.5-3µg of DNA in a variable volume of dH2O,
- sterile dH2O to make up the total volume to 10µl.

In instances where the DNA solution for digestion was very dilute, a larger overall reaction volume would be used in order to accommodate an appropriate amount in the preparation. Reactions were incubated at the required temperature (recommended by the manufacturer) for between 2 and 4 hours, before analysis using agarose gel electrophoresis.

Ligation into pCR®2.1-TOPO

DNA fragments generated by PCR were cloned using the pCR®2.1-TOPO vector (Invitrogen; Paisley, UK). The vector is supplied in linear form, with 3'thymidine overhangs, allowing efficient ligation of PCR products with 5'adenine overhangs, such as are obtained using Taq DNA polymerase. PCR products were used either unpurified, or purified via extraction from a gel. As with T4 DNA ligase, the mixture was set up to give a 3:1 ratio of vector to fragment compatible ends. The following typical reaction mixture was assembled on ice, adding the vector last, and stirred with a sterile pipette tip prior to incubation at room temperature for 30 minutes.

- 0.5-4µl of PCR product
- 1µl of salt solution (supplied by the manufacturer)
- sterile dH2O to make up the total volume to 5µl,
- 1µl of TOPO vector

Following ligation, the tube was placed on ice until ready for transformation into TOP10 competent cells (Invitrogen).

Ligation into vectors with restriction-enzyme multiple cloning sites

Compatible sticky ends from restriction enzyme-digested DNA fragments and vectors were annealed using T4 DNA Ligase, from Promega Ltd. This enzyme catalyses the formation of a covalent phosphodiester bond between a 5'-phosphoryl group and an adjacent 3' hydroxyl group. The reaction was compiled to give a 3:1 ratio of compatible ends favourable to the cloning of the insert, i.e. 3 fragment ends to every one of vector. The following guide indicates the typical mixture that was assembled in an Eppendorf tube, for incubation overnight at 4°C.

- 1µl of 10X ligation buffer (supplied with the enzyme),
- 1µl of T4 DNA ligase enzyme at 3units/µl,
- 50-100ng of vector DNA in dH2O,
- fragment to insert; sufficient to give 3/1 the number of ends
- sterile dH2O to make up the total volume to 10µl.

If the fragment for insertion was very dilute, a lesser amount of vector DNA was used, in order to preserve the ratio of sticky ends. If necessary, the ligation reaction was set up in 20µl.

2.3.5.4 Extraction, purification and sequencing of DNA

Extraction of high copy number plasmid DNA from bacterial culture

High copy number plasmid DNA was extracted from small culture volumes (up to 5ml) using the Sigma GenElute™Plasmid Miniprep kit, which produced DNA in a condition suitable for sequencing, PCR and cloning. All centrifugation in the following procedure was at 13,000rpm using a bench-top microcentrifuge.

5 ml of selective liquid LB media was inoculated with bacteria containing the plasmid DNA, and grown overnight at 37°C with constant shaking. An aliquot of this culture was taken and used for glycerol stock if required.

The rest of the culture was pelleted in several batches in a 1.5ml Eppendorf tube by centrifugation for 2 minutes. The supernatant was removed, and the cells re-suspended in 200µl of Resuspension solution, and mixed thoroughly using a vortex. 200µl of Lysis solution was then added and mixed by inversion before the tube was incubated at room temperature for 5 minutes. Following this, 350µl of Neutralisation solution was added, mixed by inversion, and centrifuged for 10 minutes to pellet the cell debris. The cleared supernatant (containing the plasmid DNA) was then applied to a Mini Spin Column in a collection tube, and centrifuged for 1 minute. After the flow through was discarded, 750µl of wash solution was added to the column and centrifuged for 1 minute more. Discarding this flow through, the column was then centrifuged for 5 minutes to dry the membrane. To elute the plasmid DNA, the column was transferred to a new collection tube, 50µl of sterile water applied to the membrane and the column left to stand for 2 minutes, before a final centrifugation for 2 minutes. The eluted DNA was stored at -20°C.

Extraction of low copy number plasmid DNA from bacterial culture

The pΔ-GUS-CIRCE vector is a low copy number plasmid, and so was extracted from a large culture volume (100-200ml) using the Qiagen Midi Prep kit. The resulting DNA was suitable for sequencing, PCR and all cloning purposes.

A flask of 100mls of selective LB liquid media was inoculated with bacteria carrying the plasmid of interest, and grown overnight with vigorous shaking at a temperature to suit the bacterial host. The culture was then transferred to sterile 50ml Falcon centrifuge tubes, and the cells pelleted by centrifugation at 6,000xg for 15 minutes at 4°C. The supernatant was discarded, and the cells re-suspended in 4ml of Buffer P1, after which 4ml of Lysis Buffer P2 was added, the tube was inverted several times to mix the contents thoroughly, and then left to incubate at room temperature for 5 minutes. A further 4ml of Neutralisation Buffer P3 was added and mixed by inversion, prior to incubation on ice for 15 minutes. The mixture was

centrifuged at 20,000xg for 30 minutes at 4°C to pellet cell debris before the plasmid-containing supernatant was removed to a clean tube, and centrifuged again for a further 15 minutes at 20,000xg, 4°C.

Before the last centrifugation step was being completed, a QIAGEN-tip 100 column was prepared to receive the cleared supernatant, by adding 4ml of buffer QBT to the column and allowing it to drain by gravity flow. The supernatant was removed from the centrifuge tube promptly and applied to the column, where it was also allowed to drain through the membrane under gravity. The QIAGEN-tip 100 was then washed twice, each with 10ml of Buffer QC, before the DNA was eluted into a sterile 15ml Falcon tube with 5ml of Buffer QF. The plasmid DNA was precipitated by mixing with 3.5ml (i.e. 0.7 vol) of room temperature isopropanol, the suspension was transferred to Eppendorf tubes and the DNA pelleted by centrifugation at 15,000xg at 4°C for 30 minutes. The pellets were washed with room temperature 70% (v/v) ethanol, centrifuged for a further 15 minutes at 15,000xg, 4°C, and the supernatant removed. The pellets were air-dried until all visible droplets of liquid had disappeared, re-suspended in 100µl of sterile, distilled water, and stored at -20°C.

Purification of DNA fragments from agarose

Fragments were purified from agarose gels following restriction digestion or PCR, using the Qiagen QIAquick® Gel extraction kit. The resulting DNA was suitable for all cloning purposes. All centrifugation steps were carried out at 14,000rpm using a bench-top microcentrifuge.

The required DNA fragments were separated as bands by electrophoresis using agarose gels in 1x TAE buffer. The bands of interest were excised by cutting out gel slices carefully using a clean sharp scalpel, whilst viewing on a trans-illuminator. Gel slices were then placed into a pre-weighed Eppendorf, and the tube weighed again to calculate the gel quantity (i.e. volume). Three volumes of buffer QG were added, and the tube incubated at 55°C for 10 minutes or until the gel slice had dissolved, vortex mixing to aid solution if necessary.

Buffer QG contained a pH indicator that revealed optimum pH by retaining its yellow colour after the gel slice dissolved. If the solution turned orange or purple, 10µl of 3M sodium acetate was added to restore optimum pH. If the fragment being purified was less than 500bp, or more than 4kb, then a single gel volume of room-temperature isopropanol was added at this stage to aid precipitation.

A QIAquick spin column was inserted into a 2ml collection tube, and the sample applied to the column membrane. After centrifugation for 1 minute, the flow-through was discarded, and 0.5ml of Buffer QG was added to the column before a further centrifugation for 1 minute, to ensure removal of any residual traces of gel. This flow-through was also discarded, and 0.75ml of Buffer PE was added to the column, followed by centrifugation for 1 minute. Finally this flow-through was discarded and the column membrane dried thoroughly by centrifugation for 5 minutes. The QIAquick column was then placed into a clean 1.5ml Eppendorf tube, and 30-50µl of sterile distilled water was added to elute the DNA. After allowing the column to stand for 5 minutes, the DNA-containing solution was collected by centrifugation for 5 minutes, and stored at -20°C.

Sequencing

All DNA sequences were obtained using the DNA Sequencing Laboratory facility at the University of Durham, using an ABI 373 DNA sequencer and dye terminator labelling reactions (Perkin Elmer Applied Biosystems). All samples were sequenced using the M13F and M13R primer sites which are included in the vectors on either side of the relevant multiple cloning site (shown in the diagrams in Appendix 3). These primers are commercially available (MWG-Biotech (Ebersberg, Germany)) and are used at a concentration of 3.2pmoles/µl. Samples were supplied as plasmids prepared as described above, diluted to a concentration of 100ng/µl.

2.3.5.5 Transformation

Transformation of chemically competent *E.coli* with plasmid DNA

The following method of making chemically competent *E.coli* cells for transformation, is as described by Ausubel *et al.* (1994). Buffers TfbI and TfbII were made up as detailed below, and filter-sterilised using 0.2µm pore Acrodisks™ (Gelman, UK) prior to use.

Buffer TfbI
30mM potassium acetate
100mM rubidium chloride
10mM calcium chloride
50mM manganese chloride
15% v/v glycerol
pH adjusted to 5.8 (with dilute acetic acid)

Buffer TfbII
10mM MOPS
75mM calcium chloride
10mM rubidium chloride
15% v/v glycerol
pH adjusted to 6.5 (with NaOH)

To prepare competent cells, a single colony from a fresh LB plate of *E.coli* strain XL1-blue was used to inoculate 100ml of sterile LB broth, and grown overnight at 37°C with vigorous shaking to provide aeration. The culture was transferred to 50ml Falcon centrifuge tubes, and chilled on ice for 15 minutes before centrifugation at 4000xg for 5 minutes at 4°C. The supernatant was discarded, and the cells were resuspended gently in 40ml (i.e. 0.4 of the culture volume) of buffer TfbI before resting on ice for 15 minutes. This suspension was pelleted at 4000xg, at 4°C for 5 minutes, the supernatant discarded and the cells re-suspended in 4ml (i.e. 0.04 of the culture volume) of buffer TfbII. The cell suspension was then rested on ice

for 15 minutes before 250µl aliquots were flash frozen in liquid nitrogen and stored at -80°C until required.

Prior to transformation, an aliquot of cells were defrosted on ice. 5µl of ligation mixture was added to the cell suspension and mixed gently before incubation on ice for 20 minutes. Cells were then heat shocked at 42°C for 30 seconds without shaking, and rested on ice again for 2 minutes. 1ml of LB broth was added to the tube, and left to shake for 1 hour at 37°C. Aliquots of 50, 100 and 250µl of the cells were spread onto LB agar plates containing an antibiotic appropriate for the selection of recombinants, and grown overnight at 37°C.

Transformation of pCR®2.1-TOPO into TOP10 One Shot™ competent cells

TOP-10 competent cells were supplied with the TOPO-TA® cloning kit from Invitrogen. The cells were stored at -80°C, and defrosted on ice when required. A 2µl aliquot of the ligation mixture was added to the cell suspension and mixed gently with a pipette tip, then incubated on ice for 30 minutes. The tube was then heat chocked at 42°C for 30 seconds, to induce uptake of the DNA, and then returned to ice for recovery for a further 2 minutes. 250µ of SOC medium (supplied with the kit) was added, and the tube incubated for 1 hour at 37°C for 1 hour, with gentle shaking. 50-100µl of cells were spread onto selective LB agar plates containing 40µg/ml X-Gal, grown overnight at 37°C, and checked by colony PCR. (IPTG is not required to induce *LacZ* in TOPO transformed cells, as the gene is transcribed by a constitutive promoter.)

Mobilisation of pΔGUS-CIRCE into *Agrobacterium* by triparental mating

Copies of the pΔGUS-CIRCE vector carrying the *HYD1* promoter deletion sequences were mobilised into *Agrobacterium* using triparental mating (Bevan 1984, Hooykaas 1988). Two days prior to triparental mating, 10ml of LB broth containing 100mg/l streptomycin and 25mg/l naladixic acid was

inoculated with *Agrobacterium* C58C3 and left at 30°C with constant shaking.

The day before mating, two 10ml LB overnight cultures containing 100mg/l kanamycin sulphate were inoculated, one with *E.coli* strain HB101 carrying the pRK2013 plasmid, and the other with XL1-blue cells carrying the pΔ-GUS-Circe plasmid with cloned insert. Both cultures were grown at 37°C with constant shaking.

For mating, 100µl aliquots from each of the three cultures were mixed together in a sterile 1.5ml Eppendorf tube, and the cells pelleted by centrifugation at 12,000 rpm for 5 minutes. The supernatant was discarded, and the pellet re-suspended in 10µl of 10mM $MgSO_4$. This droplet was spread onto a non-selective LB agar plate and allowed to incubate overnight at 30°C, this produced a bacterial lawn, mobilisation of the plasmid occurs.

Triple-selective LB agar plates were prepared containing 100mg/l kanamycin sulphate, 100mg/l streptomycin and 25mg/l naladixic acid. A patch of bacteria from the overnight LB-agar plate was streaked onto a selective plate, using a sterilised microbiological loop. Controls of each of the parental strains were also streaked, each onto a separate plate, and all plates were left overnight at 30°C. Only the *Agrobacterium* strain carrying the pΔ-GUS-Circe plasmid should grow under these selection conditions. The isolated *Agrobacterium* strain was re-streaked for single colonies, and the extracted plasmid checked by restriction analysis.

Arabidopsis transformation using the dipping method

This protocol is a modified version of that described by Clough & Bent (1998).

Plastic plant pots 3.5 inches wide were filled to above the brim with a sand-compost mixture, and a nylon mesh was placed over the soil, secured with large rubber bands. Seedlings of *Arabidopsis thaliana* ecotype Col-0

were planted into these pots through the mesh, at around 5dae, averaging 8 plants per pot. Plants were watered from above, and grown for 3-4 weeks under greenhouse conditions until all plants had bolted, and had developed an inflorescence approximately 10-15cm tall, and displaying a number of immature, unopened flower buds. Plants were trimmed of their open flowers and any young siliques prior to dipping.

A culture of *Agrobacterium* strain C58C3 carrying the promoter-reporter cassette in the pCIRCE-based vector was prepared for each construct. Culture flasks, each containing 200ml of sterile LB broth supplemented with 100mg/L kanamycin sulphate, 100mg/L streptomycin and 25mg/L naladixic acid, were innoculated with the appropriate C58C3 culture and grown for 48 hours at 30°C. The cultures were transferred to 50ml Falcon tubes, pelleted by centrifugation for 10 minutes at 3000g, the supernatants discarded, and the cells gently resuspended in 1L of 5% w/v sucrose. After re-suspension, Silwett L-77™ detergent (Lehle seeds, Texas, USA) was added to give a final concentration of 0.05% (v/v).

Holding the pots carefully to assist the mesh in retaining the soil and plant roots, the prepared plants were dipped into the bacterial solution and gently agitated for 10-15 seconds. Dipped plants were placed in transparent bags to maintain humidity, and returned to a shaded position in the greenhouse overnight. The following day, the pots were removed from the bags and returned to normal growing conditions. A second dipping, using a fresh culture of *Agrobacterium*, was made after 7 days. Following removal from the bags for the second time, plants were allowed to set seed and dry out in the greenhouse.

As the pots began to dry, each was placed into a large photographic negative bag, secured around the base with a rubber band to help prevent cross-contamination of seed, and to facilitate easy harvesting. Seeds were harvested over 1-2 weeks from each pot as the siliques matured, transferred to vented Petri dishes, the margins sealed using Micropore™ tape, and allowed to dry for up to 2 weeks at room temperature.

Dried seeds from each dipping were surface sterilised (as described in section 2.2.2), and germinated on $^1/_2MS_{10}$ plates made with bacto-agar supplemented with 35µg/ml kanamycin sulphate and 200µg/ml augmentin. Antibiotic-resistant plants stayed green, developed true leaves and showed root lengthening by around 10dae. These plants were transferred to semi-sterile conditions to recover before being planted out in greenhouse conditions to set seed; harvested seed was tested for segregation on selective plates.

2.3.5.6 Analysis of p*HYD1*::GUS constructs

Seed from plant lines showing segregation with kanamycin selection were germinated on $^1/_2MS_{10}$ plates and incubated in X-Gluc with buffer. Lines showing β-glucuronidase enzyme activity were tested for general expression patterns in seedlings and optimal incubation time in X-Gluc.

Lines were selected for further analysis, and assays made of root development, comparing growth rates against the untransformed Col-0 background, to assess any physiological consequences of T-DNA insertion. Lines showing normal root growth physiology were subjected to a comprehensive developmental analysis of p*HYD1*::GUS expression in both root and shoot tissues, throughout the developmental sequence from embryogenesis to seed maturation and senescence. Young stages were examined under sterile culture conditions as previously described. Later stages of inflorescence development and embryogenesis used seedlings grown on under greenhouse conditions.

The expression of p*HYD1*::GUS in response to exogenous phytohormones was also assessed under sterile conditions, by transferring seedlings from $^1/_2MS_{10}$ plates at 7dae, onto vertical plates supplemented with the phytohormones and inhibitor compounds listed in section 2.3.4. Plates were sealed with Micropore™ tape and returned to the growth cabinet for 7 days, after which all seedlings were harvested and stained for GUS activity.

Chapter 3

Localization and control of *HYDRA1* gene expression

3.1 Abstract

In order to investigate whether *HYD1* gene expression is associated with critical stages during radial axis formation, a molecular reporter was constructed using the β-Glucuronidase enzyme. This chapter describes the expression analysis of p*HYDRA1*::GUS, comparing full-length *HYDRA1* promoter activities from *Arabidopsis thaliana* ecotypes Wassilewskia (Ws) and Columbia (Col-0), and a deletion series of the Ws promoter. These constructs were transformed into wild-type Col-0 plants and examined both for expression throughout development, and in response to exogenous phytohormone and inhibitor treatments.

HYD1 promoter-reporter activity appeared first in the globular embryo, and showed strong expression in the root cap and root epidermis, in the stipules at the base of all true leaves, and in pollen. A weaker and more transient activity was observed in trichomes and stomata of cotyledons, true leaves and stems, and the ground tissues of roots, hypocotyls and photosynthetic lateral organs at around the point of mesophyll cell differentiation. Reporter activity may also be enhanced by light. This transcriptional information was encoded between -834bp and -215bp upstream from the *HYD1* gene. Positional cues affecting transcription were also modulated by a range of phytohormones. Analysis of the promoter for cis-acting elements highlighted a range of putative recognition motifs including those for MYB, MYC and WRKY transcription factor binding and tissue specific signals. The differentiation-associated activity of the promoter reporter, and its radial distribution, are discussed in the context of known patterning processes throughout development.

3.2 Introduction

3.2.1 Known radial patterning processes in *Arabidopsis* involve positive reinforcement with lateral inhibition

3.2.1.1 Lateral inhibition during patterning of the root epidermis resolves a radial symmetry about the longitudinal axis in *Arabidopsis*

The *Arabidopsis* primary root apex is a radially-organised structure in which newly-divided cells derived from the apical meristem have predictable fates, determined both by cues from older tissues higher up the root (Van den Berg *et al.* 1995), and by their position relative to other cells across the radial axis. In the epidermis, trichoblast cell fate is defined by positioning over cortical cell junctions (Berger *et al.* 1998). Other known radially-defined positional cues active within the root include the specification of new phloem and procambium by differentiating xylem strands (Mähönen *et al.* 2000), and initiation of lateral root primordia from pericycle cells in direct contact with underlying protoxylem (Dubrovsky *et al.* 2001).

In the root epidermis, atrichoblast (non-hair) cells differentiate and enter cell maturation ahead of trichoblast (root hair) cells, where cell division persists for slightly longer and generates a larger number of shorter cells within the cell file (Berger *et al.* 1998b, Dolan *et al.* 1993, Dolan & Costa 2001). The distinction between hair cell and non-hair cell fate is prompted by positional information relative to periclinal and anticlinal cell walls in the adjacent cortical layer beneath, and is fixed upon differentiation (Berger *et al.* 1998a).

A cascade of transcriptional regulators is involved in the specification of this pattern, many components of which have been elucidated in *Arabidopsis*.

The WEREWOLF (WER) protein is a member of the MYB family of transcriptional regulators, and is implicated as a positive regulator of non-hair cell identity (Lee & Schiefelbein 1999). WER is thought to act in conjunction with the WD40 repeat protein TTG (Walker *et al.* 1999) and the bHLH transcription factors GL3 and EGL3 to promote non-hair cell fate in a mechanism involving lateral inhibition (Bernhardt *et al.* 2003). Mutations in the *WER* gene result in roots in which all epidermal cells initiate root hairs (Lee & Schiefelbein 1999), and the cell patterning of trichoblast and atrichoblast cell files are indistinguishable morphologically (Dolan & Costa 2001). This indicates that *WER* activity positively specifies atrichoblast identity; a patterning decision made early in the cell file whilst still within the meristem, before root hair cell fate is established (Lee & Schiefelbein 1999).

The WER protein promotes transcription of the homeodomain GLABRA2 (GL2) which specifies non-hair cell fate in the atrichoblast cell file (Massucci *et al.* 1996) and the truncated MYB protein CAPRICE (CPC) which effects a lateral inhibition by moving into the adjacent trichoblast cell file, where it represses transcription of the *WER*, *GL2* and *CPC* genes (Lee & Schiefelbein 2002, Schellmann *et al.* 2002, Wada *et al.* 2002).WER directly regulates *CPC* transcription, and has been implicated in the formation of both atrichoblast and trichoblast cell types, thereby acting as a 'master regulator' (Ryu *et al.* 2005). WER-mediated transcription is thought to involve a protein complex TTG and GL3/EGL3, as these proteins are necessary for this system to function (Bernhardt *et al.* 2003).

3.2.1.2 A lateral inhibition mechanism in the *Arabidopsis* shoot epidermis involves genes in common with root epidermal patterning

Another MYB protein, GLABRA1 (GL1) is active in the shoot epidermis, apparently in a manner similar to the role of WER in the root. *GL1* is expressed only in epidermal cells of the shoot, and is necessary for the production of trichomes on leaves; the protein acts at the same point genetically as TTG, and regulates *GL2* (Oppenheimer *et al.* 1991, Larkin *et al.* 1996). Lee & Schiefelbein (2001) have shown that the transcriptional units of *GL1* and *WER* are interchangeable, and that specificity is conferred by their upstream and downstream regulatory sequences; each gene under the transcriptional control of the other's promoter was able to rescue the other's mutant phenotype. The GL1 complex (along with TTG and GL3, as in the root), targets the *TRYPTICHON* (*TRY*) gene as a lateral inhibitor; this gene encodes another truncated MYB protein, very similar in sequence to *CPC* (Schellmann *et al.* 2002).

Stomata then form in a manner subordinate to the trichome pattern. Cells in the epidermis adopt meristemoid mother cell (MMC) fate, and then undergo an asymmetric division requiring the *TOO MANY MOUTHS* (*TMM*) gene, which divides to form a meristemoid (M) and companion cell (Geisler *et al.* 2000). Stomata also form from satellite meristemoids; cells which were already part of a stomatal lineage, that later adopt meristemoid identity (Geisler *et al.* 2000, Larkin *et al.* 1997). Adjacent cells can adopt M fate, but one or both of these cells divides prior to differentiation as a guard mother cell (GMC), maintaining the spacing minimum between adjacent stomates. Cell fate identity involves overlapping expression of two genes; *TMM* in meristemoids, neighbouring cells with competence to divide, GMCs and guard cells, and *STOMATAL DENSITY AND DISTRIBUTION1* (*SDD1*) in meristemoids and GMCs (Nadeau & Sack 2002, von Groll *et al.* 2002). Differentiation then takes place

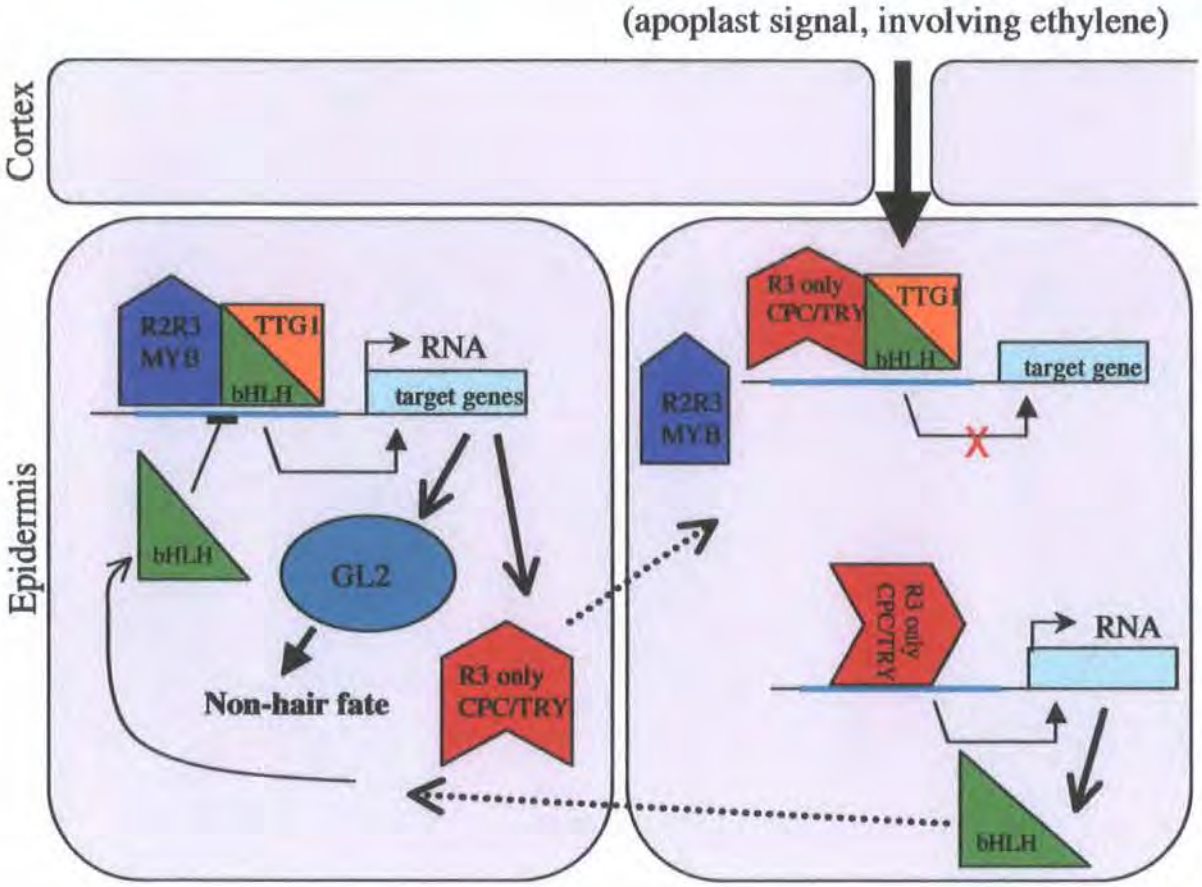

(a) non-hair cell

R2R3 MYBs: WER (root), GL1 (hypocoytl)

bHLH (MYC): GL3, EGL3

R3 only MYB: CPC, TRY, ETC1, ETC2

(b) stoma/trichoblast cell

R2R3 MYBs: WER (root), GL1, MYB23 (hypocotyl and leaf) FLP, MYB88 (leaf)

bHLH (MYC): GL3, EGL3 FAMA (leaf)

R3 only MYB: CPC, TRY, ETC1, ETC2

Diagram 3.1 MYB and MYC (bHLH) transcription factors are active in pattern definition in the *Arabidopsis* root and shoot.

This scheme illustrates early differentiation in adjacent epidermal cells in the root and hypocotyl, where MYB and MYB-like (MYC) protein cascades interact with TTG1 to transcriptionally activate target genes including GL2, and so distinguishing cells of the trichome-atrichoblast cassette from adjacent cells in the epidermal layer. This is thought to operate by a positive reinforcement - lateral inhibition mechanism. Cell fate is suppressed in adjacent cells via an R3-only truncated MYB protein, which silences the transcription of trichome/atrichoblast target genes and promotes production of other R3-only truncated MYBs. These move into adjacent cells and have a negative regulatory function, by interacting with the full length R2-R3 MYB proteins and TTG1. Genes involved in stomatal pattern definition in the leaf epidermis respond to a currently unknown relay signal across a wider field of cells than found in the hypocotyl and root (i.e. pattern is defined in non-adjacent cells).

by transition of the meristemoid to guard mother cell (GMC) fate, when activity of the *SDD1* gene ceases to be feedback regulated, producing a positive enforcement of cell fate identity (von Groll *et al.* 2002).The termination of cell division may then be controlled by the *FLP* gene (Yang & Sack 1995), which suppresses subsequent M fate, and encodes a MYB transcription factor (Lai *et al.* 2005).

3.2.1.3 Stochastic thresholds act as a mechanism defining cell fate identity during lateral inhibition

Stochastic thresholds are implicated in lateral inhibition patterning processes in the post-germination cotyledon epidermis, where meristemoids establish with an initially random distribution (Tsukaya *et al.* 1994, Geisler & Sack 2002). This spacing mechanism for stomata is affected by the trichome patterning genes (Bean *et al.* 2002), even though wild-type cotyledons lack trichomes. Further evidence for a stochastic trichome placement comes from analysis of the *TRY* gene, encoding a transcription factor that works in a non-cell autonomous manner to inhibit the adoption of trichome cell fate in adjacent pavement cells (Schellmann *et al.* 2002).

The *try* mutant epidermis has multiple trichome clusters developing from the surrounding pavement cells which form trichome basal cells in wild-type; these cells initiate hairs in the mutants producing a tightly clumped distribution. This implies that a local region of several cells is targeted in the epidermis by lateral inhibition signals. One cell within this clump will reach a stochastic threshold, triggering a positive feedback loop that promotes trichome cell fate in the committed cell, whilst suppressing this cell fate in its neighbours. The whole morphology of the trichome socket involves both basal cells in the epidermal layer and supportive cells recruited from the mesophyll beneath (Bowman 1994), suggesting a three-dimensional signal. Aloni *et al.*

(2003) noted an auxin response in developing trichome cells, highlighted by the DR5 synthetic auxin response element.

Stochastic thresholds within individual cells can be seen in the early stages of anthocyanin accumulation in mustard cotyledons; some cells respond faster to light-stimulated induction of (light quenching) flavonoid anthocyanin (Nick*et al.* 1993). Anthocyanin production is promoted by the same molecular control mechanism as shoot trichomes, namely the maize R gene homologues GL3 and EGL3, which are functionally redundant bHLH MYB transcription factors (Bernhardt *et al.* 2003).

3.2.2 Domains of differentiation are active during patterning of the plant body

Intercellular interactions rely upon the provision of routes which allow small molecules to move between adjacent cells. In plants, pores known as plasmodesmata form during cell division in the division plate which connects two daughter cells, allowing ions, small soluble molecules and even proteins and RNA to move between the two cytoplasms, connecting these cells both electrically and metabolically (Zambryski 2004, Zambryski & Crawford 2000, Lucas *et al.* 1995). The levels of connection between adjacent cytoplasms is related to the developmental stage of the cells. Studies in algae from the genus *Chara* have shown that cells which are 'differentiation synchronized' have strong cytoplasmic connections, whilst later developmental stages were less connected by degrees (Kwaitowska & Masewski 1986, Kwaitowska 1988). Sequential symplastic isolation in plant cells corresponds with the developmental control of cell fate and function, and a dynamic control of connections between fully differentiated cells allows the function of groups of cells (e.g. phloem) to fulfil specific functions in the plant body (Oparka *et al.* 1999, Pickard & Beachy 1999)

In *Arabidopsis*, differential symplastic isolation is apparent during development. Early embryogenesis through to the globular stage has a high degree of connectedness, and a common cytoplasm (McLean *et al.* 1997). Later stages have functional down-regulation of the aperture size in these connections (Kim *et al.* 2002). In the torpedo-stage embryo, these symplastic domains are resolved into four regions; a shoot meristematic zone spanning the hypocotyl-cotyledon transition region and with a freely communicating subdomain in the CZ, a zone defining each cotyledon, a zone defining the hypocotyl from the upper transition zone with the SAM to the root-hypocotyl junction, and a root zone in which the QC and root cap columella cells are strongly connected (Kim *et al.* 2005) All of these boundaries are associated with a reduced plasmodesmatal aperture, implying a specific control of symplastic movement between regions (Kim *et al.* 2005).

A serial analysis of gene expression using microarray techniques in different cells of the *Arabidopsis* root, has identified both longitudinal and radial domains according to developmental stages (Birnbaum *et al.* 2003). Cells were found to be differentiated in gene activities across the radial layers, defining domains in lateral root cap, epidermis, cortex, endodermis/pericycle, and vascular stele. Longitudinal zonation was also defined according to cell age, comprising cells of all layers across the root at the QC and initials, the zone of cell division, and the differentiation to elongation region (Birnbaum *et al.* 2003).

An examination of the *Arabidopsis* root epidermis using dye-coupling showed a strong symplastic connection within young cells of longitudinal cell files (Duckett *et al.* 1994). The youngest cells nearest to the meristem readily allowed passage of a fluorescent dye between adjacent longitudinal cell files. Progressively older cells limited the symplastic coupling to within the longitudinal cell files, and within the differentiation zone, both hair cells and non-hair cells became symplastically uncoupled from their neighbours (Duckett

et al. 1994). A different situation was found in the hypocotyl epidermis. Here, mature cells retained a strong symplastic connection with one another; injection of fluorescent dye into single hypocotyl cells resulted in uniform dye throughout the epidermal layer, although no dye moved into the root epidermis (Duckett *et al.* 2004). These results indicate a correlation between symplastic isolation and differentiation in the *Arabidopsis* root epidermis, an isolation of the epidermis between the root and shoot, and an isolation of the shoot epidermis from underlying layers, despite the presence of plasmodesmata between these cells, suggesting that the gating abilities of these pores are differentially regulated.

Other examples are known of symplastic uncoupling correlating tightly with differentiation relative to neighbouring cells. The phloem sieve-element/companion cell complexes allow movement between cells in these cell files, whilst maintaining an isolation from the surrounding tissues (Kempers *et al.* 1993). In the shoot, guard cells and surrounding epidermal cells are symplastically coupled during development, until the guard cells become isolated at maturity (Palevitz & Hepler 1985). Although guard cell walls lose their plasmodesmata as they mature, isolation appears to develop well before these pores disappear anatomically.

3.2.3 Phytohormones as additional factors in radial patterning mechanisms

3.2.3.1 Auxin is a common factor determining both apical-basal and radial polarity in the embryo

Cell position is critical in determining cell fate and body patterning, both during embryogenesis and post-embryonic growth. This means that any

individual differentiating cell must be in receipt of intercellular positional information, involving extracellular local signals. One of the best characterized plant signalling molecules is auxin; a phytohormone defining pattern and position by variation in concentration throughout the plant body, and which interacts with a multiplicity of cell intrinsic and extrinsic factors.

Auxin can be considered to be a morphogen rather than a phytohormone, as it is distributed in spatial gradients within plant organs (Jones, 1998). There is a natural maximum of auxin localization in the root apical meristem (Sabatini *et al.* 1999) resulting from a directional transport of auxin down the root via the stele into the root tip, and returning in peripheral cell layers. Auxin transport produces radial concentration gradients of this morphogen within plant tissues (Uggla *et al.* 1996). The cellular physiological response to auxin is mediated by many genes with very short half-lives, and their degradation rates are independent of exogenous auxin application (Abel *et al.* 1994, Worley *et al.* 2000).

The PIN family of proteins in *Arabidopsis* are involved in active directional transport of auxin out of cells via the auxin efflux machinery. Efflux complexes are directed to specific cell membranes during plant development, resulting in auxin fluxes which trigger complex signalling cascades (Friml 2003, Friml *et al.* 2003). *Arabidopsis* embryogenesis involves the establishment of an auxin flux between cells after the first zygotic division, promoting the establishment of an auxin circulation in the developing plant body. The initial sequence is described below.

a): flux in. The first auxin flux is generated by polar localization of PIN7 in the apical plasma membrane of the basal daughter cell, directing auxin into the apical cell (Friml *et al.* 2003). PIN1 protein is then expressed in the apical cell, and is distributed evenly over the cell surfaces as the embryo goes through its series of early divisions, allowing a free movement of auxin within the embryo proper.

b): flux out. The PIN7 protein directs auxin from the suspensor into the embryo proper. As the third layer of cells resolves from the inner cell layer, giving a 32-cell globular embryo with a three-layered spherical structure, PIN1 begins to accumulate at the 'basal' end of the embryo where it meets the suspensor, simultaneously with a reversal of the asymmetric localization of PIN7 in the suspensor cells, causing an auxin flux out of the embryo proper and into the suspensor (Steinemann *et al.* 1999, Friml *et al.* 2003). This event may have a biophysical basis; the increased surface area: volume ratio of these very small inner cells; this could result in a small relative increase in their cytoplasmic auxin level relative to their neighbours, sufficient to reach a stochastic threshold and direct PIN1 protein localization to the lower membrane, i.e. in the direction of least auxin concentration. This elongated lower central cells are histologically distinct, and define the earliest cell files of the provasculature. PIN4 protein then begins to accumulate in the adjacent suspensor cell, supporting the action of PIN1 and PIN7 by directing auxin into the suspensor (as indicated by expression of the auxin-responsive DR5 reporter) (Friml *et al.* 2000, 2002). This directs an overall downward transport of auxin, i.e. from the opposite pole of the embryo towards the suspensor.

c): flux in. A gradient of auxin develops in the globular embryo with a maximum at the basal end, and auxin-responsive reporters imply that cells at the apex (at the low point in the gradient) begin to synthesize auxin at this point. In this situation, multiple cells of the lower embryo proper are all directing their auxin content into a single upper suspensor cell. PIN7-mediated auxin transport in the suspensor proceeds at a lower rate than that of PIN1 and PIN4, resulting in a rapid build-up of auxin in the uppermost suspensor cell and specifying its fate as the hypophysis (root meristem precursor). This auxin maximum precipitates another reversal of membrane localization of the PIN proteins, hence another reversal of auxin flux back into the embryo from the suspensor. This

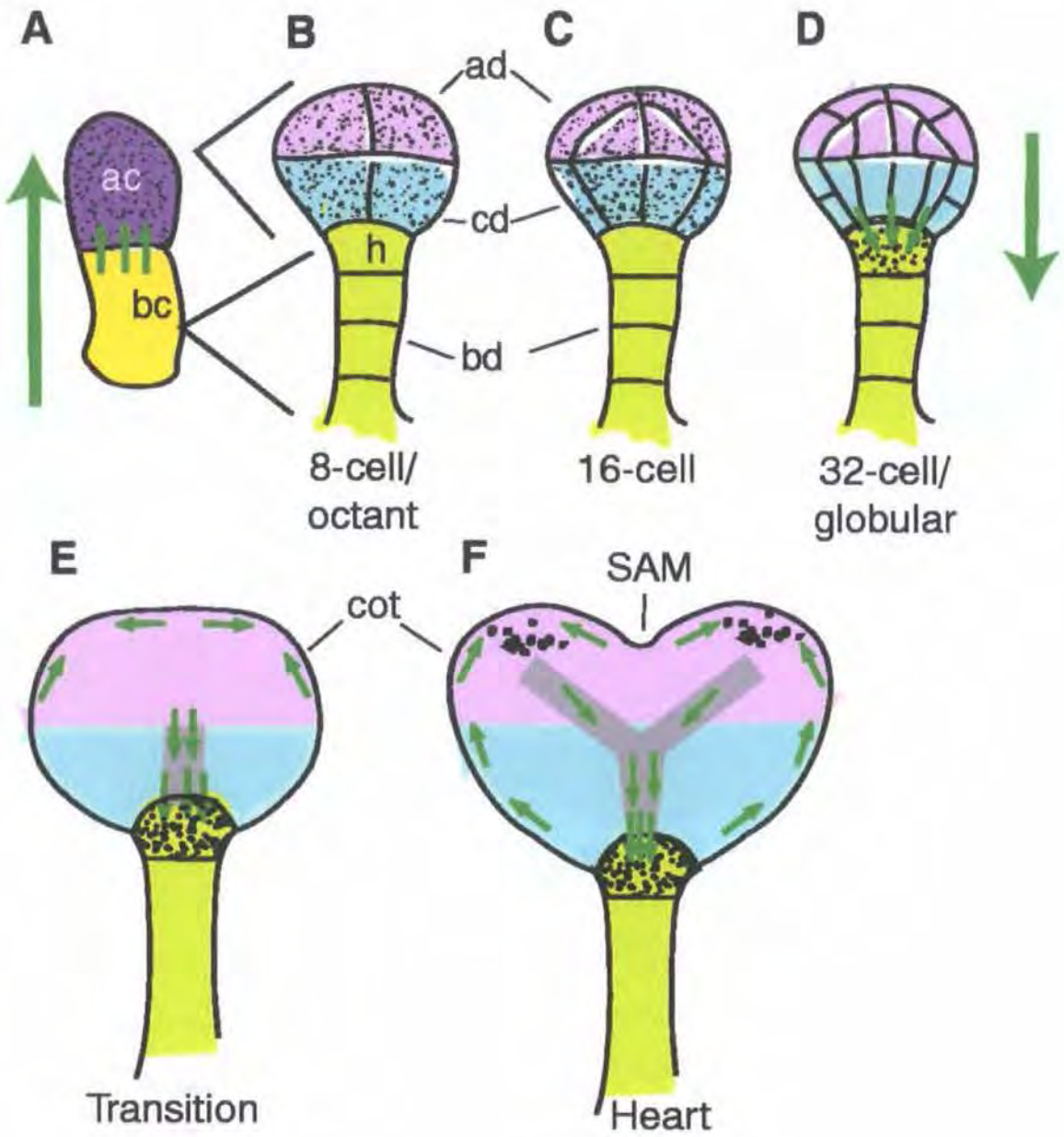

Diagram 3.2 Auxin transport relative to early events in *Arabidopsis* embryo patterning.

(A) early embryo, (B)-(F); subsequent stages, as annotated . Legend; (ac), apical cell; (bc), basal cell; (cot) cotyledon primordia; (ad) apical domain, (cd) central domain, (bd), basal domain. Green arrows indicate the direction of auxin transport,stippling indicates regions with high auxin levels, and grey areas indicate regions of vascular development. Figure from Jenik & Barton (2005); *Development* 132: 3577-3585. For further explanation see text.

means that the cell mass receives an auxin input from both the apical and the basal poles. PIN1 protein appears in a polar fashion in the protodermal layer of the upper half of the embryo, directing auxin in this layer towards the meristem flanks from both the basal region and the central apex.

4: flux central-peripheral. The embryo is now in morphological transition to the heart stage. PIN1 protein shows auxin transport directed towards the developing cotyledon primordia in the proto-epidermal layer (Steinemann *et al.* 1999, Reinhardt *et al.* 2003). The central cell files receive an input of auxin both from the apex and the hypophysis; this excess is transported laterally, first by PIN4 and then by PIN4 and PIN3, maintaining a high auxin level in the peripheral tissues around the basal pole of the embryo (Friml *et al.* 2000, 2002). A similar centripetal transport of auxin, mediated by both of these PIN proteins, is found in the post-germination root apex (Friml *et al.* 2000, 2002).

5: flux to the apex in peripheral tissues. The proliferation of cells in the inner layers of the embryonic cotyledon primordia have an even distribution of PIN1, whilst cells of the protoderm layer around the base of the primordia show PIN1 at the apical walls, directing auxin towards the cotyledon apex (Reinhardt *et al.* 2004). This results in a build up of auxin in the apical and central regions of the primordia, which promotes procambial extension into the developing organs, allowing PIN1-mediated basipetal transport out. The embryo bilateral axis is now established, and is characterized by a circulation of auxin down to the root pole in the central cell files and back towards the apex in peripheral tissues.

This circulation is maintained through embryo elongation, and is also seen during post-germination growth. Auxin is directed into the vascular system by PIN-mediated transport from the lateral organ primordia, and is transported towards the root apex. From there, it is sent radially to the periphery (Friml

2003), where the influx-implicated AUX1 protein appears to concentrate auxin into the epidermal (L1) cell layer (Bennett *et al.* 1996, Reinhardt *et al.* 2003). AUX1 has a putatively similar role in the shoot epidermis, concentrating auxin into the L1 layer, where PIN1-mediated transport directs it from the shoot meristem towards the periphery, and via the abaxial epidermis into the developing leaf primordia (Reinhardt *et al.* 2003). The developing vascular traces modulate auxin locally at the shoot apex via their active basipetal transport, resulting in transient 'hotspots' of auxin concentration at the meristem periphery which promote primordial initiation. It is conceivable that a similar mechanism of local transient auxin peaks may also promote the formation of lateral root primordia.

The location of PIN proteins is dependent upon GNOM, an auxin responsive protein which comprises part of a mechanism allowing rapid vesicle-mediated trafficking of the efflux complexes from one polar membrane to another (Steinemann *et al.* 1999). The PIN-mediated auxin fluxes that establish the provascular position at the base of the globular embryo appear as a sequence responding to an initial stimulus, such as a differential concentration of auxin in adjacent cells, resulting in directional transport from a higher auxin concentration to a lower one. A stochastic (i.e. initially random) threshold difference in auxin concentration between adjacent cells seems to trigger the reversal in PIN polarity, allowing an initial flux between cells that begins the sequence of events by which the 'circulation' of auxin within the embryo is established. As the *gnom* mutant is compromised in the vesicle-mediated trafficking of asymmetrically distributed proteins such as PIN1 (Steinemann *et al.* 1999), such a mechanism could explain the establishment of a random longitudinal polarity in the *gnom* embryo.

3.2.3.2 Phytohormones other than auxin

Ethylene biosynthesis in plants involves production of ACC by a family of ACC synthase enzymes, which define the rate-limiting step in this pathway

Tsuchisaka & Theologis (2004). ACC Oxidases are in all tissues, and rapidly convert ACC to ethylene, which then moves by diffusion through the plant body using symplastic routes (Bleecker & Kende 2000). Differential transcription of *ACS* genes are involved in ethylene biosynthesis in different tissues in response to a range of environmental stimuli (Chae & Kieber 2005). Silver ions are know to inhibit ethylene responses when applied to plant tissues (Beyer, 1976, 1979); they bind to the ethylene receptor ETR1, in competition with the Cu^{++} co-factor involved in normal ethylene signal transduction (Rodriguez *et al.* 1999). Therefore the physiological response to ethylene can be assessed by applying these compounds exogenously to developing seedlings.

3.2.4 Rationale

It was hypothesized that since the *HYDRA* genes play a critical developmental role in establishment and maintenance of cellular coordination within the radial axis, then gene expression would be predicted to occur at stages and in tissues noted for involvement in radial patterning. Promoter sequences fused to a β-Glucuronidase molecular reporter are a useful means of tracking gene expression in whole plants, as the enzyme comprises no known components which interfere with the regulation of normal gene function.

Souter *et al.* (2002) established that both *hyd1* and *hyd2* mutants are hypersensitive to auxin, are defective in ethylene- and auxin-mediated reporter gene expression, and show a partial rescue of the root phenotype with addition of Ag^{++} ions to the growth medium. He *et al.* (2003) showed that expression of *HYD2/FK* mRNA was increased in 4 dae seedlings by growth in the presence of auxin, brassinolide, gibberellin, ACC and cytokinin. It was hypothesized that p*HYD1*::GUS transcription may also respond to these phytohormones as exogenous additions to the growth media.

3.3 Results

3.3.1 Construction of a promoter-reporter series for *HYDRA1*.

The *HYD1* promoter sequence was previously isolated from the *hyd1-2* allele in its Ws background. The sequence was amplified using a primer specific to the T-DNA responsible for mutagenesis, along with degenerate primers, and recovering the promoter as a PCR product via plasmid rescue. The sequence of this recovered fragment was compared to that of the Col-0 ecotype, using the NCBI online *Arabidopsis* database resource (via the BLAST search program, after Altschul *et al.* 1997), and this comparison is presented in Fig. 3.1. The two promoters have regions of strong homology, but the Ws sequence contains an additional region of DNA (1036bp long) which is found elsewhere in the Col-0 genome, on chromosome 3.

In order to assess the effects on expression of this 'extra' segment of DNA, both full-length promoters from Ws and Col were used to produce reporter constructs. In addition, regions of -834bp, -482bp and -215bp lengths upstream of the transcriptional start were amplified and cloned using primers tagged with restriction enzyme sequences. These primer sites are highlighted in Fig. 3.1, and the full primer sequences are given in Appendix 2. The shorter promoter segments were amplified from Ws, as these sections demonstrate minimal sequence differences between the two ecotypes.

For each construct, twelve independent primary transformants were obtained using kanamycin selection, allowed to recover under semi-sterile culture, and grown on under greenhouse conditions. Their progeny were analyzed for kanamycin segregation, and the lines tested both for β-Glucuronidase

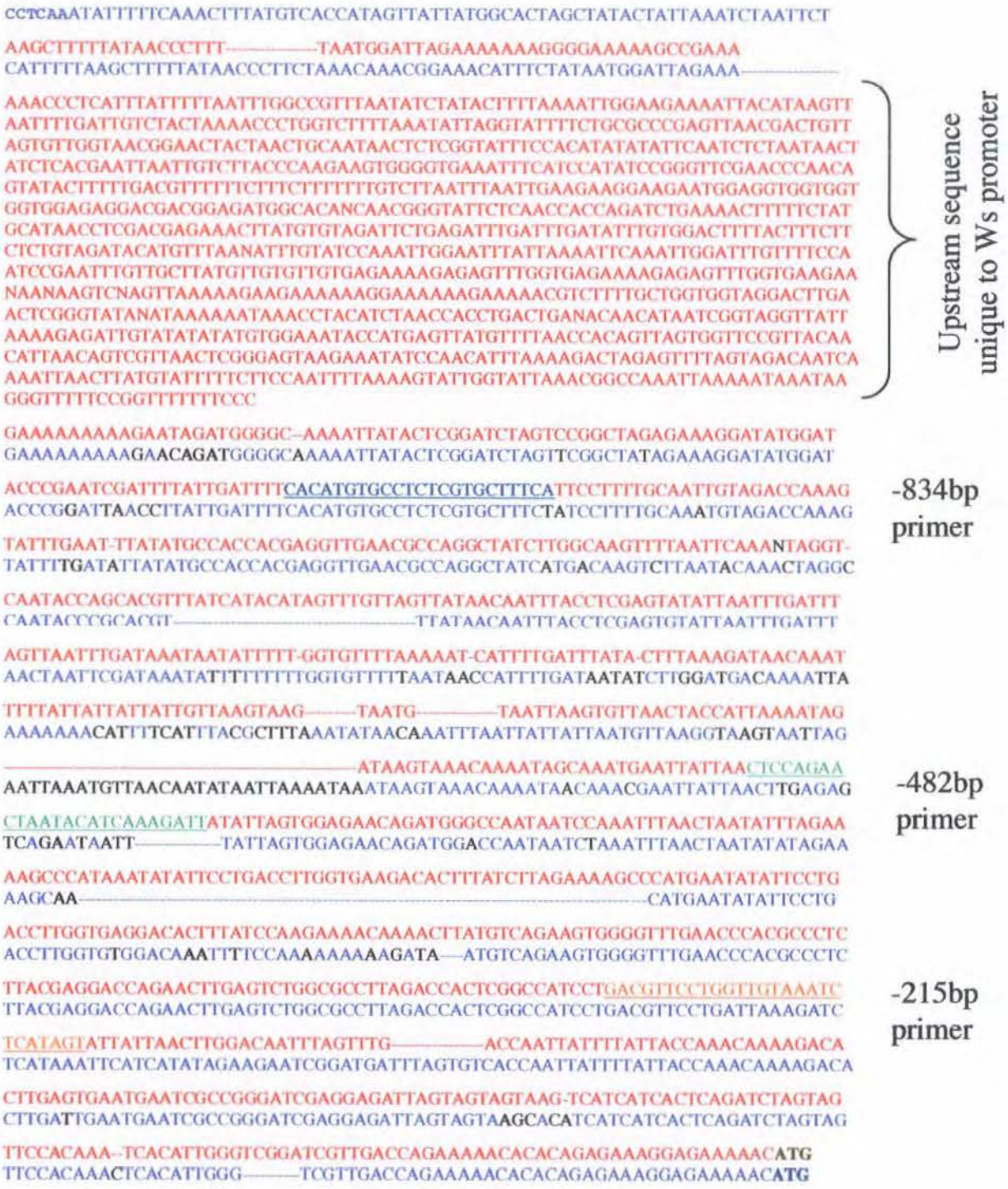

Figure 3.1 *HYD1* promoter sequences from Ws and Col ecotypes

Ws sequence in red, Col-0 in blue. Base-pair mismatches between sequences are shown in the Col-0 promoter in black type. Primer sites used to amplify promoter fragments are underlined, and indicated by margin annotations.

expression at several developmental stages, and for normal root growth and shoot morphology (data not shown). No plants carrying the -215bp constructs showed GUS expression. Single representative lines were selected for each of the remaining four constructs, and subjected to a more comprehensive developmental examination of expression. Of these, the full-length 2kb promoter from Ws was chosen to represent *HYDRA1* gene expression in the following analysis. A comparison of the expression of this reporter construct with the shorter length promoters is presented in section 3.3.3.4.

3.3.2 p*HYD1*::GUS has distinctive temporally-modulated expression patterns throughout the plant body

3.3.2.1 Expression is seen from the early globular to torpedo stages of embryogenesis, and in the root tips of emergent seedlings.

Activity of p*HYD1*::GUS appears first as a transient diffuse signal during the early globular stage of embryogenesis, persisting through the heart stage, and fades as the embryo elongates through the torpedo stage (Fig. 3.2). Transcription appears throughout the embryo proper, and may include the hypophysis, though otherwise is absent from suspensor cells (Fig 3.2; A, B). GUS activity is at its most intense in heart stage embryos. The onset of expression in early globular embryos corresponds to the first point at which irregularities arise in cell size and shape during *hydra* embryogenesis (Topping *et al.* 1997), when asymmetric cell division events become disrupted in these

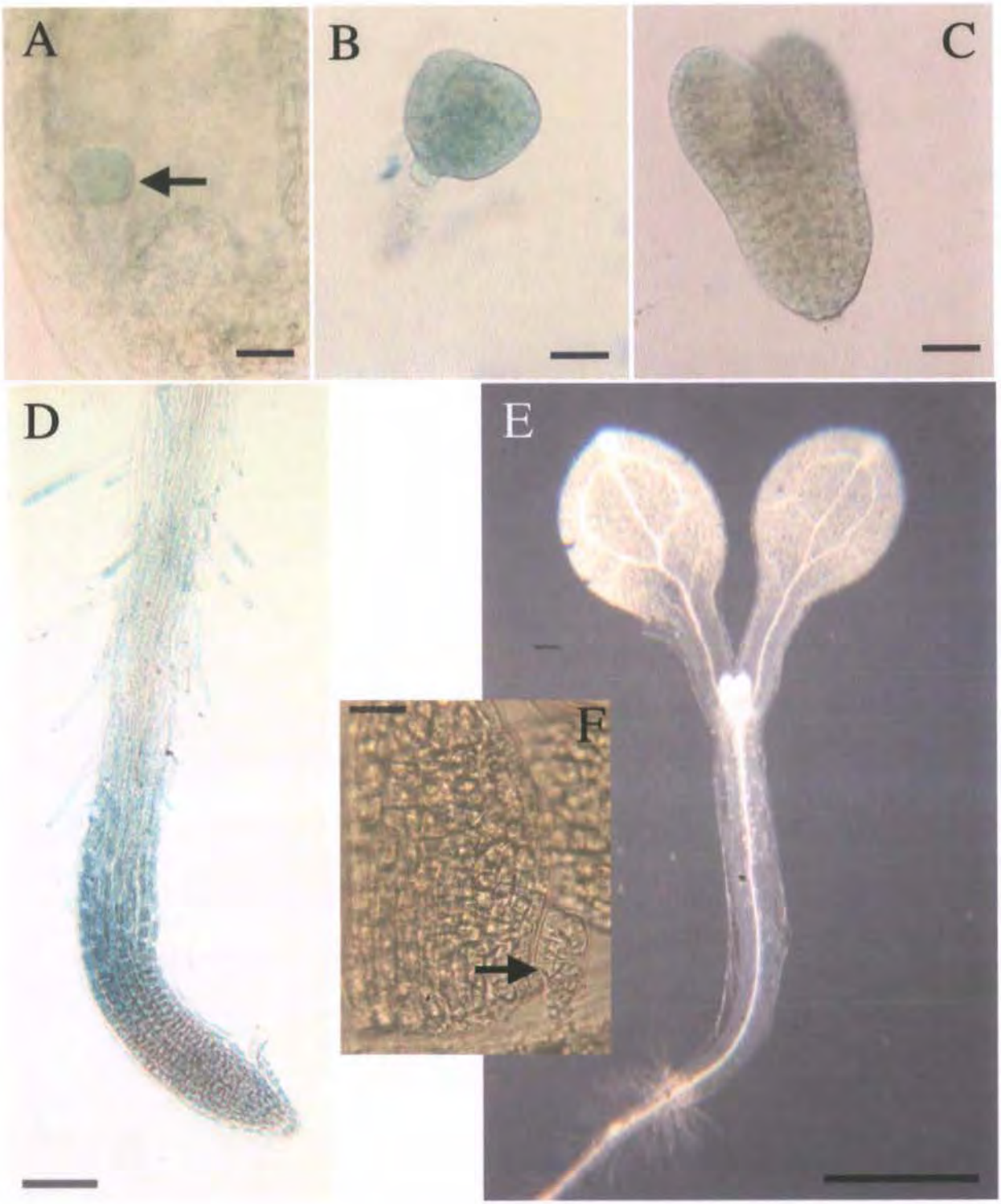

Figure; 3.2 Expression of p*HYD1*::GUS in embryos and germinating seedlings

A; globular, B; heart and C; torpedo stage embryos expressing the p*HYD1*::GUS construct. The signal diminishes in later stages of embryogenesis. In post-germination growth, GUS activity is first discernible in the emergent seedling root (D) as the cotyledons open. No shoot signal is visible at this 3dae stage, either in the cotyledons (E) or the stipules of unexpanded true leaves (F; arrow).

A-D; bar = 100μm, E; bar = 1mm, F; bar = 50μm

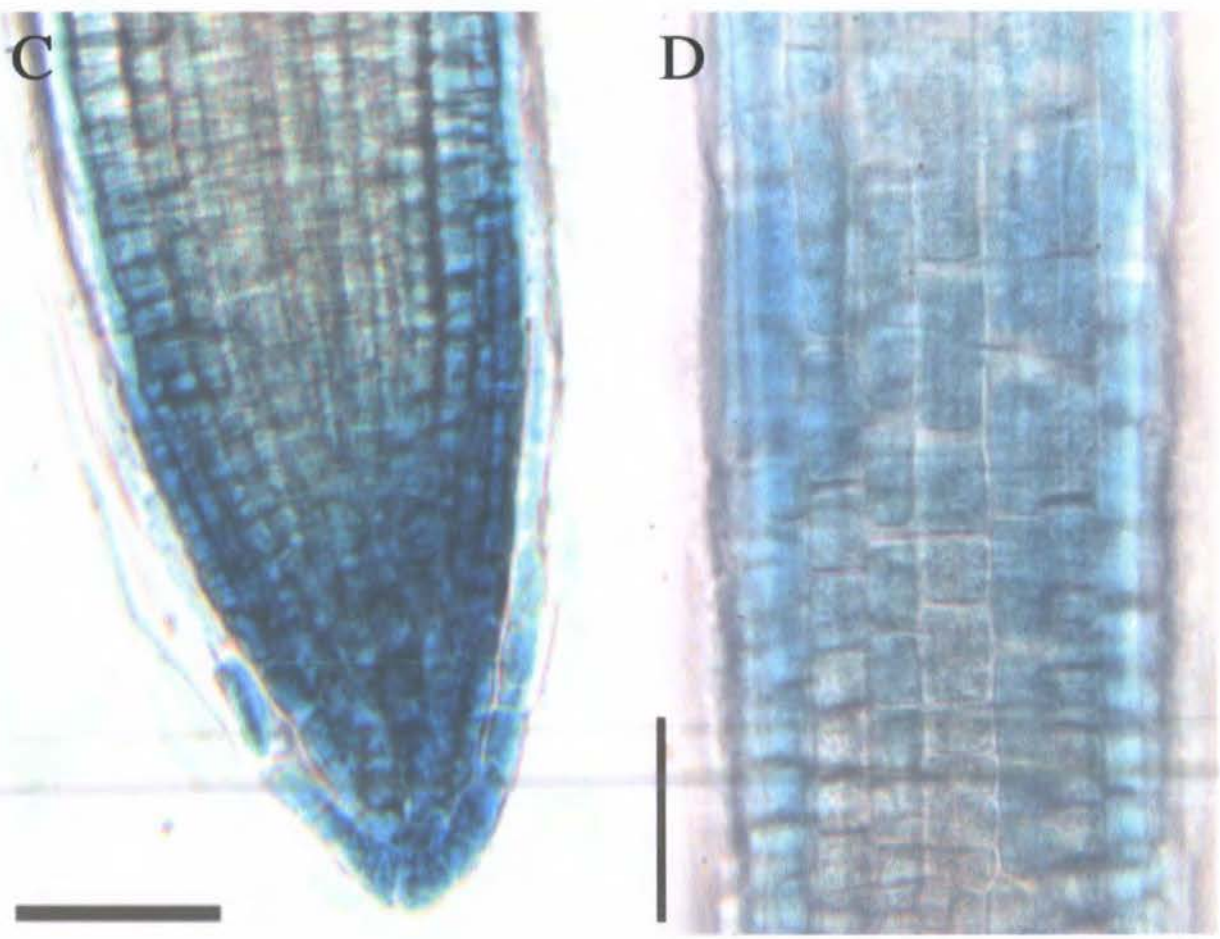

Figure 3.3 Expression of p*HYD1*::GUS in the primary root apex

A; seedling primary root apical region at 7dae, bar = 100μm.
B-D; detail of root cap (C), cell differentiation zone (D) and the lower region of the root hair maturation zone (B). Bar = 50μm.

GUS activity is strong in the root cap, and appears in the epidermal layer with a maximum in the differentiation zone. The signal then diminishes rapidly during root hair elongation, though persists longer in the trichoblasts (B) giving a 'striped' effect.

mutants (Schrick *et al.* 2000). No discernible histochemical signal was found in later stages of embryogenesis and during seed maturation.

In early post-germination growth, *HYD1* promoter activity appears first in the root apices of emergent seedlings, shown in Fig. 3.2; D. The GUS signal appears in the root cap and epidermis; strong expression is seen in the zone of cell differentiation, persisting in root hair cells undergoing tip elongation. No shoot expression is evident at emergence and cotyledon opening (Fig. 3.2; E, F), when growth is mostly via cell elongation alone (Tsukaya *et al.* 1994), though structures showing later expression such as stipules are present (Fig. 3.2; E). Guard mother cells are discernible in the cotyledon epidermis at this stage (Geisler & Sack 2002), but few are differentiated, as these organs are not yet photosynthetically active.

3.3.2.2 The p*HYD1*::GUS reporter shows strong activity in the root cap, and is expressed in a radial gradient across cell layers of the root axis during differentiation.

In primary root apices, strong p*HYD1*::GUS expression is present in both columella and lateral root cap cells (Fig. 3.3; A, detailed in C). An area of minimal histochemical staining then defines a longitudinal section of the root spanning the meristem and cell division zones, where only the epidermal cell layer carries a signal. Strong GUS activity returns in the epidermis of the cell differentiation zone, appearing first in the atrichoblasts (Fig. 3.3; D), then diminishing as the cells mature and expand, fading in the mature root prior to lateral root initiation. Trichoblast cells retain the GUS signal for longest, giving a striped effect (Fig. 3.3; B).

A similar pattern is evident in lateral root apices (Fig. 3.4; A-E). Gus activity appears after the establishment of a meristem, when the root cap and

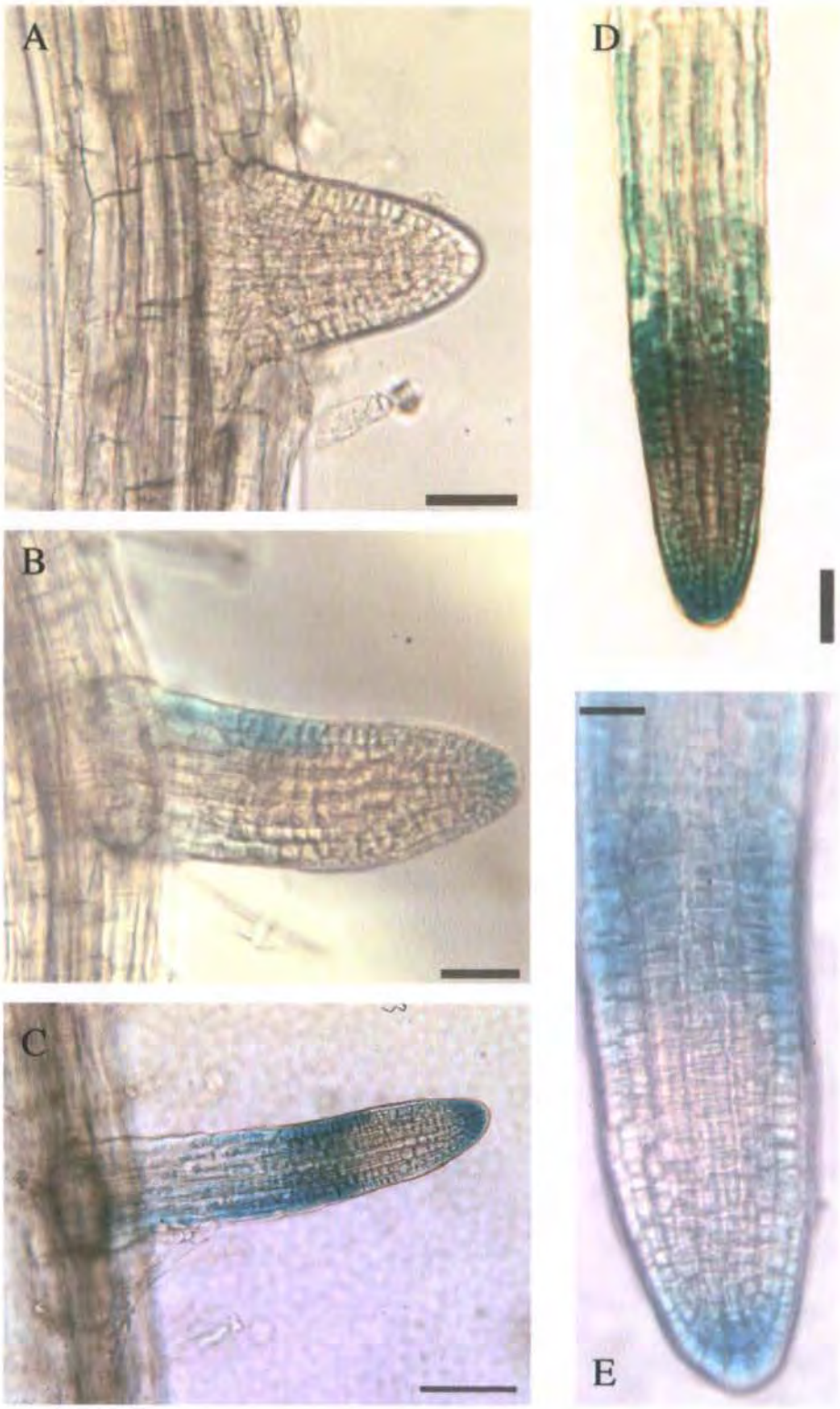

Figure 3.4 Expression of p*HYD1*::GUS in lateral root apices

A-E; young laterals of sequential age initiating along the primary roots of 7 dae seedlings. E shows detail of GUS activity in the root cap and cell differentiation zones.

A, B, D, bar = 50μm; C, bar =100μm. E, bar = 25 μm.

differentiating epidermal cells resolve a signal (Fig. 3.4; B). In established lateral roots, GUS activity appears identical to that seen in the primary root tip (Fig. 3.4; D). In 7 dae and older seedlings, the GUS signal in lateral root apices resolves first during incubation, i.e. with a stronger activity that of the primary root tip.

Fig. 3.5 shows p*HYD1*::GUS activity in transverse sections from a sequential series spanning a single primary root apex. These images reveal strong GUS expression in the root cap, around a meristem lacking histochemical activity (sections 10µm-50µm). Upon organisation of the cortex and endodermis (by 100µm in the root shown in Fig. 3.5), a signal first appears in the epidermal layer, where GUS activity is visible in the outer portions of the cells. This sub-cellular asymmetric distribution is more obvious in later sections. By 250µm, the epidermal cells are larger and show GUS activity throughout each cell, along with a weaker expression in cells of the cortex layer. At 340µm, a pronounced increase in GUS expression appears in one of each pair of trichoblast cells relative to other cells in the epidermal layer, although reporter activity is stronger in all epidermal cells at this time point. GUS activity intensifies in atrichoblasts just prior to the increase of signal intensity in trichoblast cell files.

A signal maximum is found at the mid-region of the cell differentiation zone, shown in Fig. 3.5 at 380µm; here all epidermal cells have an equally strong GUS activity. A distinct signal is now visible in the cortex and endodermal cell layers. After this maximum, the signal begins to fade in the epidermis, persisting longer in the trichoblast cell files (visible in the 460µm section), by which point the aligned cells of the protoxylem plate have resolved across the stele. The GUS signal completes a temporal wave throughout the ground tissues across the radial axis, prior to fading (600µm) as the cells enter the expansion phase.

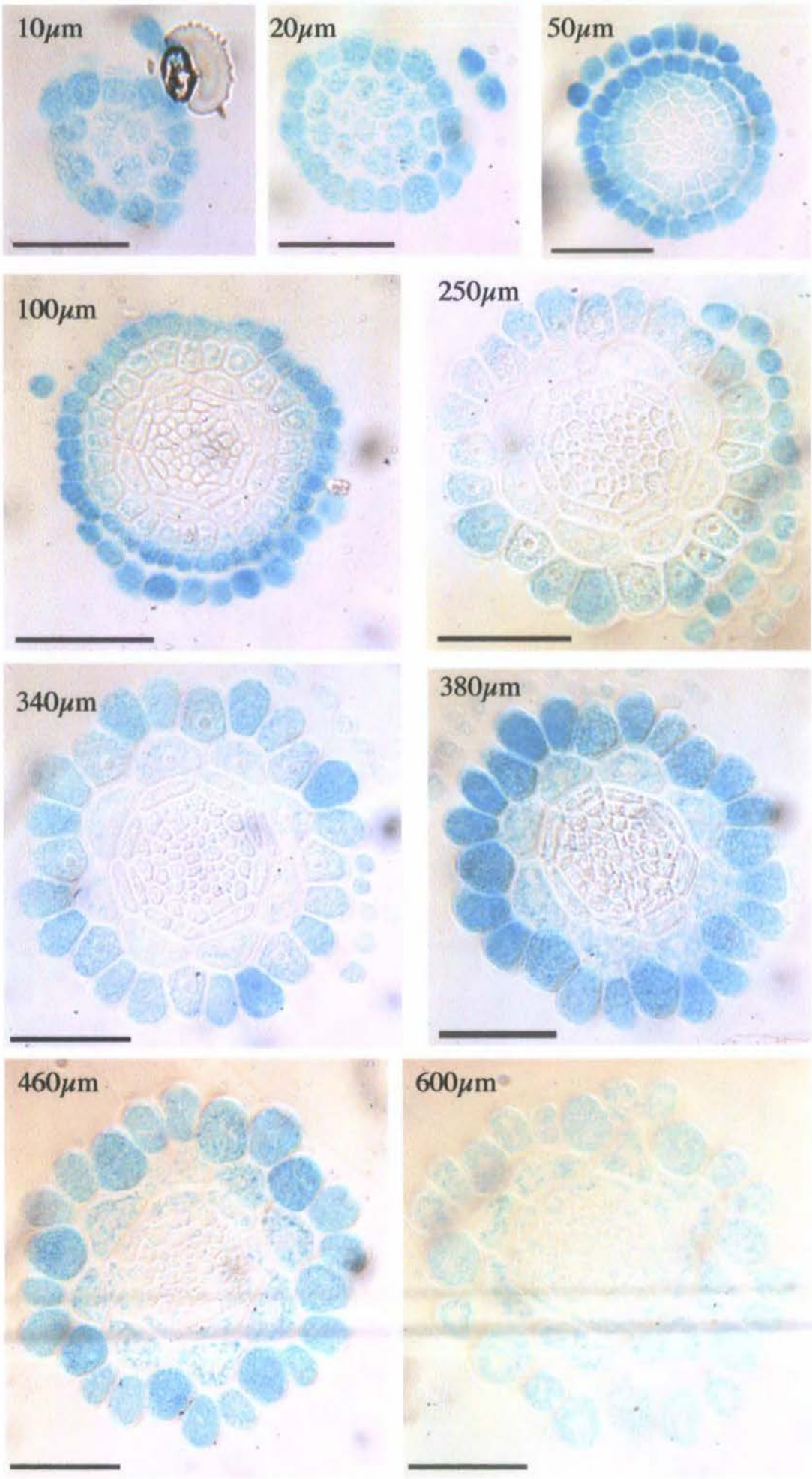
10μm
20μm
50μm
100μm
250μm
340μm
380μm
460μm
600μm

The pattern of p*HYD1*::GUS activity in the developing root indicates an association both with root cap cells, and with the temporal progression of cell differentiation during root growth. A transverse section across the root radial axis gives a developmental 'snapshot' of cells of equivalent age. The p*HYD1*::GUS reporter highlights small differences between the rates of maturity in adjacent cell files within the epidermis. In the zone of epidermal differentiation, a clear radial gradient of expression is seen across the growth axis. The rapid initial rise in GUS activity in atrichoblast cells, and the longer signal persistence in trichoblast cells after exiting the differentiation zone, further associates p*HYD1*::GUS with epidermal differentiation. This is because trichoblast cell files undergo more cell division events than the adjacent atrichoblasts (Dolan *et al.* 1994), hence cells within trichoblast cell files enter differentiation slightly later than neighbouring atrichoblasts from the same transverse section.

3.3.2.3 In the young seedling shoot, p*HYD1*::GUS expression is first seen in stipules, and is expressed transiently in the hypocotyl and cotyledons.

As the cotyledons open (between 3 and 5 dae in this study), the p*HYD1*::GUS signal is discernable first as a strong signal in the stipules (Fig. 3.6; A, J). Stipule expression persists throughout subsequent rosette development (Fig. 3.6; H, I) and into maturity of the rosette and the transition to flowering.

As the cotyledons open, a transient and diffuse GUS activity is evident in the cortex layers of the hypocotyl (Fig. 3.6; E, F), in cotyledon petioles and around the hydathode region at the apex of the cotyledon lamina (Fig. 3.6; B-D). This signal is mostly mesophyll associated, and persists at a low level between 5 and 7 dae. GUS activity appears in cotyledons, differentiating

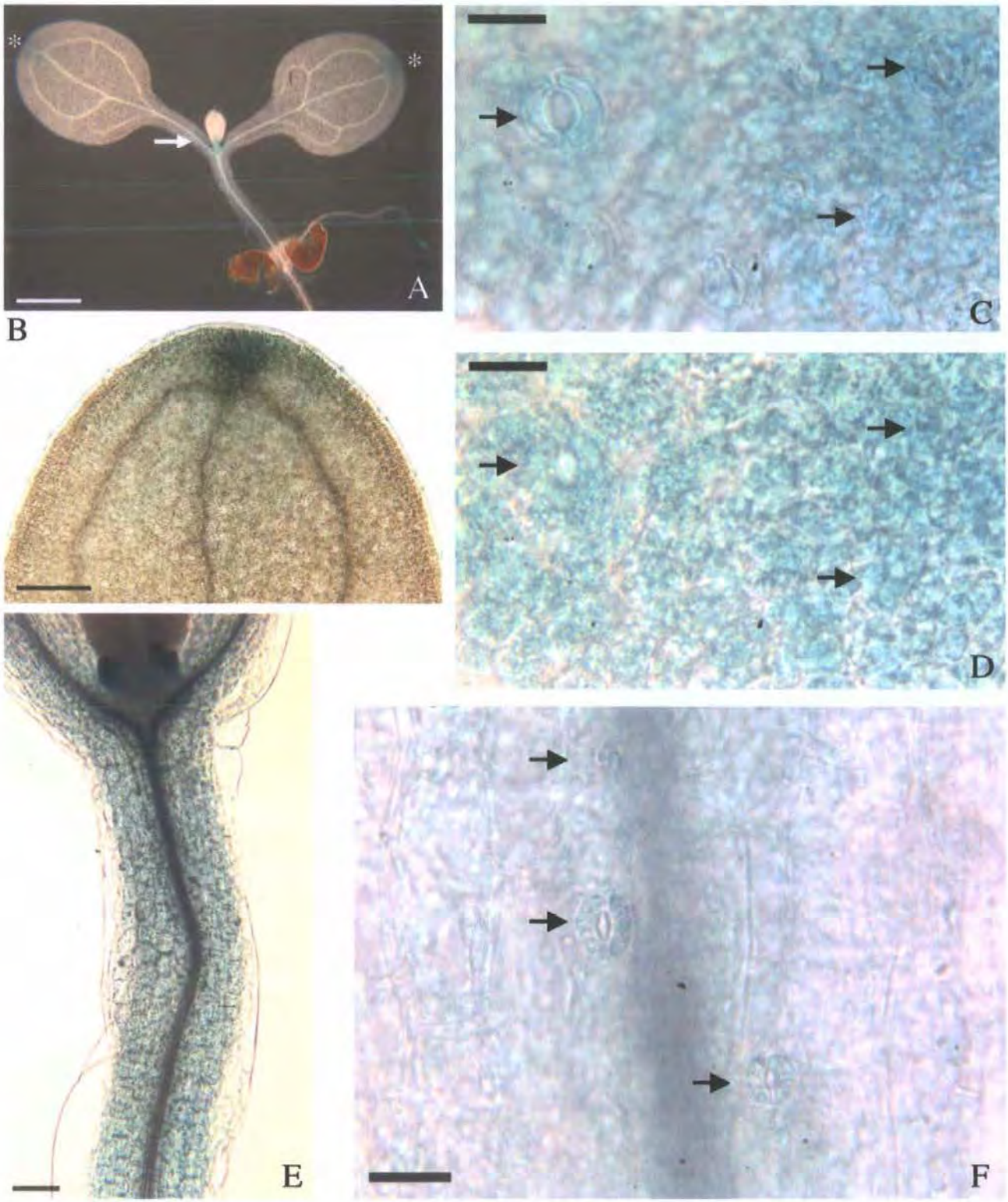

Figure 3.6 p*HYD1*::GUS expression in emergence and 5 dae shoots

A; seedling shoot region at 5 dae, with strong GUS activity in stipules (arrow) and diffuse expression staining around the hydathodes (A; asterisks, B), and in the ground tissue layers of the hypocotyl (E). The signal then resolves to differentiating guard cells (C) and the mesophyll layer beneath (D); arrows indicate equivalent positions in different focal planes. Hypocotyl expression is similarly seen in guard cells (F, arrows) and the subtending cell layers.

A, bar = 1mm; B, E, bar = 100μm; C, D, F, bar = 25μm.

guard cells and cells from the mesophyll layer beneath, as they separate to form intercellular spaces (Fig. 3.6; C, D).

In the petioles and hypocotyl, guard cells are also highlighted by GUS activity (Fig. 3.6; F), and a diffuse signal appears in the mesophyll and cortex layers of these organs respectively. This transient expression coincides with a phase of coordinated cell elongation in these structures, comprised of longitudinally oriented cell files in a radial (hypocotyl) or modified radial (abaxial-adaxial) arrangement (petiole). Epidermal patterning in the petiole is similar to that of the hypocotyl, where guard cells appearing in association with specific longitudinal cell files. Hypocotyl guard cells are positioned over cortical cell anticlinal walls as in root trichoblasts, and are under the control of the same patterning genes (Berger *et al.* 1988). Positional information directing stomatal differentiation in the *Arabidopsis* petiole is less well documented.

In the 7 dae seedling shown in Fig. 3.7; A, GUS activity has mostly faded from the hypocotyl and petioles, though is briefly seen in the vascular transition zone at the hypocotyl-cotyledon boundary. This timing coincides with the delayed differentiation of xylem strands seen in this region, associated with the vascular rearrangement from alternate in the stele to collateral in the cotyledon primary trace (Busse & Evert 1999b).

By 12 dae, at lower resolution the only GUS activity in the rosette is seen in the stipules (Fig. 3.7; B and C, detailed in D). Although GUS activity in stipules appears in conjunction with early differentiation in true leaves, this signal does not fade upon leaf maturity.

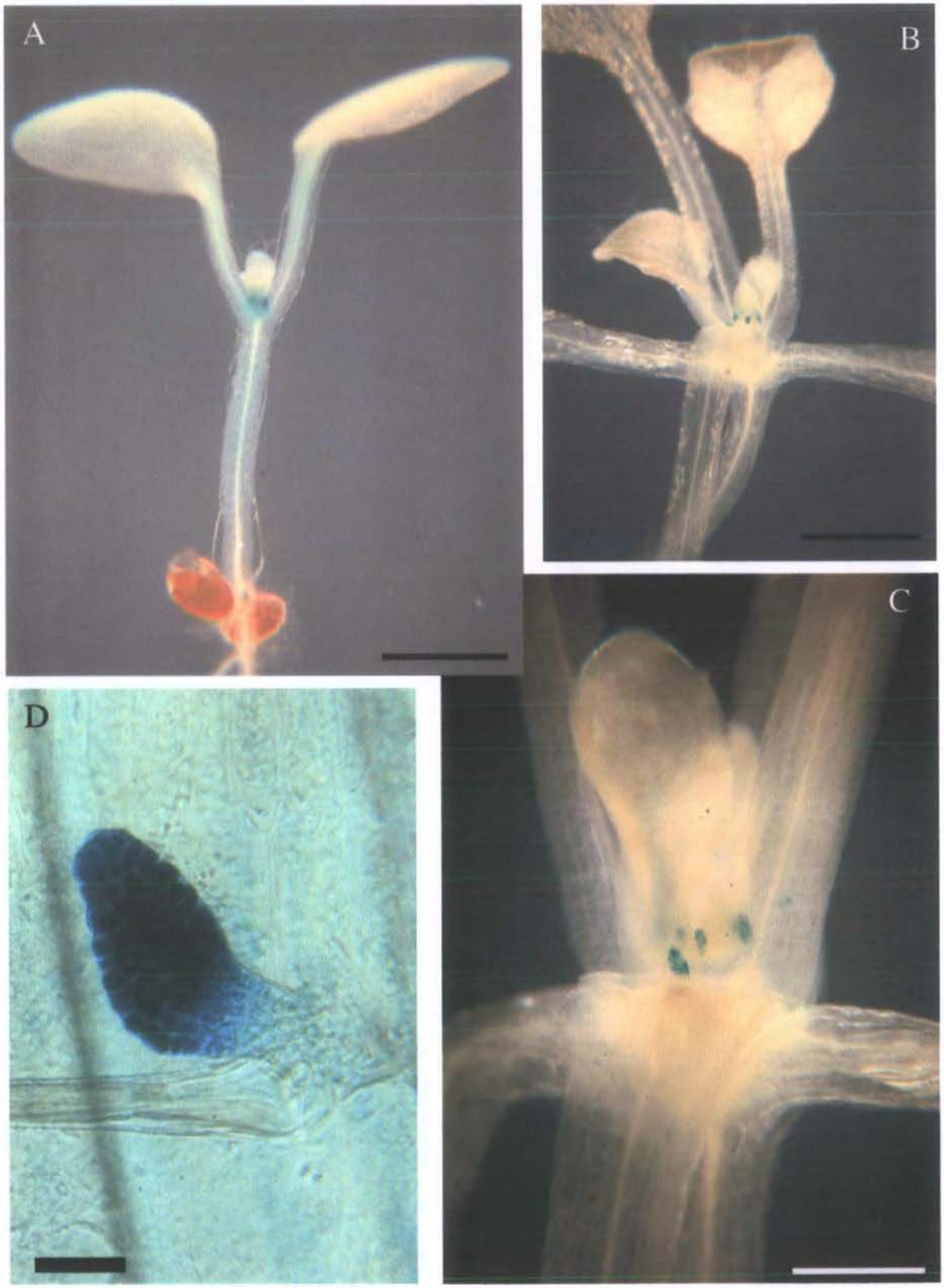

Figure 3.7 Activity of p*HYD1*::GUS in 7-12 dae shoots

A; seedling shoot 7 dae. B, shoot at 12 dae. C, shoot apical meristem region from a 12 dae plant. D, stipule detail from a second true leaf petiole base (12 dae plant).

A, B, bar = 1mm; C, bar = 0.5mm; D, bar = 50μm.

3.3.2.4 The pHYD1::GUS reporter is active in functional epidermal cells, and has a strong basipetal cell-specific expression in later rosette and cauline leaves.

The pHYD1::GUS reporter showed activity in the trichomes of juvenile rosette leaves (true leaves 1-4) from early in their differentiation. These cells carried a histochemical signature from early stages of cell expansion, prior to first branch formation (Fig. 3.8; A, B), when the cells coalign with the leaf proximal-distal axis (Hülskamp *et al.* 1994; Folkers *et al.* 1997). The trichome signal persists until cell maturity in these juvenile leaves, and is not associated with discernible reporter activity in the mesophyll layer.

A stronger and more distinctive p*HYD1*::GUS activity is seen in later (adult-phase) rosette leaf and cauline leaf development (Fig. 3.8; C-F, Fig. 3.10; B-G). These 'adult phase' rosette leaves have a progressively more complex vascular network than juvenile phase leaves with increased numbers of marginal 'teeth' corresponding to the position of hydathodes near the lamina margin; at these points the marginal cell files bear a solitary unbranched trichome (Tsukaya & Uchimaya 1997; Candela *et al.* 1999).

The first 'adult phase' rosette p*HYD1*::GUS expression appears in the trichomes of young expanding leaves in a similar manner to that seen in juvenile leaves. At a critical point from the mid-expansion phase of the lamina, the leaf develops a transient basipetal wave of diffuse GUS activity associated with the mesophyll and vasculature. This signal begins in marginal regions, and resolves in the fully expanded lamina to a zone around the primary mid-vein (Fig. 3.8; C-E) before localizing to the petiole as it elongates (Fig. 3.8; F), and fading at leaf maturity. As with juvenile rosette leaves, strong stipule staining persists throughout.

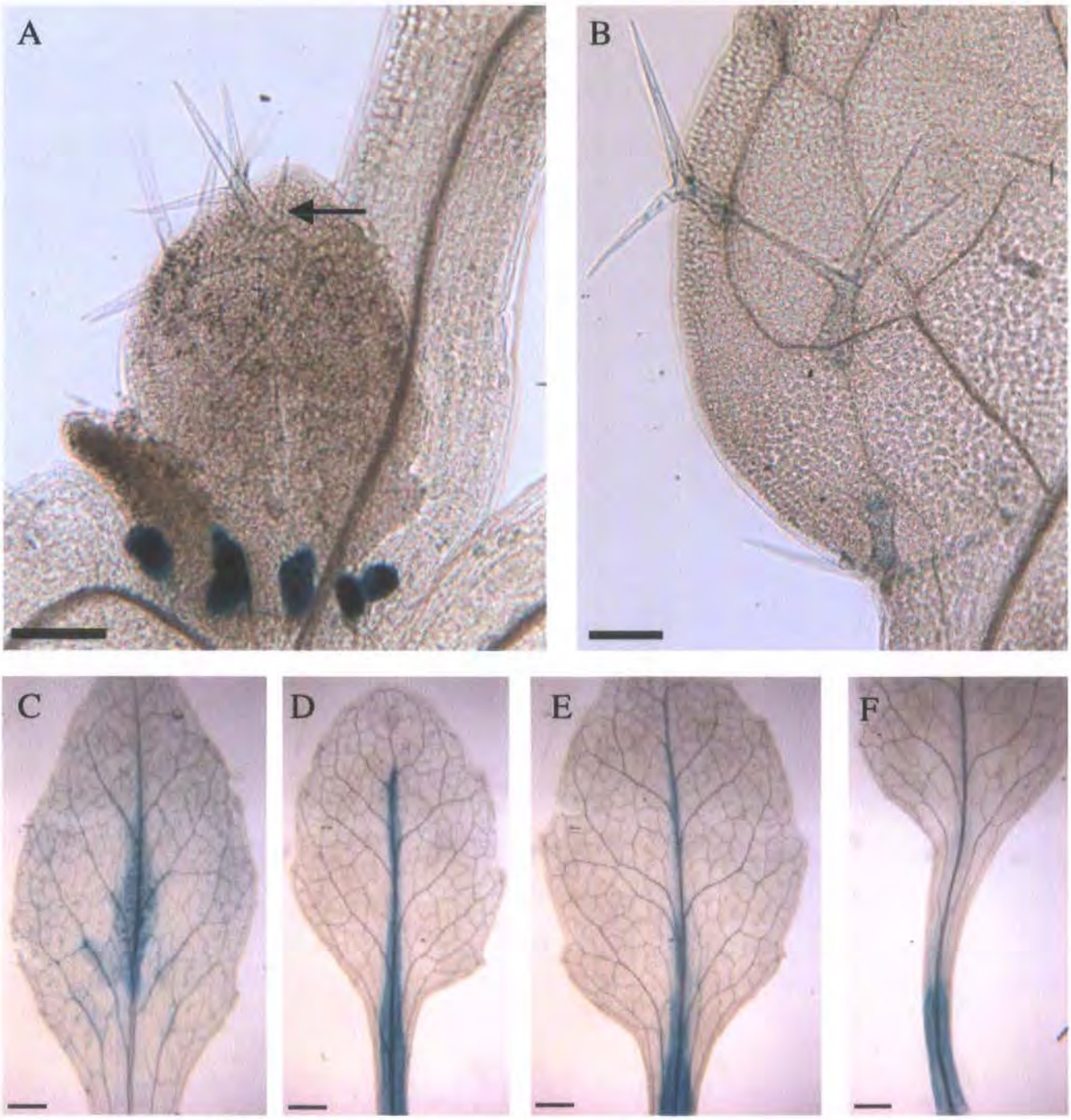

Figure 3.8 p*HYD1*::GUS activity in true leaves of the rosette

As well as the strong GUS activity in stipules, young juvenile true leaves (i.e. leaves 1-5) of the rosette also have weak, transient expression of the p*HYD1*::GUS construct in trichomes. This is seen after the cells differentiate and expand in young emerging leaves (A, arrow), persisting as branches develop in alignment with proximal-distal axis, and fading as cells reach maturity.

A different pattern is seen in adult phase leaves (true leaves 4-5 and later; C-F). This is first evident as an initial increase in the strength and persistence of the trichome signal. GUS activity then appears around the apical and peripheral regions in the mesophyll layer, and advances in a basipetal 'wave' towards the primary mid-vein and petiole; hair cells are highlighted in C, but this signal has diminished at the stage shown in D. Trichome GUS activity fades as the mesophyll signal moves basipetally.

A, B, bar = 100μm; C-F, bar = 1mm.

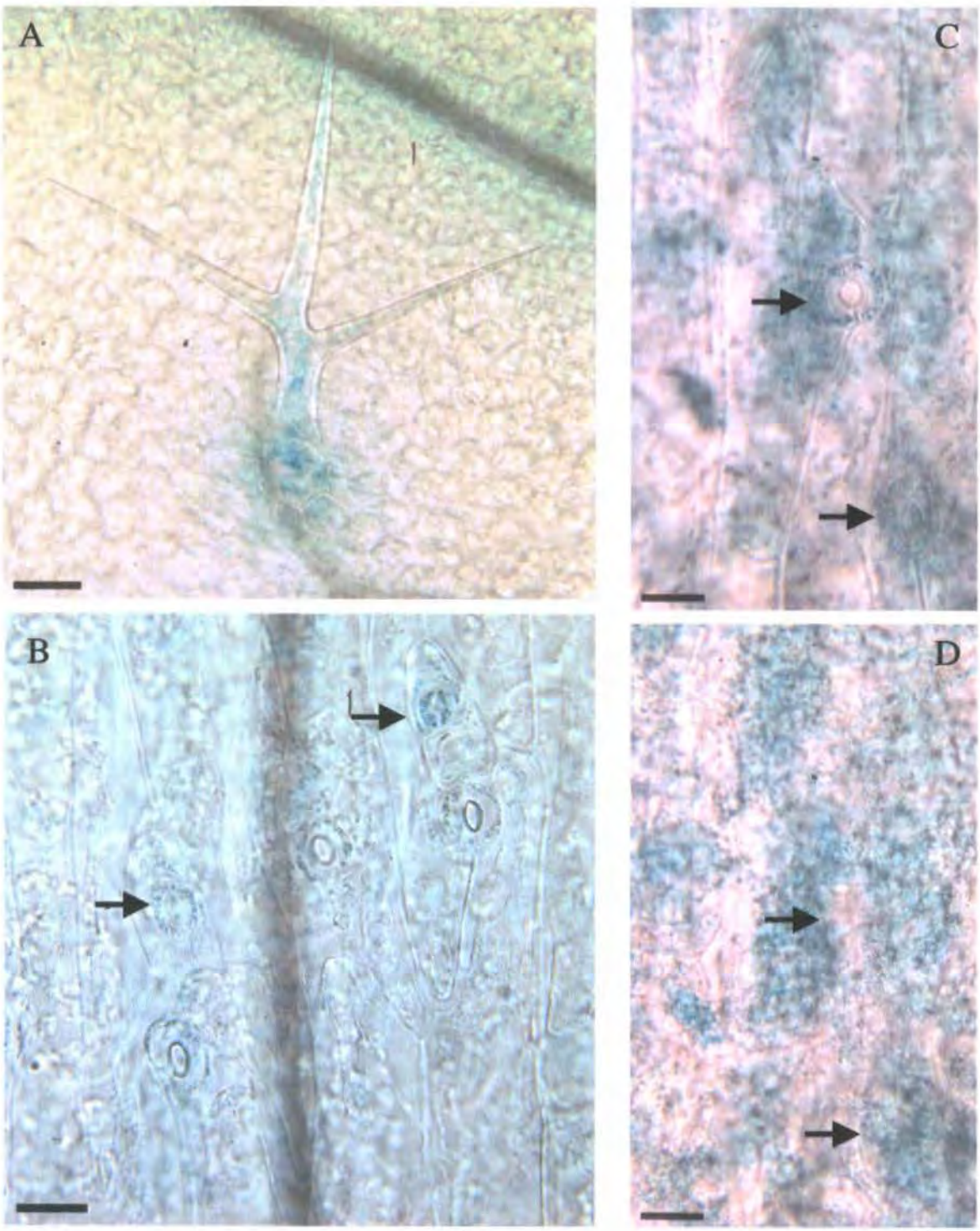

Figure 3.9 p*HYD1*::GUS activity in differentiating cells from rosette leaves

The wave of diffuse GUS activity in later expansion development of the adult phase rosette lamina and petiole (Fig. 3.8; C-F) correlates with a stronger signal in trichome basal cells (A), and differentiation of stomatal complexes in longitudinally oriented cell files of the petiole (B, C). B shows detail from the adaxial petiole epidermis from a 5th true rosette leaf; arrows indicate stronger GUS activity in young guard cells, which fades as these cells mature and expand. Where the diffuse signal in the mesophyll is more resolved, GUS activity appears in certain cells including those that separate to form intercellular spaces beneath maturing stomata; arrows indicate stomatal position in C (epidermis) and D (corresponding mesophyll).

A, bar = 50μm; B-D, bar = 25μm.

During cauline leaf development, a p*HYD1*::GUS signal is seen in stipules from the early stages of expansion, when xylem of the primary mid-vein first becomes visible (Fig. 3.10; B), followed by expression in the hydathodes in a manner that precedes formation of the first xylem loop (Fig. 3.10; C). As the lamina develops, a basipetal wave of histochemical activity is discernible, similar in character to that seen in adult phase rosette leaves. In cauline leaves the final signal resolves to the leaf central area around the primary mid-vein (Fig. 3.10; G). The difference between rosette and cauline leaf expression appears to have an anatomical basis; cauline leaves lack or have a reduced petiole in many ecotypes of *Arabidopsis,* including the Col-0 plants used in this analysis.

In both adult rosette and cauline leaves, specific localization of p*HYD1*::GUS activity appears in differentiating stomata and trichomes. In adult rosette leaves the basipetal wave is associated with strong trichome expression, which includes a transient signal in the surrounding basal cells as they elongate (Fig. 3.9; A). The strong cauline trichome signal (Fig. 3.11; C, D, E) appears to be associated with cells of the mesophyll beneath the basal cells (shown in Fig. 3.11; E, F). Again, the guard cells of differentiating stomata and the corresponding mesophyll cells beneath carry a signal in both leaf types during the formation of the intercellular spaces (Fig. 3.9;B, C-D, and Fig. 3.11; G-H). Cauline leaf expansion also includes a distinct, brief GUS signal in marginal cells (Fig. 3.9; D).

3.3.2.5 The p*HYD1*::GUS reporter shows a transient histochemical signature in sepals, during angiogenesis, in pollen grains, and during silique maturation.

The p*HYD1*::GUS reporter shows a low level of transcription in inflorescence stems, stem trichomes, and in the apices of both terminal and secondary

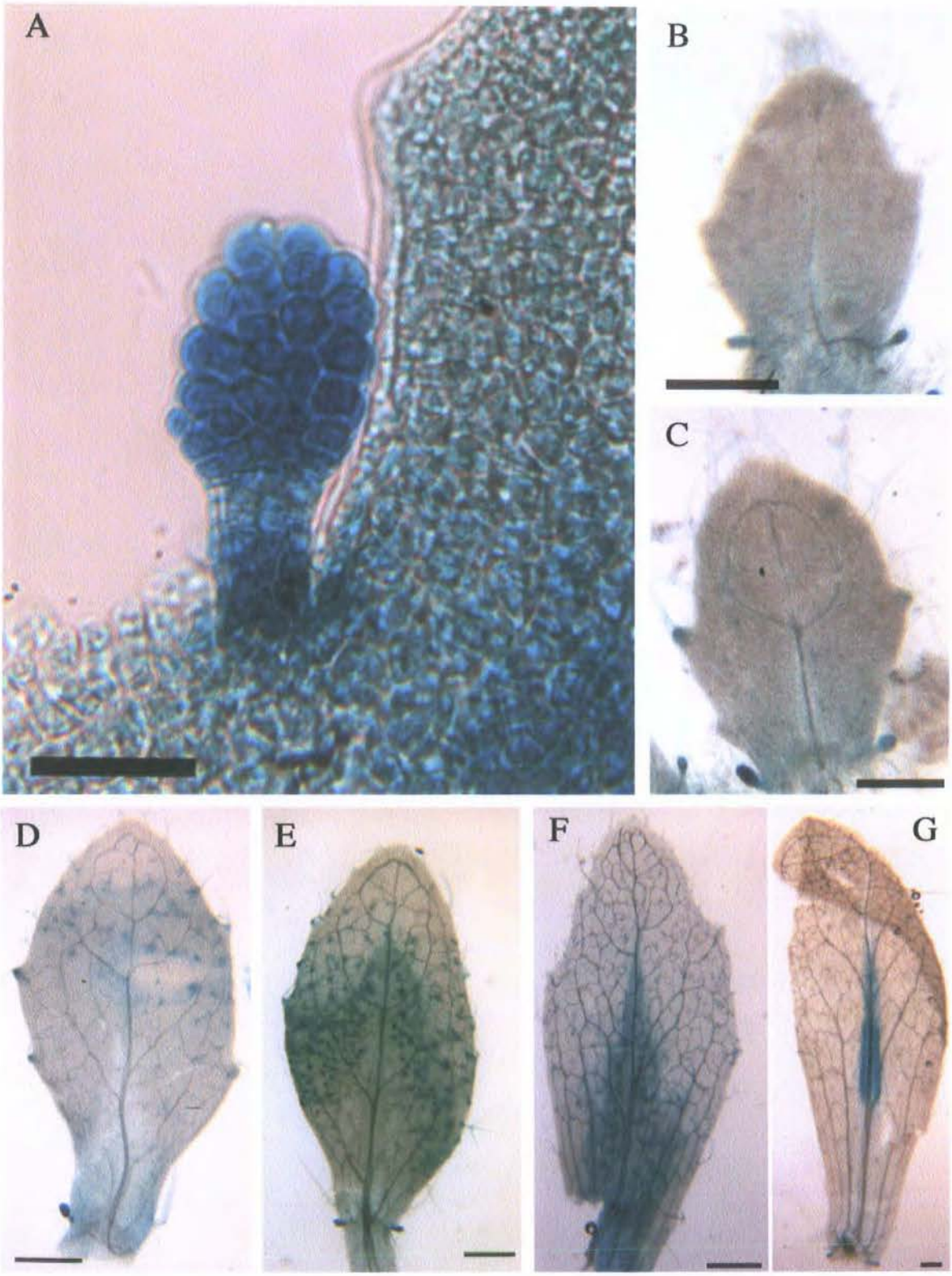

Figure 3.10 Activity of p*HYD1*::GUS in developing cauline leaves

As with rosette leaves, the first histochemical signal from the p*HYD1*::GUS construct in cauline leaves is seen in stipules shortly after primordium initiation (B, detail A). Laminar expression begins in hydathodes and trichomes (C), becoming stronger in a basipetal wave that resolves to the midvein region during later expansion growth (D-F), and fades as the leaf matures. The difference in this later signal between rosette and cauline leaves reflects the differences in petiole development between these leaf types.

A, bar = 50μm; B, C, bar = 0.25mm; D-G, bar = 0.5mm.

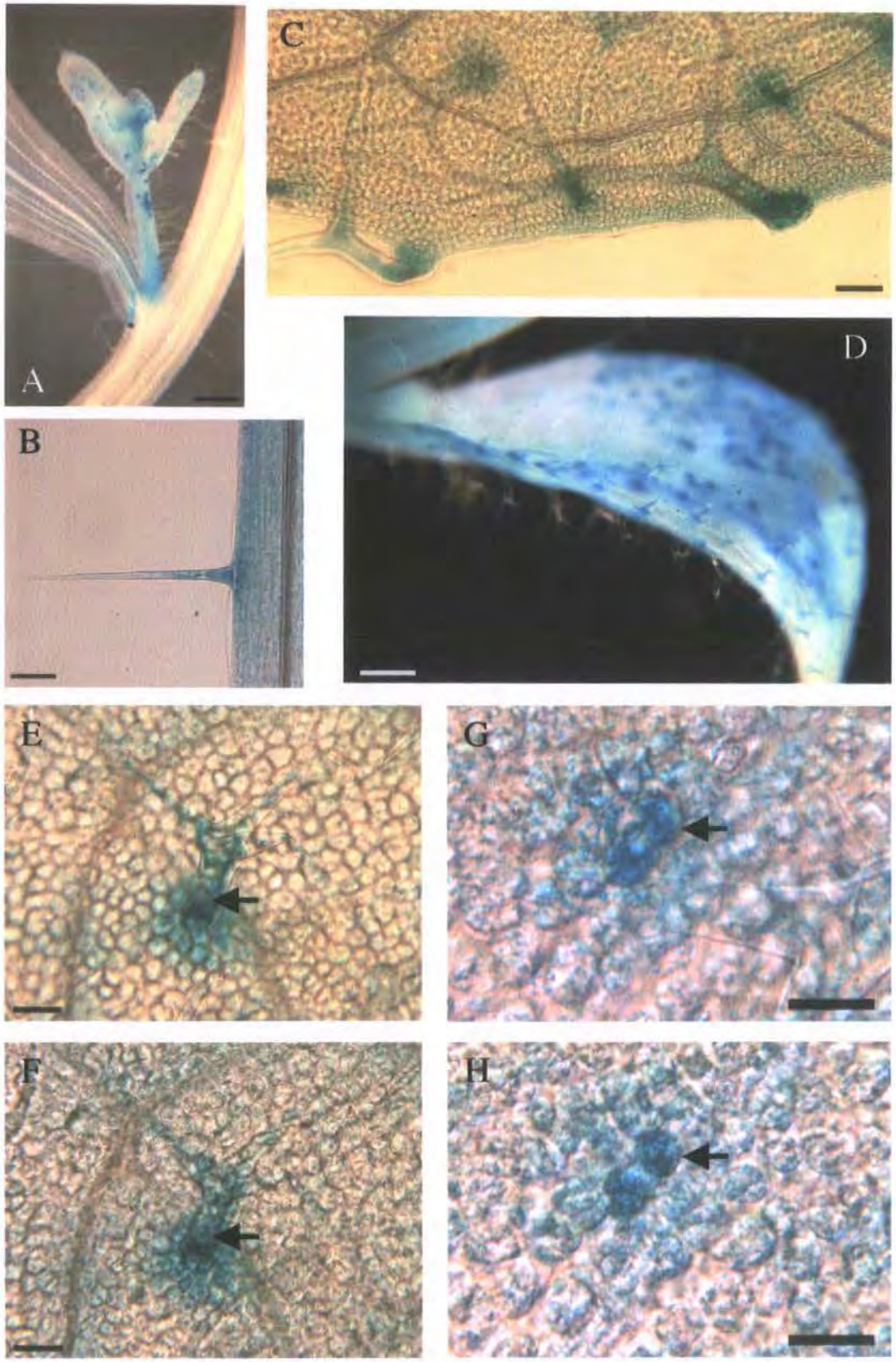

Figure 3.11 p*HYD1*::GUS in differentiating cells of cauline leaves

The basipetal cauline signal is seen strongly in trichomes (C-E), with a more transient expression associated with margin cells (C) and stomatal guard cells (G). Functional epidermal cells co-express histochemical activity with the associated mesophyll beneath, shown here in the two focal planes for a single trichome (E, F, arrows) and stoma (G, H, arrows). GUS activity is also seen in stem apices of inflorescence branches (A), associated with trichomes and the surrounding stem epidermal layer (B).

A, bar = 0.5mm; B, bar = 100μm; D, bar = 0.25mm; E-H, bar = 25μm; C, bar = 50 μm.

inflorescence branches (Fig. 3.11; A, B). In floral organ development, a brief transient GUS activity is seen in young sepals (Fig. 3.12; A), which fades rapidly after expansion of these organs, when the anthers begin to develop (Fig. 3.12; B). Histochemical localization develops more strongly in the anthers during angiogenesis (Fig. 3.12; C, D), and is particularly intense in developing pollen grains (Fig. 3.12; E, F). Transient weaker expression is also present in anther filaments (Fig. 3.12; E) during elongation growth.

A transient GUS activity is evident in the walls of young expanding siliques (Fig. 3.13; A). This signal resolves initially to the apices as the silique expands, persisting longest in the basal end and the receptacle as the pod reaches full length, and disappearing as expansion growth is completed, before maturity and desiccation (Fig. 3.13; B-E). Diffuse GUS activity was confined to the silique wall, with no signal evident in the placenta or ovules.

Siliques were harvested for GUS expression analysis from greenhouse-grown material, as plants do not set seed well when grown on $^1/_2MS_{10}$ plates. The samples shown in Fig. 3.13 were subjected to the same staining time and conditions as samples harvested from the growth chamber. The greater intensity of GUS activity in these tissues appears to be associated with greenhouse growth, and may be associated with the higher levels of light intensity experienced by greenhouse-grown material.

3.3.3 *HYDRA1* gene expression patterns are modified by phytohormone and inhibitor treatments

3.3.3.1 p*HYD1*::GUS expression is modulated by auxin-induced morphological changes, but is not clearly auxin responsive.

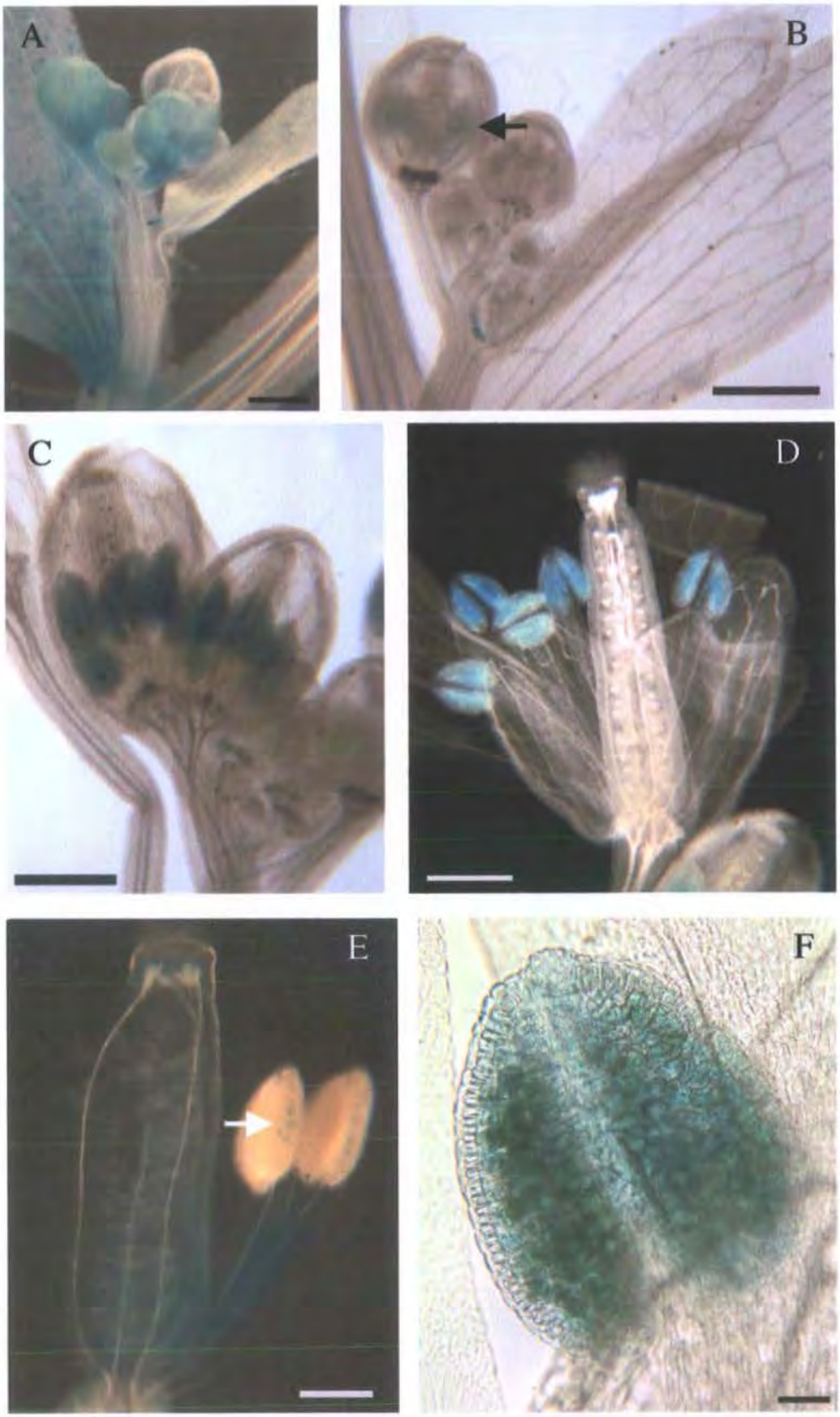

Figure 3.12 Activity of p*HYD1*::GUS in inflorescences

A; inflorescences shows diffuse transient p*HYD1*::GUS activity in young sepals, fading at maturity and shifting to young anthers (B, arrow). This increases as anthers develop (C) and mature (D). Finally, as pollen matures (E, arrow), tissue localisation resolves to pollen grains (F) and anther filaments (E).

A, bar =0.25mm; B-D, bar = 0.5mm; E, bar = 0.25mm; F, bar = 50μm.

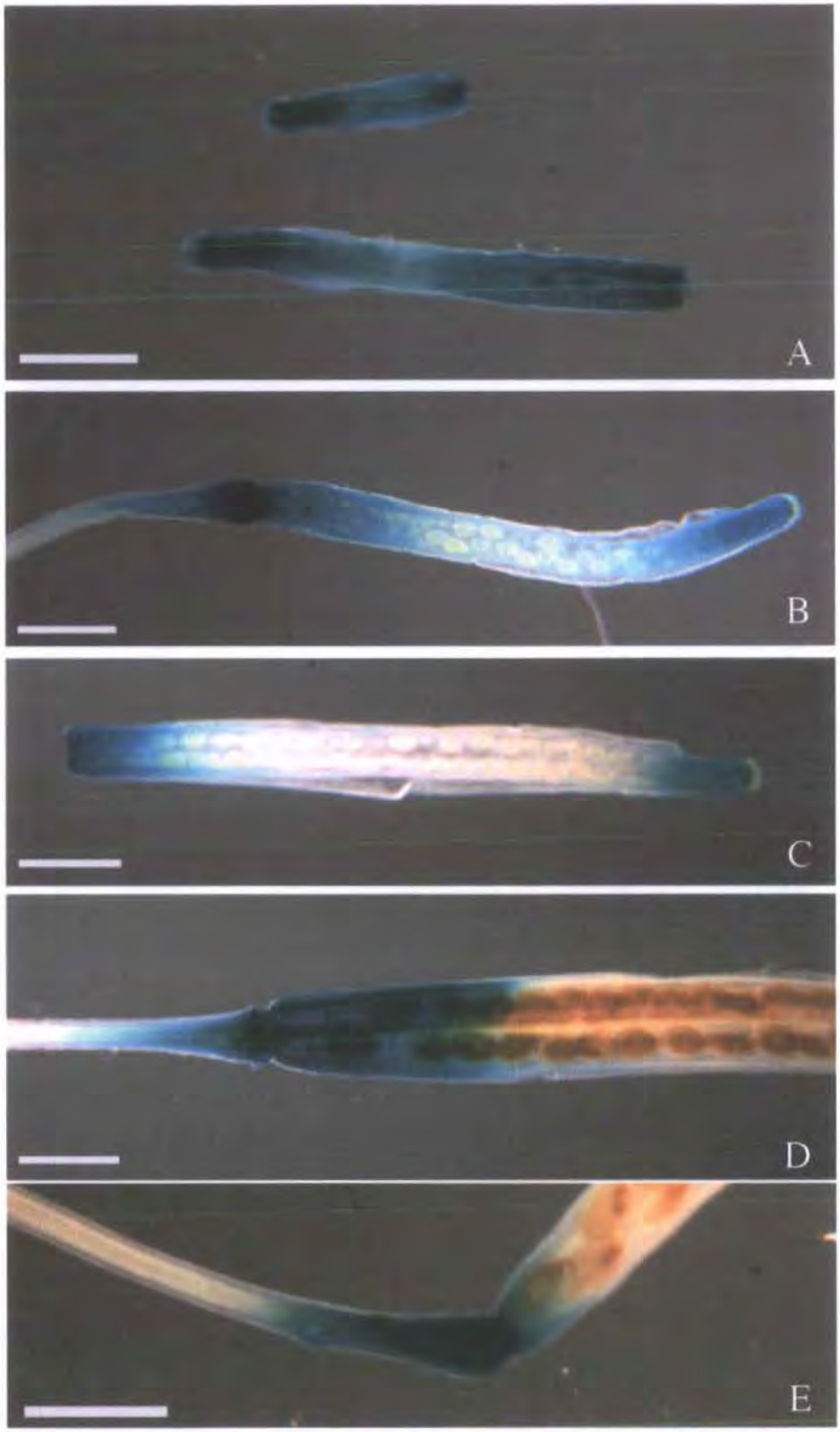

Figure 3.13 Activity of pHYD1::GUS during silique development

A-E; sequential stages of silique expansion and maturation, from plants raised under greenhouse conditions. GUS activity is seen throughout the valves of young siliques (A) resolving to the apices during expansion, and finally to the receptacle at maturity, fading as pod senescence and dessication commences.

Samples were incubated in X-gluc under standard conditions used for this reporter; the greater intensity of GUS expression in this material is associated with greenhouse grown samples, and may indicate a light-enhanced response.

Bar = 1mm

Activity of the p*HYD1*::GUS promoter in root apices is associated with tissues shown to be involved with signalling responses to auxin in roots (Sabatini *et al.* 1999); expression is also present in stipules, hydathodes (prior to xylem differentiation), and around the primary midvein of adult phase true leaves. The DR5::GUS auxin-responsive reporter also shows activity in stipules, apical hydathodes, and in the vicinity of the primary midvein of true leaves (Aloni *et al.* 2003). To assess whether the *HYD1* promoter activity is modulated by an auxin-responsive component, plants carrying the p*HYD1*::GUS constructs were subjected to exogenous treatment with an active auxin (1-NAA) and its reputedly inactive analogue (2-NAA).

Fig. 3.14 C-F shows p*HYD1*::GUS roots after treatment with (1-NAA). There is little effect on reporter expression at 1μM 1-NAA, though at 10μM 1-NAA, a strong increase in GUS activity is seen in tandem with an increased lateral root initiation. This change in root tip expression displaced the GUS maximum from root cap and differentiating epidermal cells into the former site of the root apical meristem and cell division zone. 10μm of 1-NAA induced strong GUS peaks in the apices of both primary and lateral root tips (Fig. 3.14; E, F). A similar though less severe modification of expression resulted from treatment with 10μm of 2-NAA (Fig. 3.15; B, C). Induction of lateral primordia by exogenous auxin, and associated alterations in GUS activity, were more pronounced along the primary root than on lateral roots present before treatment.

The auxin 1-NAA (and its relatively inactive analogue 2-NAA) enters plant cells by diffusion (Delbarre *et al.* 1996), and therefore penetrates throughout treated tissues. Were p*HYD1*::GUS expression to respond directly to exogenous auxin, a modified histochemical signal would be expected at lower concentrations of 1-NAA. Instead, the response was only obvious at high exogenous concentrations, and GUS localization showed similar positional modulation by 2-NAA. The modification of p*HYD1*::GUS expression seen in this

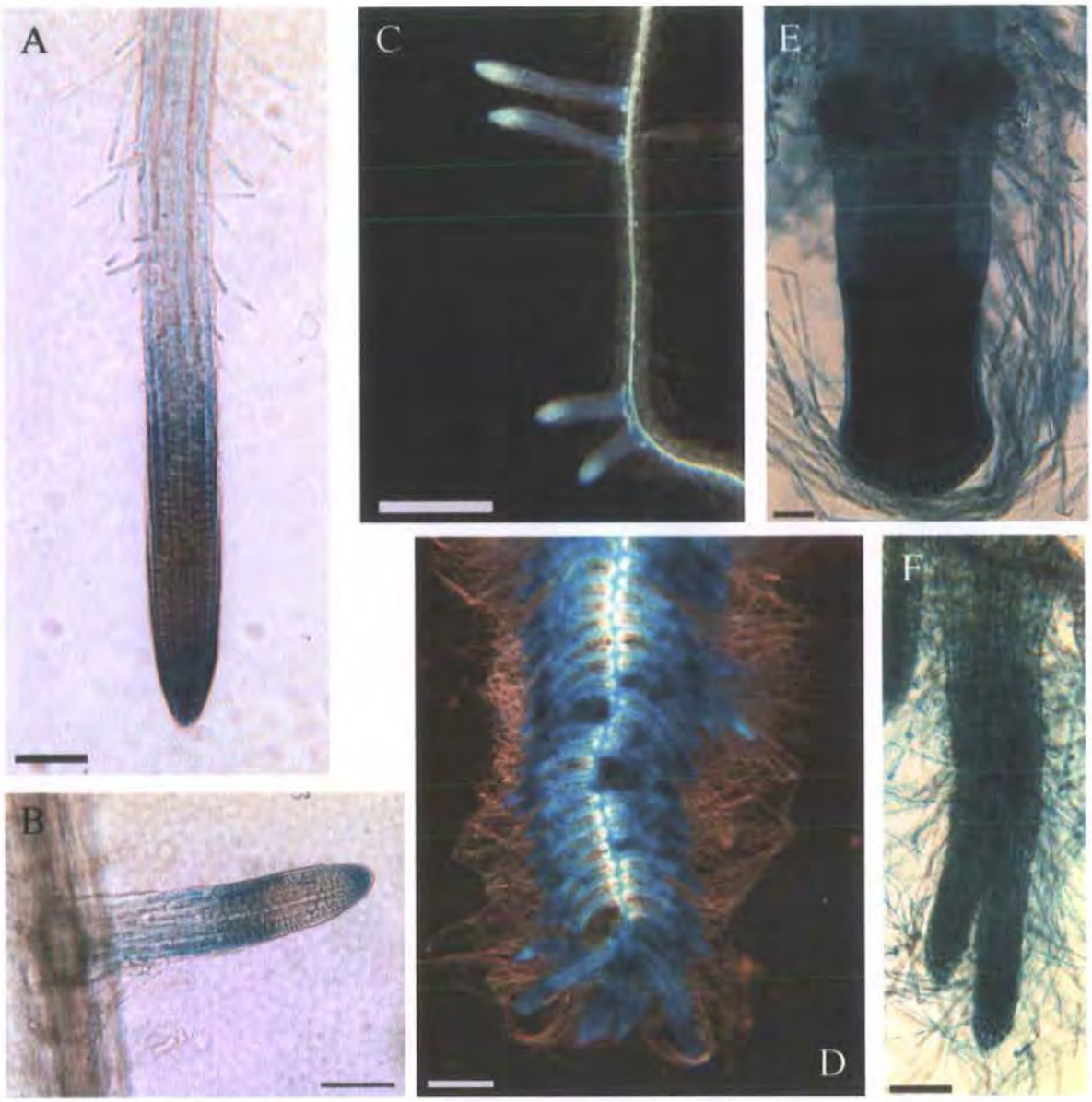

Figure 3.14 Response of p*HYD1*::GUS to exogenous 1-NAA (an active synthetic auxin)

A; primary, and B; lateral untreated root apices. C-F; roots treated with 1-NAA.

There is little effect on expression of p*HYD1*::GUS at 1μM 1-NAA (C), but at 10μM a dramatic increase in GUS activity is associated with laterals induced to form along the primary root (D, detailed in E). This change highlights the zone of cell division, which has minimal expression in control root tips. Secondary laterals from anchor roots (F) show less increase in signal but the same zonal translocation.

A, B, bar = 100μm; C, D, bar = 0.5mm; E, F, bar = 50μm.

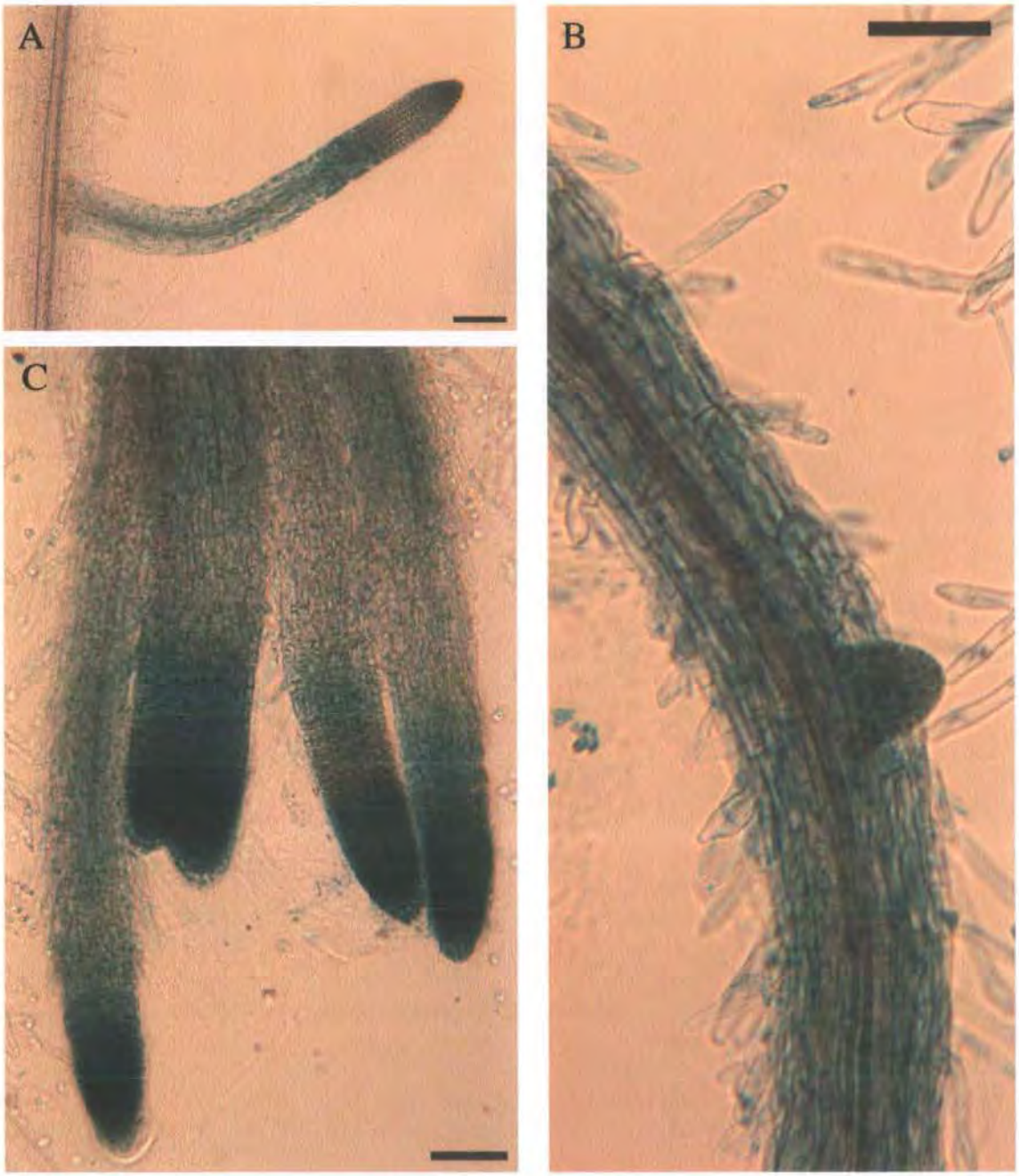

Figure 3.15 Response of p*HYD1*::GUS to exogenous 2-NAA (an inactive synthetic auxin)

A-C; roots treated with the (relatively inactive) 2-NAA. (These plants are to be compared to the results of treatment with the active auxin analogue 1-NAA,and the untreated control seedlings, both shown in Fig. 3.14.)

The analogue 2-NAA had no effect at 1μM (A), though 10μM resulted in a partial increased GUS activity in laterals from the primary root (B) and anchor root (C), in conjunction with morphological change, implying some auxin-related activity for this compound.

A-C, bar = 100μm.

study may therefore result from changes in positional signals, resulting from an overwhelming of endogenous cues defined by auxin distribution, rather than through an auxin-induced response.

3.3.3.2 Inhibition of polar auxin transport moves p*HYD1*::GUS expression in parallel with known alterations of positional cues.

To assess the effects of auxin transport on reporter expression, plants carrying the p*HYD1*::GUS construct were treated with TIBA and 1-NOA. Exogenous application of these compounds results in an altered auxin transport within the plant body. For example, Sabatini *et al.* (1999) showed an alteration in expression of the auxin-responsive reporter DR5::GUS in auxin-transport inhibited lateral root tips. DR5::GUS is seen in the root cap columella of untreated root apices. These authors noted that exogenous inhibition of auxin transport induced a proximal shift and expansion of the DR5::GUS signal into the former site of the quiescent centre and zone of cell division in 4 dae seedling roots, incorporating the epidermis. They also showed a similar change, in the absence of treatment, in lateral roots of the *aux1* mutant. These experiments show that both chemical and mutational modification of auxin movement causes a relocation of the normal positional cues defined by auxin gradients.

1-NOA specifically inhibits the auxin influx carrier AUX1, with minimal effects on auxin efflux (Imhoff *et al.* 2000). It neither affects PIN1-associated auxin efflux, nor has auxin-like activity (Parry *et al.* 2001). AUX1 is thought to unload free auxin (IAA) from mature phloem in the root, and deliver it directly to the root meristem via the protophloem cell files. In the *aux1* mutant, accumulation of free auxin at root apices is impaired (Swarup *et al* 2001).

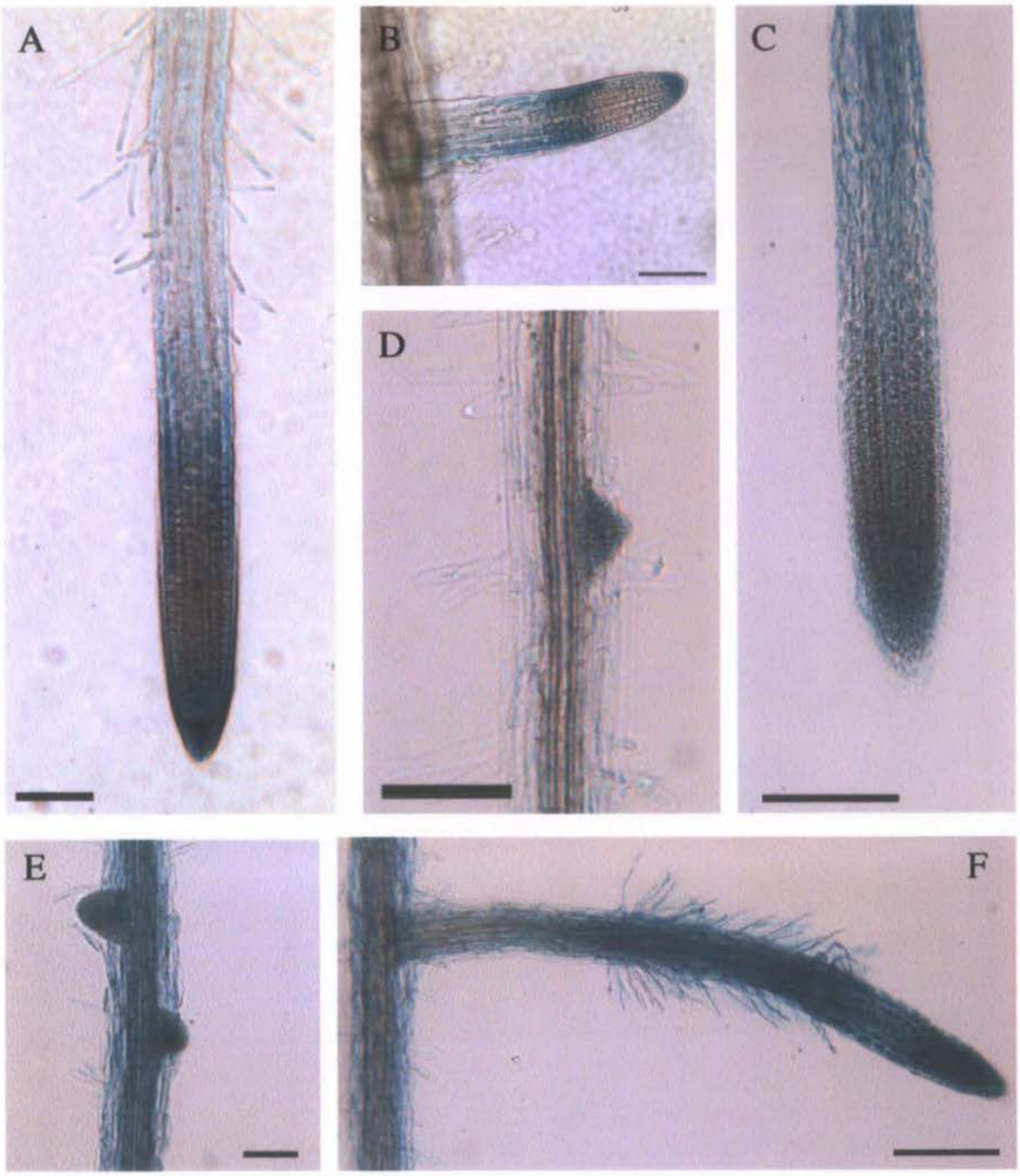

Figure 3.16 Effects of 1-NOA (an auxin influx inhibitor) on expression of p*HYD1*::GUS in root tissues

A: primary and B; lateral root apices from untreated plants, compared with the primary apex (C) and lateral root apices (D-F) of plants treated with 1-NOA.

NOA accentuates GUS activity in younger sections of lateral roots (as seen in F), particularly in root hairs.

A-F, bar = 100 μm.

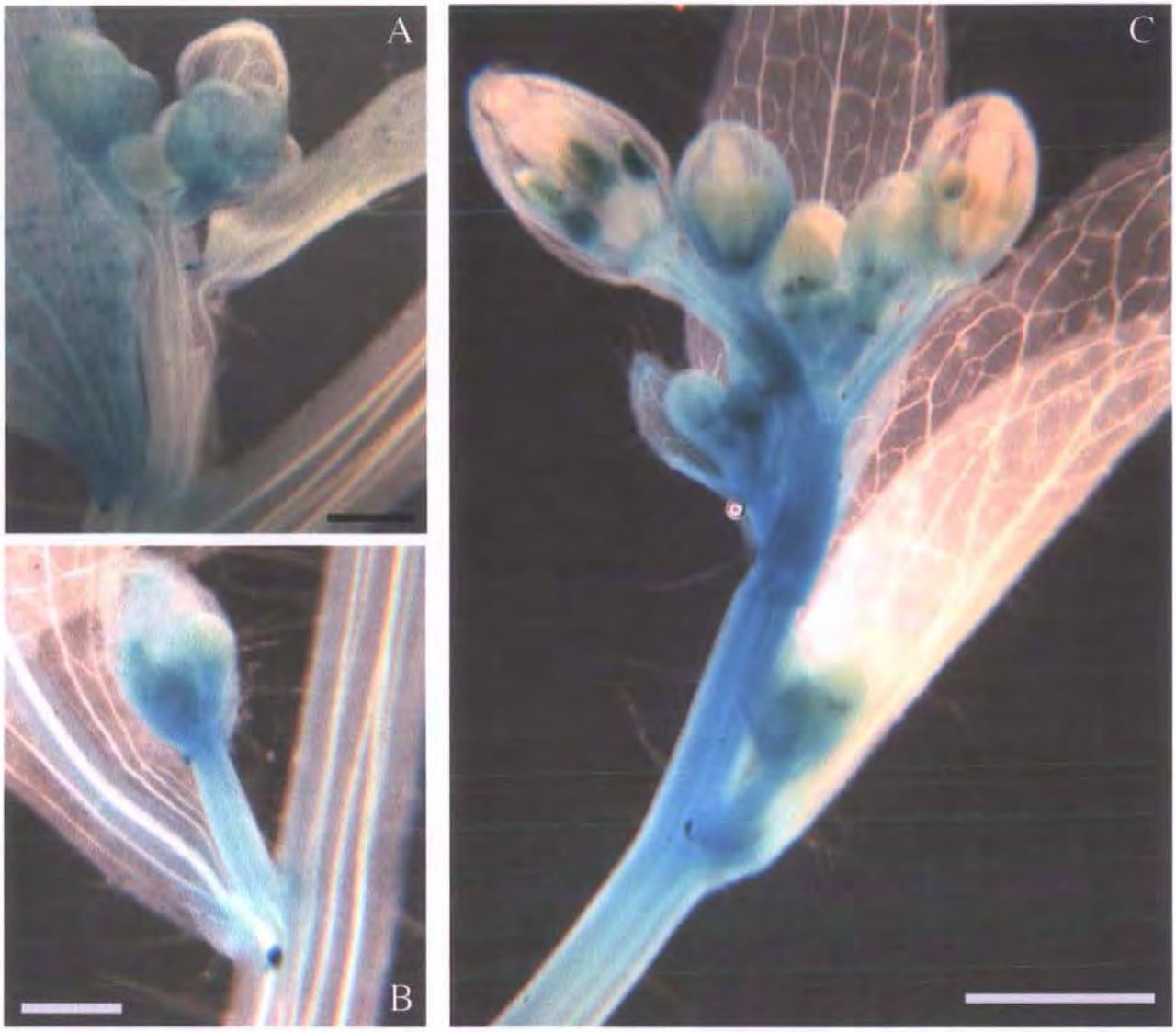

Figure 3.17 Effects of exogenous 1-NOA (an auxin influx inhibitor) on shoot expression of p*HYD1*::GUS

A; inflorescence apex from an untreated plant, compared with B and C; inflorescence apices from plants grown in the presence of 10 μM 1-NOA.

The auxin influx inhibitor 1-NOA has relatively little effect on histochemical localization in the floral organs, although the inflorescence stem apices show an increased p*HYD1*::GUS activity.

A, bar = 0.25mm; B, C, bar = 0.5mm.

Treatment with NOA had no obvious effect on *HYD1* promoter activity in the primary root apex (Fig. 3.16; C). In contrast, changes were discernable in lateral roots; treatment produced a stronger and more persistent signal in lateral root tips and epidermis including a persistent signal in root hairs (Fig. 3.16; D-F), with dense GUS activity in the former lateral root tip cell division zone. Emerging lateral roots showed GUS activity (Fig. 3.16; D, E) from younger stages of primordial initiation than in untreated plants. This signal was not localized to root cap and differentiating cells as in the controls, and showed some up-regulation in the lateral root cell division zone. In the shoot, an increased signal was seen only in the apical portions of inflorescence stems (Fig. 3.17; B, C).

TIBA inhibits auxin efflux (Thompson *et al.* 1973; Cande & Ray, 1976, Geldner *et al.* 2001) and mimics the reduction in polar auxin transport caused by the *pin1* mutation of *Arabidopsis* (Okada *et al.* 1991), though does not have auxin-like activity. TIBA treatment resulted in a substantially enhanced histochemical signal in the apices of p*HYD1*::GUS primary and lateral roots (Fig. 3.18; C, D). The primary root showed substantially increased GUS activity at the tip, with a strong signal visible in a transverse band across the root over the former position of the quiescent centre (Fig. 3.18; C, arrow), and persisting in mature root hair cells. These observations imply induction of *pHYD1*::GUS by auxin trapped in the root apex by efflux inhibition, suggesting a disruption of the radial auxin gradient present in this area under normal physiological conditions. In young lateral root tips treated with TIBA, cellular differentiation of expression was lost, replaced by a dense signal extending proximally from the root cap into the zone of root hair maturation (Fig. 3.18; D).

Some mature sections of the main root showed blocks of GUS activity, associated with inner cell layers around the stele (Fig. 3.18; E). This pattern is similar to that found by Sabatini *et al.* (1999) when transgenic plants

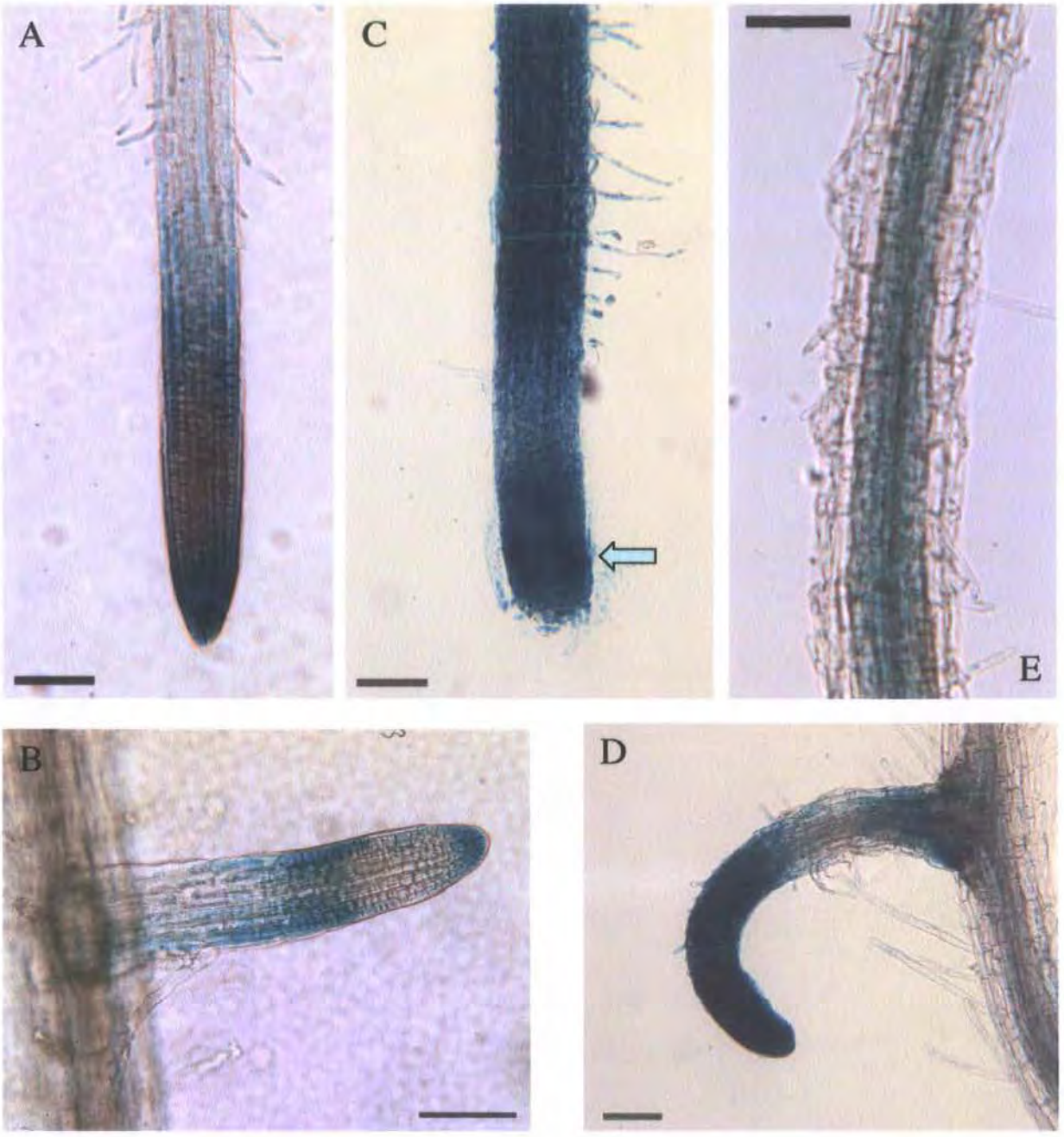

Figure 3.18 Effects of TIBA (an auxin efflux inhibitor) on root expression of p*HYD1*::GUS

A: primary and B: lateral root apices from untreated plants, compared with the primary apex (C) and lateral root apices (D-F) of plants treated with 1-NOA.

In TIBA-treated plants the GUS signal is increased substantially in the whole root tip region, and appears in the inner cell layers in certain sections of more mature root (I). Note the band of enhanced histochemical activity in the former cell division zone of the primary root apex (C, arrow).

A-E, bar = 100 μM

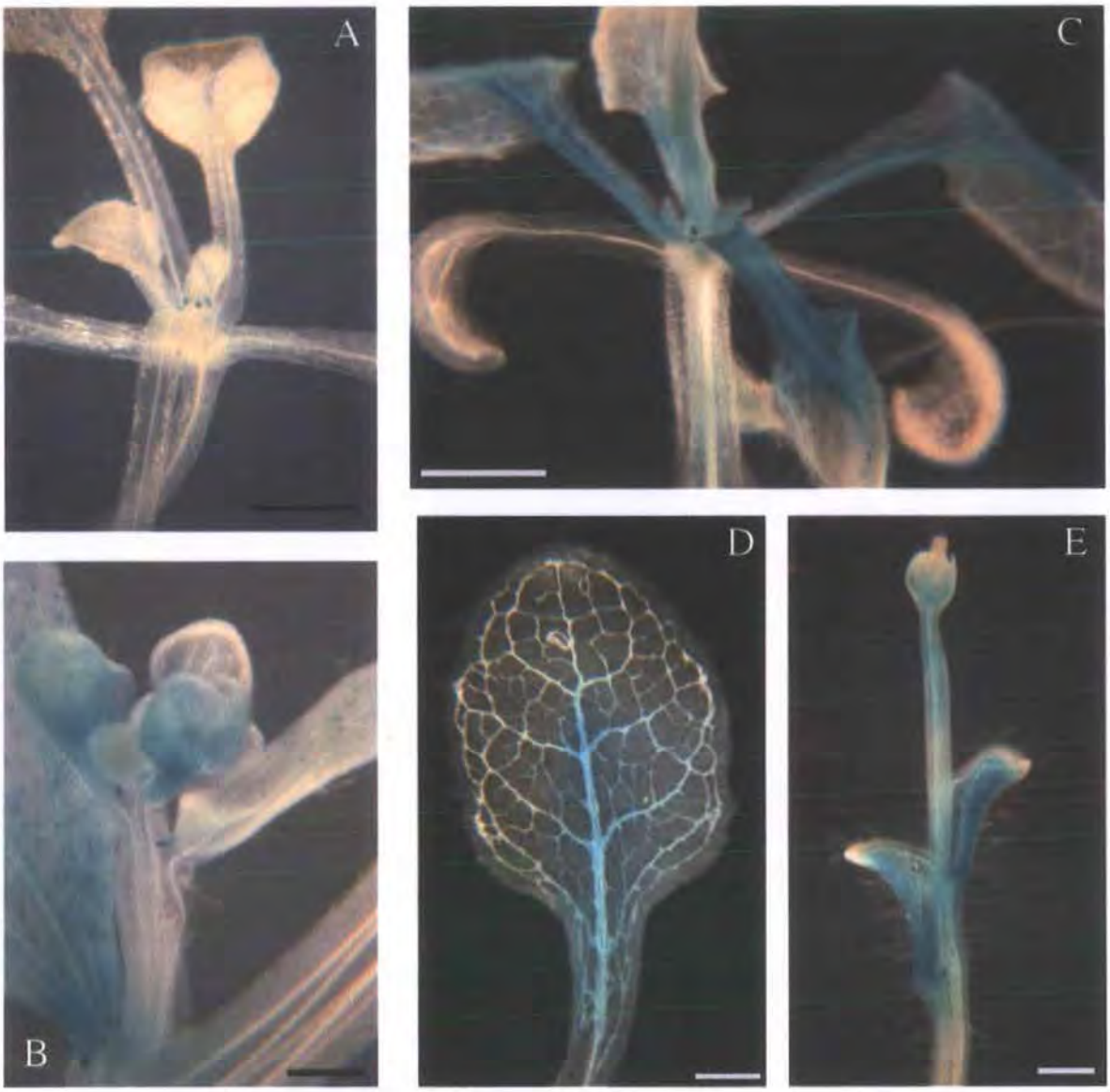

Figure 3.19 Effects of TIBA (an auxin efflux inhibitor) on shoot expression of p*HYD1*::GUS

A; rosette, and B; inflorescence apex from an untreated plant. C; rosette, D; adult phase rosette leaf, and E; an inflorescence apex, from plants treated with 25 μM TIBA.

TIBA strongly accentuates the transient basipetal signal in the mesophyll layer from p*HYD1*::GUS activity in adult phase rosette and cauline leaves, and causes the signal to linger around the primary midvein region and petioles, which are wider than in untreated plants. Floral organ development is also severely retarded by TIBA treatment, although no clear change in signal localization is evident (E).

A and B, bar = 1mm; C, bar = 0.25mm; D and E, bar = 0.5mm.

carrying the DR5 reporter were subjected to prolonged exposure to 50μM NPA (an alternative auxin efflux inhibitor).

The shoot tissues of TIBA-treated p*HYD1*::GUS transgenic plants showed a persistence of the transient staining seen in untreated plants around the central mid-vein of later rosette and cauline leaves (Fig. 3.19; C-E).

In the present study the p*HYD1*::GUS reporter had a similar positional response in roots treated with both auxin and with inhibitors of auxin movement, namely a displacement of signal out of the columella and into the former cell division zone of the root meristem, with up-regulation in other tissues known to be involved with the movement of auxin in roots, such as the root hair cell files. The similarity in patterning between these treatments suggests that the p*HYD1*::GUS reporter is not auxin responsive, but its distribution is modified by auxin-induced changes in positional information. In addition, some differences in response were found between primary and lateral root apices, implying either a differential modulation of auxin transport between these tissues by the inhibitor compounds, or an innate differential response threshold within the plant body.

3.3.3.3 Cytokinins up-regulate p*HYD1*::GUS expression in both the root and shoot, and cause a proximal shift in the root apical histochemical maximum.

To assess the transcriptional response of p*HYD1*::GUS to cytokinin, plants carrying the reporter construct were treated with benzyl-amino purine (BAP). The addition of BAP to the growth medium produced significant changes in histochemical activity. In the primary root tips (Fig. 3.20; A-D), 1μM BAP produced a discernable modification of GUS localization, specifically reducing the root cap signal. The 10μM treatment resulted in a strong increase in

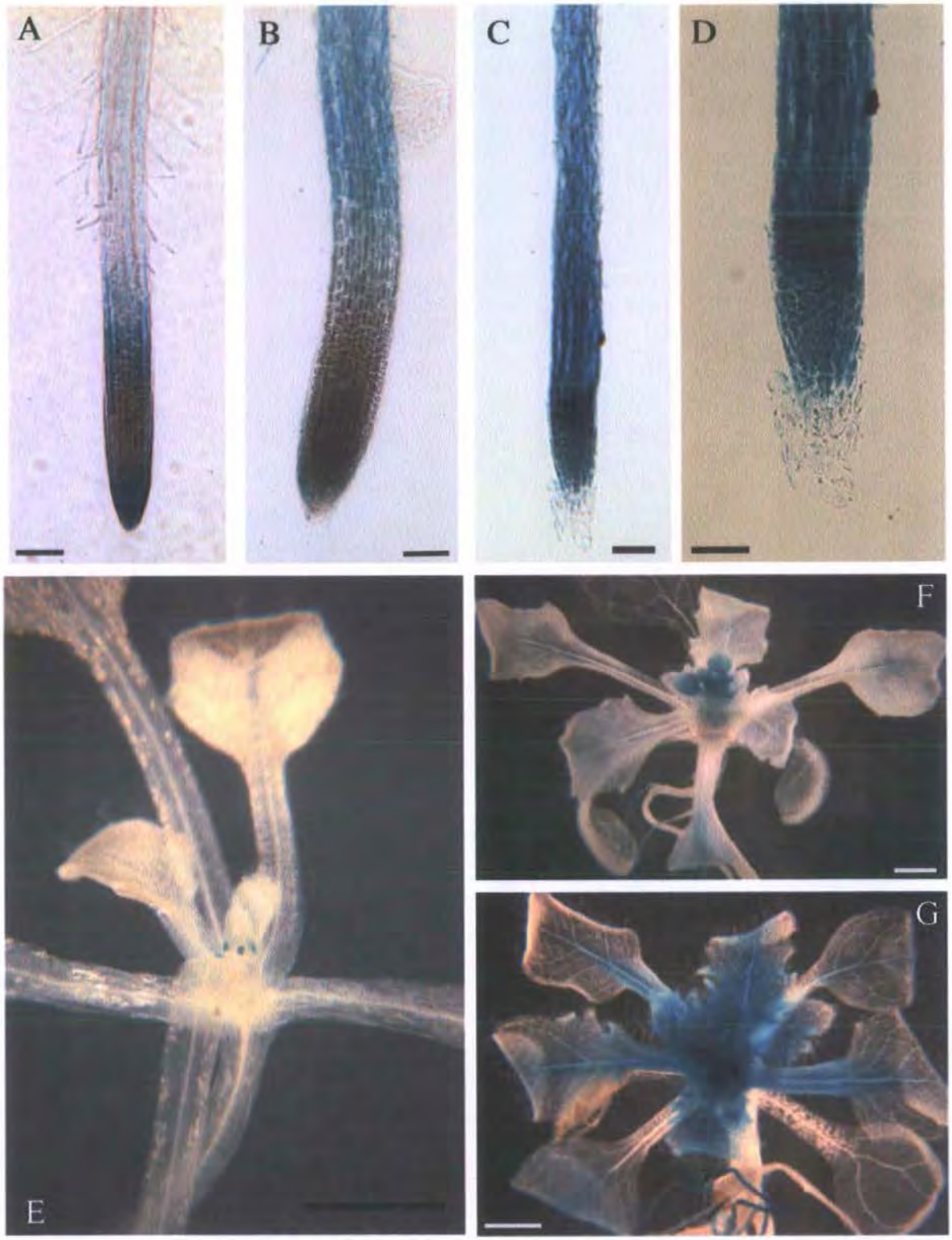

Figure 3.20 Activity of p*HYD1*::GUS in response to exogenous benzyl-amino purine (BAP) treatment

Primary root tips show increased intensity of p*HYD1*::GUS expression in response to BAP (B; 1μM and C, 10μM BAP) compared to an untreated root (A). The histochemical localisation has shifted into the elongation zone with 10μM BAP treatment, detailed in D. Rosette expression is also increased around the stipules (F; 1μM) and into the zone around the primary midvein of the rosette leaves (G: 10μM) compared to untreated plants (E).

A-C, bar = 100μm; D, bar = 50μm; E-G, bar = 1mm.

overall signal and a modulation of the staining maximum away from the root cap columella into the former cell division zone (Fig. 3.20; D). A similar pattern was seen in lateral roots (not shown).

In the shoot, a slight increase in GUS activity was evident at 1μM BAP (Fig. 3.20; F), mostly as a diffuse signal around the stipules and in sepals. At a 10μM concentration, plants showed intensification and persistence of p*HYD1*::GUS expression around the primary midvein and petioles of the rosette leaves (Fig. 3.20; G), where a transient signal is seen in untreated plants. There was also an increase of the diffuse sepal expression signal, but stamens were unaffected.

Cytokinin treatment appears to increase the activity of the *HYD1* promoter in both root and shoot tissues, with a loss of normal zonal resolution in root apices. In shoots the enhancement and persistence of the transient signal seen in the mesophyll of lateral organs in untreated plants is similar to the effects produced by inhibition of auxin transport described in section 3.3.3.2.

3.3.3.4 Exogenous ACC enhances *HYD1* gene promoter activity in primary roots and shows strong GUS expression in root hair cells.

To assess the response of reporter expression to ethylene, transgenic p*HYD1*::GUS plants were treated with the ethylene precursor ACC. Plants carrying the *HYD1* reporter, when treated with ACC, promoted strong GUS activity in the primary root apex, with 1μM, 10μM and 100μM concentrations giving a progressive increase in intensity (Fig. 3.21; A-D). Most intense histochemical localization was seen in a zone extending proximally from the columella to the site of root hair emergence. At lower concentrations, the reporter appeared to be differentially associated with root hair cells in the

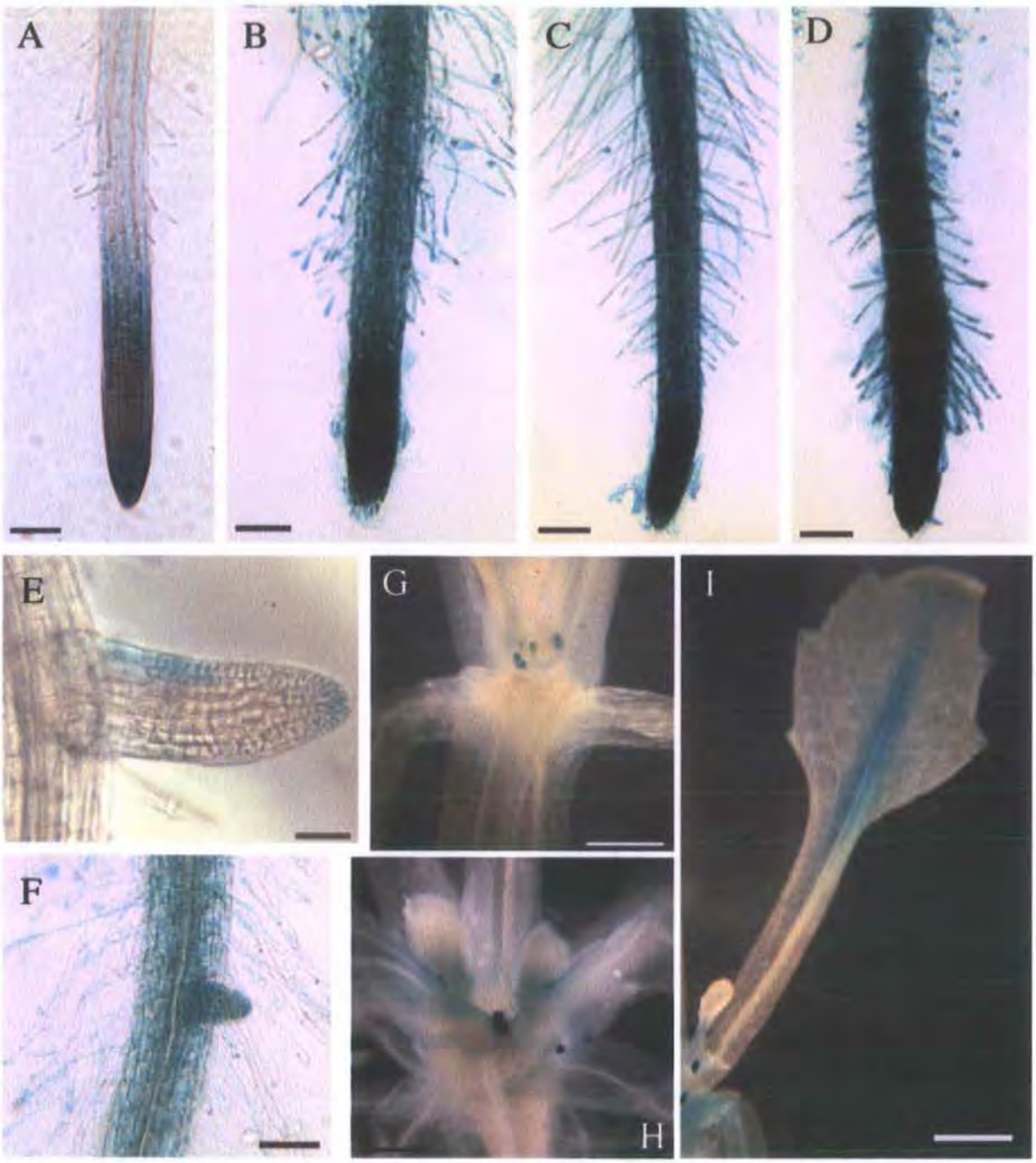

Figure 3.21 Response of the p*HYD1*::GUS reporter to exogenous ACC (ethylene precursor) treatment

A-D; primary root tips (A, untreated; B, 1μM, C, 10 μM and D, 100μM ACC), and E, F; laterals formed from the primary root (E; untreated lateral root, and F; lateral root grown in the presence of 1μM ACC).

Primary root apices showed increased p*HYD*1::GUS activity in response to increased ACC concentration. The main root epidermis and laterals had a diffusely increased signal, in association with enhanced root hair production and hair tip elongation.

In the shoot, stipules had an enhanced and less precisely localized GUS activity with addition of ACC (H; 1μM, I; 100μM), compared to untreated plants (G). Higher concentrations resulted in a persistence of diffuse activity around the primary midvein, as shown in I; this signal is seen transiently in the later expansion growth of untreated vegetative leaves. Note also in I that the hydathodes have retained a GUS signal; this was not seen during late leaf expansion in untreated plants.

A-F, bar = 100μm; G-I, bar = 0.5mm.

more mature tissues further from the apex (these cell files are just visible in Fig. 3.21; B and C). 100μM ACC treatment obscures this resolution, giving a dense GUS activity throughout the epidermis (Fig. 3.21; D) in association with ethylene-induced proliferation of root hairs (Tanimoto *et al.* 1995).

Lateral roots did not have the same intensity of signal response to ACC, though at all exogenous concentrations a diffuse, non-specific p*HYD1*::GUS activity was seen in emerging laterals (Fig. 3.21; F) at a younger stage than in untreated roots (Fig 3.21; E). Older portions of the main root were unaffected by lower concentrations of ACC, but at 100μM zones of strong GUS activity appeared in association with induced initiation of laterals.

In the shoot, ACC produced an enhanced expression in and around the stipules (Fig. 3.21; H) in comparison to untreated plants (Fig. 3.21; G), and a greater persistence of the transient signal seen in hydathodes, primary mid-vein and petioles of adult phase rosette leaves (Fig. 3.21; I). Inflorescences were unaffected.

The dose-responsive increase in intensity of p*HYD1*::GUS activity with addition of ACC suggests a direct enhancement of *HYD1* transcription by ethylene in all tissues in relation to the expression pattern seen in untreated plants. Positional cues do not appear to be modified, as areas showing reporter activity in untreated plants still show maxima on ACC, although with an enhanced background. An indirectly enhanced expression was also evident associated with ACC-induced proliferation of root hairs.

3.3.3.5 Inhibition of ethylene perception by silver ions causes a loss of cell-specific resolution in p*HYD1*::GUS expression

Silver ions (as silver thiosulphate) were used to inhibit ethylene perception; this treatment modified the position of reporter expression, and reduced cell-specific resolution of p*HYD1*::GUS in both primary and lateral root tips. Gus activity was induced uniformly from the root cap through the former zone of cell division (which lacks a signal in untreated roots) and into the root hair cell differentiation zone in both primary and lateral root apices (Fig. 3.22; B-C, E-F). This pattern spatially mimics the results found with ACC treatment, though was not dose-responsive, implying that the lower Ag^{++} concentration blocks all available ETR1 receptors. In contrast to the ACC-induced response, no resolution in the modulation of reporter expression was observed between primary and lateral root apices. The differential highlighting of trichoblast cell files seen in untreated plants was less obvious in samples grown in the presence of silver thiosulphate.

In contrast, shoot-specific changes were evident in response to the addition of silver ions. Adaxial trichomes, and mesophyll cells of the primary midvein and petiole in adult phase rosette leaves and cauline leaves, had an increased and prolonged persistence of GUS activity which increased incrementally in response to Ag^{++} application (Fig 3.23; C, D). An increased diffuse GUS signal was also noted in inflorescence stems around the branching nodes (Fig 3.23; E) and in the anthers and sepals of inflorescences (Fig 3.23; F).

Inhibition of ethylene perception by silver diminished resolution of cell-specific identity by p*HYD1*::GUS in roots, and prolonged the transient wave of GUS activity in shoots associated with later leaf expansion. Taken together with the responses to ethylene described in section 3.3.3.4, these results suggest an ethylene-responsive component to p*HYD1*::GUS expression in roots,

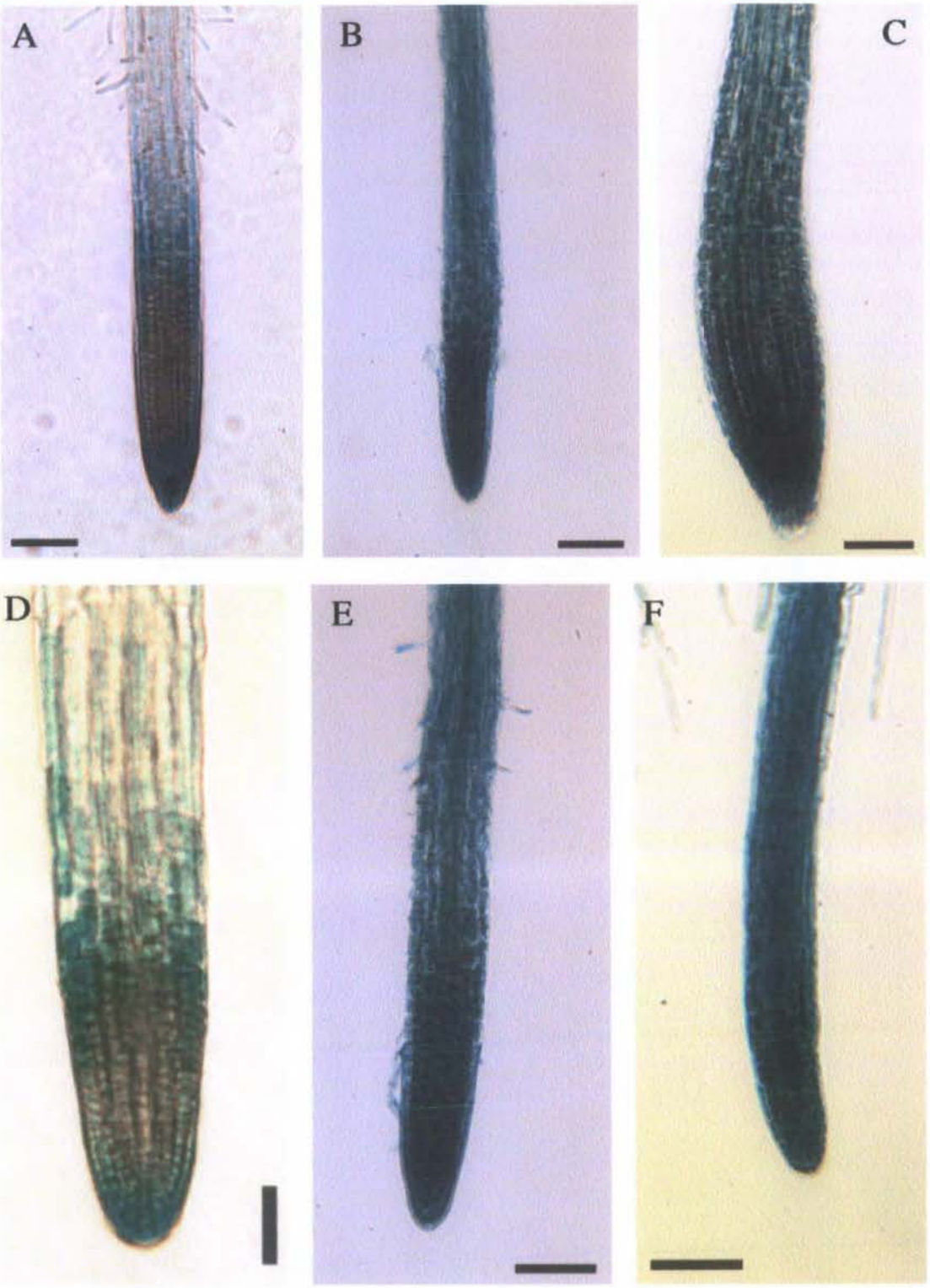

Figure 3.22 Effects of exogenous silver ions (inhibiting ethylene response) on p*HYD1*::GUS reporter activity in roots

Primary roots (A-C) showed a minimally increased, and lateral root tips (D-F) a strongly increased intensity of p*HYD1*::GUS expression around their apices, in response to the presence of silver ions. A, D, untreated roots; B, E, 10 μM, and C, F, 100μM silver thiosulphate.

A-F, bar = 100μm.

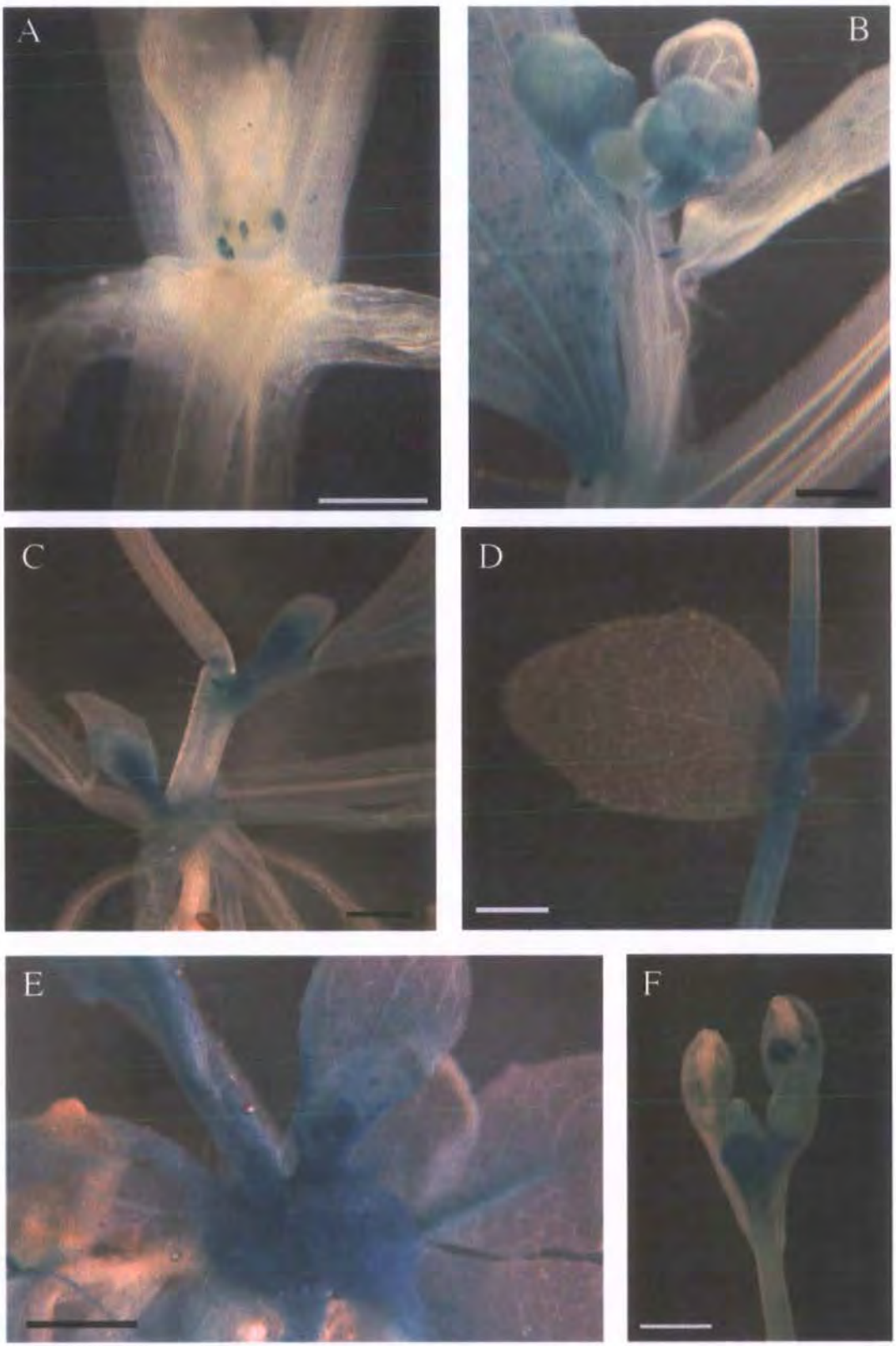

Figure 3.23 Effects of exogenous silver ions (inhibiting ethylene response) on p*HYD1*::GUS reporter activity in shoot tissues

Shoot tissues from seedlings grown on media containing silver thiosulphate resulted in a modified p*HYD1*::GUS reporter activity. Stipule regions and inflorescences showed an increased histochemical signal and an expanded distribution in response to increasing concentrations of exogenous Ag^{++} (C, 10μM; D, 100μM; E and F, 10μM) compared to untreated plants A, B).

A, bar = 0.5mm; B, bar = 0.25mm; C-F, bar = 1mm.

in a manner additive with cell-specific cues for positional transcription. Shoot expression is elevated both by enhanced ethylene levels and reduced ethylene perception, suggesting the activation of transcription via cross-talk between other signalling systems in aerial parts of the plant.

3.3.3.6 ABA treatment provokes reduced primary root expression, enhanced lateral root expression, and modifies the position of p*HYD1*::GUS in rosettes and inflorescence apices.

In the primary root apex, p*HYD1*::GUS expression appeared to become progressively less intense with increasing ABA treatment (Fig. 3.24; B-D), though this was difficult to interpret at lower concentrations by visual analysis, (Fig. 3.24 B and C). There was also some variation between plant samples in the modulation of GUS activity by ABA.

In contrast, p*HYD1*::GUS activity in lateral (Fig. 3.24; F-I) and anchor root tips (Fig. 3.24; E) showed an obvious and concentration-dependent enhancement of expression with application of ABA. At lower exogenous ABA concentrations (Fig. 3.24; G, H) a diffuse, apparently non-specific GUS activity is seen throughout the root apex. At 10μM exogenous ABA, a very strong signal is induced, extending throughout the apex from the columella to the zone of cell extension in all young lateral roots (Fig. 3.24; H). In anchor root apices, this was modulated in association with the shortened and slightly radially-swollen morphology resulting from ABA treatment (shown in Fig. 3.24; E).

In shoots, growth in the presence of exogenous ABA resulted in increased diffuse staining around rosette stipules (Fig. 3.25; B, C) and around the primary mid-vein of the rosette leaves. This was more pronounced in juvenile

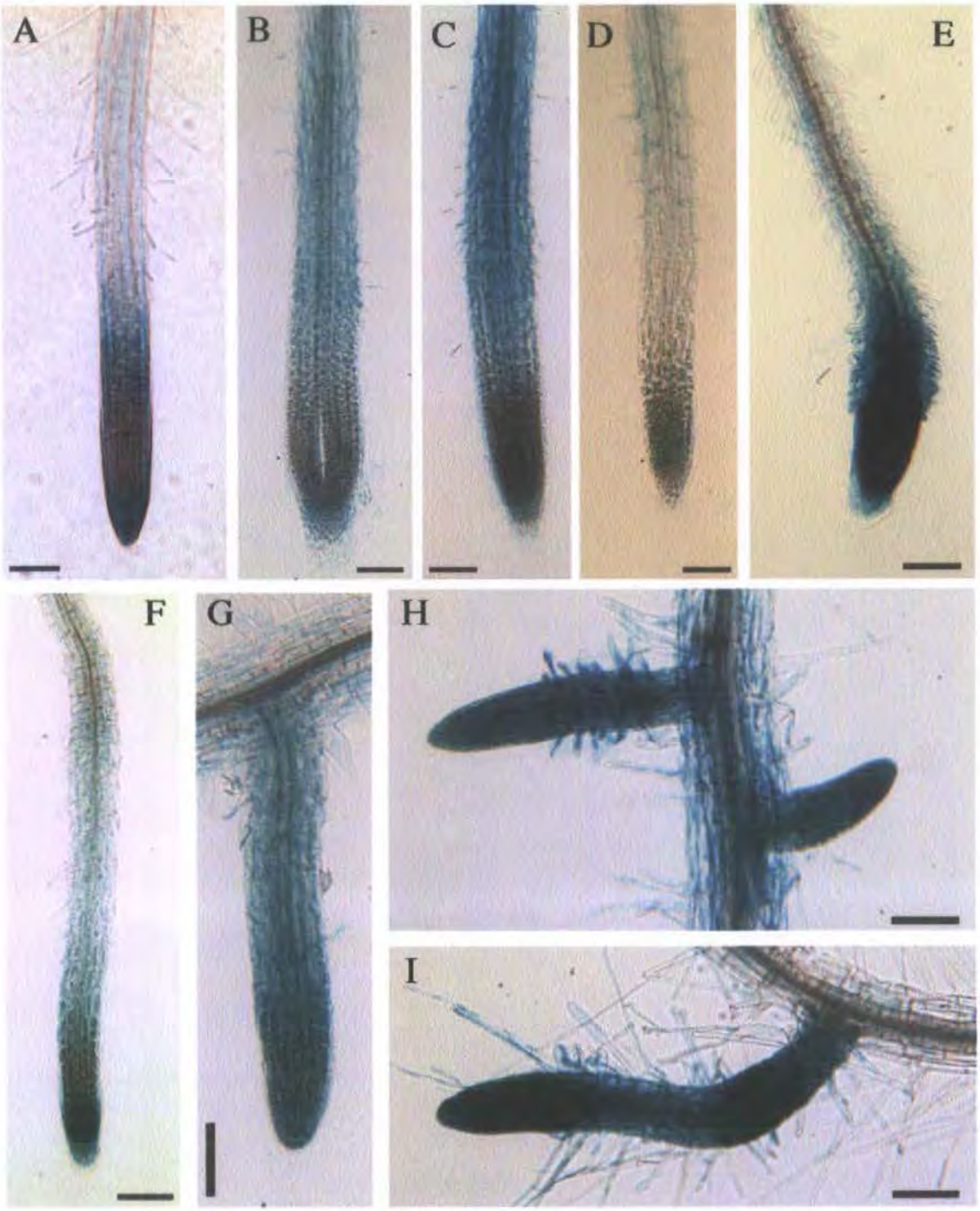

Figure 3.24 Response of p*HYD1*::GUS root expression to exogenous ABA treatment

Primary (A-D), anchor (E) and lateral root tips (F-I) in plants expressing the p*HYD1*::GUS reporter construct, in the presence of varying concentrations of exogenous ABA, as follows. A and F, no treatment; B and G, 0.1μM; C and H, 1 μM; D, E and I, 10μM.

The ABA-treated primary root tips B-D appeared to have reduced GUS activity in response to 10μm ABA, but lower concentrations did not show conclusively modulated expression when compared to the primary tip from an untreated treated plant (A). In contrast, a strong increased expression was seen in the tips of anchor roots (as in E) and young laterals from the main root (G-I), compared to the untreated young lateral (F).

Bar = 100μm.

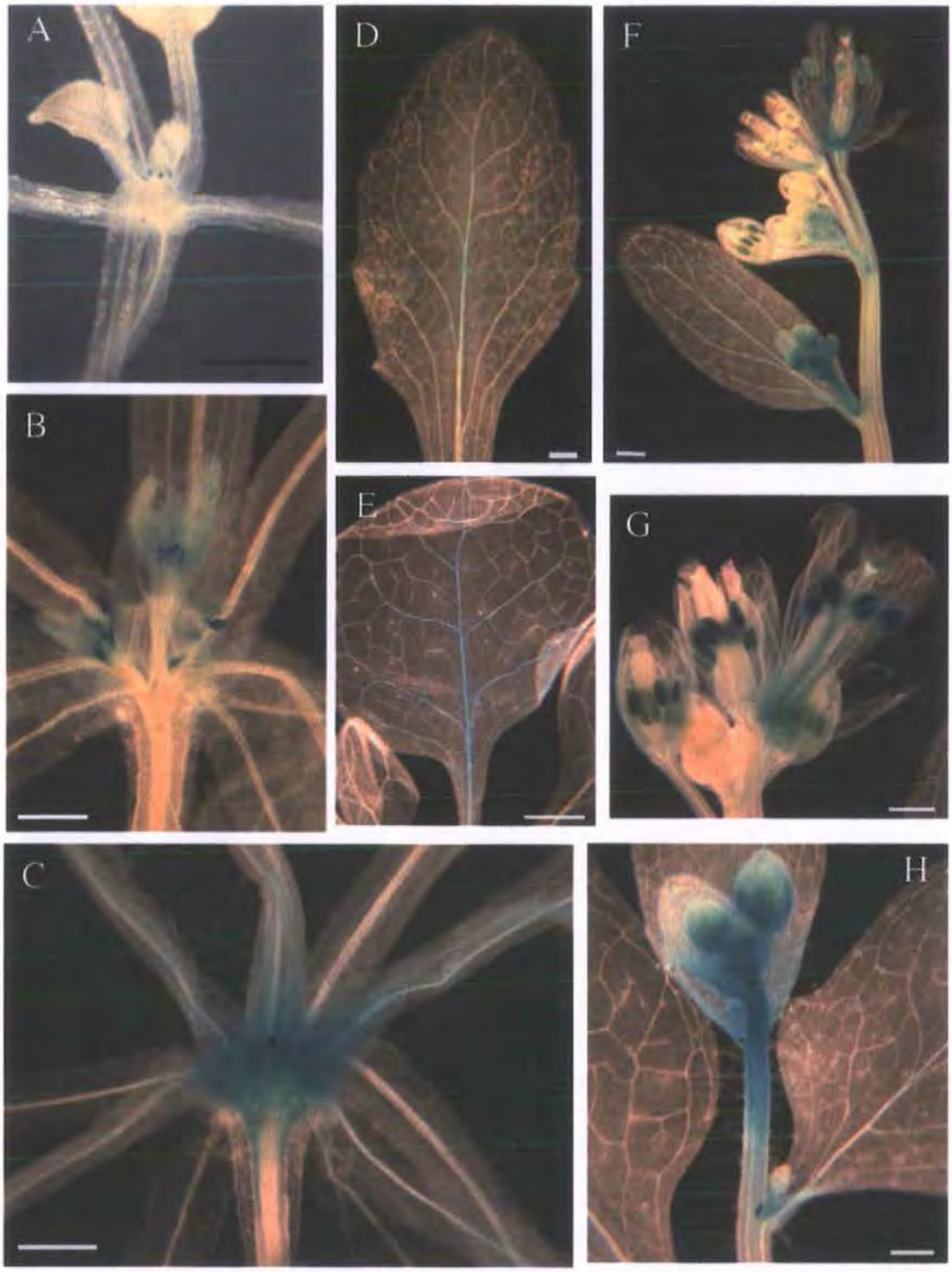

Figure 3.25 Response of shoot activity of the p*HYD1*::GUS reporter to exogenous ABA treatment

Exogenous ABA causes increased expression of p*HYD1*::GUS in and around rosette stipules B, 0.1μM), and petiole bases and the inner cell layers of the upper hypocotyl (C, 10μM) compared to untreated plants (A). In rosette leaves, low ABA concentrations promoted a diffuse staining around the primary mid-vein (D; 5th true leaf, 0.1μM), which resolved to the lower order vasculature at higher concentrations, particularly in juvenile leaves (E; 2nd true leaf, 10 μM). In the inflorescence, increased staining was seen in anthers, filaments, sepals and terminal inflorescence stems (F, 0.1μM; G, 1μM and H, 10μM ABA).

A, bar = 1mm; B-H, bar = 0.5mm.

than adult phase leaves (Fig. 3.25; D, E), and resolved into the lower order vasculature at higher ABA concentrations. Stronger histochemical activity was also evident in the stem apices of inflorescence branches (Fig. 3.25; F, H) in young sepals, and in maturing anthers and filaments (Fig. 3.25; G).

This analysis suggests that ABA modulates reporter expression in roots by enhancing expression in lateral apices whilst not affecting or reducing staining in the primary root tip. Enhanced GUS activity was also evident in shoot tissues, particularly in stem apices, with a strong signal in anthers. Higher concentrations of exogenous ABA resulted in the displacement of the GUS signal into vascular strands of juvenile but not adult phase rosette leaves. This phenomenon is distinct from the expression pattern observed in untreated plants, and may indicate a differential response to hormonal or positional cues between juvenile and adult leaf phases in the presence of high ABA concentrations.

3.3.3.7 GA treatment reduces p*HYD1*::GUS activity in primary roots, has no affect on lateral root expression, and enhances the signal in inflorescence apices

In p*HYD1*::GUS roots treated with increasing concentrations of GA_3, the patterning of reporter expression was unaffected, although the intensity of signal diminished in the main root hair cell files and around the primary root tip (Fig. 3.27; A, C-E). Lateral roots appeared unaffected by the addition of GA_3 (Fig. 3.27; B, F-G). In contrast, shoot expression demonstrated a strong up-regulation in the apical portions of inflorescence stems, in stems at cauline branch nodes, and in the young sepals and anther filaments of inflorescences (Fig. 3.27; H-K). Rosette leaves were unaffected. This strong shoot response was evident at the lowest concentrations of additional GA_3 used (0.1μM, shown

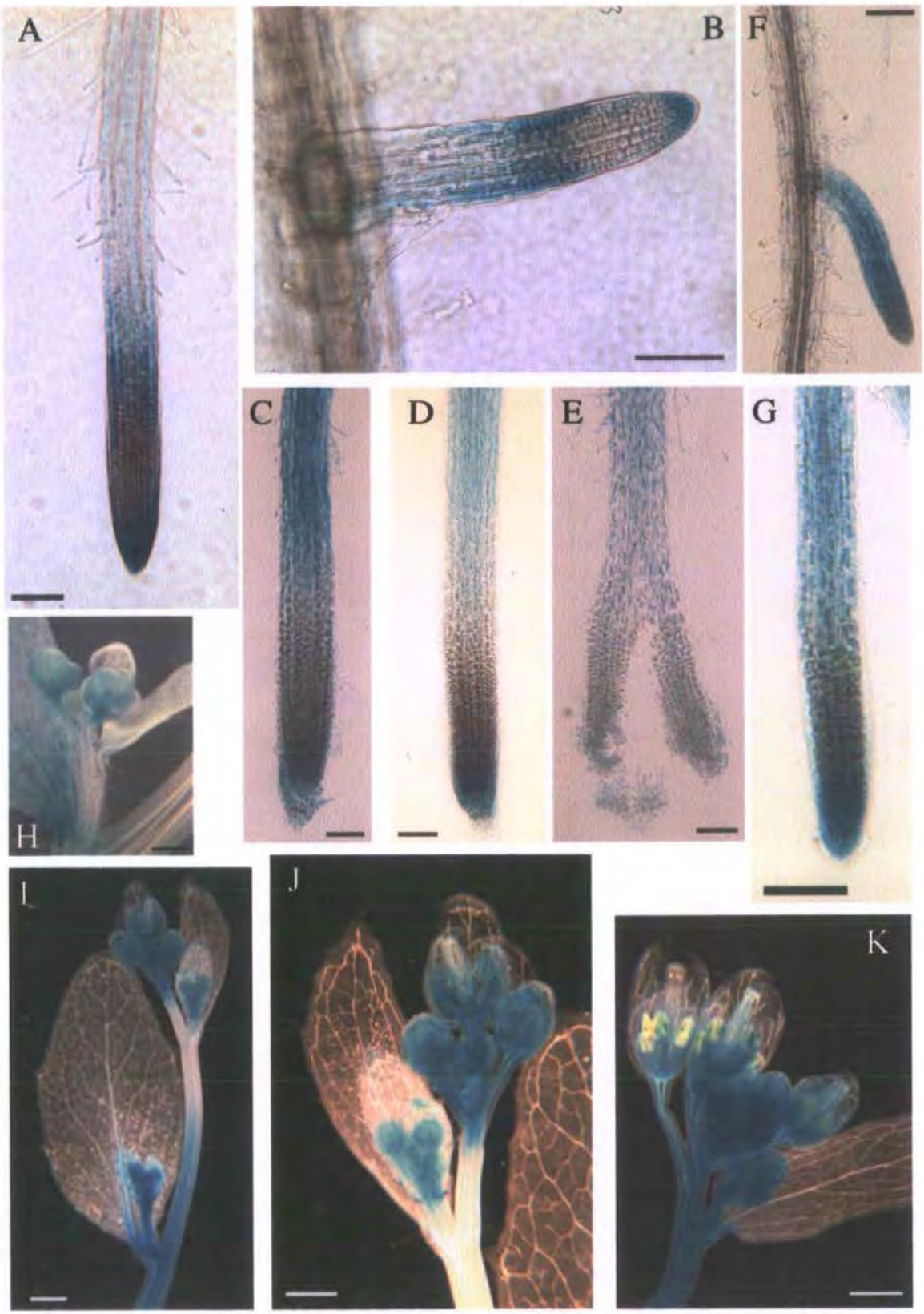

Figure 3.27 Modulation of p*HYD1*::GUS activity in response to exogenous GA_3

Untreated primary (A) and lateral (B) root tips, compared to roots from plants treated with GA_3. Primary roots treated with 0.1 μM (C), 1μM (D) and 10μM (E) demonstrated a reduced intensity of expression with increasing GA, whilst laterals (F; 0.1 μM and G; 10μM) appeared unaffected. Inflorescences showed a more intense histochemical activity with additional GA_3 (I, 0.1 μM; J, 1μM and K, 10μM) when compared with untreated plants (H).

A-G, bar = 100μm; H, bar = 0.25mm; I-K, bar = 0.5mm.

in Fig. 3.27; I), and was not visibly enhanced by further addition of exogenous hormone.

Morphology and positional information appeared normal in GA-treated plants, hence it seems likely that these results indicate a GA responsive component to p*HYD1*::GUS expression, which has opposite effects in the root and shoot. The reporter response in GA-treated root tips showed a similar dose responsive decrease in primary apices, but a differential response in laterals, where ABA treatment increased GUS activity but GA did not affect it. This means that the well documented effect of these two hormones is not reflected in modulation of *HYD1* promoter activity in root tissues. Neither is this antagonism apparent in p*HYD1*::GUS shoots, as both treatments enhanced staining in terminal inflorescence apices, though this was more marked with GA than ABA. However staining rosette leaves did not show an obvious GA-responsive component, as was seen with ABA treatment.

3.3.3.8 Epibrassinolide up-regulates p*HYD1*::GUS expression in lateral root apices

Exogenous addition of 0.1µm, 1µm and 10µm epibrassinolide (EBR) produced a dwarfed seedling morphology and modification of root form, as previously reported (Clouse *et al.* 1993; Clouse and Sasse, 1998; Müssig *et al* 2003), though did not significantly modulate the location of signal produced by the p*HYD1*::GUS construct. Primary roots and the mature tissues of the main root appeared to show a slightly reduced GUS signal intensity with the addition of EBR (Fig. 3.28; A-D), though this was not clearly dose-responsive in the samples examined. In contrast, lateral root tip GUS activity intensified in direct response to increased exogenous EBR (Fig. 3.28; E-J). Reporter activity was strongest in the lateral root cap, and was so intense in 10µM treated lateral root apices that the zonal resolution seen in untreated lateral apices

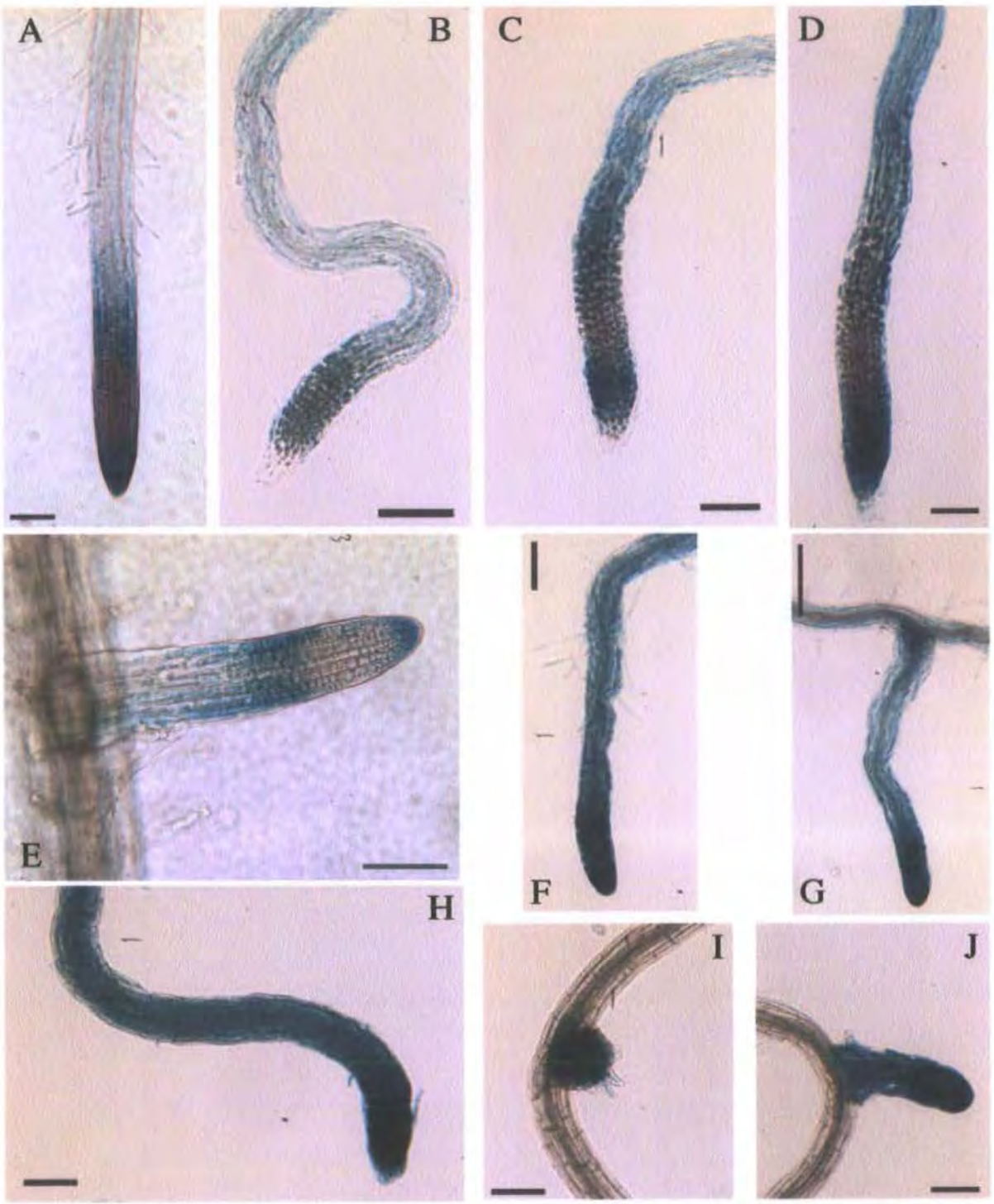

Figure 3.28 p*HYD1*::GUS activity in response to exogenous Epibrassinolide

A-D, primary root tips and E-J, laterals; A and E are untreated controls. All other roots are from plants treated with epibrassinolide as follows; B and F, 0.1μM; C and G, 1μM; H-J, 10μM.

Primary root tips appeared slightly paler than controls in response to increased exogenous phytohormone, whilst laterals showed a strong increase of p*HYD1*::GUS expression. The zonation seen in untreated lateral root apices was much less distinct in treated plants, where strong GUS activity extended proximally from the root cap into differentiating trichoblast cell files.

Bar = 100μm.

could no longer be seen (Fig. 3.28; J). These findings imply a modulation of transcription of *HYD1* in roots by EBR, with distinct effects between primary and lateral root apices, but no affect on shoot expression.

3.3.4 *HYDRA1* gene expression is driven by conserved sequences within 1kb, and modulated by phytohormones within 2kb upstream of the transcriptional start.

3.3.4.1 Developmental expression in driven mostly by promoter elements within 1kb upstream of the HYDRA1 gene

All p*HYD1*::GUS constructs (Columbia -1.2kb, Ws -2kb, Ws -834bp, and Ws -482bp) were analyzed for developmental expression, with the exception of the shortest construct (Ws -215bp), which showed no GUS activity at any developmental stage. Table 3.3 summarizes the expression patterns for these constructs, defining comparative GUS intensity on a subjective scale from "very weak" to "strong".

The general expression pattern is similar in roots for all promoter sequences, with a slightly stronger signal discernable in lateral root apices than primary apices (lateral root tips are the first structures to show visible GUS activity during X-Gluc incubation for all reporters). The Ws -2kb promoter maintains a signal more strongly in mature root tissues than the other promoters.

Shoot expression was also similar between the longer promoters, whilst shoot transcription of the -482bp sequence was mostly confined to the stipules. All

Table 3.3 Comparison of deletion constructs for p*HYD1*::GUS

Tissue	Promoter			
	Col -1.2kb	Ws -2kb	Ws -834bp	Ws -482bp
ROOTS				
Primary root cap	+ + +	+ + +	+ + +	+ + +
Lateral root cap	+ + + +	+ + + +	+ + + +	+ + + +
Cell division zone	-	-	-	-
Differentiation zone	+ + +	+ + +	+ + +	+ + +
Maturing trichoblasts	+	+ +	+	+
HYPOCOTYL				
Hypocotyl guard cells	+ transient	+ transient	-	-
Hypocotyl cortex	+ + transient	+ + transient	-	-
COTYLEDONS				
Hydathode mesophyll	+ transient	+ transient	+ transient	-
Young guard cells	+ transient	+ transient	+ transient	-
ROSETTE				
Stipules	+ + + +	+ + + +	+ + + +	+ + + +
1st true leaf trichomes	+ transient	+ transient	+ transient	+ transient
3rd true leaf trichomes	+ transient	+ transient	+ transient	+ transient
6th true leaf; trichomes	+ + transient	+ + + transient	-	-
midvein mesophyll	+ + transient	+ + transient	-	-
petiole mesophyll	+ + transient	+ + transient	-	-
petiole guard cells	+ transient	+ transient	-	-
CAULINE LEAVES				
Stipules	+ + + +	+ + + +	+ + + +	+ + + +
Hydathodes	+ transient	+ transient	-	-
Trichomes	+ + transient	+ + + transient	-	-
Guard cells	+ transient	+ transient	-	-
Margin cells	+ transient	+ transient	-	-
Mesophyll	+ + transient	+ + transient	-	-
INFLORESCENCE				
Stem apex	+	+ +	-	-
Stem epidermis	+	+	-	-
Stem trichomes	+	+ +	-	-
Sepals	+ + transient	+ + transient	+ transient	+ transient
Petals	-	-	-	-
Anthers	+ +	+ + +	+	+
Filaments	+ +	+ + +	-	-
Pollen	+ + + +	+ + + +	+ + + +	+ + + +
Carpels	-	-	-	-
Silique	+ + + +	+ + + +	+ + + +	+ + + +
EMBRYOS				
Globular	+	+	+	+
Heart	+ +	+ +	+ +	+ +
Torpedo	+	+	+	+

Key; - = no GUS activity detected, + = very weak activity, + + = weak activity, + + + = clear GUS signal, + + + + = strong signal.

constructs had strong and persistent GUS activity in stipules of all true leaves, and in anthers, pollen and siliques. Trichomes were highlighted in both rosette and cauline leaves by all promoters other than the -482bp promoter, which also lacked the transient diffuse signal seen in sepals and cotyledons. The full-length Col-0 and Ws promoters, and the -834bp promoter, produced transient GUS activity in the mesophyll around the midvein and petiole of maturing rosette leaves and cauline laminas, although staining was not as intense in the -834bp construct. These mesophyll signals were coordinated with differentiation of functional cells in the epidermis, implying a role for *HYDRA1* in inter-layer communication, and possibly with the generation of appropriate spacing during centrolateral expansion in leaves.

All constructs produced a strong signal in developing pollen grains, and a transient GUS activity throughout the embryo proper in the globular and heart stages of embryogenesis.

3.3.4.2 The Ws -2kb promoter contains elements that respond to signalling cues within the plant body

As shown in Table 3.3, general expression was similar in most tissues for all constructs in the *HYD1* deletion series in the absence of exogenous hormone and inhibitor treatments, with the highest degree of signal similarity in root tissues and embryos. The full-length Col-0 promoter construct and the shorter Ws (-834 and -482bp) reporters were also treated with exogenous phytohormone and inhibitor compounds, as described in section 3.3.4.1 above. Not all of the deletion series showed the changes in expression observed in the full-length Ws-2kb construct. The observed responses of these different promoters are summarized in Table 3.4. Histochemical localization in the root apices showed most similarity between constructs, with a maintenance of the differential responses seen between primary and lateral roots.

Tissue	1-NAA	2-NAA	TIBA	1-NOA	BAP	ACC	Ag++	ABA	GA_3	EBR
Col -1.2kb										
Primary root	+++	+	++			+++				
Lateral root	+++	+	+++	+		+				
Rosette			+	+	+	+				
Cauline/stem			+			+				
Inflorescence				+		+				
Ws -2kb										
Primary root	+++	+	++		++	+++	++	-	-	-
Lateral root	+++	+	+++	++	++	+	++	+++		+++
Rosette			+	+	++	+	+	+		
Cauline/stem			+		+	+	+	+	++	
Inflorescence				+	+	+		++	+++	
Ws -834bp										
Primary root	+++	+	+						-	
Lateral root	+++	+	++						-	
Rosette					+				-	
Cauline/stem						-			-	
Inflorescence						-				
Ws -482bp										
Primary root	+++	+	+							
Lateral root	+++	+	++							
Rosette					+					
Cauline/stem						-				
Inflorescence						-				

Table 3.4 Comparison of p*HYD1*::GUS deletion responses to exogenous phytohormone and inhibitor treatments

Key; [blank] = no change from untreated plants, + = increased activity, + + =strongly increased activity,
+ + + = very strongly increased activity, - = reduced activity.

Auxin (NAA) treatment affected all constructs by elevating expression in root tips, in association with the auxin-induced morphological changes and enhanced lateral initiation. Inhibition of auxin transport produced some similarities in root expression from all promoters, suggesting that auxin is providing positional cues which affect the root localization of p*HYD1*::GUS even though reporter activity in roots was not auxin dose-responsive. The impacts to shoot expression of altered auxin distribution through transport disruption (TIBA and 1-NOA) were evident only in the Col-0 and Ws full length promoter sequences. This could suggest a more direct shoot-based response to auxin signalling, controlled by elements beyond -834bp upstream from the transcriptional start.

Treatment with cytokinin (BAP) induced a strong response in Ws -2kb root apices, and around the primary mid-vein and petioles of older rosette leaves and cauline leaves. The Col-0, -834 and -482 Ws promoters exhibited no discernable response to treatment in root expression, and showed only a slight increase in the rosette stipule signal. This could suggest that a cytokinin responsive element is present in the unique section of the -2kb Ws promoter.

Elevated levels of ethylene (as ACC) produced similar strong root expression from both WS and Col-0 full-length promoters, and an increased signal intensity around stipules with these constructs. The shorter Ws constructs showed no modification in root GUS expression with ACC treatment, and the shoot signal was unaffected in rosettes, with a possible reduction in the diffuse activity seen in inflorescence apices and sepals. Treatment with Ag^{++} ions to decrease ethylene signal perception resulted in some elevated root expression from the Ws -2kb promoter, with a loss of the zonation present in untreated root tips. Again this modulation was not seen in the roots of the Col-0 or shorter Ws reporters. The promoter segment common to Ws-2kb and Col-1.2kb may therefore contain an ethylene responsive element, though the response to silver ions suggests that the Ws -2kb unique region carries

elements responding to signalling systems active in a reduced ethylene environment, perhaps with a role in defining positional cues in the root.

An ABA response was raised solely from the Ws -2KB promoter, with no changes obvious in plants carrying the other constructs. This suggests the presence of a positive-responding ABA element in the unique Ws promoter sequence.

GA treatment produced increased transcription of p*HYD1*::GUS in the apices of inflorescence branches with the Ws -2kb promoter, and a slight diminishing of signal in primary roots but not lateral roots. The Col-0 and Ws -482 promoters showed no change in expression when compared to untreated plants, but the Ws -834 promoter lost its stipule signal in the rosette. Because the Col and Ws-2kb promoters, and the shorter -482bp promoter all have normal stipule expression with GA treatment, it appears likely that this is an artefact peculiar to the -834bp plant line. Alternatively, though it could result from a repressor element in the -834 sequence, which is overridden by elements in the full length promoters.

The sequence unique to the Ws-2kb promoter appears to carry a positive cis-acting element which up-regulates reporter expression in lateral roots in response to epibrassinolide. No change in either shoot or root expression was noted in the other promoter constructs.

The observations described in sections 3.3.4.1 and 3.3.4.2 are summarized in Fig. 3.29. This scheme shows the full-length -2kb Ws promoter, annotated to show the regions containing the transcriptional instructions defined by this analysis, and further information from section 3.3.4.3 below.

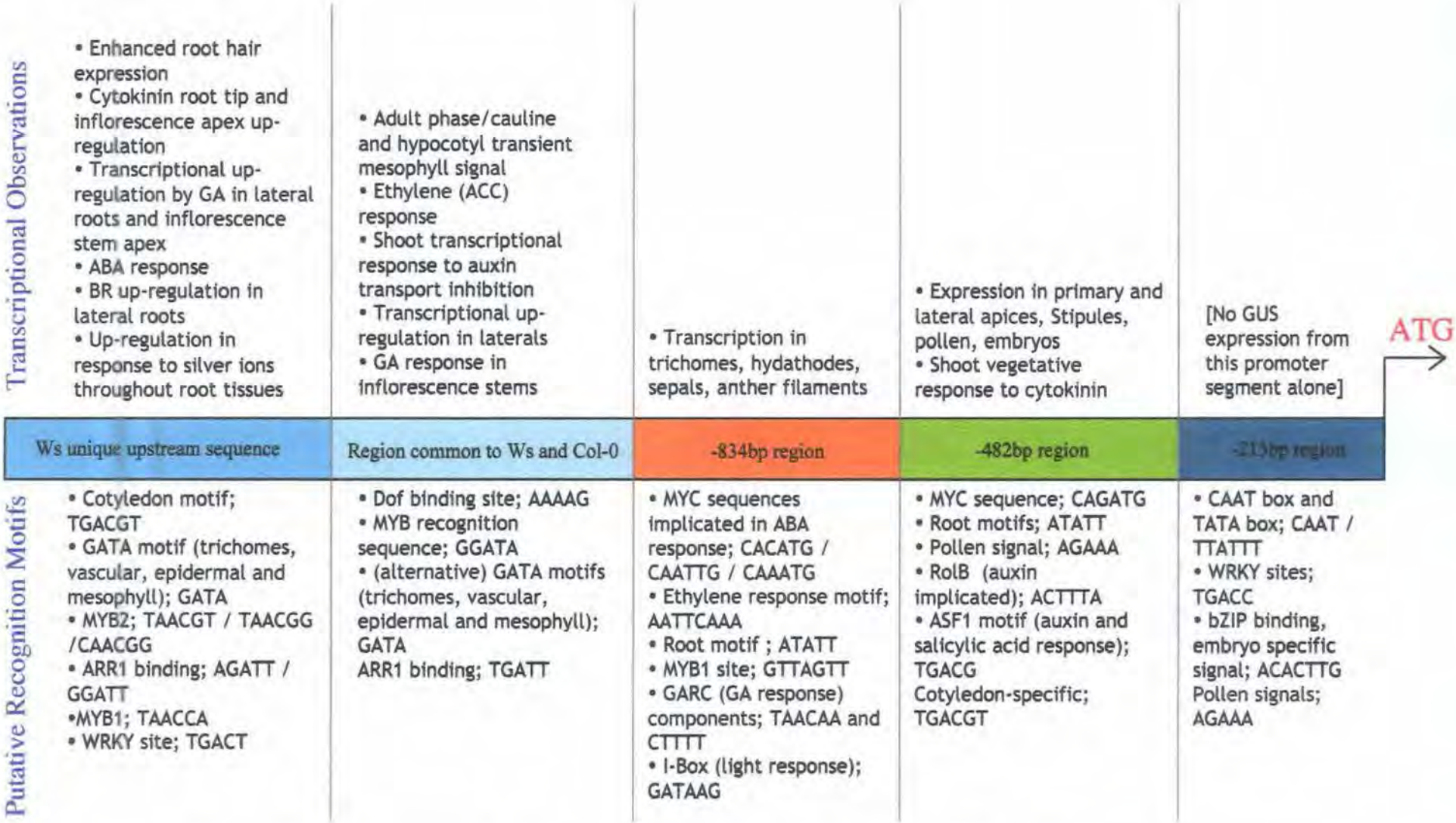

Figure 3.29 Annotated scheme of the *HYD1* -2kb promoter from Ws

3.3.4.3 Putative cis-acting elements are present in the *HYDRA1* promoter

The Ws -2kb promoter sequence was examined for the presence of putative transcriptional recognition motifs and cis-acting elements. Sequence analysis was performed using the PLACE database (after Higo *et al.* 1999), using the online search facility at www.dna.affrc.go.jp/PLACE. A selection of the putative motifs returned by this search are noted as annotations in Fig. 3.4, and their positions in the Ws -2kb sequence are highlighted in Appendix 4. These findings are summarized below, grouped according to function. Where a number of possible motifs are present, such as in the case of TATA and CAAT boxes, only the most likely functional examples have been included in the selection and described below.

Initiation of transcription

The first -150bp of the *HYD1* promoter contains a putative CAAT box activating sequence (Shirsat *et al.* 1989). This is 14bp upstream of a putative TATA box, the binding site for RNA polymerase II. This TATA motif, found at -160bp from the translational start in the *HYD1* promoter sequence, is equivalent to that of a glutamine synthetase gene from *Pisum sativum* (Tjaden *et al* 1995). The CAAT and TATA putative sites were present in both the Ws and Col-0 promoter sequences.

Positional information and signalling response motifs

A number of putative recognition sequences thought to specify transcription in specific tissues during plant development were found by searching the database.

Several GATA motifs are present upstream of the -482bp primer binding site in both Ws and Col-0. They are associated with tissue specific expression in trichomes, vascular elements, epidermal and mesophyll cells, and are also

light-regulated (reviewed by Gilmartin *et al.* 1990). If these sequences are active in the *HYD1* gene promoter, then their additive effects and position offers an explanation as to why leaf and shoot expression is weaker in the -834bp construct, and confined to stipules in the -482bp construct. The light-responsive component could also contribute to the stronger staining seen in greenhouse-grown material, as compared to seedlings raised under artificial light.

Two WRKY transcription factor binding motifs are present in the Ws and Col-0 common promoter sequence close to the transcriptional start, with an additional site present upstream in the Ws unique sequence. WRKY transcription factors are involved in various signalling pathways in plants, including salicylic acid-induced pathogenesis response (Yu *et al* 2001), GA-implicated sugar responses (Sun *et al* 2003) and transcriptional responses to environmental stress (Chen *et al.* 2002).

There are copies of the motif AAAAG in both Col-0 and Ws promoters within the first -1kb; this sequence was found to be a recognition motif in maize for Dof proteins; a subclass of zinc finger transcription factors implicated in the control of guard cell specific gene expression (Plesch *et al.* 2001). Dof transcription factors are unique to plants, and several of their typical binding motifs can be seen in the *HYD1* promoter. They regulate many types of genes, and may contribute to stimulus-response and tissue-specific gene expression (Yanagisawa and Schmidt, 1999; Yanagisawa 2000). The location of Dof binding motifs in the *HYD1* promoter is consistent with the transient expression seen in developing guard cells of the -834bp promoter and full-length constructs.

A pollen-specific transcriptional activating sequence (AGAAA) isolated from tomato (Bate and Twell, 1998), is present six times within the first -400bp upstream of the *HYD1* promoter, and could explain the strong expression of p*HYD1*::GUS in developing pollen grains. Similarly, a cotyledon-specific

element isolated from *Vigna mungo* (Yamauchi 2001) is present within the first -250bp, and could contribute to the transient staining seen in cotyledons. However activity of the -482bp promoter did not include an obvious cotyledon signal, and so this element, if active, is not the only motif required to activate transcription in cotyledons.

The ATATT motif, first found in the 35S promoter, has been evaluated in tobacco, and found to confer root-specific expression (Elmayan and Tepfer, 1995). Multiple copies of this motif are present within the first -800bp of the *HYD1* promoter though are absent in the first -215bp segment; additional copies are found in the upstream sequence unique to the Ws-2kb promoter. These motifs may contribute both to the distinctive root expression activity seen in all but the -215bp promoter construct, and could be involved in the persistence of the signal seen in mature root hair cells of the Ws-2kb construct.

Another set of putative root-specific motifs is represented by the AAGAT and CTCTT sequences, found in both Ws and Col promoters between -800 and -400bp from the transcriptional start. These sequences were isolated as putative binding sites for nodulin proteins in soya bean (Sandal *et al.* 1987; Stougaard *et al.* 1990). They have been associated with root organ-specific expression in infected cells of root nodules, and are present in the promoters of leghaemoglobin genes in *Vicia faba; Medicago truncatula; Glycine max* and *Sesbania rostrata* (Vieweg *et al.* 2004; Fehlberg *et al.* 2005).

One copy of the ACACTTG motif is found in both the Ws and Col sequences, within the first -200bp of the transcriptional start. This sequence was identified in the carrot *Dc3* gene promoter; it usually confers embryo-specific gene expression, and is thought to bind bZIP transcription factors (Kim *et al* 1997). The bZIP ("leucine zipper") transcription factors are also implicated in transcriptional responses to ABA in *Arabidopsis*; for instance the *ABI5* gene

encodes a bZIP protein which regulates a number of genes active during later embryogenesis (Finkelstein and Lynch, 2000; Lopez-Molina and Chua, 2000).

Other putative binding sequences for MYB, and MYC transcription factors, an ARR1 (cytokinin response) sequence, an ethylene response motif, and putative auxin response contributory elements are present within the *HYD1* promoter.

3.3.5 Summary of Results from Chapter 3

The earliest expression seen from the p*HYD1*::GUS reporter is during the development of the globular embryo, when the radial axis is established. Post-germination promoter activity highlights radially-positioned cells and organs such as root trichoblasts and stipules, and is expressed as a radial gradient across the differentiation zone of root apices.

In shoot tissues, the pHYD1::GUS reporter also defines fields of cells at stages of inter-layer co-ordination during centrolateral expansion of photosynthetic lateral organs (cotyledons, rosette leaves, cauline leaves and sepals), and during the expansion growth of longitudinally oriented cell files in petioles, stem apices, anther filaments and siliques. This signal is most distinct in adult phase leaves, which have greater vascular patterning complexity than juvenile leaves. The *HYD1* promoter activity seen in the young hypocotyl, cotyledon hydathode region, and during later leaf expansion, is associated with differentiation of functional epidermal cells (trichoblasts, trichomes and guard cells), and cells from the associated sub-epidermal layers. This activity was absent during the transient diffuse signal associated with organ expansion of sepals and siliques, even though both have stomata, and sepals possess trichomes.

Cotyledons and sepals both have a very simplified vascular patterning comprising only primary and secondary order vascular strands; they also lack stipules. Sepals differ from cotyledons in that they lack an apical hydathode,

and their vascular patterning can have both open and closed loops (shown in Fig. 4.1.7, K and L.). These simple lateral organs showed the weakest and most transient GUS signal.

Reporter expression suggests a role for the HYD1 protein during angiogenesis and pollen development. Transcription may also be increased in response to light, and may be synchronized with the onset of photosynthetic competence in lateral organs. Petals lacked a GUS signal; they are notable as the only dorsiventrally flattened lateral organs in *Arabidopsis* which are neither transpirationally or photosynthetically active. They neither develop stomata, nor contain chlorophyll.

HYD1 promoter activity was modulated by exogenous phytohormone treatments in both root and shoot tissues, though not always in the same manner. Expression was not found to be clearly responsive to exogenous auxin, but was modified by auxin-associated changes in positional information. Cytokinin treatment increased transcription in both roots and shoot tissues, and modified the signal's position in roots. Ethylene provoked a substantial increase of p*HYD1*::GUS expression in the primary root, and alteration of ethylene levels modified pattern resolution in both primary and lateral root apices. The aerial parts of the plant showed increased expression with both higher and lower ethylene levels, suggesting interaction with other signalling systems. Exogenous GA and ABA appeared to have antagonistic effects on reporter activity in roots but not in shoot tissues. Transcriptional responses were differentiated between primary and lateral root tissues by exogenous inhibitors of auxin transport, ethylene, ABA, GA and BR, but not by auxin or cytokinin.

The *HYD1* gene promoter contains putative cis-acting motifs which correlate with some aspects of the developmental expression of its molecular reporter, and which may contribute to the modulation of this expression by endogenous plant phytohormone and morphogenic signalling systems.

3.4 Discussion

3.4.1 Developmental activity of the pHYD1::GUS promoter-reporter

3.4.1.1 *HYD1* promoter-reporter activity has a radial and temporally modulated distribution

The first transcription activity from the p*HYD1*::GUS reporter is found in the early globular embryo, where a transient diffuse signal is seen throughout the embryo proper. This activity corresponds to the first signs of cellular patterning anomalies in the plant body of both *hydra* mutants (Topping *et al.* 1997, Schrick *et al.* 2000), and is synchronized with the appearance of molecular genetic signals which resolve and pattern cell layers across the radial axis (Helariutta *et al.* 2000, Nakajima *et al.* 2001, Di Laurenzio *et al.* 1996).

HYD1 transcription is strongly active in the root cap and epidermis close to the root apex, with a reduced but distinct signal in the adjacent cortex and endodermis at the point of coordinated cell differentiation across the radial axis. A similar low level signal then appears briefly in the vascular stele in a non-cell specific manner, before fading as the root enters the expansion phase. This signal therefore constitutes a radial gradient, strongest in the differentiating epidermis, and decreasing in intensity through the inner layers towards the centre. Pattern definition in these cells is coordinated by cues defining positional information between these radial layers in *Arabidopsis* (Berger *et al.* 1998a, Schellmann *et al.* 2002, Rerie *et al.* 1994, Massucci *et al.* 1996).

The epidermis of wild-type rosette and cauline leaves are differentially patterned across the radial axis, with trichomes appearing preferentially on adaxial surfaces in young leaves, and modulating their position according to developmental phase (Telfer *et al.* 1997, Chien & Sussex 1996). The p*HYD1*::GUS signal appears early in trichome differentiation, and is visible in these cells from early expansion of the first pair of rosette leaves. In the mid-phase of leaf expansion, both rosette and cauline leaves show GUS activity in trichomes and differentiating stomata, along with cells of the mesophyll beneath. A later mesophyll signal progresses down the leaf longitudinal axis in a basipetal fashion, prior to later laminar expansion and maturation. Activity was also found in inflorescence stem apices, sepals and siliques, where a transient signal, associated with the mesophyll, was noted and developed in these organs during the rapid expansion phase.

3.4.1.2 Vegetative and cauline leaves resolve a strong and persistent *HYD1* transcription in stipules from early in leaf formation, establishing gene activity at radial positions around the shoot axis.

Auxin has long been implicated in patterning around the shoot apex, and has recently been reinterpreted as a radial rather than apical-basal signal by Reinhardt *et al.* (2000). Expression of the auxin-responsive DR5::GUS reporter commences first in stipules and later in hydathodes of the developing *Arabidopsis* leaf (Aloni *et al.* 2003), interpreted by these authors as indicating the production of free auxin in at these sites. DR5 develops a persistent signal in the apical hydathode, but not in lateral hydathodes until after xylem differentiation of the primary midvein (Aloni *et al.* 2003). The DR5 stipule signal is absent from the youngest and oldest leaves of the mature rosette.

In contrast with DR5, p*HYD1*::GUS activity appeared early as a strong signal in stipules of rosette and cauline leaves, temporally just before expression

described for DR5::GUS. This stipule signal persisted even after leaf maturation and the transition to flowering, unlike DR5. *HYD1* promoter activity was also noted transiently in hydathodes; the first hydathode signal was found in emergent cotyledons just prior to xylem differentiation, and again in emergent adult rosette and cauline leaves ahead of vascular differentiation. The onset of p*HYD1*::GUS stipule expression was closely associated with its transient expression in the apical hydathode, and rapidly appeared in lateral hydathodes, again as a transient signal. This implies that activity of the *HYD1* gene corresponds with cell differentiation ahead of auxin production in hydathodes and stipules, i.e. is radially positioned around the shoot apex in locations associated with auxin radial cues, but is not positioned in response to those cues. However the *HYD1* promoter sequence does contain putative auxin response elements.

3.4.1.3 Regions of *HYDRA* gene activity appear to be complementary to other known sterol biosynthesis components in shoots, and may overlap in roots.

The differences in the *hydra* mutant phenotype between rosette and cauline leaves, despite a similar GUS activity from the *HYD1* promoter, may result from phase-specific functional redundancy between *HYDRA* genes and other sterol biosynthesis components. A study of the transcriptional behaviour of *HYD2* has not been reported in these later developmental stages. A superficial analysis of younger stages presented by He *et al.* (2003) appeared to indicate a diffuse signal throughout the cotyledons and hypocotyl, and also around the root apex of 4 dae seedlings. *HYD2* promoter activity was also described by Jang *et al.* (2000) as associated with regions of active cell growth. This would suggest a similar transcriptional activity between the two *HYDRA* genes.

GUS promoter-reporter fusions of the three *SMT* genes revealed a similar expression which appeared strong in the apical portions of rosette leaves,

although *SMT1* appears to resolve to the lower order vasculature in more mature organs; a phenomenon not commented upon by the authors (Carland *et al.* 2002, Diener *et al.* 2000). *SMT2* and *SMT3* showed similar rosette transcription to *SMT1,* and an apically distributed expression in sepal mesophyll, although like *HYD1* this signal was much weaker than the leaf signal (Carland *et al.* 2002). The *smt2* and *smt3* mutants have a less severe phenotype than *hydra* and set viable flowers, although seed set is reduced in relation to wild-type, and the upper margins of sepals have a sinuous aberrant morphology. In roots, the SMT reporters were shown in association with root apices, although again *SMT1* was visible in the vascular system of roots, in regions where lateral root primordia were just becoming visible (Diener *et al.* 2000). This signal in root primordia is complementary to that observed in *HYDRA1.* RNA transcriptional analysis of *SMT1* and *SMT3* appears to show enhanced expression in the shoot apex, although GUS activity was not seen in these tissues; this may suggest that downstream regions of the *SMT* transcript influence its function.

Schrick *et al.* (2002) found *hyd1-hyd2/fk* double mutants to have a near identical phenotype to the single *hydra* mutants, whilst double mutants between *hydra* and the *smt1/cph* mutant produced an embryonically lethal result, and *hydra* mutations in combination with the downstream mutation *dwf1* were rarely seedling viable, suggesting independence of function. Considering these results in conjunction with the complimentary distribution of p*HYD1*::GUS and *SMT* promoter-GUS activity profiles suggests some complementarity in zonal gene expression. Both *HYD* and *SMT* reporters showed a basipetal maturation in leaves; perhaps these enzymes target different tissues within the mesophyll layer; p*HYD1*::GUS resolved to cells associated around the primary midvein, but not the vascular system itself as seen with p*SMT1*::GUS.

3.4.2 *HYD1* transcription is associated with aspects of developmental timing and cell differentiation

3.4.2.1. *HYD1* gene activity is associated with differentiation of epidermal cells

Expression of p*HYD1*::GUS is found in specific functional cells of the epidermis of both shoot and root, and in the subtending ground tissue layers, corresponding to the developmental timing of differentiation in these cells.

In roots, p*HYD1*::GUS activity commences in epidermal cells prior to their emergence from the meristematic region, as defined by the limits of the lateral root cap. Upon emergence into the differentiation zone, a GUS maximum appears in atrichoblasts of the root epidermis, first in one and then the other of the adjacent atrichoblast pairs of adjacent cell files, revealing a small temporal difference in maturation. After the atrichoblast cell files have developed their signal, the trichoblast cell files similarly develop a maximum. When all epidermal cell files show their strongest activity, a synchronous weaker but distinct signal appears throughout the cortex layer beneath. The trichoblast cell file signal persists beyond the stage at which the atrichoblast signal has diminished. This reflects the greater persistence of cell division, and the later entry into differentiation, noted in the trichoblast cell files (Berger *et al.* 1998b). This temporal modulation of expression between cell files suggests a precise correlation between the adoption of fate decision in cells of the root epidermis and an associated activation of *HYD1* transcription.

In the shoot, the first sign of GUS activity appears after 4 dae both in the stipules of the first true leaf pair (which are already differentiated), and in the cotyledon hydathode region, where differentiating stomata carry a signal synchronously with associated mesophyll cells beneath. As the true leaves

begin to expand, the first cells in the epidermis to differentiate are the trichomes, which similarly develop p*HYD1*::GUS activity. Trichomes are initiated in the leaf epidermis with a non-random spacing, comprising an average minimum distance of three cells between each hair cell (Hülskamp *et al* 1994.). Similarly the initiation of meristemoids (stomatal precursors) is influenced at the tissue level by the trichome spacing mechanism (Bean *et al.* 2002). Spacing of both stomata and trichomes are compromised in *hydra* mutant rosette leaves, resulting in paired trichomes, variably clustered stomata, and variable patterning of the trichome basal cells.

3.4.2.2 *HYD1* may mediate targets for lateral inhibition through modulation of differentiation timing

Transcription of the p*HYD1*::GUS reporter is associated with differentiating functional cells. In the epidermis, reporter activity appears in trichomes, stomata, and successively in atrichoblast and trichoblast cell files of the root epidermis, targeting cells in which differentiation is slightly asynchronous with their neighbours. Wenzel *et al.* (2001) and Wenzel & Rost (2001) demonstrated that cells of the root cap in the open root apical meristem of *Trifolium*, and the closed root meristem of *Arabidopsis*, all differentiate in 'waves' around the circumference of the root, generating a synchronized spiral formation. This pattern was so regular in *Arabidopsis* that Wenzel & Rost (2001) suggest that a timing mechanism is in operation in the initials around the QC and their daughters. This wave pattern is also visible in the appearance of p*HYD1*::GUS expression in the root cap cells of the serial transverse sections shown in Fig. 3.2.2.2. Another 'timing' mechanism could involve the generative phyllotactic spiral around the shoot apex, where the rapid appearance of the pHYD1::GUS stipule signal is synchronized with the onset of cell differentiation in the expanding leaf primordium.

In the root epidermis, each cell file functions independently and generates a gradient of cells of increasing age ascending the root, with earlier cessation of

cell division and transition to differentiation in the atrichoblasts (Berger *et al.* 1998b). The p*HYD1*::GUS expression shown in the sequence in Fig. 3.2.2.2 highlights some atrichoblast cells differentiating ahead of their neighbours, although the transition into full differentiation is rapid across the root radial axis. Similarly the p*HYD1*::GUS signal persists in the trichoblast cell files, and is strongest at the developmental time point corresponding to the onset of symplastic isolation. An equivalent sequence appears in the shoot epidermis, with p*HYD1*::GUS initially in trichomes, and later in stomatal guard cells. This implies an active *HYD1*-implicated differentiation stage in association with p*HYD1*::GUS reporter expression, indicating symplastic isolation and patterning in cells known to be defined by a MYB transcription factor cascade.

3.4.2.3 *HYD1* promoter activity in later laminar development corresponds to the onset of differentiation in the mesophyll

A rapid, diffuse and transient signal from p*HYD1*::GUS is seen throughout the ground tissue leavers of the hypocotyl and cotyledon petioles, with stomatal-specific expression in the epidermis. In leaf development, a diffuse and transient basipetal mesophyll signal from *pHYD1*::GUS appears from around the apices of rosette and cauline leaves, synchronous with the reduction seen in cell division activity during leaf development, and the transition to leaf expansion (Pike *et al.* 1991, Donnelly *et al.* 1999). A similar signal appears in sepals, again synchronized with the onset of rapid organ expansion prior to differentiation. This suggests an association of *HYD1* activity with differentiation in the mesophyll layer.

The p*HYD1*::GUS expression in ground tissues of the hypocotyl and cotyledons is in the context of an absence of cell division in these tissues (Tsukaya *et al.* 1994, Gendreau *et al.* 1997). Upon germination, hypocotyl and cotyledon tissues differentiate and enter a coordinated expansion phase. The diffuse p*HYD1*::GUS signal seen in the ground tissue layers of these structures implies

a role for *HYD1* in the early differentiation and transition to elongation in these longitudinally organized cell files.

3.4.2.4 HYD1 may have a role in phase-related development

Arabidopsis, as with most plants, exhibits age-related shape changes in leaf morphology (heteroblasty) with increasing age. Differences are seen between juvenile, early adult and later adult phase rosette leaves; successive increases in vascular complexity are accompanied by a modulation of trichome distribution (Tsuge *et al.* 1996, Telfer *et al.* 1997). Wild-type sepal trichomes are found on the abaxial surface, whilst juvenile rosette leaves carry adaxial trichomes, later adult and cauline leaves have trichomes over both surfaces, and cotyledons show an absence of hair cells. The initiation of trichomes on cotyledons of mutants such as *lec1* (Meinke 1992) modulates the subsequent heteroblastic progression, implying that cotyledons are the first components of a heteroblastic series (Tsukaya *et al.* 2000). Trichome spacing and distribution is also influenced by both the light regime and GA signalling (Chien & Sussex 1996).

The *HYD1* reporter showed a modulation of activity which was minimal in cotyledons and the first true leaves, became stronger in early adult phase leaves of the rosette, and was most pronounced in cauline leaves. All true leaf trichomes and differentiating stomates carried a GUS signal, which appeared to increase in intensity as the leaves progressed from juvenile to adult phase. Trichomes of the inflorescence stem also showed GUS activity, often in association with adjacent cells at the trichome base. Sepal expression was reduced in relation to cotyledons, and unlike true leaves and stems, the trichomes and stomates did not express GUS activity. These patterns of expression suggest that p*HYD1*::GUS transcription is phase related, and the increased expression intensity of the diffuse mesophyll signal in older

leaves may be related to signals associated with the greater complexity of adult and cauline phase leaves.

3.4.3 Hormonal modulation of transcription and putative cis-acting elements

3.4.3.1 The *HYD1* promoter contains putative recognition sequences that may contribute to its radial and temporal expression

The *HYD1* promoter sequence contains a number of putative target sequences found to specify directed expression in other genes, promoting transcription in roots, trichomes, cotyledons, pollen and embryos. A number of MYB and MYC recognition sequences are found within the first -1000bp, and bZip binding domain within -200bp of the transcriptional start suggest that gene expression is also modulated by the many MYB transcription factors involved in specifying cell fate identity in the epidermis. Anomalies in the *hydra* mutant phenotype correspond to these regions, confirming the transcriptional pattern of the reporter construct. Other putative response motifs are present, which are implicated in light response and various plant signalling systems.

The *HYD1* promoter bZip recognition sequence is a motif used as a target along with MYB sites for transcriptional activation by homeodomain proteins. The TGACG sequence is a binding site for the ASF-1 transcriptional activator; two copies are present in the *HYD1* promoter from Ws and one copy in the Col sequence. These motifs are found in many promoters, are involved in the transcriptional activation of several genes by auxin and /or salicylic acid (Despres *et al.* 2003). The ASF-1 binding site, found in the CaMV 35S promoter, is recognized by the TGA family of bZIP transcription factors (Xiang

et al. 1997, Klinedinst *et al.* 2000), which have putative roles in plant stress responses (Redman *et al.* 2002).

The majority of plant homeodomain (HD) transcription factors contain a b-Zip (basic leucine zipper) motif, first identified in animal systems. In the many *Arabidopsis* HD-Zip proteins found within the genome, the relative positioning and electrostatic configuration of the homeodomain region and putative leucine zipper is identical to that between leucine zipper and DNA binding motifs in animal bZip transcription factors (Schena & Davis 1992). These authors suggest that as the plant HD-Zip combination may mediate aspects of development that are unique to plants, such as the coupling of development to environmental signals.

GATA sequences are in suitable positions in the *HYD1* promoter to contribute to the p*HYD1*::GUS transcriptional activation in leaf mesophyll and functional epidermal cells. Sequences with a GATA core consensus have been found in petunia, rice and *Arabidopsis* (Gidoni *et al.* 1989, Reyes *et al.* 2004), and are thought to interact with type IV zinc finger DNA binding proteins (Teakle *et al.* 2002).

WRKY transcription factor recognition sequences are present in the *HYD1* promoter close to the transcriptional start. WRKY proteins may have a role in the developmental interactions involved in between-cell patterning; for example, the TTG2 WRKY transcription factor is expressed strongly in trichomes and atrichoblasts, and contributes to the lateral inhibition processes which define fate commitment in these cells (Johnson *et al* 2002). WRKY activity has been implicated in GA-mediated sugar responses (Sun *et al.* 2003). As stipule p*HYD1*::GUS expression is initiated concurrently with the onset of photosynthetic competence in the shoot, WRKY elements may be involved in driving this transcriptional activation.

Of course, any conclusions about the possible functions of putative cis-acting elements identified by bioinformatic analysis must be treated with caution, and requires direct experimental evidence from future mutational and protein binding studies. Nevertheless, this analysis generates hypotheses on which such future studies can be based.

3.4.3.2 Transcription of the *HYD1* reporter is modulated differentially in different parts of the plant body and may indicate functional distinctions between primary and lateral root growth.

In addition to the phase-related temporal variation in the transcriptional activation of p*HYD1*::GUS in shoot tissues, variation was also noted between primary and lateral root apices. The positional expression was essentially similar in both cases, with GUS maxima visible in all cell files of the root cap, and in the differentiation zone of the epidermis, with a lesser signal in the underlying cortex. The GUS activity in lateral root apices as compared to primary roots revealed a more rapidly produced signal upon incubation in X-Gluc.

Auxin treatment of wild-type roots results in a differential morphological response between the main root and laterals formed prior to treatment; the primary root produces multiple laterals along its length in response to 1-NAA, whilst anchor roots and established laterals from the main root undergo minimal morphological changes. Similarly the modulation of *pHYD1*::GUS transcription was more severe in laterals formed as a result of synthetic auxin treatment. However as these phytohormone experiments used exogenous concentrations substantially in excess of physiological auxin levels, the auxin-responsiveness of the p*HYD1*::GUS reporter is not clear. Modulation of root expression was also differentiated upon inhibition of auxin influx; the primary root did not show altered GUS activity but a mildly increased GUS activity was found in laterals. Efflux inhibition resulted in primary root apices developing

a band of intense GUS activity across the former meristematic zone, whilst lateral roots showed a much stronger and non-specific up-regulation throughout the apical region.

Cytokinin was the only treatment to show similar up-regulation of p*HYD1*::GUS expression in all primary and lateral apices. Other exogenous signals produced contrasting results. ACC treatment enhanced primary root activity but did not affect lateral root expression. GA reduced the primary root signal but did not affect the lateral signal, and both ABA and epibrassinolide produced a reduced primary root signal and a strongly enhanced signal in laterals. The *HYD1* promoter activity, and the different morphological responses to exogenous auxin in the wild-type control and reporter background, suggest that differences in auxin and other signalling responses between primary and lateral roots in *Arabidopsis* point to a complex differential regulation between these meristems.

3.4.3.3 A putative auxin response motif is present in the *HYD1* promoter which may be involved in the control of transcription, although reporter activity is not dose-responsive to the addition of exogenous auxin

The ACTTTA motif, bound by the Dof protein NtBBF1, was found necessary for tissue-specific expression of the *Arabidopsis* rolB oncogene (Baumann et al 1999). The *HYD1* locus has one copy in the Col-0 promoter sequence, and three in Ws. The *rolB* gene, when inactivated, totally suppresses root induction by *Agrobacterium rhizogenes* (White *et al* 1985). A link is implied between hormonal and developmental control of the expression of *rolB*, which is modified by treatment with exogenous auxin (Maurel et *al* 1990; Binns and Constantino 1998). The ACTTTA sequence is one of the regulatory elements necessary for the *rolB* auxin response (Baumann et al 1999), and expression of this gene is seen at the end of the globular stage of embryogenesis

(Chichiriccò *et al.* 1992) at the point when embryo cells acquire the capability to respond to auxin (Lo Schiavo *et al.* 1991). However as p*HYD1*::GUS activity is seen from the early globular stages of embryogenesis, reporter activity does not correspond with activation via this regulatory sequence.

The behaviour of the *HYD1* reporter to exogenous auxin did not suggest a primarily auxin-responsive behaviour, as the modulated expression pattern corresponded with the morphological changes induced in the plants at higher exogenous NAA concentrations. However the positional cues were modified by auxin transport inhibition, including a zone of dense activity in the primary root apex with TIBA treatment, in the area of the former meristem, where heightened activity from PIN proteins directs auxin from the centre to the periphery and generates a radial gradient. If the enhanced activity of the *HYD1* gene in this region is to increase the production of sterols, which then promote vesicle trafficking and hence auxin transport, this suggests that the up-regulation of reporter activity in this apical region suggests a function in feedback control, promoting the transport of auxin in this zone where auxin movement and the resultant zonation is crucial for meristem function.

3.4.3.4 Ethylene contributes to but does not cause the radial anomalies seen in *hydra*

Inhibition of ethylene perception by silver diminished resolution of cell-specific identity by p*HYD1*::GUS in roots, and prolonged the transient wave of GUS activity in shoots associated with later leaf expansion. Taken together with the p*HYD1*::GUS responses to ethylene described in section 3.3.4, these results suggest a strong ethylene-responsive component to p*HYD1*::GUS expression in roots, in a manner dependent upon positional cues which are modified by ethylene. Shoot expression is elevated both by enhanced and reduced ethylene levels, suggesting the activation of other signalling systems in aerial parts of the plant.

Two copies of the ethylene responsive enhancer element AATTCAAA is present in the Ws promoter but not in the Col-0 sequence. This motif, found in carnation *GST1* and tomato *E4* genes, is related to senescence and fruit ripening respectively in these species (Itzhaki et al. 1994, Montgomery et al. 1993). As both the Ws and Col-0 full-length promoter constructs raised a transcriptional activation in targeted tissues when treated with ACC, the presence of this element cannot account for the observed results. Rather, these observations could be explained by considering the putative binding of ethylene response factors to MYC and MYB sites as reported by Chakravarthy *et al.* (2003). No change was seen in roots, and a negative transcriptional response to ACC was seen in shoot tissues of the -834 and -482 promoters, which is not explained by the positioning of MYC and MYB sites. It is clear from these observations that ethylene activation of the *HYD1* promoter is complex, and may involve the interaction of a number of interacting signalling systems.

3.4.3.5 Transcription of the *HYD1* gene is activated by cytokinins and may comprise part of a cytokinin response pathway

The *HYD1* promoter carries a number of the NGATT recognition motifs for the *Arabidopsis ARR1* gene, encoding the transcription factor responsible for activating cytokinin immediate response genes (Sakai *et al.* 2000) in conjunction with other cytokinin-induced factors (Ross *et al.* 2004). These sequences are present in the -1kb *HYD1* promoter common to both Ws and Col-0, with a further four sites in the unique upstream Ws sequence.

3.4.3.6 The *HYD1* promoter contains recognition motifs for MYC, MYB and MYB-related families of transcription factors which may modulate expression by GA and ABA.

MYC and MYB sequences have been shown to be involved in the ABA response in both *Arabidopsis* and tomato (Abe *et al* 2003, Chakravarthy *et al.* 2003), though ethylene cross-talk is implicated, as these sequences are also bound by an ethylene responsive factor (Chakravarthy *et al.* 2003).

Four MYC sites are common to both the full-length Ws and Col promoter sequences, including the CACATG consensus found to bind a drought and ABA-induced MYC transcription factor (rd22BP1) in the promoter of the *rd22* gene of *Arabidopsis* (Yamaguchi-Shinozaki and Shinozaki, 1993; Abe *et al* 1997; Busk & Pages 1998). Another two MYC sites are present in the Ws unique upstream sequence.

MYB1 proteins are implicated in water stress responses and possibly ABA response in maize (Urao *et al.* 1993, Abe *et al.* 2003). Both ecotypes carry MYB1 recognition motifs; the MYB1 binding site TAACAA is present in the first -1kb of the *HYD1* promoter from both Col-0 and Ws ecotypes, and other MYB transcription factor binding sites The TTACTG and TTACGG sequences, found to be MYB2 transcription factor binding sites in *Arabidopsis*, are present in the Ws upstream unique sequence.

Two motifs (GGATA) found to be the core recognition sequences of a MYB homologue from *Solanum tuberosum* (Baranowskij *et al.* 1994), are present in tandem within -1kb of the transcriptional start in both Ws and Col-0 promoters. An "I-box" sequence (GATAAG) lies just upstream of the -482bp primer site in both Ws and Col sequences; this motif is recognized by a novel class of MYB-like proteins in tomato, and is involved in light response (Giuliano *et al.* 1988; Donald and Cashmore, 1990; Rose *et al.* 1999).

The TAACAA MYB consensus, present in both the Ws and Col -1kb *HYD1* sequences, was defined as a cis-acting DNA element, responsive to GA and ABA in an antagonistic fashion (Skriver *et al.* 1991). This motif is bound *in vitro* by a GA-responsive MYB protein in barley aleurone cells (Ogawa *et al* 2003).

Along with the Dof 'pyrimidine box' CTTTT sequence, these motifs constitute a number of elements bound by a group of GA-response proteins suggested to comprise a GA-responsive complex (GARC) in barley aleurone (Mena *et al.* 2002), and to have partial roles in GA-implicated sugar repression (Morita *et al.* 1998).

3.4.3.7 The phytohormone-responsive upstream promoter sequence from Ws may be indicative of a transcriptional modulation mechanism targeting multiple genes

The *HYD1* gene is located on chromosome 1 of the *Arabidopsis* genome (Topping *et al.* 1997). The *HYD1* promoter was cloned from a T-DNA insertion mutant in the Ws ecotypic background, and the sequence compared to that of Columbia using the NCBI online information sources. This analysis revealed differences in the *HYD1* promoters from the two ecotypes. Most of the first -900bp upstream of the transcriptional start showed strong homology between the two promoter sequences, beyond which the Ws promoter contained a unique segment, 1036bp long, which was found elsewhere in the Columbia genome, on chromosome 3. This upstream region was found to be transcriptionally responsive to multiple exogenous phytohormone treatments. This finding shows the result of a chromosomal rearrangement, and may indicate a point of interaction between these chromosomes within the nucleus. Such rearrangements are frequent in the Brassicaceae (Coghlan *et al.* 2005). These phenomena are likely to be exacerbated in laboratory ecotypes of *Arabidopsis*, where generation turnover is more rapid than under normal ecological conditions, and genetic mixing is minimised between siblings; such a situation present idealized conditions under which to expect an accelerated 'genetic drift'.

3.4.3.8 Activity of the p*HYD1*::GUS reporter may be influenced by innate differences in environmental responsiveness between primary and lateral root apices.

The *HYD1* promoter-reporter construct showed a different modulated activity in primary and lateral root apices in response to treatment with exogenous phytohormones and inhibitors. This may result from differentiation of physiological function between these organs. The root system of maize, which is typical of grasses, consists of distinct types of roots which are formed at different developmental stages and initiate from different locations along the growth axis. Primary roots as well as seminal lateral roots are formed during embryogenesis, whereas crown roots and brace prop roots arise post-embryonically from stem tissue (Hetz *et al.* 1996, Hochholdinger & Felix 1998). Considering the often dry and ephemeral nature of grassland habitats, this suggests the possibility of functional specialism between components of the root system, namely a deeper primary root for access to water at lower levels in the soil, and other roots at higher levels for both stability and mineral nutrition (as the soil zone containing the most bacterial activity is concentrated in the upper layers which receive most organic input).

Soil pH has a profound effect on the availability of nutrients in soil solution, and phosphorus is known to be a limiting factor in many limestone soils (Tyler 1992). *Arabidopsis thaliana* is a species found growing in dry or well drained, often nutrient-poor (i.e. base-poor) conditions throughout the temperate zones of the northern hemisphere (Bowman 1994). Its ability to survive under relatively extreme conditions mean that it is often a coloniser of bare soil and ephemeral habitats, an ability which is reflected in one of its common names; 'wall cress'. These conditions, also favoured by a number of grass species, mean that soil mineral availability is low, and utilisation by the plant requires a local pH modification of the 'rhizosphere' zone around the root, and an adaptation of the available root absorptive surface area. Therefore a differentiation within the overall structure of the *Arabidopsis* root system,

allowing root specialism for e.g. water absorption and nutrient sourcing, would give the plant a competitive advantage within this ecological niche.

Dolan *et al.* (1993) note a greater variation in cell numbers in cortical and epidermal layers of lateral roots as compared with the primary root apex. These authors note that larger numbers of cortical cells are coupled to fewer epidermal cells, implying that the cell file numbers in a given tissue are not solely determined by the available space. Variable anatomy between primary and lateral roots has also been described in pea (Esau 1965, Torrey 1955). The primary root of pea has an invariable triarch vascular pattern; however the laterals can vary between diarch and pentarch, in association with variation in size of the developing lateral root primordium, (Torrey 1955). Dolan *et al.* (1993) suggest that this indicates an autonomous developmental plasticity in pea lateral roots which is responsive to environmental factors; a possibility which can also be inferred in *Arabidopsis*.

Studies in *Arabidopsis* have shown that nitrate supply directly modulates the architecture of the root system (Zhang *et al.* 1999, Zhang & Forde 2000). A uniform nitrate supply promotes uniform lateral root growth at all points on the main root system, and uniform high nitrate availability limits lateral root growth uniformly. In roots grown in conditions where the longitudinal growth axis of the root passes through zones of nitrate availability in a nitrate starved situation, then lateral root growth is accelerated in the region of higher nitrate. The *ARABIDOPSIS NITRATE REGULATED1* gene, encoding a MADS domain transcription factor, is transcribed within 30 minutes following nitrate treatment of nitrate-starved roots, implying that nitrate is functioning as a signalling molecule (Zhang & Forde 1998). Studies in tobacco have revealed that this signalling modulates the partitioning of growth between shoot and root (Scheible *et al.* 1977). Other studies have demonstrated the modulation of root architecture by other nutrient regimes (Robinson 1994, Leyser & Fitter 1998). This evidence offers support to the idea of a nutrient-absorbing specialism in lateral root development.

Research into signalling responses in *Arabidopsis* root development has concentrated on the root apex as a functional unit, comprising signalling interactions which respond to external stimuli such as gravity, and internal signals such as PIN-mediated longitudinal and radial auxin gradients. Such studies have not commented on differential responses between primary and lateral root apices. Gravity response requires auxin, and involves a sensing of the position of starch amyloplasts in columella cells of the root apex, although the nature of the signalling interaction is unclear (Chen *et al.* 1999). In order that the lateral roots do not compete with the same soil zone as the primary root, they grow horizontally from the main stem prior to commencing a gravitropic response. The differences in auxin-related modulation of p*HYD1*::GUS between primary and lateral apices may reflect differential gravity and auxin sensitivities in different root apices, as basipetal and lateral auxin transport are contributors, though is not the sole cause, of root gravitropic curvature (Young *et al.* 1990, Rashotte *et al.* 2000).

Chapter 4

Pattern coordination in the *hydra* plant body

4.1 Abstract

Analysis of the p*HYD1*::GUS deletion series in chapter 3 revealed a developmentally modulated promoter activity occurring in a radially distributed manner throughout the plant growth axis. No meristematic GUS activity was observed; rather the *HYD1* promoter appears to have an active role in differentiation of peripheral tissues, appearing in the root cap, stipules and functional epidermal cell types of roots and shoots from the point of cell fate commitment, and transiently as a mesophyll signal corresponding to the timing of final differentiation throughout that cell layer. The strong and persistent stipule signal corresponds with regions where organ expansion is coordinated in a manner which preserves the radial (abaxial-adaxial) axis. This chapter makes a further investigation of the role of the *HYDRA* genes in radial development, by examining the *hydra* mutant phenotype with specific reference to the cell types highlighted by the p*HYD1*::GUS reporter, and patterning processes involving coordination between cells.

The *hydra* phenotype exhibits considerably morphological variation between siblings; this is associated with radial mis-coordination between and within longitudinally aligned cell files during embryogenesis and early seedling development. Extreme examples include dissociation or duplication of the apical-basal axis, accompanied by anomalous cell layer coordination in the ground tissues. Vascular coordination was poor throughout development and stems from patterning problems at the point of procambial coordination; these phenomena being most severe in vegetative structures. Disjunct and dissociated xylem vessels were seen typically in association with persistent ectopic cell division activity.

Misalignment of polarly-aligned cells in the epidermis was evident from *hydra* mutant cellular morphology and cortical microtubular arrays. Functional

epidermal cells demonstrated a range of morphologies and expansion anomalies, which reflect tissue-level disorganization within the organ. These patterning problems were found to be confined to vegetative rather than reproductive phase organs in the mutant plants.

Poor radial coordination around the mutant vegetative shoot apex produces anomalies in phyllotactic patterning, with ectopic and multiple adjacent clusters of primordia initiating over the meristem region, particularly in association with vascular patterning anomalies in the hypocotyl-cotyledon transition zone. Developing primordia also showed a variable and sometimes reversed organ radial polarity, as revealed by promoter-reporters for genetic markers of abaxial and adaxial tissue identity. These mis-expression phenomena were also evident from embryogenesis.

4.2 Introduction

4.2.1 Longitudinal cell files are coordinated across the radial axis throughout development

4.2.1.1 Longitudinally-coordinated vascular and endodermal cell files connect the root and shoot in juvenile seedlings

Differentiation of cell types in the *Arabidopsis* root epidermis are co-ordinated within each radial layer according to their cell file, giving a definable relationship between the longitudinal cell file identity within the epidermis and its radial relationship to the cortical cell files beneath. Root atrichoblast (non-hair cell) files occur in contact with a cortical periclinal cell wall, and the trichoblast (hair cell) files lie over the anticlinal junctions between cells (Dolan *et al.* 1993). These epidermal-cortex relationships also define epidermal cell file identity in the hypocotyl, where stomata differentiate within the trichoblast cell files at positions defined by root patterning genes (Berger *et al.* 1998), shown in Diagram 4.1.

The cell files of the hypocotyl epidermis branch contiguously at the shoot apex to form the abaxial epidermis of the cotyledon petioles (Gendreau *et al.* 1997). The mesophyll layer and cortex layers of the hypocotyl and cotyledons are also in continuity. Within the cotyledon, the vascular procambium differentiates in connection with both the vasculature and endodermis of the hypocotyl (Gendreau *et al.* 1997, Wysocka-Diller *et al.* 2000).

The root-hypocotyl junction marks an anatomical transition in *Arabidopsis*; this longitudinal region is distinguished by a transition in the ground tissue from one cortex cell layer to two (Dolan *et al.* 1993, Scheres *et al.* 1994). The epidermis over this region contains between 4 and 7 shortened cells per

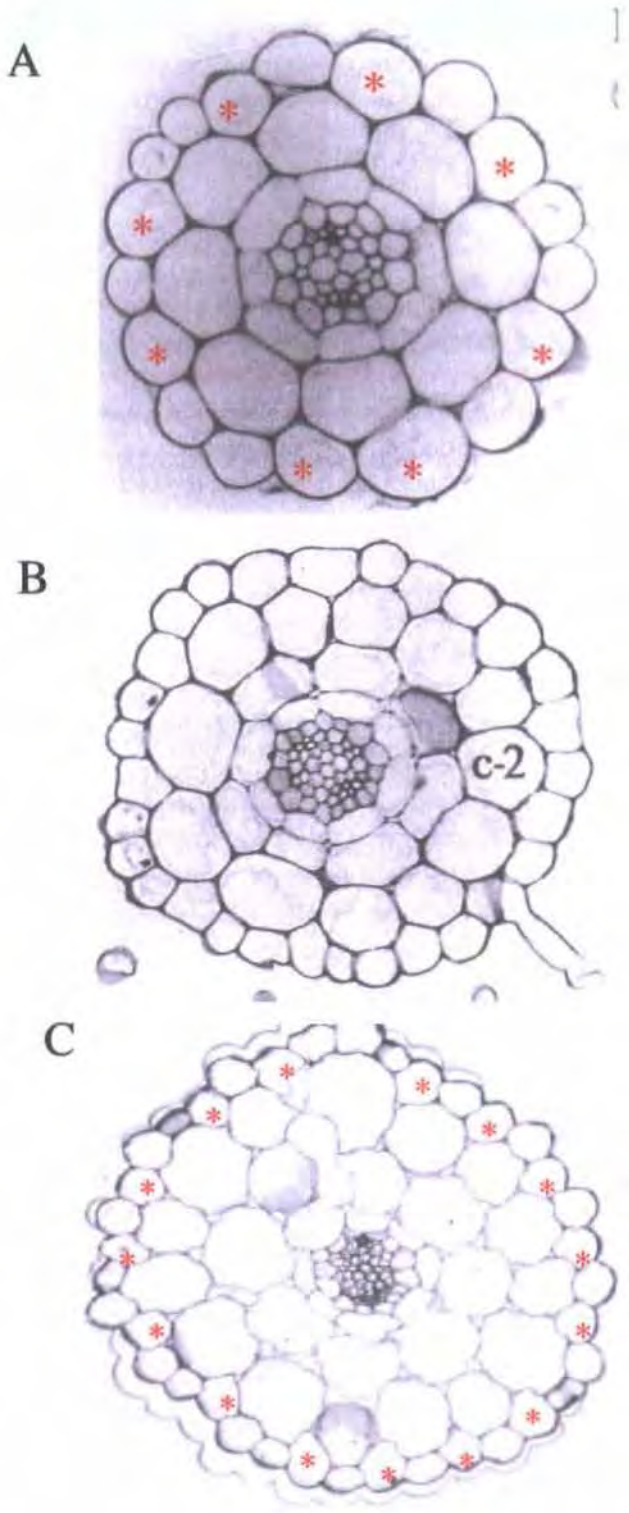

Diagram 4.1 Transverse sections of root and hypocotyl tissues in *Arabidopsis thaliana*

A shows a mature primary root, B shows the patterning at the root-hypocotyl transition where the additional cortex layer has differentiated (indicated by c-2), and C shows the hypocotyl in transverse section. Asterisks indicate cells in the epidermis which lie adjacent to the junction between cells of the cortex below. A-C, x100.

longitudinal cell file, and the numbers of cell files make a similar transition from around 18 in the root below to 34 in the hypocotyl (Dolan *et al.* 1993, Geldner *et al.* 1997). Epidermal patterning over this region does not show the same spatial relationship between layers as in the two tissue types above; here, all epidermal cells differentiate as root hairs, although they do not show the usual lengthening prior to tip initiation (Dolan *et al.* 1993, Scheres *et al.* 1994).

Continuity of the epidermis is maintained as a single radial layer over this transition zone, although longitudinal cell files are modulated transversely in the pattern to accommodate the increased cell numbers. The endodermis layer with its Casparian band is continuous across this boundary, and expresses the SCARECROW (SCR) protein from the root apex up the root pole and into the shoot (Di Laurenzio *et al.* (1996); the endodermal cell files flanking the stele separate at the hypocotyl-cotyledon transition boundary and extend into the cotyledon and leaf primordia on the abaxial side of the vascular trace in continuity with the bundle sheath around leaf vascular elements (Wysocka-Diller *et al.* 2000).

In the hypocotyl and leaf primary traces, the endodermis (also known as the starch sheath) contains sedimenting starch amyloplasts, and is involved in gravity sensing (Fukaki *et al.* 1998). The endodermis layer expressing SCR protein maintains proximity with the vasculature as it bifurcates in the upper hypocotyl and extends into the cotyledons within the abaxial mesophyll (Wysocka-Diller *et al.* 2000). As vascular differentiation 'invades' into the mesophyll of expanding leaf primordia, expression of SCR defines the associated bundle sheath, and appears to be recruited from the undifferentiated cell mass along with the vascular trace (Wysocka-Diller *et al.* 2000).

4.2.1.2 Vascular strands modify their patterning across the radial axis at the *Arabidopsis* juvenile shoot apex

The vascular traces form connected conduits of cell files from the shoot to the root, and throughout all structures of the plant body. These long files of similar cells are comprised of xylem vessels and phloem sieve tubes, with openings in their connecting cell walls within each cell file (Esau 1977). All vascular traces at the SAM form in direct continuity with the hypocotyl vasculature (Pike & López-Juez 1999). They differentiate by recruitment of new cells within undifferentiated cell masses, and extend into newly forming leaf primordia in an acropetal manner, first via procambial cell file specification, then the elongation of cell files, followed by differentiation of the vascular elements (Busse & Evert 1999a, 1999b). Phloem vessels differentiate synchronously throughout their length, whilst xylem elements initiate points of differentiation at intervals along the established phloem trace, later joining into a continuous network by completing xylem cell fate adoption throughout the procambial strand (Esau 1977, Busse & Evert 1999a).

The vascular strands of the post-germination *Arabidopsis* seedling undergo a radial transition at the hypocotyl-cotyledon junction, changing their patterning across the transverse axis from an alternate arrangement in the root and hypocotyl, to a collateral pattern in the cotyledon traces (Busse & Evert 1999b). The phloem traces and xylem plate form bifurcating strands in the upper hypocotyl, and reorientate so that two phloem strands, one strand from each phloem pole combines with one of the xylem strands and form the cotyledon primary trace. The xylem trace twists as it makes this transition, so that the older protoxylem at the outer edge of the stele come to lie on the inner (adaxial) side of the cotyledon, and younger metaxylem differentiate between the protoxylem and the phloem (by the abaxial surface). This transition from alternate to collateral is complete at around a third of the length into the cotyledon midvein. All subsequent leaf vascular traces derive

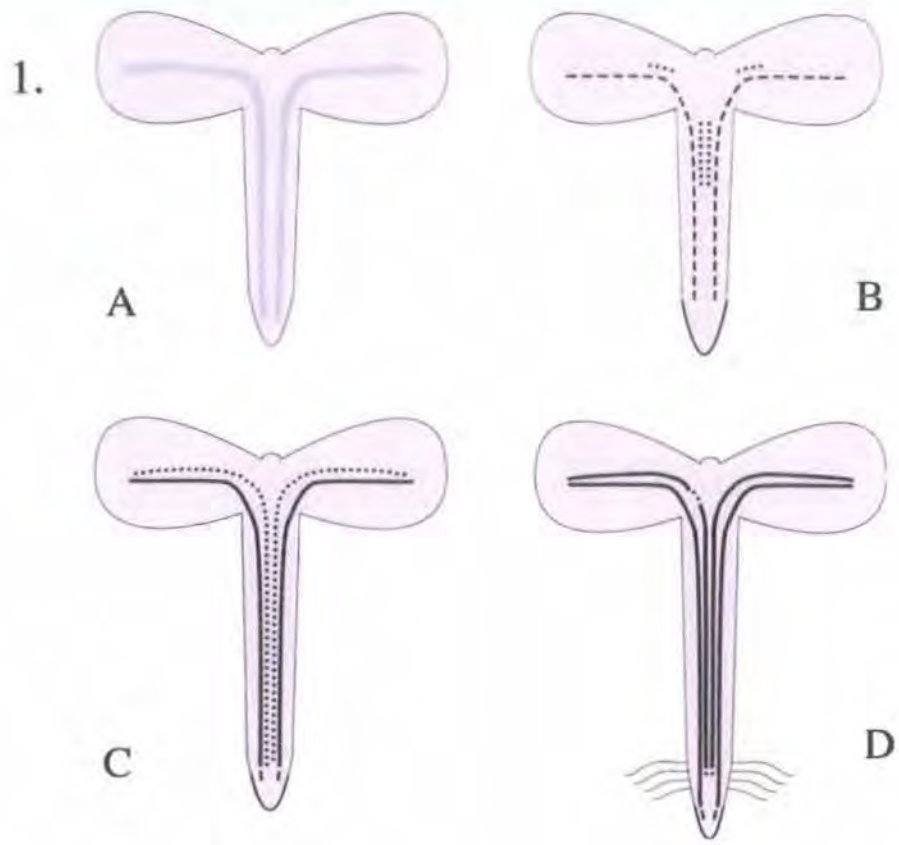

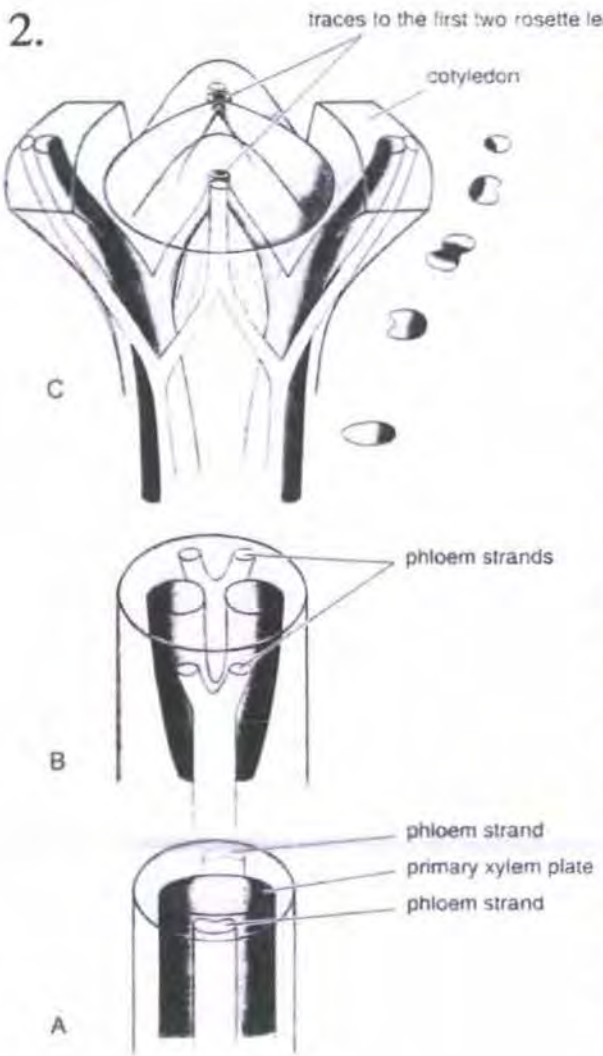

Diagram 4.2 Vascular differentiation in juvenile *Arabidopsis* seedlings

1. A-D; pattern of differentiation of the first phloem and xylem elements in the mature embryo (procambium only) (A), at 2.5dae (B), at 2.75dae (C) and 3dae (D). Immature phloem strands are shown by dashed lines, and immature xylem by dotted lines.
2. A-C; diagram illustrating vascular transition in the connection between hypocotyl and cotyledons. In the hypocotyl, the vascular arrangement for most of its length is alternate (diarch) (A) with phloem on either side of the xylem plate. Strands bifurcate in the upper hypocotyl (B), and a pith separates the xylem into two units. (C), xylem reorientates around the phloem across the hypocotyl-cotyledon transition; successive sections (protoxylem darker than metaxylem) show the strand inverting in the radial plane (exarch to endarch) and reorientating in relation to the phloem from alternate to collateral. Diagrams from Busse & Evert (1999a, 1999b).

from this new branching pattern, in continuity with the vasculature of the upper hypocotyl. A similar restructuring of the pattern is found in other dicotyledons (Busse & Evert 1999b, Esau 1977).

The pattern in the leaf traces that result from this vascular transition are distinguishable as having an abaxial-adaxial differentiation across the radial axis. As all subsequent leaf organs initiating around the SAM periphery form continuous vascular traces with this pattern, meaning that the presence of a vascular trace in a new primordium conveys an anatomical dorsiventrality to the tissue, in the plane of the radial axis.

4.2.1.3 Secondary development in many dicotyledons including *Arabidopsis* modifies the radial patterning from its juvenile form.

Many dicotyledons and some monocotyledons undergo a secondary vegetative development. This growth is via the 'lateral meristems', which take the form of radial cell layers around the longitudinal axis, and initiate specific tissues rather than whole organs (Steeves & Sussex 1989).

In the hypocotyl and cotyledon tissues of young *Arabidopsis* seedlings, the only cell division events to occur are associated with post-germination differentiation of stomata in the epidermal layer (Gendreau *et al.* 1997, Tsukaya *et al.* 1994). No divisions take place within the mesophyll layers of either tissue; all growth in the epidermis, cortex and endodermis involves expansion, accompanied by rounds of endoreduplication in the cells of the longitudinal cell files (Gendreau *et al.* 1997). This implies that the hypocotyl epidermis, cortex and endodermis are juvenile structures.

Subsequent 'secondary growth' generates a differently organized tissue in the internode stem. After completion of extension growth, the *Arabidopsis* hypocotyl undergoes secondary thickening. The epidermal, cortical and

endodermal cell layers gradually disintegrate; cell walls rupture, whilst growth in the stele develops from two types of radially-arranged 'lateral meristem' tissues. The first of these, termed the 'vascular cambium' is derived from thin walled cells between the primary xylem and phloem traces in the juvenile stele, and comprises cells which are thin in cross section. As thickening progresses, these cells form an oval ring with the phloem on their outside and the xylem on their inside. As this arrangement matures, strands become distinct within the hypocotyl, comprising of clustered phloem sieve elements and companion cells, and associated xylem on the inside of the vascular cambium (Bowman, 1994). This new arrangement of the vasculature across the radial axis of the plant, shown in Diagram 4.3, is similar to the collateral arrangement of vascular bundles within the leaves. The second type of tissue, lying beyond the phloem further to the margin of the radial axis, is derived from the pericycle. This tissue layer, the 'phellogen', generates epidermal layers of cells by periclinal divisions, producing multiple layers of outer cells, known collectively as the 'periderm' (Dolan *et al.* 1993, Gendreau *et al.* 1997).

A similar situation is found in secondary growth of the *Arabidopsis* root; as in the hypocotyl, signs of disintegration of the outer layers are evident in 3-4 week old seedlings (Dolan *et al.* 1993). New root primordia are the first sign of a modification of the original pattern, and form from the pericycle. As the lateral root develops, it bursts out through the intervening layers of endodermis, cortex and epidermis, sometimes appearing to cause mechanical damage to these cell layers (Dolan *et al.* 1993, Dubrovsky *et al.* 2001).

Post-germination lateral organs around the SAM are contiguous with vascular strands arising from the internodes within this secondary pattern; procambial strands 'invade' from established traces into the new primordia as they arise, connecting the leaf organ to the existing network via two phloem strands, one from each of the two adjacent primary leaf traces. This pattern reiterates the continuity with the tissues below, as seen at the root meristem. Lateral root

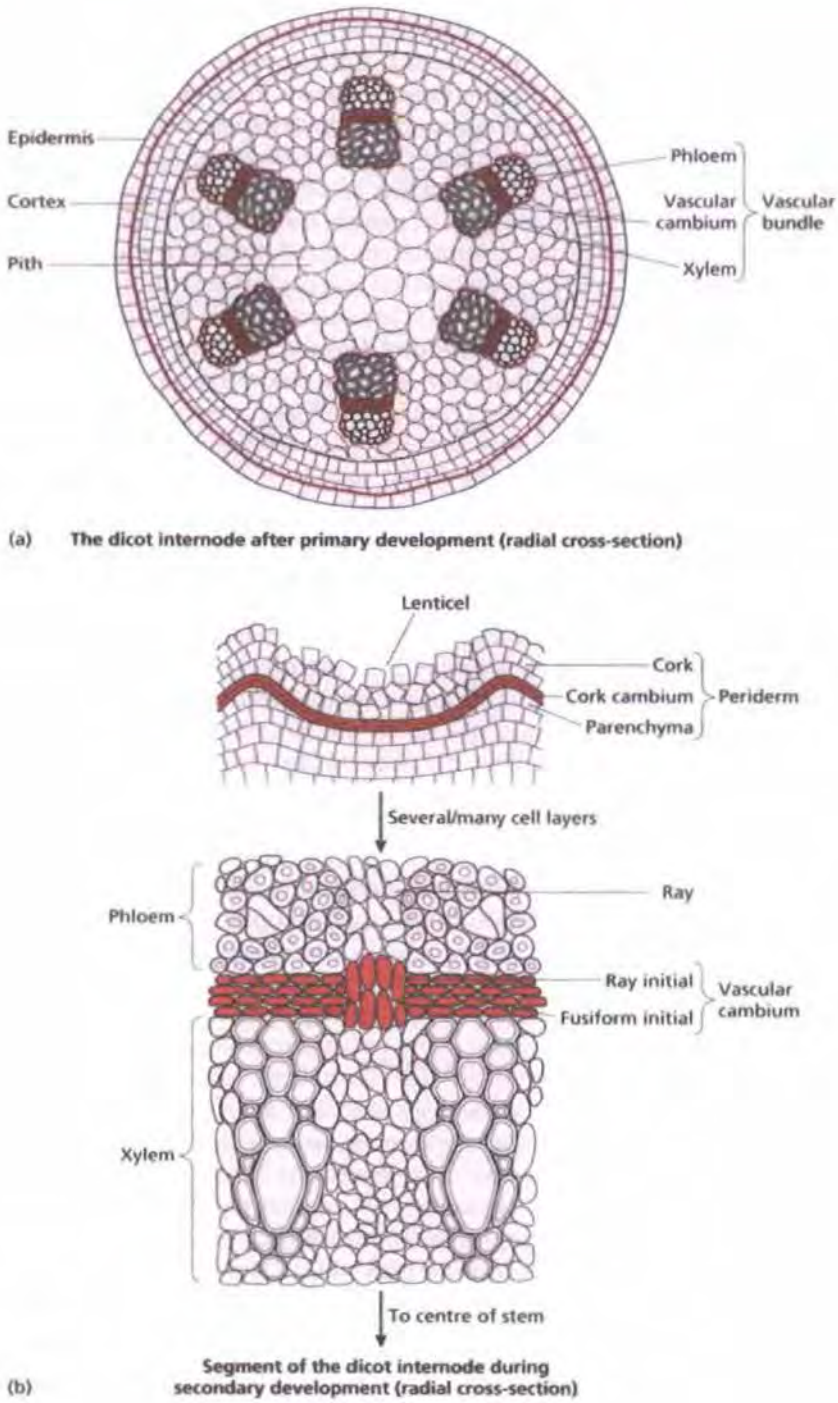

Diagram 4.3 A comparison of primary and secondary development across the longitudinal axis in dicotyledons

(a), primary and (b), secondary development of a generalized dicotyledon internode.
Diagram from Leyser & Day 2003.

primordial form from a single cell file (Dubrovsky *et al.* 2001). New leaves have longitudinal cell files in line with the existing vascular pattern (Pike & López-Juez 199, Busse & Evert 1999b), and epidermal patterning is under the control of many of the same genes that pattern the radial root (Larkin *et al.* 1994, 1996, Massucci *et al.* 1996, Fyvie *et al.* 2000, Schellmann *et al.* 2002).

These common mechanisms imply that leaves are radially patterned organs like roots, and are subsequently modified to undergo centrolateral expansion between the longitudinal cells of the margin by dorsiventral expansion signals. This means that heteroblasty (the change from juvenile to adult organ morphologies) and the phase-dependent differentiation of distinct organ types such as petals, (concurrent with associated changes in the distribution of functional epidermal cells,) can be viewed as modification of the basic radial pattern.

4.2.2 A radially differentiated morphology and physiology is evident within organs and tissues

4.2.2.1 Radial differentiation in gene expression controls patterning in the *Arabidopsis* epidermis

The plant epidermis differentiates types of distinct cells which fulfil multiple roles in environmental interaction. In the shoot, stomatal guard cell pairs control epidermal pore opening and size, allowing gas exchange essential for photosynthesis, whilst controlling water loss from the organ in response to environmental cues. Root hair cells comprise environmental exchange surfaces with functions both in an absorptive activity for uptake of water and mineral solutes, and with a secretory function, supplying proteinaceous compounds into the 'rhizosphere' zone surrounding the root, where bacterial metabolic activity makes many insoluble minerals and trace elements

available in soluble form, suitable for uptake by the plant. Stomata can also appear in a modified form for secretory purposes, such as at hydathodes (guttation points) and nectaries (for control of nectar secretion under favourable conditions).

Stomata, root hairs and shoot trichomes are under the control of a common set of patterning genes (Berger *et al.* 1998a, 1998b, Schellmann *et al.* 2002, Rerie *et al.* 1994, Massucci *et al.* 1996), in a mechanism where cell fates are promoted by mutually-inhibiting cassettes of molecular cues. These data can be interpreted as identifying two functional 'cassettes' for cellular function, namely an 'exchange' mechanism involving epidermal control of transpiration and gas or solute exchange (root hairs and stomata), and a 'barrier' mechanism (atrichoblasts and the pavement cell/trichome arrangement). The resolution between these functional cassettes is determined at the level of tissue patterning, respectively involving a simple radial organ (the root tip) and a modified radial organ (the developing shoot lateral organ).

Arabidopsis wild-type plants do not carry trichomes on their cotyledon surfaces, but the activity of the trichome/atrichoblast barrier cassette is still evident, as the tissue level spacing of stomata is modified in these organs by mutations at the (atrichoblast) *GL1* and (trichome) *TRY* loci, respectively producing ordered and clustered stomatal patterns (Bean *et al.* 2002). Trichomes and stomata have never been found arising from adjacent cells in wild-type plants. As trichomes appear before stomates in epidermal differentiation, this implies that the exchange (stomata/root hair) cassette is subordinate to the barrier (trichome/atrichoblast) pattern. The placement of stomates in the *Arabidopsis* hypocotyl epidermis has been found to rely upon the same molecular cues as those that define root hair position (Berger *et al.* 1998a). The hypocotyl, like the root, is a simple (unmodified) radial organ.

In the *Arabidopsis* root epidermis, a distinction between hair cells (trichoblast cell files) and non-hair cells (atrichoblast cell files) is made anatomically and

genetically. Atrichoblasts develop where the epidermal cells have contact with periclinal walls of the cortex layer beneath, whilst trichoblasts arise over cortical cell junctions (see Diagram 4.1). This anatomical arrangement is found throughout the young *Arabidopsis* root (i.e. prior to secondary meristem activation), with the exception of the root-hypocotyl transition zone. The alternating 'striped' arrangement of root hair and non-hair cell files seen in *Arabidopsis* is not common to the higher plants as a whole; rather hair cells appear to have a more random placement in most taxa, suggesting that the striped pattern has evolved independently in several dicotyledon clades (Dolan & Costa 2001) The monocot resolution between cells involves an asymmetric cell division within the longitudinal cell file, where the larger cell adopts atrichoblast cell fate and the smaller cell adopts trichoblast fate (Clowes 2000). Similarly, in the shoot epidermis of rice, asymmetric divisions resolve guard mother cells (stomatal precursors). This mechanism involves a rice homologue of the *Arabidopsis* SCR protein, necessary for asymmetric divisions that resolve the cortex and endodermal cell layers of the developing root (Di Laurenzio 1996, Kamiya *et al.* 2003).

Trichomes are thought to protect the plant from predators and the disease causing organisms they carry. Some plant species have trichomes adapted for certain functions, such as entrapment of small insects as a source of extra nutrition as in *Drosera* species, or to convey protection from herbivores, such as the venom-laden hairs of *Urtica dioicia*. *Arabidopsis* trichomes are thought to act as a 'simple barrier over the leaf surface'(Glover, 2000). Their main function may be to slow down air movement in order to maintain humidity over the leaf surface; trichome growth is exaggerated under conditions of drought stress, developing a dense thicket of hairs over the lamina.

Trichomes are found over the surfaces of vegetative lateral organs in *Arabidopsis* in characteristic arrangements according to the placement of the leaf in developmental phase transition. This transition, known as heteroblasty, is characterized by a successive increase in vascular complexity,

and additional numbers of hydathodes in the network (Tsukaya *et al.* 2000). Juvenile rosette leaves carry these hair cells only on their upper (adaxial) surfaces, later rosette leaves produce trichomes on both abaxial and adaxial surfaces, and cauline leaves develop trichomes preferentially on abaxial surfaces (Telfer *et al.* 1997, Chien & Sussex 1996). This differential distribution is influenced by both the light regime and GA signalling (Chien & Sussex 1996). Stomatal distribution also varies between the surfaces of the lamina; fewer stomates form on the (more exposed) adaxial than abaxial surfaces. As stomatal distribution is influenced by patterning genes from the 'atrichoblast/trichome' cassette, this implies that the spatial organization of cellular patterning processes in the leaf epidermis is defined by cues affecting the organ radial axis.

Trichome formation over both adaxial and abaxial surfaces can be considered in terms of the water conservation needs of the different phase leaves, i.e. the greater vascularization of later rosette and cauline leaves would predispose their surfaces to a more rapid transpiration loss. The desiccation risk is most extreme in cauline leaves, which are further above ground than leaves of the rosette, and so are more exposed to wind desiccation. Other desiccation responses include curling of leaves (which further preserves a humid microclimate beneath the abaxial surface where rosette leaf stomates are at higher density) and anthocyanin production. As *Arabidopsis* is a colonist of desiccation-prone habitats (as indicated by one of its common names; 'wall cress'), trichome growth is one means of morphological adaptation to its dry habitat.

4.2.2.2. Lateral organs are generated around the root radial axis

The cell division zone of the *Arabidopsis* root apical meristem is defined longitudinally by the limits of the lateral root cap cell files (Hauser & Bauer 2000). Cells then undergo differentiation and co-ordinated longitudinal

expansion, retaining the relationship between adjacent cells within and between layers in transverse 'modules'.

The first lateral roots initiate soon after the modules complete elongation. Within the pericycle, one or two cells from a cell file adjacent to a protoxylem pole become 'founder cells' and proliferate rapidly This cell division activity forms a mass of cells which rapidly develops tissue organization (Malamy & Benfey 1997). The new root primordium then bursts out through the intervening layers of endodermis, cortex and epidermis, sometimes appearing to cause mechanical damage to these cell layers (Dolan *et al.* 1993, Dubrovsky *et al.* 2001). Emerging laterals have a similar morphology and cell arrangement to that of the primary root, including a diarch vasculature.

Similarities in primordial initiation exist between shoot and root tissues. In *Arabidopsis,* both lateral roots and leaf primordia initiate from a small number of founder cells (Reinhardt *et al.* 2000, 2004, Dubrovsky *et al.* 2001). They form within a finite distance form their apical meristems and can be induced by ectopic application of auxin; also auxin transport inhibition arrests organ initiation in both systems (Casmirio *et al.* 2000, Reinhardt *et al.* 2000). Subsequent proliferation within the leaf primordium produces multiple small cells into which procambial cells expressing p*AthB8*::GUS 'invade' (Baima *et al.* 1995, 2001, Kang & Dengler 2002, Scarpella *et al.* 2004).

4.2.2.3 Lateral inhibition in organ generation at the shoot apex controls radial position and dorsiventral alignment

Leaf primordia arising singly from the peripheral zone of the SAM in one of the classic phyllotactic arrangement (helical, or alternate), can be numbered P_1, P_2, P_3 etc in order of increasing age. The position in this helical phyllotaxy of the next incipient primordial initiation can be predicted in wild-type shoot apices; the next to arise is designated I_1, followed by I_2. Classic surgical

experiments have attempted to interfere with this leaf positioning. Separation of the P_1 primordium from the meristem by a tangential incision resulted in I_1 arising at its normal position, but I_2 appearing at a greater angle with I_1 (Snow & Snow 1931). These and other experiments involving puncturing of presumptive primordial positions (Wardlaw 1949 and others, reviewed in Steeves & Sussex 1989), led to the idea of a field of lateral inhibition around the existing primordia, which prevented the adoption of primordial fate in these tissues. The involvement of dorsiventrality in the phyllotactic process was first demonstrated by the finding that young incipient primordia from *Solanum* could be induced to develop as radially symmetrical finger-like structures when surgically separated from the meristem (Sussex 1951, 1955).

Reinhardt *et al.* (2003) suggest that the developing primordia function as 'sinks' for auxin, which means that auxin in the L1 layer of the SAM is drawn away by active transport in the xylem. This provides a means by which an area of the peripheral zone could establish a higher auxin accumulation, at a minimum distance from the existing primordia (at positions P_1 and P_2), corresponding to the I_1 position.

> *"Auxin accumulation at I_1 induces a new primordium, which in the course of the plastochron, will grow out and itself become a sink for auxin. This mechanism represents a combination of positive feedback (auxin accumulation) and lateral inhibition (withdrawal of auxin from adjacent tissues) that could conceptually be compared with the short range activator and long range inhibitor in reaction-diffusion mechanisms."* (Reinhardt *et al.* 2003)

The implications of this work mean that the dorsiventral patterning and vascular development of new primordia is also involved in and affected by lateral inhibition, coordinated with the phyllotactic series. Reinhardt *et al.* (2004) repeated the classic experiments of the Snows using laser ablation of primordia on tomato apices; this less damaging procedure resulted in changes

in the divergence angle as previously reported, but also shifted the meristem centre away from the wound, and caused major changes in the vertical growth of the apices. These authors conclude that the P1 and P2 primordia are sufficient to specify the general location of I1, whilst the directly contacting neighbours (P3 and P4 in tomato apices) control its delimitation and hence exact position. They also found that isolation of the meristem from all primordia but P1 produced leaves widened across the centrolateral axis.

4.2.2.4 The dorsiventral organization of leaves requires signalling cues involving START-domain transcription factors

Leaf primordia are radially partitioned from very early in their inception by the SAM. Dorsiventral patterning genes appear in the cotyledon primordia during embryogenesis, and persist in post-germination primordial formation. The mechanism by which abaxial-adaxial identity is established is unclear, but appears to involve homeodomain proteins of the HD-Zip III class (Prigge *et al.* 2005). Some of these proteins; PHABULOSA, PHAVOLUTA and REVOLUTA (PHB, PHV and REV) promote adaxial cell fate in *Arabidopsis*, and are also required to establish the shoot apical meristem (Emery *et al.* 2003). Gain of function mutations in these proteins were found to affect a putative sterol binding (START) domain (McConnell *et al.* 2001), although these mutations also modify the binding site of micro-RNAs (miRNAs) involved in post transcriptional mRNA cleavage (reviewed by Bartel 2004). These miRNAs are abaxially located in leaf primordia, and are presumed to restrict HD-Zip expression to the adaxial side of the developing leaf (Tang *et al.* 2003). However a meristem-derived signal is required to maintain leaf dorsiventral morphology, transmitted in the L1 layer, as demonstrated by the laser ablation of these cells by Reinhart *et al.* (2004). Abaxial domain transcription factors of the *YABBY* and *KANADI* classes working antagonistically to the adaxial-promoting HD-Zip III genes (Eshed *et al* 2001, 2004, Kumaran *et al.* 2002) do not encode a START domain motif.

The microsurgical removal of the L1 layer of tomato apices effectively isolated the young primordia from the meristem, and resulted in an abaxialised radialization, even at later stages of identity (Reinhardt *et al.* 2004), confirming the theories of Bowman *et al.* (2002) that the meristem produces an adaxialising signal. Micro-RNAs have been implicated in the control of abaxial identity by down-regulating the abaxial mRNA levels of adaxializing proteins such as PHABULOSA in *Arabidopsis* and ROLLED LEAF1 in maize (Kidner & Martienssen 2004, Juarez *et al.* 2004). Whatever the nature of the meristem adaxialising signal, it is required during an extended period of leaf development, as surgical isolation of the primordium from the meristem L1 layer can abolish the dorsiventral pattern in the later maturing parts of the leaf (Reinhardt *et al.* 2004).

The collateral arrangement of xylem and phloem in the vascular strand of the *Arabidopsis* leaf has an abaxial-adaxial asymmetry. Both the *KANADI* and *PHB/PHV/REV* families of genes show polar expression in the vasculature, respectively in phloem and xylem, and both functions are required for the polar development of vascular strands (Emery *et al.* 2003, Juarez *et al.* 2004). Another HD-Zip III, again with a START domain, is the *AthB8* gene, defining pre-provascular cell fate ahead of both phloem and xylem differentiation (Scarpella *et al.* 2004). *AthB8* is the earliest known transcriptional signal in provascular cell fate commitment, and expression studies demonstrate an 'invasion' of p*AthB8*::GUS reporter activity advancing acropetally from the established vascular system into the youngest leaf primordium (Scarpella *et al.* 2004). A layer of SCR-expressing cells follows this vascular advance, recruiting cells from the pro-mesophyll layer on the abaxial side of the procambial strand (Wysocka-Diller *et al.* 2000).

4.2.3 Rationale

The tissue localization of the p*HYD1*::GUS reporter in wild-type plants implies a cell-type specific gene activity for *HYDRA1* in the plant body, which is modulated throughout embryogenesis and post-germination development. The reporter specifically highlighted the root cap and differentiating epidermis, with a differential timing of expression between trichoblast and atrichoblast cell files that reflected the distinctions in their differentiation timing and symplastic isolation. This distribution is in contrast to reporter activity for other sterol biosynthesis genes such as the SMTs (Diener *et al.* 2000, Carland *et al.* 2002), and the higher resolution examination of *HYD1* reporter activity than previously reported (Souter *et al.* 2004) suggests a different interpretation of tissue expression than as reported by these authors. In shoots, stipule expression appeared strongly at a very early stage of leaf differentiation, and persisted throughout development in these organs. A more transient signal resolved specific cells in functional epidermal cells of the leaves and stems. In contrast, a transient expression which did not highlight specific cell types was evident in sepals.

In order to assess the role of HYDRA-mediated sterols in development, this chapter examines pattern definition in the *hydra* mutant plant body, with particular reference to the cells highlighted by *HYD1* reporter activity.

4.3 Results

4.3.1 Sibling variation and duplication of the longitudinal axis

4.3.1.1 Mutants at the *hydra* loci demonstrate substantial sibling variation

Fig. 4.1 shows a representation of the range of morphological inter-sibling variability found in the *hydra* phenotype. The shoot can have from one (Fig. 4.1; A) to multiple SAMs (Fig. 4.1; F) and may have a duplicated primary root axis (Fig. 4.1; C, E), although not in all seedlings. A subset of the population have prong-shaped structures which arise either from the hypocotyl as in Fig. 4.1; D, or from around the SAM during later post-germination growth. Another variable characteristic is SAM position, shown in Fig. 4.1; E; in this example the SAM is displaced towards the outer margin of the upper hypocotyl radial axis opposite the formation of a single cotyledon. Some siblings have a morphology where most of the cotyledon-like structures are fused into a large, often lobed structure; this formation also results in variation in SAM positioning.

Other *hydra* seedlings, appearing rarely within the population of siblings, have more extreme phenotypes than those represented in Fig. 4.1. These 'rarities' are usually very short lived (not surviving for more than one week), and can include the following.

a. Seedlings with a ring of fused cotyledon material, producing a 'golf-tee' shape, reminiscent of *Brassica juncea* embryos cultured in the presence of auxin transport inhibitors (Liu *et al.* 1993.

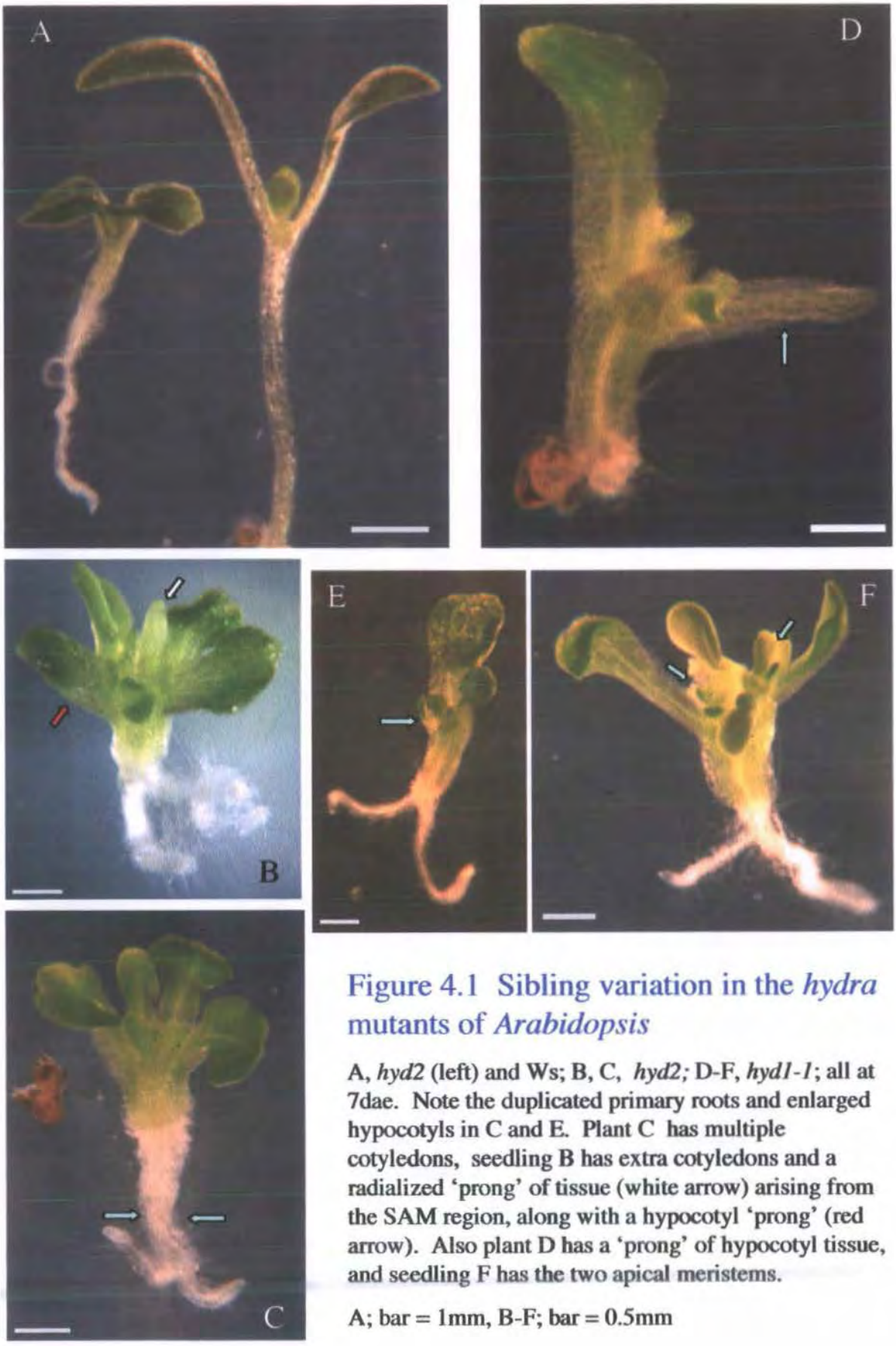

Figure 4.1 Sibling variation in the *hydra* mutants of *Arabidopsis*

A, *hyd2* (left) and Ws; B, C, *hyd2;* D-F, *hyd1-1*; all at 7dae. Note the duplicated primary roots and enlarged hypocotyls in C and E. Plant C has multiple cotyledons, seedling B has extra cotyledons and a radialized 'prong' of tissue (white arrow) arising from the SAM region, along with a hypocotyl 'prong' (red arrow). Also plant D has a 'prong' of hypocotyl tissue, and seedling F has the two apical meristems.

A; bar = 1mm, B-F; bar = 0.5mm

b. Seedlings with a rounded apex and no cotyledons, producing a structure that is reminiscent of the inflorescence apices of *pin1* mutants (Okada *et al.* 1991).
c. Seedlings with one or two cotyledons and almost no root, with a morphology similar to *monopteros* (Mayer *et al.* 1991).
d. Barrel-shaped seedlings, with short roots, and with rudimentary or much reduced cotyledon primordia-like structures at the apex.

The *hydra* mutants demonstrate a variation in longevity (Table 4.1, derived from data in Appendix 5). In comparison, none of the control plants died under these culture conditions over the time-span of the experiment. Siblings were selected as 3 dae seedlings, and so this data does not account for mutants which may have aborted either during embryogenesis or during the transition to post-germination growth. It is likely that pre-emergence abortion accounts for some siblings, as within different heterozygous parental lines, a variable number of mutants arise, from the classic 3:1 ratio, to a much smaller proportion of overall seedlings. A small number of mutants, associated with the more extreme morphologies, died within a few days of germination. Other seedlings die over a range of timescales; it is unclear from later sibling survivors whether this is predictable in association with early morphology, other than in cases with extreme patterning defects.

Of the seedlings surviving in the longer term, siblings of *hyd1* usually retained some growth of the primary root, although this was slower than growth seen from both anchor roots (at the root-hypocotyl junction) and laterals from the main root axis. In *hyd2*, where primary root meristems demonstrate less viability than *hyd1* (Souter *et al.* 2002), longer-lived siblings showed almost all continued root growth from post-germination anchor roots and laterals. Where death of the primary root apex occurred, this was followed rapidly by signs of senescence in the cotyledons and oldest true leaves of the rosette in both *hyd1* and *hyd2*. This phenomenon was seen most frequently in *hyd2*, and all of the 'survivors' in the longevity study listed in Table 4.1, showed

senescence in the cotyledons. A cessation of root growth preceded shoot death in all cases.

Of the siblings which survived under tissue culture conditions beyond around 40 days, a further subset of these produced inflorescences. All wild-type plants (n=20), taken from both *hydra* backgrounds, had bolted by 25 dae under the same conditions. Bolting in the mutants was severely delayed in comparison with wild-type plants grown under the same conditions (data not shown).

Lifespan (dae)	*hyd1-2* (n = 94, median = 36-42)	*hyd2* (n = 97, median = 22-28)
3-6	2.1%	9.3%
7-13	17.0%	21.6%
14-21	11.7%	18.6%
22-28	8.5%	15.5%
29-35	10.6%	17.5%
36-42	16.0%	2.1%
43-50	4.3%	-
51+ (surviving)	28.7%	14.4%

Table 4.1; Longevity in *hydra* siblings

4.3.1.2 Sibling variation is associated with variable duplication or dissociation of the hypocotyl stele

Wild-type seedlings show a coherent close association of vascular strands within a central stele in the hypocotyl (Fig. 4.2; A); this association extends to the root apex, where new cells from the meristem are recruited into the established cell files. The vascular strands of the hypocotyl stele bifurcate

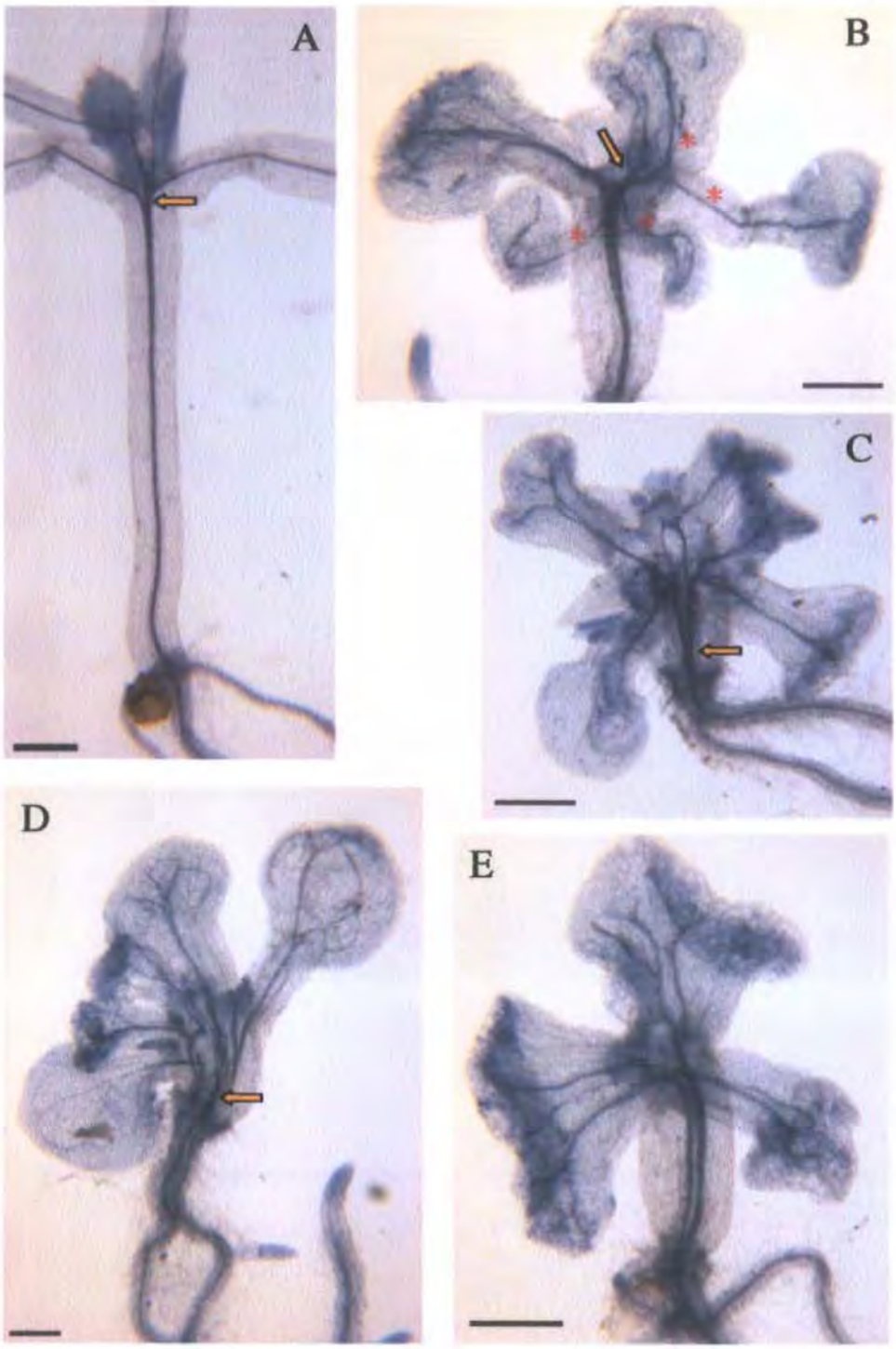

Figure 4.2 Variable stele dissociation and axis duplication between *hyd1* siblings

A; wild-type hypocotyl detail from an 8dae plant, stained with aniline blue. The coherent vascular trace within the hypocotyl stele branches at the apex into the cotyledon vascular traces. B-E *hydra1*, 8dae seedlings, with some true leaves removed to show the upper hypocotyl region. A-E, bar = 0.5mm.

B appears to have a coherent vasculature within the stele; one primary strand dissociates above the usual branch point (arrow) giving multiple cotyledon structures (asterisks). The trace in C dissociates above the root-hypocotyl junction, giving a wide apical meristem area. E; a duplicated axis is evident in both hypocotyl and root. D; extreme strand dissociation results in a barrel-shaped hypocotyl above a duplicated root axis.

near the shoot apex beneath the presumptive SAM in the hypocotyl-cotyledon transition zone, forming the primary vascular traces of the cotyledons, and conferring a bilateral symmetry onto the seedling.

A range of patterning phenomena were found in the *hydra* mutant hypocotyl stele (Fig. 4.2; B-E). The range of sibling phenotypes include;

1. Dissociation of the vascular trace above the primary branch point beneath the SAM (as in Fig. 4.2; B). In this example, four cotyledon-like structures have resolved from dissociation of a single primary trace, whilst the opposite side of the SAM the trace has remained coherent, resulting in a single cotyledon.

2. Dissociation within the hypocotyl stele between the SAM region and the root-hypocotyl junction, as shown in Fig. 4.2; C and D. In example C, the hypocotyl trace divides from near the base giving two strands, and a widened hypocotyl structure towards the SAM region. These strands divide again at the hypocotyl apex, resulting in a total of five cotyledons, again of variable size. Plant D has a more severe dissociation of strands from the hypocotyl base. In this instance multiple traces are evident within the radially swollen hypocotyl, which have further divided at or near the shoot apex into multiple cotyledons and true leaf primordia. (Most true leaves were removed from this sample, to allow visualisation of the hypocotyl).

3. Duplication of the whole longitudinal axis from the apex to the base, giving two primary roots, each with a stele, as in Fig. 4.2; E. In this case, hypocotyl morphology appears similar to that of the plant in Fig. 4.2; B, which lacks an obvious strand dissociation.

It is interesting to note that no *hydra* siblings showed root axis dissociation or duplication in the absence of hypocotyl patterning defects, implying that

duplication of the longitudinal axis was determined in a 'top-down' manner by patterning further towards the shoot apex.

A categorization of this patterning phenomenon was made between the populations of *hydra* siblings, shown in table 4.2. Seedlings were harvested at 8 dae, stained and cleared, and scored for the three categories above. These data show that the axis dissociation and duplication phenomena are common to both *hydra* mutants, although full axis duplication occurs more frequently in the *hyd1-2* population. Each category contained a range of morphologies, varying particularly with regard to cotyledon numbers, i.e. strands dissociated within the hypocotyl may or may not further divide nearer to the apex, resulting in variable numbers of cotyledons. Scoring was conducted according to the location of the first signs of axis dissociation, meaning that strands with dissociations in the hypocotyl and in the cotyledon traces were preferentially tallied into the 'within the hypocotyl stele' category. Very rarely, siblings with axis duplication extending part of the length of the root axis were found, although no examples of this phenomenon were present in the data set in table 4.2.

	hyd1-2 (n = 221)	*hyd2* (n = 178)
Strand dissociation above the SAM only	54 (24.4%)	48 (27.0%)
Dissociation within the hypocotyl stele	134 (60.7%)	120 (67.4%)
Full axis duplication	33 (14.9%)	10 (5.6%)

Table 4.2 Axis dissociation and duplication in *hydra* siblings

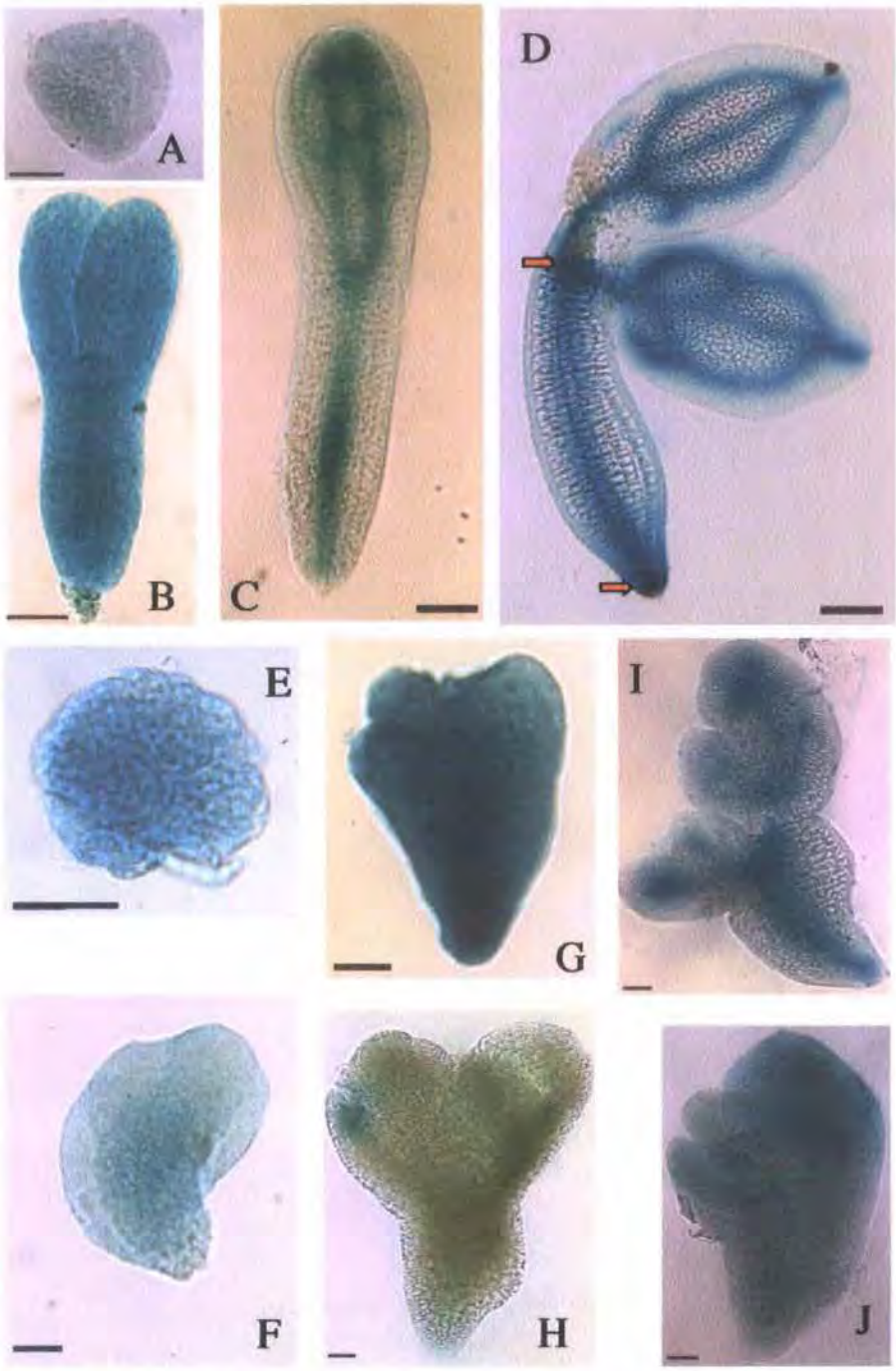

Figure 4.3 Procambial traces in *hydra* mutant embryos

A-J; wild type (A-D) and *hyd2* (E-J) embryos carrying the p*AthB8*::GUS procambial marker.

In wild-type, this construct is first expressed diffusely throughout the embryo at the globular-heart stage transition (A), becoming stronger in the young torpedo stage (B), and resolving to show the position of provascular traces as the embryo elongates and matures (C, D). Arrows in D show peaks of GUS activity in the root cap and SAM.

In *hydra*, expression is seen in globular (E) and heart (F) stage embryos, and becomes stronger through the torpedo stage (G). Later stages show anomalies in the patterning of the provascular trace. H shows a peak of expression in a cotyledon-like structure. J shows indistinct diffuse staining in super-numerary cotyledons. I has bifurcation of the primary vascular traces resulting in lobed cotyledon-like structures, and a diffuse reporter expression in the laterally-expanded mid to upper hypocotyl region; this may correspond to hypocotyl vascular strand dissociation in the seedling.

A-C, E-,; bar = 50μm; D, bar = 100μm.

Although strand dissociation above the SAM region in *hyd2* appears higher than in *hyd1*, a greater number of these showed duplications of the cotyledon primary axis without forming separate organs, giving a lobed or enlarged cotyledon lamina. No examples of axis duplication were observed in the wild-type (Ws) background for either of these mutants.

4.3.1.3 Anomalies in formation of the longitudinal axis are evident in provascular strand formation during embryogenesis

The morphology and body organization of the emergent *Arabidopsis* seedling is under the control of patterning events during embryogenesis. The position of the stele corresponds to that of longitudinally-oriented procambial (provascular) cell files formed during the globular-heart transition. A subset of these cells differentiate first in the emergent seedling as the phloem traces, followed by the xylem (Busse & Evert 1999a, b). In order to investigate the establishment of procambial patterning in the embryo, the p*AthB8*::GUS reporter was introduced into a *hydra* mutant background. The AthB8 protein is an HD-Zip transcription factor, and its promoter-reporter construct shows expression in cells prior to their adopting vascular procambial cell fate (Baima *et al.* 1995, Baima *et al.* 2001).

Fig. 4.3 compares the expression of p*AthB8*::GUS in wild-type and *hyd2* mutant embryos. In wild-type (Fig. 4.3; A-D), GUS activity is first seen during the heart stage, increasing during the torpedo stage, and then resolving to the procambial traces in the pro-cotyledons, hypocotyl and root. By the late torpedo stage (Fig. 4.3; C) the procambial strand position is well defined, and reporter activity persists into the maturation stage embryo (Fig. 4.3; D), when a particularly strong expression is visible in the root cap and shoot meristem (arrows).

A variable expression pattern emerges from the activity of p*AthB8*::GUS in *hyd2* mutant embryos (Fig. 4.3; E-J). Expression at the globular-heart stage transition shows diffuse GUS activity throughout the embryo, whist later stages can develop high levels (G) or minimal levels of signal (H), the latter showing a peak near the apex of one of the super-numerary proto-cotyledon structures. More mature embryos may have a rudimentary procambial trace, although may not demonstrate normal patterning (I), or a diffuse signal which is located in one region of the embryo (such as the proto-cotyledons as in J). These findings suggest that the patterning processes allowing the definition of the procambial strands have been disrupted.

4.3.2 Vascular strand coherence and integrity of longitudinally oriented cell files in *hydra* mutant seedlings

4.3.2.1 Xylem vessels of the stele have variable longitudinal integrity in the *hydra* hypocotyl and root

During post-germination growth, in the majority of *hyd2* mutant siblings the hypocotyl stele carries a coherent procambial trace, as shown by the p*AthB8*::GUS reporter in Fig. 4.4; B and C. In contrast to wild-type (Fig. 4.4; A), where the xylem strands have differentiated as single continuous cell files, the *hydra* mutant hypocotyl is characterised by incomplete and isolated sections of xylem within this defined provascular field (Fig. 4.4; B and C, arrows). Xylem vessels of the mutant root stele can also have discontinuous sections in their xylem traces (Fig. 4.5; E), whereas the wild-type root maintains its integrity (Fig. 4.5; D). Discontinuities in root xylem are less frequent than in hypocotyls from seedlings of this age class. Again the

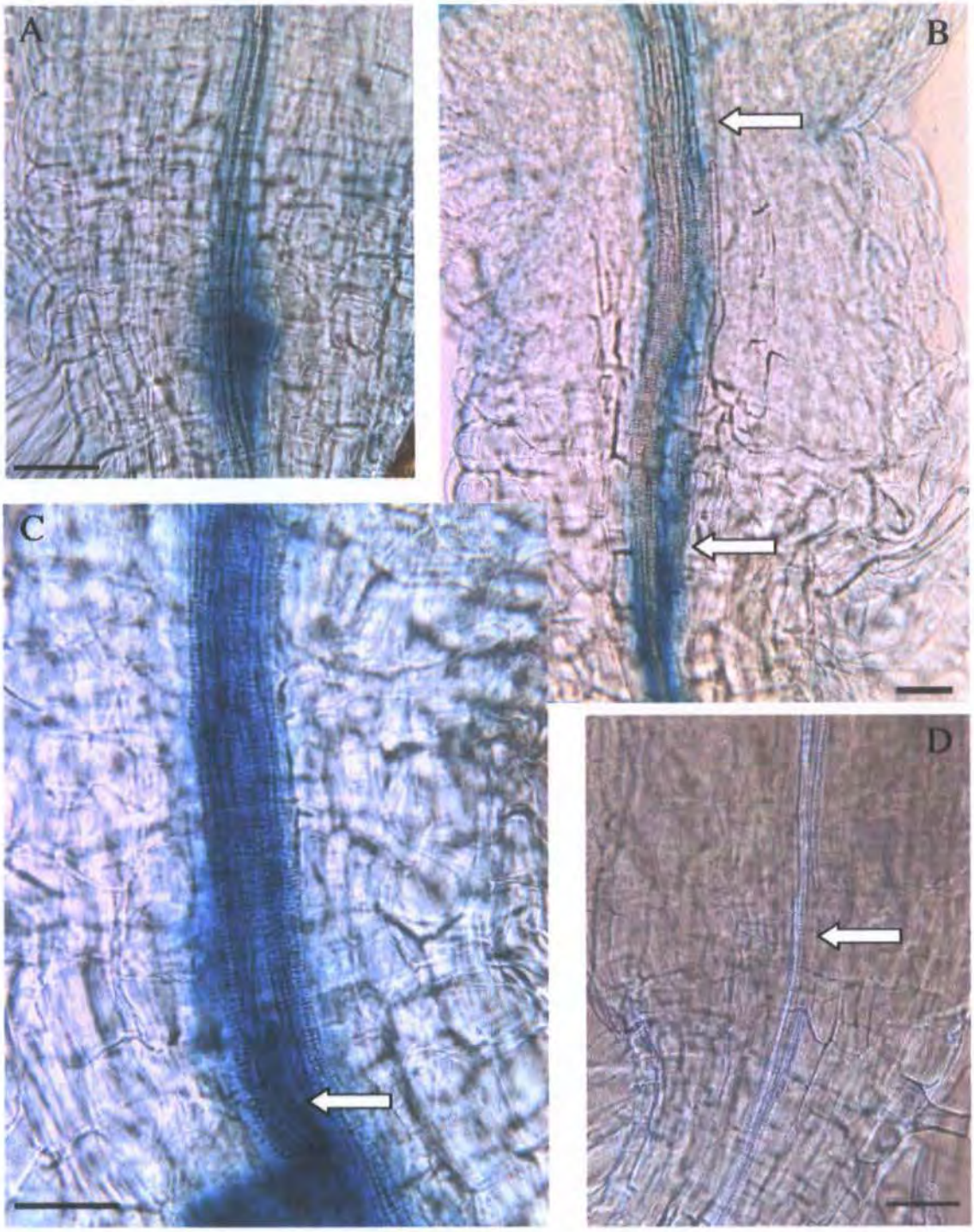

Figure 4.4 Compromised xylem integrity in the lower hypocotyl of *hydra* mutant seedlings

A-D, root-hypocotyl junction in wild type and mutant seedlings. A; Ws, and B and C; *hyd2*, all 5dae plants carrying the p*AthB8*::GUS reporter of procambial tissue identity. D; *hyd1* at 3dae, cleared tissues.

Vascular strands form continuous files of cells in the wild type hypocotyl and root stele; as radial expansion takes place, new vascular cell files form in tight association with the existing pattern (as in A (Ws); the staining peak marks an initiating anchor root primordium.) In *hydra* mutants, vascular discontinuities are often seen in the xylem (B-D, arrows), although procambial traces, as shown by p*AthB8*::GUS activity, appear coherent.

Bar = 50μm.

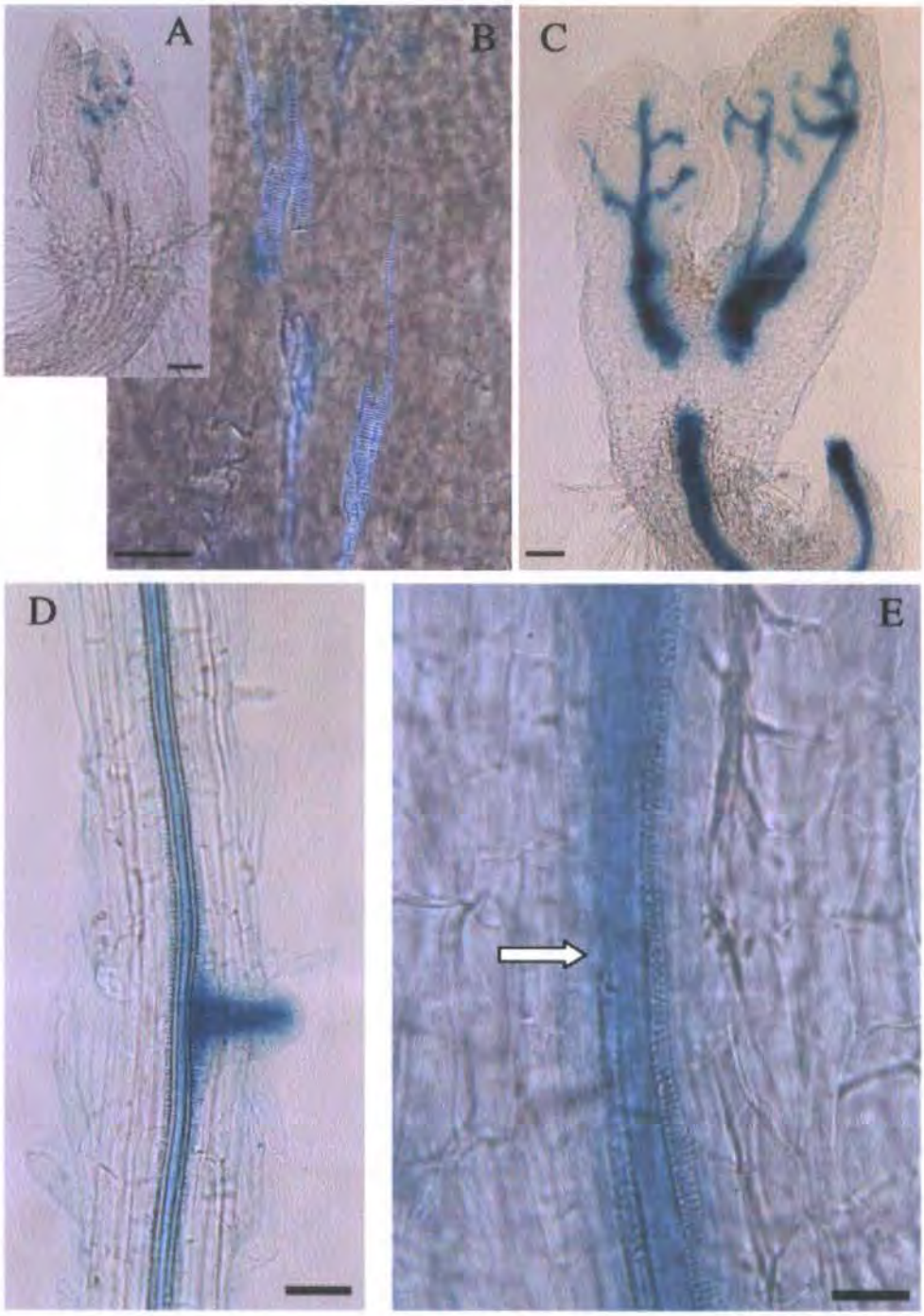

Figure 4.5 Compromised xylem and procambial integrity in the hypocotyl and root of *hydra2*

A; *hyd2* 3 dae plant expressing the p*CYC1At*::CDB::GUS reporter. This image demonstrates that hypocotyl vascular continuity problems, resulting from patterning events during embryogenesis, are also associated with a disruption of local signals promoting post-germination cell division. B; DIC image showing detail of the mid hypocotyl region of plant A. C; 3 dae *hyd2* seedling expressing the p*AthB8*::Gus provascular marker, is an extreme example where the entirety of the hypocotyl stele is broken between shoot and root regions. This time the provascular trace is incomplete; such examples are rare and represent extremes in the range of sibling variation. Xylem discontinuities can also be seen in roots. D = wild-type, and E = *hyd2*; mid-roots of 5dae plants show broken strands of xylem in *hyd2* (arrow).

A, C, bar = 100 μm; B, D, E, bar = 50μm.

procambial trace demonstrates a broad coherence along the longitudinal axis in the vicinity of these discontinuities.

The 3 dae *hyd2* seedling in Fig. 4.5; C has a broken procambial trace between the root and shoot in the region of hypocotyl-cotyledon transition; this plant represents a rarely-observed extreme within the range of sibling variability. Note that at the free vein ends, p*AthB8*::GUS shows peaks of activity. It is possible that siblings with patterning problems of this nature are amongst the individuals showing post-germination early death, or may more usually fail to germinate.

The *hyd2* seedling shown in Fig. 4.5; A, detailed in B, has extreme xylem incoherence in the hypocotyl, although the root xylem trace appears intact in this example. This seedling shows expression of the *CYC1At*:CDB:GUS reporter of cells at the G2 and M phases of the cell cycle, i.e. undergoing active division (Hauser and Bauer, 1999). The main reporter activity is around the shoot apical meristem region, although occasional ectopic cell divisions are visible in the vicinity of these isolated xylem vessels. Wild-type hypocotyl growth at this stage proceeds by cell elongation at this stage (Gendreau *et al.* 1997), with the only cell division events highlighted by this reporter involving stomatal ontogeny from division of meristemoid mother cells in the epidermis. It would appear that the extreme vascular discontinuity in this sibling is not caused by ectopic cell division, but is associated with a local modulation of the cues co-ordinating division and differentiation between cells.

4.3.2.2 Cotyledons in *hydra* mutants show anomalous patterning, and xylem traces demonstrate increased levels of 'noise' (i.e. reduced between-cell co-ordination within the cell file)

The basic template of cotyledon vasculature in *Arabidopsis* comprises a primary midvein which bifurcates at the apex to form marginal loops of

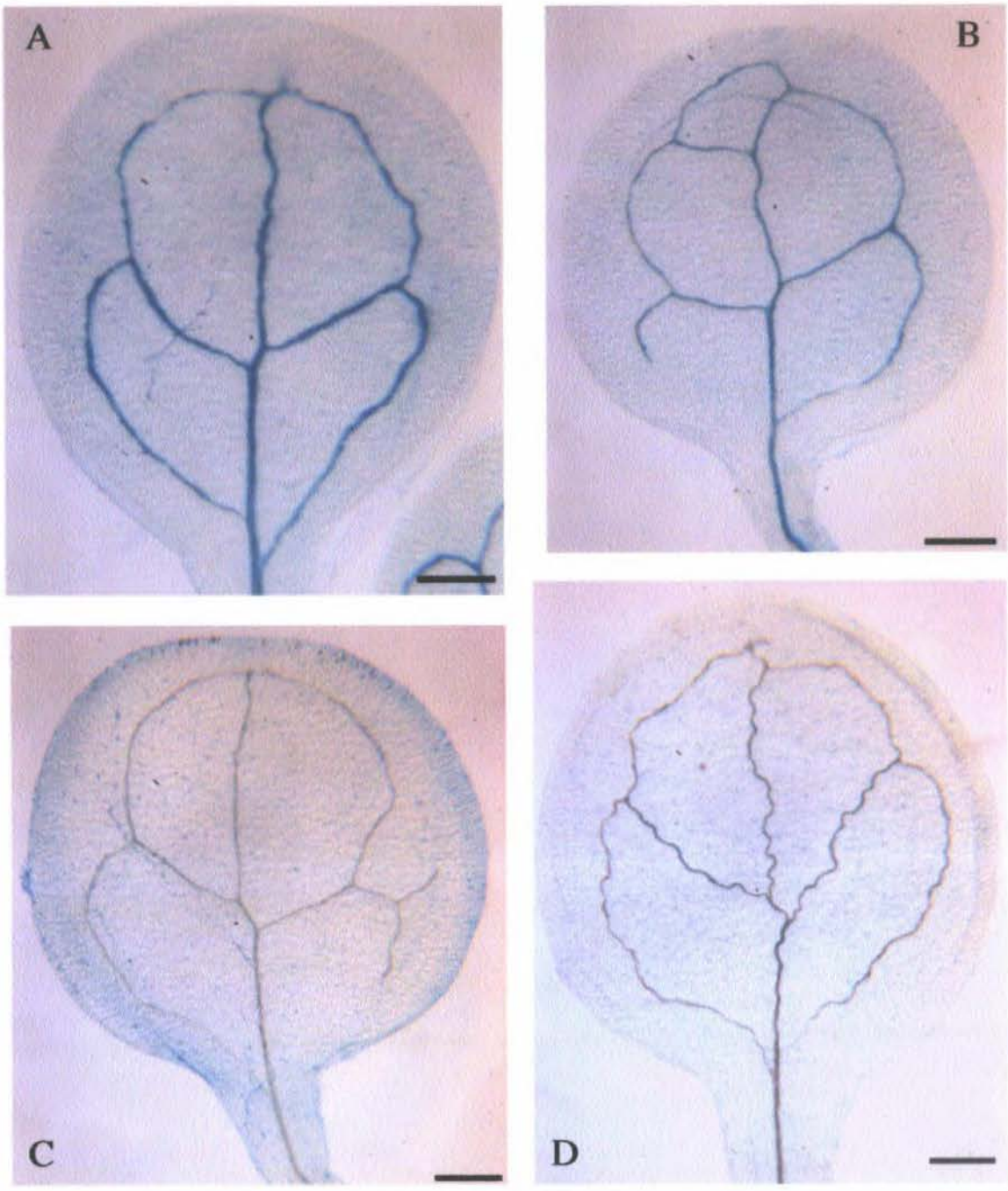

Figure 4.6 Cotyledon vasculature in wild-type seedlings

A-D; cotyledons from wild-type plants at 5dae, A and B showing expression of the p*PIN1*::GUS construct (bar = 0.25mm).

The 'classic' vascular patterning shown in A is variable between seedlings, with different cotyledons carrying irregular loops (B), open loops (B and C) and wavering vascular traces (D). Vascular patterning can vary between the two cotyledons of an individual wild-type seedling. This suggests that wild-type vascular differentiation has a high degree of plasticity, and relies upon local cues to recruit and coordinate undifferentiated mesophyll into coherent cell files, forming a continuous network.

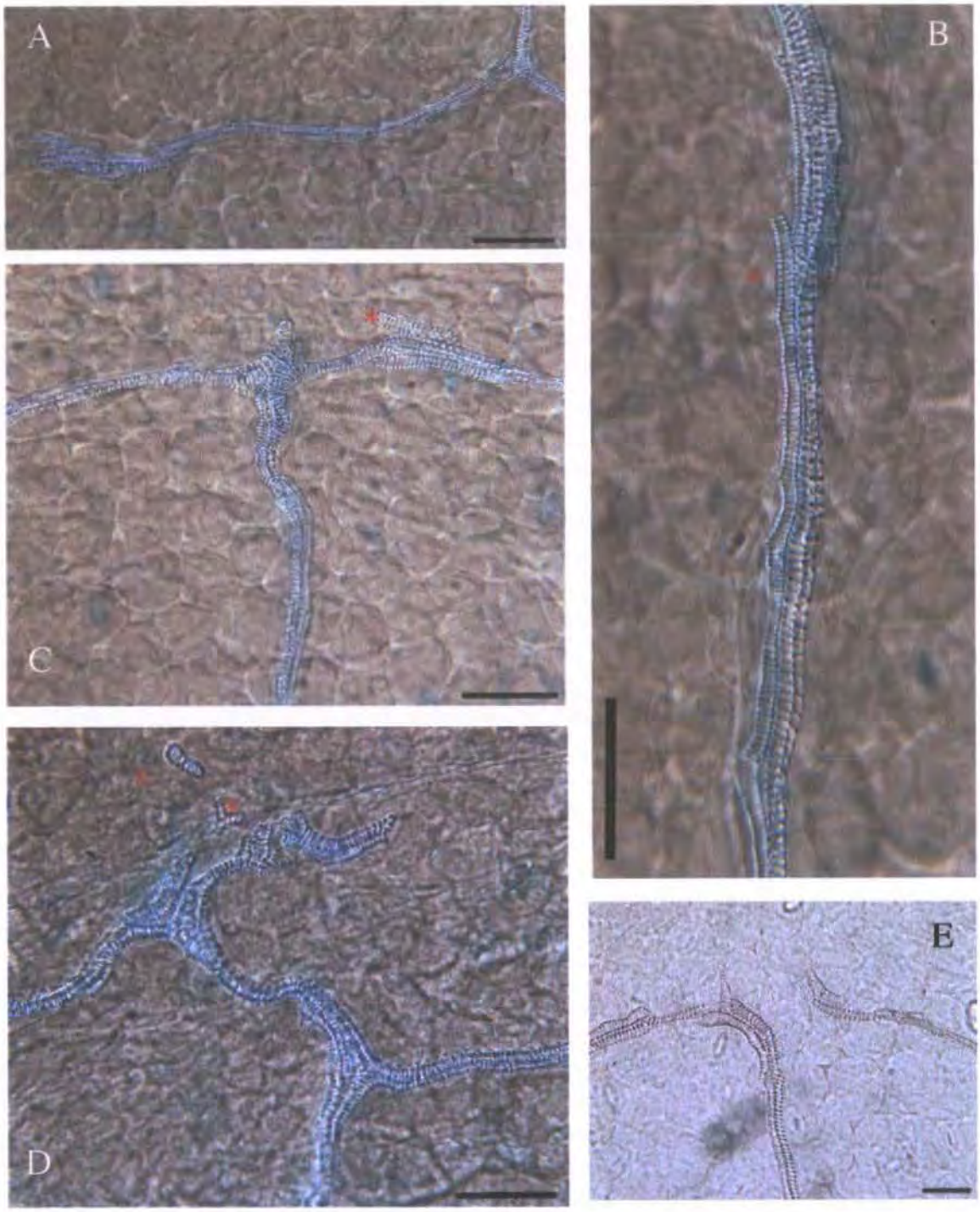

Figure 4.7 Xylem detail from wild-type cotyledon vasculature

A-E; DIC images of vasculature in cleared tissues from wild-type cotyledons (bar = 50μm).

B; mid-vein, A; free vein ending and C; hydathode from the cotyledon shown in Fig. 4.6; C. D and E; hydathodes from other cotyledons at 7 dae. Asterisks show the position of vessels which appear dissociated or poorly coordinated with other xylem cells.

Plasticity is evident in the development of the vascular trace in wild-type plants, resulting in xylem 'noise' at vein endings, in parts of the primary vascular strand, and most frequently at the apical hydathode. As the wild-type cotyledon mesophyll layer does not undergo cell division in post-germination growth, these patterns result from recruitment and subsequent cell differentiation events.

secondary venation (as in Fig. 4.6; A). Wild-type cotyledons show some variation in this pattern (Fig. 4.6; B-D), and variably form some open loops in the secondary vasculature in certain organs. Often there is a difference in the vascular trace formed in the two cotyledons from an individual seedling. A higher-resolution of these vascular traces reveals variation in the coherence of the files of xylem vessels comprising the strand (Fig. 4.7; A-E). Areas where the greatest degree of this variation can be seen, (hereafter referred to as 'noise'), correspond to the positions of the apical hydathodes. Here, differentiation produces a range of phenomena (Fig. 4.7; C, D, E), including individual vessels isolated on the margin of the strand (C), incomplete closure of the secondary trace with the primary midvein (E) and isolated xylem vessels between the main vascular trace and the laminar margin (D). Lesser amounts of noise in the cotyledon trace are evident in the primary midvein (Fig. 4.7; B), and at free vein endings (Fig. 4.7; A).

In *hydra* mutant cotyledons, a much more varied cotyledon pattern is seen (Fig. 4.8; A-H). These examples are taken from seedlings showing expression of the p*PIN1*::GUS reporter construct, which marks the positioning of *PIN1* transcription. This marker highlights the xylem patterning in these mutant cotyledons, revealing a range of traces which include extra secondary loops, large numbers of free vein endings, and some examples of dissociated or duplicated primary strands, all in tandem with a modification of the shape of the lamina. In some of these cotyledons (A, E, H) the reporter highlights sections of xylem isolated from the main traces. These vascular 'islands' are separated by a much larger intervening area of mesophyll than the occasional isolated xylem cells seen in wild-type hydathode regions.

At higher resolution, the mutant xylem vasculature reveals a substantially greater degree of noise in both primary midveins (Fig. 4.9; A-D) and hydathodes (Fig. 4.9; D, F, G). Examination of a xylem 'island (Fig. 4.9; E) shows many of the characteristics of this lower level of co-ordination, with cells of variable size and shape, clustered in a range of orientations relative to

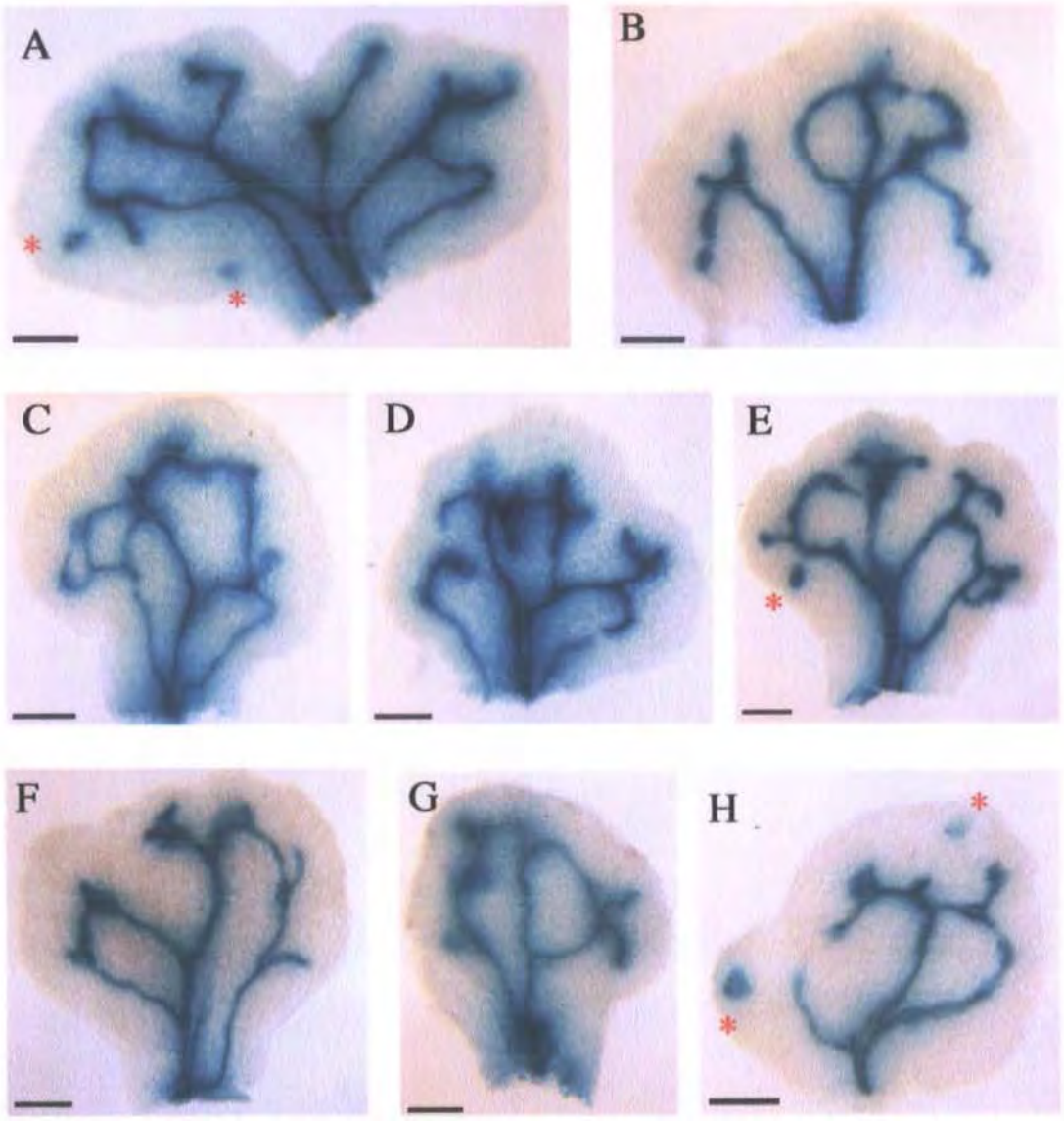

Figure 4.8 Cotyledon vasculature in *hydra2*

A-H; *hydra2* cotyledons from 5dae plants expressing the p*PIN1*::GUS construct.

Several of these examples have dissociated (A, B) or duplicated A, D, E, F, H) primary vascular strands, and isolated areas of xylem (A, E, H; asterisks). A similar variability in vascular patterning, again with isolated sections of xylem, can be seen in true leaves of older *hydra* specimens.

A-H, bar = 0.25mm.

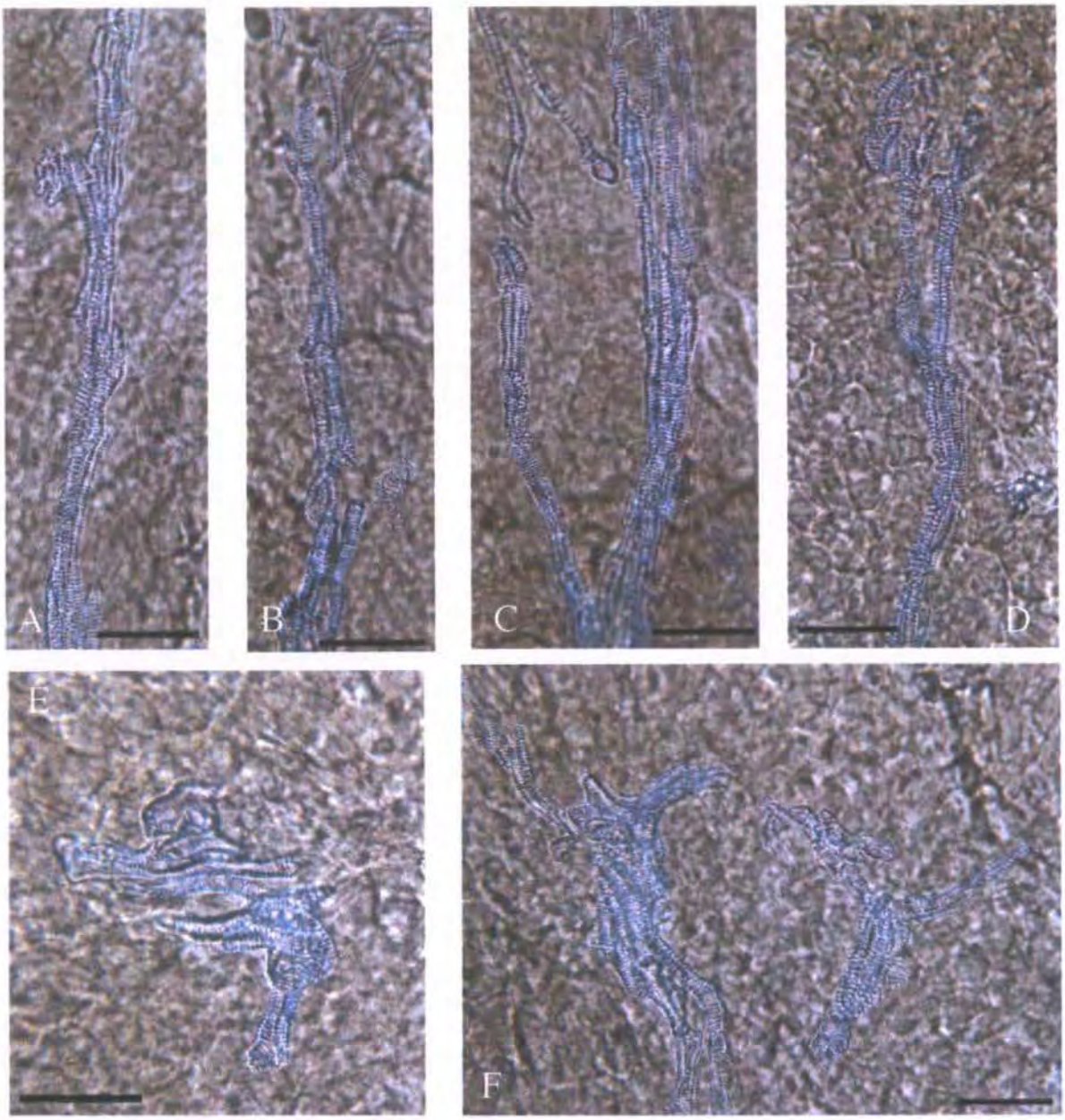

Figure 4.9 Xylem detail from *hyd2* cotyledon vasculature

A-G; DIC images showing vascular detail from *hydra1* cotyledons, taken from 7 dae plants cleared with chloral hydrate.

A-C; primary midveins, D, F and G; cotyledon apical hydathode regions, and E; a vascular 'island', of disconnected xylem tissue. The *hydra* mutant xylem traces show a greater degree of 'noise' than wild-type (Fig. 4.7).

Bar = 50μm.

each other. The main strands also show variability in vessel size and orientation, with cells running parallel with each other, or contorted into a more varied strand morphology than seen in wild-type plants. All of the examples in this figure have been taken from *hyd2*; a similar spectrum of vascular anomalies can be found in the xylem traces of *hyd1* mutants.

4.3.2.3 Duplication of the cotyledon primary axis and multiple cotyledon formation is found in the presence of dissociated vascular strands in the upper hypocotyl

A closer examination of the hypocotyl-cotyledon transition zone shows a substantially increased level of xylem 'noise' in *hydra* hypocotyls over this region. Fig. 4.10; A-D compares wild-type and mutant traces, again in association with localization of the p*AthB8*::GUS procambial marker. Wild-type plants have a distinct point of bifurcation in the xylem traces (Fig. 4.10; A, B). The *hyd2* sibling shown in Fig. 4.10; C also appears to have a coherent vascular trace in the stele, branching in an ordered manner to produce the cotyledon traces, although subsequent strand development in the cotyledons show anomalies. This plant, detailed in Fig. 4.10; D, has an upper hypocotyl containing xylem vessels which with good longitudinal integrity up to this point, although a reduction in co-ordination is evident at this point. As the strands separate, the xylem vessel elements have not connected with the cotyledon trace. In the cotyledon lamina (Fig. 4.10; C) some enlarged and isolated xylem cells are visible in the vicinity of the primary midvein. The provascular trace appears normal in the upper hypocotyl, although has discontinuities in the cotyledons.

Fig. 4.11; B-E shows further examples of *hyd2* siblings at 7 dae, again expressing the p*AthB8*::GUS reporter. In wild-type plants (Fig 4.11; A) the cotyledon traces form tightly associated strands in the elongating petioles and the primary vasculature of the first true leaf pair is in continuity with the

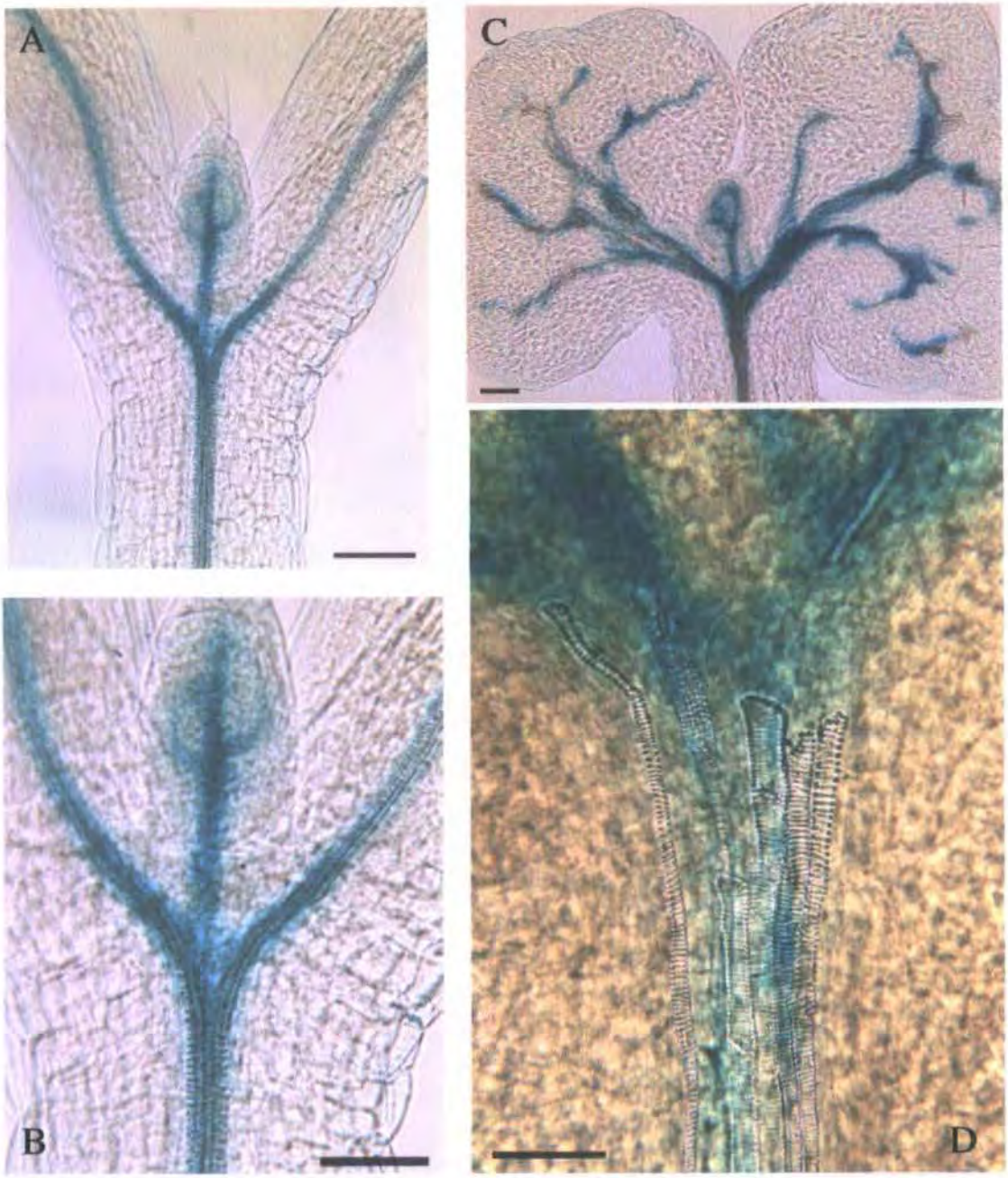

Figure 4.10 Vasculature of the wild-type and *hydra* upper hypocotyl at 3 dae

A-D; seedlings expressing the p*AthB8*::GUS procambial tissue marker.

A = wild-type at 3dae, B = detail of A. Vascular strands from the stele branch in the upper hypocotyl beneath the shoot apical meristem region, to form the two cotyledon primary vascular traces. The primary procambial trace of the first two true leaf primordia appear between these branches (A, arrow) in continuity with the cotyledon traces ahead of vascular differentiation.

The 3 dae *hyd1* seedling shown in C has vascular strands which lack co-ordination at the branch point (detailed in D), and resulting in the anomalous primary mid-vein pattern seen in the cotyledons.

A, C; bar = 10μm, B and D; bar = 50μm.

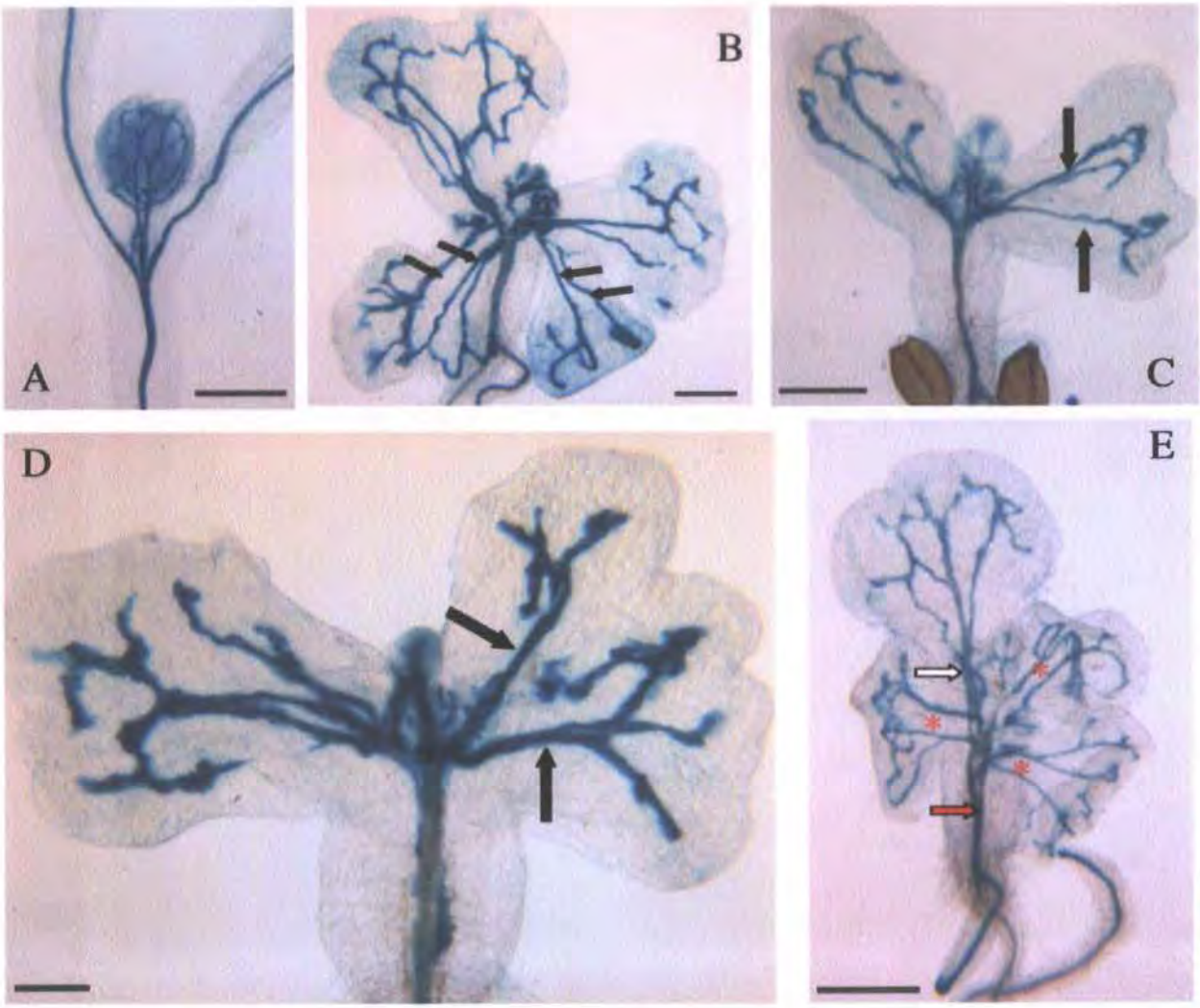

Figure 4.11 Cotyledon and true leaf vascular traces in *hydra2* at 7 dae

A, Ws and B-E, *hydra2* seedlings at 7dae, expressing the p*AthB8*::GUS procambial tissue marker.

Plant B shows vascular dissociation in the upper hypocotyl stele, with traces diverging into four cotyledons, of which two have subsequent primary vascular duplications (arrows). Plants C and D show strand divergence after initial branching of the vascular traces in the upper hypocotyl; both have duplicated primary vasculature in the right-hand cotyledon (arrows). In plant E, strand dissociation begins in the lower hypocotyl (red arrow); several traces diverge from the stele at different points, each forming a cotyledon with two parallel primary vascular strands (asterisks). The remaining cotyledon of this seedling has an extra primary vascular strand, which appears to have been 'adopted' from a diverging strand further down the stele (white arrow), and is associated with development of an extra lobe on the cotyledon.

A; bar = 100μm; B, C, E, bar = 0.5mm; D, bar = 0.25mm.

branch point of the cotyledon traces, with subsequent true leaves taking cues from these positions.

The *hyd2* seedlings in Fig. 4.11; B-D have apparently good coherence in the upper hypocotyl stele, but show multiple examples of dissociation in the cotyledon primary traces, producing duplicated midveins in widened petioles. Leaf shape is modified concurrently with this patterning anomaly, as shown in these examples. The seedling in Fig. 4.11; E has strand dissociation beginning from lower in the hypocotyl stele than the examples seen in B-D. This sibling has three cotyledons with apparent duplications of the primary midvein (asterisks), and one larger cotyledon with an extra lobe; in this organ a dissociated strand from below the petiole that appears to have joined with a secondary vascular loop from the lamina (indicated by the white arrow).

4.3.2.4 Longitudinally-oriented epidermal cell files demonstrate variable co-ordination across the radial axis

Cell files of the hypocotyl epidermis in wild-type plants show an ordered pattern of tightly aligned longitudinally oriented cell files (Fig. 4.12;C). This contrasts with the patterning of the *hydra* mutant hypocotyl. In the example from *hyd1* in Fig. 4.12; A, cells show anomalies in longitudinal alignment including single, unusually large cells spanning two cell files above (red arrows), and elongated cells with a curled morphology that appear to have changed the direction of their expansion axis, resulting in a question-mark shape (white arrows). In the *hyd2* epidermis, other anomalies in cell size can be seen in the hypocotyl (Fig. 4.12;B); curled cells, and cells shifting alignment across cell files (white arrows) are found near files of smaller cells that appear between other longitudinal cell files (red arrows).

A disruption of longitudinal cell files can also be seen in the *hydra* root epidermis (Fig. 4.13; B and C), where wild-type root epidermal cells show a

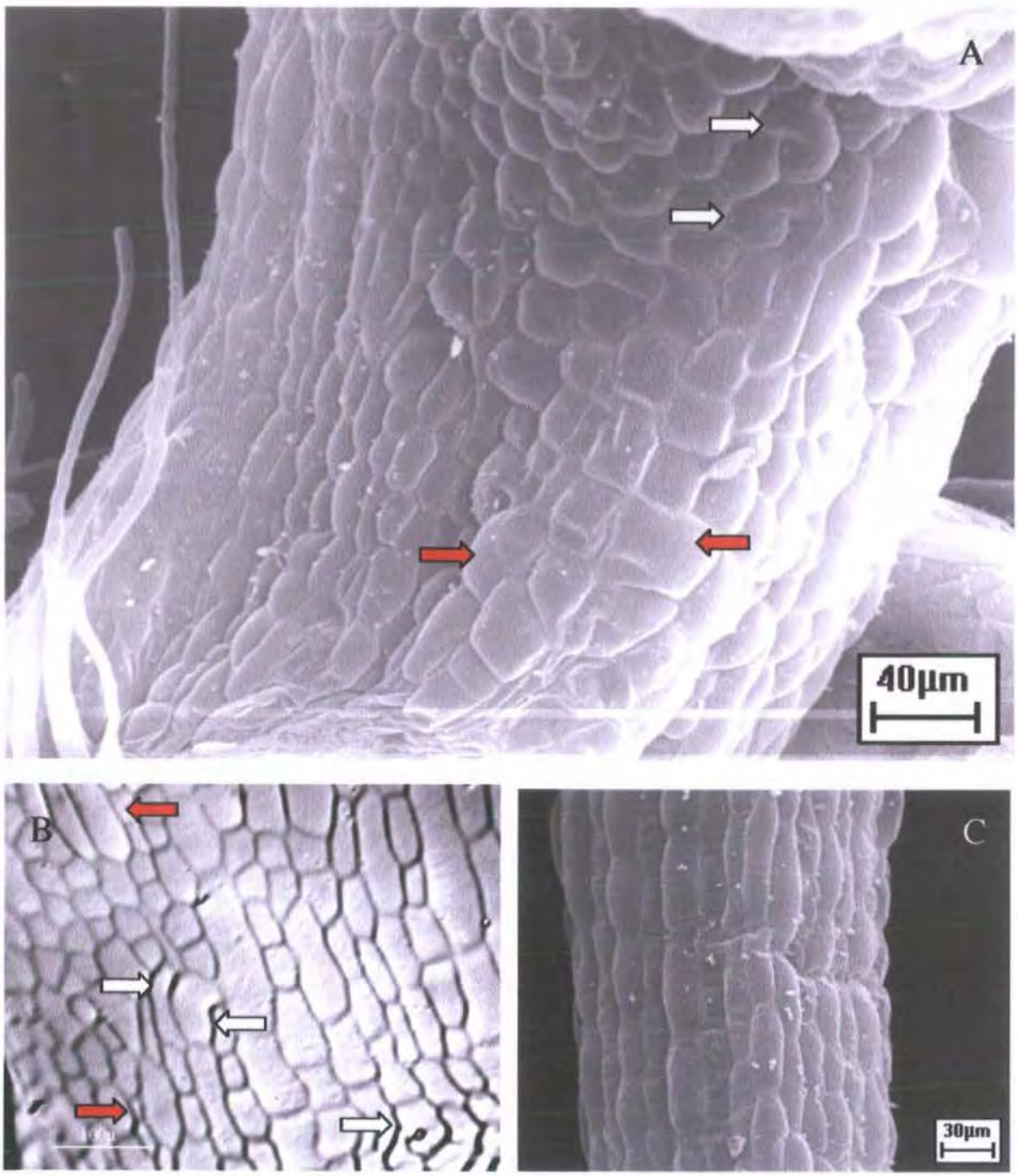

Figure 4.12 Epidermal cell files of the *hydra* mutant hypocotyl

A-C; hypocotyl epidermis from 5 dae seedlings.

Longitudinal epidermal cell files show disrupted coordination in both *hyd1* (A) and *hyd2* (B), whereas wild type plants have coherent files of cells which maintain apical-basal alignment by undergoing coordinated expansion growth. The *hydra* mutants have anomalous cell sizes (red arrows) and strangely shaped cells which appear to result from modification of the direction of expansion growth (white arrows).

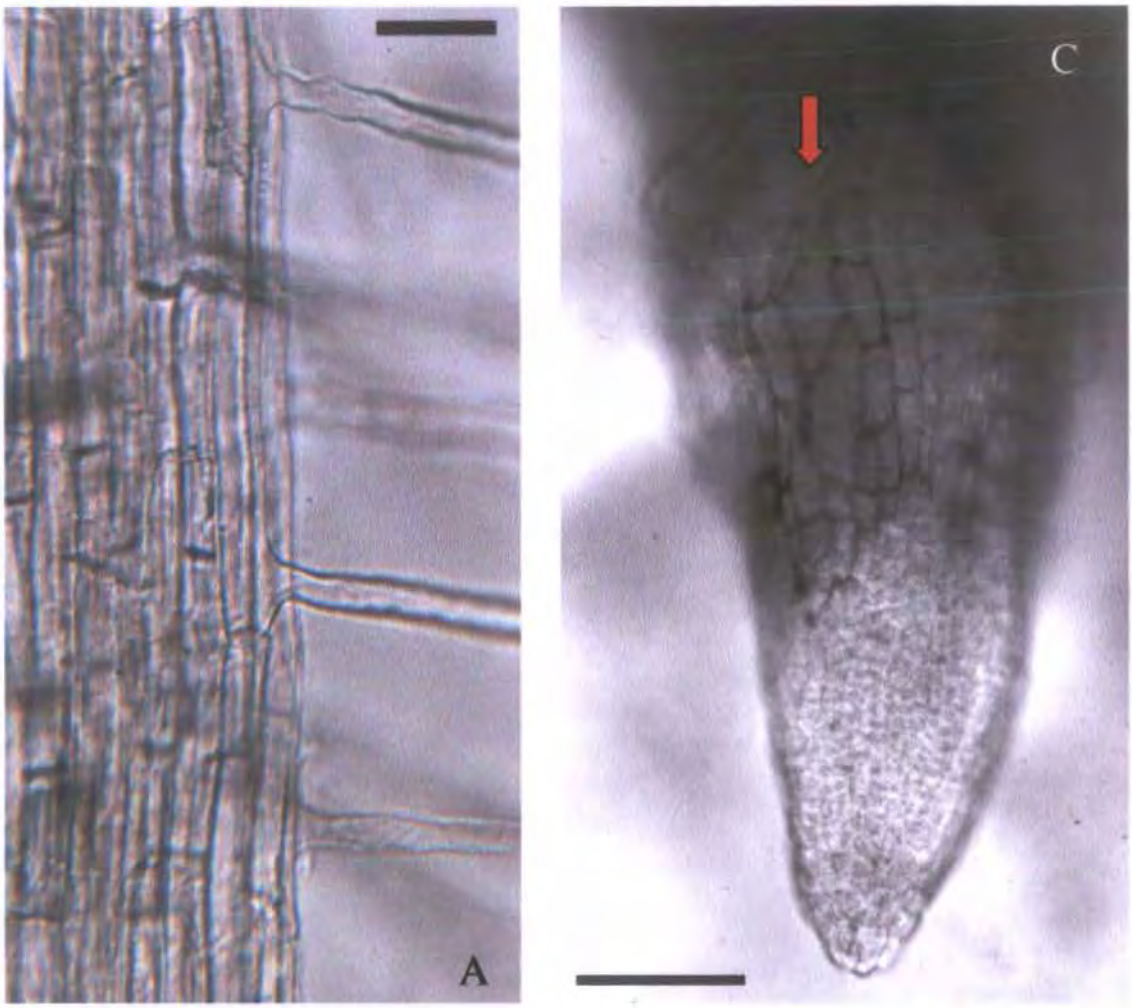

Figure 4.13 Epidermal cell files at the wild-type and *hyd2* root apex

As in the hypocotyl (Fig. 4.12), signs of disruption can also be seen in longitudinal cell files of the *hydra* root epidermis.

A-C; roots at 5 dae, grown in agar. Misalignment of longitudinal cell files is shown here in the *hyd2* primary (B) and lateral roots (C) (arrows).

In contrast, wild-type (A) maintains longitudinal integrity of cell files shown here after root hair elongation and cell maturation.

A, bar = 50μm; B, C, bar = 100μm.

similar longitudinal integrity as in hypocotyl tissues (Fig. 4.13; A). Both of the *hydra* mutants are able to initiate lateral roots, although their positioning along the main root is varied (not shown). Lateral roots appear less radially swollen than mutant primary root apices (seen in the examples in Fig. 4.13; B and C, taken from the same plant). The most viable and rapidly growing mutant laterals are anchor roots, formed at the root-hypocotyl junction.

4.3.2.5 *hydra* inflorescence stems and floral organs have a mostly coherent longitudinal cellular alignment and organ morphology, with slight variability between flowers in the centrolateral axis.

The *hydra* siblings which make the transition to flowering, initiate the bolts from axillary meristems, (shown in the dissected rosette of the seedling from Fig. 4.14; A), rather than from the primary apex. Internode length is reduced in relation to wild-type seedlings, and the bolts develop only single floral meristems in cauline axils, rather than secondary branches. Cauline internodes are reduced, so that few cauline leaves appear as distinct form the rosette in un-dissected seedlings, although subsequent internode elongation is improved.

In contrast with the production of vegetative lateral organs, the lateral organs of *hydra* inflorescence stems appear to have a normal gross morphology. Flowers appear very similar to wild-type both in the organ morphology and the whorled arrangement of these organs (Fig. 4.14; B). Anthers and carpels (Fig. 4.14; D) are also similar to wild-type organs (Fig. 4.14; C), although with slight increases in 'noise' in the xylem strands in some samples (e.g. Fig. 4.14; D, arrow). Cauline leaves (Fig. 4.15; C-E) are reduced in size in relation to wild-type (Fig. 4.15; A), and according with their size, show a reduced vascular complexity. However, the cauline xylem traces are substantially more coherent than vasculature from rosette leaves. Hydathodes in these organs showed greatest levels of xylem dissociation (Fig. 4.15; E), but 'islands of

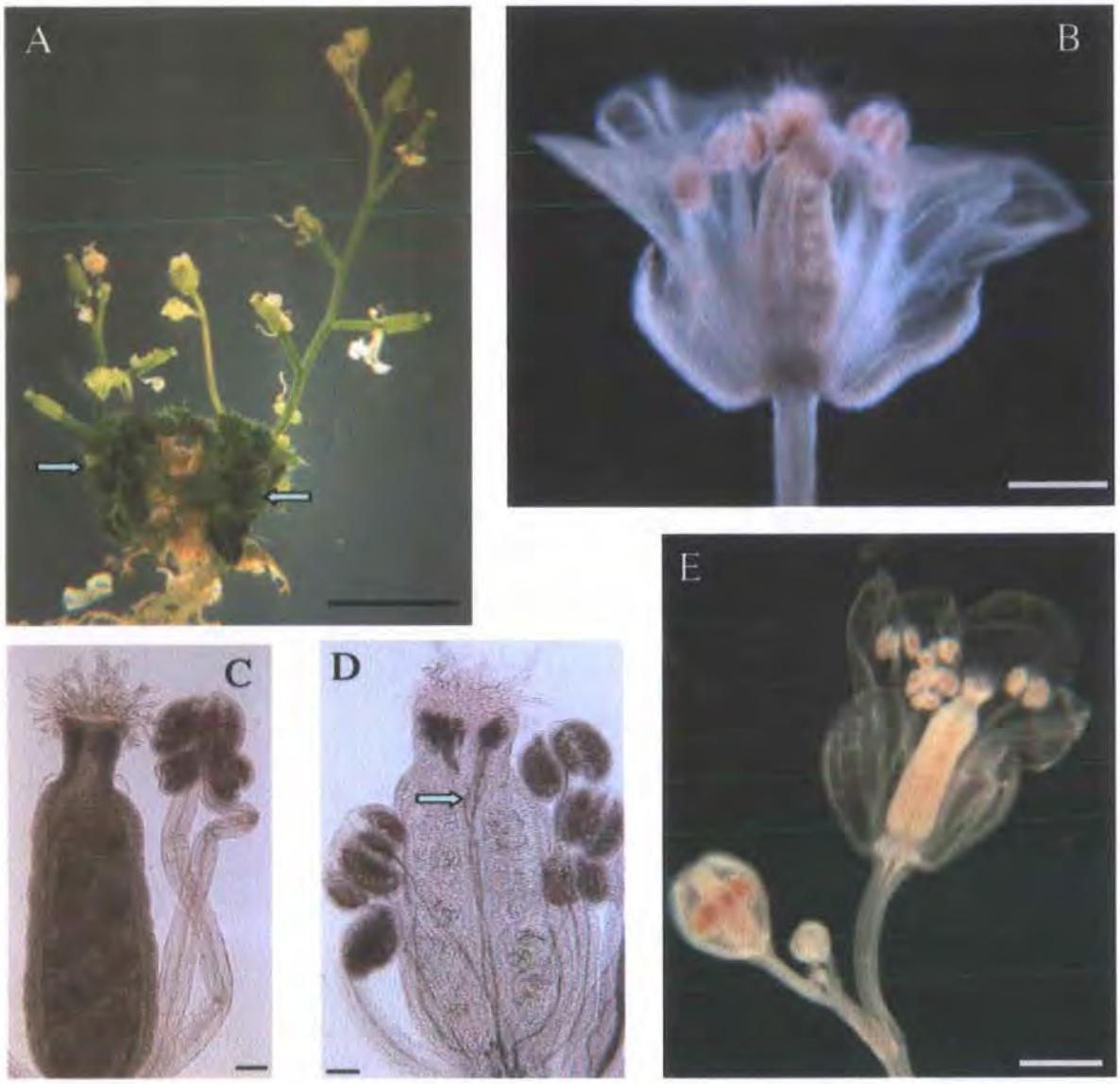

Figure 4.14 Inflorescence morphology in wild-type and *hydra* seedlings

A subset of *hydra* siblings initiate inflorescence stems between 4 and 6 weeks after germination. This transition to bolting occurs much later in the mutants than in wild-type plants grown under the same conditions (on supplemented media).

The *hyd1* 50 dae seedling shown in A has been dissected to remove the primary SAM; all *hydra* inflorescences initiate from axillary meristems as in this example (arrows). Internode length is reduced substantially in comparison to wild-type, and a single floral meristem forms in cauline axils (rather than secondary branches).

Floral morphology (*hyd2*, B) is similar to wild-type (E), and anther and carpel morphology appears normal (C, Ws and D, *hyd2*).

A, bar = 4mm; B, E, bar = 0.5mm; C, D, bar = 100μm.

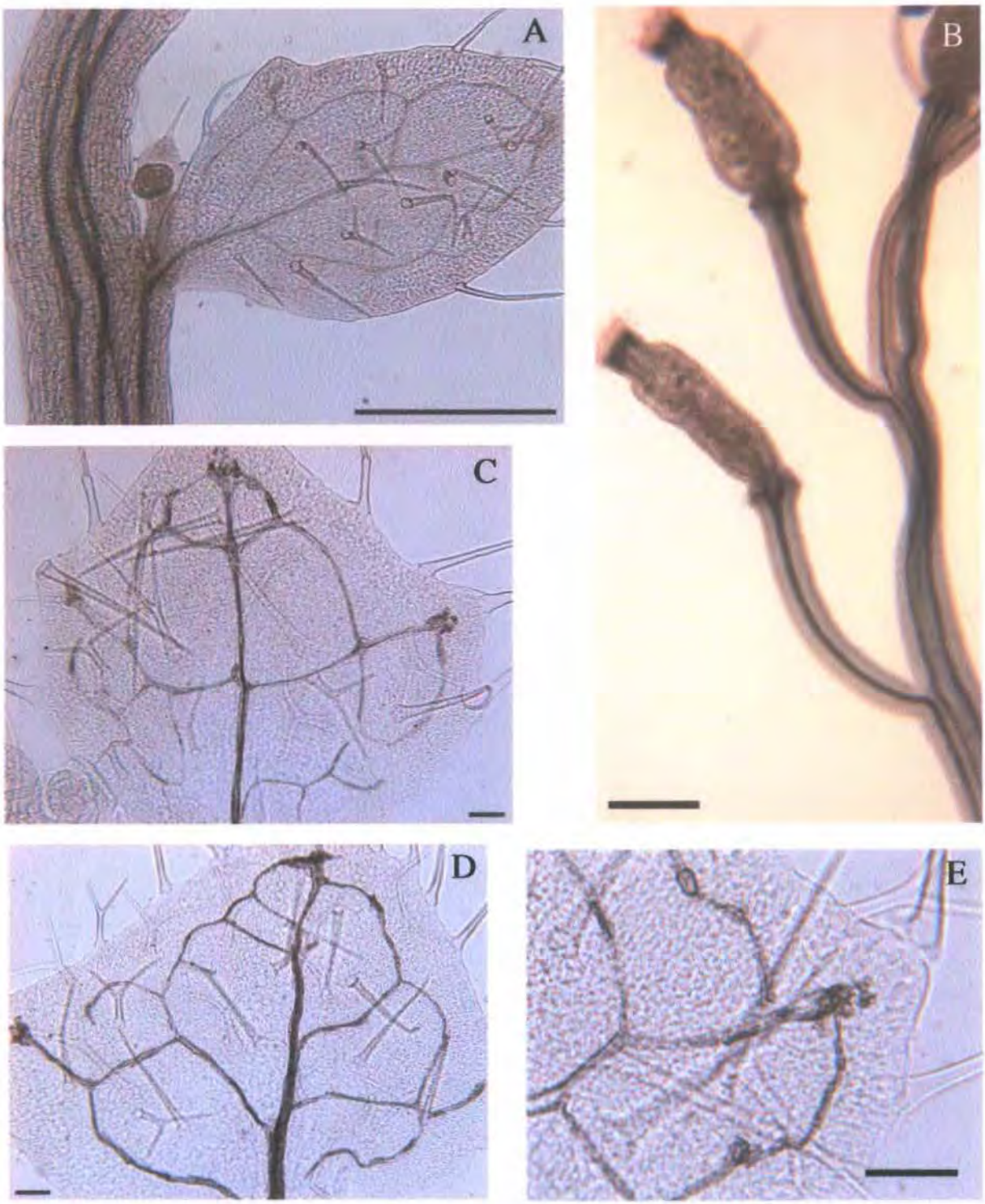

Figure 4.15 Xylem traces in wild-type and *hydra2* cauline leaves

The *hydra* mutant inflorescence bolts maintain coherent vascular strands, as in wild-type, although the *hydra* shoots are substantially reduced in size. The vasculature at nodes of wild-type bolts (A) branch away from the cauline trace in the leaf axil. The *hyd2* trace (B) shows strand dissociation proximally (towards the rosette) at both cauline and floral meristem nodes.

Cauline leaves of *hyd2* (C, D) have greater coherence of vascular patterning, compared to cotyledons and true leaves of the rosette, and lack vascular islands, though still demonstrate greater 'noise' in the trace than wild-type A). This is most pronounced at the hydathode regions, as in E.

A, B, bar = 0.5mm; C-E, bar = 100μm.

isolated xylem were absent from the cauline traces, in contrast to mutant rosette leaves. Coherent vascular traces were also present in the inflorescence stems (Fig. 4.15; B).

Vascular patterning in sepals (Fig. 4.16; F-I) is similar to that observed in wild type organs (Fig. 4.16; A-B and C-D), with an array of open and closed loops. Mutant sepal vasculature showed an increased in 'noise' in the xylem traces (Fig. 4.17; C-D) comparable to the xylem noise of mutant cauline leaves. This was particularly noticeable in organs of irregular width; in Fig. 4.16; G, some enlarged xylem vessels can be seen at the free vein endings.

Sepal morphology did vary slightly between mutant inflorescences. Flowers contained consistently four sepals in the whorl, although these were not always of even size, i.e. in some floral organs, the boundaries between organs were unevenly spaced around the meristem. The sepals shown in Fig. 4.16; G and H, were taken from the same flower; here the whorl had unevenly sized organs in the circumferential plane, with one wide, one narrow and two normally-sized organs which were partly fused at the base. In this example, as in others, sepal length was as wild-type. In other floral organs, including other flowers from the same seedling, sepal widths appeared usually much more even, and similar to wild-type (e.g. Fig. 4.16; F and I). The upper margin of some hydra sepals appeared uneven, with marginal protrusions (as in Fig. 4.16; F), or a serrated margin (as in the organs of uneven width, in Fig. 4.16; G and H), although this was also noted occasionally in wild-type examples (Fig. 4.16; A), although this character was less pronounced there.

Mutant petal morphology was indistinguishable from that of wild-type organs. In Fig. 4.16; J-N, the vascular traces show a greater pattern variability in mutants than in wild-type, with larger numbers of open loops, although wild-type petals did include these pattern phenomena. Petal xylem vascular strands were coherent, and appeared indistinguishable from wild-type (Fig. 4.17; E-F). Some examples of sepals with serrated margins were found,

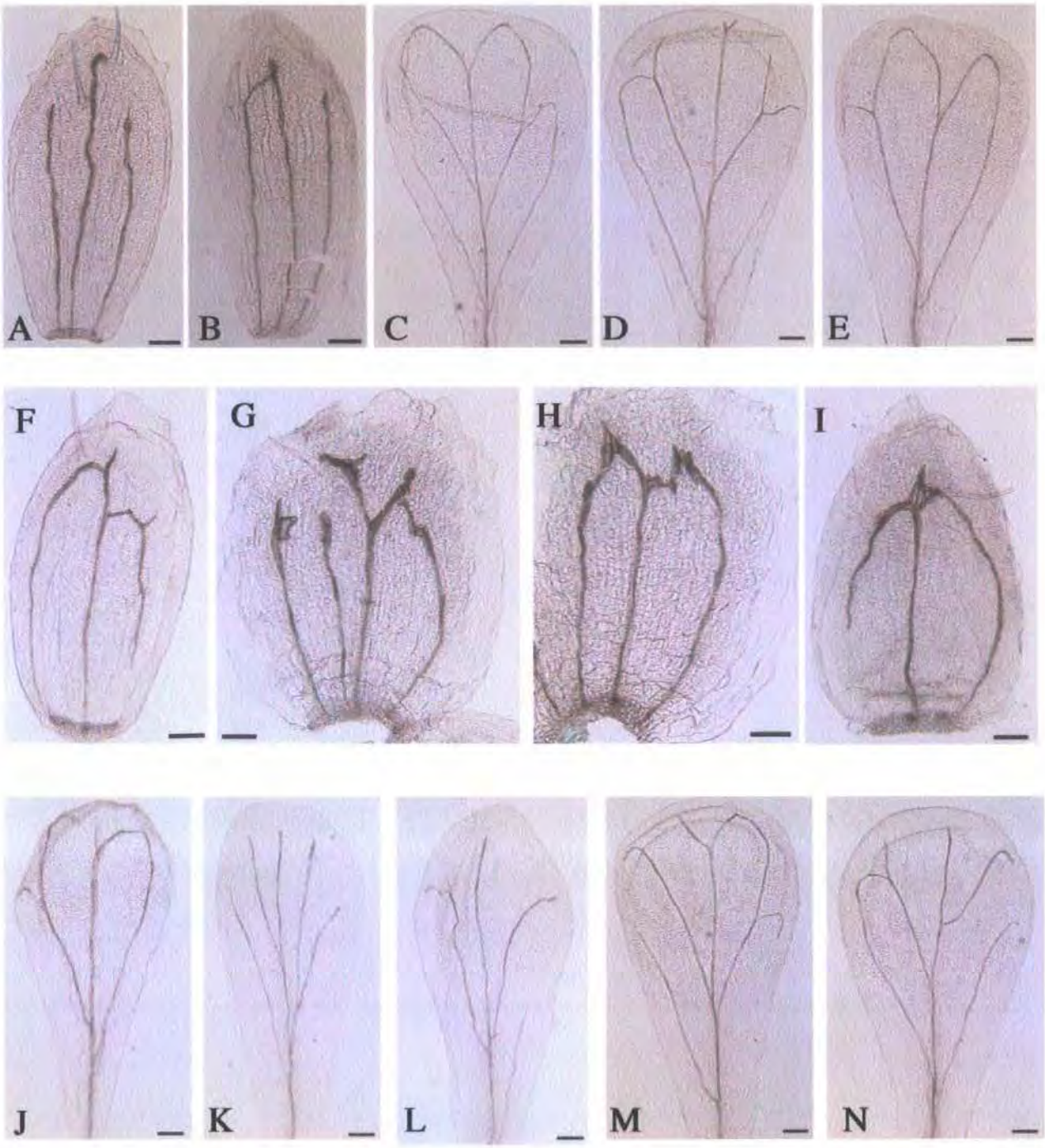

Figure 4.16 Vascular patterning in *hydra* inflorescence lateral organs

A-E; Ws sepals (A, B) and petals C- E). F-N; *hyd2*, sepals (F-I) and petals (J-N). All tissues are cleared using chloral hydrate prior to staining with safranin-O. Bar = 100μm

As in cotyledons, petal and sepal vasculature in wild-type plants show variation within a general conserved pattern characterised by a series of mostly open (sepal) or closed (petal) loops.

Sepal vasculature in *hydra* mutants shows a greater degree of noise than wild-type. These organs can vary in width in the mutants, and show some morphological variation; the sepals G and H are taken from the same inflorescence.

Petals show minimal differences in vasculature between mutants and wild type; although mutant traces (J-N) have more pattern variation and a greater frequency of unclosed loops. Wild-type petals also include these pattern variants, although not at the frequency observed in *hydra* petals.

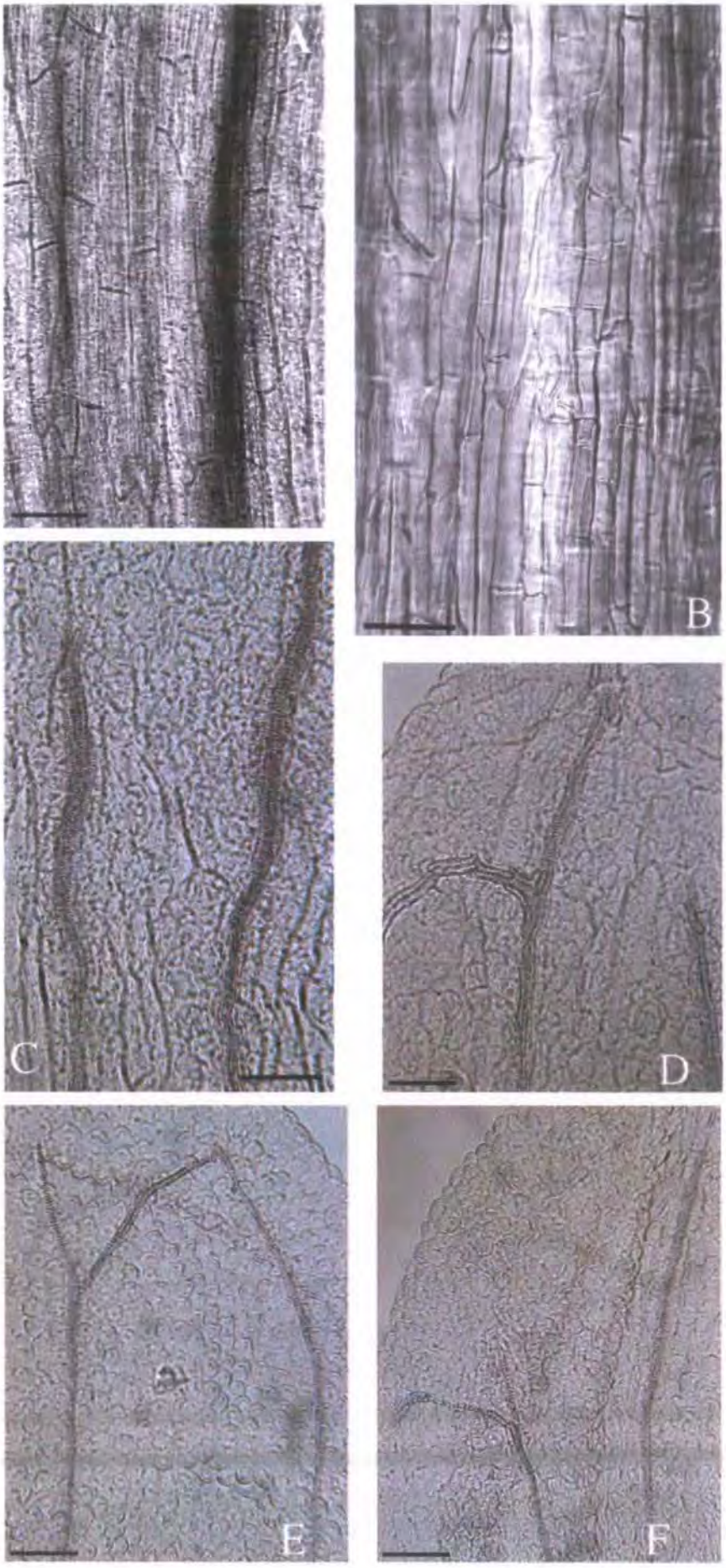

Figure 4.17 Longitudinal coherence in inflorescence stem epidermal cell files and sepal and petal vasculature

Longitudinally organised files of cells show greater integrity in the mutant inflorescence than in root and hypocotyl tissues.

The *hyd2* inflorescence stem epidermis (B), has mostly coherent cell files similar to those observed in wild-type stems (A).

xylem traces in sepals show a slightly greater degree of 'noise' in mutants (D: *hyd2)* than in wild-type (C: Ws), although *hydra* does not develop vascular 'islands' in these organs, unlike in rosette leaves.

In contrast, strand coherence in mutant petal vasculature (F) is indistinguishable from wild-type (E).

A, B, bar = 50μm; C-F, bar = 100μm.

similar to those described for petals in *cvp1* (Carland *et al.* 2002). However some wild-type petals from the *hydra* parental background also demonstrated this phenomenon (not shown).

Longitudinally oriented cells of the mutant inflorescence stem epidermis showed some size variation, and had shorter cells than those of the wild-type, although with similar longitudinal integrity (Fig. 4.17; A and B).

4.3.3 Cell division and expansion in longitudinal cell files

4.3.3.1 The coordination of cell division events throughout development demonstrates spatial and temporal anomalies in *hydra* mutants

In wild-type plants, cell division events (shown by expression of the *CYC1At*::CDB::GUS protein fusion) are visible in the root upon seedling emergence, and quickly establish a distribution around the apical meristem that is maintained throughout the life of the growing root (Fig. 4.18 A, C and E). In the shoot, cell division appears actively in the true leaf primordia after cotyledon opening, at around 2 dae (Fig. 4.18; B), and continues in these developing organs in a basipetal fashion (Fig. 4.18; D, F). No obvious cell division events shown by this reporter were observed in the cotyledons and hypocotyls of seedlings up to 7 dae. Early post-emergence growth of the cotyledon and hypocotyl is dominated by cell expansion; limited numbers of division events occur in the epidermis between 2 and 7 dae, in association with differentiating stomata (Tsukaya *et al.* 1994, Geisler & Sack 2002, Gendreau *et al.* 1997).

Figure 4.18 Cell division events in wild-type early seedling development

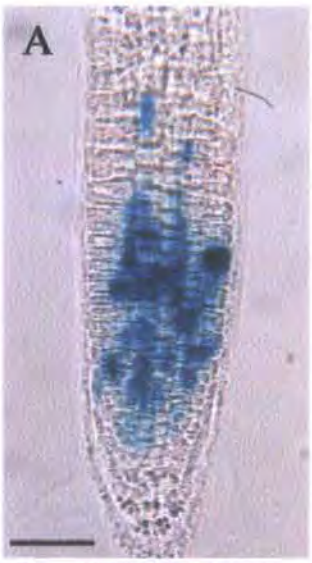

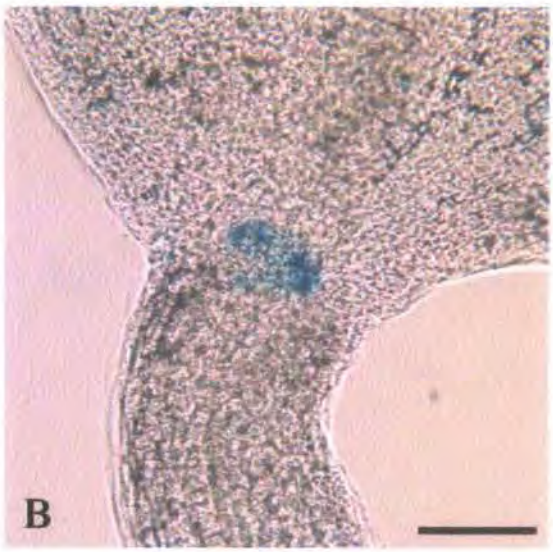

A-F: wild-type plants expressing the *pCYC1At*::CDC::DB::GUS reporter (marking cell division events) in primary root apices at emergence (A), and persisting in the root meristem, seen here in primary root tips from seedlings at 3dae (C) and 7dae (E).

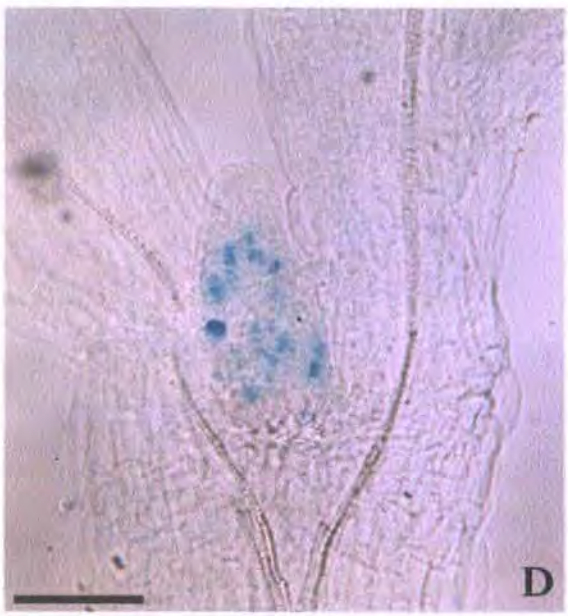

Cell division events are not seen in the shoot until 2dae (B), when development of the first pair of true leaf primordia commences. Division events are visible throughout these organs at 3dae (D), after which most of the cell population at the the leaf apex enter the expansion phase.

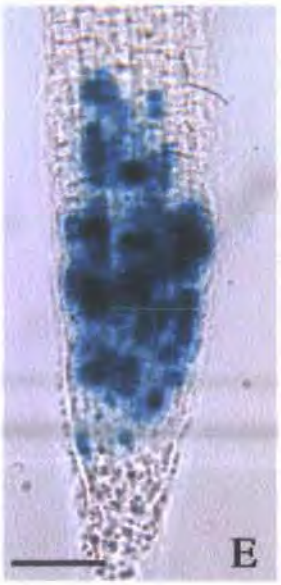

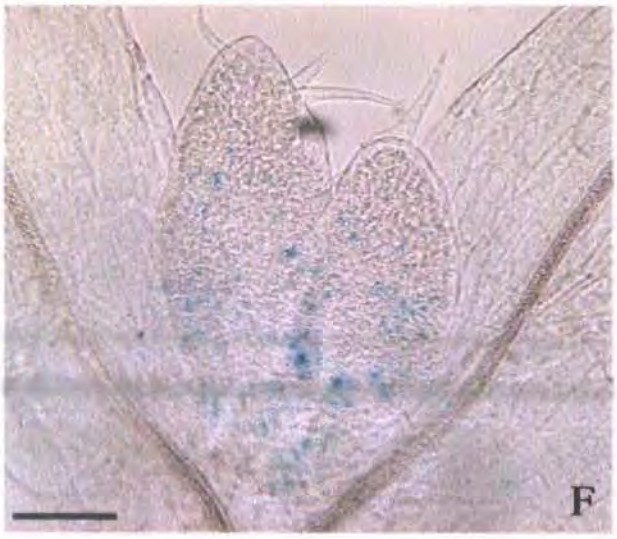

In the 7dae seedling (F) apical cells show signs of differentiation (e.g. trichomes in the epidermis). Occasional cell divisions associated with differentiating stomata are seen in the upper and central lamina epidermis, with a zone of more active division in the younger cells of the lower leaf, closest to the SAM.

A, C, E, bar = 50μm; B, D, F, bar = 100μm.

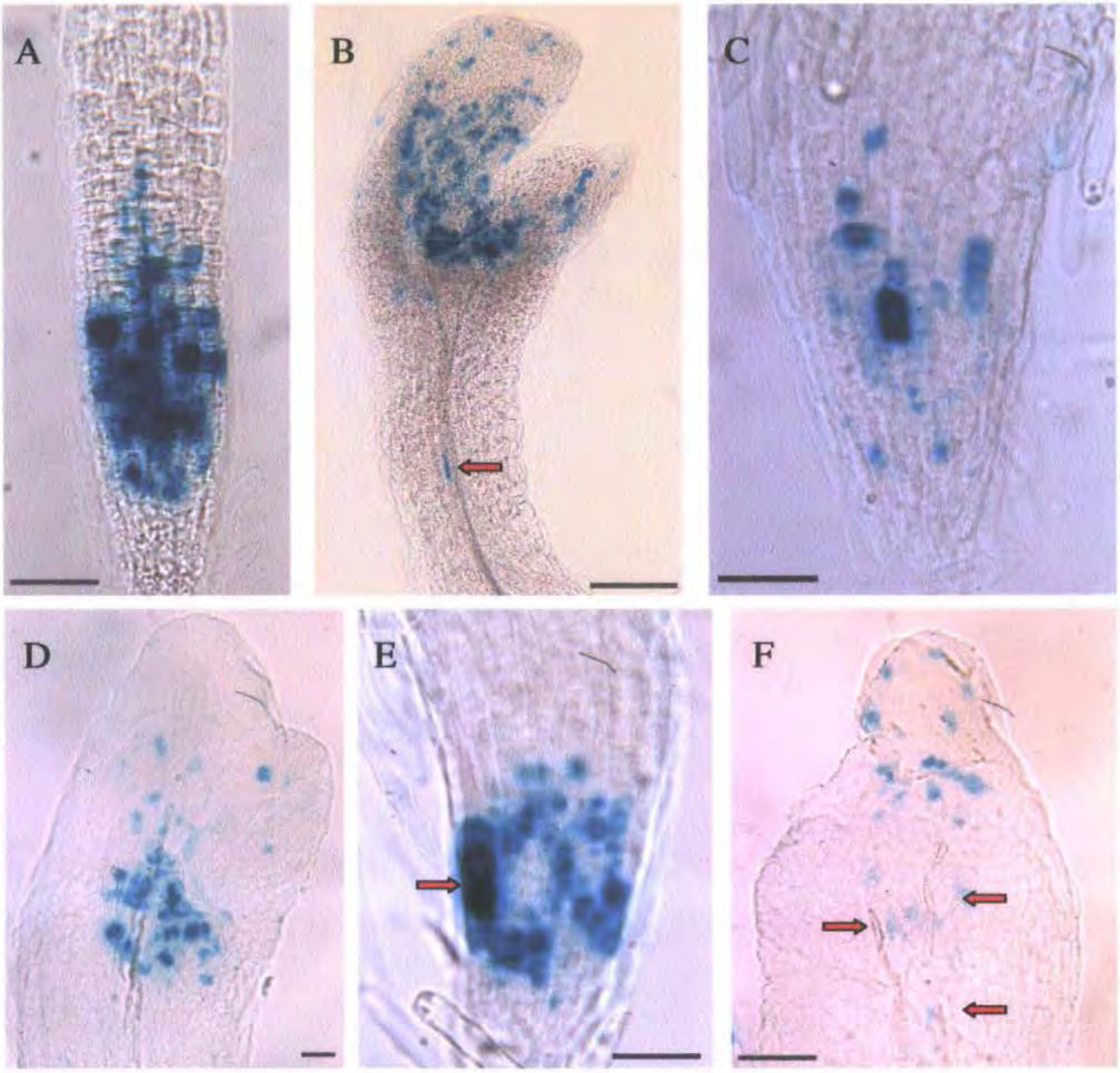

Figure 4.19 Cell division events in *hydra* 3 dae seedlings

A-F; ***hydra*** seedlings expressing the p*CYC1At*::CDB::GUS reporter. A and B; root and shoot apices from the same ***hyd1*** seedling, C and D, E and F, root and shoot apices from the same ***hyd2*** seedlings, all at 3dae.

In this early phase of growth (up to 3 dae). cell division patterns are highly variable in mutant root apices though have fewer anomalies in ***hyd1*** (A) than in ***hyd2*** (C, E). A is an exceptional example; most ***hyd1*** siblings have a less regular cell division pattern, resembling the roots of ***hyd2*** (C, E). In the sibling populations of both mutants, the incidence of cell division events can be less than in wild type (as in C), or broadly similar but with local 'hotspots' as in E, arrow.

Sibling shoots of both ***hyd1*** (H) and ***hyd2*** (D, F) consistently show increased cell division events, with ectopic reporter expression in cotyledons, and less frequently in hypocotyls (B, F, arrows).

A, C-F, bar = 50μm; B, bar = 200μm.

In 3 dae seedlings of both *hyd1* and *hyd2* (Fig. 4.19; A-F), the pattern of cell division events is highly variable. The primary root apex shown in Fig. 4.19; E, from a *hyd2* seedling, is representative of the patterning seen in the young root apices of both mutant sibling populations. However in *hyd1*, a few examples, such as that shown in Fig. 4.19; A, have a division pattern more reminiscent of wild-type plants, and in the *hyd2* population, some root apices display a much reduced number of division events (e.g. Fig. 4.19; C).

By 7 dae, cell division events in root apices of the two mutant populations show greater variation than in the younger seedlings. In *hyd2* (Fig. 4.20; B, D, F), a number of siblings have primary root tips with almost no continued cell division (D, F) whilst others retain a viable pattern (B). In the *hyd1* population, most siblings show viable primary root meristems with frequent cell division events (Fig. 4.20; H, J). Cell division was more evenly distributed around lateral root apices of both *hyd1* and *hyd2*, suggesting a greater viability of the meristems in these structures (not shown).

In the 3 dae shoot apices of *hyd1* (Fig. 4.19; B) and *hyd2* (Fig. 4.19; D, F), cotyledons show substantial and variable *CYC1At*::CDB::GUS expression, including ectopic cell division in the hypocotyl. Young leaf primordia (as in Fig. 4.19; B and D), show stronger expression than in wild-type shoots; these seedlings are characterised by a spread of division activity across the SAM region. By 7 dae, heightened reporter expression is retained around the SAM and in young primordia of both mutants, although ectopic GUS activity in cotyledons has reduced, and is seen at certain 'foci', associated with the vascular trace (Fig. 4.20; *hyd1* shown in G and I, *hyd2* in A, C and E). In mutant expanding true leaf primordia there was no obvious basipetal resolution of cell division activity as seen in wild-type young true leaves. There was no obvious relationship between the rates of cell division activity seen in the root and shoot apices of these siblings.

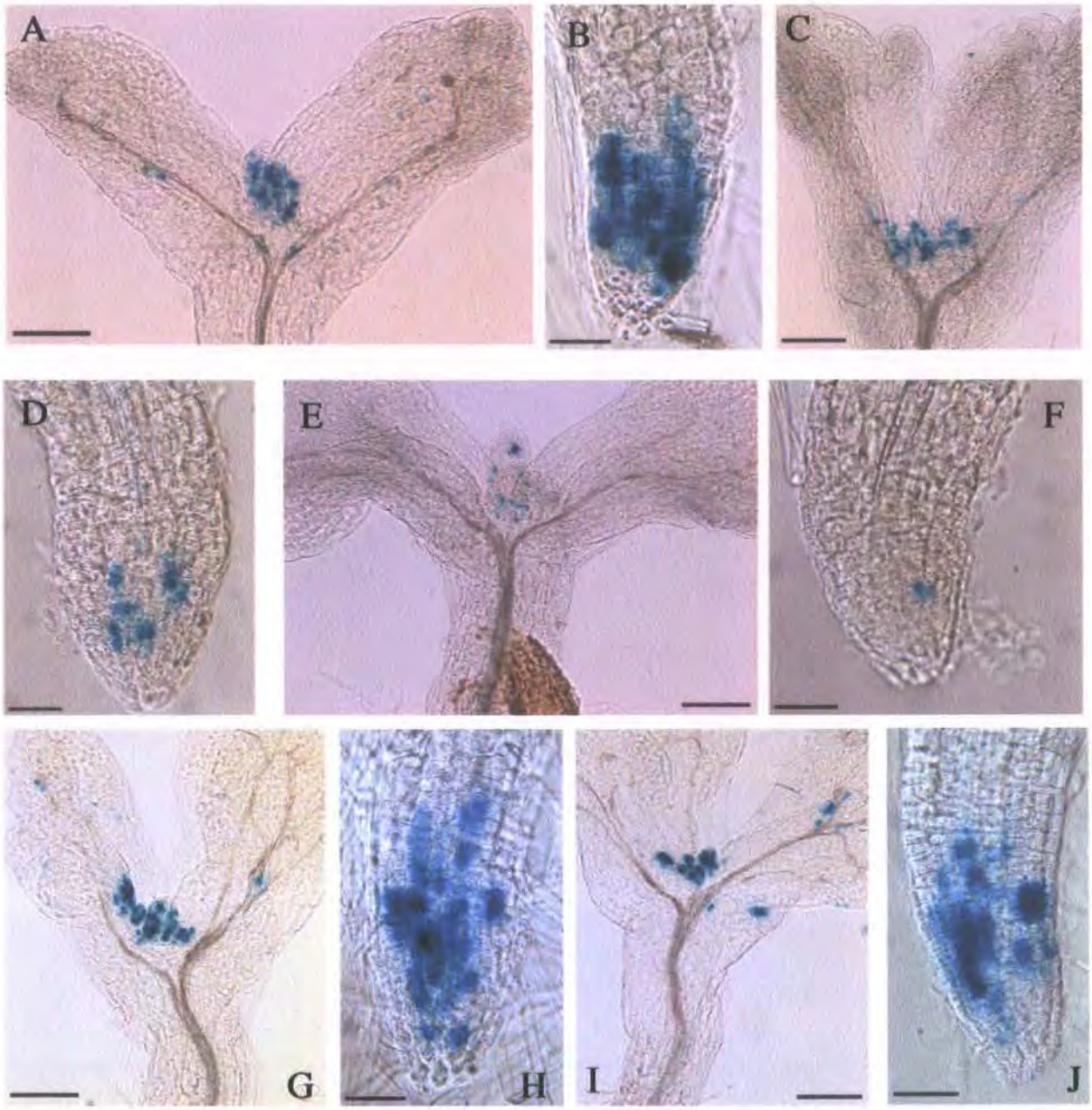

Figure 4.20 Cell division events in *hydra* seedlings at 7 dae

A-J; *hydra* 7dae seedlings expressing the p*CYCAt*::CDC::DB::GUS reporter, here shown in shoot and root regions of the same *hydra* seedlings. A-B, C-D and E-F; *hyd2*; G-H and I-J, *hyd1*.

Shoots of siblings from both *hyd1* (G, I) and *hyd2* (A, C, E) have persistent ectopic cell division events in cotyledon tissues at 7dae.

The *hyd1* primary root apex (H, J) retains its cell division pattern correlating with viability of the primary root meristem. Lateral roots form along the main root and anchor roots develop at the root -hypocotyl junction at this stage. Lateral root apices in *hyd1* have similar cell division patterns to *hyd1* primary roots (not shown).

In roots of *hyd2* (B, D, F) a slowing of cell division in some sibling primary root apices correlates with slowed growth from the root apical meristem, whilst reporter activity remains strong in initiating laterals and anchor roots (not shown).

A, C, E, G, I, bar = 200μm. B, D, F, H, J, bar = 50μm.

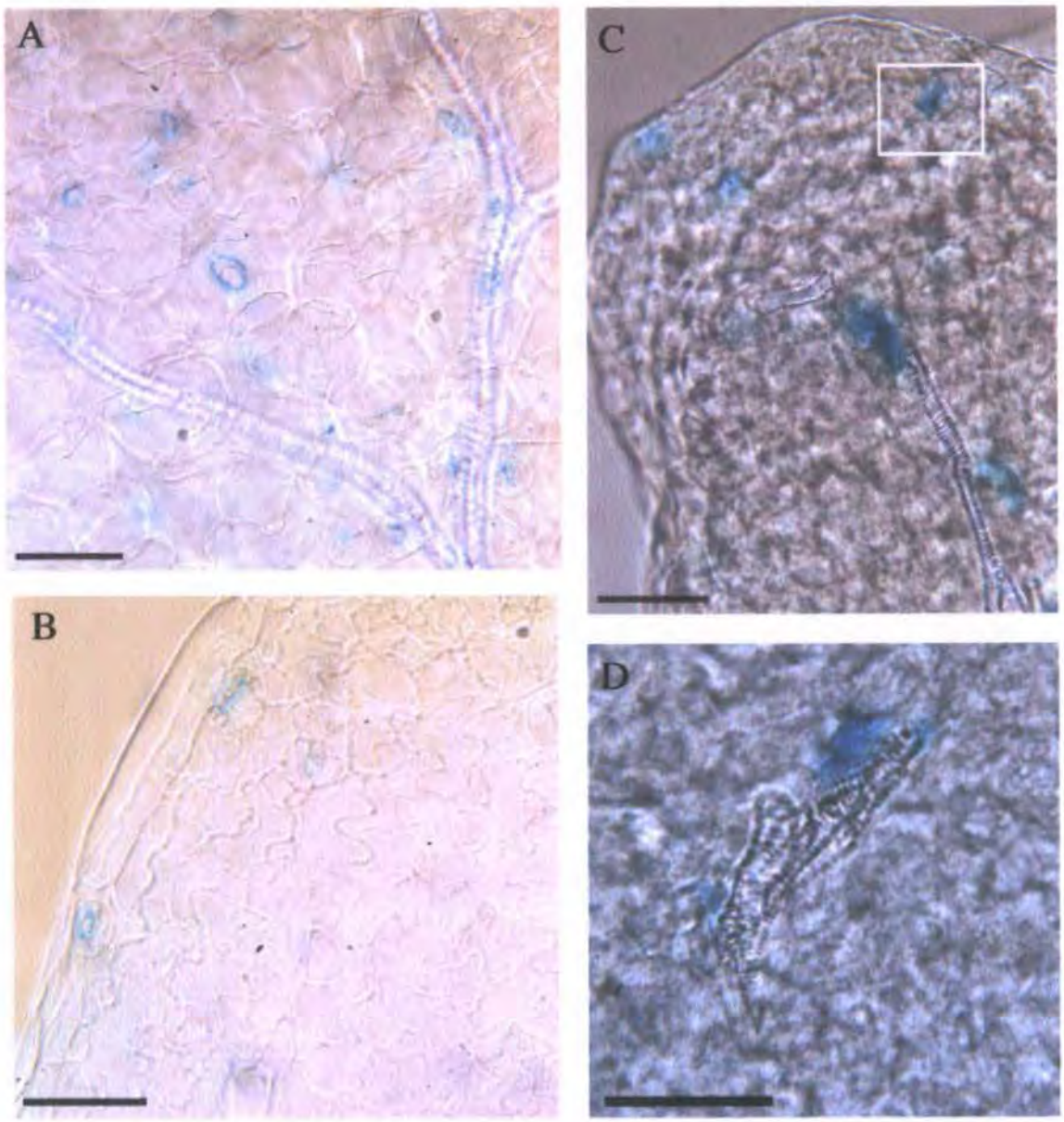

Figure 4.21 Cell division in wild-type and *hyd2* cotyledons

A; wild-type cotyledon adaxial epidermis from the central lamina near the primary mid-vein, and B; marginal region just below the cotyledon apex, both from 7 dae plants expressing the p*CYC1At*::CDB::GUS reporter of cell division events. Between 5 and 8 dae, transient cell-specific expression of this reporter occurs in the cotyledon epidermis in association with stomatal differentiation. No cell division events are evident in any other epidermal cell types or in the mesophyll cell layer. The division events highlighted in A and B show stomatal guard cell pairs, with residual GUS activity following their formation from division of a guard mother cell.

C; *hyd2* cotyledon at 7 dae showing ectopic expression of the same reporter. Regions of GUS-expressing cells are visible in both the epidermis and mesophyll. D shows the boxed area highlighted in C, where cells are dividing in proximity to an isolated section of xylem. These ectopic mesophyll division events are usually in association with dissociated or disjunct xylem vessels.

A-D, bar = 50μm.

4.3.3.2 Ectopic cell divisions in *hydra* cotyledons are associated with areas of dissociated and discontinuous xylem

In wild-type plants expressing the *CYC1At*::CDB::GUS (Fig. 4.21; A and B), higher resolution examination of the cotyledons revealed limited GUS activity in the guard cells of recently differentiated stomata. In contrast, regions of persistent GUS activity in *hydra* 7 dae cotyledons were in the mesophyll layer, associated predominantly with discontinuities in the xylem strands (Fig. 4.21; C-D, Fig. 4.22; A-D). No such expression was found in wild-type. Rarely, cell division events were seen in the *hydra* mesophyll without proximity to vascular islands or disjunctures (Fig. 4.22; D) and elsewhere in the epidermis, in association with stomatal differentiation (Fig. 4.22; E).

4.3.3.3 Ectopic and misaligned cell division events in the mutant hypocotyl and root stele are associated with disruptions in the alignment of longitudinal cell files.

No expression of the cell division reporter *CYC1At*::CDB::GUS were observed in hypocotyls of 3-7 dae wild-type seedlings (Fig. 4.23; A), although histochemical activity was visible elsewhere in the plant body. In roots, wild-type plants show division events associated with the stele at points where lateral roots initiate, and proliferation of a cell mass is generated from founder cells in the pericycle (Fig. 4.24; C).

A closer examination of ectopic cell division events in *hydra* mutant hypocotyls showed cell division events in the stele of the upper hypocotyl in the vicinity of branching points in the xylem vascular strands (Fig. 4.23; B, D). Vascular-associated reporter activity was also seen in other locations where vascular branching occurred, as in Fig. 4.24; A, showing the mostly coherent vascular

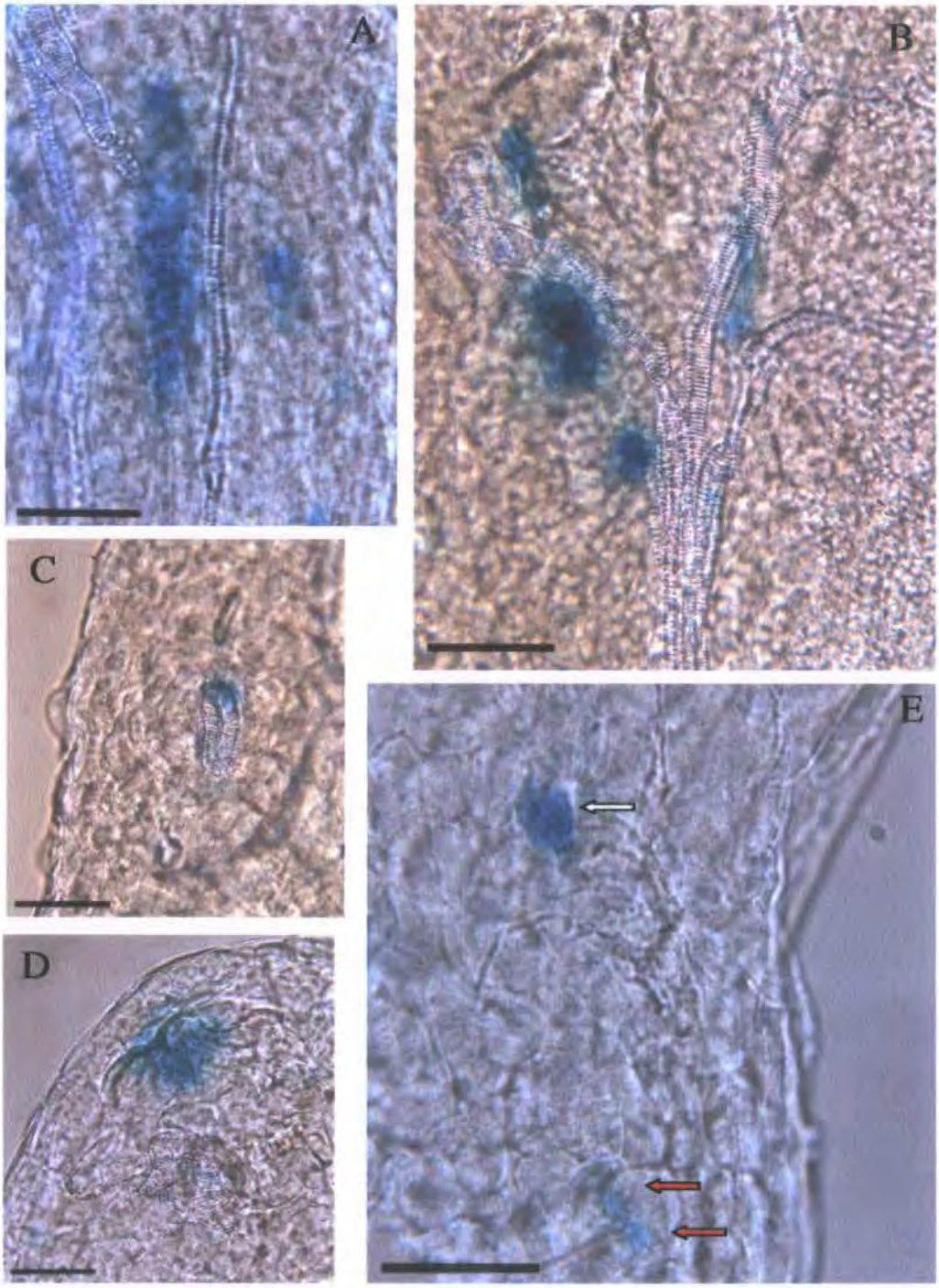

Figure 4.22 Ectopic cell division detail in the *hydra2* cotyledon

A-E; detail from cotyledons of *hyd2* plants at 7 dae expressing the p*CYC1At*::CDB::GUS reporter. Bar = 50μm.

A and B show cotyledon primary mid-vein regions, where the cell division marker is seen in association with dissociated xylem strands.

C details a 'vascular island' of unconnected xylem.

D highlights a group of dividing mesophyll cells beneath a raised area of the lamina; these cells are not obviously associated with any differentiated xylem vessels, though disconnected xylem cells are just visible in the mesophyll layer nearby.

E shows an area of petiole epidermis, where a relatively normal reporter expression can be seen. The single white arrow shows a stoma whose guard cells have recently formed from a guard mother cell. The two red arrows highlight a clustered pair of more mature stomata, which have retained a residual GUS signal.

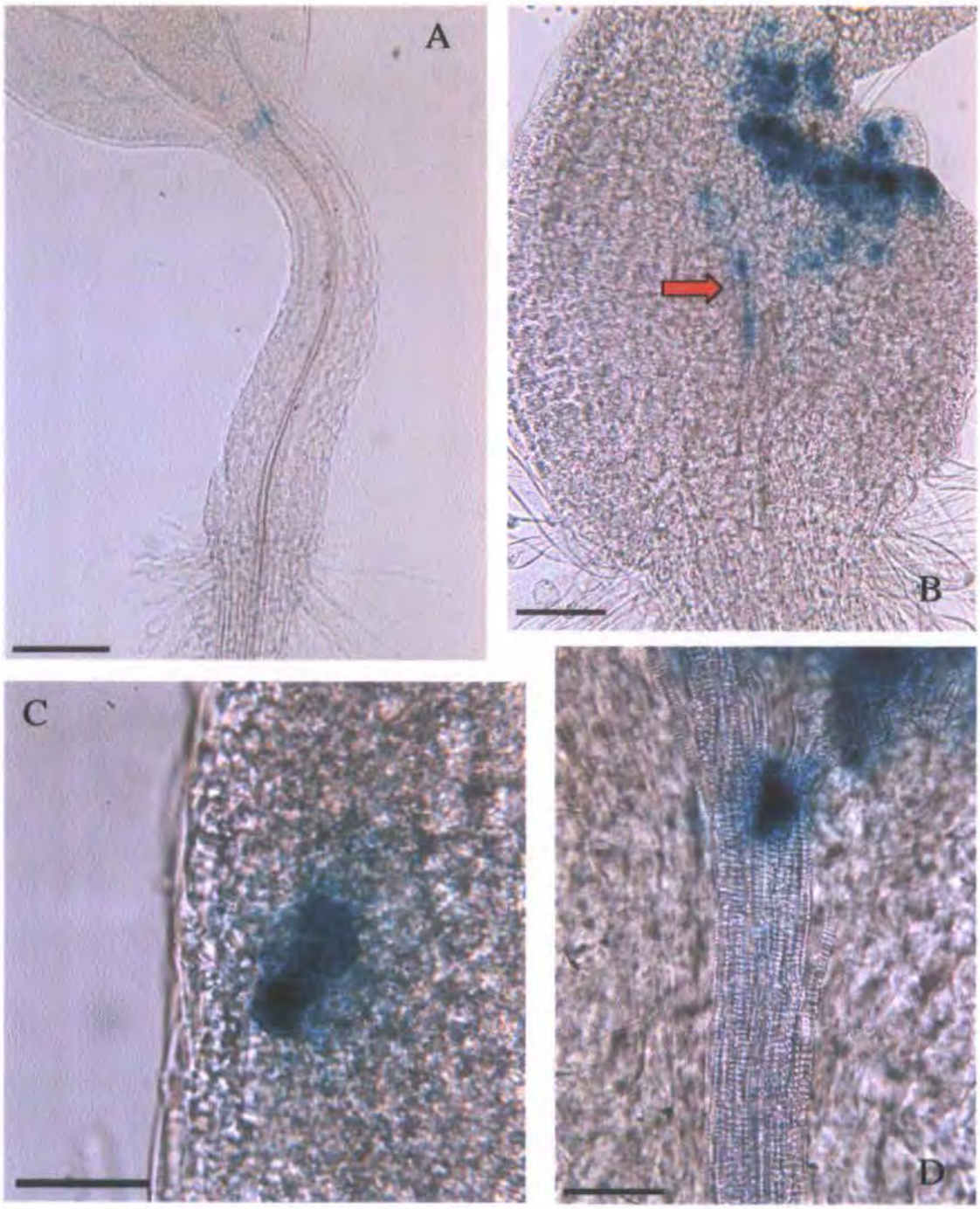

Figure 4.23 Ectopic cell division events in the *hydra* hypocotyl

A; wild-type hypocotyl region from a 3 dae seedling showing expression of p*CYC1At*::C:DB::GUS in dividing stomatal precursors of the cotyledon epidermis, and in the developing first pair of true leaves.

B; hypocotyl region of a 3 dae *hyd2* seedling, showing cell division in association with the hypocotyl stele (arrow). Such ectopic cell division events are also visible in *hyd2* 7 dae seedlings. C shows a mis-oriented ectopic cell division event spanning two longitudinal cell files in the hypocotyl epidermis, whist the GUS activity in D highlights the upper hypocotyl stele at the point of vascular branching.

A, B, bar = 100μm; C, D, bar = 50μm.

trace in a mutant cotyledon at the petiole-lamina junction where a secondary vascular loop rejoins the primary trace.

In *hydra* roots, examples of clustered cell division can be seen in association with the stele (Fig. 4.24; D), in this example, in close proximity to a single cell division event (arrow). Further down the stele of this root (at the bottom of the picture), a xylem discontinuity is visible. The cell division pattern in this root region may correspond to the initiation of two adjacent root primordia - a phenomenon observed in both *hydra* mutants (not shown).

4.3.3.4 Some cell division events in longitudinally aligned epidermal cell files show signs of disruption in longitudinal alignment

The dividing cell in Fig. 4.23; C is in the hypocotyl epidermis of a *hyd2* seedling at 7 dae. This ectopic division event, highlighted by the *CYC1At*::CDB::GUS reporter, is from the mid-hypocotyl epidermis, and its expansion axis appears to be at an oblique angle to the cell file orientation in this region. An epidermal cell division in the mutant hypocotyl such as this, which is clearly not associated with stomatal ontogeny, is a rare event, and so may result from a local modification of cues within the epidermis at this point, or tension within the cell mass.

Fig. 4.24; B shows detail of the root apex from a *hyd2* seedling at 7 dae. Although present in wild-type root apices, columns of simultaneously dividing cells, as can be seen in this example, are more frequent in *hydra* root apices. The example shown includes a disrupted cell file, where one cell appears displaced (indicated by an asterisk). It is unclear from the sample whether this cell is from an epidermal cell file, or from the lateral root cap. The column of cells highlighted by the reporter appears to have expanded laterally

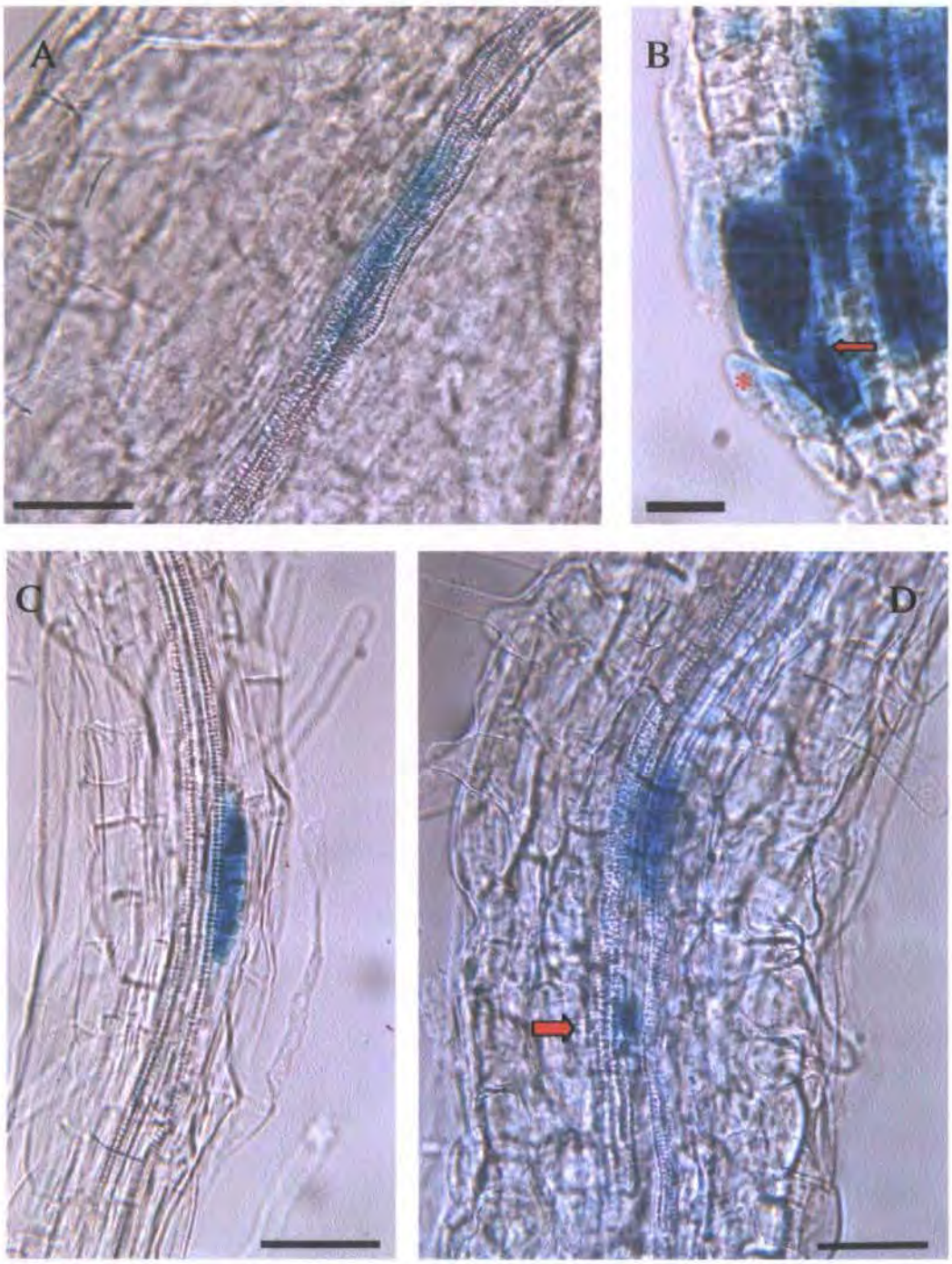

Figure 4.24 Ectopic cell division in the *hydra* cotyledon petiole and root

A; *hyd2* 7 dae cotyledon petiole just below a 'node' of strand dissociation. C; wild-type root, and B, D; *hyd2* roots at 7dae, all showing expression of the p*CYC1At*::CDB::GUS reporter. A, B, bar = 50μm; C, D, bar = 20μm.

The *hydra* root epidermal cell highlighted by the arrow in B appears to have shifted its alignment to encompass both its own and the adjacent epidermal longitudinal cell file. The cell originally from this cell file has been displaced sideways (asterisk). It is unclear whether the displaced cell has been forced out of alignment by the dividing cell, or whether misaligned expansion displaced it from its original cell file, leaving space for the dividing adjacent cell to 'invade'.

Division events adjacent to the root xylem pole in the wild type root shown in C are producing a founder population of cells which will become a lateral root. Lateral root initiation also appears to be taking place in *hydra* (D), although with an extra cell division event in the stele nearby (arrow).

into the gap (or may have expanded and pushed the adjacent cells out alignment), and are now dividing.

4.3.3.5 Mutant trichoblast cell files have compromised longitudinal expansion, and demonstrate various cell shape anomalies in root hair initiation

Wild-type trichoblast cell files are positioned according to radial patterning cues in the root epidermis, involving position relative to the cortical cell junctions in the cell layer beneath. The point of root tip initiation then appears to be positioned in an apical-basal fashion, towards the lower transverse cell wall, i.e. at the end of the cell's long axis closest to the root apex.

In the *hydra* root epidermis, cell files have variable longitudinal integrity, visible in the more mature sections of root shown in Fig. 4.25;B (*hyd1*), and E and F (*hyd2*). As can be seen from these images, not all cell files produce root hairs in *hyd2* as was originally thought (Souter *et al.* 2002), although the mutant roots do have prolific hair production. The roots shown in Fig. 4.25 have been grown in agar on microscope coverslips, allowing a closer examination of root morphology 'in situ'. These photographs show that mutant trichoblast cell files can have radial misalignment across the root longitudinal axis, and that radial position appears modified within certain cell files over the length of the root.

In the *hyd2* root shown in Fig. 4.25; E, two parallel longitudinal cell files, marked by white arrows at the top of the photograph, can be followed visually to a single large cell, (white asterisk), below which a single cell file includes a trichoblast cell showing radial swelling and two root hair tips (red arrow). Immediately to the right of the white asterisked cell, the opposite patterning phenomenon is visible; two files of enlarged cells below appear joined to a

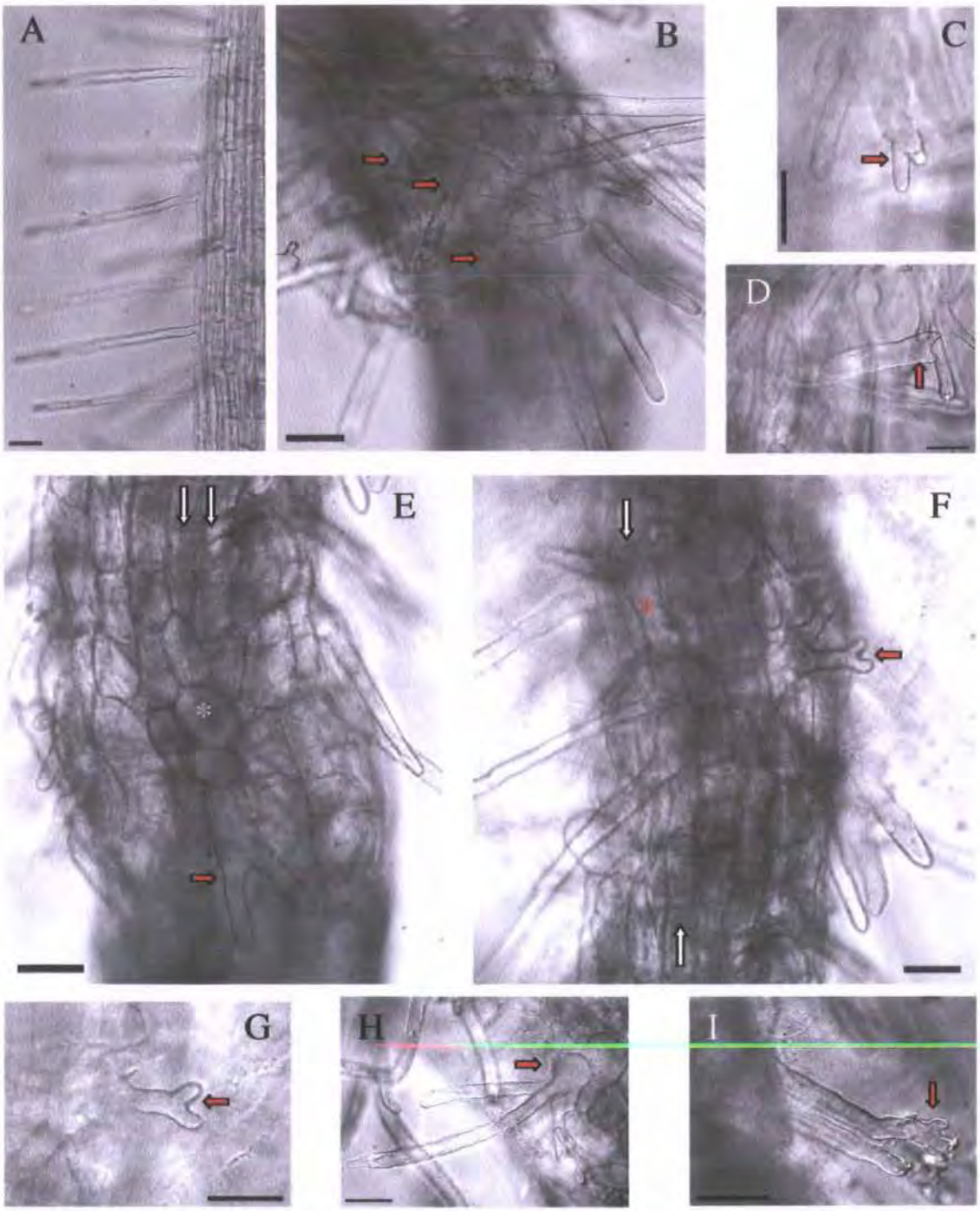

Figure 4.25 Trichoblast morphology in wild-type and *hydra* primary roots

A: Ws, B-D; *hyd1*, and E-I; *hyd2* primary root trichoblasts, from plants grown in agar on coverslips to visualise 'in-vivo' morphology. Bar = 5μm.

Root hairs occur at substantially increased frequencies in all *hydra* mutant siblings; hairs form in both trichoblst and atrichoblast cell files, and are consistently at higher densities around primary roots than laterals. The morphology of these hair cells is variable. Tip elongation can proceed normally in some examples, although the position of initiation relative to the cell's longitudinal axis may be compromised. Anomalies include post-elongation branching of the growing root tips (arrows), and initiation of multiple growing tips in tandem from different regions of the same trichoblast cell (e, asterisk). In roots of both *hyd1* (B) and *hyd2* (E, F), variation in epidermal cell sizes corresponds to disrupted longitudinal alignment of the cell files, with the majority of cells only partially elongated in the longitudinal axis. White arrows in E and F mark longitudinal cell files where some, but not all cells, have adopted trichoblast cell fate. The white asterisk in E indicates a cell associated with two files above and one (trichoblast) file below.

single cell file above, the junction of 'movement' in alignments being at the same point as the highlighted cell files just described. The section of root shown is within the root hair maturation zone; many root hairs can be seen, although not all of the cells have an obvious trichoblast cell fate.

In another *hyd2* root (Fig. 4.25; F), the white arrows indicate a longitudinal cell file with apparent integrity over the distance shown in the photograph. In this cell file, several cells have differentiated as trichoblasts with a single root hair emerging from each. The red asterisk highlights one of these cells, where the root tip has emerged from the uppermost end of the cell, i.e. near the cell wall furthest from the root apex, implying a reversed polarity of the cell contents relative to the growth axis. All cells in this file show reduced longitudinal expansion.

In terms of trichoblast cell size and shape, a range of phenomena are seen in these examples. Many root hair cells from both *hyd1* and *hyd2* (Fig. 4.25; B-I) show branching from later points of tip growth, i.e. after emergence from the trichoblast. To the left of Fig. 4.25;E, is a single trichoblast cell, marked by a red asterisk, with multiple root hair tips emerging from its surface over both its longitudinal and transverse orientations.

4.3.3.6 Variable axes of expansion, as indicated by cortical microtubular arrays, are found in adjacent cells of longitudinally organized epidermal cell files

Between 2-7 dae, hypocotyl cells in *Arabidopsis* undergo a co-ordinated expansion growth that begins near the root -hypocotyl junction and proceeds in a wave up the hypocotyl towards the SAM. A radial (transverse) transect across the hypocotyl in wild-type plants would thus give a subset of cells in the same co-ordinated phase of cellular expansion. Microtubules of the plant cytoskeleton form transverse helical arrays around the margins of actively

expanding cells; these arrays correlate with the direction of transverse parallel microfibril depositions in the cell wall (Ledbetter & Porter, 1963), and are formed at right angles to the direction of cell expansion. Although there is some debate as to whether these cortical arrays of microtubules control the orientation of cellulose microfibrils (reviewed by Wasteneys, 2002, 2004), their organized arrangement has been used frequently as an indicator of the direction of anisotropic cell expansion (e.g. Lloyd *et al.* 2000).

Fig. 4.26; A shows a section of hypocotyl tissue from a 5 dae wild-type seedling expressing the GFP::TUA6 fusion protein, which highlights the cortical microtubules (Ueda *et al.* 1999). In wild-type actively expanding cells (Fig. 4.26; A), the microtubules are organized in helical arrays, transversely to the direction of cellular expansion growth. In hypocotyl cell files, this cellular expansion is co-ordinated with the longitudinal axis of the seedling.

In contrast, cells of the *hyd1* hypocotyl (Fig. 4.26; B-D) show a very different pattern, both in the arrangement of the cell files, and in the direction of the microtubular cortical arrays within these cells. The double-ended arrows in Fig. 4.26; C and D reveal the apparent axis of expansion in these cells. Cells can be seen in which;

1. expansion appears to be aligned with the longitudinal axis,
2. in a direction approximately transversely to the longitudinal axis, and
3. non-random arrangements of the microtubules are visible but no clear expansion axis is evident.

Figure 4.27; A shows the expression of GFP::TUA6 in a section of the cotyledon adaxial epidermis from a *hyd1* seedling at 5 dae. A number of features are visible; in the centre of this epidermis, some giant cells are visible (marked by asterisks), apparently still undergoing expansion, although not in the plane of the cotyledon lamina. The identity of these cells is unclear, although they may have been originally associated with longitudinal cell files of the petiole. Elsewhere in the lamina a randomised pattern of microtubules can be seen in

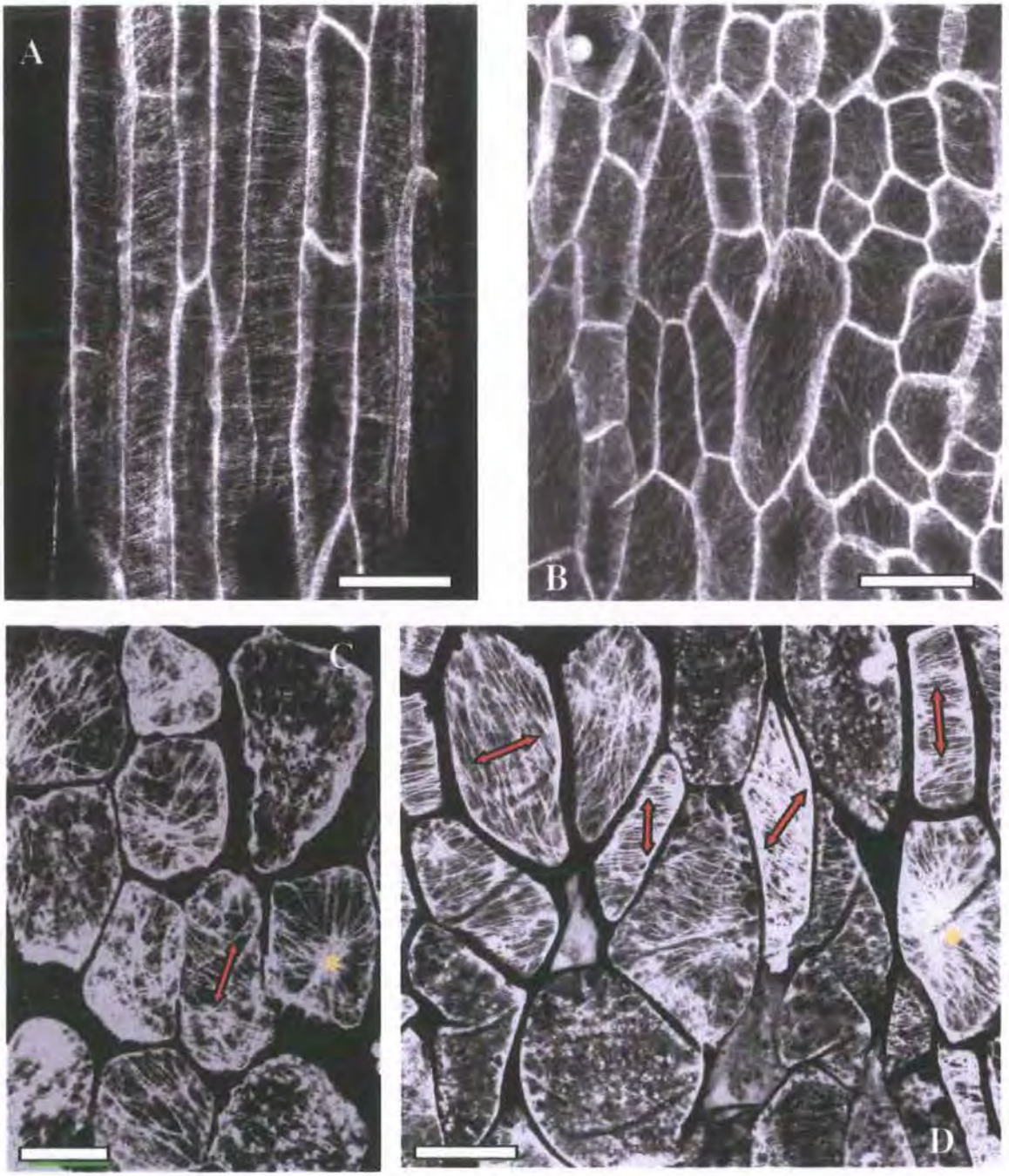

Figure 4.26 Expansion axes in hypocotyl cells from wild-type and *hyd1*

A; wild-type hypocotyl epidermis at 5 dae showing expression of the GFP::TUA6 protein fusion, showing the position of cortical microtubular arrays in longitudinally expanding cells. B-D; *hyd1* hypocotyl cell detail from 5dae (B) and 8 dae plants (C, D) expressing the same protein-fusion construct.

The organisation of cortical microtubules in actively growing cells correlates with the expansion axis in longitudinal cell files of wild-type plants (A). Using these microtubular arrays as an indicator of directional cell expansion, it is evident that in *hyd1* the intercellular alignment of expanding cells is compromised (B). C and D show variable states of cellular expansion in older tissues; these mid-hypocotyl epidermal cells appear to still be undergoing an active expansion in various orientations (red arrows), whilst other cells show a randomised pattern of microtubules, as is seen at this stage in wild type (not shown). Some cells have highly organized microtubular cortical arrays without a clear directionality (asterisks).

A, B, bar = 50μm; C, D, bar = 20μm.

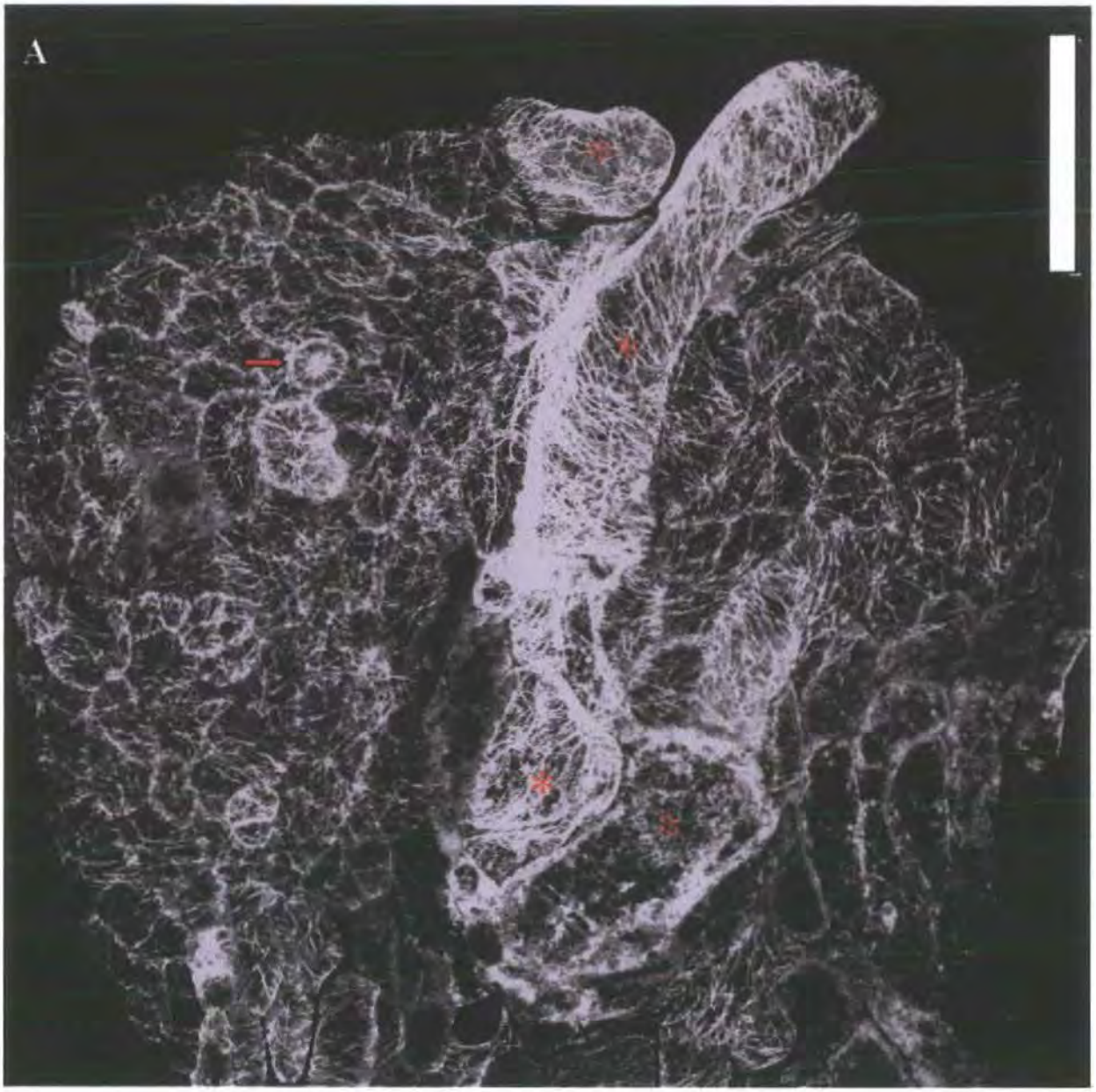

Figure 4.27 Microtubule detail in giant cells from the *hyd1* cotyledon epidermis

A; *hyd1* cotyledon adaxial epidermis at 5dae showing expression of the GFP::TUA6 protein fusion. Bar = 50μm.

The 'giant' cells in the centre of the lamina (red asterisks) indicate a misplaced marginal or central longitudinal epidermal cell file. Other smaller longitudinally-oriented epidermal cells near the petiole are visible at the base of the picture beneath these giant cells.

A differentiated stoma is visible (arrow), and shows a radial arrangement of microtubules spanning the guard cell pair around the pore aperture. Pavement cells, where visible, show microtubules in randomised patterns. Both of these cell types have similar microtubular arrangements to those of cells from wild-type cotyledon epidermis (not shown).

pavement cells, and a radial arrangement within guard cell pairs of functional stomata; these patterns are similar to that of microtubules in wild-type cells (Ueda *et al.* 1999).

4.3.4 Cell layer identity and integrity across the radial axis

4.3.4.1 Axis duplication and dissociation affects cell layer organization in *hydra* seedlings

A transverse section of the wild-type seedling hypocotyl at 7 dae reveals a well-ordered arrangement of cell layers across the radial axis (Fig. 4.28; C). In this picture, the bilateral polarization of the vascular tissues within the stele of the juvenile seedling are visible; denser staining phloem cells are separated by xylem. The stele is enclosed by the pericycle, then an endodermis, and in the hypocotyl two layers of cortex separate these layers from the epidermis (Gendreau *et al.* 1997). The longitudinal alternating 'ridge and furrow' formation of the hypocotyl epidermis, reported by Gendreau *et al.* (1997) is visible in this section. A similar arrangement of radially-coherent cell layers is found in the *Arabidopsis* juvenile root, although here a single cortex layer of typically eight cells lies between the epidermis and endodermis (Dolan *et al.* 1993).

Fig. 4.29 shows a hypocotyl transverse section from *hyd1* at 7 dae. Here, phloem poles are visible within the stele, separated by xylem, although the shape of the stele is distorted in the radial axis. Pericycle and endodermal cells appear to be present around parts of the vasculature, although radial integrity of these layers is unclear. Beyond this, a substantial proliferation of cortex has occurred, so that the radial patterning of these layers is distorted,

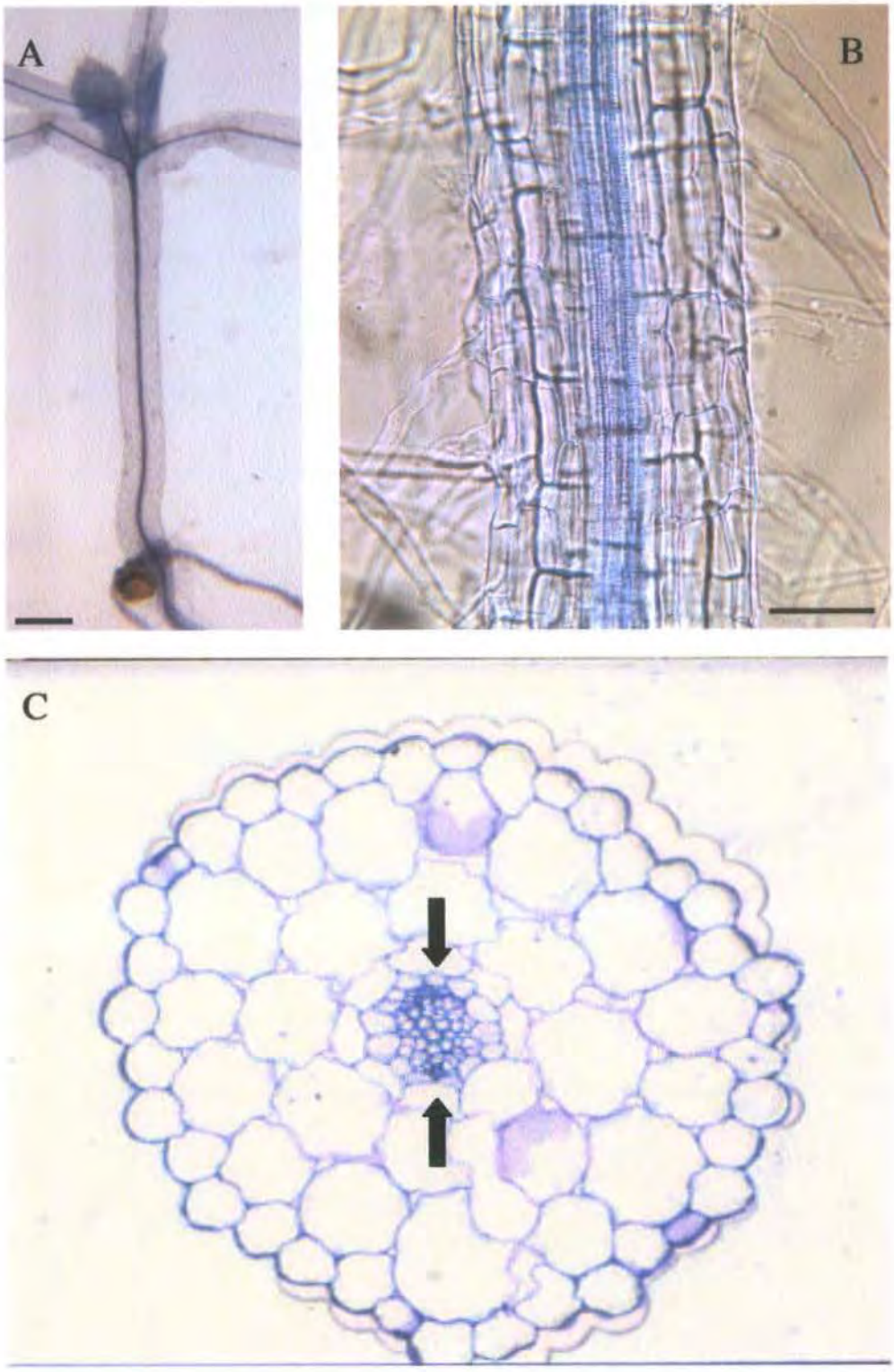

Figure 4.28 Patterning of the longitudinal axis in the wild-type hypocotyl and root tissues

A; anilne blue-stained and cleared wild-type seedling hypocotyl, 7dae. B; DIC image of wild-type root pole, and C; transverse section of the lower hypocotyl from 7dae plants. The stele in these radially-organised tissues contains xylem and phloem poles which define a bilaterally symmetrical radial axis (B; arrows mark the phloem poles, with a clear pericycle layer between).

A, bar = 0.5mm; B, bar = 50μm; C, section at x200 magnification.

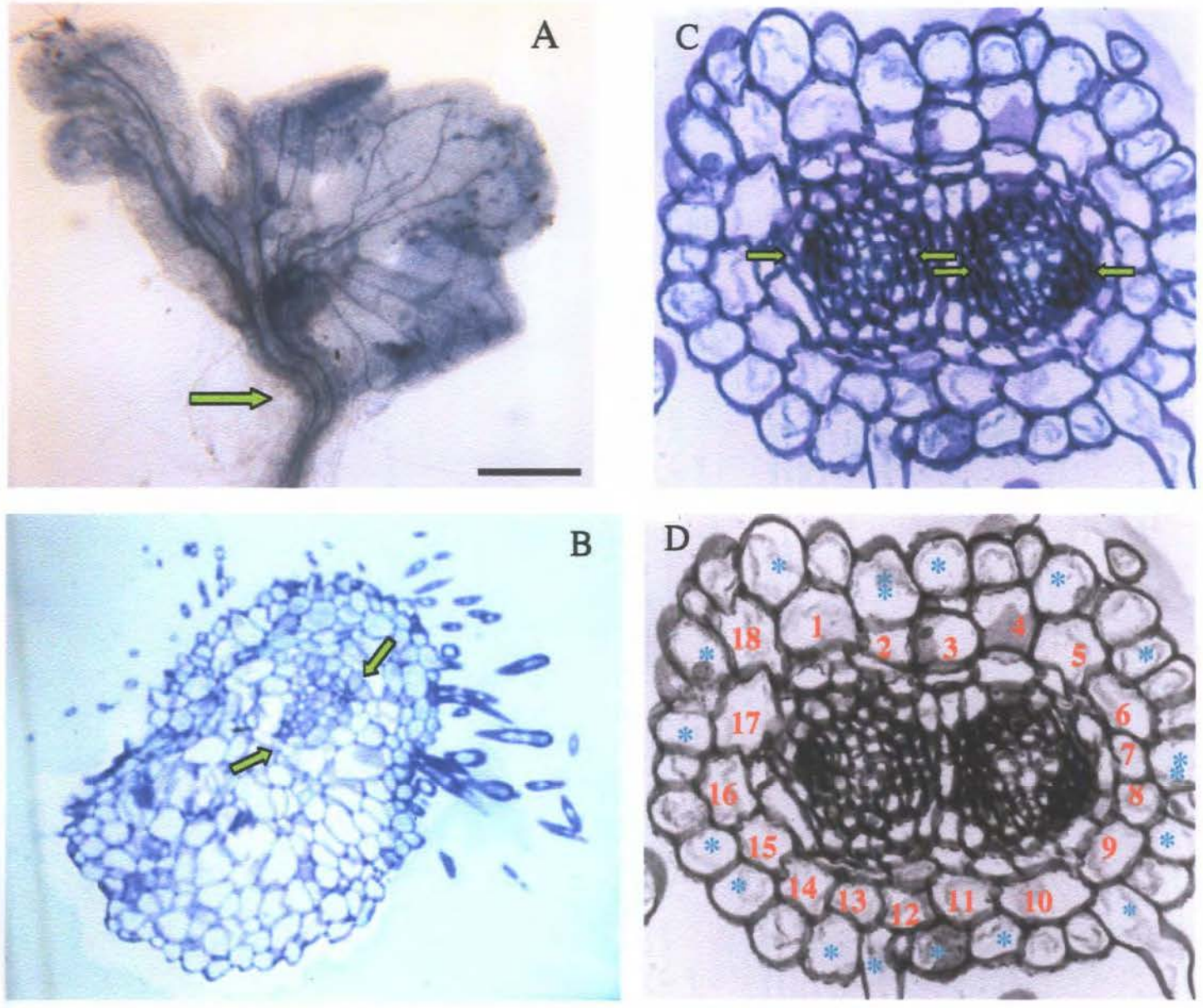

Figure 4.29 Longitudinal axis duplication in *hydra* seedlings

and in parts of the section, appear to be lost, replaced by a mass of disorganised cells of various sizes.

The root transverse section shown in Fig. 4.29; C is taken from a seedling with full duplication of the longitudinal axis; this plant has two steles which extend from the shoot apex, through the hypocotyl to the root apex, as in the seedling pictured in Fig. 4.29; A. The duplicated steles each retain a coherent pericycle, around and between which the endodermis extends, also forming a single cell layer which appears to have retained its integrity. Between the steles, two layers of endodermal tissue lie adjacent to each other. Single cell layers of cortex and epidermis are found beyond these central layers, which also appear to have a radial integrity.

Fig. 4.29; D shows the same root section as in C, with colour coding of the radial cell layers, and annotations added to show cortex (numbered 1-18), and epidermal cells positioned over junctions in the cortical layer beneath (asterisks). Although radial integrity of the cell layers appears intact in this root, the radial patterning cues between the cortex and epidermis are modified by the super-numerary proliferation of cortex cells, and their variable size in cross section. Instead of the alternation of each trichoblast cell file bordered on each side by a pair of atrichoblasts, as seen in wild-type root patterning (Dolan *et al.* 1993), this *hydra* mutant root shows an epidermis where a number of adjacent cells potentially receive cues from the cortex that will promote trichoblast cell fate. Two cells in this section, marked with double asterisks, overlap two cortical cell junctions.

4.3.4.2 Dissociation of the vascular strands in the hypocotyl stele are associated with an enlarged and distorted shoot apical meristem

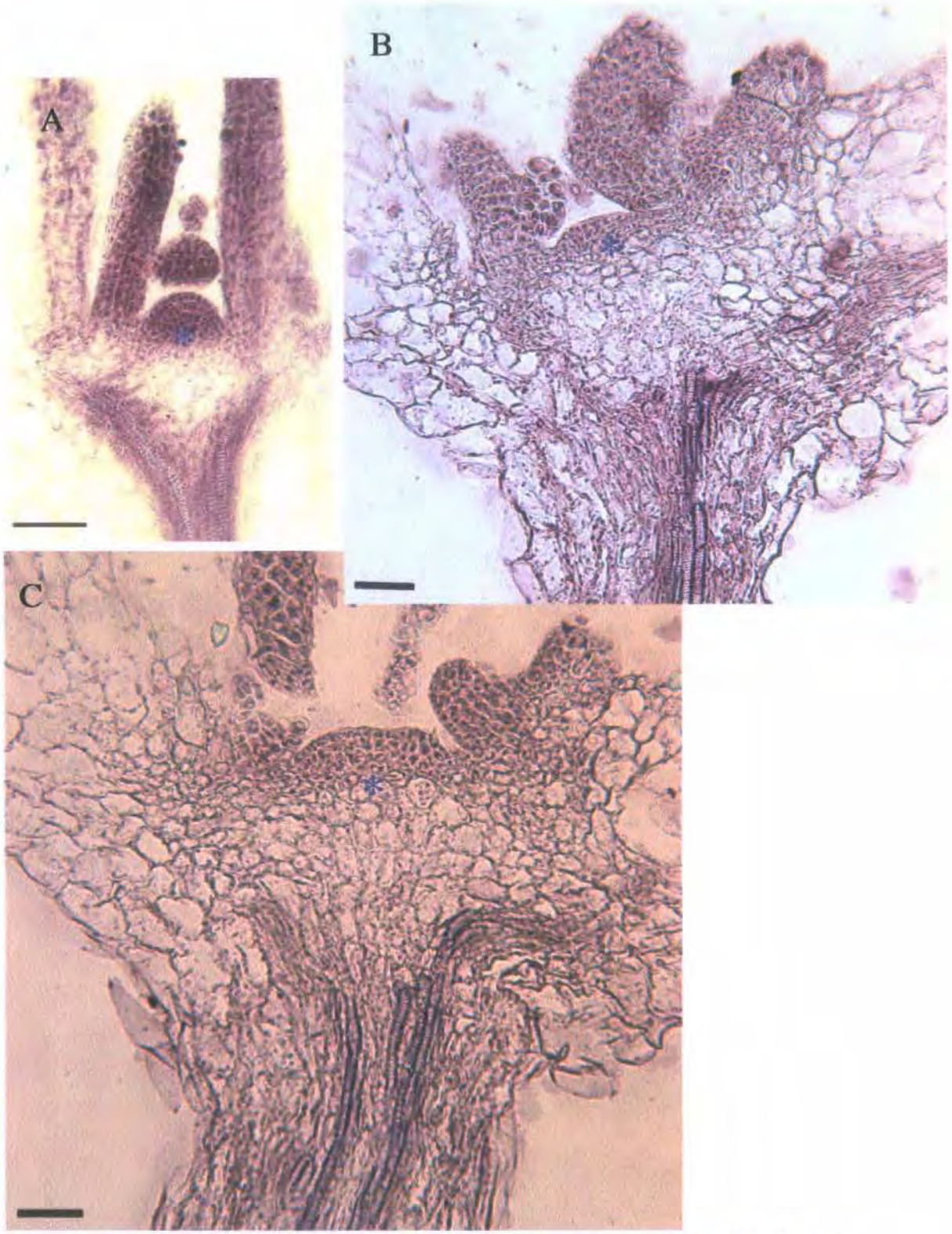

Figure 4.30 Shoot apical meristem patterning in Ws and *hyd2*

A-C; 10μm longitudinal paraffin sections of Ws (A) and *hyd2* (B-C) shoot apices from 8dae seedlings, stained with safranin and fast green. Bar = 5μm.

The Ws seedling in A shows the expected domed SAM (asterisk), formed above the region in the stele where the vascular strands branch into the leaf traces. The true leaves arise spaced around this region of stem cells in an ordered manner. B and C show longitudinal sections of the same shoot apex of a plant with two cotyledons with strand dissociation and radial thickening in the hypocotyl. Here the SAM (asterisk) is substantially enlarged in a transverse direction, and forms a distorted shape with an increased number of primordia.

In wild-type plants the vasculature of the upper hypocotyl stele divides symmetrically to form the cotyledon traces, and above this division point, the shoot apical meristem forms as a dome-shaped structure, visible in the longitudinal section in Fig. 4.30; A. In the domed SAM, small densely stained layers of cells are present, comprising the L1-L2 ('tunica') and L3 ('corpus') above a zone of larger, vacuolated cortex ('pith') cells, which appear pale in this picture. Densely staining cells are also visible surrounding the vascular strands of the stele.

Longitudinal sections of the shoot apex from *hyd2* plants (Fig. 4.30; B and C, Fig. 4.31 A and B) show a range of morphologies in this region.

The sections in Fig. 4.30; B and C were taken from seedlings which appeared to have a coherent hypocotyl stele. In C, the stele has already dissociated before it reaches the branching point below the meristem, and a correctly positioned though widened SAM is visible. In B, the stele appears to have branched asymmetrically across the bilateral axis, producing a thickened cotyledonary structure to the right, and a distorted and expanded SAM, displaced here to the left.

Another asymmetrically branched stele is shown in the mutant apex sectioned in Fig. 4.31; B, this time resulting in a widened shoot apex that has separated to form two SAMs, between which a leaf-like structure appears to comprise a disorganised densely-staining cell mass. In this seedling, the vascular trace appears to show a range of xylem vessel sizes; these elements do not appear coherently aligned into traces, although this is difficult to interpret as the stele is not centrally located within the hypocotyl, and so does not appear in the section.

The *hyd2* section in Fig. 4.31; B shows even less coherent cellular organization; vascular traces are not visible in the hypocotyl near the meristematic zone, which is substantially expanded in its transverse

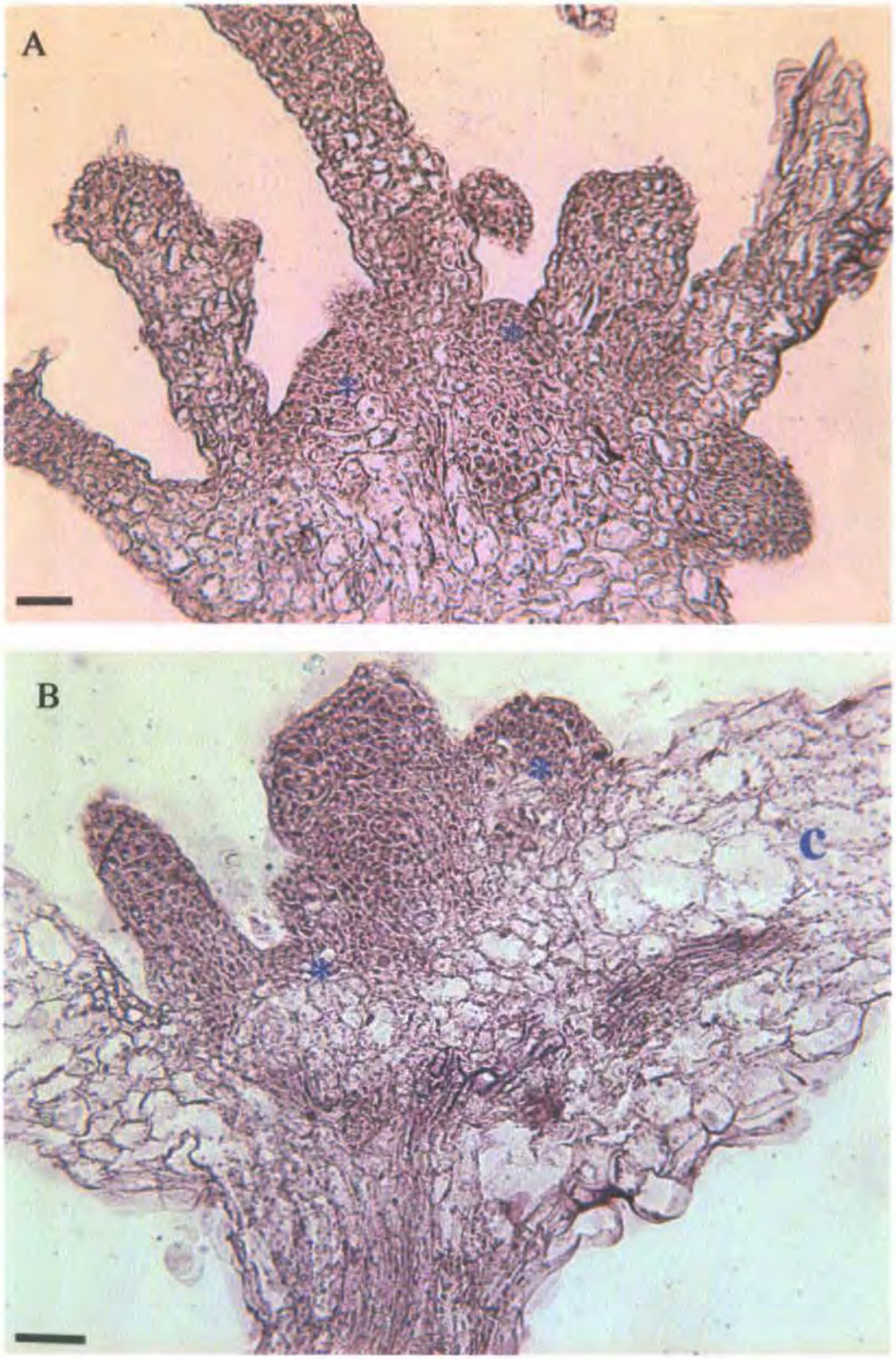

Figure 4.31 Multiple shoot apical meristems in *hyd2* siblings

A and B; 10μm longitudinal paraffin-embedded sections of shoot apices from 8dae *hyd2* seedlings, stained with safranin and fast green. Bar = 5μm.

In both of these examples, SAM regions appear (asterisks) separated by a developing leaf organ. In plant A, thickening of the hypocotyl region is associated with dissociated strands in the stele and a wide shoot apex. Plant B developed substantial thickening of one cotyledon-like structure (c); deformation of the SAM region appears to be associated with this distorted morphology.

orientation. An abundance of densely stained meristematic tissue is visible, resolved into two SAMs in the plane of the section, between and around which young expanding primordia have emerged from multiple points over the apex. This example has the least clear separation of meristematic tissue from the cells of the cortex beneath.

4.3.4.3 The endodermal cell layer of the root retains its identity in relation to the vascular stele, even in the presence of duplicated longitudinal axes.

The specification of the *Arabidopsis* endodermis in the developing embryo requires the SHORTROOT (SHR) protein, produced in cells of the procambium, and transported into the adjoining cell layer, where it promotes production of the SCARECROW (SCR) required for separation of cells into cortex and endodermal cell layers (Nakajima *et al.* 2001, Di Laurenzio *et al.* 1996, Wysocka-Diller *et al.* 2000). SCR then maintains the endodermal layer in the post-germination root apex by acting longitudinally to control the asymmetric periclinal cell division of cortical initial daughter cells that generates two cell layers; the cortex and endodermis (Di Laurenzio *et al.* 1996).

Fig. 4.32; A shows a wild-type root apex from a 3 dae seedling, expressing the SCR::GFP fusion (Wysocka-Diller *et al.* 2000). This optical section shows a clear endodermal signal in the root, which in three dimensions appears as a sheath encasing the stele.

The SCR::GFP reporter was introduced into mutants of both *hyd1* and *hyd2*. In both of these mutants, root apices showed a normal localization of the GFP signal, indicating that the endodermal cell layer identity is maintained in a single cell layer around the stele in these mutants (Fig. 4.32; B-E). This pattern still appears to define a single cell layer in roots which are radially swollen (Fig. 4.32; C), and in examples where duplication of the stele has

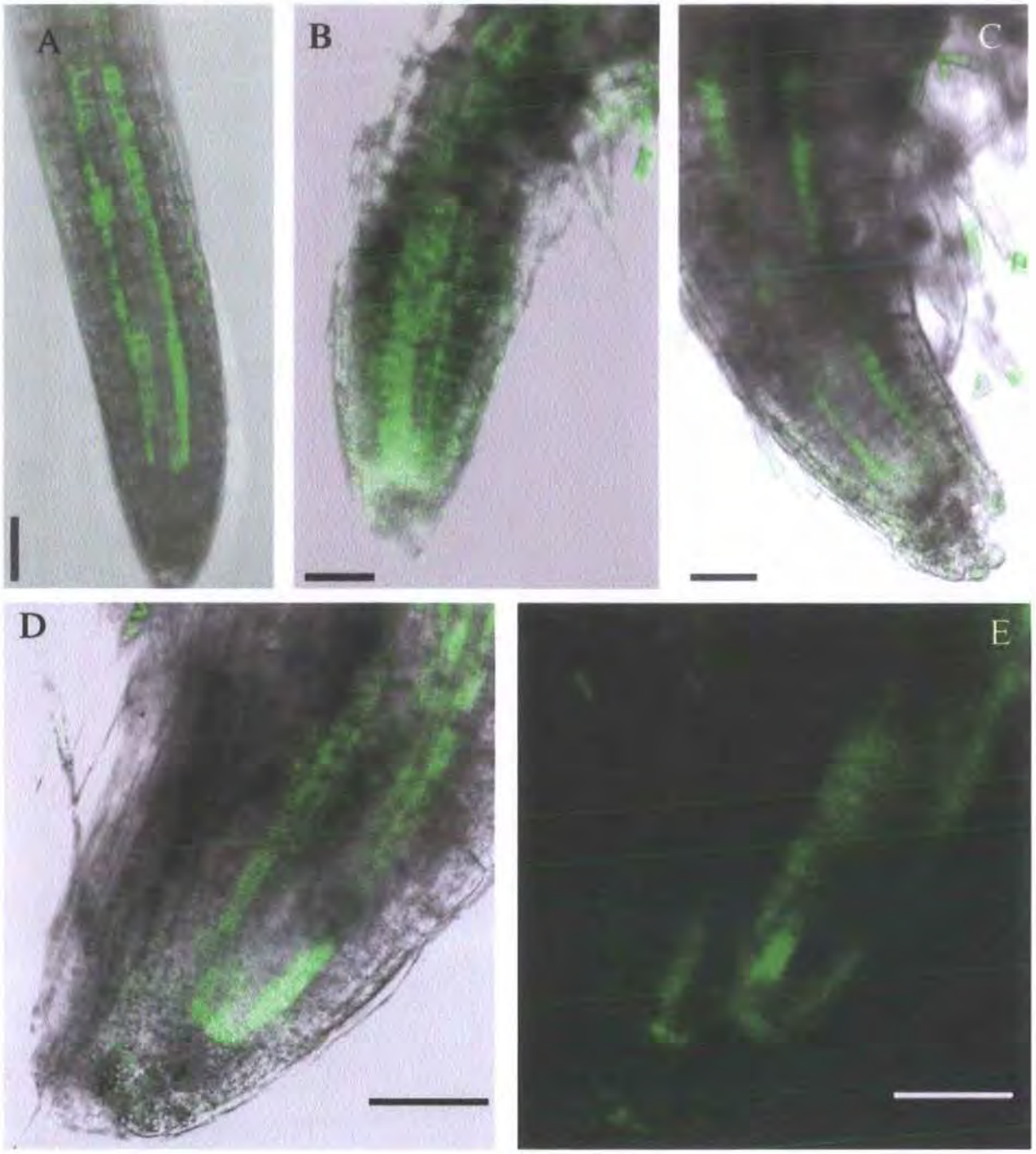

Figure 4.32 *SCR*::GFP expression in wild-type and *hydra* root apices

A; wild-type, B-D; *hyd2*, showing expression of SCR::GFP (as a z-stack) superimposed over the transmission image of the root apex. D shows a seedling with full longitudinal axis duplication, with the Z-stacked GFP image separately in E. All plants are 3dae, bar = 50μm.

The wild-type root shown in A spans a stacked longitudinal section of 30μm thickness. This shows a partial section of the endodermal GFP signal which encircles the stele. The *hyd2* root in B shows a median longitudinal z-sacks with GFP expression in a mostly coherent endodermal layer as it spans the root axis, although with some diffuse spread of the signal, which may indicate a distortion of the cell layer. In C, another hyd2 seedling, the optical longitudinal section shows a single endodermal layer as in wild-type, despite radial thickening of the upper root. Neither of these seedlings produced a hypocotyl GFP signal.

Seedling D shows a *hyd1* 3dae root apex with duplicated longitudinal axes, as shown in the sectioned plant from Fig. 4.29; C. The GFP signal suggests that two steles produce endodermal cues that in concert resolve a single layer of SCR::GFP expression (i.e. endodermal identity) encircling both axes but not including the cells that separate the two steles.

taken place (Fig. 4.32; D and E). in this example, which is anticipated to have a similar transverse patterning to that seen in Fig. 4.29; C, it appears that only the outer endodermal cells are expressing GFP, and the endodermal cells in contact with the endodermis around the adjacent stele are not producing GFP.

Wysocka-Diller *et al.* (2000) have used the SCR::GFP reporter to examine the patterning of the shoot endodermal layer (known as the starch sheath in shoot tissues), by counter-staining with propidium iodide to highlight other cell layers. Although wild-type seedlings were able to withstand this pre-treatment, the *hydra* mutants appeared particularly sensitive to propidium iodide, and did not maintain a satisfactory GFP expression with treatment, even in very young seedlings where reporter activity appears most strong. For this reason, the GFP images presented in Fig. 4.32 are overlain onto the transmission image of the unstained root apex. No satisfactory images were obtained of the mutant hypocotyl and shoot apex using this reporter, although whole mounted seedlings under fluorescence did appear to have some GFP activity, implying that at least some cells of the hypocotyl had endodermal cell layer identity.

4.3.5 Primordial initiation and phyllotaxy

4.3.5.1 Mutants at the *hydra* loci have more rapid rates of true leaf initiation than wild-type plants

Mutants from populations of both *hyd1* and *hyd2* were transplanted at 4 dae, grown on vertical plates, and harvested at 12 dae to be scored for numbers of initiating true leaves. Multiple primordia formed in these seedlings, not all of which showed a rapid expansion (see 4.3.5.2 below). Leaves were counted by examination with a dissecting light microscope, and scored for structures

where leaf lateral expansion was apparent. These frequency data are summarised below; the original data are presented in Appendix 6.

Ws (n = 20)	*hyd1* (n = 68)	*hyd2* (n= 61)
5.10	9.35	7.67

These data show a more rapid rate of leaf initiation in the *hyd1* population than in *hyd2*, although both mutants produce leaves more rapidly than their wild-type backgrounds. There is a very wide range in the data, with the higher scoring plants having duplicated shoot apical meristems.

4.3.5.2 Mutants at the *hydra* loci demonstrate anomalies in primordial initiation and position around the vegetative shoot apical meristem

Patterning cues derived from the position of existing cotyledons and true leaves around the wild-type SAM influence subsequent primordial positions in wild-type plants. Mutant seedlings with two cotyledons and relatively normal shoot morphology were selected to study *hydra* phyllotaxy, in order that the structures associated with influencing the position of subsequent primordia should be normally located. In choosing siblings for this study, it was noted that the *hyd2* population comprise a much greater proportion of plants with two cotyledons than seen in the *hyd1* population.

A comparison of *hydra* mutant plants with wild-type seedlings reveals a variably distorted phyllotaxy (Fig. 4.33; A-F). Plants analyzed for this data were selected at 4 dae and grown on fresh culture plates until 12 dae, fixed in FPA for 30 minutes to remove chlorophyll from the emerging primordia (to aid visualization) and examined using a dissecting stereomicroscope with top illumination.

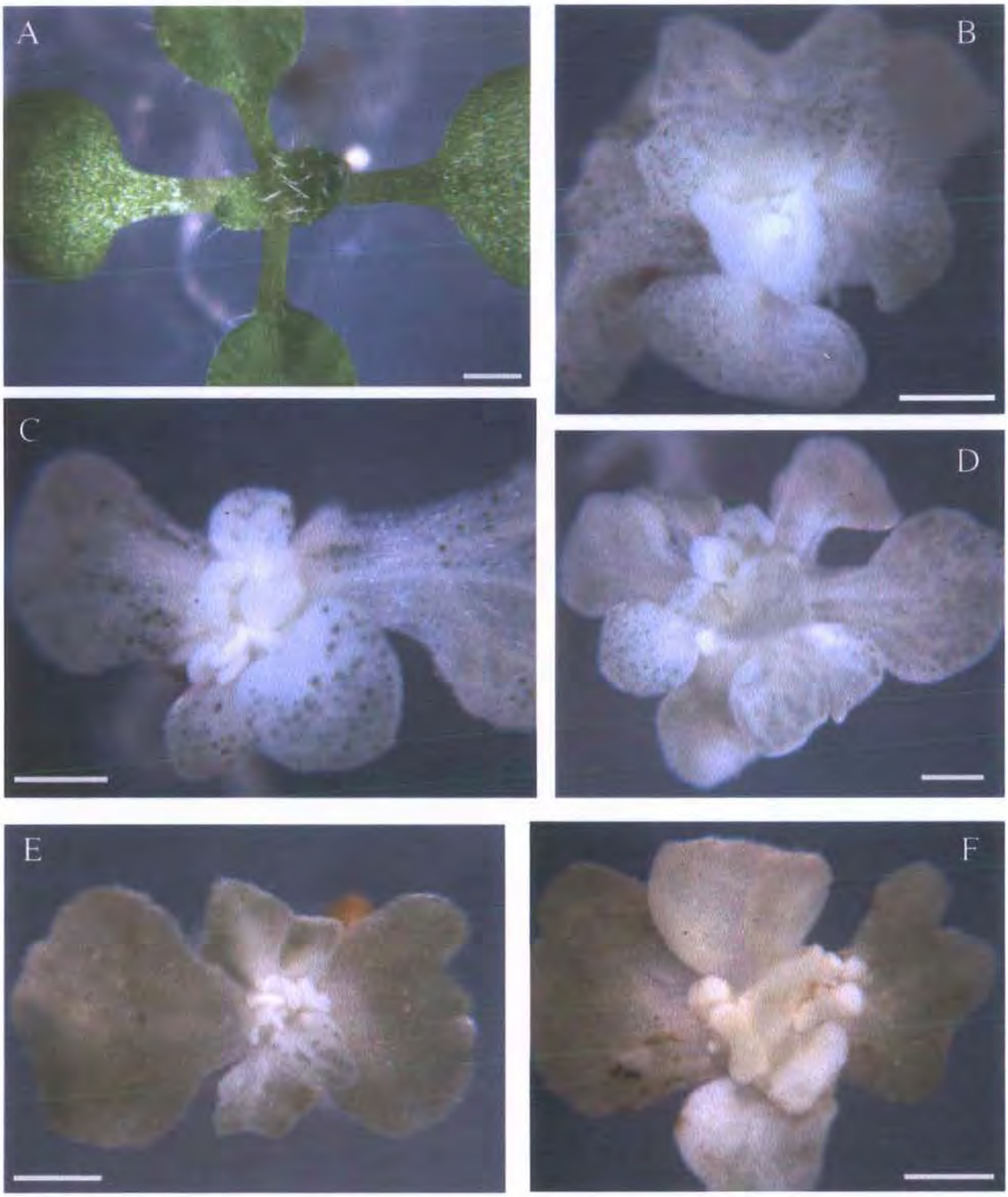

Figure 4.33 Primordial initiation in wild-type and *hydra* seedlings

A; Ws, B-D; *hyd1* and E, F; *hyd2*, all at 12dae, bar = 0/5mm. Plants B-D were incubated in acid fixative (FPA) for 30 minutes to remove chlorophyll and visualise young primordia.

These seedlings were selected at 4 dae as plants with two cotyledons and no obvious signs of axis duplication, in order to give a result comparable to the two-cotyledon morphology of wild-type. In many cases, plants were able to initiate the first pair of true leaves in the expected positions, though few subsequent primordia continued to follow the expected pattern. The plant shown in B has retained a classic spiral and was the only sibling to do so in 28 *hyd1* seedlings examined. Similar phenomena were found in *hyd2*. Siblings developed simultaneous points of primordial initiation around the SAM, in association with an increasingly distorted shoot apex.

From this sub-population, occasional plants were found, such as the *hyd1* seedling shown in Fig. 4.33; B, with what appears to be a normal phyllotaxy. In this example the leaves initiate and expand around a central SAM in a spiral arrangement, as in wild-type (Fig. 4.33; A). However, even in this individual, the rate of leaf initiation was more rapid than in wild-type.

Other plants shown in Fig. 4.33 have variable numbers of extra primordia, which do not arise in a predictable phyllotactic order. The *hyd1* plant in Fig. 4.33; C, and the *hyd2* sibling in Fig. 4.33; E, both have developed a widened SAM where multiple primordia are appearing without an apparent focus or obvious timing to the phyllotactic sequence. In both seedlings it appears that the first 3-4 true leaves have formed in approximately correct positions, suggesting that the relative positional cues from the cotyledon positions are functioning as in wild-type plants.

In the seedlings shown in Fig. 4.33; D (*hyd1*) and F (*hyd2*), at least two separate meristem regions are apparent. In D, there appears to be a clear separation of the shoot axis, with two points of origin for expanding leaves. In F, points of initiation appear to be located on the laminae of the cotyledons, in the region of the lamina-petiole junction (although expansion of the petioles is not apparent in this seedling).

These plants demonstrate that primordial initiation in *hydra*, and meristem formation and maintenance, are not responding to the normal positional cues which control these processes. Although certain individuals with a single SAM can demonstrate an apparently normal phyllotaxy in the positioning of the first 2-5 true leaves, the rate of primordial initiation appears to be independent of the phyllotactic pattern in these mutants.

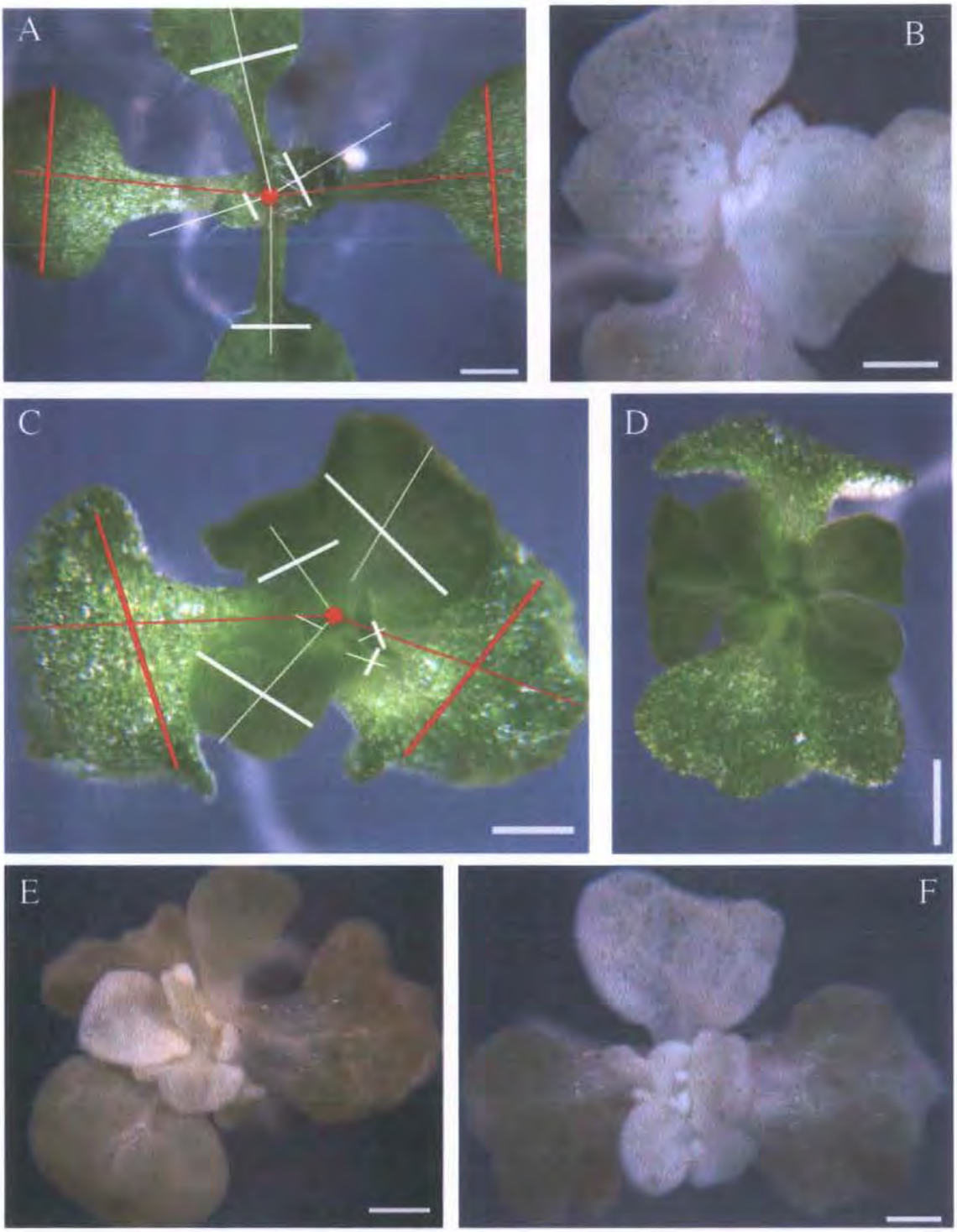

Figure 4.34 Misalignment of the *hydra* leaf longitudinal axis

A, Ws; B-D, *hyd1* and E, F, *hyd2* seedlings at 12dae, bar = 0.5mm

A; lines drawn along the longitudinal leaf axes from the origin of the phyllotactic spiral show how wild-type primordia expand their dorsiventral axis at right angles to the long axis of the leaf, i.e. at 90° to these lines. True leaves (white lines) take their positional cues from the cotyledon positions (red lines).

In *hydra,* alignment of the leaf axes is not easily predictable. The *hyd1* seedlings shown in B-D have two cotyledons, and would be expected to produce a phyllotactic spiral with centrolateral alignment as demonstrated in A. The seedling in C has lines drawn along the leaf axes across the direction of transverse expansion as in A. Similar problems with primordial alignment can be seen in both *hyd1* and *hyd2* siblings.

4.3.5.3 Expanding true leaves around the *hydra* SAM show misalignment of the centrolateral expansion axis.

Wild type leaves that initiate around a single SAM show not only a predictable phyllotactic sequence, but maintain their axis of longitudinal expansion in a co-ordinated fashion so that the centrolateral axis of the leaf is at right angles to the direction of shoot growth (Fig. 4.34; A).

In *hydra* mutants, seedlings show a distortion of this alignment (Fig. 4.34; B-F). The seedling in Fig. 4.34; C has been annotated in the same manner as the wild-type plant in Fig. 4.34; A, to show the leaf axes in relation to a point of phyllotactic origin, i.e. the presumptive SAM. Although these true leaves may have initiated their primordia in correct positions relative to the SAM, subsequent development has modified the alignment of the leaf apical-basal axis in relation to the phyllotactic origin, and hence the centrolateral axis has become skewed in relation to the shoot apex. These observations may be interpreted as being associated with a successive distortion of the SAM region during shoot development.

4.3.5.4 Ectopic meristems form on the proximal laminae of the cotyledons and in the marginal zone of the SAM in many *hydra* siblings

In wild-type plants, seedlings develop a singe SAM at the shoot apex, around which the expanding true leaves develop in a 'hooded' formation, protecting the meristems shown in Fig. 4.5.4; A. The small structures visible in this SEM image are stipules. In contrast, the young primordia of *hydra* mutants were never observed to develop this hooded morphology. Instead, many plants carry regions of multiple primordial initiation, as can be seen in both *hyd1* (Fig. 4.35; B-E) and *hyd2* (Fig. 4.36; A-E).

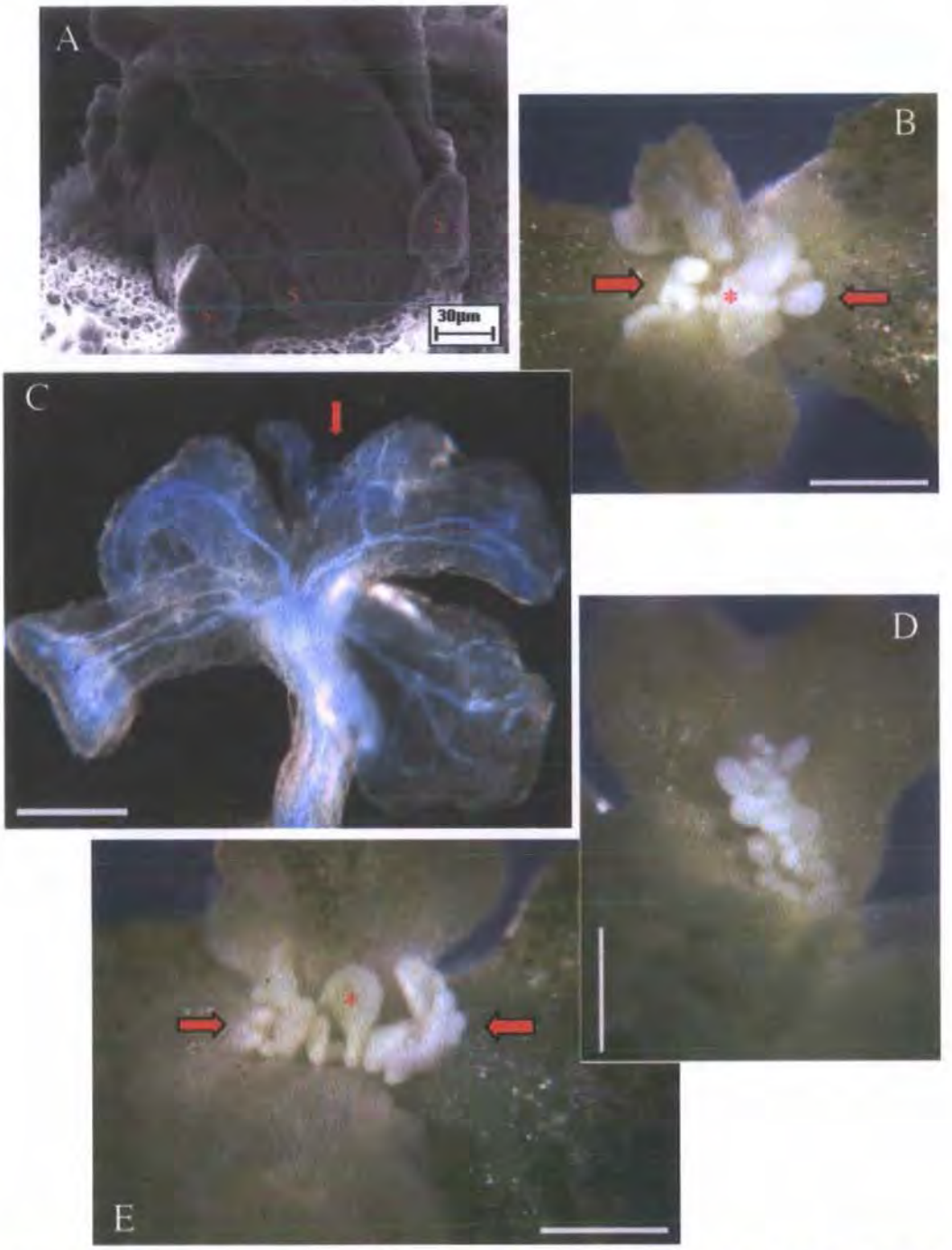

Figure 4.35 Ectopic meristems at the *hydra1* hypocotyl-cotyledon boundary

A; Ws shoot apical meristem from 11dae plant, older leaves removed. Primordia initiate around the SAM in regular and predictable positions, forming young leaves which enfold the meristem region. The small structures at the base of these leaves are stipules (S), which form at the margins of laterally expanding primordia.

B-E; *hyd1*, bar = 0.5mm. B and E (12 dae) have several points of primordial initiation; the central SAM position (asterisk) is flanked by ectopic primordial initiation points at the base of the cotyledon petioles (arrows). B also shows a third collection of primordia on a small lobed region towards the top of the picture.

C shows an 8dae plant with the first true leaves removed, revealing an ectopic meristem (arrow) initiating on the lower lamina of a lobed cotyledon. A secondary vascular strand from the cotyledon is visible, and has branched upwards towards the primordia.

D shows the petiole region of a 12dae cotyledon, initiating primordia above the expected position of the primary mid-vein.

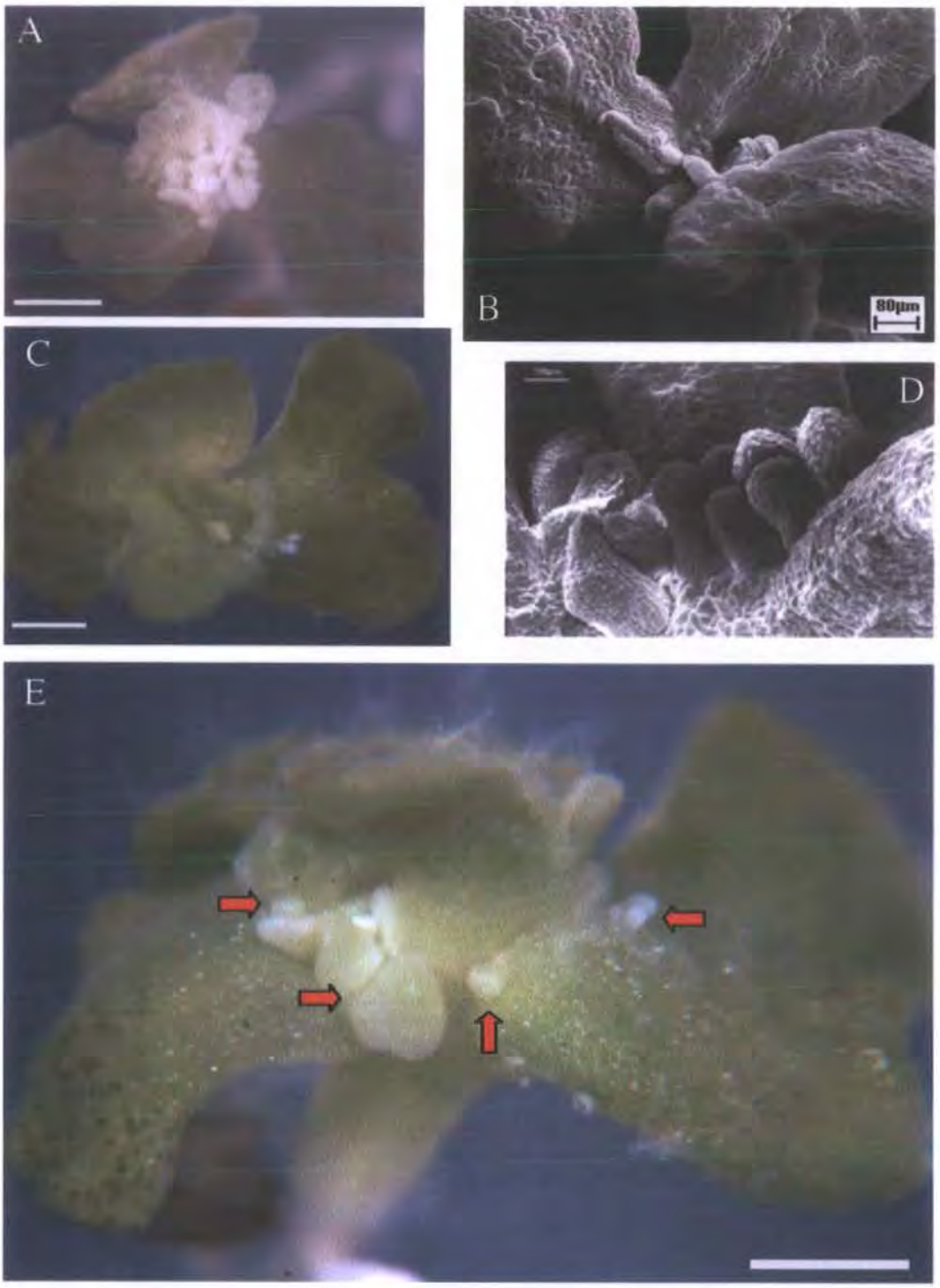

Figure 4.36 Ectopic meristems on *hydra2* cotyledons

A-E, *hyd2*; B and D at 7 dae, A and C are 12dae. E shows plant C in side view, bar = 0.5mm.

As in *hyd1*, *hyd2* seedlings also form ectopic meristems. A shows a shoot region initiating multiple SAMs. The seedling shown in B has elongated growths appearing on the cotyledon shoulder. D shows a different seedling, with multiple young primordial structures that do not show signs of dorsiventral flattening as in wild-type. C shows an apical SAM in the expected position between cotyledons, along with further primordial on the lobed cotyledon to the right. This same plant, shown in E, has multiple points of ectopic primordial initiation at the meristem flanks, around the meristem-petiole junctions (arrows).

Siblings of the *hydra1* mutant populations, such as those shown in Fig. 4.35; B and E, display regions of primordial initiation at the shoot apex (marked by red asterisks), alongside additional meristems at the base of the cotyledon lamina (shown by arrows). In these two examples, a minimal longitudinal expansion of the cotyledon petiole has taken place. In other examples, for instance Fig. 4.35; C and D, clusters of ectopic primordia can be seen at the junction of the cotyledon petiole and lamina (C), and along the presumptive route of the primary midvein of a laterally-enlarged cotyledon petiole. Similar examples are seen in *hyd2* (Fig. 4.36; A-E). In all of these examples, ectopic meristem initiation appears to take place only in tissues of the cotyledon, most usually in positions associated with the primary midvein, although primordia also arise elsewhere around the cotyledon-hypocotyl transition zone, as can be seen indicated by arrows in Fig. 4.36; E.

Almost all 12 dae seedlings examined had additional primordia, although not all to the extent shown in these examples. It is unclear from the phenotype of older seedlings whether all of such clusters of ectopic primordia continue to develop. Where they occur, they are always found on the cotyledon adaxial surface, in proximity to the meristem zone, and can be variably positioned on these cotyledons surfaces in a lateral fashion, i.e. around the radial periphery of the shoot apex. Only flattened *hydra* cotyledons appeared to initiate ectopic meristems (i.e. not all cotyledons have an abaxial-adaxial flattened morphology, some forming 'prong' shapes). No examples of ectopic meristem formation were found on true leaves, or on cotyledon laminae away from the hypocotyl-cotyledon transition zone.

4.3.5.5 Ectopic meristem initiation takes place in association with extra or misplaced branching events in the zone of vascular transition between the hypocotyl and cotyledons

Examination of the position of ectopic meristem formation in relation to the vasculature of *hydra* mutants was carried out using seedlings expressing the p*AthB8*::GUS provascular tissue marker. This reporter highlights the provascular traces of very young primordia, and so ectopic primordia and meristems are made visible in cleared tissues by reporter activity. Analysis of *hydra* siblings revealed that ectopic meristem formation and initiation of additional primordia occurs within the vascular transition region.

In wild-type *Arabidopsis,* differentiation events after germination re-orientate the xylem plate from exarch in the hypocotyl (provasculature on the outside) to endarch (provasculature on the inside of the radial axis, i.e. the adaxial side) in the cotyledon. This takes place in conjunction with a rearrangement of the spatial relationship between xylem and phloem from alternate to collateral (Busse & Evert 1999a, 1999b). The zone of transition is restricted to a very short portion of the upper hypocotyl, cotyledonary node and cotyledons (Busse & Evert 1999b). The vascular system of the first pair of true leaves, and subsequent development of the rosette, develops only after establishment of the vascular pattern in the root-hypocotyl-cotyledon unit (Busse and Evert 1999b).

Development of the first pair of true leaves does not take place until vascular connections have been made between the differentiated vasculature of the cotyledons and the true leaf primordia. This involves formation of a pair of procambial strands, each one connected to each of the cotyledon traces; these are first visible anatomically at around 4 dae, followed by differentiation of the first phloem elements at 6 dae, and xylem at 8 dae (Busse and Evert 1999b). Each subsequent rosette leaf trace is connected to strands associated with two other leaves, including the cotyledons, lower on the axis in a manner similar to that of the first two rosette leaves; this can be made out in the third true leaf trace of the wild-type plant shown in Fig. 4.37; A.

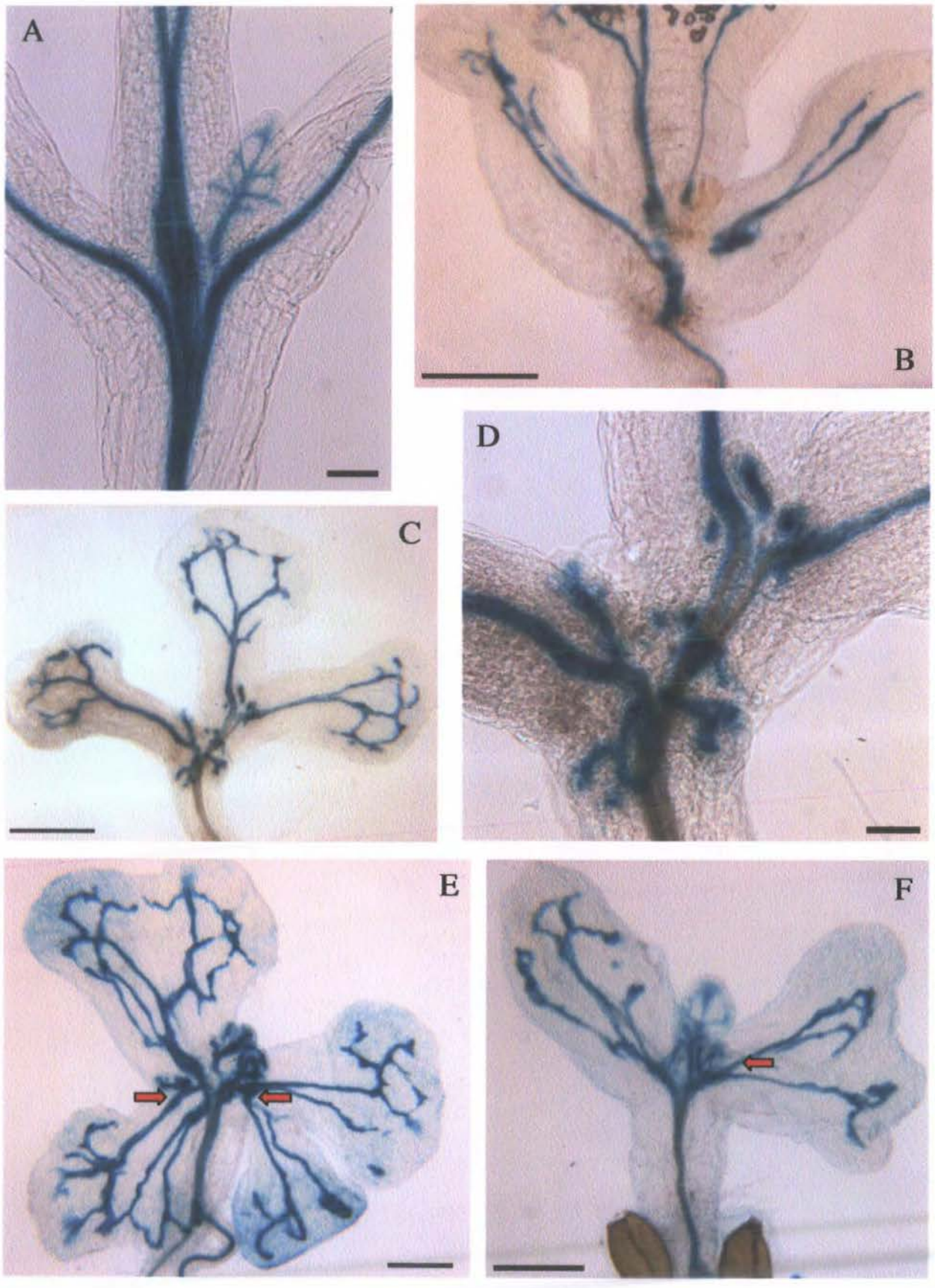
A
B
C
D
E
F

Examination of primordial initiation in *hydra*, in relation to this zone of hypocotyl-cotyledon vascular transition, revealed that the anomalous phyllotaxy found in *hyd* mutants is associated with mis-positioning of vascular branching in this region. Unlike wild-type, *hyd* mutants may produce multiple primordia at these points, with or without an obvious meristematic zone between them. Primordia did not initiate at branch points between radialized cotyledonary structures in the absence of xylem differentiation, although some of these structures had a provascular trace shown by p*AthB8*::GUS. This suggests that initiation of true leaf primordia is associated with the transition zone only where cotyledons have xylem differentiation, implying that a differentiated vasculature with both phloem and xylem may have signalling implications for meristem establishment.

Primordial initiation was not seen on cotyledon surfaces away from the hypocotyl-cotyledon transition zone, neither in association with true leaves. In examples of seedlings where vascular dissociation has taken place further down the stele producing duplicated parallel primary vascular traces in the cotyledon petiole (as shown in Fig. 4.37; G), or dividing a short distance into the cotyledon petiole (Fig. 4.37; H), no ectopic primordia were observed.

Clear ectopic branching events in the transition zone, such as in the example shown in Fig. 4.37; C-D, were found in association with large ectopic meristem formations (i.e. clusters of primordia). In other examples, where the stele divided into multiple cotyledon traces, smaller meristems with a lesser number of true leaves could be seen at each branch point (Fig. 4.37; E, detailed in F).

An association between two coherent apical-basal vascular traces appears to be necessary for meristems to develop. The 11 dae seedling shown in Fig. 4.37; B has an incomplete pattern where the provascular traces of the cotyledons do not meet the single trace through the hypocotyl stele and into one of the cotyledons; this seedling lacks a branch point in the upper stele,

and also lacks any signs of primordial development, although the presence of cotyledons does suggest that lateral-radial patterning took place during embryogenesis. Seedlings with two coherent apical-basal vascular strands in the stele, even where these strands are dissociated, can produce an apical SAM, as in the *hyd1* seedling shown in Fig. 4.41; E which has duplicated axes forming two distinct shoot apices. Each axis has a single apical SAM with an apparently normal phyllotaxy.

4.3.6 Dorsiventrality

4.3.6.1 Transverse sections of *hydra2* cotyledons and true leaves reveal variably sized cells, unusually large or absent air spaces, and variable dorsiventral organization within the mesophyll.

Transverse sections across the laminae of cotyledons and true leaves from wild-type plants (Fig. 4.38; A and B) reveals a dorsiventral differentiation within the mesophyll cell layer. Towards the adaxial (upper) lamina, a dense layer of slightly elongated palisade cells can be seen, below which towards the adaxial lamina, a less obviously organized spongy mesophyll are packed in such a way that air spaces are generated within the leaf organs. A paradermal section across the lamina (Fig. 4.38; C) shows that these air spaces appear in a regularly-spaced arrangement, and lie within the same plane of the leaf as the vascular traces. This differentiation of the palisade and spongy mesophyll represents one of the several developmental characteristics that confers a dorsiventral axis onto the developing lateral organ (Pike & López-Juez 1999), and palisade anatomy is present in very young primordia prior to the onset of centrolateral expansion (Pike *et al.* 1991).

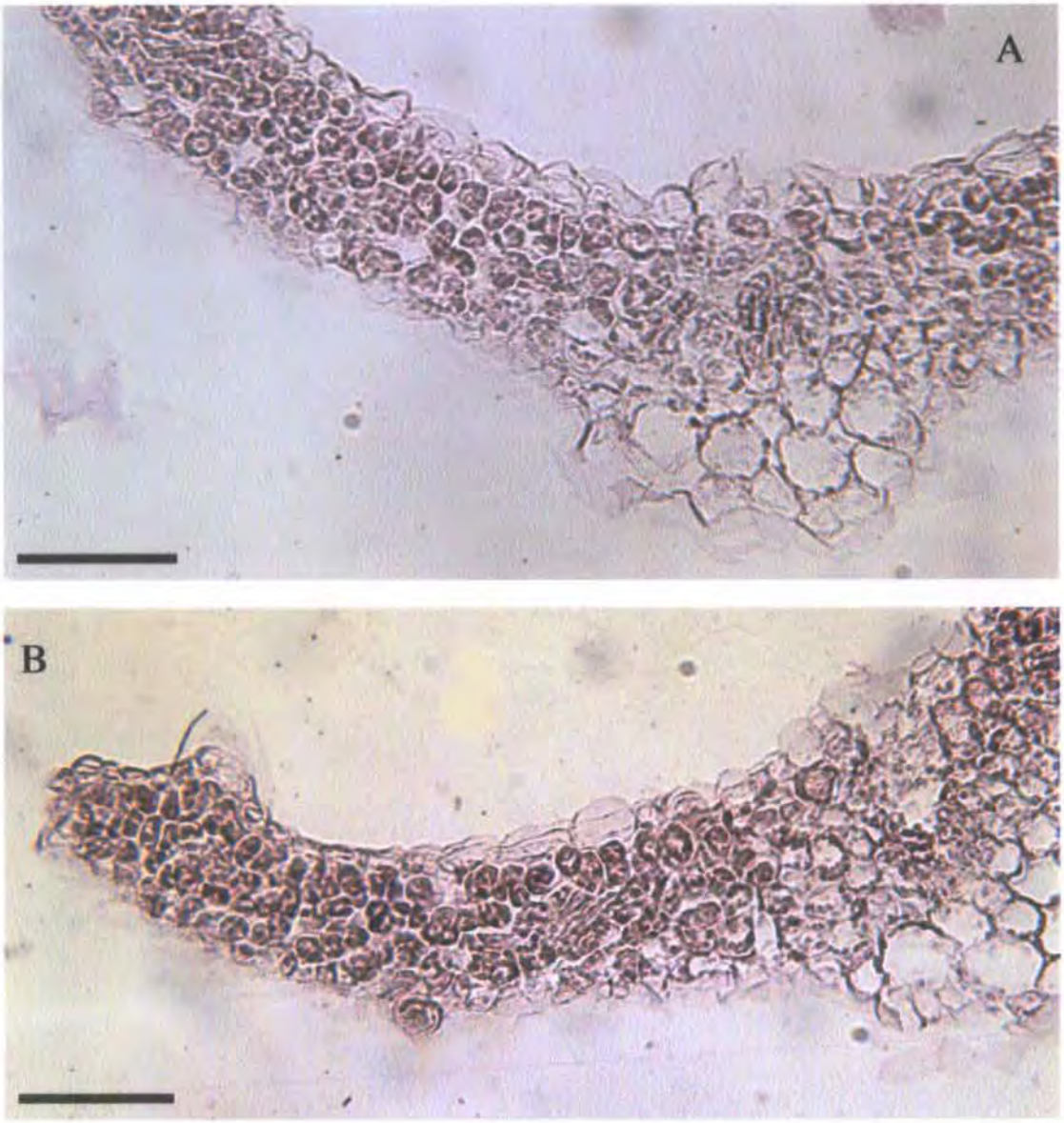

Figure 4.38 Distribution of cells in the wild-type lamina

A-C; Ws sectioned material from 8dae plants, bar = 50μm.

A; cotyledon, and B; young expanding true leaf transverse sections, showing dorsiventral organisation of the cell layers within the mesophyll. A dense layer of palisade cells are visible beneath the adaxial epidermis, with developing intercellular spaces beneath. C; paradermal section through a mature cotyledon showing the distribution of air spaces and chloroplasts in cells of the mesophyll layer.

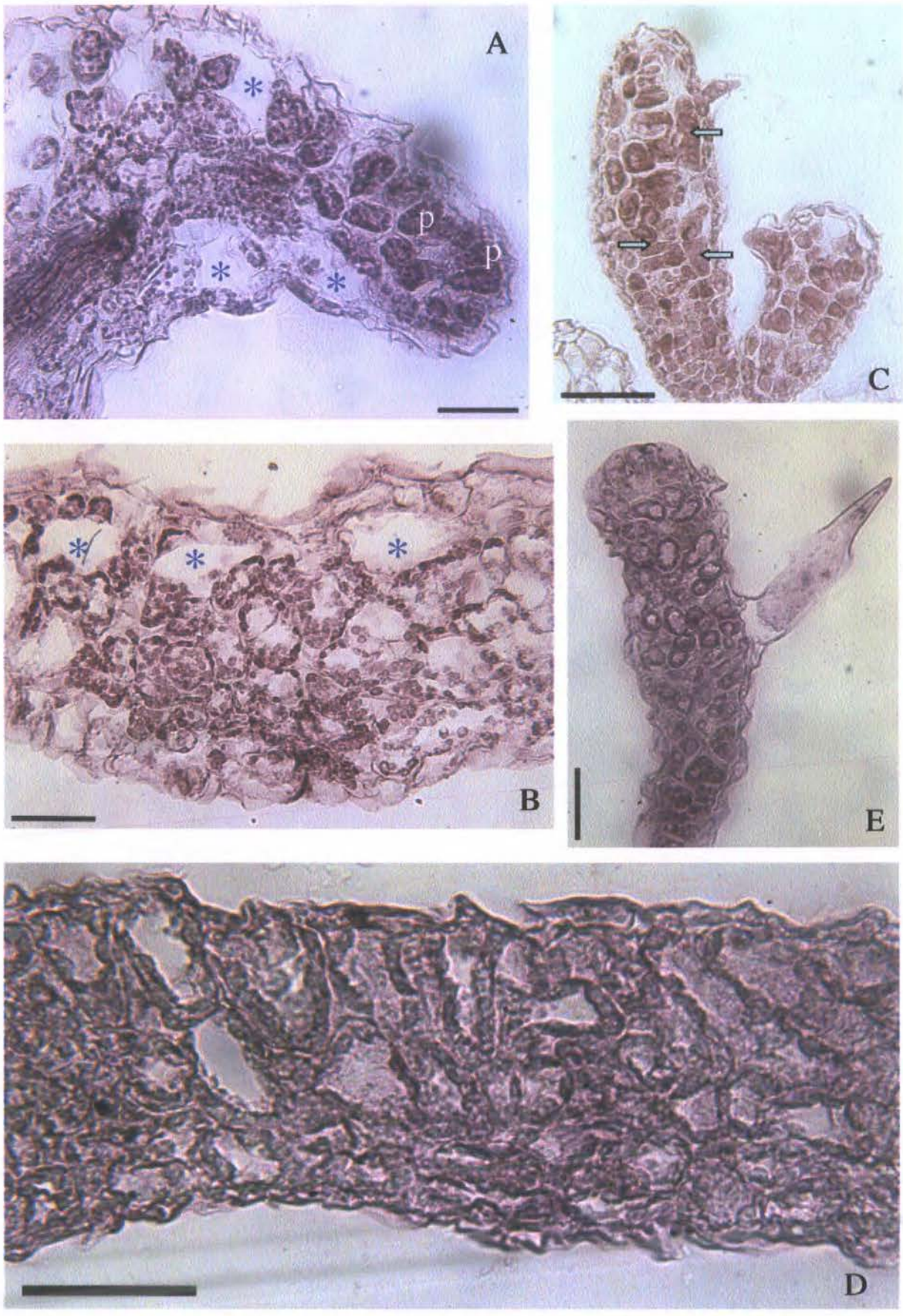
A
p
p
C
B
E
D

In cotyledon and true leaf tissues of *hyd2*, a much less regular arrangement of cells is seen (Fig. 4.39; A-E). Their internal anatomy suggests that there is a problem in co-ordinating the behaviour of mesophyll cells across the dorsiventral axis in these mutants. In Fig. 4.39; A, the *hyd2* cotyledon shown lacks a well-defined leaf margin. Instead, a variable arrangement of enlarged mesophyll with an elongated shape and putative palisade cell identity (marked p) are clustered towards the margin zone in two layers, with only the upper layer arranged in the expected dorsiventral orientation. These cells appear much larger than mesophyll from the wild-type cotyledon (Fig. 4.38; A, C), and are packed with chloroplasts. Other plastid-dense cells are present, comprising the bundle sheath around the vascular strand visible in the left of the picture. Several large intercellular spaces are visible, marked with asterisks, bordered by spongy mesophyll with a more usual arrangement of plastids around the cell margins.

The *hyd2* cotyledon section in Fig. 4.39; B does not have any elongated cells with putative palisade identity. Instead the whole transverse section of the lamina appears to be comprised of spongy mesophyll, some showing unusual density of plastids, although the size of these organelles appears consistent. Again, enlarged air spaces are present, marked by asterisks. The *hydra* cotyledon section in Fig. 4.39; D (from the mid lamina) appears unusually thickened, and filled with variably sized mesophyll cells, many of which have excessive numbers of plastids. The layer of cells beneath the adaxial epidermis are larger than cells close to the abaxial epidermis; this distinct but poorly-defined dorsiventral orientation suggests a putative palisade identity. No air spaces are evident.

A longitudinal section of young expanding true leaves of wild-type *Arabidopsis*, prior to epidermal differentiation and the generation of intercellular air spaces (Fig. 4.38; B) shows a regular arrangement of cell layers within the lamina. In young true leaves of *hyd2*, dorsiventrality appears to be present, as defined by the presence of adaxial trichomes (Fig. 4.39; C), although with an

irregular cellular arrangement in the mesophyll, and a lamina of variable thickness. This leaf section has some elongated cells with putative palisade identity, although they are variably oriented within the organ (arrows). The mutant leaf shown in Fig. 4.39; E, has a putative palisade layer adjacent to the adaxial lamina with the cells' long axes in an approximate and variable alignment with the dorsiventral axis. The margin of this leaf is thickened, and has a cluster of what appear to be palisade cells, oriented is at right angles to the dorsiventral axis.

4.3.6.2 Functional stipules, as highlighted by the DR5::GUS reporter, are rare in *hyd1* and appear to be absent from *hyd2*

In wild-type *Arabidopsis,* stipules are small structures that arise from the leaf tissue at the margins of true leaf primordia, close to the junction between the expanding leaf blade and the shoot apical meristem. They differentiate rapidly, maturing ahead of xylem differentiation in the primary midvein, and undergo no or minimal expansion during subsequent laminar growth. Their function is unknown, but their ultrastructure reveals these structures to comprise cytoplasmically-dense cells with high metabolic activity (Bowman 1994). As stipules are morphologically distinguishable between the onset of centrolateral expansion of the primordium, and prior to trichome differentiation in the adaxial epidermis, this implies that they are early morphological markers of centrolateral expansion, and their presence suggests an established abaxial-adaxial axis in the developing leaf.

The DR5::GUS fusion construct combines a highly active synthetic auxin response element with the β-Glucuronidase reporter gene, (Ulmasov *et al.* 1997). During true leaf development, the first signs of DR5::GUS reporter expression appear in stipules ahead of primary xylem differentiation and DR5::GUS activity in the apical hydathode (Aloni *et al.* 2002). The present study uses DR5::GUS expression as a morphological marker of stipule

differentiation, indicating the onset of functional metabolic activity in these structures. Wild-type plants show a strong expression of DR5::GUS in the stipules of developing leaves, as shown in Fig. 4.40; A. This 10 dae wild-type seedling has strongest reporter activity in the stipules, with a less active GUS signal in the apical hydathode and developing vascular traces.

Fig. 4.40; B-D show seedlings of *hyd1* at 10 dae, expressing the DR5::GUS reporter. The seedling in B has strong GUS activity in the stipules of both true leaves, although close examination of the photographs shows a weaker signal in the second stipule pair. A variable expression is seen in the developing leaf traces of this plant, and the apical hydathodes, seen clearly in wild-type, are not clearly resolved in the mutants. This plant demonstrated the best stipule definition of the whole *hyd1* sample, of approximately 40 seedlings at this age class. Other *hyd1* siblings, such as those shown in Fig. 4.6.2; C and D, revealed a less defined reporter activity. Seedling D has activity in one tiny stipule-like structure, and little reporter activity in the primordia, although root expression was strong. Seedling C shows a more typical GUS activity, with a few variable peaks in primordia, and ectopic expression in localized points in the cotyledons. No *hyd1* siblings were found with DR5::GUS stipule expression in any later initiating leaves after the first true leaf pair, i.e. stipules were absent from leaves formed from post-germination primordia.

DR5::GUS activity in *hyd2* highlighted an absence of functional stipules throughout the sibling population; neither were non-functional putative stipule structures anatomically resolved in the samples examined. Reporter activity elsewhere in the seedlings showed substantial variation between siblings, some examples of which are visible in Fig. 4.40; E-G. These mutants demonstrated variable ectopic reporter expression in cotyledons and young true leaves.

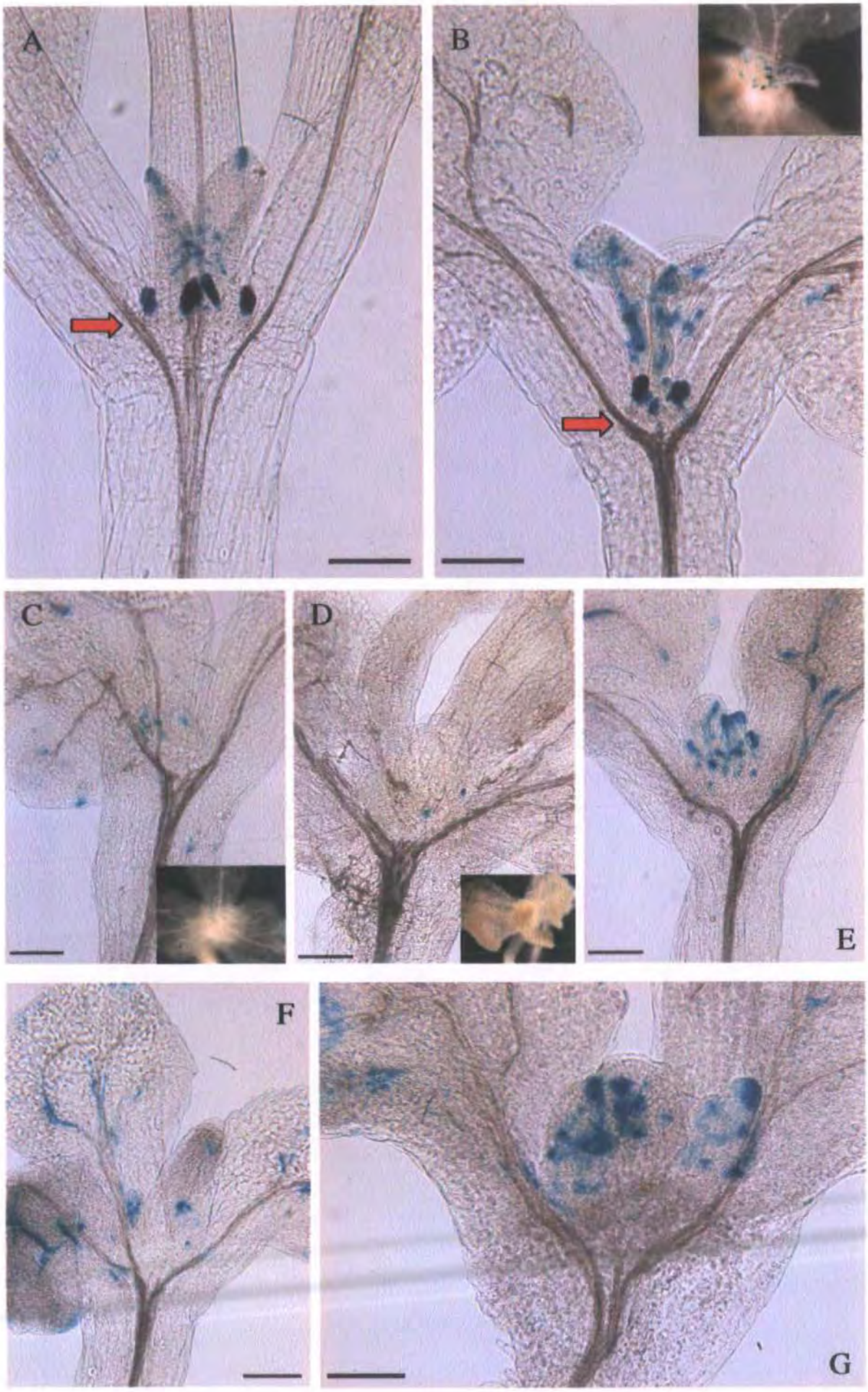
A
B
C
D
E
F
G

4.3.6.3 The p*REV*::GUS marker of primordial adaxial tissues, shows variably increased GUS activity in *hyd2* but not in *hyd1*, although both sibling populations show mis-positioned adaxial cues.

For this analysis, wild-type plants showing p*REV*::GUS reporter activity were selected from the *hyd* mutant backgrounds, so that any differences in expression due to ecotype (as seen in *rev* mutant alleles by Otsuga *et al.* 2001), would be incorporated into the controls. No differences in reporter activity in seedlings from the *hyd1* and *hyd2* backgrounds were noted. In wild-type, the p*REV*::GUS reporter defines the meristematic zone of the shoot apical meristem and adaxial tissues of very young primordia (Fig. 4.41; B). Expression was also seen in the hypocotyl and root stele (not shown), in provascular strands of true leaves ahead of xylem cell differentiation, and as a diffuse signal in the region of pith that separates the bifurcated vascular strands of the stele from the SAM above (Fig. 4.41; D-F). A brief and transient expression in cotyledon vascular traces at 3 dae faded rapidly as the xylem strands differentiated, and was not evident by 7 dae in these structures (Fig. 4.41; A, C).

Activity of the p*REV*::GUS reporter was used in this study to define adaxial tissue identity in very young true leaf primordia of *hydra* mutant plants. Examples were chosen that appeared to have a single SAM in association with a coherent longitudinal axis, and include several plants where the axis is clearly duplicated but each axis has a correctly-positioned SAM within two longitudinally coherent cotyledon-hypocotyl-root strands.

In *hyd1*, reporter activity was enhanced relative to wild-type in association with vascular disorganization in the cotyledon laminae (Fig. 4.42; A), but with only mild up-regulation in the stele. In seedlings with fully duplicated axes (Fig. 4.42; C), each axis retained the integrity of the stele signal, and in plants where the longitudinal axis was dissociated (Fig. 4.42; E) a pale diffuse GUS

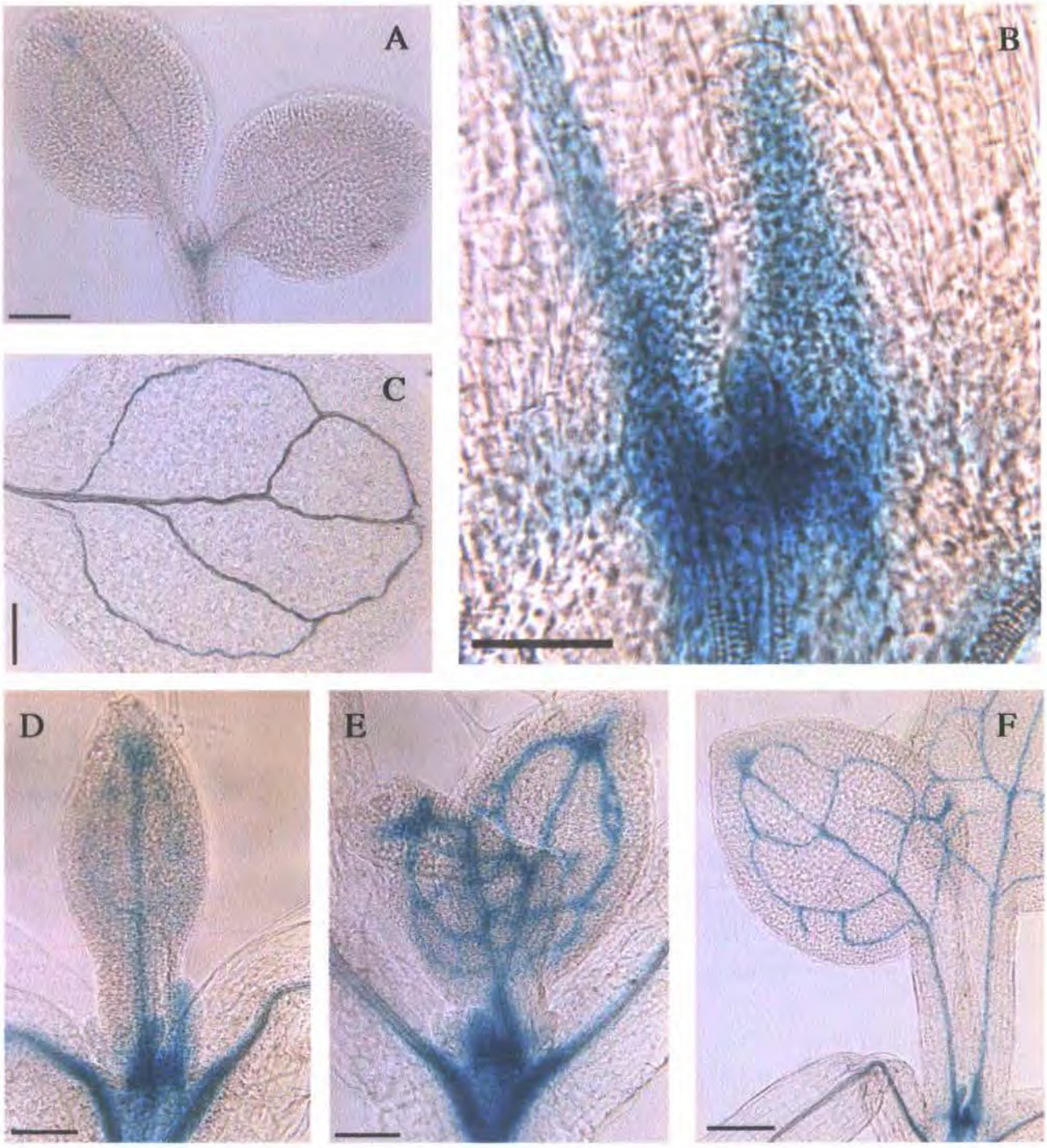

Figure 4.41 Expression of p*REV*::GUS in wild-type seedlings

A-F; wild-type plants expressing the p*REV*::GUS reporter, highlighting the vascular system in both root and shoot tissues, and defining adaxial tissue identity in young vegetative primordia.

A; 3dae seedling with transient expression in cotyledon vasculature. In 7 dae seedlings the SAM region shows adaxial definition in emerging true leaf primordia (B), and a diminishing signal in the cotyledons (C). As young true leaves expand (D-F), the vascular trace is defined by reporter activity ahead of xylem differentiation.

A, C, F, bar = 200μm; B, bar = 50μm; D and E, bar = 100μm.

activity was seen, suggesting that the normal signal has been 'spread out' in these siblings. Adaxial orientation appeared variable between *hyd1* primordia. Fig. 4.42; D, shows a shoot apex whose primordia appear skewed in relation to the SAM. The primordium marked with an asterisk seems to have a minimal adaxial signal, whist the closely spaced primordium adjacent (arrow) has an enhanced GUS activity which is skewed towards the asterisked primordium, and away from the SAM. Because these two primordia have initiated so close together, and because the adaxial signal is misplaced to a position within their adjacent tissues, it is possible that these two structures are resolving in response to cell recruitment cues below from a single vascular sympodium. Adjacent primordia appear to be adaxialised correctly in relation to the meristem position. This SAM is from the left-hand duplicated axis of the seedling pictured in Fig. 4.42; C, where the differentiation of the cotyledons associated with this axis is poor.

Fig. 4.42; B shows the meristem region of plant A. The primordium marked with an asterisk, and all the primordia visible in the photograph, appear to have an adaxial signal on the anticipated abaxial side. This problem is common to the whole meristem implies that the misplacement of an abaxial-adaxial signal is a peripheral SAM-associated phenomenon. A complete reversal of abaxial and adaxial tissue identity such as this has been reported for gain of function mutations in the adaxialising *REV*, *PHB* and *PHV* genes (Emery *et al.* 2003, McConnell & Barton 1998, McConnell *et al.* 2001) and loss of function in *KANADI* genes (Emery *et al.* 2003). This plant (Fig. 4.42; A) has indistinct vasculature in the cotyledons; primary traces are marked by the reporter, and appear coherent, but have not completed xylem differentiation, and neither formation of secondary loops nor clear lateral expansion has taken place in these organs.

In contrast, primordia from the two SAMs in the seedlings shown in Fig. 4.42; E, detailed in Fig. 4.42; F and G, have correctly positioned adaxial cues. In this example, the two cotyledons associated with each axis, each with a single

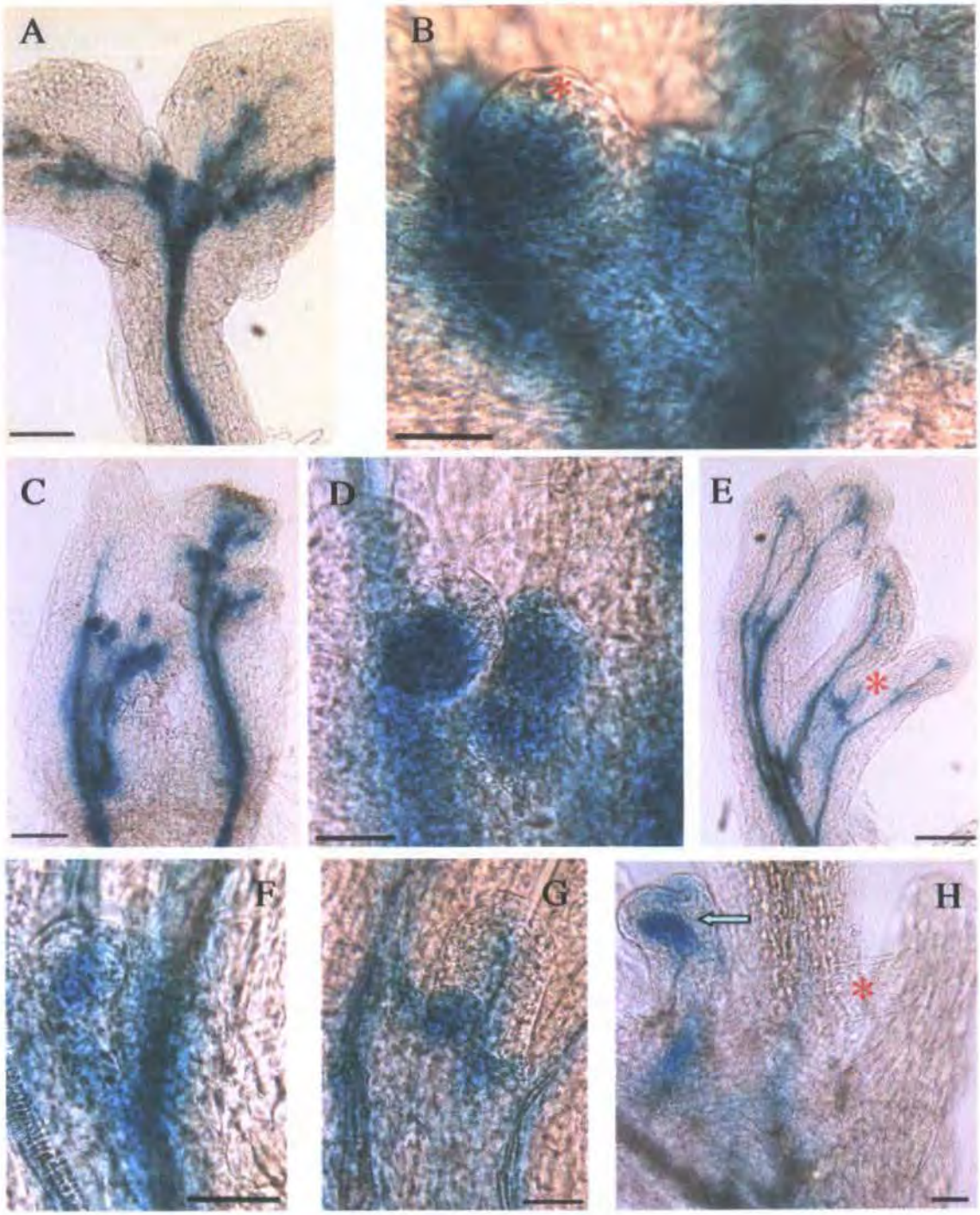

Figure 4.42 Activity of the p*REV*::GUS reporter in *hydra1* siblings

A-H; p*REV*::GUS activity in ***hyd1*** seedlings. A-G are from 7dae seedlings, and H shows detail from a 12dae shoot apex. B shows primordia detail from A, D shows detail of the SAM region from the duplicated axis to the left in C, and F and G show SAM regions from plant E. A, C and E, bar = 200μm; B, D, F-H, bar = 50μm.

The primordium marked with an asterisk in B appears to have a reversed dorsiventrality, with reporter expression on the abaxial side, away from the SAM. Duplication of the longitudinal axes do not affect p*REV*::GUS expression (C and E), but strand dissociation in the second axis (asterisk in E, detailed in G) corresponds to diffused weak activity around the SAM. This plant has better adaxial definition in primordia around the less dissociated axis (G). The asterisk in H highlights a prong-shaped structure lacking reporter activity; this structure has initiated and expanded next to a misshapen leaf (arrow) carrying an unusual expression peak, and appears to show an adaxialized structure next to an abaxialized prong.

SAM, have a coherent primary and secondary vascular pattern, although signs of 'noise' in xylem development are visible. The right-hand axis has dissociated further down the stele than the left-hand axis, which also shows some anomalies in the positioning of its stele vasculature.

The final *hyd1* example, shown in Fig. 4.42; H, is taken from a 12 dae seedling with two cotyledons between which an extra un-vascularized 'prong' of cotyledonary tissue has formed, visible to the right of the picture. This example has been included in the results figure because of the two primordia shown respectively by an arrow and an asterisk. The asterisked structure is an elongated 'prong' of tissue lacking any apparent vascular differentiation, and lacking an adaxialising (or vascular) signal from p*REV*::GUS. The arrowed primordium has also elongated away from the SAM, forming a narrow structure with a cone-shaped apex. This structure has a morphology reminiscent of that described to result from gain of function mutations in the adaxialising genes *REV*, *PHB* and *PHV* (Emery *et al.* 2003, McConnell & Barton 1998, McConnell *et al.* 2001), and shows a peak of p*REV*::GUS activity near its apex.

In *hydra2*, activity of p*REV*::GUS was substantially increased in relation to both wild-type (Fig. 4.41; A-F) and *hyd1*, and was particularly strong in seedlings with wider vascular strands in the stele (Fig. 4.43; C). Primordia showed strong GUS expression throughout the apical meristem region, and had little differentiation between abaxial and adaxial surfaces of these organs (Fig. 4.43; F, H). In 12 dae wild-type plants, most p*REV*::GUS activity had faded in the first pair of true leaves after vascular differentiation. This signal persisted in *hyd2* true leaves from siblings of this age class, possibly suggesting a delayed progression of differentiation in the *hyd2* mutants. The difference in intensity of reporter activity between the *hydra* sibling populations suggests that some mutant-specific process, e.g. a sterol-mediated patterning phenomenon, is operating to different degrees in *hyd1* and *hyd2*.

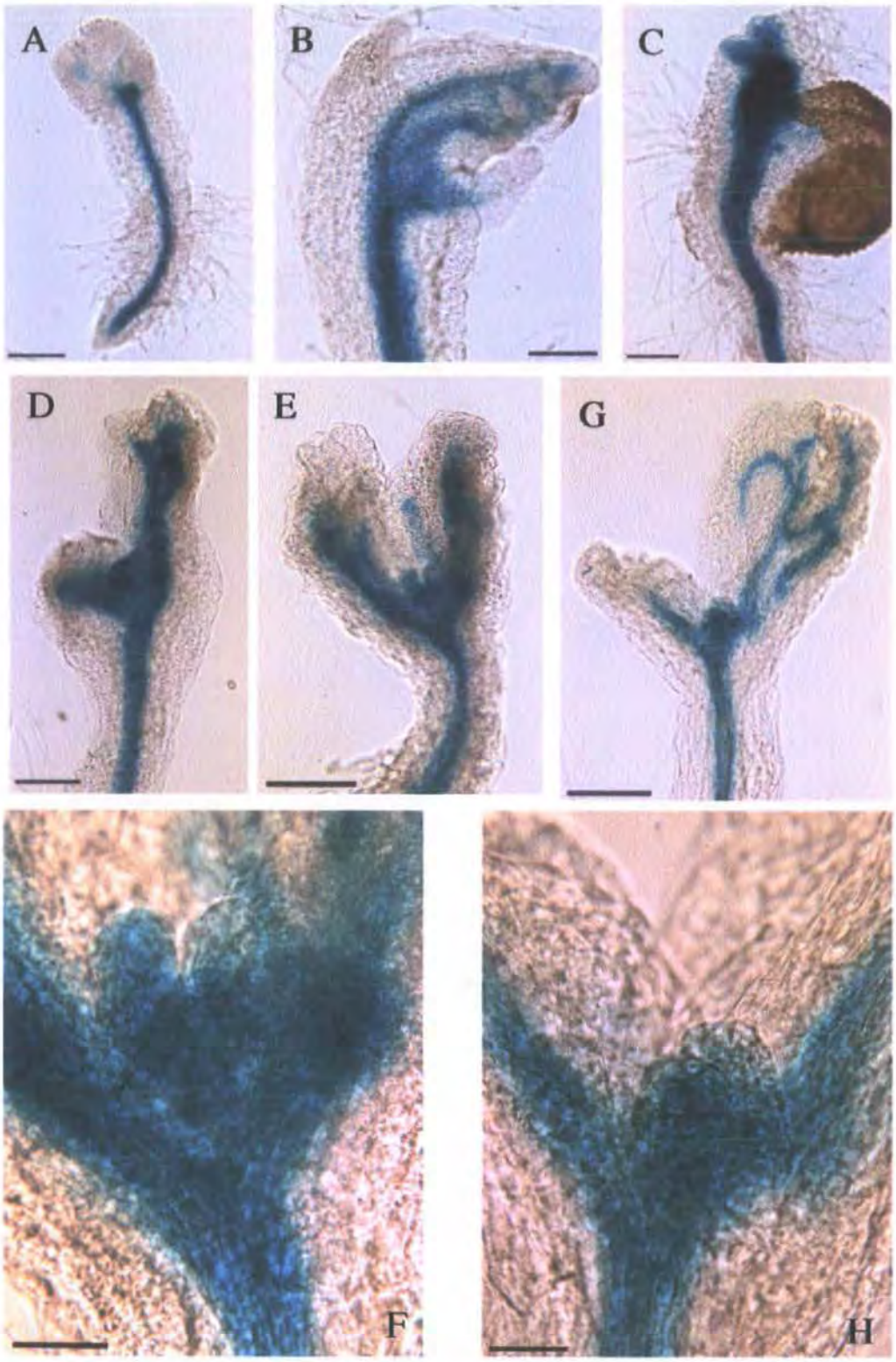

Figure 4.43 Activity of the p*REV*::GUS reporter in *hydra2* siblings

A-H, p*REV*::GUS activity in *hyd2* seedlings at 3dae (A-C) and 7dae (D, E, G). A-E, G, bar = 200μm; F, H, bar = 50μm.

The *hydra2* vascular traces carry a stronger and more persistent p*REV*::GUS histochemical signal than wild-type, evident from the stele in G-I and cotyledons in D, E and G. F shows detail of primordia from E, and H shows the SAM region from G. Reporter definition of adaxiality is less clear in these mutants than in wild-type plants, appearing to be obscured by high levels of histochemical activity.

4.3.6.4 Expression of the p*PHB*::GUS reporter of adaxial tissue identity is substantially enhanced throughout primordia from *hyd1*, whilst GUS activity in *hyd2* appears on abaxial surfaces of cotyledons and true leaf primordia.

Wild-type plants from the *hyd* mutant backgrounds, expressing the p*PHB*::GUS reporter of adaxial tissue identity, have a different developmental expression from that seen with p*REV*::GUS. Reporter activity appears in differentiating vasculature of the hypocotyl and cotyledons in very young seedlings (between emergence and cotyledon opening), and in young primordia after xylem differentiation is apparent in the cotyledon-hypocotyl primary trace (Fig. 4.44; A, C). By 7 dae, this signal has faded, leaving an adaxial-specific signal in new primordia, and a late-appearing signal in the expanding true leaves that appears in association with the definition of tertiary vascular complexity (Fig. 4.44; D and E).

In *hyd1*, p*PHB*::GUS reporter activity is stronger in 3 dae seedlings than in wild-type, and is seen particularly associated with primordial structures distributed around the shoot apical meristem (Fig. 4.45; A and B). This expression has substantially intensified in 7 dae seedlings (Fig. 4.45; C-G), where strong GUS activity is present throughout young primordia, and extends into the cotyledon primary vascular traces. Intensity of GUS expression does show some sibling variation, although even in seedlings with a less intense reporter activity, all primordia appear to have an indiscriminant expression of this adaxial signal (Fig. 4.45; F and G). A diffuse GUS signal did extend from the meristem region partly into the meristem peripheral tissues of the cotyledons and hypocotyl stele, although this seemed unaffected by variations in vascular strand cohesion in the hypocotyl stele (Fig. 4.45; C-E).

A very different reporter expression was found in siblings of *hyd2* (Fig. 4.46; A-G). Histochemical intensity varied substantially in 3 dae mutant seedlings,

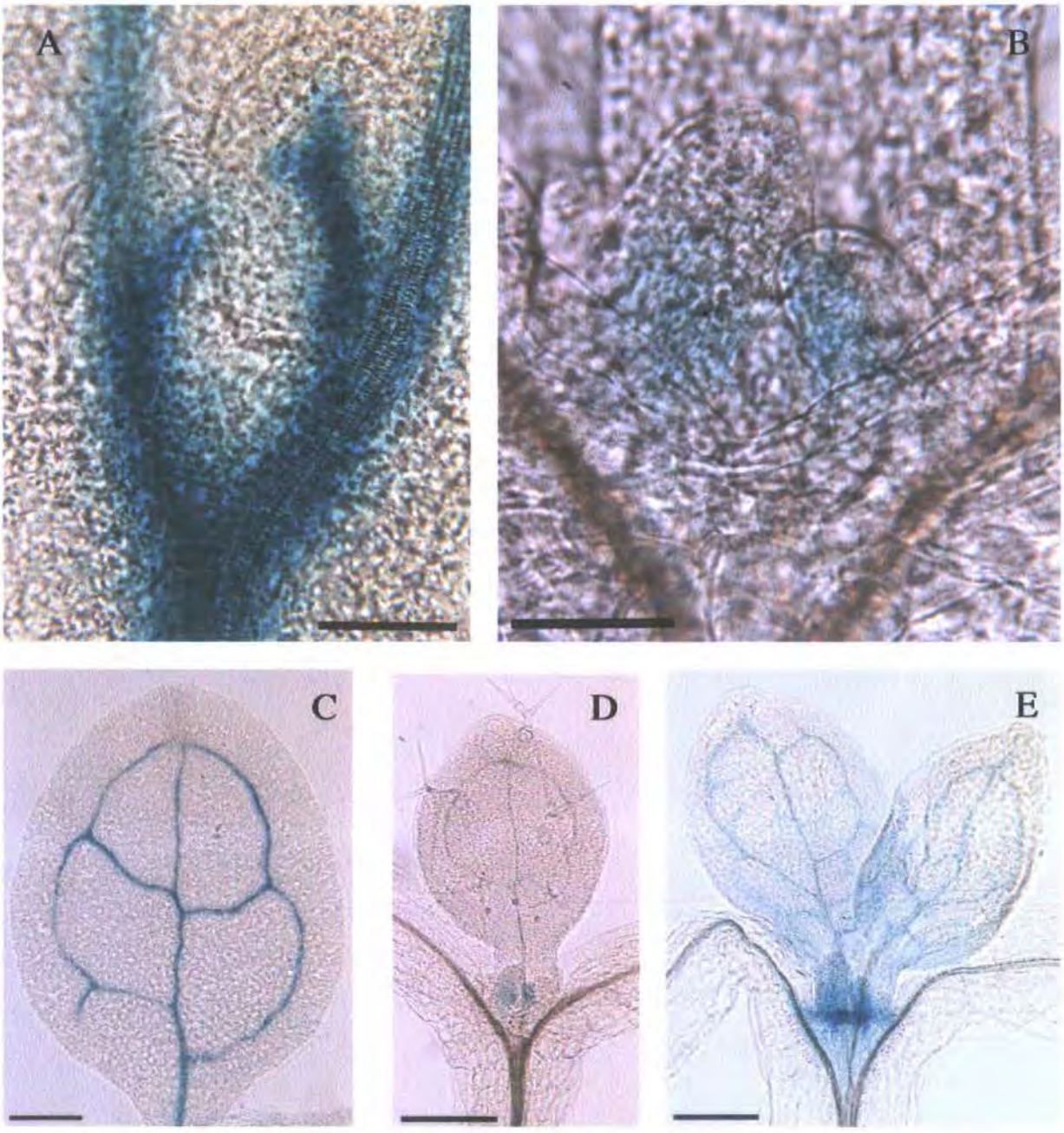

Figure 4.44 Expression of p*PHB*::GUS in wild-type seedlings

A-E; wild-type plants showing expression of the p*PHB*::GUS reporter, highlighting adaxial tissue identity in young vegetative primordia. SAM regions from 3 dae (A) and 7dae (B) plants show reporter definition of the adaxial surfaces of emergent true leaves prior to centrolateral expansion. At 3dae, the vascular trace is also defined in cotyledons (C), with a low level of GUS activity evident in the vasculature of true leaves as they expand and mature (D, E, showing true leaf detail from 7dae seedlings).

A, B, bar = 50μm; C-E, bar = 200μm.

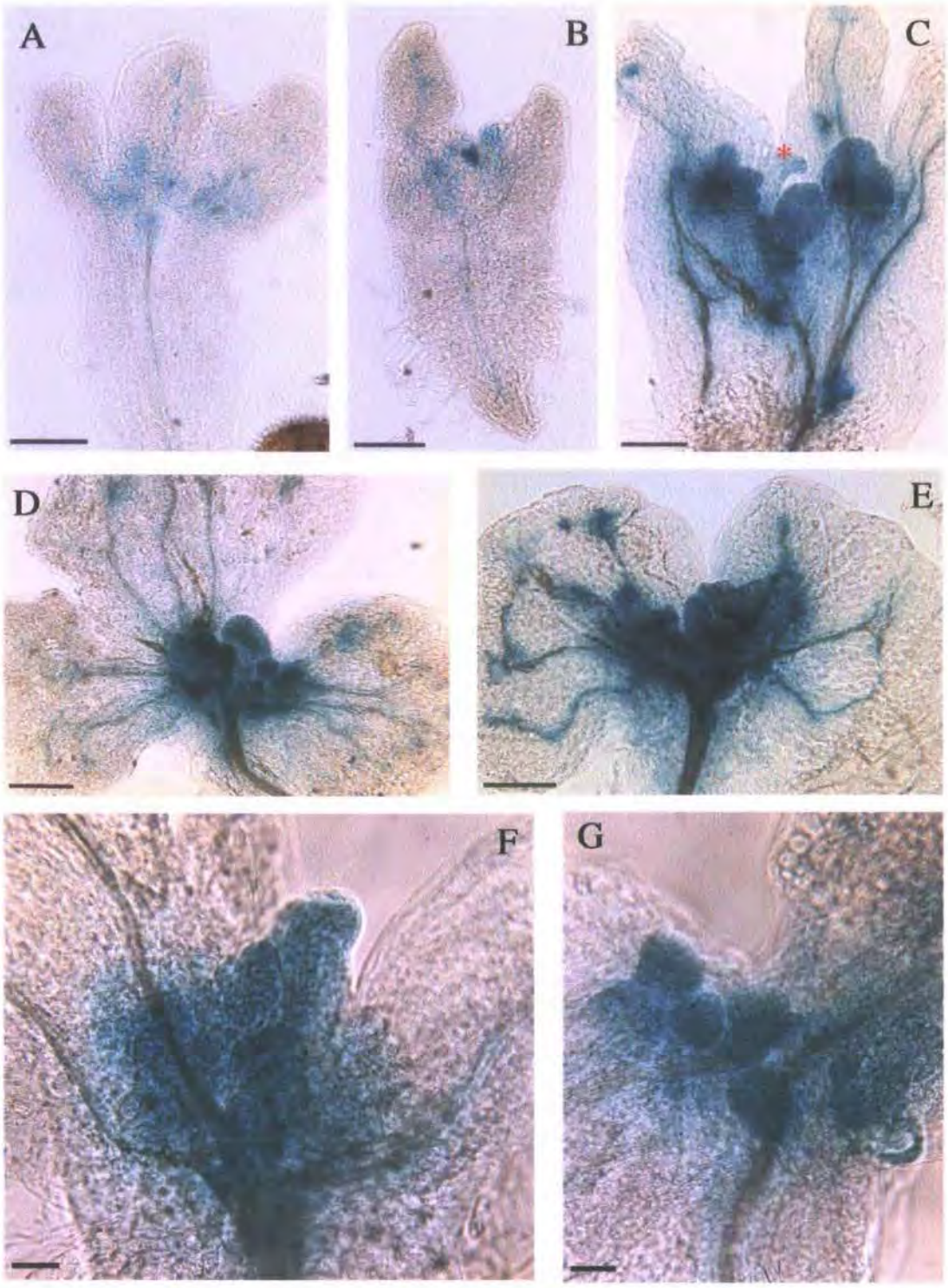

Figure 4.45 Expression of the p*PHB*::GUS reporter in *hydra1*

A-G; *hyd1* seedlings at 3 dae (A. B) and 7 dae (C-G), showing expression of the p*PHB*::GUS reporter. At 3 dat *hyd1* seedlings have stronger primordial expression of the reporter than wild-type plants, and by 7 dae this signal has substantially intensified so that both cotyledon vasculature and the whole of the SAM region comprises densely stained tissue (as in D and E). There is little discernible difference between abaxial and adaxial tissue in these young primordia, even in siblings with slightly less intense histochemical activity, such as F and G.

Dissociation of the hypocotyl longitudinal axis serves to displace the histochemical signal over a wider area as in C, although with a reduced intensity. A prong-like structure without obvious vascular differentiation is present in this seedling (asterisk), and carries only a background GUS activity, implying that this structure does not have adaxial identity.

F-J; bar =200μm, K, L; bar = 50μm.

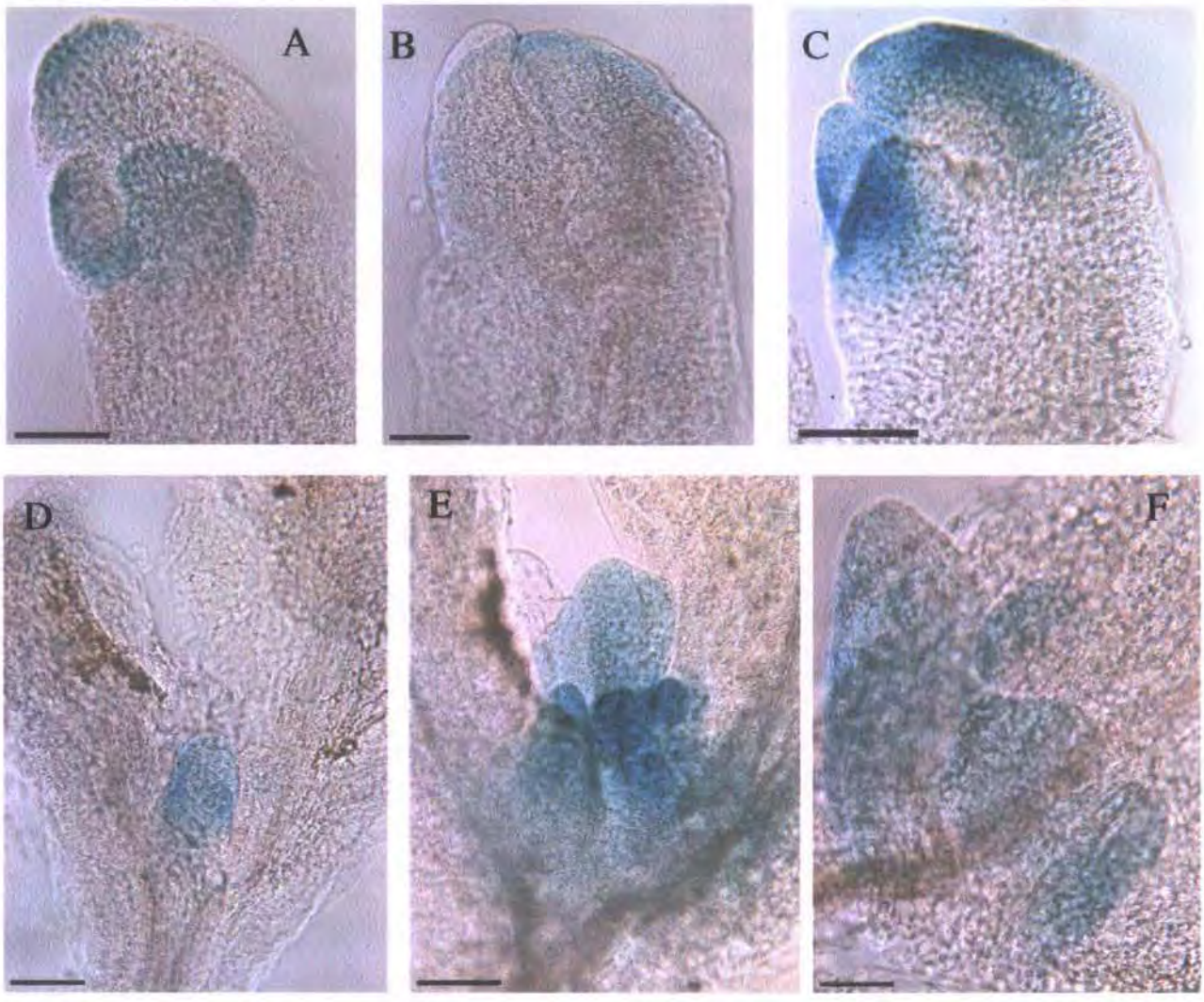

Figure 4.46 Expression of p*PHB*::GUS in *hydra2*

A-G; *hyd2* seedlings at 3 dae (A-C) and 7 dae (D-G), showing expression of the p*PHB*::GUS reporter. A-D, bar = 100μm; E-G, bar = 50μm.

The *hyd2* expression patterns differ from those of wild-type and *hyd1*. Rather than an indiscriminate signal around the SAM, the abaxial surfaces of young *hyd2* 3 dae cotyledons show GUS activity, with variation in intensity between siblings (A-C). By 7 dae, reporter activity has diminished in cotyledons, and highlights young primordia at an intensity similar to wild-type, although without clear adaxial positional identity. Primordia may carry GUS activity across the primordial dorsiventral axis (D, E), or show a mis-oriented or adaxially-positioned signal (F and G).

with very few individuals within the population showing GUS expression. Of those which did show reporter activity at 3 dae, this was confined to the abaxial tissues of the cotyledons (Fig. 4.46; A-C), in complete reversal of the molecular-genetic signal distribution found in wild-type plants from the mutant background. In 7 dae *hyd2* mutant shoot apices, most plants showed primordia with abaxially positioned reporter activity (Fig. 4.46; D, F, G). Siblings with a greater proliferation of primordia around the SAM showed a more intense GUS expression and a less discriminate GUS localization, often with a signal across the whole primordial dorsiventral axis (Fig. 4.46; E). These observations imply a reversal of the dorsiventrality of *hyd2* leaves. A reversed dorsiventrality has also been reported for gain-of-function mutants at the closely related *PHB* and *PHV* loci (McConnell & Barton 1998, McConnell *et al.* 2001).

4.3.6.5 Expression of the abaxial marker p*YAB3*::GUS is down-regulated in *hyd* seedlings, and highlights a variable radially-reversed positioning of abaxial cues in both mutants.

Semi-dominant gain of functions at *PHB* and *PHV* loci result in an adaxialization of lateral organs and a loss of *YABBY* gene activity defining abaxial cell fate (Siegfried *et al.* 1999). In wild-type plants the p*YAB3*::GUS reporter defines the abaxial sides of young leaf primordia (Fig. 4.47; A, B), and is seen in association with the expanding region near the lower leaf margin (closest to the basal plate meristem) as a transient basipetal signal (Fig. 4.47; B, C).

Fig. 4.48: A-F shows p*YAB3*::GUS reporter activity in *hyd1*. A similar distribution of expression was found in *hyd2*, where visible, although expression of this transgene was so substantially reduced in the *hyd2* sibling population that few examples were visible (data not shown). The *hyd1* plants shown in Fig. 4.48; A and B have variable GUS activity in their primordia,

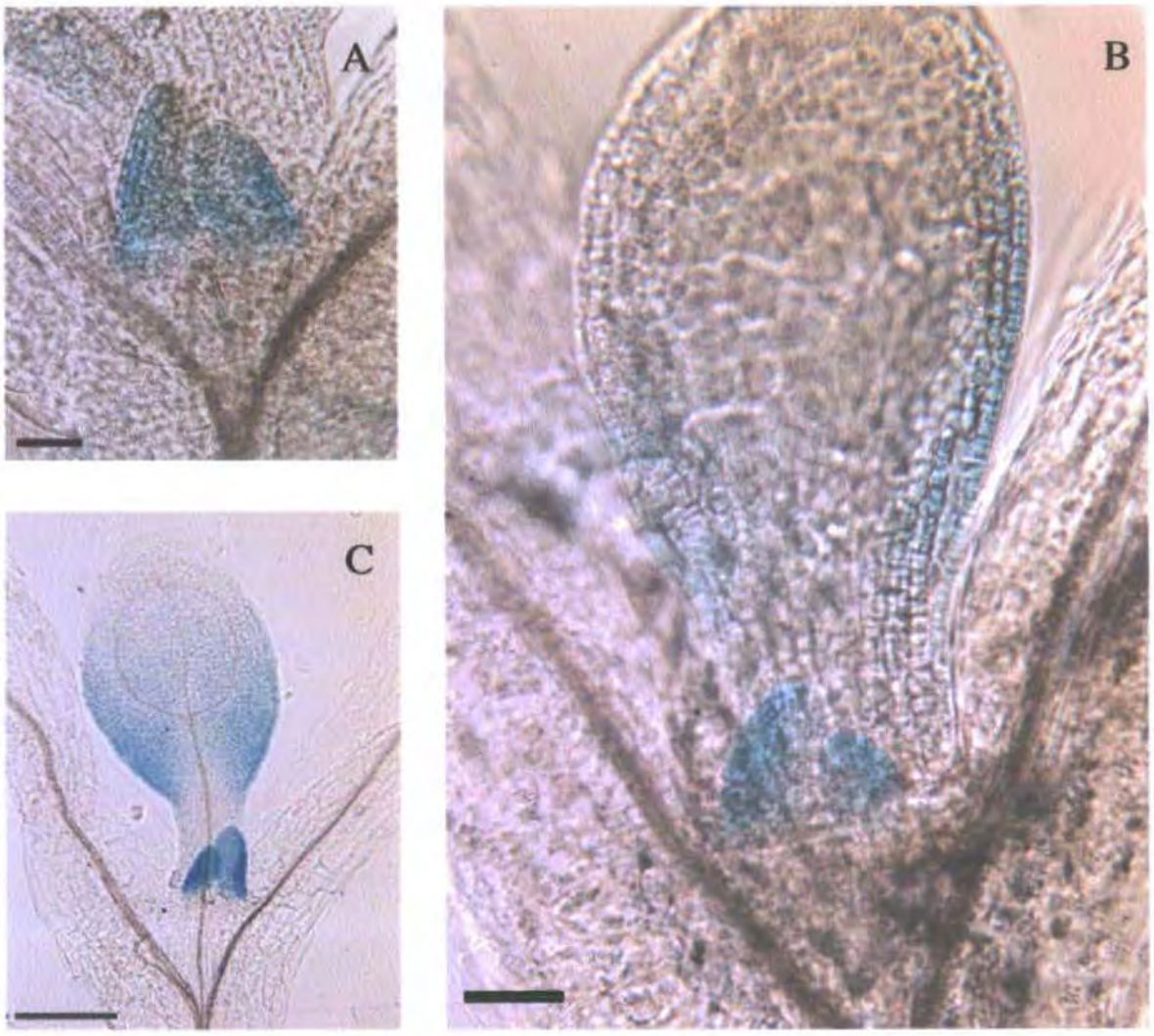

Figure 4.47 p*YAB*::GUS expression in wild-type

A-C; wild-type shoot apical meristem regions from 7dae seedlings, showing expression of the p*YAB*::GUS reporter construct. A and B; bar = 50μm, C; bar = 200μm.

The *YABBY* genes define abaxial tissue identity in the very young true leaf primordia of wild-type plants, and shows a basipetally and marginally-oriented signal in the abaxial epidermis of the expanding lamina, as in B and C. As the true leaf continues to expand, activity is quickly lost from the leaf tissues.

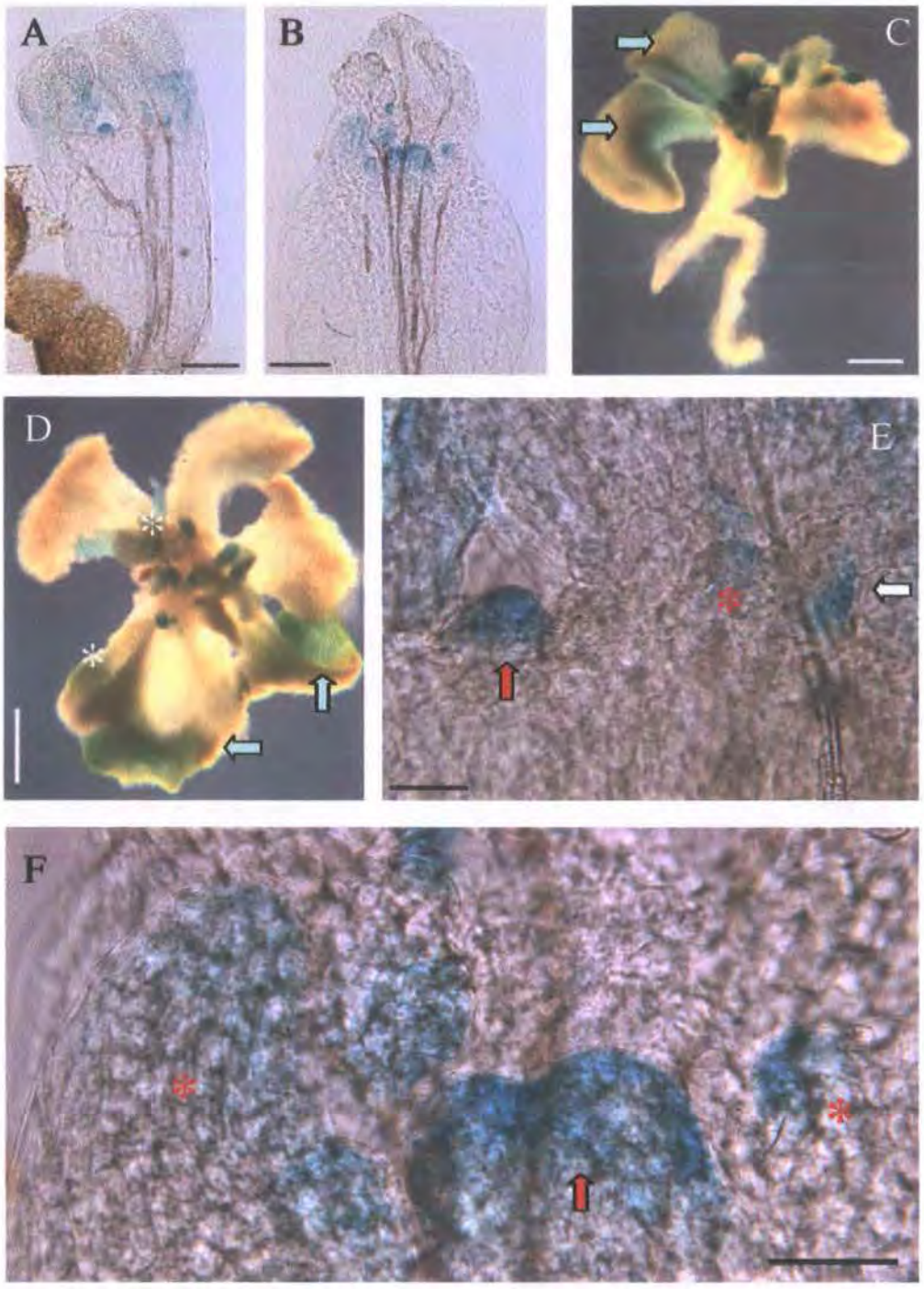

Figure 4.48 Activity of the p*YAB*::GUS reporter in *hydra* seedlings

A-F; *hyd1* plants showing expression of p*YAB*::GUS. A and B; 7 dae seedlings, bar = 200μm. E shows detail of the young primordia in plant A, and F the SAM region from plant B, bar = 50μm. Activity of p*YAB*::GUS is reduced in *hyd1*, and substantially reduced in *hyd2*, in relation to wild type plants.

SAM regions from 7dae *hyd1* plants in (E showing A and F showing D), indicate variably skewed or reversed abaxial tissue identity definition in primordia. A has two SAMs, whilst B appears to have one expanded SAM across an expanded radial axis. E (white arrow) shows a primordium with correct abaxial orientation adjacent to primordia with the abaxial signal on their adaxial side (asterisk) or throughout the developing organ (red arrow). F (arrow) shows two fused primordia with a GUS signal from their apical region extending down the right side of the composite organ. The 13dae plants in C and D, subjected to a prolonged incubation in X-Gluc, have areas of persistent ectopic GUS activity in correct positioning relative to the SAM (C), or remote from the meristem (D). Asterisks indicate prongs of abaxialized tissue.

shown in more detail in Fig. 4.48; E and F. Primordia are visible with an adaxial positioning relative to the SAM (red asterisks). The two red arrows are indicating a primordium in H with reporter expression throughout, and a pair of fused primordial structures in F, where GUS activity is seen near the apex of the organs. The white arrow in E indicates a primordium with apparently correct adaxial positioning, although expression in this structure is reduced in relation to that seen in wild-type primordia (Fig. 4.47; A and B).

Unlike wild-type, which shows a diminished GUS activity once laminar expansion has progressed, the 13 dae *hyd1* seedlings shown in Fig. 4.48; C and D, have a persistent expression of p*YAB*::GUS, some in tissues not adjacent to the meristem. In seedling C, expression is seen in association with the adaxial lamina of two leaves indicated by the arrows, and appears normally positioned. Elsewhere in this seedling, lobed outgrowths from the cotyledon far from the meristem are carrying reporter activity; these are just visible to the right of the picture. In seedling D, the arrows indicate regions of 'abaxial' tissue growth near the apices of substantially thickened cotyledons. Asterisks highlight radialized (abaxialised) organs formed from the SAM region, carrying reporter expression.

4.3.6.6 Embryos of both *hyd1* and *hyd2* show variable mis-positioning of adaxial and abaxial tissue identity markers

During embryogenesis, wild-type and *hydra* mutant expression for the abaxial p*YAB3*::GUS reporter (Fig. 4.49), and the adaxial reporters p*REV*::GUS (Fig. 4.50) and p*PHB*::GUS (Fig. 4.51) show substantial positional differences.

Activity of p*YAB*::GUS was reduced in *hyd* embryos relative to wild-type, in a manner which mimicked the reduction in shoot expression. The severity of mis-expression appears to correspond to the severity of disruption of the bilateral symmetrical morphology of later stages of embryogenesis. The

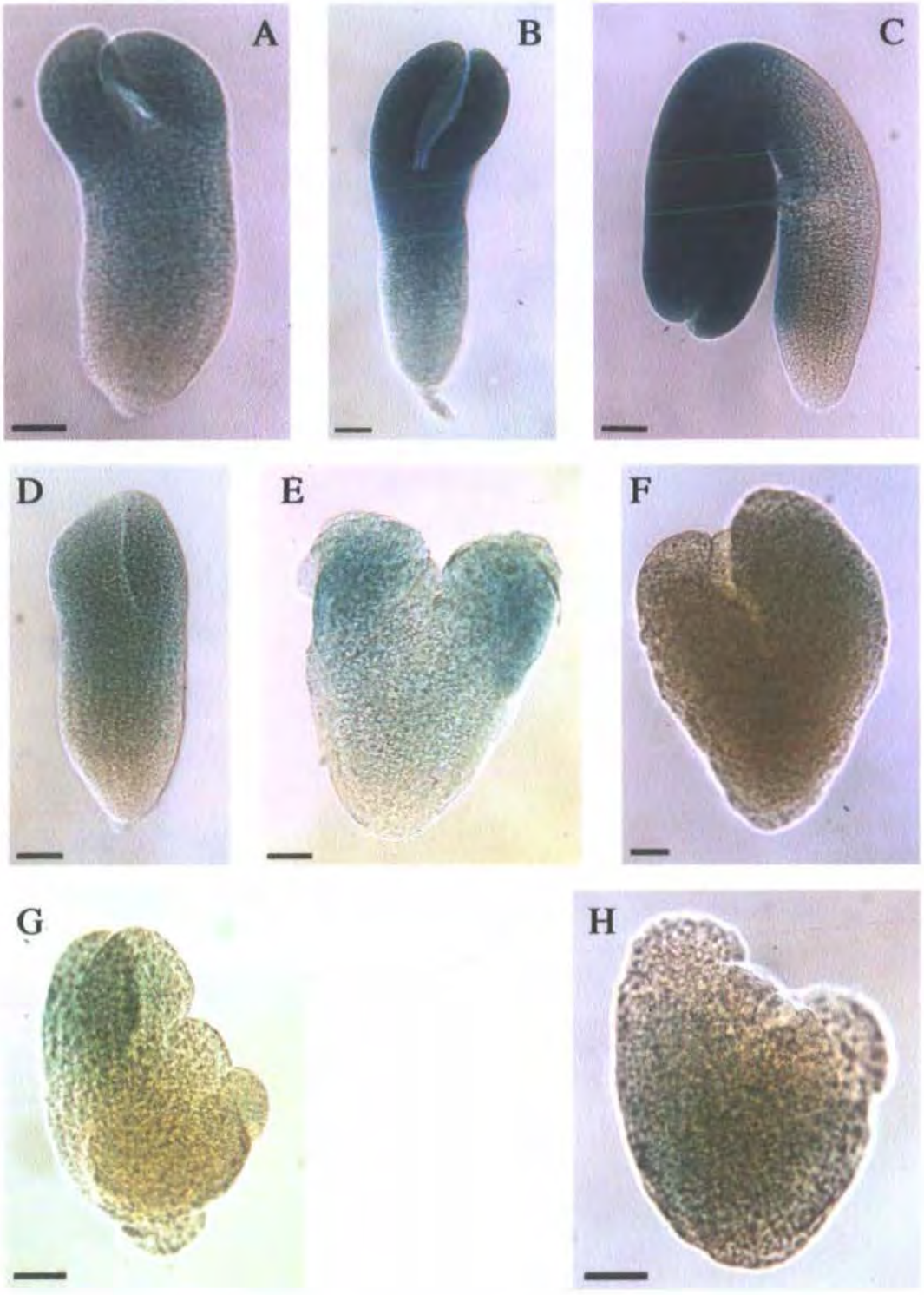

Figure 4.49 Abaxial positional information from the p*YAB*::GUS reporter in wild-type and *hydra* embryos

A-H; wild-type (A-C) and *hyd2* (D-H) embryos showing expression of the p*YAB3*::GUS reporter, bar = 50μm.

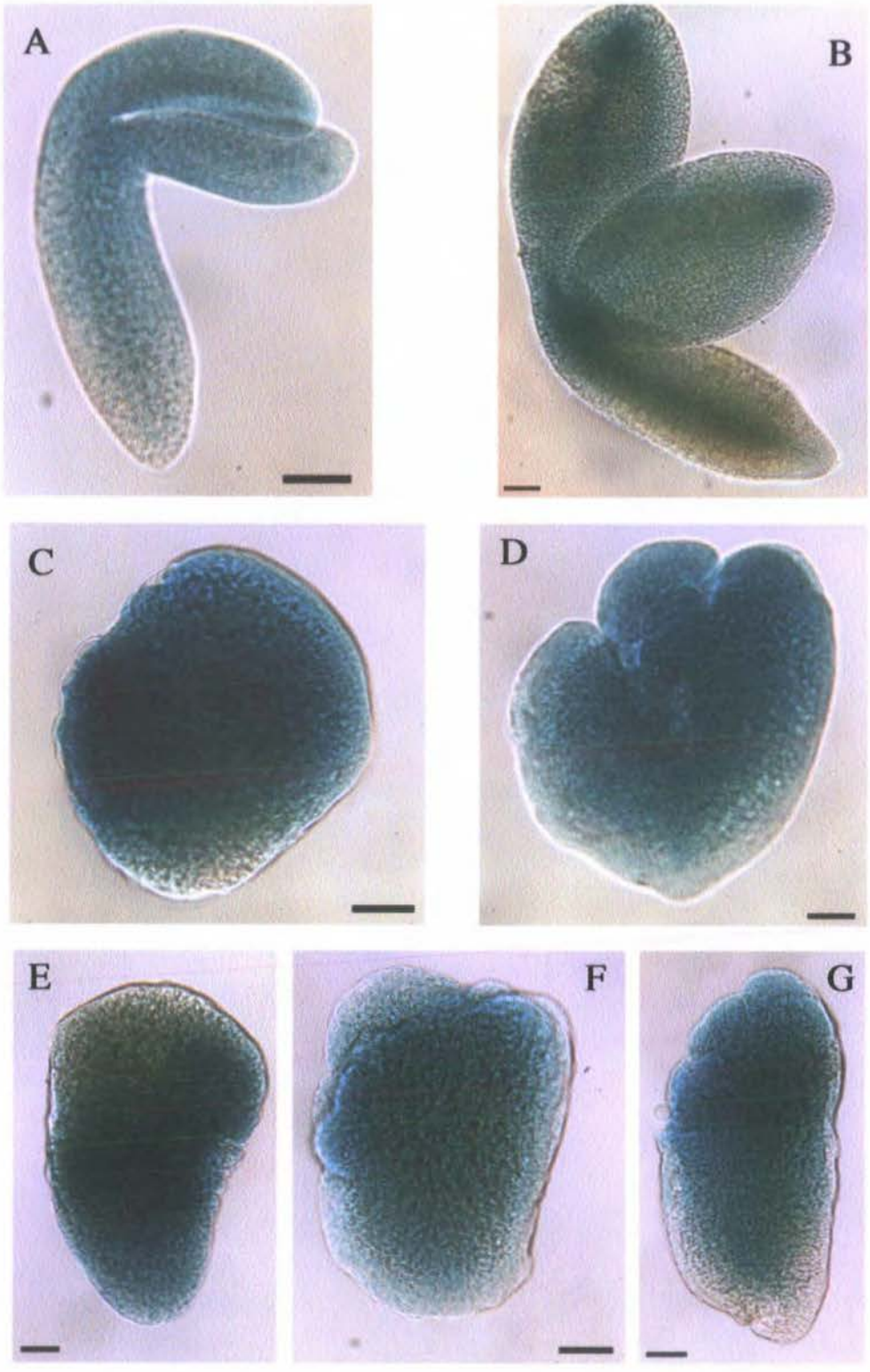

Figure 4.50 Positional information from the p*REV*::GUS reporter in wild-type and *hydra* embryos

A-G; wild-type (A, B) and *hyd1* (C-G) embryos showing expression of the p*REV*::GUS reporter, bar = 50μm.

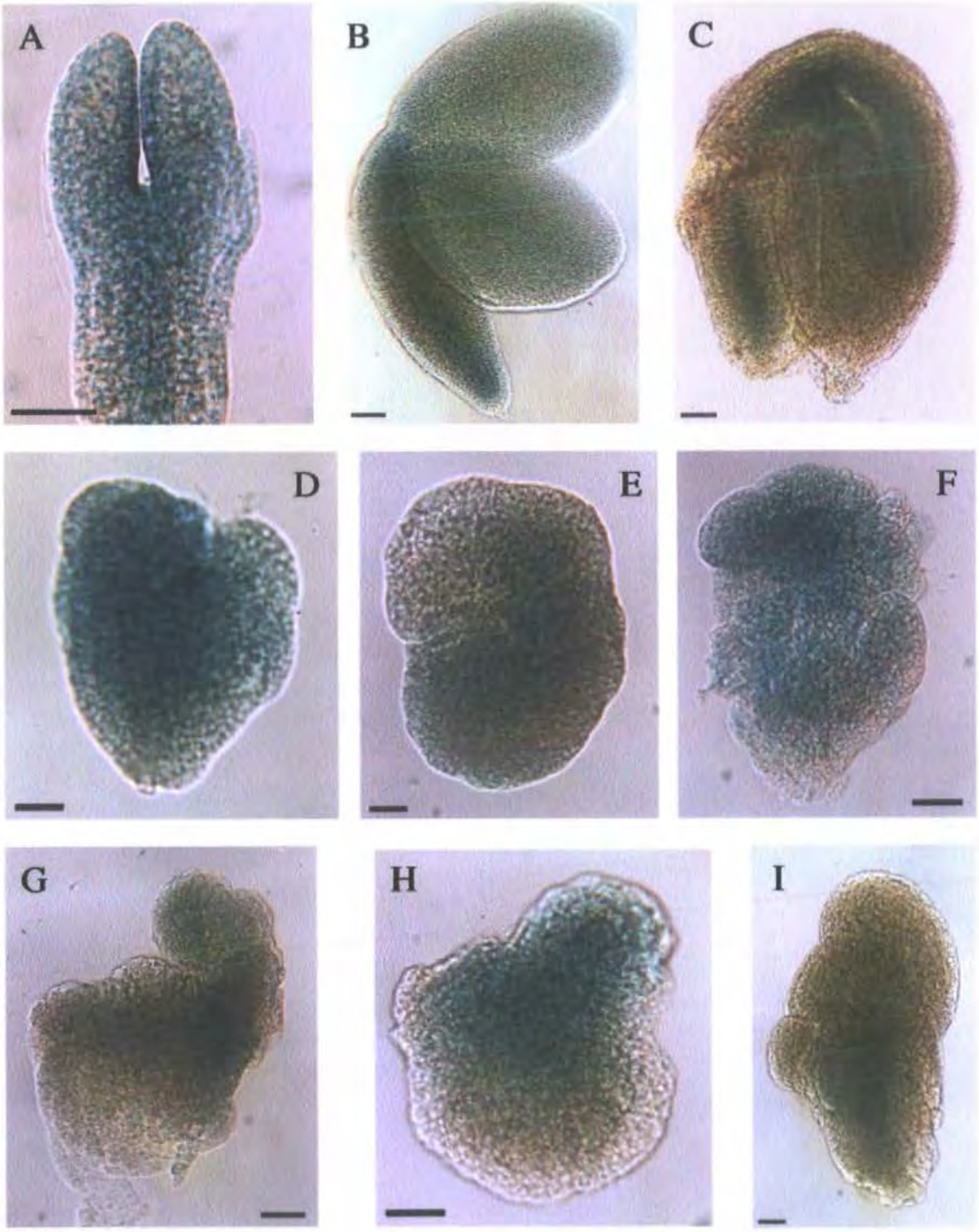

Figure 4.51 Positional information from the p*PHB*::GUS reporter in wild-type and *hydra* embryos

A-C; wild-type, and D-I; *hyd2* embryos showing expression of the p*PHB*::GUS reporter, bar = 50μm.

relatively bilaterally symmetrical mutant embryos in Fig. 4.49; D and E showed apical expression in approximately abaxial positions in the cotyledons. Others showed a reduced signal skewed to one side of the longitudinal axis (Fig. 4.49; F and G) or in the basal peripheral tissues, away from the cotyledons (Fig. 4.49; H).

Embryos of *hyd* mutants showing expression of the p*REV*::GUS reporter (Fig. 4.50; C-G) had a consistent strong elevation of GUS activity relative to wild-type (Fig. 4.50; A, B). Reporter activity was seen throughout the mutant embryo apex and longitudinal axis, irrespective of differences in morphology.

Expression of the p*PHB*::GUS reporter in *hydra* embryogenesis (Fig. 4.51; C-I) showed similar expression intensity to that seen in wild-type (Fig. 4.51; A-C), although no clear adaxial definition was seen in any of the mutant embryos. Expression was slightly up-regulated in *hyd* embryos with a better bilateral symmetry (Fig. 4.51; D), and was variably asymmetrically positioned in developing cotyledon primordia (Fig. 4.51; F-H), or diffusely in line with the apical-basal axis (Fig. 4.51; E, I).

4.3.7 Co-ordination between cells during lateral expansion

4.3.7.1 Lateral organs of the *hydra* mutant rosette show multiple anomalies in organ gross morphology

The leaves of *hydra* mutants are small and compressed in the proximal-distal axis, reaching approximately 5-10% of the length of wild-type leaves (Topping *et al.* 1997). Both cotyledons and true leaves of the *hydra* mutant shoot have variable gross morphology. Many siblings from both mutant populations have

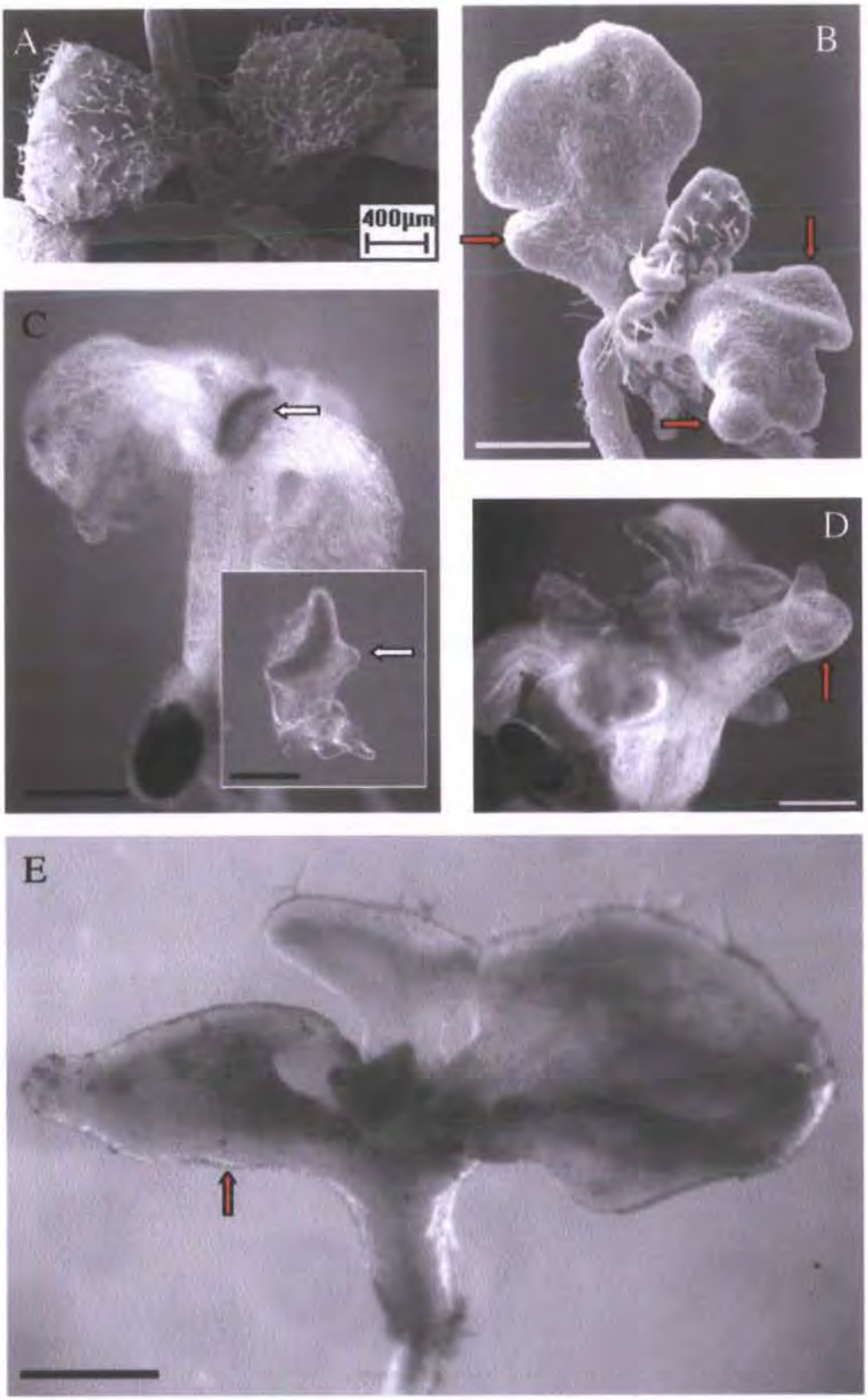

Figure 4.52 Variable leaf morphology in *hydra* mutants

A; Ws at 7 dae (bar = 0.4mm), B; *hyd2* at 7 dae, bar = 0.5mm. C-F; *hyd2*, 8 dae plants, all bar = 0.5mm. Inset of C; bar = 0.25mm.

The simple shape of cotyledons in wild-type is often distorted in *hydra* cotyledons (red arrows) to produce extra lobes (B), structures thickened in the dorsiventral axis (D), or in extreme cases, elongated into a tube shape (E). These phenomena are also observed in true leaves; the young true leaf in C (white arrow) is growing with the adaxial surface facing away from the shoot apical meristem; removal of this leaf from the parent (inset) reveals expansion growth on the abaxial side in the form of 'prong' of tissue (arrow), and a substantial radial thickening of the petiole.

uneven lobe formation in cotyledons, shown in Fig. 4.52; B (arrows). True leaf primordial development also demonstrates a variable morphology and lobe formation.

Radialized structures (as seen in Fig. 4.48; D) may form in cotyledon positions, or from primordia in the post-germination SAM. Some leaves develop an elongated structure bearing a flattened or cone shaped apex; a modification of this pattern is seen in the young true leaf in Fig. 4.52; C. This organ has an apparently reversed dorsiventral orientation, with what appears to be the adaxial lamina facing away from the meristem; dissection of this organ reveals an ectopic projection of tissue developing from the presumptive abaxial surface. The cotyledon-like structure in Fig. 4.52; D is difficult to interpret, consisting of an almost geometrical projection of tissue with lamina-like laterally flattened growths near the apex. The seedling shown in Fig 4.52; E has a cotyledon to the left of the picture with a cone-shaped morphology, the open end closest to the shoot apical meristem. Other lateral organs around this apex appear normal.

There does not appear to be a correspondence between lateral organ shape around the same apex. As can be seen in these examples, morphological anomalies in leaf shape can arise from the same SAM region as relatively normally- shaped leaves, and the leaves from any one individual can be highly heterogeneous. This variation in *hydra* leaf shape appears most associated with differences of lateral expansion, i.e. due to the orientation of the centrolateral axis.

4.3.7.2 The variation in cotyledon and leaf morphology is associated with anomalies in laminar vasculature

Wild-type *Arabidopsis* plants develop leaves around the SAM in a heteroblastic sequence, as can be seen in Fig. 4.53; A. This plant, showing vascular-

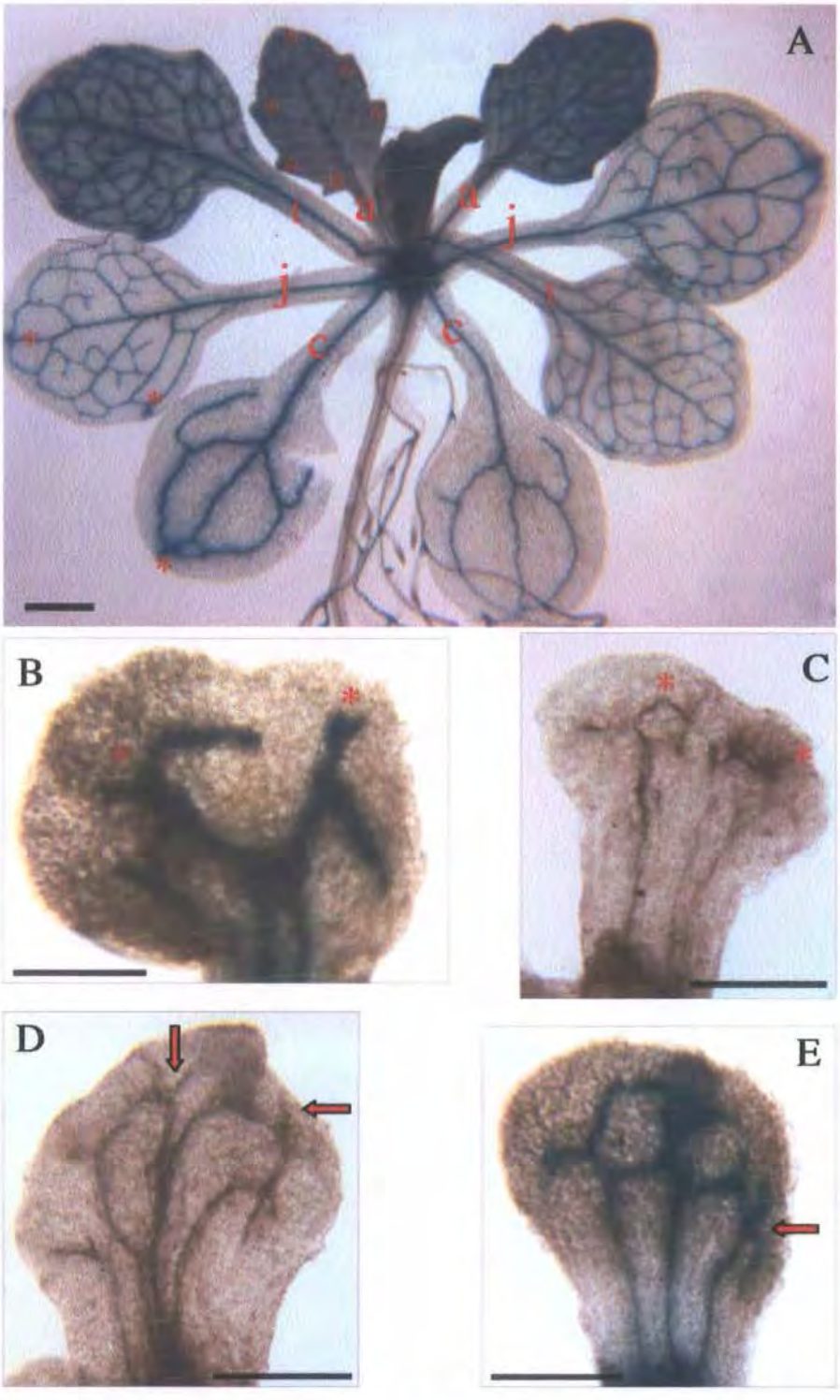

Figure 4.53 Leaf morphology and vascular patterning in wild-type seedlings and in cotyledons of *hydra* mutants

A; wild-type seedling, B and E; *hyd2* cotyledons, expressing the p*PIN1*::GUS reporter construct. C and E; *hyd1* cotyledons, stained with safranin-O. Wild-type annotations indicate cotyledons (c), juvenile (j), transition (t) and adult phase (a) true leaves through a heteroblastic series.

All samples taken from 15dae plants. A; bar = 1mm, B-E; bar = 0.5mm.

associated reporter activity for the p*PIN1*::GUS construct, illustrates heteroblastic phase change from the juvenile (j) to adult (a) true leaves, as indicated in the figure. Cotyledons (c) have the simplest vasculature and shape, and also have only one apical hydathode. The First true leaf pair are juvenile, and have a simple vasculature in a slightly modified oval lamina, with between one and two hydathodes per lamina in this example. The adult phase leaves arising latest, have a more complex vasculature associated with a serrated margin, where each 'tooth' is a module of the developing organ, associated with a lateral hydathode.

The modular nature of leaf development in *Arabidopsis* is shown by the sequential vascular differentiation during laminar expansion. In emerging primordia, the first pattern to be established is the primary midvein. Initially a procambial trace condenses simultaneously along the longitudinal axis of the primordium from the point of vascular origin (in continuity with adjacent established vasculature in the upper hypocotyl) to the apical hydathode, close to the leaf apex. Anatomically distinguishable secondary loops of vascular procambium then form ahead of xylem differentiation along this primary trace. The xylem strand appears along the route of the primary midvein, and then bifurcates at the apical hydathode position. The next near-simultaneous xylem strands appear following the procambial traces of secondary loops, which extend marginally from the tip of the primary strand, to rejoin the main strand at a point approximately central to the lamina (Pike & López-Juez 1999, Scarpella *et al.* 2004). (These two stages of xylem differentiation can be seen in the young cauline leaves in Fig. 3.10; B and C.) Further laminar expansion allows a second loop of secondary vasculature to form, giving a pattern reminiscent of the cotyledon traces. Wild-type true leaves continue to expand and differentiate the xylem traces in a basipetal direction, adding sequential secondary loops to the existing pattern.

Lateral hydathodes can be seen in the true leaf traces of Fig. 4.53; A (asterisks), in association with a pattern extending beyond the cotyledon-like

template of two secondary loops (although the presence of the p*HYD1*::GUS reporter signal in the first lateral hydathode pair, shown in Fig. 3.10; C, suggests that hydathode differentiation precedes second pair of loops in the basic cotyledonary pattern). In Fig. 4.53: A, only one of the first pair of true leaves (marked with the letter j) has an additional hydathode. The next pair of true leaves are in a transitional stage (t) and have each resolved two pairs of lateral hydathodes. The presence of hydathodes in older, adult-phase leaves appears co-ordinated with a stronger development of secondary venation, and may be associated with an increased transport efficiency in the vascular network. This implies a putative role for hydathodes as secondary 'organising centres' beyond the basic cotyledonary pattern in modular leaf development.

In *hydra* mutants, the simple oval shape of the cotyledon is modified, in a manner that corresponds with a modification of the vascular trace in these organs (Fig. 4.53; B-E). Specifically, lobed or partially-lobed morphology is seen in association with a duplication of the apical hydathode, in the vicinity of a bifurcation or dissociation of the primary midvein. (Apical hydathode positions are marked with asterisks in Fig. 4.53; B and C.)

The morphology of *hydra* mutant true leaves is also variable, and shows a similar range of misplaced or duplicated hydathodes, often in association with patterning anomalies in the primary midvein. The very young true leaves in Fig. 4.54; A-F have duplications in the apical hydathode, and are typically associated with branching (A and D) or dissociation (C) of the primary vasculature. The putative double hydathode at the leaf apex in B demonstrates a reduced expression of the p*PIN1*::GUS reporter in this organ. The leaf shown in Fig. 4.54; C has the greatest extent of laminar expansion in any of the examples shown; despite the increased laminar size, no sign of tertiary vascular strands are present, and the secondary xylem traces visible have a higher proportion of free vein endings than seen in wild-type.

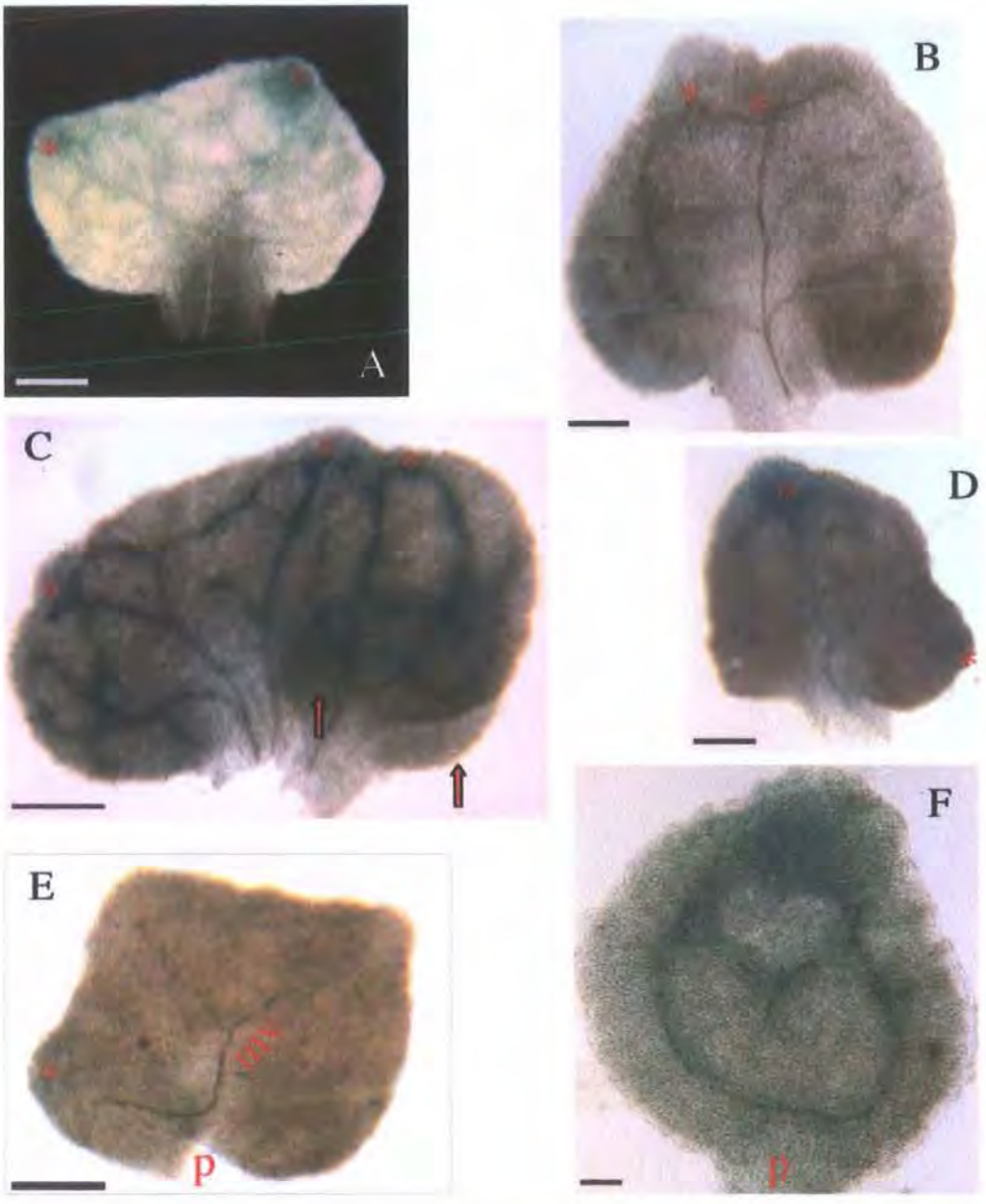

Figure 4.54 True leaf morphology and vascular patterning in *hydra* mutants

15dae true leaves from *hyd1* (A, C, E and F) and *hyd2* (B, D), taken from plants carrying the p*PIN1*::GUS reporter construct, marking tissue localization of expression of the PIN1 auxin transport protein, Variations in the histochemical intensity of this marker result from transcriptional differences between tissues.
Heteroblasty of wild-type vegetative leaves is a developmental transition associated with increasing vascular complexity, defined by increasing numbers of marginal 'teeth' (arrows) indicating the presence of hydathodes (*). In *hydra* mutants, no clear heteroblasty is evident, though various vascular and morphological anomalies can be found. The young leaf in E, taken from a plant with strong reporter expression, has a dim peak of p*PIN1*::GUS activity marked by an asterisk. This point in the tissue may be functioning as a hydathode, as it appears to mark the termination of a primary midvein (mv). This differentiating vascular strand is not associated with the petiole position (p). K similarly lacks a primary midvein associated with the petiole position. Here a has differentiated in a ring shape, with no apparent connection to the main vascular network.

A, B, D, E, bar = 0.25mm; C, bar = 0.5mm; F, bar = 100μm.

Other patterning defects affecting the differentiation of the primary midvein, also have implications for reporter activity. Fig. 4.54; E has a poorly differentiated primary midvein which does not correspond to the leaf apical-basal axis. The organ in Fig. 4.54; F, shows a rounded lamina with a horse-shoe shaped strand of xylem running across the organ, at right angles to the petiolar position (p).

The laterally enlarged leaf in Fig 4.54; C has a complex morphology involving the formation of a secondary lamina bisecting the original lamina at right angles (arrows). This lamina appears to have several putative primary midveins in different regions, and may be the product of simultaneous development in adjacent primordia, (such as those seen in Fig. 4.48; F).

In all of these examples, the positioning or duplication of the apical hydathode, and its relationship to the primary midvein, appears to define the subsequent basic patterning and laminar shape. Where the apical hydathode is in approximately the correct position as in Fig. 4.53; E, a patterning reminiscent of wild-type cotyledons results in this *hyd2* organ, although not with perfect patterning or laminar shape. It is interesting to note that even in these variably distorted leaf morphologies, hydathodes always appear at marginal positions.

4.3.7.3 Anomalous morphology of *hydra* cotyledons are associated with misplaced marginal cells in the epidermis.

The cotyledon adaxial epidermis at emergence consists of a uniform field of cells with equal opportunity to differentiate and adopt stomatal or pavement cell fate (Bean *et al.* 2001, Geisler & Sack 2002). The pattern of differentiated cells seen over the wild type cotyledon adaxial lamina is visible in Fig. 4.55.1; A. This epidermal layer differentiates above a mesophyll in which all growth is by cell expansion alone, and not associated with cell

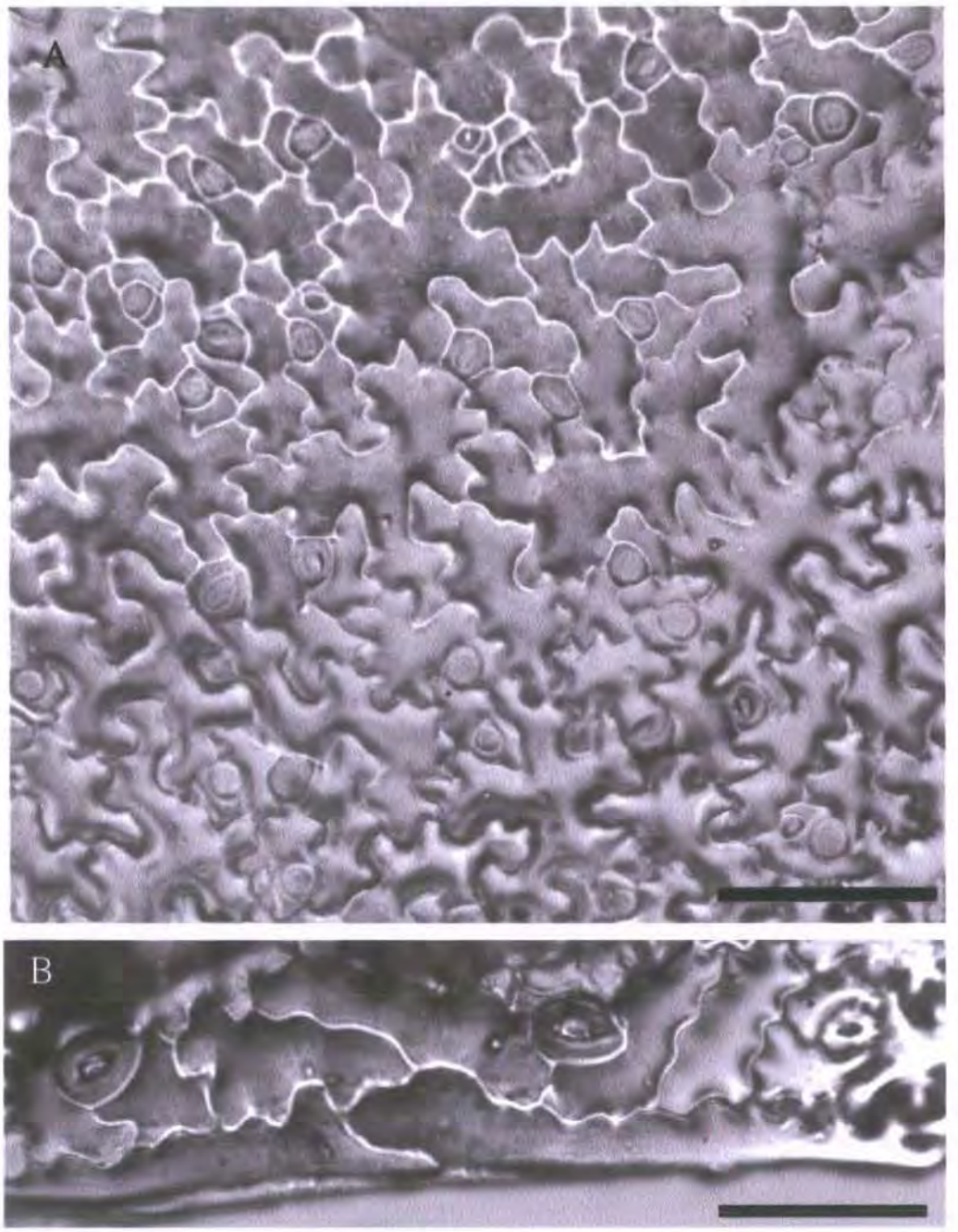

Figure 4.55.1 Patterning of the cotyledon adaxial surface in Ws

4.55.1: A, B; Ws, bar = 100μm; composite images of agarose epidermal impressions of cotyledon adaxial surfaces, taken from 8 dae plants.

Cotyledon cells originate during embryogenesis; at germination the adaxial cell layer comprises a uniform field of cells bordered by longitudinal cell files which differentiate into marginal cells (B). Between these margins, cells are recruited either to meristemoid mother cell fate, or become pavement cells, giving the characteristic pattern shown in A.

4.55.2: C and D (next page) show composite images of agarose epidermal impressions from *hyd1* cotyledon adaxial surfaces at 8 dae. C, bar = 100μm; D, bar = 200 μm.

In *hydra* mutants, the cotyledon epidermis appears to have a variable, possibly randomised positioning of marginal cell files. C has misplaced marginal cells towards the right of the image. D has a more normal margin cell positioning, between which the cells have differentiated as a field containing either pavement cells, or stomatal complexes.

division (Tsukaya *et al.* 1994). This field of mesophyll is bounded by elongated marginal cell files, positioned at the junction between the adaxial and abaxial epidermal layers (Fig. 4.55.1; B). Marginal cells form a continuous longitudinally-aligned boundary around the entire lamina, and are continuous with longitudinal cell files of the petiole, although their margins inter-digitate with the adjacent pavement cells, as can be seen in Fig. 4.55.1; B. Solitary stomata differentiate at intervals within these cell files, as also seen in specific cell files of the petiole epidermis.

The adaxial patterning of two *hyd1* cotyledons at 8 dae are shown in Fig. 4.55.1; C and Fig. 5.44.2, composed as composite pictures from multiple digital images of agarose impressions of the cotyledon surfaces.

In the cotyledon shown in Fig. 4.55.1; C, almost the entire right hand side of the lamina is comprised of elongated cells in approximate cell files. These cells appear to be morphologically similar to marginal cells from wild-type, show isolated stomates, and inter-digitate with adjacent pavement cells. To the far right, and to the left of this lamina, the anticipated field of pavement and stomatal complexes are visible. Note the distorted and asymmetrical shape of this lamina.

The cotyledon adaxial lamina shown in Fig. 4.55.2 has a much more even surface, with a correct positioning of its marginal cell files. Although leaf length is substantially reduced, as in all *hydra* vegetative lateral organs, epidermal patterning is much more even, with a reduced range of cell sizes evident. Laminar expansion has proceeded in the centrolateral direction, as can be seen from the elongated shape of certain pavement cells, and a regular leaf shape has resulted, although with a shorter morphology with regard to the longitudinal axis.

Similar examples were found in cotyledons from other siblings of both *hyd1* and *hyd2* (not shown). In these samples, the correct placement of margin

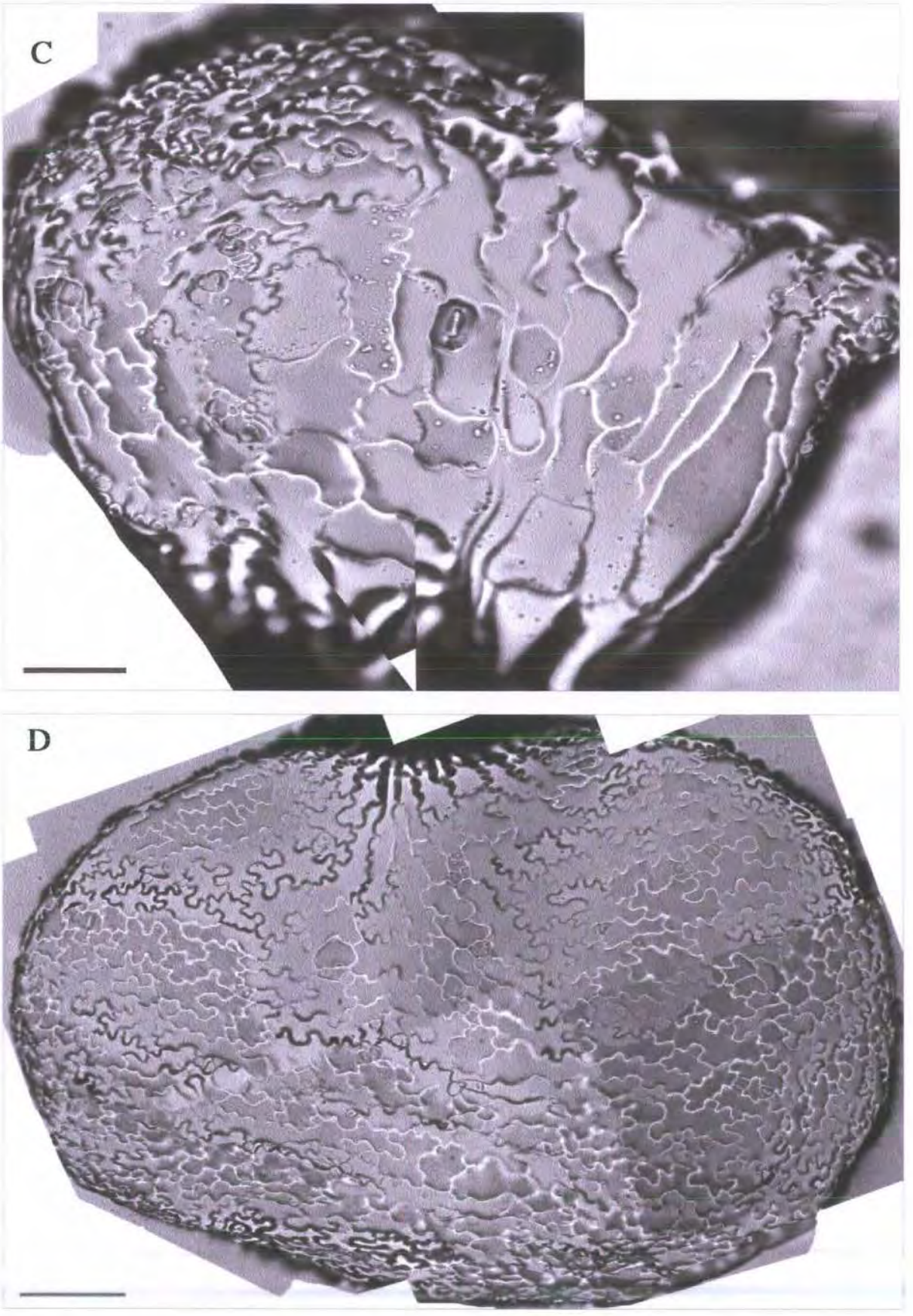

Figure 4.55.2 Cotyledon adaxial surface patterning from *hydra1*

cells was accompanied by a regularly-shaped and approximately symmetrical though shortened lamina. In contrast, a misplacement of the marginal cells accompanied an asymmetrically proportioned lamina with compromised centrolateral expansion. Varying degrees of marginal cell misplacement were found, implying that positioning is the result of a randomised patterning process. As the cotyledons form within zones defined by dorsiventral cues at the margins of the embryonic SAM, positioning of these marginal cell files in *hydra* cotyledons results from radial-bilateral patterning anomalies during embryogenesis.

4.3.7.4 Xylem vessel discontinuities in *hydra* cotyledons and true leaves are associated with longitudinal cell file misplacement in the epidermis

In the cotyledons and true leaves of seedlings from both the *hyd1* and *hyd2* sibling populations, enlarged clusters of longitudinally organised epidermal cells, often associated with anthocyanin pigmentation, are found in variable positions over the laminar surfaces. In the examples from *hyd2* shown in Fig.s 4.56 and 4.57, these enlarged cells can be seen to comprise sections of co-ordinated cell files of varying lengths. Such cells are not observed in all lateral organs from a single seedling; rather, they are associated with distortions of cotyledon or leaf morphology. Anthocyanin production is also pronounced in these regions of epidermal cell mis-patterning. From their shape and positioning, it is likely that these cells are either misplaced marginal cells (in cotyledons) or misplaced longitudinal cell files found both at the margins and over the primary midvein in the adaxial epidermis of true leaves.

Fig. 4.56; A-D demonstrates the relationship between these cells and the xylem vascular trace of a 12 dae *hyd2* cotyledon. The vascular trace of this cotyledon is visible in the dark-field image in Fig. 4.56; A. The epidermis

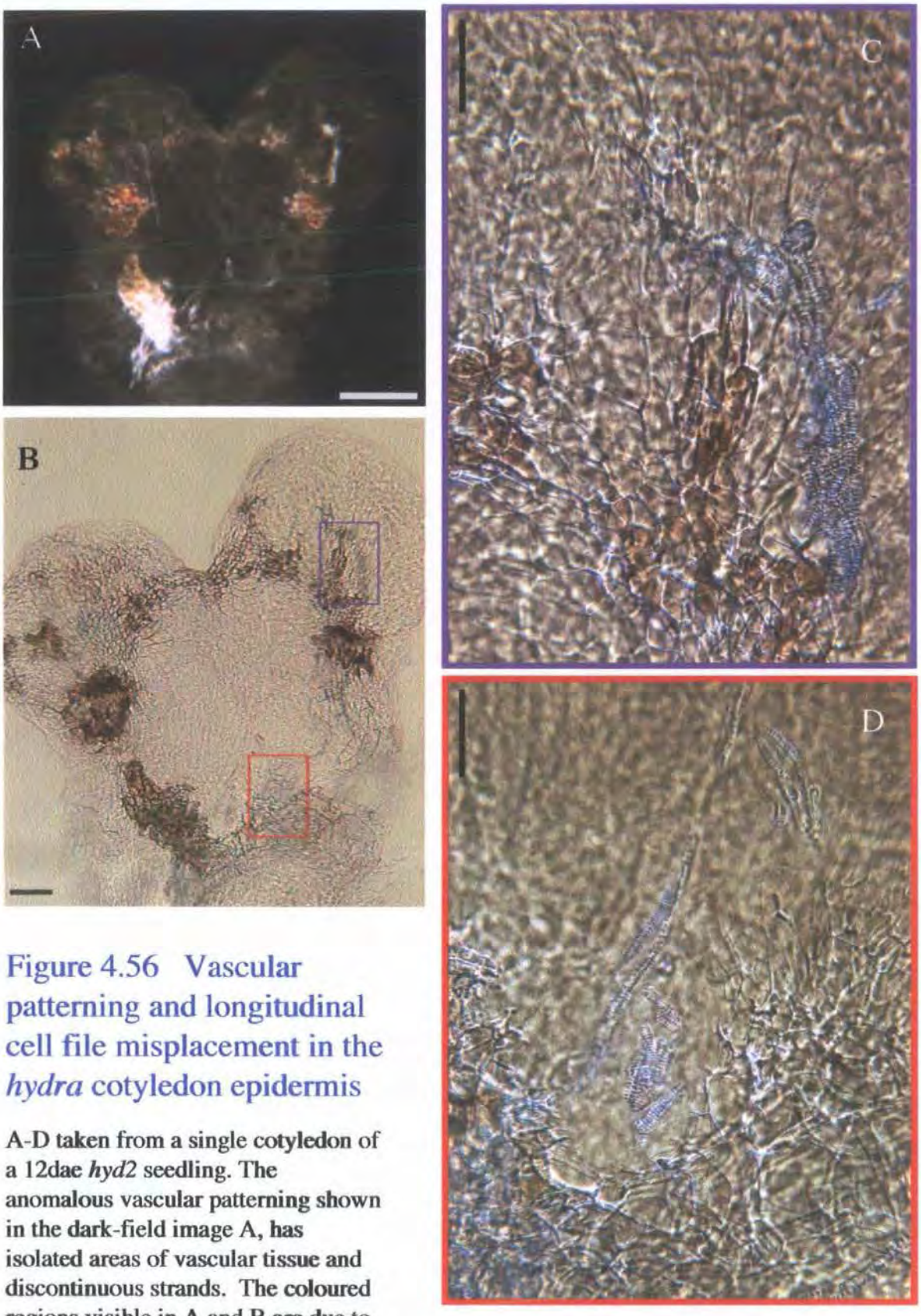

Figure 4.56 Vascular patterning and longitudinal cell file misplacement in the *hydra* cotyledon epidermis

A-D taken from a single cotyledon of a 12dae *hyd2* seedling. The anomalous vascular patterning shown in the dark-field image A, has isolated areas of vascular tissue and discontinuous strands. The coloured regions visible in A and B are due to anthocyanin accumulation

These misplaced longitudinal cell files may be misplaced marginal cells. C and D; overlain images showing detail of vascular strand anomalies and epidermal patterning from two focal plains; the red and purple borders corresponding to the marked rectangles on picture B.

A; bar = 0.25mm, B; bar = 100μm, C and D; bar = 50μm.

shows anthocyanin accumulation in association with many but not all of the enlarged cells visible in Fig. 4.56; B. Two areas are highlighted in this picture by coloured rectangles; these are shown at higher magnification in C and D, where the epidermal focal plane has been overlain onto the Nomarski image of the xylem vessels beneath. In both of these locations, areas of isolated xylem (vascular islands) are visible.

A similar situation is seen in the true leaf, also from a 12 dae *hyd2* plant, shown in Fig. 4.57; A-D. This leaf has a most unusual morphology, with four lobes having formed around a central midvein which is bifurcated at a point low down the leaf axis. The arrows over the darkfield image in Fig. 4.57; A indicate the edges of these lobes. The lightfield image in Fig. 4.57; B shows these lobes in relation to the presence of the enlarged longitudinal cell areas in the epidermis, and the coloured rectangles define the areas detailed in Fig. 4.57; C and D. The enlarged cells and pigmented cells indicated by the arrow are forming a margin to one of the lobes; this aggregation of cells is situated close to the primary midvein at the lamina-petiole junction (at the base of the photograph), implying that these cells may originate from longitudinal epidermal cells over the primary midvein. In this leaf the lobed laminae are of normal thickness, the longitudinal cells at these lobe margins appear coherent, and include occasional trichomes visible in Fig. 4.57; B. These laminae around the central axis of this leaf appear to have expanded in a centrolateral direction relative to the primary midvein.

Fig. 4.57; D reveals that a xylem strand from the main trace has differentiated towards the largest aggregation of these marginal cells. The elongated area of pigmented cells to the left of the primary midvein in Fig. 4.57; B, is shown in more detail in D. Here the epidermal cells are associated with an area which has developed extreme vascular noise in the xylem trace, with vessels oriented in unclear branching patterns.

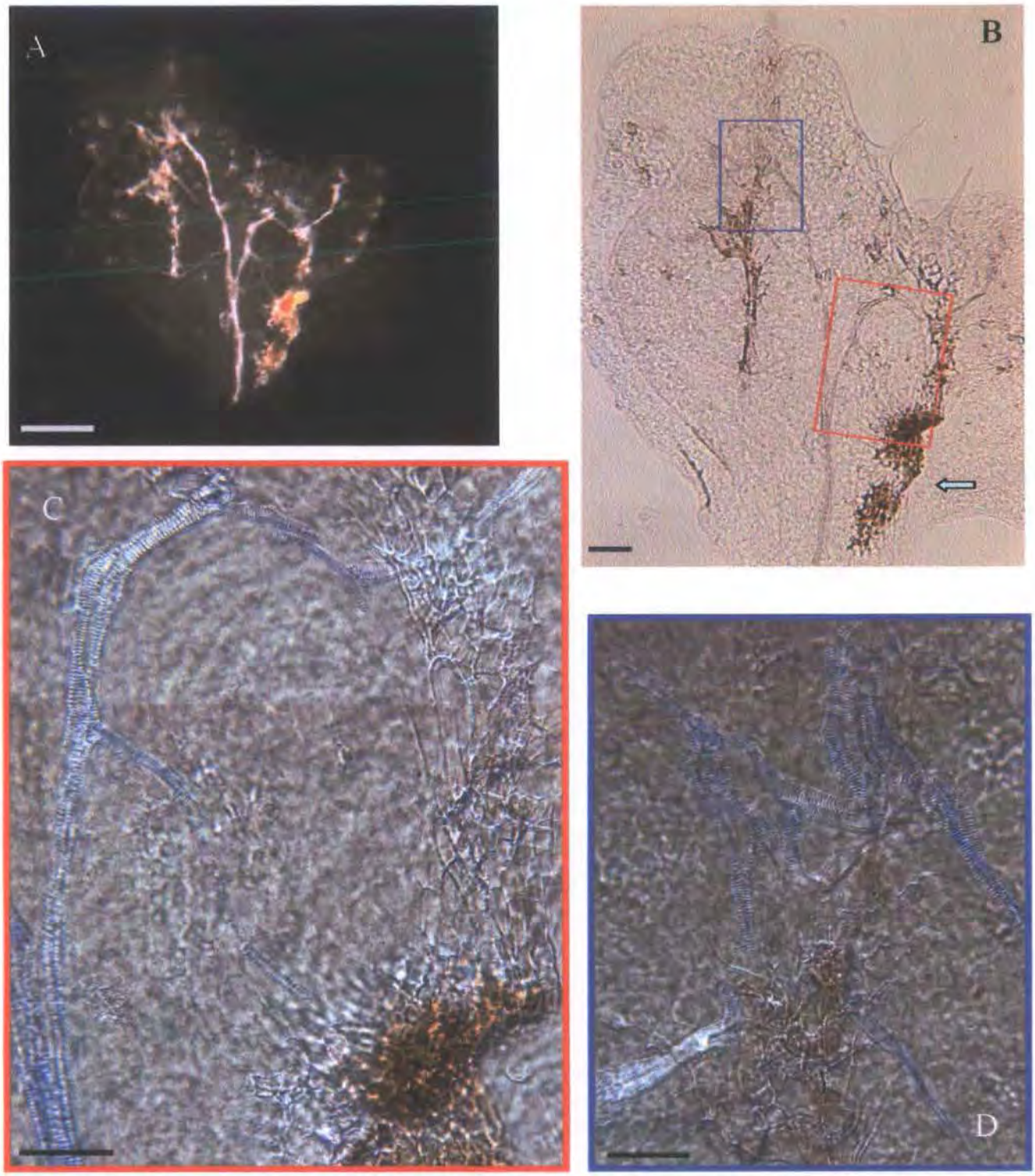

Figure 4.57 Vascular patterning and longitudinal cell file misplacement in the *hydra2* true leaf epidermis

A-D taken from a single true leaf from a 12dae *hyd2* seedling, cleared with chloral hydrate. The leaf has multiple lobes associated with a divergent primary vascular strand and subsequent anomalous development (A), and highly stained epidermal cells which are shown in the light field image B to be misplaced longitudinal cell files. The arrow indicates a lobe margin comprised of large cells, pigmented with anthocyanin. C and D; overlain images showing detail of vascular strand anomalies and epidermal patterning from two focal plains; the blue and orange borders corresponding to the marked rectangles on picture B. (C = orange, D = blue).

A, bar = 0.25mm; B, bar = 100μm; C and D, bar = 50μm.

4.3.7.5 Vascular discontinuities in *hydra* rosette leaves are associated with incomplete xylem differentiation along procambial traces and ectopic phloem-associated callose

The p*AthB8*::GUS reporter of pre-procambial cell fate is the earliest marker of vascular development discovered to date (Scarpella *et al.* 2004). Cellular expression of this transgene initiates from an established vascular strand, and extends distally (towards the apex) from a proximal position, invading through un-patterned cells in young primordial mesophyll (the 'ground meristem') by adopting cells to make a continuous trace, along which the anatomically-resolved elongated shape of the provascular cells then appears in simultaneous modules (Scarpella *et al.* 2004).

The p*PIN1*::GUS reporter highlights the transcription of the *PIN1* gene, comprising a component of the auxin efflux machinery (Palme, K; *pers. comm.*, Friml 2003). Expression of this marker is found in association with xylem vascular traces, and is correctly positioned in the vicinity of xylem vessels in both *hydra* mutants and in their respective wild-type backgrounds (shown in Fig.s 4.6 and 4.8). The p*PIN1*::GUS reporter highlights isolated sections of xylem, shown in the cotyledon trace in Fig. 4.58; A, with detail of these two sections in Fig. 4.58; B and C. These pictures show that expression of the auxin transport machinery corresponds to the position of xylem differentiation, and vascular islands of isolated xylem are highlighted by p*PIN1*::GUS expression.

Fig. 4.58; D and E show wild-type plants expressing the p*AthB8*::GUS transgene. In very young expanding primordia, the primary and secondary traces appear ahead of xylem differentiation (Fig. 4.58; D), with an even GUS activity throughout the traces. After expansion of the first true leaf pair and xylem differentiation in the secondary vasculature, most p*AthB8*::GUS

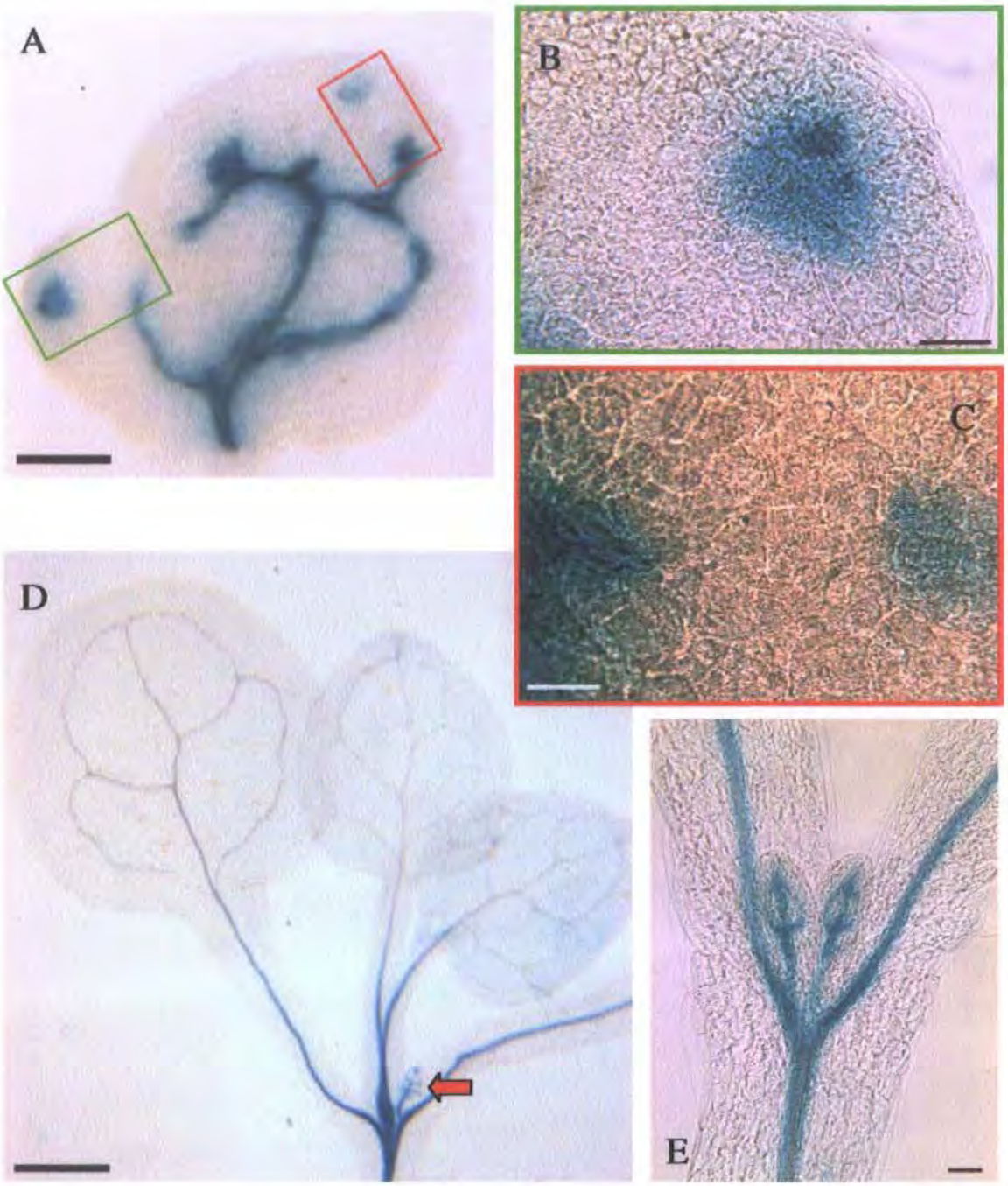

Figure 4.58 Vascular and provascular traces in wild-type and *hydra*

D and E show wild-type plants at 3 dae (E) and 10dae (D), carrying the p*AthB8*::GUS provascular tissue marker. As true leaves form, the first sign of vascularization is the establishment of a primary provascular strand, followed by the first secondary loops (visible in E). The third true leaf of seedling D (arrow) shows differentiation of the next provascular secondary loops. By 10 dae (D), provascular strand differentiation has mostly ceased in the laminas of the cotyledons and first true leaves, but is retained in the petioles and hypocotyl.

A; *hydra2* cotyledon from 5 dae plant expressing the p*PIN1*::GUS marker, showing the location of expression of the PIN1 auxin transport protein, highlighted areas detailed in B and C. In this cotyledon, marginal cell files are correctly placed at the edge of the lamina (visible in B), and the isolated vascular sections are putatively located at the most apical point of each of the two lobes, where hydathodes may form.

A, bar = 0.25mm; B, C and E, bar = 50μm; D, bar = 0.5mm.

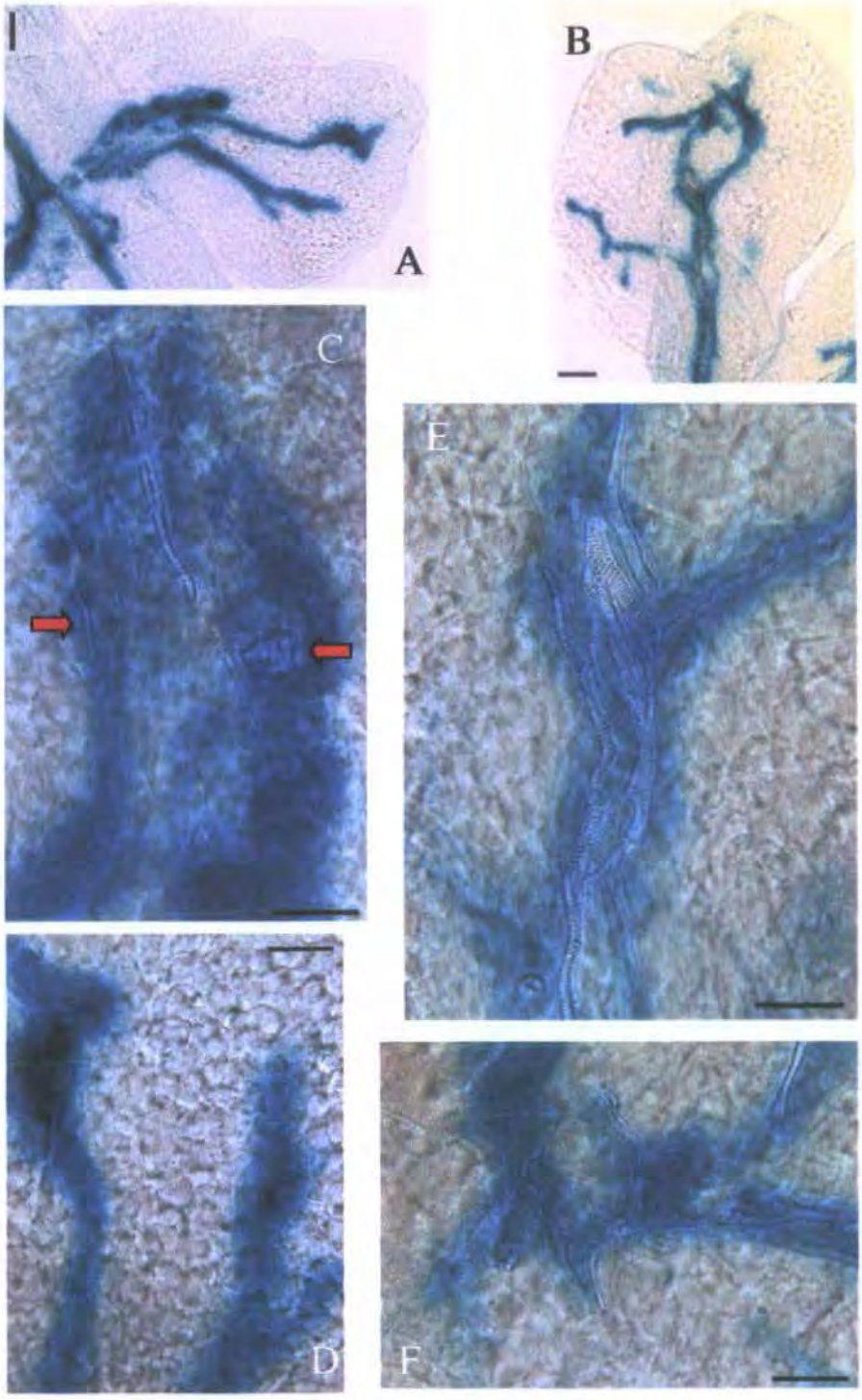

Figure 4.59 Detail of provascular and xylem correlation in *hyd2* cotyledons

A-F; detail from *hydra2* cotyledons at 5 dae, expressing the p*AthB8::*GUS construct. C shows the duplicated primary mid-vein, and D the hydathodes of the cotyledon shown in A. Similarly, cotyledon B has a dissociated primary vascular strand (E) and exaggerated 'noise' in xylem differentiation (F). A, B, bar = 100μm; C-F, bar = 50μm.

Although the activity of this reporter suggests a substantial enhanced expression of *AthB8* in *hydra*, the provascular traces are largely coherent in *hydra* mutant cotyledons and vegetative leaves. Xylem differentiation does not entirely reproduce this pattern; isolated sections of xylem are often seen (e.g. C, arrows), suggesting that vascular discontinuities arise at the differentiation stage, rather than during pattern establishment.

expression is seen in the hypocotyl and petioles, with little further activity in the lamina (Fig. 4.58; D).

In *hydra* cotyledons expressing the p*AthB8*::GUS reporter (Fig. 4.59; A-F), the expression of p*AthB8*::GUS is uneven along the length of the pre-procambial pattern. These cotyledons have zones of enhanced GUS activity at the apices of the primary strands, in the regions associated with hydathode differentiation (e.g. Fig. 4.59; D). Along the primary traces in the examples shown, an exaggerated 'noise' is seen in the differentiating xylem. Xylem formation within a strand is not continuous, as the cells mature individually and join into a coherent trace as the population of proto-xylem all differentiate (Scarpella *et al.* 2004, Aloni 2001).

However the high degree of xylem noise seen in the primary midveins shown in Fig. 4.59; C and E, are not due to part-completion of this process. The trace in E shows a highly disparate strand without close association between the longitudinal cell files, and forming a pattern which varies from the procambial pattern defined by the p*AthB8*::GUS reporter. In C, vessel discontinuities are seen again across a region without reporter expression, and involving the differentiation of misshapen cells such as the vessel indicated by the arrow in Fig. 4.59; C.

An examination was made of the correspondence between xylem vessels and callose deposition, corresponding to the traces of sieve elements of the phloem. The aniline blue-stained phloem traces correspond precisely with the xylem traces in wild-type roots (Fig. 4.60; A-B) and leaves (Fig. 4.61; A), as observed by Carland *et al.* (1999). A different situation was found in the *hydra* mutants, corresponding to variations in xylem vascular integrity. In the root stele, in areas where xylem discontinuities are visible, callose fluorescence was seen diffusely all around the vessel position, and also highlighted cell walls of surrounding cells (Fig. 4.60; B-D). In mutant cotyledons (Fig. 4.61; B-D) and true leaves (Fig. 4.61; E, F), sections

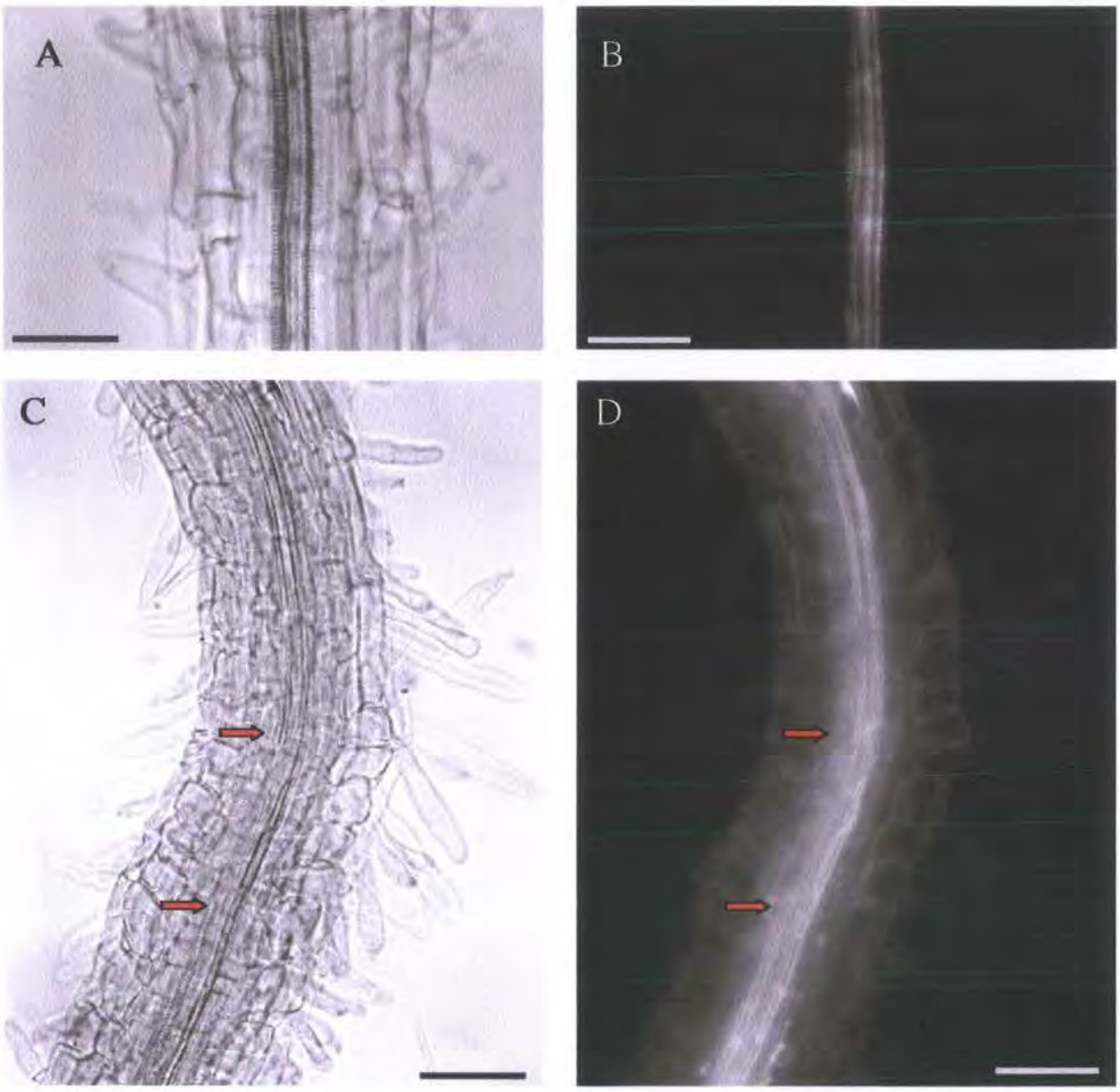

Figure 4.60 Phloem-associated callose in roots of wild-type and *hyd1*.

A and B; light-field and UV fluorescence images of the same section of the mid-root from an 8 dae wild-type seedling. The tissue has been stained with aniline blue to allow the visualisation under UV light of callose deposition around phloem sieve elements. In Ws plants, xylem differentiation appears tightly coupled with the position of callose (i.e. the phloem sieve elements).

C and D; *hyd1* main root from an 8 dae seedling treated with the same procedure. In the light-field image (C), a discontinuity in the xylem strand is just visible (between the arrows). This corresponds to an area of diffuse fluorescence when the same tissue is viewed under UV (D). Note that a residual fluorescence is retained throughout the *hydra* root under UV, in contrast to wild-type where peripheral tissues are not visible.

A-D, bar = 100μm.

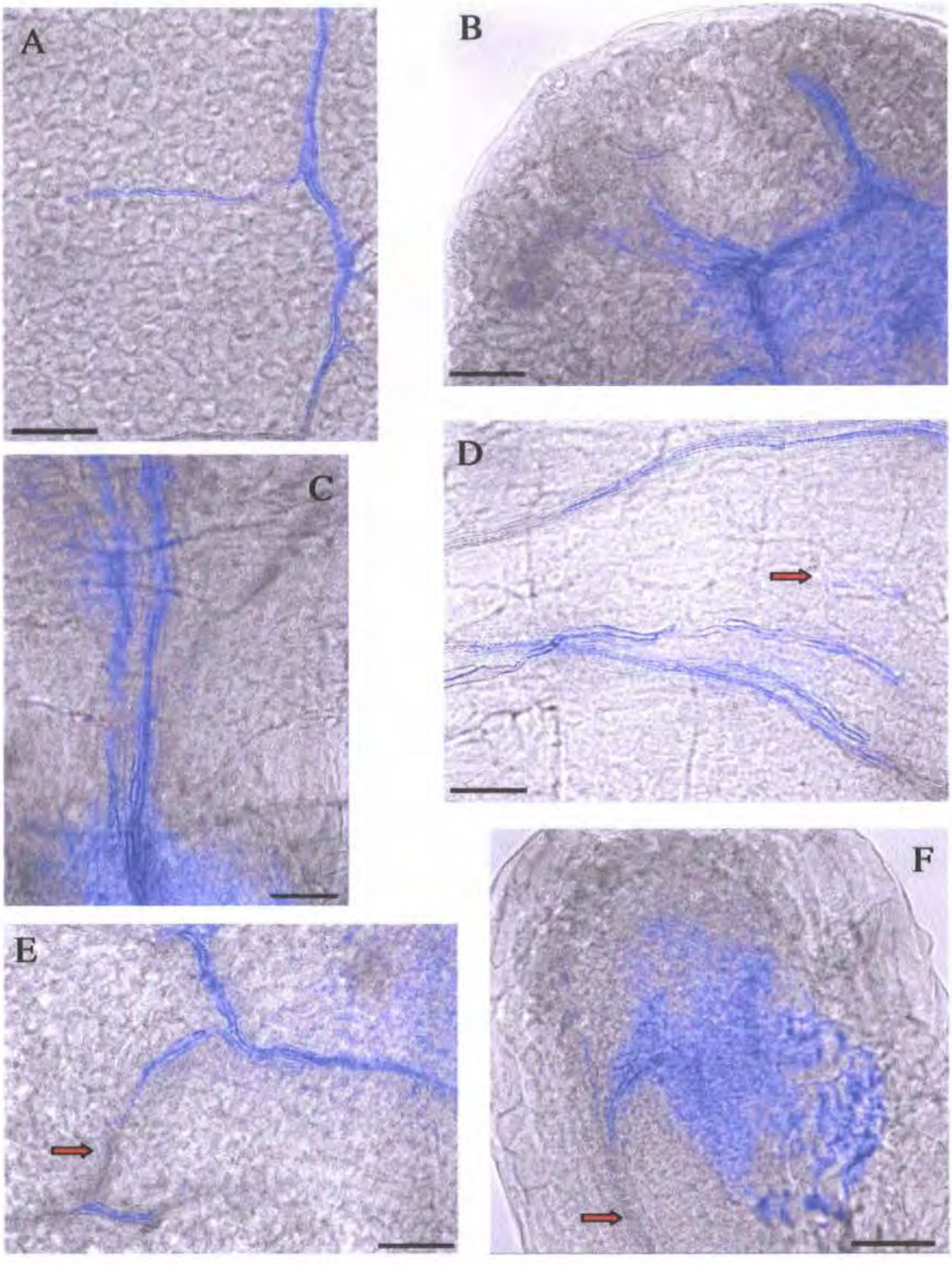

Figure 4.61 Phloem-associated callose in wild-type and *hyd1* vegetative lateral organs

A-F; superimposed images of light-field and artificially coloured fluorescence of tissues treated with aniline blue to visualise callose under UV light. Bar = 100μm.

A: wild-type aureole from a first true leaf, showing close association between xylem vessels and phloem sieve elements.

B-F; *hyd1* cotyledon (B-D) and first true leaf (E-F) tissues. Where xylem has differentiated, fluorescence mostly reveals a corresponding phloem trace. Dissociated or discontinuous xylem strands are associated with diffuse deposition of callose (B, C, F),. Occasional phloem elements appear without accompanying xylem (D, arrow). Note also in E and F (arrows) the presence of an apparently continuous section of xylem without associated callose fluorescence.

continuous xylem traces with minimal noise were typically followed by a coherent fluorescence from the phloem (D and E), although not always (as in Fig. 4.61; F, arrow). Where isolated xylem vessels formed, (Fig. 4.61 D, arrow), the phloem signature was also seen. Elsewhere, a non-specific diffuse region of fluorescence was visible in the lamina in regions of high xylem noise and poor strand cohesion (Fig. 4.61; O). Where free vein endings formed in distorted laminae (Fig. 4.61; B, F) a broad area of disorganised callose deposition could be seen without associated differentiation of xylem vessels.

This suggests that the coherent pre-procambial pattern indicated by coherent (though uneven) expression of p*AthB8*::GUS may not be translated into a continuous procambial trace, as both the early-differentiating phloem (shown by callose), and later-differentiating xylem vessels have strand anomalies, and the correlation between the positioning of these cell types is more variable in the mutants than in wild-type. Phloem differentiates at a lesser auxin threshold than xylem; also the p*AthB8*::GUS reporter is induced by auxin (Baima *et al.* 1995, Mattsson *et al.* 2003). The phenomena seen in the mutant vascular traces could therefore suggest an anomalous auxin distribution within the *hydra* mutant lamina.

4.3.7.6 Lateral spacing mechanisms defining the distribution of trichome 'foci' appear normal in *hydra* true leaves, although ectopic trichomes appear on cotyledons.

Trichomes arise on the epidermis of true leaves in *Arabidopsis* from very early in leaf development (Fig. 4.62; A). Trichomes arise in wild-type laminae with a characteristic spacing, whereby as the lamina expands new cells within the spaces adopt hair cell fate. The spacing mechanism is thought to be generated *de novo* (Larkin *et al.* 1996, Schnittger *et al.* 1999), and appears to function via a mechanism involving lateral inhibition (Schellmann *et al.* 2002). Examples of new secondary trichomes in wild-type true leaf epidermis can be

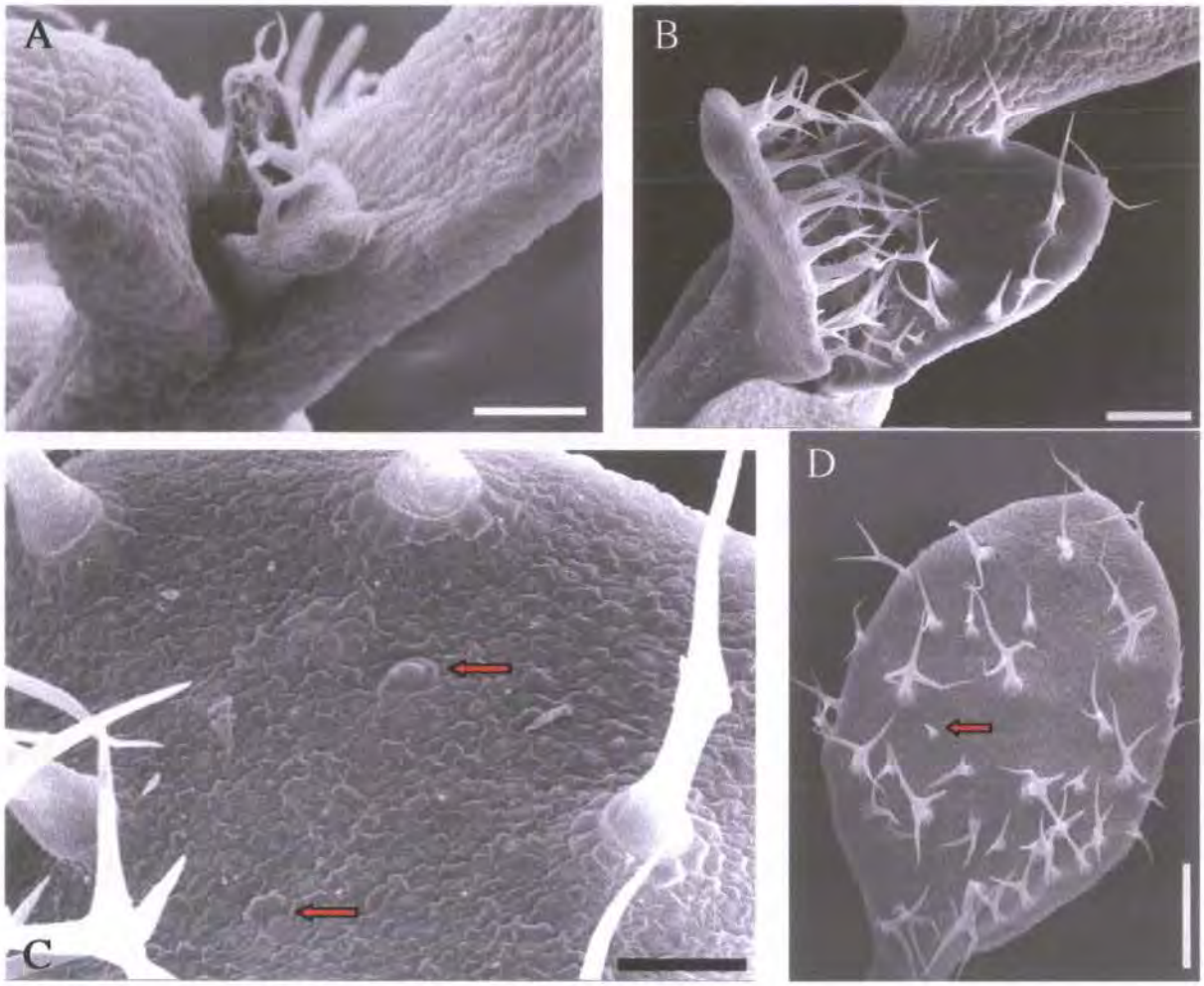

Figure 4.62 Trichome distribution over the wild-type lamina

A-D; wild-type Ws plants, showing trichome distribution on the first pair of true leaves at 5dae (A), 7dae (B, detail C), and a first true leaf from an 11 dae seedling (D).

In wild-type plants, the first pair of young true leaves emerges between 3- 5dae; trichomes appear on the adaxial surface soon after commencement of the lateral expansion of the primordium (A).

As the lamina grows, new trichomes form between older ones (B, detail C arrows). The older leaf in D shows a later stage of centrolateral expansion, with emergence of new trichomes (arrow) further down the lamina. Commitment to trichome cell fate in an undifferentiated epidermal cell triggers lateral inhibitory signals that prevent adjacent epidermal cells from becoming trichomes. Instead, the adjacent cells become pavement cells, and expand to form a ring of basal cells around the developing trichome.

A, C, bar = 100μm; B and D, bar = 200μm.

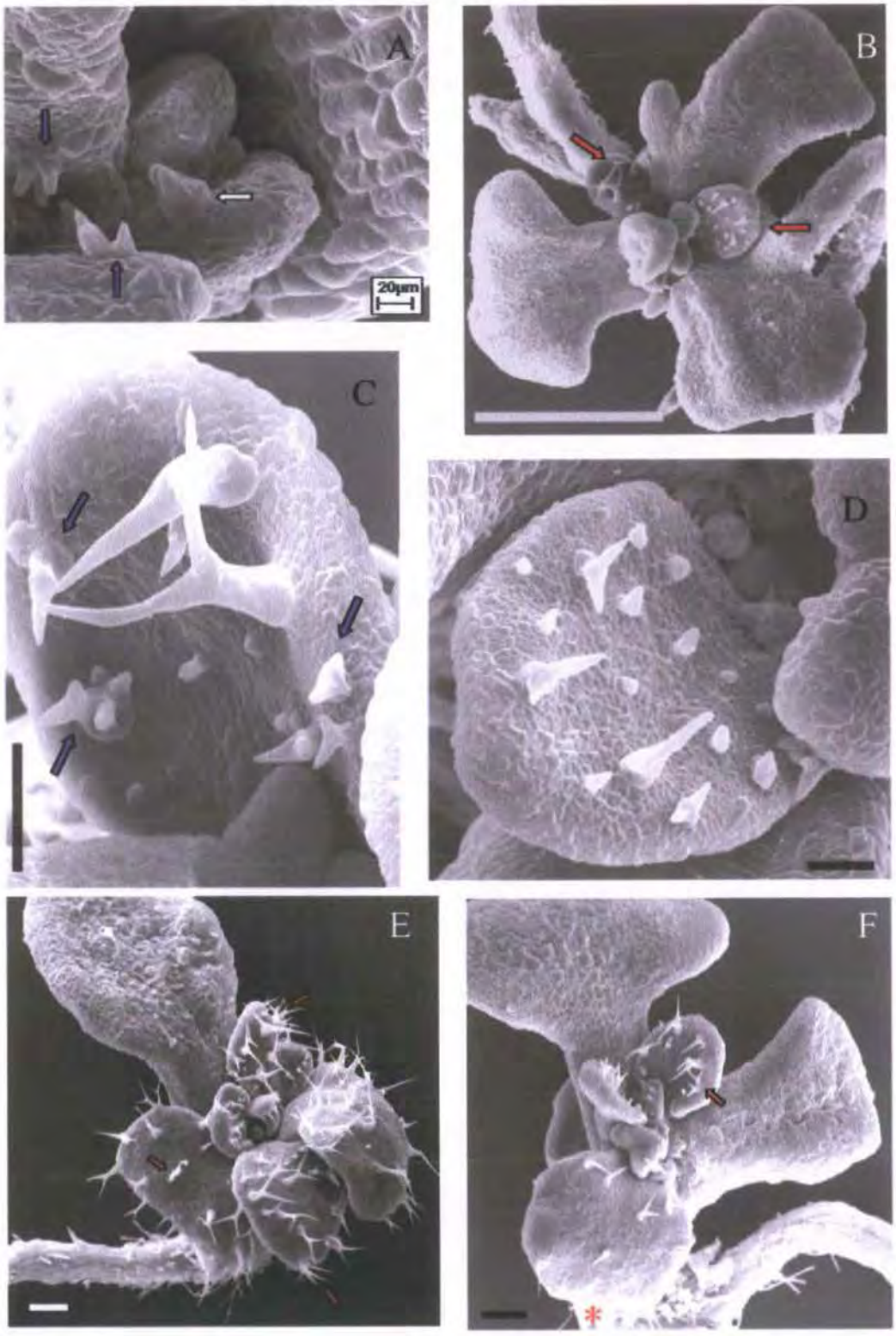

Figure 4.63 Trichome spacing in young true leaves of *hydra2*

The young leaves of the 5dae ***hyd2*** plant in A show young trichomes forming in clusters from adjacent epidermal cells (purple arrows). Note also the unusual inflated shape of the young trichome to the right (white arrow).

C and D show detail of the young true leaves indicated on the 7 dae *hyd2* seedling in B. Leaf D shows an even distribution over the laminar surface. C shows less regular spacing, and anomalous cell morphologies (arrows). The 7 dae *hyd2* seedlings in E and F have variable trichome distribution between the emerging young true leaves, with further examples of paired trichomes (arrows).

B, bar = 0.5mm; C- F, bar = 100μm.

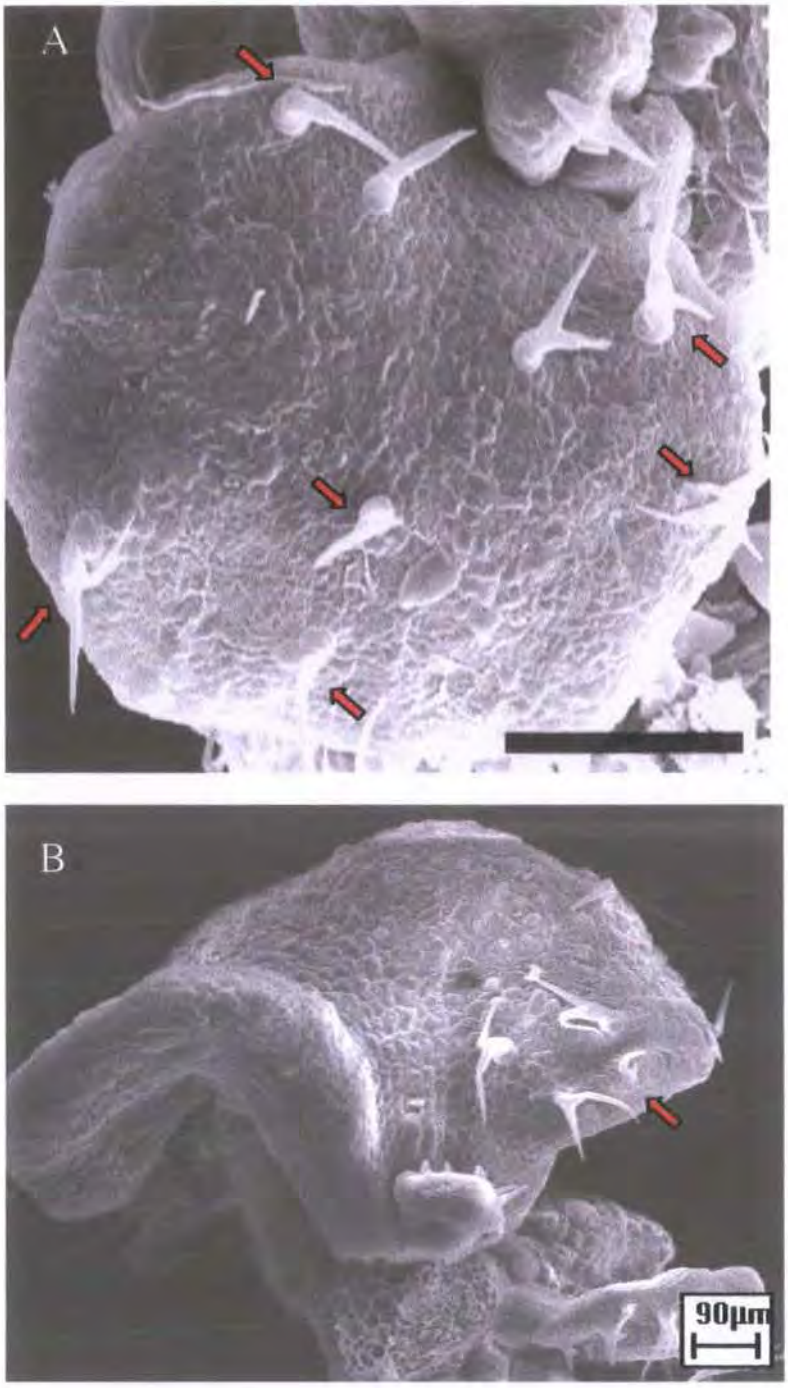

Figure 4.64 Cotyledon trichomes in *hydra2*

A and B; cotyledon detail from 7 dae *hyd2* plants

The cotyledons in A and B carry trichomes over a proportion of their adaxial surfaces (arrows). Wild-type cotyledons do not carry trichomes, and so these phenomena in *hydra* may indicate a 'mixed phase' phenotype. However as trichomes have only been found post-germination in *hydra*, this suggests that these misplaced hair cells may not result from similar phase-associated defects seen in the *lec* and *fusca3* mutants of *Arabidopsis*, in which trichomes appear during embryogenesis.

A, bar = 100μm.

seen in Fig. 4.62; C and D. *Arabidopsis* wild-type plants to not develop trichomes in the cotyledon epidermis.

In the true leaf epidermis of *hyd2*, shown in Fig. 4.63; A-F, leaves produce regularly spaced trichomes, although some arise in pairs, and hair cell morphology is variable. If the single or paired trichomes are taken as one 'spacing unit', then the patterns of spacing generation over the *hydra* lamina appear to be relatively normal. However lateral inhibition has been shown to act very locally, promoting trichome cell fate commitment within one cell whilst inhibiting this same cell fate in adjacent cells (Schellmann *et al.* 2002), suggesting that this local differentiation signal may be compromised in the *hydra* epidermis. This does not offer an explanation for the appearance of trichomes on *hydra* cotyledons, as detailed in Fig. 4.64.

Where trichomes arise ectopically on *hydra* cotyledons, they are not found over the entire lamina (Fig. 4.64; A and B) as in true leaves. The example shown in Fig. 4.64; B has a region of trichomes to the right of the lamina, whilst most of the rest of the surface of this organ is free of hair cells. Cotyledon trichomes in *hydra* mutants arise post-germination, and have never been found in embryos. This is in contrast to known mutants with cotyledon trichomes which are interpreted as a 'mixed phase' phenotype, i.e. *lec1*, *lec2* and *fus3* (Meinke 1992, Meinke *et al.* 1994, Keith *et al.* 1994).

4.3.7.7 Trichomes and basal cells in the *hydra* adaxial epidermis have variable defects in morphology and patterning

Wild-type trichomes differentiate and then expand in association with a ring of basal cells, visible around the trichome base in Fig. 4.65; A. A closer examination of *hydra* trichome morphology shows a range of anomalies both in the variable morphology of the hair cells themselves, and in the variable co-ordination of the trichome with its surrounding epidermal cells.

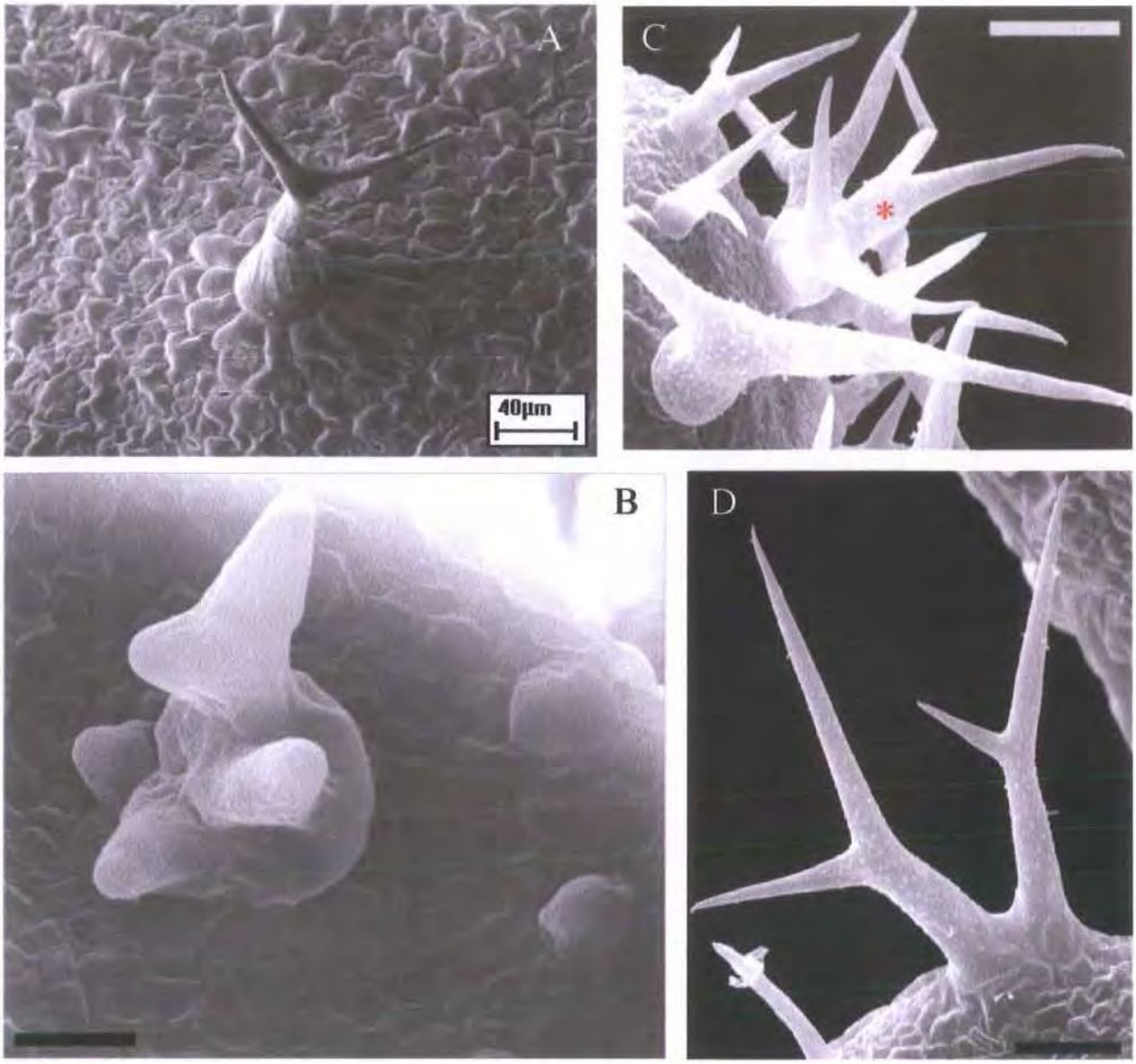

Figure 4.65 Trichome morphology and basal cell patterning in wild-type and *hyd2*

A; young trichome (at the first branching stage) from Ws, 7 dae, showing the elongated arrangement of basal pavement cells in towards the hair cell. B-D; trichome detail from *hyd2* plants at 7 dae. B, bar = 20μm; C and D, bar = 30μm.

B shows a young trichome prematurely initiating multiple branches. Two trichomes are beginning to emerge in the epidermis to the right.

The trichome marked by an asterisk in C looks like three fused trichomes; all of these branches appear to originate from a single cell (as in B), and their branch direction has no clear orientation relative to the leaf longitudinal axis.

The pair of trichomes shown in D appear to be two cells separated by a cell wall. In this case, branches are aligned along the same axis.

Trichome morphology in *hydra* may develop normally, may result in variably inflated and swollen hair cells that initiate branches prematurely (Fig. 4.65; B), may develop a reduced number of branches (Fig. 4.65; A, arrows) or none, or may resolve as 'twins' separated by a cell wall (Fig. 4.65; C, D, Fig. 4.66; B). Patterning of trichome basal cells in *hydra* mutants also show variation. The cell patterns visible in the epidermis in Fig. 4.66; D and E, show respectively a ring of cells round a single (D) and twinned (E) trichomes. In both of these examples, poor and uneven cell expansion has taken place; surrounding these basal cells the epidermis appears to contain many small undifferentiated cells with variable patterning.

The group of young trichomes in Fig. 4.66; A lack well differentiated basal cells, although most do appear to have a ring of pavement cells which have adopted basal cell identity. An exception is the 'trichome' marked by an asterisk; this mis-shapen cell appears to extend into the surrounding lamina over the area where the basal cells would be anticipated to have formed.

The base of the mature trichome shown in Fig. 4.66; C does have some elongated pavement cells, although not all have a clear cell fate. The white arrow indicates a file of marginal cells which appear to become 'adopted' by the trichome basal cells. To the right of this picture, the red arrow indicates pavement cells which are in the marginal position and would be anticipated to form a continuous cell file with the cells to the left. One of these pavement cells has also been 'adopted' at the end nearest the trichome and contributes to the ring of basal cells, forming an elongated section at one end.

These examples suggest that hair cells of the *hydra* leaf epidermis have difficulty both in regulating their morphology, and in co-ordinating differentiation between adjacent functional cells.

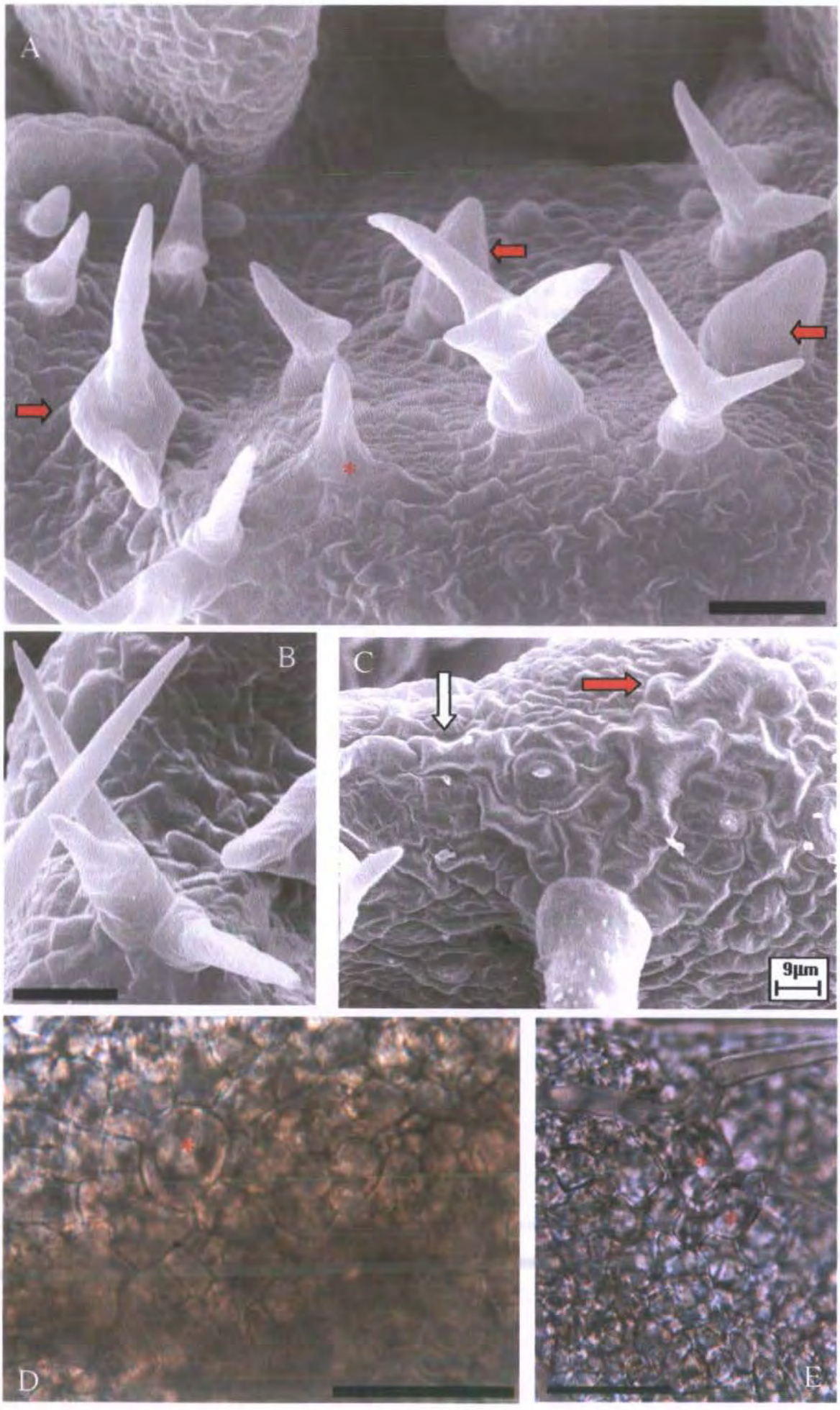
A
B
C
9µm
D
E

4.3.7.8 Stomata in the *hydra* cotyledon epidermis demonstrate anomalies in spacing and morphology

The agarose impression of a section of wild-type cotyledon adaxial epidermis in Fig 4.67; A, shows the result of a spacing mechanism that generates a separation between stomata so that no two stomata can form without an intervening cell (Geisler *et al.* 2000, Berger & Altmann 2000). Stomata at various stages of differentiation are visible, from fully functional guard cell pairs, to young stomates just differentiated, and occasional meristemoids prior to adopting guard mother cell fate.

In the *hydra* cotyledon epidermis, a different pattern resolves. The *hyd1* cotyledon adaxial pattern visible in Fig. 4.67; B, shows adjacent clusters of stomata (red asterisks), a guard cell pair comprised of unevenly sized cells (red arrow) and an apparently unpaired solitary guard cell (white arrow). The stoma with the uneven guard cell sizes is situated at the centre of what appear to be an elongated area of pavement cells, all oriented towards the stoma position.

Examples from the *hyd2* cotyledon adaxial epidermis are shown in Fig. 4.68. In Fig. 4.68; A, a cluster of stomata are visible (asterisk) close to variably spaced single stomates. The structure visible in Fig. 4.68; B appears to be guard-cell-like, although appears continuous with a pavement cell from the epidermis. The uneven surface of the adaxial epidermis is illustrated in Fig. 4.68; C, where a raised section of expanded tissue has created a 'hole'. Note the distortion of orientation of the stoma in the epidermis to the right.

The abaxial cotyledon epidermis detail from *hyd2* shown in Fig. 4.69; A illustrates more of the variety in stomatal formation seen in these mutants. Single, enlarged stomates are visible between clusters of variably sized stomata. Where clusters form, they appear to have arisen from many cells (as

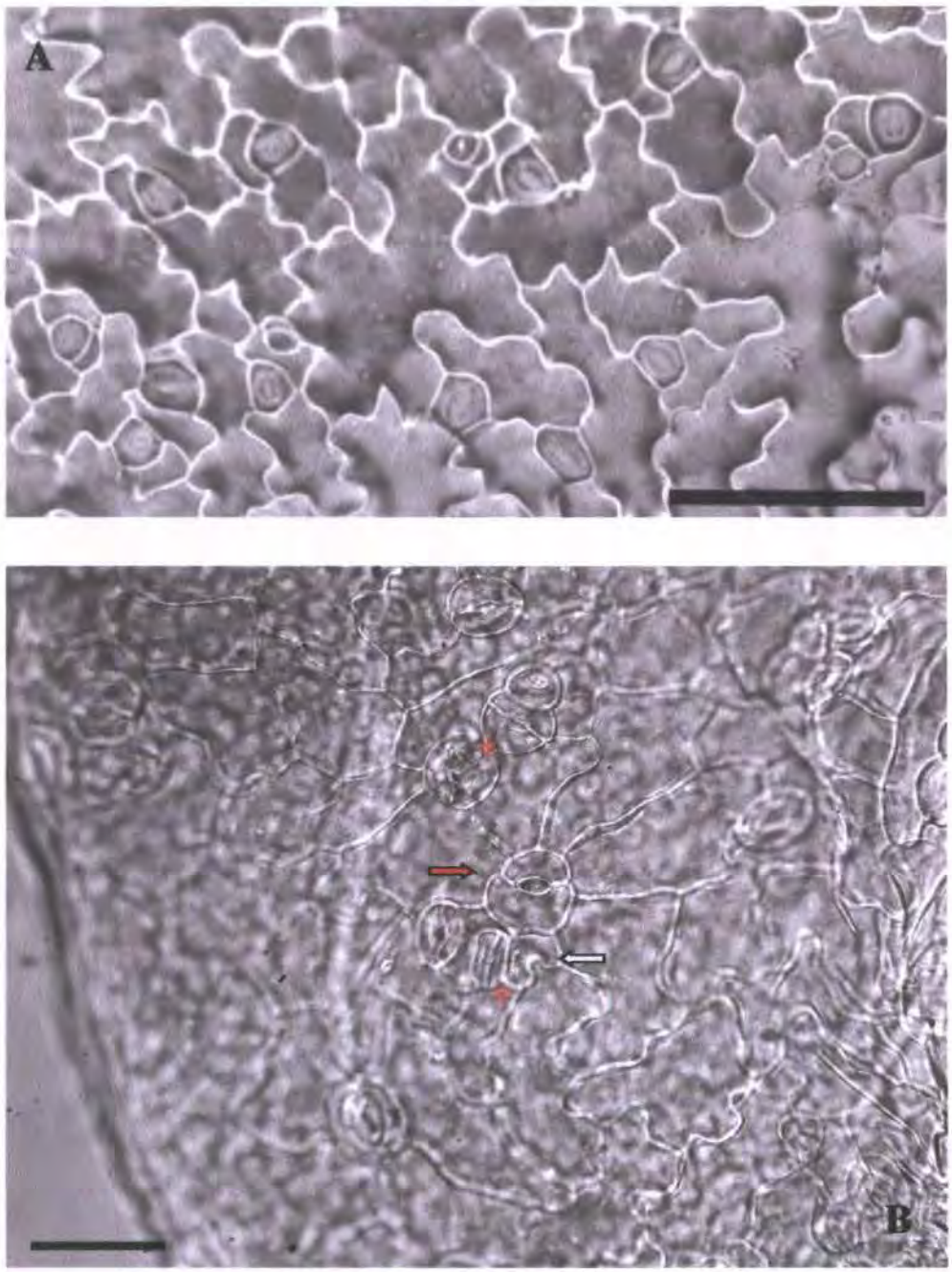

Figure 4.67 Stomatal spacing in the wild-type and *hydra1* cotyledon epidermis

A; Ws stomatal pattern taken from the centre of a cotyledon adaxial surface from an 8 dae plant (composite image assembled from agarose epidermal impressions), bar = 100μm. Stomatal complexes are evident here at different stages of differentiation. As complexes develop, the adoption of meristemoid (stomatal precursor) cell fate is inhibited in cells adjoining other meristemoids or guard mother cells. This generates a stomatal distribution close to, but not exactly random, in which all stomata are separated by at least one intervening cell.

B; patterning of the *hyd1* cotyledon adaxial surface at 8 dae, bar = 50μm. Note that in this plant, stomata are seen adjoining (asterisks), and in the centre of the picture some unusual guard cells are evident, with a pair of guard cells of unequal size (red arrow) and a single cell which appears to have adopted guard cell identity, but lacks its partner cell (white arrow). Other anomalies are evident, including misshapen pavement cells around this stomatal complex, forming a pattern more reminiscent of trichome basal cells than the usual interlocking pavement cells between stomata seen in the wild type epidermis.

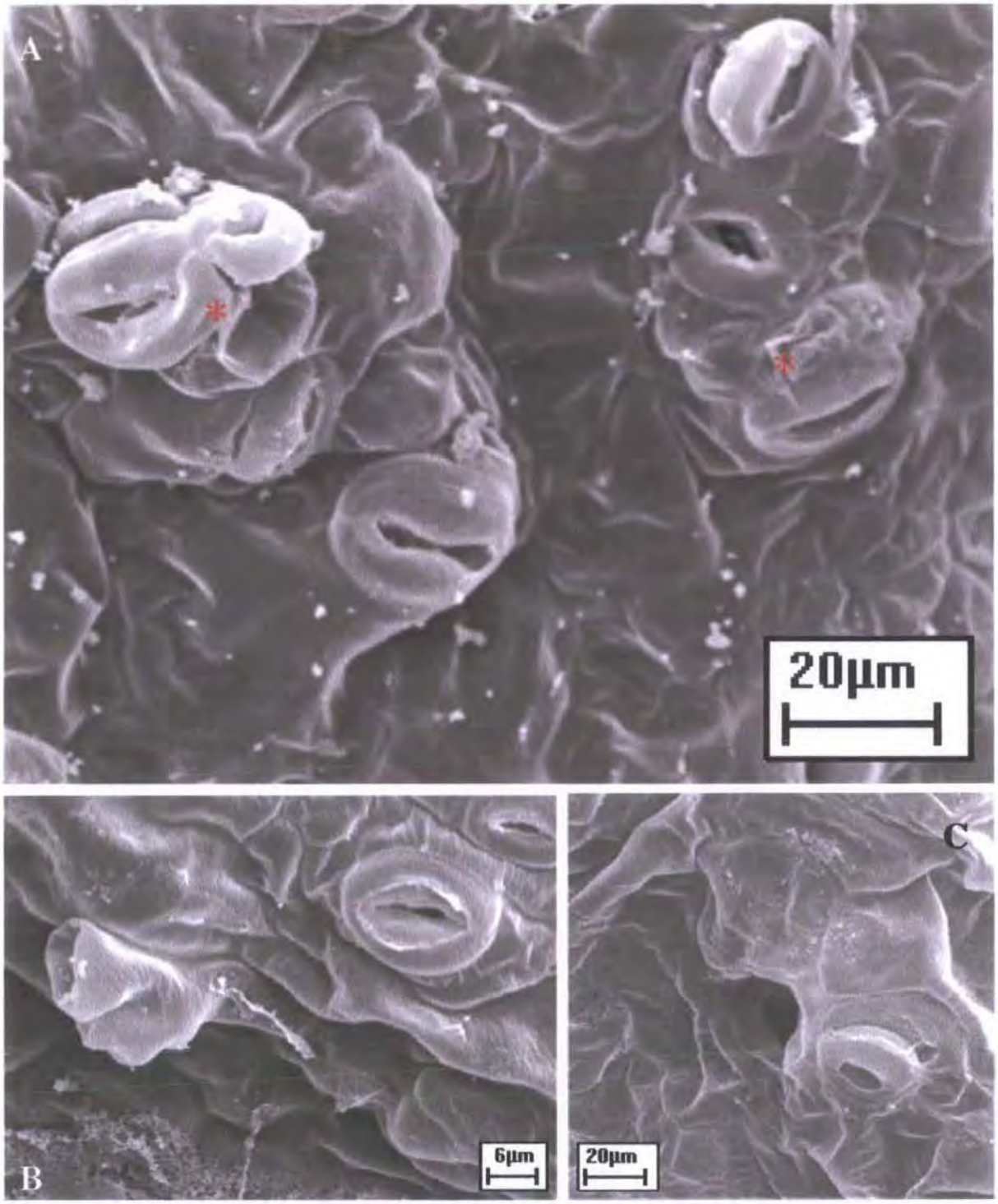

Figure 4.68 Stomatal detail from the *hyd2* cotyledon adaxial lamina

A-C; stomata from cotyledon adaxial surfaces of *hyd2* seedlings at 5 dae (A, B) and 11dae (C).

Clusters of stomata are evident in A, forming raised areas of leaf surface.

The cell seen to the left in B is difficult to interpret, but may result from a situation where division and differentiation of guard cell pair have become mis-synchronised.

The large single stoma in C has been pushed sideways by a section of lamina, forming a raised and uneven region above the usual surface. The 'hole' is not an artefact; these phenomena are often seen in mature laminae in associated with raised or uneven regions of the mutant leaf surface. Such modification of the adaxial lamina is common in the cotyledons of both *hyd1* and *hyd2* seedlings, which continue to develop after normal leaf maturation is complete. These raised sections of epidermis may be associated with points of persistent ectopic cell division in the mesophyll.

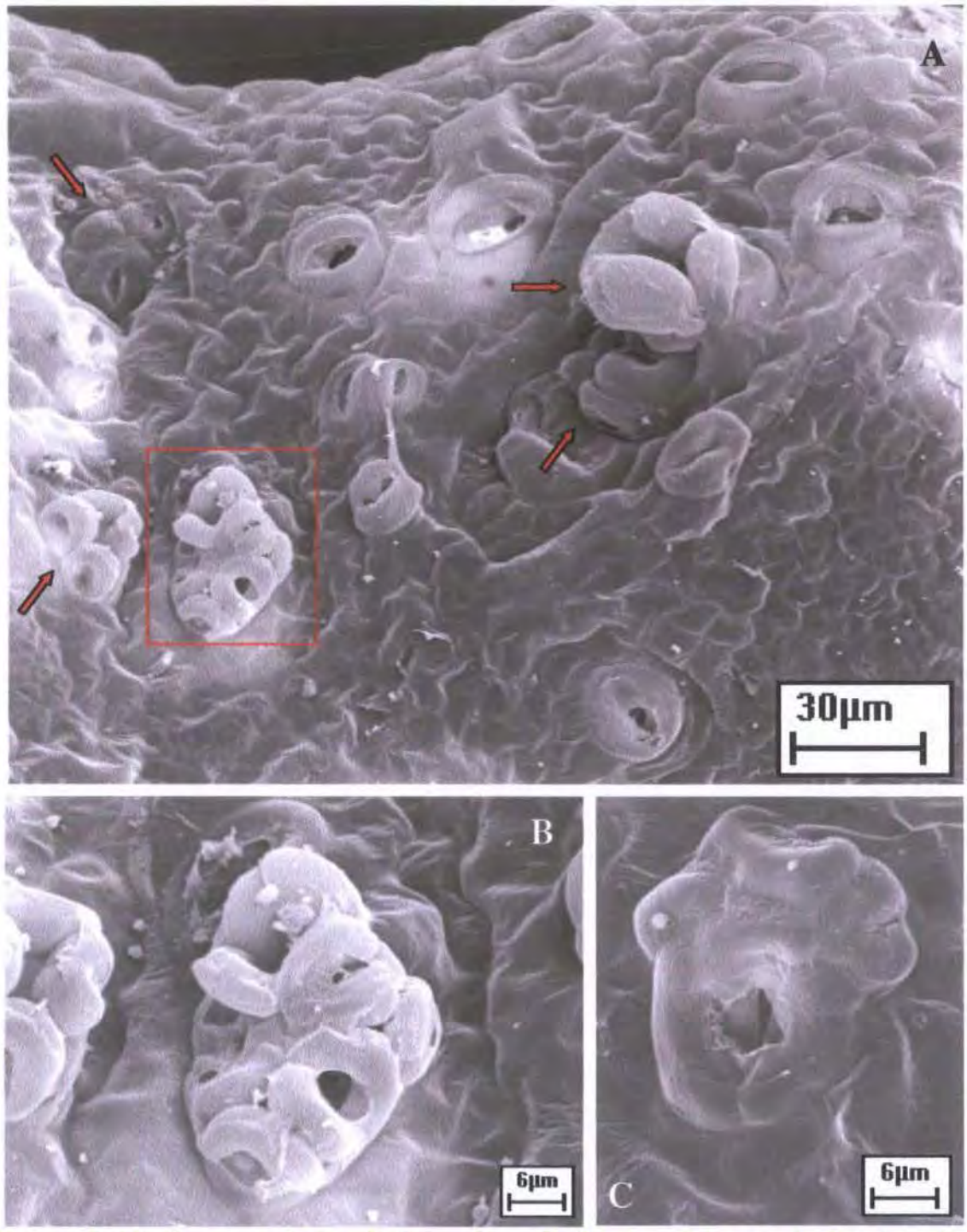

Figure 4.69 Stomatal detail from the *hyd2* abaxial cotyledon lamina

A-C; stomata from cotyledon abaxial surfaces of *hyd2* plants at 7 dae. B shows detail of the stomatal cluster defined by the box in A.

The abaxial lamina of wild-type cotyledons carries greater numbers of stomata than the adaxial surface, and is more uneven. However, the stomatal spacing observed in wild type plants still applies, with no two adjacent cells adopting guard cell fate.

The *hydra* lamina shown in A shows further exacerbation of the stomatal spacing problems seen on adaxial surfaces, with extensive formations of clustered guard cells forming three-dimensional mounds (box, arrows). The cluster shown in C appears to consist of multiple guard cell pairs, and may represent a an earlier stage of cluster development than that seen in A and B.

in B and C), or comprise numerous, few, or only two stomates. These numbers within the cluster encompass a range of phenomena known from other stomatal patterning mutants, namely *too many mouths* (*tmm*), *stomatal density and distribution1* (*sdd1*) and *fourlips* (*flp*) (Geisler *et al.* 2000, Berger & Altmann 20000, von Groll & Altmann 2001, Yang & Sack 1995, Larkin *et al.* 1997).

4.3.7.9 Poor co-ordination of asymmetric cell divisions during stomatal ontogeny in *hydra* mutants can result in adjacent cells adopting meristemoid identity

Stomata arise in post-germination *Arabidopsis* cotyledons from in a randomised pattern from undifferentiated epidermal cells adopting meristemoid mother cell fate (Geisler & Sack 2002, Bean *et al.* 2002). They may proceed to become guard mother cells and differentiate as a single stoma without further division, or may go through a series of co-ordinated asymmetric divisions to produce further small meristemoid cells and larger companion cells. This process is co-ordinated between cells in the epidermis, in order that no two meristemoids lie adjacent to each other. If this happens, one of the meristemoids will divide again, orienting the daughter meristemoid away from the other (Geisler *et al.* 2000). A number of stages in this ontogeny are represented in agarose impressions from wild-type epidermis, shown in Fig. 4.70; A-E. Whilst these images are not of sequential cell division and differentiation patterns, the range of examples illustrates that stomatal ontogeny is proceeding normally in these wild-type plants taken from the *hyd1* mutant background.

Fig. 4.71; A-C, D-F and Fig. 4.72 A-C show sequential agarose impressions from regions of the *hyd1* cotyledon adaxial epidermis, and reveal the ontogeny processes contributing to formation of stomatal clusters in these mutants. It

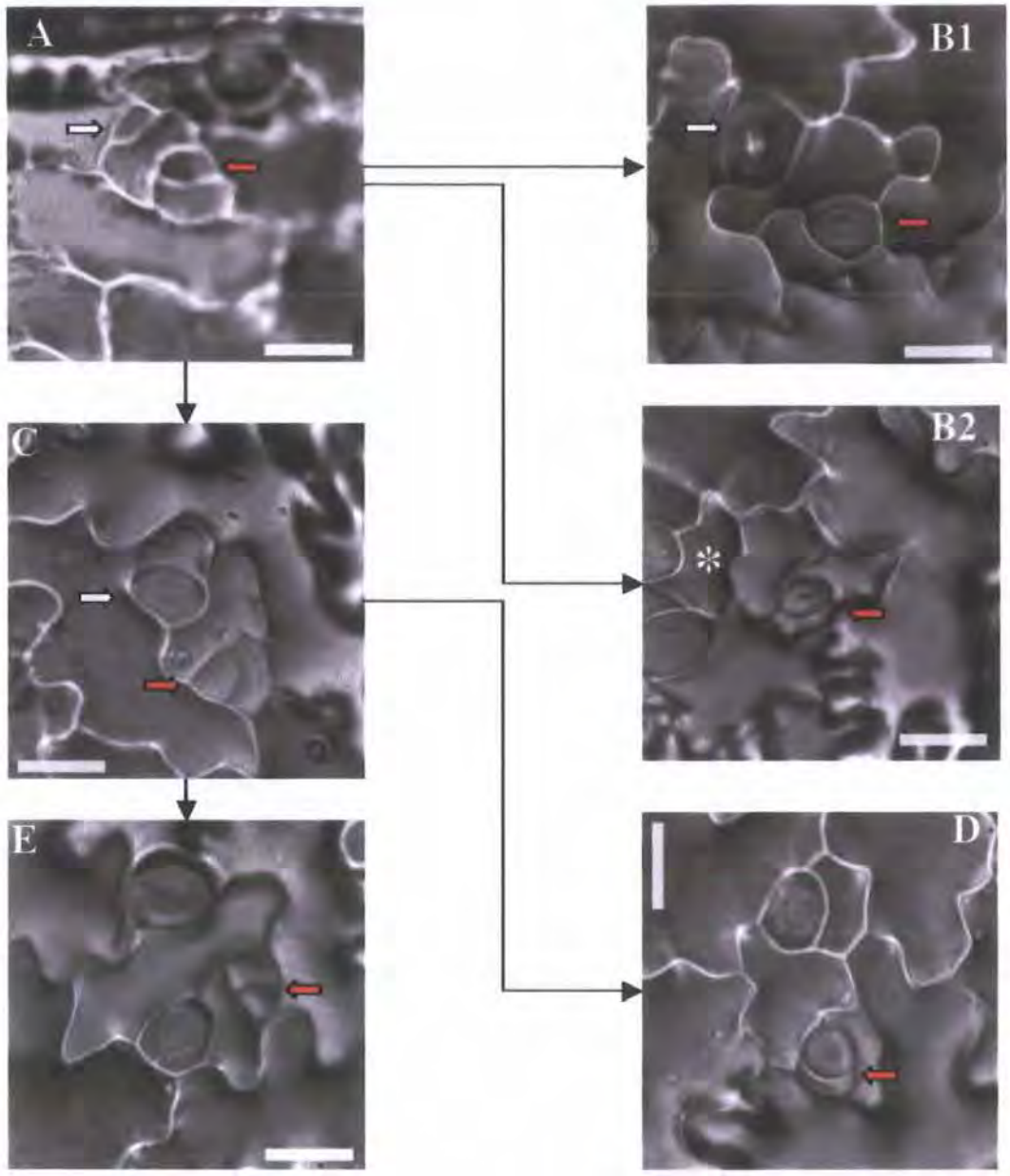

Figure 4.70 Stomatal ontogeny in the Ws cotyledon adaxial epidermis

A-E; agarose impressions of stomatal complexes at various representative stages of development (i..e. not sequential), taken from different regions of wild-type cotyledon adaxial surfaces between 4 and 8 dae, bar = 20μm.

In wild-type cotyledons, stomata develop after germination within a field of undifferentiated epidermal cells where meristemoid mother cell (MMC) or pavement cell fate is available. MMC's undergo an asymmetric division to produce a small triangular shaped meristemoid and a neighbouring cell (A, red arrows). The direction of this division appears to be random when no neighbouring cells have adopted guard mother cell (GMC) fate.

A-B1; meristemoids have adopted guard mother cell fate, and divided to produce two guard cells (white arrows) without further meristemoid formation.

A-B2; one meristemoid has divided again to generate an extra cell before differentiating as a guard mother cell (white arrow), generating a stomate. In this example, the asterisked cell (in a similar position to the red arrowed cell in A) lies adjacent to other stomata and so has not adopted GMC fate.

A-C-E; meristemoids can divide up to three times, in a spiral pattern, developing a stomatal complex, or exit the process (as in C-D) at an earlier stage.

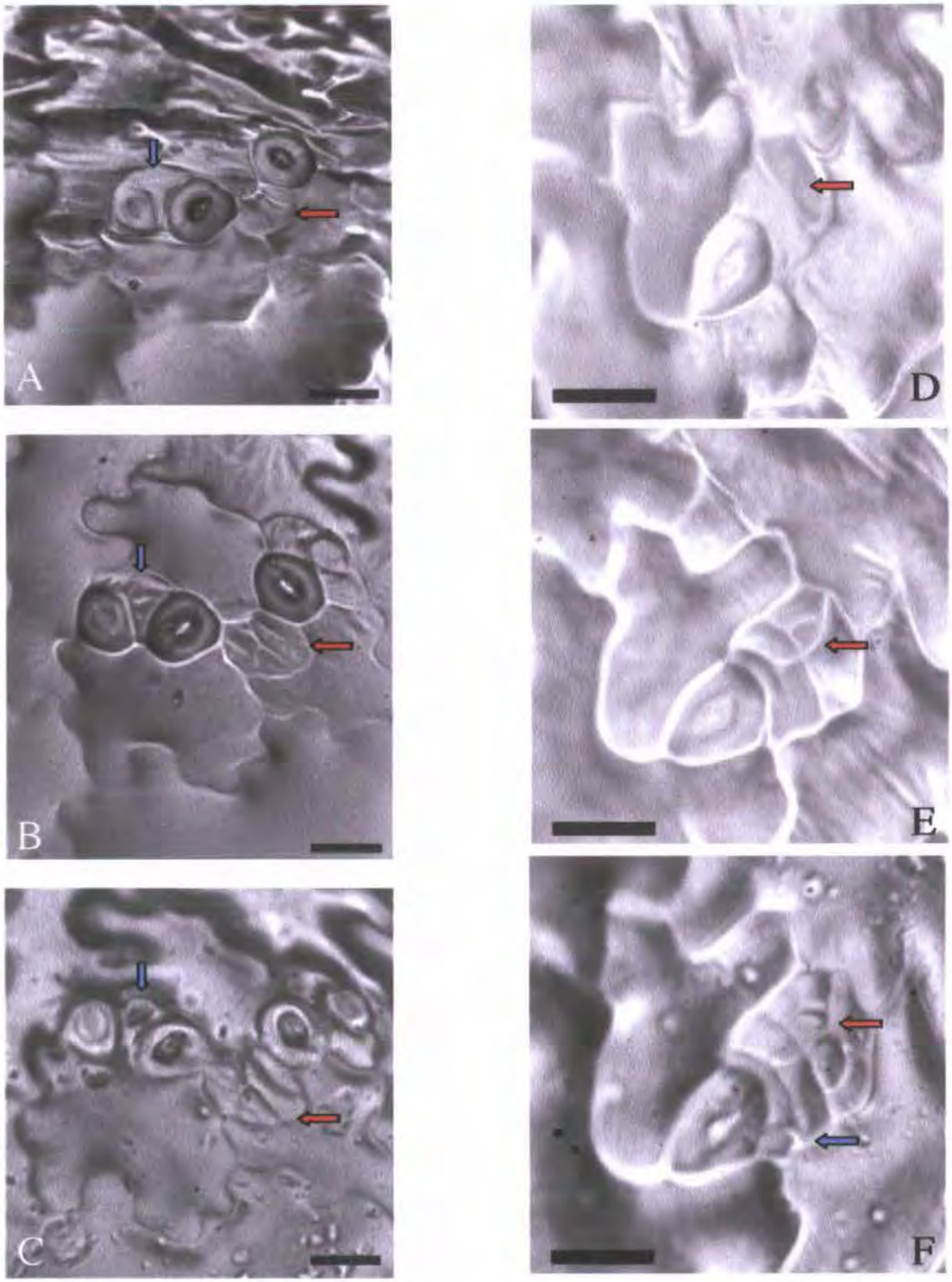

Figure 4.71 Stomatal ontogeny in *hydra1* cotyledons

A-C and D-F; sequential agarose impressions of stomatal complex formation in *hyd1* between 6 and 8 dae, bar = 20μm.

A-B-C; the field of cells indicated by the red arrows undergoes simultaneous divisions producing daughters of roughly equal size (A-B), and then two of cells make classic meristemoidal asymmetric divisions (B-C). To the left, a larger cell (blue arrow) separates two differentiated stomata. Between B and C (within 24 hours) this cell has differentiated as an additional stoma, in contact with the first two.

D-E-F; the field of cells indicated by the red arrow undergoes divisions to place two triangular meristemoid cells adjacent to each other, and a further meristemoid appears adjacent to a stoma (blue arrow).

is evident from these pictures that both the orientation of cell division and cellular expansion proceed variably in *hyd1*.

In Fig. 4.71; A-C, the cell indicated by the blue arrow, which separates the two stomates in F, has adopted meristemoid cell fate, and differentiated directly into a stoma itself by C, apparently without an intervening cell division to generate a separating companion cell. In this same cluster, the red arrow shows a series of divisions which have resolved two small asymmetric meristemoids which are well spaced from each other and the adjacent stomata, and other symmetric divisions producing cells which may or may not adopt meristemoid cell fate.

In contrast, the series in Fig. 4.71; D-F shows a series of cell division events which has produced two adjacent small triangular shaped meristemoids (red arrow). Fig. 4.71; F also shows another meristemoid (blue arrow), formed from two rapid divisions of a companion cell, and positioned adjacent to a differentiated stomate.

The series in Fig. 4.72; A-C shows a group of cells around a differentiated stomate which undergo a series of rapid divisions without differentiation, but which are producing a distortion of the epidermal surface. Such a series, accompanied by a later simultaneous differentiation of the many small cells which result, may prefigure some of the larger stomatal clusters as shown in Fig.s 4.68 and 4.69.

The stoma in Fig. 4.72; D is substantially enlarged with respect to other stomata in the epidermis. This example is surrounded by enlarged, elongated cells which appear to comprise a region of misplaced marginal cell files. Within this zone, the stoma shown has enlarged along with these other cells, producing a 'giant' morphology.

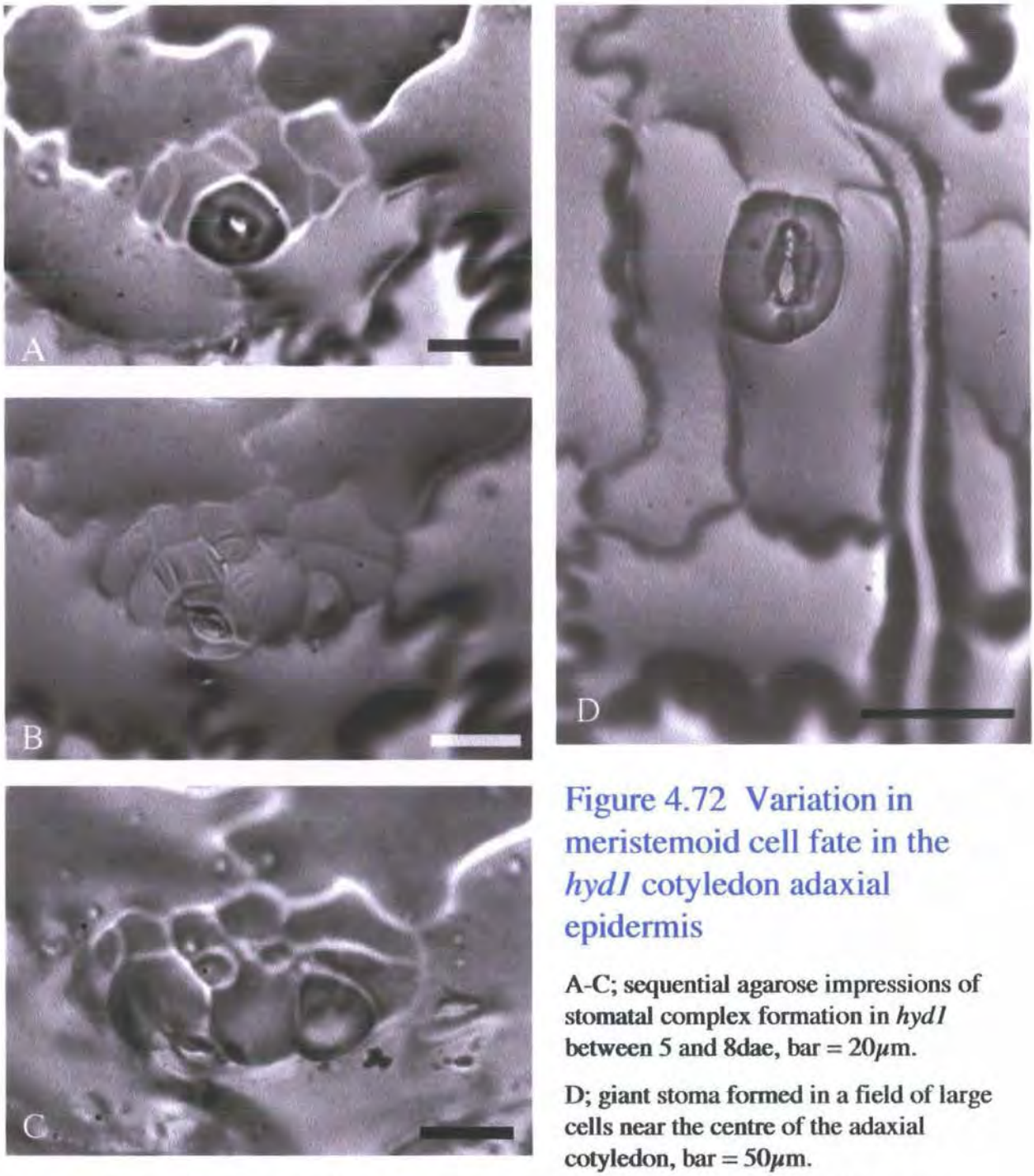

Figure 4.72 Variation in meristemoid cell fate in the *hyd1* cotyledon adaxial epidermis

A-C; sequential agarose impressions of stomatal complex formation in *hyd1* between 5 and 8dae, bar = 20μm.

D; giant stoma formed in a field of large cells near the centre of the adaxial cotyledon, bar = 50μm.

A-C; a filed of dividing cells lies adjacent to a differentiated stoma. These cells undergo various divisions, and appear to expand under the established guard cell pair so that it is pushed sideways, and a mound of cells develops behind it.

D; giant stoma, found in an area of cells which may be misplaced marginal cells on the adaxial cotyledon surface. In the absence of cell division events associated with stomatal complex formation in this region of the lamina, this stoma become substantially larger than any of the other stomata from the same cotyledon adaxial surface.

4.3.7.10 Epidermal patterning in the lateral organs of *hydra* inflorescence stems show normal patterning of functional cells in the epidermis.

Fig.s 4.73 and 4.74 details the epidermal patterning found in cauline leaves, sepals and petals from *hydra* mutant inflorescence stems, showing examples from *hyd2*.

In contrast to lateral organs of the rosette, no patterning anomalies were found in functional epidermal cells (stomata and trichomes) of either cauline leaves or sepals. Fig. 4.73; A shows a section of adaxial epidermis from a *hyd2* cauline leaf. Although the pavement cells in this epidermis are much smaller than in wild-type, patterning processes appear to be functioning normally. No clustered trichomes or stomata were found in the cauline epidermis, although rosette leaves from the same plants showed clusters formed from both cell types. The adoption of a ring of pavement cells in association with trichome development was normal (Fig. 4.73; A and B, white arrows), although these cells were compromised in expansion, along with the reduced size of the whole cauline lamina. Where these cells were un-expanded, they were observed to be of even size around the trichome base. All cauline leaves had clearly differentiated marginal cell files, within which differentiated trichomes could be seen (Fig. 4.73; C) as in wild-type.

As with cauline leaves, patterning of the sepal epidermis in *hydra* showed no clustering of stomata or trichomes. The arrangement of cell files within the epidermis was indistinguishable from wild-type (Fig. 4.74; A and B), and the equivalent cell lengths reflected the similar size of wild-type and mutant sepals. A similar situation was observed in the petal epidermis (Fig. 4.74; C and D), where the mutant pattern appeared identical to that of wild-type organs over both abaxial and adaxial surfaces. No stomata or trichomes are

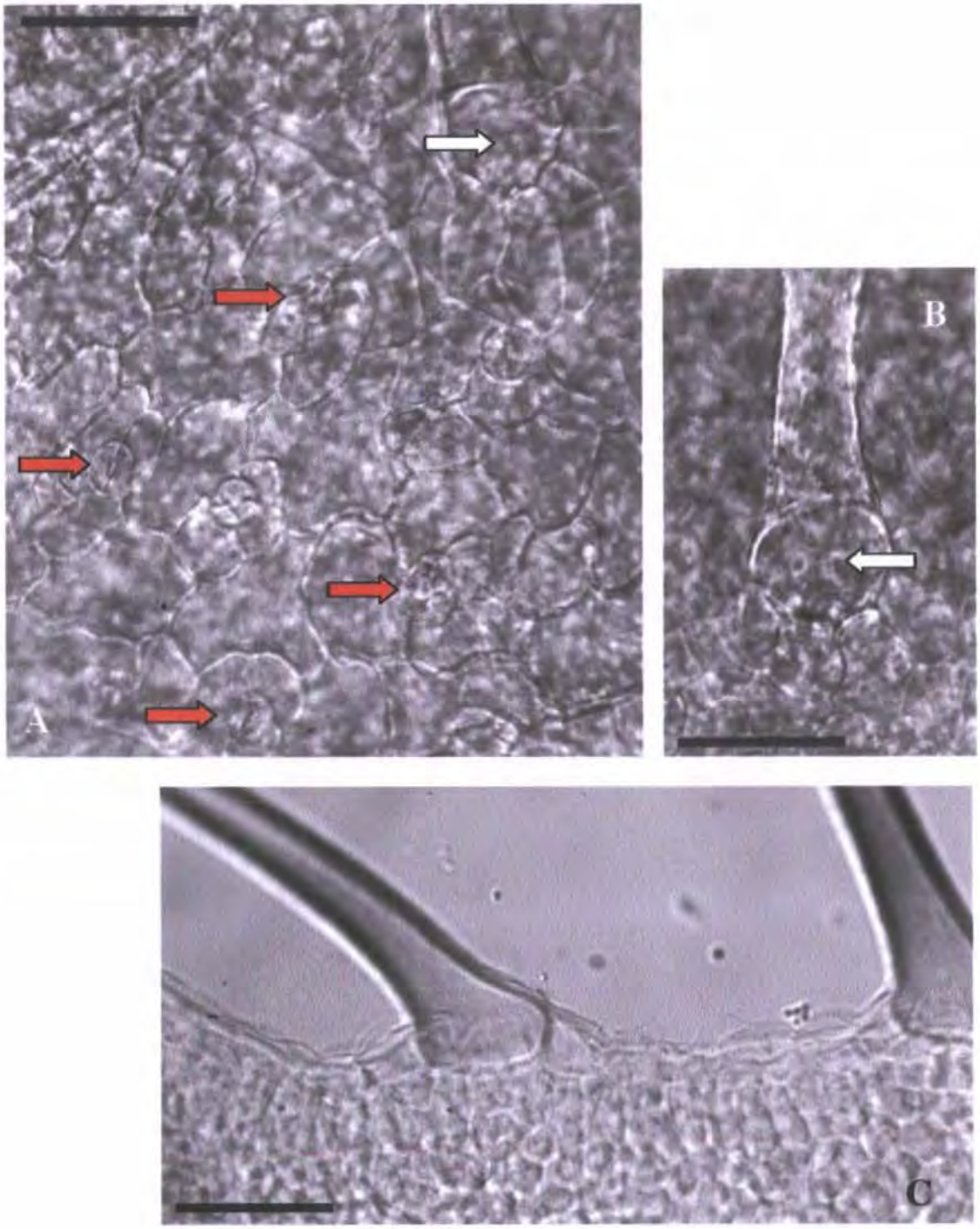

Figure 4.73 Epidermal detail from *hyd2* cauline leaves

A-C shows epidermal detail from cauline leaves of *hyd2*, bar = 50μm.

Unlike cotyledons and rosette leaves, no clustered stomata were observed in these organs. Red arrows show individual stomates. Trichomes appear normal and are found as single cells in the epidermis, with a normal arrangement of accessory cells (A, B; white arrows) although these cells are not elongated as in wild-type. Margin cells appear to form coherent cell files at the laminar adaxial-abaxial boundary, and show normal patterning (C). However these leaves are much smaller than wild-type, and have a longitudinally shortened morphology (shown in Fig. 4.15).

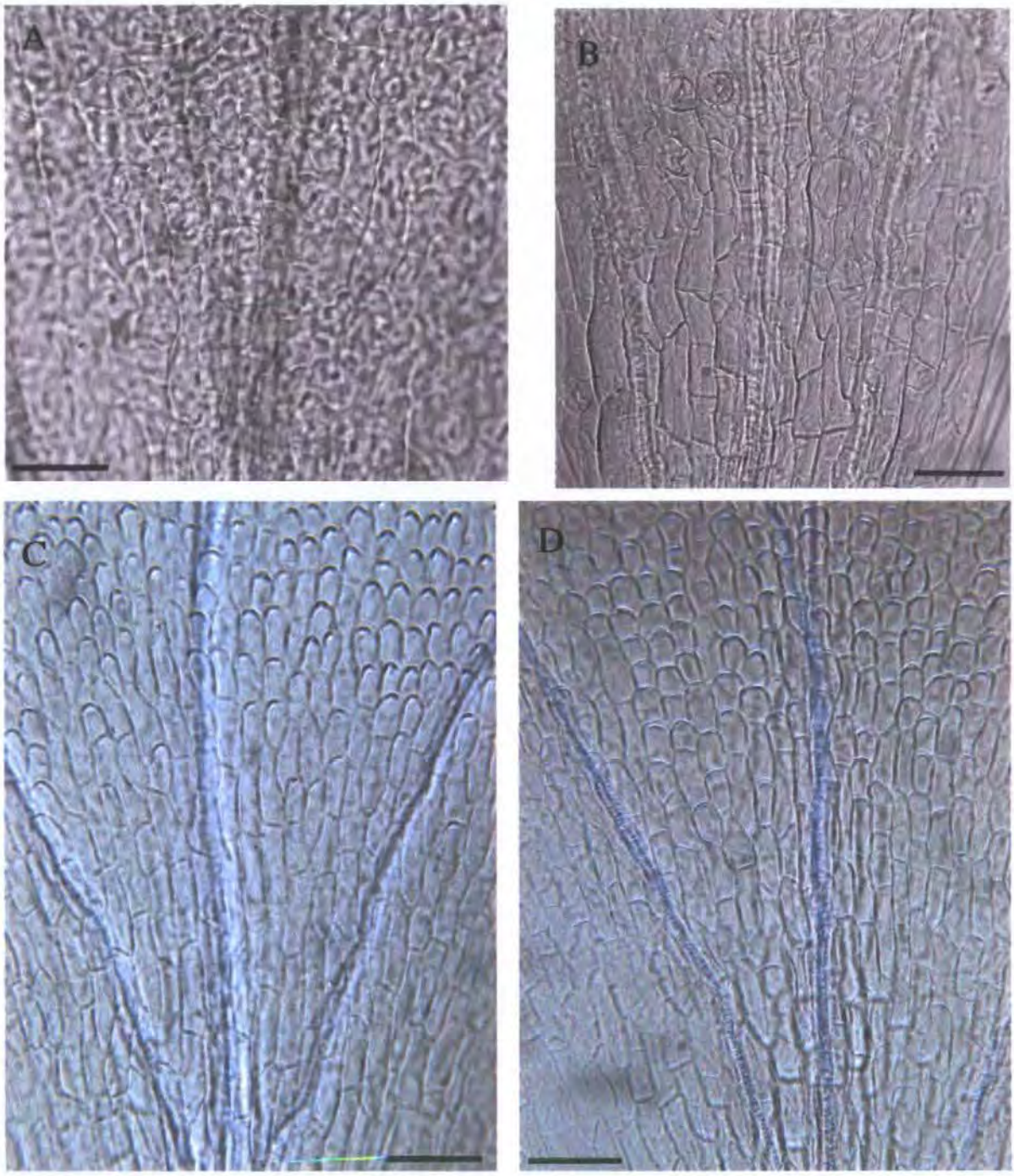

Figure 4.74 Patterning in wild-type and *hydra* mutant sepal and petal epidermis

A; Ws and B; *hyd2* sepal epidermis,C; Ws and D *hyd2* petal epidermis, bar = 50μm.

The wild-type sepal epidermis is comprised of longitudinal files of cells; growth appears mostly longitudinal with longitudinally oriented cell files across the lamina, and minimal lateral expansion. Stomata differentiate within these cell files in a pattern reminiscent of the petiole epidermis of true leaves (A). Petals do not carry stomata; their longitudinally arranged cell files have elongated cells towards the base of the organ, and more isodiametric cells with conical surfaces towards the petal apex (C).

Epidermal patterning appears normal in the lateral organs of *hydra* bolts. No clustered stomata were found in any *hydra* sepals examined, and the range of cell sizes within the mutant epidermis looked very similar to the wild-type cell population (B). In *hydra* petals, no discernible differences were evident between wild type and mutant epidermal cells (C).

found in the petal epidermis, unlike other flattened lateral organs of the inflorescence stem.

These findings imply that the *HYDRA* genes have a distinct role in the co-ordinated differentiation of cells during the resolution of epidermal patterning of rosette lateral organs, but are not involved, or are redundantly involved, in patterning of lateral organs in the inflorescence stem. However there does still appear to be a requirement for correct *HYDRA* gene function normal expansion of the cauline leaves, unlike inflorescence lateral organs. This may indicate that sterols are involved in two processes, namely epidermal pattern definition of rosette leaves (and possibly cauline leaves in a redundant fashion), and vegetative lateral organ expansion.

4.3.9 Summary of Chapter 4

The morphology of *hydra* mutants demonstrates multiple anomalies associated with radial mis-coordination of longitudinal cell files throughout the growth axis. This results in variable duplication or dissociation of the stele and primary vascular traces in the shoot, resulting in the development of a range of sibling morphologies characterised by supernumerary cotyledons, variably sized SAMs, adjacent or clustered and precocious primordial initiation, and poor meristem maintenance. Ectopic SAM formation was seen specifically within the hypocotyl-cotyledon transition zone, and was promoted by anomalous branching events in the upper hypocotyl stele. Variable leaf shapes are associated with radial patterning difficulties at the shoot apex in tandem with dissociation of the leaf vascular primary traces.

Mis-positioning of dorsiventral cues were revealed by reporters of *YABBY*, *PHABULOSA* and *REVOLUTA*, including a complete reversal of abaxial-adaxial marker positioning in young primordia of some siblings. Most siblings also

lacked functional stipules, and showed poor abaxial-adaxial organization of the mesophyll in cotyledons and true leaves.

Multiple patterning processes reliant upon intercellular communication were disrupted, including longitudinal cell file coherence in the epidermis, disjunct and isolated xylem, variably clustered stomata, paired trichomes, misplaced marginal cell files and variably shaped epidermal cells in both shoot and root. Ectopic cell division events, and excessive proliferation of cells in expanding primordia, imply a lack of co-ordinated transition to the differentiation stage. There appears to be a correlation between marginal misplacement and xylem disjuncture. Microtubule cortical arrays within cells of the longitudinally-oriented epidermal cell files implied poor co-ordination of expansion axes, and longitudinal cell expansion was compromised throughout the growth axis.

Asymmetric division of meristemoids during the ontogeny of stomatal clusters in rosette lateral organs appeared to function normally, although placement of division planes variably put stomatal precursors next to differentiated stomates. Cells of various shapes appeared to become satellite meristemoids, and proceeded to guard mother cell fate next to other differentiated guard cell pairs.

Patterning anomalies found in cotyledons and true leaves of the rosette were not replicated in cauline leaves or inflorescence lateral organs. Flattened lateral organs which showed activity of the p*HYD1*::GUS reporter (cauline leaves, sepals, silique valves) displayed 'noise' in the xylem trace, although this was minimal in comparison to rosette leaves, and developed no patterning anomalies in functional cells of the epidermis, again in contrast to the rosette organs.

Radial organization of the root appears subordinate to the vascular organization of the stele. Increased root hair production is associated in the mutants with an increased number of cortex and endodermal cells within the

radial layers, and poor epidermal cell file organization corresponds to organizational difficulties in the cortex cell files. In addition, some trichoblast cells show shape anomalies including swelling at the site of root hair initiation, branching of root hairs, and occasional polarity reversal or tip initiation at multiple points along the cell's longitudinal axis. Points of mis-coordination within longitudinal cell files and sites of vascular discontinuity appear to act as foci for localized ectopic cell division, particularly in cotyledons and in the region of vascular transition in the upper hypocotyl.